# WORKSHOP IN SAMPLING REQUIREMENTS

# FOR MONITORING AND EVALUATION

# OF WATERSHED MANAGEMENT PRACTICES

Presented by

Simons, Li & Associates, Inc.

Daryl B. Simons
Ruh-Ming Li
Thomas P. Ballestero
Kenneth G. Eggert

Sponsored by

U.S. Environmental Protection Agency
Environmental Research Laboratory
Athens, Georgia

In cooperation with

U.S. Environmental Protection Agency
Water Planning Division
Office of Water Regulations and Standards
Washington, D.C.

May 20-21, 1981
Arlington, Virginia

TABLE OF CONTENTS


Page

I. INTRODUCTION . . . . . 1.1

1.1 Course Objectives . . . . . 1.1
1.2 Physical Processes Governing Watershed Response . . . . . 1.2

1.2.1 Introduction . . . . . 1.2
1.2.2 Spatial Representation of Watersheds . . . . . 1.6
1.2.3 Model Components . . . . . 1.16

1.3 Procedures for Evaluation of a Monitoring Network . . . . 1.24
1.4 References . . . . . 1.25

II. CONCEPTUAL DESIGN OF A MONITORING SYSTEM. . . . . 2.1

2.1 Introduction . . . . . 2.1
2.2 Data Needs . . . . . 2.1

2.2.1 General . . . . . 2.1
2.2.2 Specific Needs. . . . . 2.2

2.3 Direct Measurements. . . . . 2.8

2.3.1 General . . . . . 2.8
2.3.2 Collection and Processing of Surface Water Data . . 2.8

2.3.2.1 Gage Datum . . . . . 2.9
2.3.2.2 Maintenance of a Gaging Station. . . . . 2.9
2.3.2.3 Recording and Documentation of Data. . . . 2.10
2.3.2.4 Servicing Stage Recorders. . . . . 2.10
2.3.2.5 Discharge Measurements . . . . . 2.15
2.3.2.6 Equipment. . . . . 2.17
2.3.2.7 Current Meter Measurements . . . . . 2.18
2.3.2.8 Velocity Measurements. . . . . 2.18
2.3.2.9 Development of Rating Curves . . . . . 2.21
2.3.2.10 Requirement for Discharge Measurement at a Range of Stage. . . . . 2.27
2.3.2.11 Operation and Maintenance of Crest-Stage Gages. . . . . 2.27
2.3.2.12 Discharge Measurements at Low-Flow Partial-Record Stations. . . . . 2.29

2.3.3 Collection and Processing of Water Quality Data . . 2.31

2.3.3.1 General. . . . . 2.31
2.3.3.2 Sampling Techniques. . . . . 2.32
2.3.3.3 Field Evaluations. . . . . 2.33
2.3.3.4 Chemical Samples . . . . . 2.35
2.3.3.5 Sediment Sampling. . . . . 2.35
2.3.3.6 Site Selection . . . . . 2.36
2.3.3.7 Stream Sampling Stations . . . . . 2.39

TABLE OF CONTENTS (continued)


2.3.3.8 Total Collection Devices . . . . . 2.39
2.3.3.9 Suspended Sediment Samplers and. . . . . 2.41
Measurements . . . . . 2.41
2.3.3.10 Bed-Material Samplers. . . . . 2.50

2.4 Meteorological Data. . . . . 2.52

2.4.1 Site Requirements . . . . . 2.52
2.4.2 Air Temperature . . . . . 2.54
2.4.3 Air Humidity. . . . . 2.55
2.4.4 Wind. . . . . 2.56
2.4.5 Solar Radiation . . . . . 2.57
2.4.6 Barometric Pressure . . . . . 2.59
2.4.7 Rainfall Measurement. . . . . 2.60

2.4.7.1 Site Selection . . . . . 2.61
2.4.7.2 Factors Affecting Accuracy . . . . . 2.62
2.4.7.3 Nonrecording Gages . . . . . 2.64
2.4.7.4 Recording Gages. . . . . 2.66

2.5 References . . . . . 2.68

III. SPATIAL AND TEMPORAL CORRELATION . . . . . 3.1

3.1 Introduction . . . . . 3.1
3.2 Correlation in Time, the Autocorrelation Function . . . . 3.2

3.2.1 Introduction and Theory . . . . . 3.2
3.2.2 Loss of Information by Discretization . . . . . 3.6

3.2.2.1 Discrete Point Sampling . . . . . 3.8
3.2.2.2 Average Sampling . . . . . 3.11

3.2.3 Effect of the Sampling Interval on the Correlogram 3.11
3.2.4 Miscorrelation: Effects of the Misuse of Data and the Misinterpretation of the Autocorrelation Function . . . . . 3.14

3.2.4.1 Intermittent Processes . . . . . 3.14
3.2.4.2 Jumps and Trends . . . . . 3.14
3.2.4.3 Measurement Accuracy (Effect of Truncation) and Autocorrelation . . . . . 3.17

3.2.5 Effects of Reservoirs on Correlation Structure . . 3.18

3.2.5.1 Introduction . . . . . 3.18
3.2.5.2 Water Quantity Variables . . . . . 3.18
3.2.5.3 Water Quality Variables . . . . . 3.22

3.2.6 Note on Sampling Frequency Design . . . . . 3.26

TABLE OF CONTENTS (continued)


3.2.6.1 Introduction . . . . . 3.26
3.2.6.2 Water Quality Sampling Frequency . . . . . 3.26
3.2.6.3 Concepts for Designing Sampling Frequency 3.28

3.2.7 Conclusion for Temporal Correlation . . . . . 3.28

3.3 Spatial Correlation: The Cross-Correlation Function . . . 3.28

3.3.1 Introduction and Theory . . . . . 3.28
3.3.2 Effect of Spatial Correlation on the Amount of Information Obtained from a Gaging Network . . . . 3.31
3.3.3 Use of Cross Correlation for Network Design and Application to a Raingage Network . . . . . 3.34

3.3.3.1 Introduction . . . . . 3.34
3.3.3.2 Geographic Effects on the Spatial Variability of Rainfall . . . . . 3.34
3.3.3.3 Topographic Effects on the Spatial Variability of Rainfall . . . . . 3.42
3.3.3.4 Small-Scale Spatial Variability of Precipitation . . . . . 3.44

3.3.4 Spatial Variability of Streamflow . . . . . 3.48
3.3.5 Spurious Correlation . . . . . 3.48

3.4 References . . . . . 3.50

IV. QUALITY OF DATA . . . . . 4.1

4.1 Introduction . . . . . 4.1
4.2 Data Quality Assessment Through Physical Process Analysis . . . . . 4.2
4.3 Data Inhomogeneity . . . . . 4.4

4.3.1 Introduction . . . . . 4.4
4.3.2 Testing for Data Inhomogeneities . . . . . 4.4

4.3.2.1 Qualitative Test For Inconsistencies . . 4.4
4.3.2.2 Testing for a Jump . . . . . 4.5
4.3.2.3 Detection of Trends . . . . . 4.16

4.4 Correction of Data Inhomogeneities . . . . . 4.23

4.4.1 Introduction . . . . . 4.23
4.4.2 Filling of Missing Data . . . . . 4.23
4.4.3 Measurement or Recording Errors . . . . . 4.27
4.4.4 Jumps . . . . . 4.27
4.4.5 Trends . . . . . 4.29

4.5 References . . . . . 4.29

TABLE OF CONTENTS (continued)

V. PHYSICAL PROCESS SIMULATION: I. WATER AND SEDIMENT ROUTING . . 5.1

5.1 Introduction . . . . . 5.1
5.2 Water and Sediment Routing . . . . . 5.2

5.2.1 Formulation of the Water and Sediment Model . . . . 5.2
5.2.2 Formulation of Excess Rainfall Calculations for MSED1 . . . . . 5.4
5.2.3 Derivation of Analytical Kinematic Wave Equations for MSED1 . . . . . 5.9
5.2.4 Sediment Determination for MSED1 . . . . . 5.24

5.2.4.1 Overland Sediment Transport Capacity . . . 5.24
5.2.4.2 Channel Sediment Transport Capacity . . . 5.29
5.2.4.3 Determination of Sediment Supply . . . . . 5.29
5.2.4.4 Determination of Sediment Yield . . . . . 5.30

5.2.5 Mathematical Derivation of the Numerical Kinematic Routing Procedure for MSED3 . . . . . 5.30
5.2.6 Channel Infiltration Routine for MSED3 . . . . . 5.35
5.2.7 Sediment Routine for MSED3 . . . . . 5.35

5.2.7.1 Governing Equation for Sediment Routing . 5.36
5.2.7.2 Numerical Procedure for Sediment Routing . 5.38

5.2.8 MSED2 . . . . . 5.39

5.3 Water and Sediment Input Data Requirements . . . . . 5.40

5.4 References . . . . . 5.41

VI. PHYSICAL PROCESS SIMULATION: II. INTERSTORM AND PESTICIDE MODELS . . . . . 6.1

6.1 General . . . . . 6.1
6.2 Interstorm Process . . . . . 6.1

6.2.1 Evaporation . . . . . 6.2
6.2.2 Evapotranspiration (ET) . . . . . 6.7
6.2.3 Electrical Analogue . . . . . 6.13
6.2.4 Heat Transfer by Convection . . . . . 6.21

6.3 Interception and Infiltration . . . . . 6.23

6.3.1 Interception . . . . . 6.23
6.3.2 Infiltration . . . . . 6.27
6.3.3 Infiltration Parameters . . . . . 6.33

6.4 Data Requirements for Interstorm Model . . . . . 6.35
6.5 Pesticide Loading . . . . . 6.36
6.6 Data Requirements for Pesticide Model . . . . . 6.45
6.7 References . . . . . 6.50

TABLE OF CONTENTS (continued)

VII. APPLICATION OF EVALUATION PROCEDURES . . . . . 7.1

7.1 Introduction . . . . . 7.1
7.2 Data Availability and Data Gaps . . . . . 7.1
7.3 Analysis of Existing Data Network . . . . . 7.6

7.3.1 Geometry and Channel Data . . . . . 7.6
7.3.2 Soil Data . . . . . 7.7
7.3.3 Vegetation Data . . . . . 7.14
7.3.4 Climatic Data . . . . . 7.17
7.3.5 Hydrologic and Hydraulic Data . . . . . 7.33
7.3.6 Nutrients and Herbicides-Pesticides . . . . . 7.49

7.3.6.1 Nutrients . . . . . 7.49
7.3.6.2 Herbicides-Pesticides . . . . . 7.54

7.4 References . . . . . 7.59

VIII. CASE STUDY II: APPLICATION OF A PHYSICAL PROCESS MODEL . . 8.1

8.1 General . . . . . 8.1
8.2 Data Needs . . . . . 8.1
8.3 Available Data and Gaps . . . . . 8.1
8.4 Model Application and Results Using Collected Data . . . 8.3

8.4.1 General . . . . . 8.3
8.4.2 Small Watershed Simulation . . . . . 8.3
8.4.3 Medium Watershed Simulation . . . . . 8.10

8.5 Use of the Model for Data Synthesis and Evaluation . . . 8.10

8.5.1 Time of Concentration Determination . . . . . 8.10
8.5.2 Sensitivity Analysis . . . . . 8.15
8.5.3 Correlation in Simulated Runs . . . . . 8.20

8.6 Summary . . . . . 8.28

8.7 References . . . . . 8.35

# I. INTRODUCTION

## 1.1 Course Objectives

The objective of this short course, as the name implies, is the design and evaluation of monitoring networks. Four points that are addressed are:

1. If data are to be collected, what will they be used for?
2. If a watershed is to be studied, how is the sampling program designed?
3. If water supply data have been gathered, how are they interpreted? (What do you have?)
4. How are measurements evaluated?

The design of any monitoring network must be based not only upon the overall objective (i.e., designing a major hydraulic structure), of which monitoring is a part, but also upon the physical processes governing watershed response.

The most overlooked yet the most important aspect of designing a monitoring network is that there is usually no adequate available data on the processes which are to be monitored (i.e., time series, maximum value, minimum value, variation, etc.). Sometimes there are regional average values which can be found or calculated (regional mean rainfall, computing average annual runoff with mean discharge per square mile, etc.). Many recent publications base network design on statistical data. Unfortunately the statistics must come from observed data in order to be computed in the first place. A significant aid to monitoring network design is the utilization of physical process models to synthesize data and then to use the synthesized data for the network design specificities (what data to collect, what time step, where should the gages be located, etc.). Physical process models may not initially have all the required information in order to synthesize data, and thus this information would necessitate interim monitoring of watershed processes and characteristics in order to calibrate model parameters, or some information may be obtained by borrowing statistical parameters from other watersheds (i.e., soil permeability).

The evaluation of a data monitoring network must be performed in order to ascertain whether or not the monitoring network is collecting data suitable to satisfy the monitoring objective. For example, if the monitoring objective were to simply detect water quality criteria violations, the most important

monitoring design consideration to satisfy this objective is selection of the sampling frequency. Guidelines have been suggested for this case based upon the average daily streamflow and the type of water quality variable being measured (see reference 1). Other design criteria for this example would be the location of the gage, homogeneity of the data, and representative nature of the data (is the data realistic for the process which it was obtained from?). After the gage has been in operation, it may be evaluated to see if all of the design considerations have been satisfied and also whether it can identify or has identified water quality violations. Meeting the monitoring objectives is very important since usually the overall objective must base future decisions on the data base. An example might be designing a hydraulic structure based on three years of data. Typically, in this case, estimates of certain magnitude events are made with probabilistic or physical process models and the structure is then designed based on the estimates. The estimates could not be made without a data base since the models used to estimate the events must be designed and calibrated with observed data. If the observed data is of poor quality or insufficient, the hydraulic structure will be poorly designed (over- or underdesigned).

Design and evaluation of monitoring networks are integral parts of accomplishing watershed objectives.

These topics will be covered in the next section.

## 1.2 Physical Processes Governing Watershed Response

### 1.2.1 Introduction

The management of watersheds and river basins for the optimum benefit of the people in general requires a complete knowledge of the interrelations between ecology and environment. The watershed response to developments, either natural or man-induced, must be anticipated correctly if progress is to be made toward wise use of our natural resources. The increasing interests in predicting watershed response has accelerated the progress in the mathematical modeling of water hydrographs and yields. Concern for protecting the natural environment has also increased research in the field of predicting watershed sediment yields. Further, degradation, aggradation and movement of sediment and other pollutants in watersheds are closely related to water movement. In fact, no sediment yield can be predicted without the knowledge of water

routing and yield. This section describes several methodologies for calculating water yield and storm water routing from watersheds which were developed at the Engineering Research Center, Colorado State University, under the general direction of Daryl B. Simons and Ruh-Ming Li.

The physical processes governing watershed response are very complicated. Many past studies have utilized a statistical interpretation of observed response data. The unit hydrograph method for water routing and the hydraulic geometry equations for stream morphology are examples of these types of studies It is often difficult to predict the response of a watershed to various watershed developments or treatments using these methods, because they are based on the the assumption of homogeneity in time and space. Mathematical modeling using the governing physical processes may be used as an alternative means of estimating the time-dependent response of watersheds to precipitation with varying vegetative covers and land use. The principal advantage of the mathematical simulation approach is that the parameters that are used to vary watershed response may be physically defined. Such a definition enables the user to predict changes in watershed response arising from alterations in the watershed environment. The principal disadvantage of the simulation approach in comparison to purely statistical methods is size and complexity of simulation models. However, the speed and availability of modern computers largely answer this problem. In addition, the availability of inexpensive and powerful hand-held programmable calculators places many sophisticated simulation methods in the hands of both researchers and application-oriented engineers.

Physical process simulation models represent the system being modeled by decomposing it into its respective components. By dividing a system into its respective components, "lumping" of processes or parameters can be avoided. By simulating the selected phenomena through separate components, each individual process can be analyzed and refined or altered to meet the needs of the user. Consequently, as each process component is upgraded, the model becomes more representative of the physical system. Only a limited number of physical process models are presented. However, because they are physical process component models, the processes involved are similar between the models. Differences do exist between some components, making some models more complex or versatile than others. Basically two modeling approaches are described below. The selected water routing approaches are: (1) high-resolution watershed storm water routing and yield model, and (2) simplified watershed

routing and yield models. A number of other approaches are available, but research has shown that these cited models contain the most sensitive physical processes.

The above general approaches share essentially the same basic physical process. The main differences are in the formulation, implementation and degree of detail that may be represented. The high-resolution model was first developed by Li (1974) and subsequently published by Simons, Li and Stevens (1975) and updated by Shiao (1978). The model routes storm runoff water from overland flow surfaces and then through the channel system of a watershed. This is done using mathematical formulations of the water continuity equations and certain assumptions about the flow. This model is termed high resolution because it uses a finite-difference solution technique to solve the water discharge at selected times and points on the overland flow surface and channel system. The watershed for this model can be subdivided into numerous overland flow surfaces and the channel represented by several connected segments.

The simplified models, in contrast to the high-resolution model, require a watershed to be represented by a channel and two contributing planes or a combination of two-plane and single-plane watersheds connected by a channel system. This much simpler representation of the watershed provides for easier application, but may create problems if the watershed is extremely nonhomogeneous or anisotropic. This model uses an analytic formulation to route water from the overland flow planes (Simons, Li and Eggert, 1977). Use of the single two-plane one-channel model is warranted for watersheds that are fairly homogeneous and are subject to spatially constant rainfall. The combined watershed model may be used for larger, more heterogeneous drainages that may be modeled as a group of differing, yet internally homogeneous, subwatersheds.

Simulation of continuous time hydrology requires modeling of the interstorm period. The processes included in the interstorm model are evaporation, evapotranspiration and soil moisture redistribution. This model is designed to interface with the storm water and sediment runoff model. The interstorm model may be used to establish initial conditions for runoff and predict soil moisture contents required for nutrient and pesticide loading calculations.

The interstorm model is a mechanistically based simulation requiring daily meteorological inputs. It is based on a model originally presented by

Goldstein, Mankin and Luxmoore (1974) with substantial modifications to the storm infiltration calculations. This model approaches the evapotranspiration-soil moisture flow-evaporation problem by utilizing an electrical circuit analog. Flow of water through the system is assumed analogous to the current, the water as hydraulic potential is assumed analogous to the voltage, and the plant-soil atmosphere characteristics are parameterized into resistances to water flow. In addition, the model uses climatic data to predict evaporation rates. Soil water content is updated daily, layer by layer, to provide correct parameters for infiltration. Transpiration is modeled simply by continuity. Water absorbed by the roots is delivered to the atmosphere. On days when rainfall occurs, the additional hydrologic processes of interception and infiltration are simulated. With initial soil and interception conditions specified by the daily routines, interception and infiltration calculations are performed on rainfall hyetographs to produce an excess rainfall hyetograph to be routed as surface water runoff. When using the interstorm simulation, its infiltration and interception calculations are substituted for those normally performed in the runoff model.

Pesticide yields from field surfaces is modeled using a mechanistically based approach presented by Leonard and Wanchope, 1980. This model was developed on simplified concepts of processes and designed to be responsive to different management options. Foliar- and soil-applied pesticides are separately described so that different decay rates can be used for each source of the same chemical if necessary. Usually pesticide residing on foliage dissipates more rapidly than that from soil. Also decay rates can be made site-specific if information is available. Movement of pesticides from the soil surface as a result of infiltrating water is estimated using differences of rainfall and runoff for the storm and pesticide mobility parameters. Pesticide in runoff is partitioned between the solution or water phase and the sediment phase. This aspect is particularly important when examining management options that limit sediment yield.

The discussion of these routing and yield simulations begins in Section 1.2.2 with a description of the spatial representations required by the individual methods. This section is followed by a description of the physical process components and general layout of the simulators. An important feature of both the high-resolution and simplified models is the method used for estimating excess rainfall. This method involves both interception and infiltra-

tion processes. The greatest differences between the high-resolution and simplified models occur in the water routing methods. Both kinds of models use kinematic wave routing for overland and channel flow. However, the simplified models use the method of characteristics solution to the kinematic wave problem for some or all of the water routing. The high-resolution model uses a numerical solution to the kinematic wave problem for all water routing.

All of these methods exist as specific computer programs at SLA; however, the general theory presented is not intended as a program description, but rather a general approach that may be used in a variety of watershed simulation problems.

### 1.2.2 Spatial Representation of Watersheds

Because most watersheds are nonhomogeneous in topography, soils, vegetation, and other features, it is necessary to segment each watershed into units which can be treated as being homogeneous. Similarly, the channel system in a watershed can be represented by one or more segments, each having a characteristic location, shape, slope and roughness.

The location, area, length, and slope of each watershed unit are usually obtained from the available topographic maps. The following steps can be used in collecting the geometric data from topographic maps. Two types of watershed segmentation are considered. For the high-resolution model, the watershed is subdivided into square grids of a selected size (Simons, Li and Ward, 1978). The size of these grids or cells is chosen to conform with the watershed geometry and represent the accuracy of the input data and required output. Node points of the grid system represent sampling points where topographic, soils, and vegetative data are selected. The channel system is represented by straight line segments between node points. The sampled information is computer processed to produce a segmented watershed of overland flow cells with corresponding length, slope, width, and soil and vegetative indices, and a channel system described by lengths, slopes, and locations. Gravity flow logic, cell and channel aspect are used to determine flow directions in the watershed. On a much smaller scale, the slope, lengths, widths and flow directions of roadways can be prepared from maps, construction plans, or field measurements. For the simplified watershed models consisting of planes and channels, a different approach is used to abstract the geometry for model input. This approach can be used on small or large watersheds. On

large watersheds multiple sets of two-plane one-channel watersheds may be present (Simons, Li and Spronk, 1978). A method is presented below that is applicable to single watersheds or subdivided watersheds.

Geometric Representation for High-Resolution Model. The first problem encountered in numerical modeling of watershed response is to determine representative response units for mathematical computations. Simons and Li (1975) have approached this problem by developing a watershed segmentation program based on a grid system. The grid size is chosen so that the watershed boundary and channel segments can be approximated by grid lines (Figure 1.1). The overland flow units are the grid units inside the watershed boundary and the channel units are segments of channel between grid intersection points.

From the contour lines, the elevations of the land surface at the grid points are determined (Figure 1.2). These elevations, along with the locations and bed elevation of the stream channel, are input to the developed computer program. In addition to elevation data, vegetation and soil code numbers can be input for each grid point (Figure 1.2). The computer program then performs the following functions:

1. The slope and the slope azimuth of each overland flow unit are computed.

2. It is assumed that the water flows in the opposite direction of the slope gradient to the next overland flow unit or to the adjacent channel. Thus, water cascades from overland unit to overland unit and then into the channel system. The program identifies the cascade sequence (arrows in Figure 1.1).

3, The computational sequence for the flow is established by the program. The method employed is simply to follow the logics of gravity flow and flow continuity.

4. If data on the vegetation type, soil type, canopy cover density, and ground cover density are available, the variations of these factors inside a watershed can be established in the program. This is executed by decoding the vegetation and soil codes and assigning previously input parameters to each type code. These parameters may include soil porosity, soil depth, and selected vegetation measures.

In order to save computer storage capacity and processing time in the water and sediment routing computations, an additional computer program to combine small grid units into larger response units is developed. With this treatment, the flow is conceptually routed from overland flow units to channel units and to the selected watershed outlet.

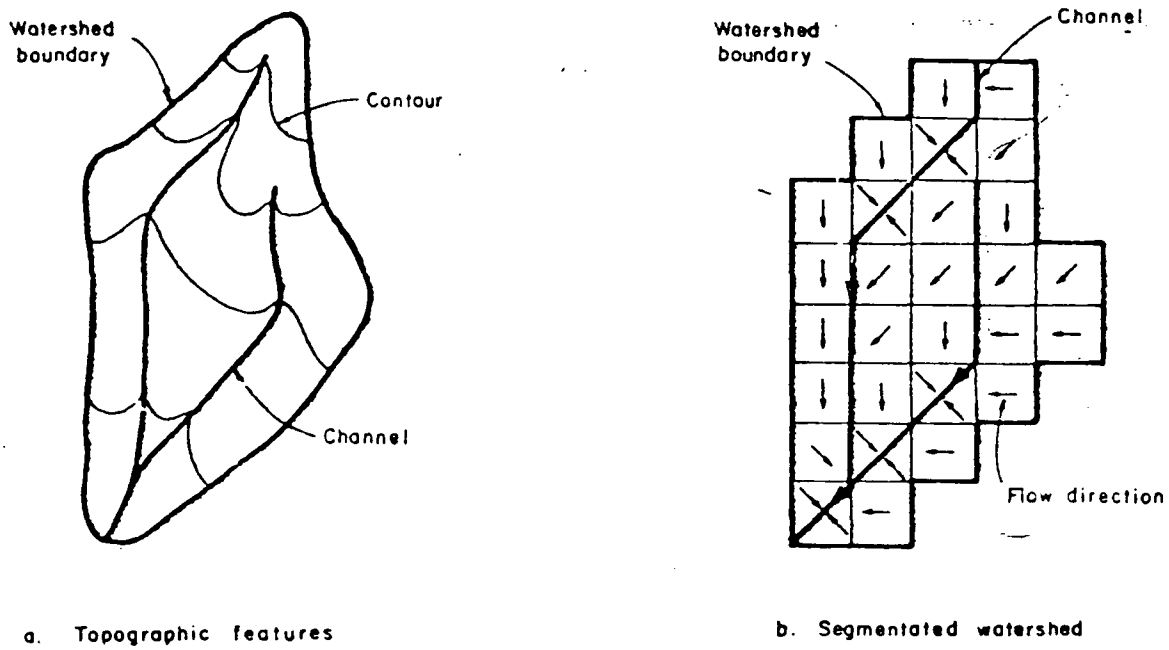


Figure 1.1 Example of watershed segmentation.

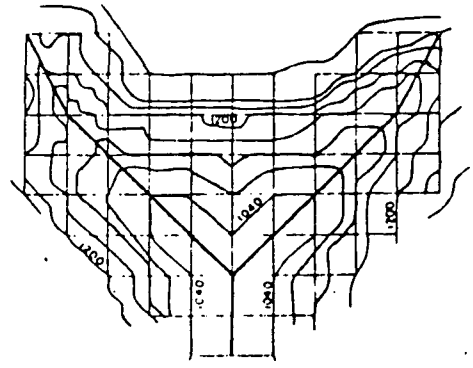


(a) Topographic Map Contour Interval = 40'

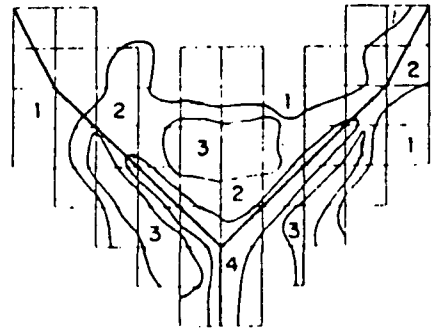


(b) Soils Map Numbers are soil type codes

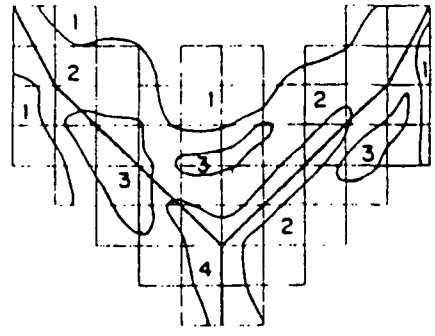


(c) Vegetation Map Numbers are vegetation type codes

Figure 1.2 Input data for hypothetical watershed.

This segmentation method is essential not only in water and sediment routing, but also for introducing the information from snowmelt computations, landslide hazard mapping, forest fire hazard mapping, forest inventory studies and snow avalanche hazard identification into the routing model. Moreover, if such factors as soil properties, vegetation cover, type of management treatment, or rainfall vary within the watershed, these variations can be handled easily and with the least manual input by segmenting the watershed with a grid system. The developed segmentation method provides input data on watershed geometry and computational sequence required for the simulation model to predict water and sediment routing and yield from small watersheds.

Often the manual determination of the response unit is preferable for non-computer oriented personnel. Such a manual determination should follow the similar logic used in the computer segmentation method. The flow path can be drawn perpendicular to contour lines. The manual determination of hydrologic response unit is subject to the individual's perception and is time consuming for applications to complicated watersheds. It is recommended that the manual determination be limited in application to small and simple watersheds.

Another characteristic of the channel system that must be numerically defined is the wetted perimeter-flow area relationships for each channel segment. This relationship is needed for use in water and sediment routing in the channel. The relationship is most often expressed in the power form as

$$P = a_1 A^{b_1} \tag{1.1}$$

where $P$ is the wetted perimeter, $A$ is the flow area, and $a_1$ and $b_1$ are statistically determined values. Data needed for development of Equation 1.1 are measurements of the channel cross section. These measurements are the horizontal distance from a datum mark or a bank to a point in the channel and the elevation change between the point and the mark. In a complex application where many stream cross sections are involved, the values of $a_1$ and $b_1$ for each channel segment may be found by a fitting routine contained within the simulation program. As an alternative, $a_1$ and $b_1$ may be determined beforehand using a small calculator program.

Geometric Representation for Simplified Model. The two types of simplified watershed simulation use essentially the same geometric

representation. The watershed must be subdivided in such a manner to allow approximation of the land surface by planes that extend to the watershed boundary and one or more interconnecting channels. The simpler of these two models uses an "open-book" representation wherein the watershed is transformed into a single two-plane unit with a central channel. The more complex model uses a number of such units in combination with single planes and interconnecting channel segments.

At Colorado State University these two simplified models have been developed and named ANAWAT and MULTWAT. The former is an acronym for Analytical Watershed Model and is the simpler single open-book representation. The latter name is an acronym for Multiple Watershed Model and is the more complex formulation. These acronyms are only introduced here to simplify later reference to these two model approaches. The basic method of transforming the contour map geometry into planes and channels, however, is the same for both models. This technique is described below for ANAWAT and then extended for the MULTWAT case. The process is illustrated by Figure 1.3 and presented in a step-by-step form below.

1a. Divide the watershed into units which can be considered homogeneous by using the available topographic, soil type, and vegetation type maps for the watershed. The size of the division is based on the resolution needed and the availability of data.

1b. Divide the watershed using the channel system. This division is often at the user's discretion, but should be based on homogeneity in the channel segment or its contributing side slopes. This homogeneity may be the channel segment gradient or similar soil types on the contributing side slopes.

2. Delineate the main channel in the unit. Extend the channels at least to the last distinct end points. Such an end point is often noted as the last distinct "V" on the contour line for tributary channels. In small watersheds determining the correct path along which to extend the channel may be difficult. In larger watersheds the extension of the channel may be apparent all the way to the basin boundary. Therefore, the extension of the channel for measurement purposes is arbitrary. A general consideration may be:

   (a) Small watersheds - extend the channel to the last distinct "V" and no further.

   (b) Medium sized watersheds - extend the channel from the last "V" one-half the distance to the watershed boundary.

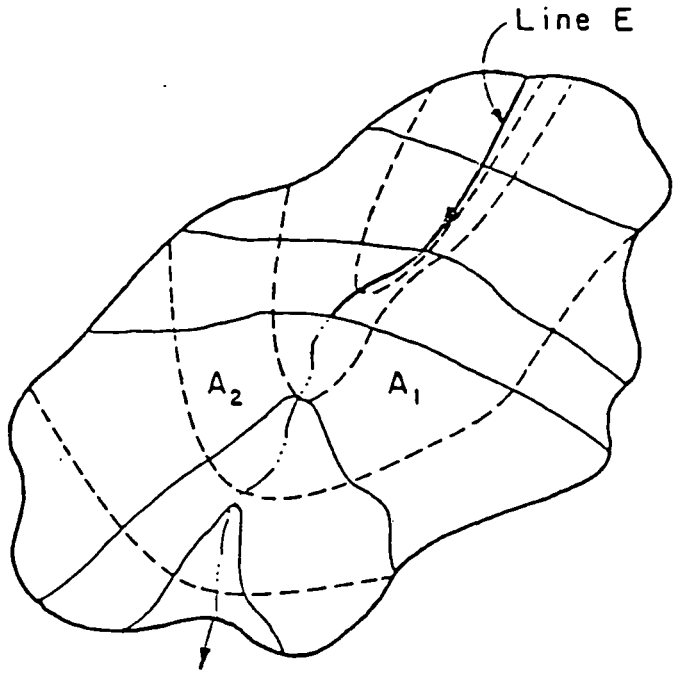


(a) Original Subwatershed Topographic Map

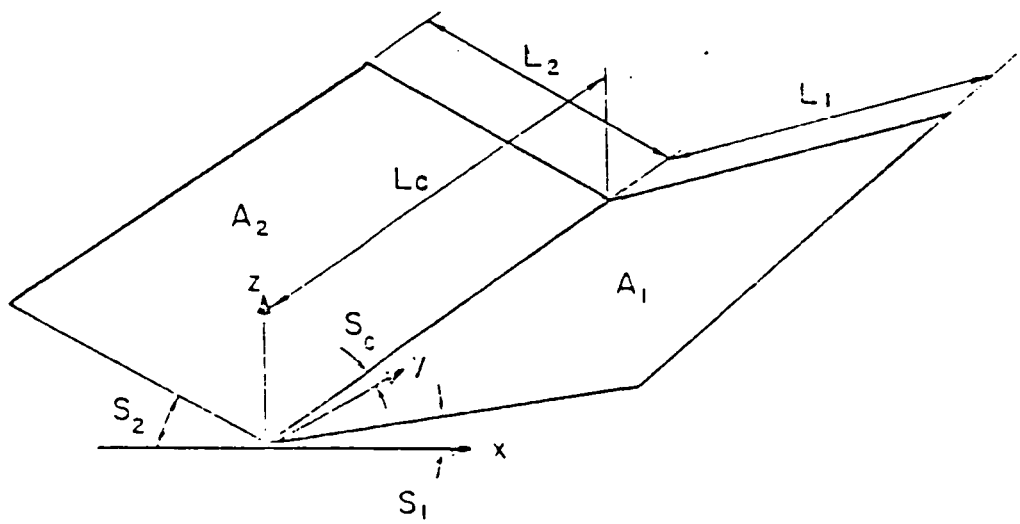


(b) Openbook Plane Representation

Figure 1.3. Geometric representation of a subwatershed unit.

(c) Large watersheds - Extend the channel from the last "V" to the watershed boundary.

No distinction is made on watershed size as this is a factor that is dictated by experience. In general, however, a small watershed may have a maximum size of one hundred acres, medium would be 100 to 1000 acres, and large, anything more than 1000 acres.

If a channel extension is made, the extension must perpendicularly cross the contour elevations to insure that the water is following the shortest path to the channel. Measure the channel segment length.

3. Sketch in the boundaries between contributing side slopes to the different channel segments. The enclosed contributing areas are now the watershed subdivisions. Each channel has a left and right subdivision when looking downstream.

4. Determine the channel segment slope as the ratio of elevation difference at the channel end points to the channel length.

5. Determine the area of the left and right contributing subdivisions by using the channel as the dividing line. For small and medium sized watersheds, an artificial dividing line may need to be constructed as an extension from the assumed channel end point to the watershed boundary. Make sure this division remains perpendicular to the topographic contours.

6. Determine each subdivision width as sum of subdivision area divided by channel length as determined in Step 4.

7. Subdivide the channel into several (5-20) equally spaced sampling points. At each sampling point lay out sampling lines from the channel to the watershed or response unit boundary. Sampling lines are drawn perpendicular to contour lines and represent flow lines that cross equipotential lines in a flow net. The sampling lines are the potential routes water would follow when flowing across the subdivision. Determine the slope as elevation change on the sampling line. Form the product of sampling line length times slope. Sum these products for the sampling lines in each response unit.

8. For small or medium sized watersheds, a single slope sampling line will be extended from the end point of the channel. This sampling line should coincide with the artificial dividing line constructed in Step 6. Because the area above the assumed channel endpoint represents an overland flow plane, it is treated as being equally divided between the two response units. To do this, add the slope-length products for this sampling line to the summed slope-length products for each subdivision. Also add the length of the sampling line to the summed lengths of the sampling lines of each subdivision. These additions will incorporate the effects of this headwater overland flow plane into each of the subdivisions.

9. Determine the average slope of each subdivision as the summed slope-length products for the unit divided by the summed sampling line lengths, or

$$\bar{S} = \frac{\sum_{i=1}^{n} S_i \times \ell_i}{\sum_{i=1}^{n} \ell} \qquad (1.2)$$

where $\bar{S}$ is the average of overland slope, $n$ is the number of sampling lines, $S_i$ is the slope of line $i$, and $\ell_i$ is the length of line $i$. The consistent step-by-step procedure presented above will provide a digitized watershed amenable to analysis by watershed modeling.

An example of the above procedure is presented below.

Example: Small Watershed (See Figure 1.4).

Area = 4.01 acres

Length of channel to "V" = 418 ft

Slope of channel to "V" = 0.108

| | Acres | Average Width (ft) | Weighted* Average Slope |
|---|---|---|---|
| Left side | 2.64 | 275.5 | 0.172 |
| Right side | 1.37 | 142.4 | 0.205 |

*includes artificial extension 192.5 feet long with slope of 0.26. Ten sampling lines utilized.

As mentioned earlier, ANAWAT has the capability of simulating the storm water runoff from a single plane or from the "open book" geometry as shown in Figure 1.3. MULTWAT classifies the single-plane units as planes and the "open book" units as subwatersheds. Storm water runoff hydrographs from the ANAWAT units serve as inputs to the interconnecting channel units. Water in the channels is routed by using a numerical solution to the nonlinear kinematic wave approximation. A method to account for channel losses due to infiltration is included in the channel routing procedure. The necessity of using a numerical channel routing routine rather than an analytical routine is due to the occurrence of kinematic shock. The analytical solution cannot be applied in situations where kinematic shock occurs.

There are four types of response units in MULTWAT: (1) a single plane ANAWAT unit, (2) an "open book" ANAWAT unit, referred to as a subwatershed,

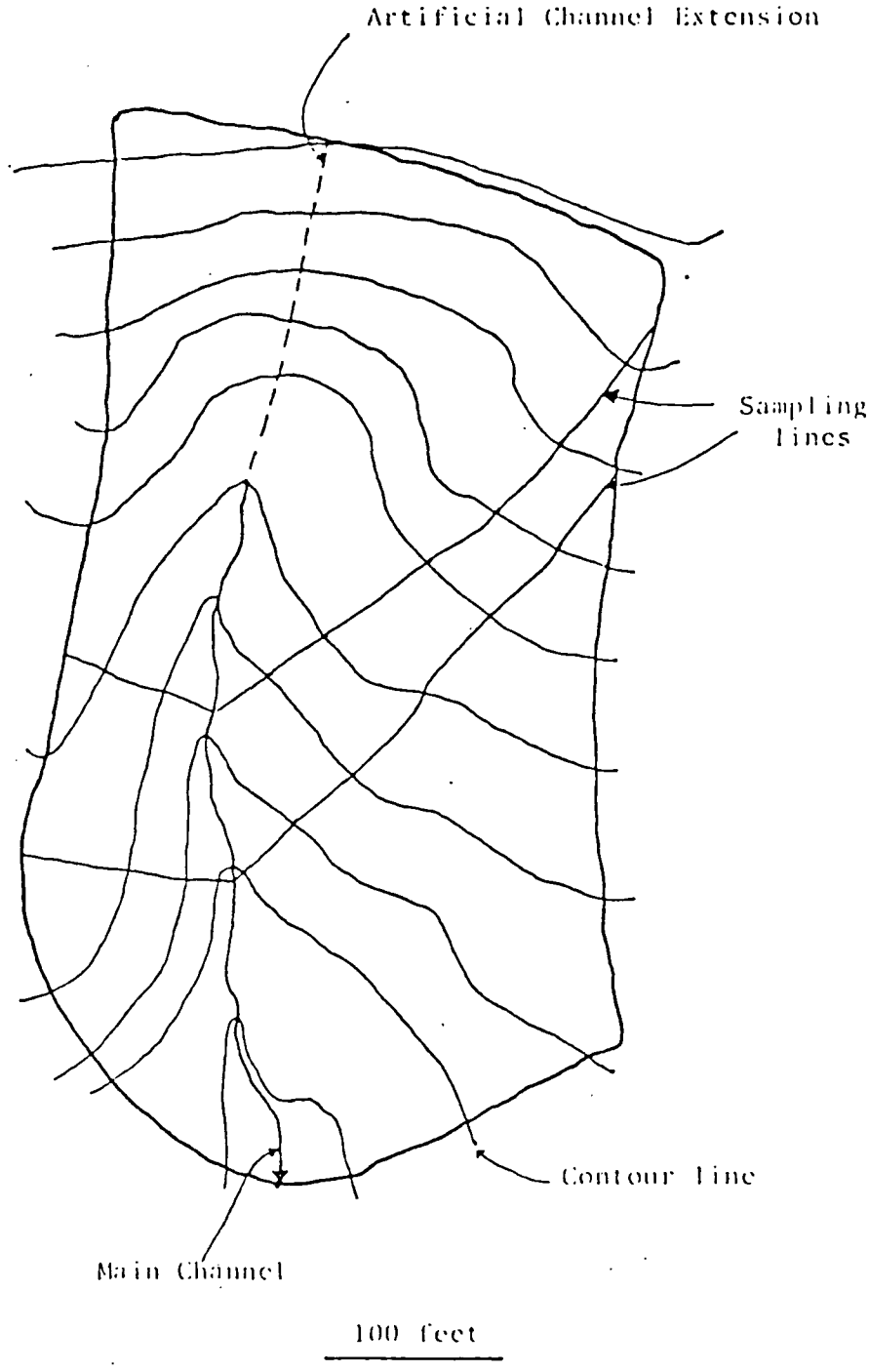


Figure 1.4. Important features for developing a small watershed representative geometry.

(3) a channel, which is a larger channel interconnecting the other units, and (4) a connection. A connection unit is used when only the lowest part of a basin is being modeled and the response of the upstream portion of the basin is input as a hydrograph recorded or simualted at the gaging station dividing the upper and lower parts of the basin. The method of obtaining the size and slope of planes and channels was given above. As an example of the transformation of a larger, more heterogeneous watershed into a system of planes and channels, Figure 1.5 shows a map of Walnut Gulch, Arizona, a watershed selected for development and testing of MULTWAT. The boundaries of the planes and subwatersheds are marked to illustrate how a large watershed can be represented by a system of these units interconnected by channel units. Figure 1.6 shows a schematic diagram of Walnut Gulch Watershed, represented by planes, subwatersheds, and channels.

### 1.2.3 Model Components

As mentioned earlier, both the high-resolution and simplified models contain essentially the same physical process components; however, the implementation of the process varies considerably due to the differences in water routing methods. The components and basic model structure are presented below. This discussion is a description of existing models, but may be used as a blueprint for the development of similar models.

#### High-Resolution Model

Once the watershed has been numerically defined by the above segmentation procedure, overland flow units and channel flow units in the watershed can be determined. Simons and Li (1975) developed a watershed sediment model which is primarily applicable for surface erosion simulation. It simulates the land surface hydrologic cycle, sediment production, and water and sediment movement on small watersheds. Conceptually, the watershed is divided into an overland flow part and a channel system part. Different physical processes are important for the two different environments. In the overland flow loop, processes of interception, evaporation, infiltration, and overland flow water routing to the nearest channel are simulated. In a channel system loop, water contributed by overland flow is routed. A flow chart presenting the interrelationship of these processes is shown in Figure 1.7. A brief summary of the components is given below. The model described in Figure 1.7 also contains sediment routing and erosion components.

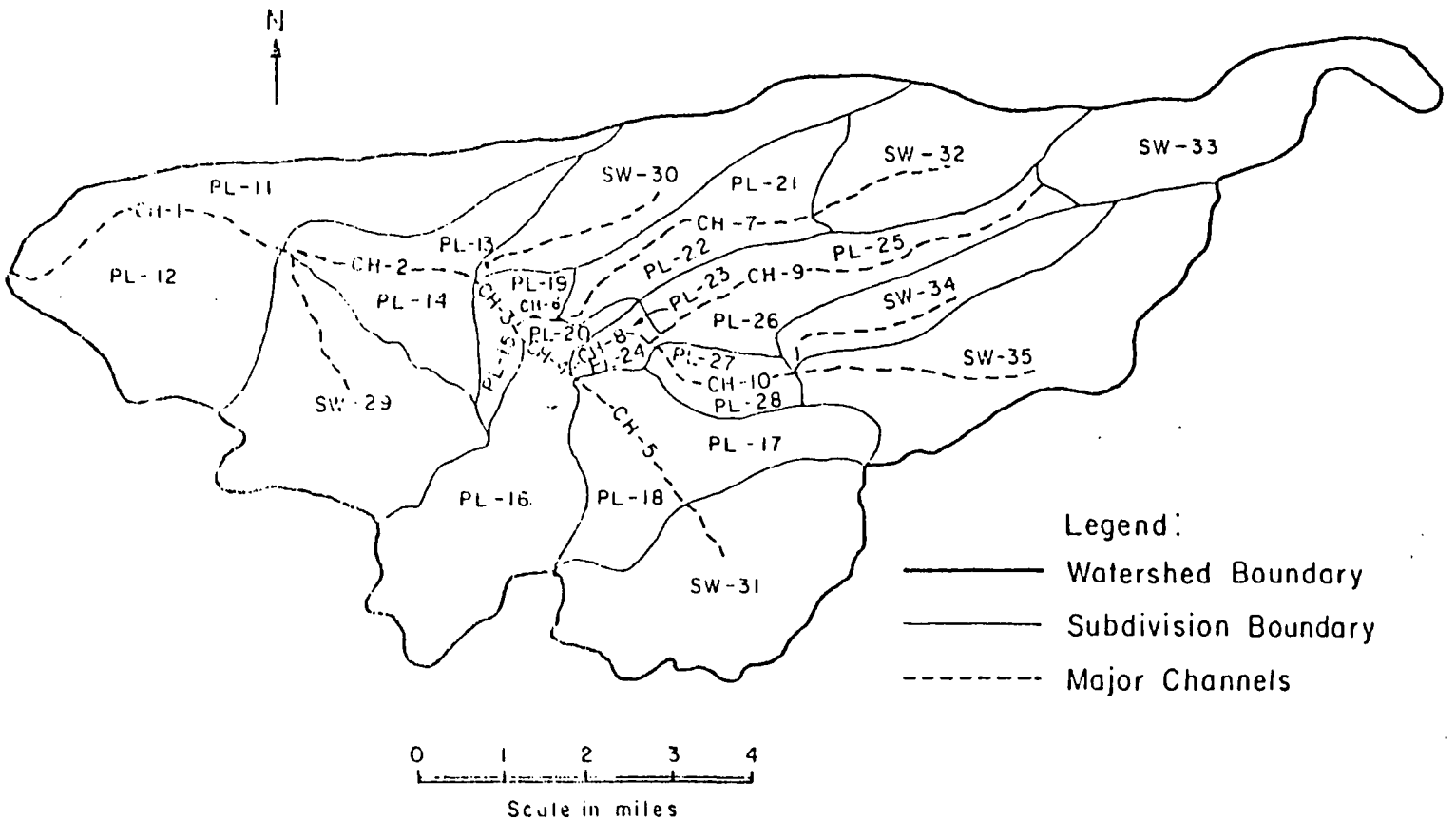


Figure 1.5. Response units for Walnut Gulch, Arizona, watershed.

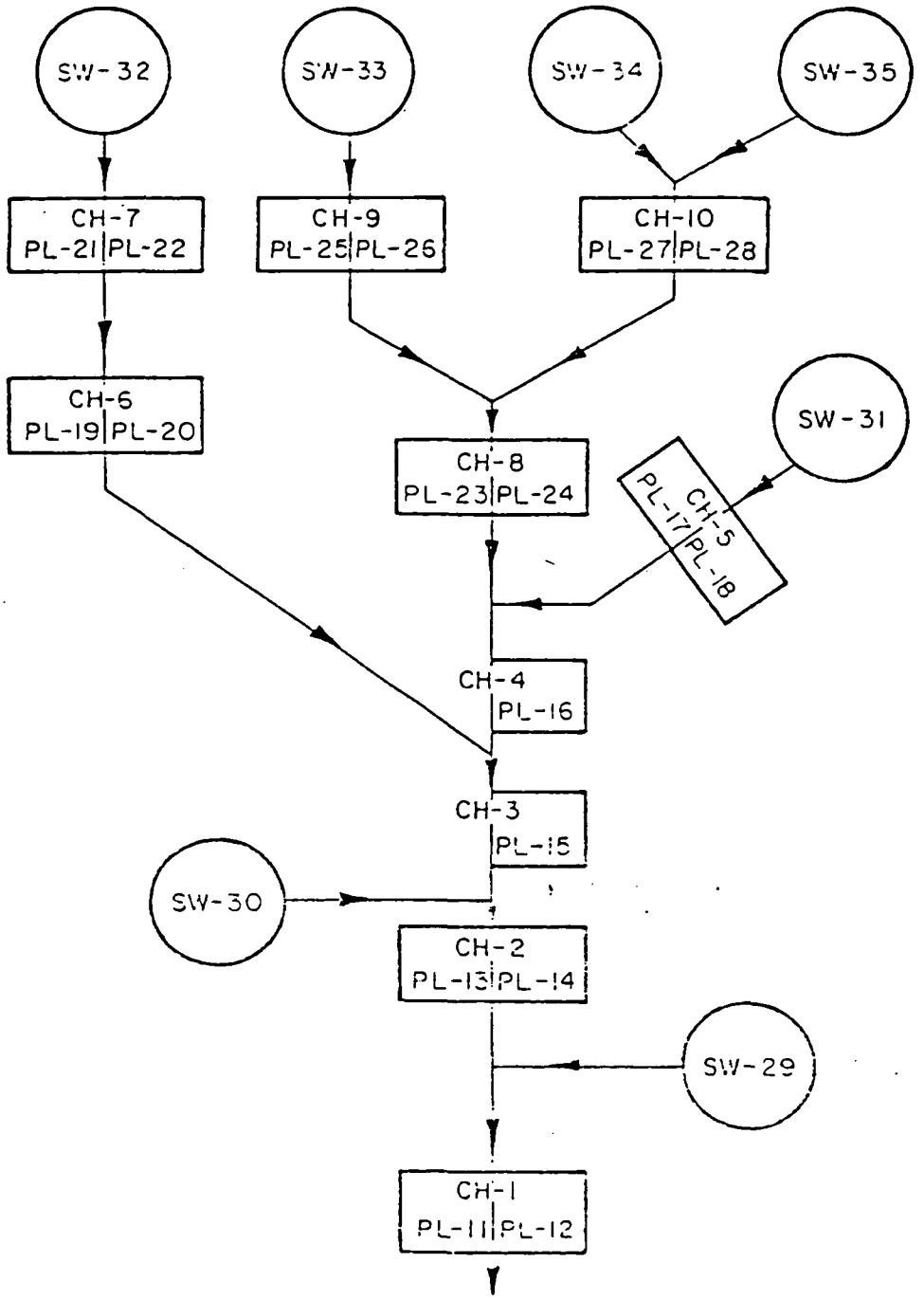


Figure 1.6. Schematic diagram of the Walnut Gulch response units.

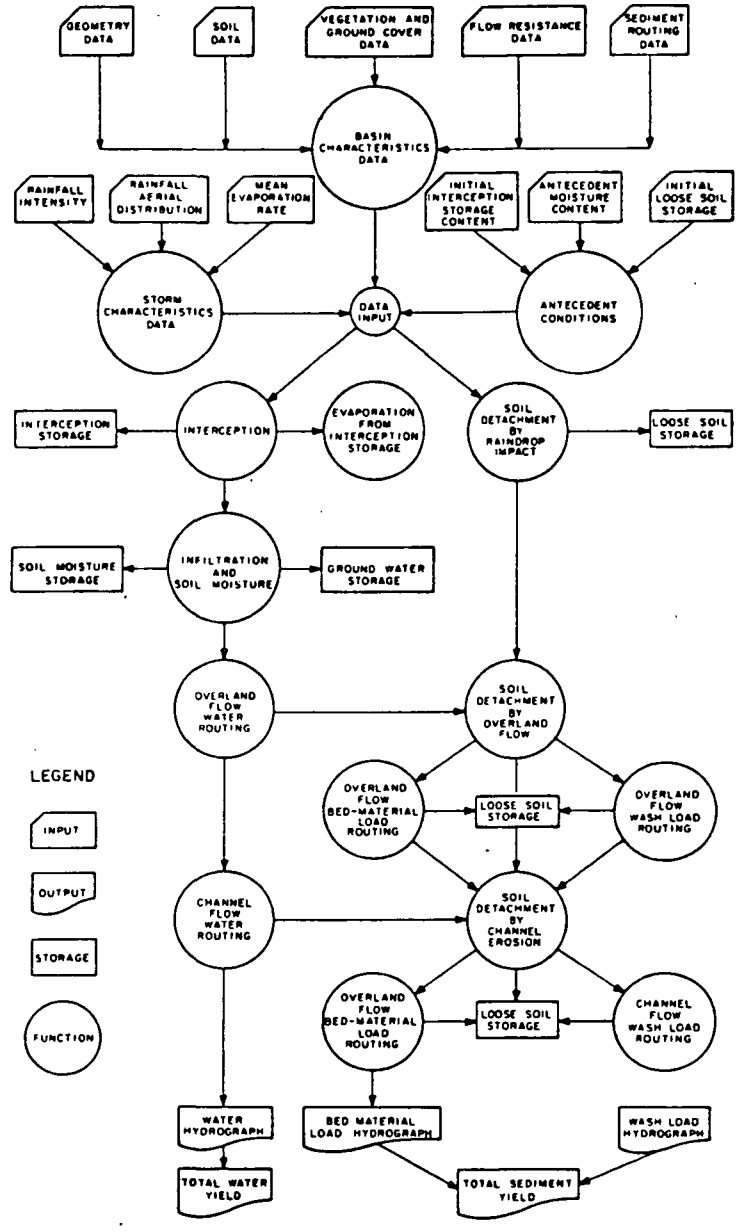


Figure 1.7. Flow chart for the watershed sediment and routing model.

Overland Flow Loop

There are three components in the overland flow loop: interception, infiltration, and overland surface water.

Interception Component. In this component the interception amounts due to the crown and forest floor are computed and the net rainfall is determined from the rainfall input. The interception loss includes the constant interception storage and the continuous evaporation from the interception surfaces. The evaporation is usually negligible during the storm. The interception storage is formulated to be a funciton of canopy cover density, ground cover density, and vegetation type.

Infiltration Component. This component of the model simulates the process of infiltration. The infiltration rate is computed by an approximation of Darcy's Law assuming that a distinct wetting front exists and is formulated to be a function of saturated hydraulic conductivity, average capillary suction pressure, soil porosity, antecedent moisture content, and moisture content in the wetted zone. Therefore, the rate of rainfall excess can be determined from the net rainfall and infiltration rates.

Overland Surface Water Routing Component. With this component the overland surface water runoff resulting from the mean rainfall excess is routed to the nearest channel. The routing procedure is based on the continuity of water, a momentum equation of kinematic wave approximation, and a set of resistance functions for different hydraulic conditions. The total resistance to flow is assumed to be a sum of the drag resistance due to ground cover and the shear stress acting on the soil bed. The computation is carried out by a nonlinear finite-difference scheme developed by Li et al. (1975a) and the computation results include the mean flow depth, bed shear stress and flow discharge at computation points as a function of time and space point.

Channel Water Routing Component. This component of the model routes the water down the creeks in the channel system and computes the hydrograph at the watershed outlet. The lateral water inflows to the channel system are the overland surface water flows. The channel water routing procedure and the finite-difference scheme are similar to those used in the overland flow loop.

Simplified Models

The simplified models contain the same physical processes listed above, but these routines are applied to subunits that are in general much larger

than those of the high-resolution model. In addition, these routines are uncoupled in the sense that they are used to calculate the process response for the entire event on a given unit before passing on to the next physical process. For example, infiltration for the entire storm is calculated before passing the entire rainfall excess function on to overland flow routing. This is as opposed to the time step-by-time step calculation of the high-resolution model. Therefore, some resolution is sacrificed for a gain in computational speed.

The physical processes modeled for each type of unit are shown in Table 1.1. The processes involved in the plane and subwatershed units are identical except for the analytical channel routing performed for the subwatershed units. The only processes considered for the channel units are numerical routing and channel infiltration.

Much of the rain falling during the first part of a storm is intercepted by the vegetal ground cover. Precipitation intercepted by vegetation or other ground cover eventually evaporates, and the amount of rainfall reaching the soil surface is less than the recorded amount. The amount of interception loss depends on the percentage of the ground that is covered by canopy and ground cover, and their respective water holding capacities. It is assumed that interception starts at the beginning of a storm and continues until the potential intercepted volume is filled.

A portion of the rainfall reaching the ground moves through the soil surface into the soil. This process is defined as infiltration. The model used to simulate this process is based on the Green and Ampt infiltration equation (Li, Simons and Eggert, 1976).

Using an approximate explicit solution to the Green-Ampt equation for time-varying rainfall given by Eggert, Li and Simons (1979), a function for infiltration with respect to time is developed. Thus, the infiltration occurring during a selected time period can be determined if the soil characteristics are known.

An analytical solution to the continuity, momentum, and cross section geometry equations is used to route water in the plane and subwatershed units. The method presented is identical to the routing scheme presented by Simons, Li and Eggert (1977). However, the routing of water with the conditions of

Table 1.1. Physical Processes Considered for Each Type of Unit

| | Plane | Subwatershed | Channel |
|---|---|---|---|
| Physical Processes Considered | 1. Interception | 1. Interception | 1. Channel Infiltration |
| | 2. Overland Infiltration | 2. Overland Infiltration | 2. Overland Channel Routing |
| | 3. Analytical Overland Routing | 3. Analytical Overland Routing | |
| | | 4. Analytical Channel Routing | |

continuous infiltration is developed and incorporated. Due to the assumed "open book" geometry, both overland and channel routing are required. Excess rainfall, the amount of rainfall not intercepted or infiltrated, serves as the input to the overland flow routing scheme. Results of the overland flow routing are then used as the lateral inflow into either a subwatershed or a channel unit.

The partial differential equations for overland flow are solved by the method of characteristics. The characteristic paths along which the solution is valid can be calculated in either the upstream or downstream direction. This allows a user to find the discharge at the downstream boundary for any given time.

A numerical procedure for water routing developed by Li, Simons and Stevens (1975) is used for the channel units. Routing is accomplished by a second-order nonlinear scheme developed to numerically solve the kinematic wave equation. A numerical routing procedure rather than an analytical procedure is used for the channel units because analytical solutions are restricted by the formation of kinematic shock. Kinematic shock results when characteristic paths intersect. Physically this may be described as a faster moving parcel of water overtaking a slower moving parcel of water as they both travel downstream. Analytic solutions for problems that have kinematic shock display discontinuities in the hydrographs. Due to this restriction, a simple numerical routing procedure is necessary for the channel units.

Stability of a numerical procedure refers to whether the computational errors, due to the finite-difference approximation of the partial differential equations, accumulate to an unbounded error. If the errors do not grow unbounded, the procedure is stable. The numerical scheme that is used has proved to be unconditionally stable and can be used with a wide range of time to space increment ratios without loss of significant accuracy. However, the physical significance of the time and space intervals should be considered when selecting their values.

An infiltration routine is combined with the numerical channel routing procedure to account for channel seepage losses. The channel infiltration procedure is similar to the overland infiltration procedure because both are based on the Green-Ampt infiltration equation (1911). The major difference between the two routines is that the depth of the water in the channel situation cannot be neglected as in the overland situation.

This description has listed the components of a MULTWAT model. The same description applies to the simple ANAWAT model up to the numerical channel routing scheme. Since the single open-book representation does not require an upstream inflow to any channel segment, a numerical channel routing is not required.

## 1.3 Procedures for Evaluation of a Monitoring Network

The methodology discussed in this workshop combines graphical, statistical, and physical process modeling techniques to analyze and evaluate existing and proposed data collection networks. Graphs are used extensively since they rapidly display the relationships between data types, sampling sites, data and time. Plots of input and output measurements, such as rainfall and runoff, water and sediment discharge, and nutrient concentrations and soil depth, permit comparison of the physical link between the measured quantities. Analyses based on the distance between stations at a fixed sampling interval show the spatial variation in data while analyses based on time at a selected site show the temporal variation of the data. A combination of the two allows a better understanding of the network and the data. Similarly, mass accumulation curves, such as used for rainfall, show both temporal and spatial relationships between sites. Trend graphs and data compared to time allow appraisal of key sampling times and uptrend or downtrend shifts in values.

Graphic procedures provide rapid insight into a data collection system when there is existing information at several sites. However, for sparse or proposed systems this type of information may not exist. In such cases, use of physical process models can aid design and evaluation by simulating and analyzing data at selected sites and times. This information can be used in lieu of the actual data if the physical process model accuratley represents the system being evaluated. Physical process models can also provide useful information regarding system variability, travel time of floods, magnitudes and durations of flow, sediment transport, nutrient movement, changes in soil moisture, and fluctuations in climate. Not only can process models be used to simulate the output data but also to detect and check the accuracy of input data.

By combining visual techniques including graphical presentation and use of physical-process models, a unified approach to evaluate data collection networks can be achieved. In this way, collection networks can be evaluated.

This method is applicable to many situations.

General data network evaluation procedures consist of the following steps.

1. Data needs should be identified for intended application or modeling.

2. Data needs should be compared with measured data.

3. Data gaps must be identified, and it must be determined if missing data can be derived from the measured data or from other records.

4. Graphical and statistical techniques should be utilized to compare data between sites at different sampling intervals and with time. Statistical techniques include autocorrelation, cross correlation, maximum values, minimum values, means, standard deviations, ranges of data, linear and nonlinear relationships between data, and order of magnitude comparisons. Graphical comparisons can be time series plots, such as hydrographs auto and cross-correlograms relating correlation coefficients with time, space, or both (Lecture 3), dimensionless mass accumulation curves, changes in magnitude of a measured variable with location, bar graph distributions, and relationships between two variables.

5. Correlograms and other graphical and statistical aids can be used to check on the spatial and temporal adequacy and the physical significance of the data.

6. Erroneous data should be checked, eliminated, or modified so physically inconsistent data are not used in further analyses.

7. If data are not available at certain locations and for specified times, then mathematical models may need to be employed to generate records for those sites or times. For example, if a discharge measurement station is to be built at a certain location or if a current station records stage height every hour, a stream flow simulation model can generate hydrographs at the station resulting from different levels of storm input for analysis.

8. The simulated data base by physical process simulation models may be used to conduct the same analyses as listed in Step 4.

## 1.4 References

Grimsrud, G.P., et al., 1976, User Handbook for the Allocation of Compliance Monitoring Resources, Office of Air, Land, and Water Use, USEPA, Document EPA-600/5-76-012, Washington, D.C., December, pg. 9.

# II. CONCEPTUAL DESIGN OF A MONITORING SYSTEM

## 2.1 Introduction

In order for any monitoring network to be designed and implemented, the overall objective as well as the monitoring objective should be analyzed to assess what type of data is required to fulfill these objectives. An overall objective is of broad scope; for example, a water supply system or a sewage treatment system. A much smaller objective which is formulated under the overall objective is the monitoring objective. Examples are: streamflow measurement; water quality measurements; precipitation measurements; etc. It must be kept in mind that the overall objective determines the nature of the monitoring objective. For example, if the overall objective was enforcement of water quality laws, the monitoring objective would be to monitor the water quality variables in the jurisdiction area; but how is the monitoring to be done? In this case, sampling every night may miss industrial pollution loads, and monitoring upstream of industrialized areas would do the same. Here the overall objective conceptually defines the sampling frequency and spatial location of the monitoring network. The exact number, location and sampling frequency for monitoring stations must bow to social, political, legal and financial considerations.

When computer modeling is the overall objective (or an objective on a higher level than the monitoring objective), there are certain specific data which are required by the model(s) and these needs must be fulfilled through the monitoring objective. In the light of any constraints placed on the monitoring network (financial, legal, etc.), data measurements may be made directly or indirectly. These types of measurements will be discussed after describing data needs. Details of performing direct measurements of hydrologic parameters are discussed in following sections.

## 2.2 Data Needs

### 2.2.1 General

Data for water, sediment and chemical yields from agricultural lands can be divided into several groups including watershed and channel geometry, soil, vegetation, climate and meteorology, hydrology, hydraulics, and man's influence. As models vary so do the specific inputs for each. Specific needs will be discussed in following subsections.

Data needs should not be determined carelessly because of the time, money, and instrumentation necessary to collect information. Careful consideration must be made so that each piece of information is justified and prioritized with respect to other data. Modeling needs are usually dictated by the model inputs. So, the person using the model must know the essential model inputs.

Typical data for modeling are listed in Table 2.1. Although general, this list shows there are numerous factors to consider in designing a data collection system. Typical data collection methodologies are listed in Table 2.2. Although the list is brief, it does indicate that a number of measurement devices are needed for data collection.

Data for modeling of rainfall, runoff, sediment yield, dissolved oxygen, and nutrient transport in agricultural watersheds require complex collection networks. Seldom are enough data collected to fully meet most users' needs. Consequently, some models may be untested or unverified. Therefore, it is important to define data needs, data priorities, and data availability to determine linkage between data collection and ultimate use. The first step is to define the specific data needs.

### 2.2.2 Specific Needs

Data needs vary from model to model. For example, the models being developed at Colorado State University that describe rainfall, runoff, sediment yield, dissolved oxygen, and nutrient processes require specific information (Simons et al., 1979). Four separate models comprise the overall mathematical model. The primary model is a water balance and evapotranspiration model that computes infiltration of layered soils and operates on a daily basis in the watershed. If a rainfall event occurs on a certain day, control is passed to an event-based water and sediment routing and yield model that used antecedent conditions from the water balance model. In addition to these hydrologic-hydraulic models there are two water quality models. One is for dissolved oxygen and thermal loading and the other is for nitrogen and phosphorous. These models also use inputs from the two water and sediment models. As indicated in Table 2.3, data needs vary among models and not all data are used for inputs. Some are used for calibration and/or verification of the model. Fortunately, use of a physical process model allows calibration with a limited number of events with measured data.

Table 2.1. Data Parameters for Modeling Water and Sediment Yield

I. Watershed and Channel Geometry Data

1. Area of watershed
2. Slopes and lengths of channels and land surfaces
3. Channel cross sections
4. Geological or man-made control
5. Watershed and channel network

II. Soil Characteristics

1. Soil type
2. Distribution of types
3. Porosity
4. Grain size distribution
5. Infiltration characteristics
6. Soil moisture data

III. Vegetative Cover Data

1. Density or coverage
   a. Canopy cover
   b. Ground cover
2. Cover interception of rainfall
   a. Canopy cover
   b. Ground cover

IV. Climatic Data

1. Rainfall hyteographs
2. Snowmelt rate
3. Evaporation rate
4. Air temperature
5. Humidity
6. Wind
7. Solar radiation

V. Hydrologic and Hydraulic Data*

1. Water discharge hydrographs
   a. Timing
   b. Peak
   c. Volume
2. Resistance to flow parameters
3. Sediment yield
4. Grain size analysis of transported sediment

*Most of this catagory of data are required for model calibration and/or verification.

Table 2.2. Typical Data Collection Methods

| Type of data | Methodology |
|---|---|
| Rainfall | Measured by automatic recording rain gauge or meteorological radar |
| Evaporation | Measured by evaporation pan |
| Solar Radiation | Measured by radiometer |
| Air Temperature | Measured by thermometer |
| Soil Temperature | Measured by thermometer |
| Infiltration | Measured by infiltrometer |
| Flow Discharge | Measured by weir, current meter, or rating table for a calibrated section |
| Water Surface Elevation | Measured by an automatic recording bubble gauge or in a stilling well |
| Flow Velocity | Measured by current meter or dye dilution method |
| Sediment Discharge | Measured by automatic pump sampler or standard depth-integrating samplers |
| Flow Resistance Parameter | Manning's equation, comparison to USGS publication, equation for 'n' |
| Location of the Channel | Measured by plane surveys or from USGS maps or aerial photographs |
| Channel Cross Section Geometry | Measured by hand level-survey rod, sag tape, or transit-stadia rod |
| Channel Bed Profile | Measured by sonic soundings and transit-stadia rod |
| Rock Outcrops and Man-made Control | Measured by geological survey or from available geological maps |
| Bed and Bank Samples | Determined by composite soil samples |
| Watershed Geometry | Determined from topographic maps |
| Vegetation Distribution | Determined from aerial photographs or a vegetation map |
| Soil Type Distribution | Determined from soil survey maps and field investigations |
| Soil Moisture | Measured by neutron probe or gypsum blocks |
| Sediment Source | Color infrared or black and white photographs |

Table 2.3. Data Needs for Colorado State University Physical Process Models

| Data group | Water balance model | Water and sediment storm model | Nutrient model | Dissolved oxygen model |
|---|---|---|---|---|
| Geometry and Channel Data | | | | |
| Watershed area | | X | | |
| Length of overland slopes | X | X | X | X |
| Width of overland slopes | X | X | X | X |
| Gradients of overland slopes | | X | X | X |
| Length of channel sections | | X | | |
| Gradient of channel sections | | X | | |
| Measured, representative channel cross sections | | X | | |
| Elevation of watershed | X | | | X |
| Soil Data | | | | |
| Distribution of soils | X | X | | |
| Types of soils | X | X | | |
| Number of soil layers | X | | | X |
| Thickness of layers | X | | | X |
| Initial water content of layers or top layer | X | X | | |
| Saturated hydraulic conductivity of each layer or top layer | X | X | | |
| Tensiometer measurements (desorption curve) for each layer | X | | | |
| Temperature for tensiometer data | X | | | |
| Field moisture capacity for each layer | X | | | |
| Intrinsic permeability of top layer | | | X | |
| Porosities of soil layers on top layer | X | X | | |
| Specific gravity of soil | | | X | X |
| Temperature of top layer | | | | X |
| Thermal conductivity of soil | | | | X |
| Grains size analysis of top layer | | X | | X |

Table 2.3. (Continued)

| Data group | Water balance model | Water and sediment storm model | Nutrient model | Dissolved oxygen model |
|---|---|---|---|---|
| Soil Data (continued) | | | | |
| Concentrations of nitrogen and phosphorus species in soil and litter layer | | | X | |
| Vegetation Data | | | | |
| Types | X | X | | |
| Distribution | X | X | | |
| Density of ground cover | X | X | | |
| Density of canopy cover | X | X | | |
| Storage of ground cover | X | X | | |
| Maximum and minimum storage of canopy cover | X | X | | |
| Albedo of vegetation | X | | | |
| Yearly growth cycle of canopy | X | | | |
| Average leaf length of dominant species | X | | | |
| Maximum and minimum leaf area | X | | | |
| Root cross sectional area per unit area of soil in each layer | S | | | |
| Fraction of roots in each layer | X | | | |
| Annual litter input to ground surface | | | X | |
| Litter layer thickness | | | X | |
| Average litter temperature | | | X | |
| Nitrogen content of litter | | | X | |
| Phosphorous content of litter | | | X | |
| Specific gravity of litter | | | X | |
| Climatic Data | | | | |
| Daily solar radiation | X | | | X |
| Average daily temperature | X | X | X | X |
| Average daily humidity or vapor pressure | X | | X | |

Table 2.3. (Continued)

| Data group | Water balance model | Water and sediment storm model | Nutrient model | Dissolved oxygen model |
|---|---|---|---|---|
| Climatic Data (continued) | | | | |
| Total daily precipitation | X | | | |
| Average wind speed | X | | | |
| Air pressure--for year as function of altitude | X | | | |
| Specific heat of air | X | | | |
| Rainfall storm hyetographs | X | X | | |
| Nitrogen species input from rainfall | | | X | |
| Surface water temperature | | | | X |
| Hydrologic and Hydraulic Data | | | | |
| Storm and daily runoff hydrographs | X | X | | |
| Overland flow resistance | | X | | |
| Channel flow resistance | | X | | |
| Storm sediment yield | | X | | |
| Sediment yield from litter layer | | | X | |
| Runoff temperature | | | | X |
| Grain size and analyses of sediment | | X | | |
| Sediment detachment coefficient for rainfall and runoff | | X | | |
| Dissolved oxygen content in runoff | | | | X |
| Nutrient concentration in runoff | | | X | |
| Rate of addition of BOD in runoff | | | | X |
| Man's Influence | | | | |
| Cropping patterns | Man's influence may affect all of the physical qualities controlling water runoff, sediment yield, and nutrient transport from watersheds. The effects can be quantitized by assessing the impact of man's activities on the different measurable variables. | | | |
| Land use changes | | | | |
| Timbering activities | | | | |
| Modification of drainages | | | | |
| Nitrogen application | | | | |
| Phosphorous application | | | | |

It is not always possible or necessary to collect every piece of identifiable data. Several types of data can be estimated or synthesized from a single measurement or description as well as from experience or data from a nearby watershed. For example, a soil type description such as sandy loam or sandy clay allows initial estimates of erosion potential, porosity, moisture conditions, and hydraulic properties. These estimates may be refined later with measurements or through model calibration. Sensitivity analyses of the model with respect to the different inputs will aid in determining the most important data.

## 2.3 Direct Measurements

### 2.3.1 General

Direct measurement of a process is defined as the procurement of data for a variable by measuring the variable itself. An example of this is measurement of precipitation by use of a rain gage. Direct measurements are the most important type of data since any model based upon the measured data may be calibrated with the use of the direct measurements. For example, rainfall-runoff models may be calibrated on observed storm rainfall and the resultant hydrograph. Often this calibration occurs through model parameters which are vaiables that are measured indirectly or insufficiently. Indirect measurement will be treated in the next section. Insufficient measurement of a variable means exactly what its name implies, that there is not enough information about the variable to support concrete statements, but that the information available is used for generalized statements. For example, soil properties, (conductivity, porosity, etc.) may be measured at two or three locations in a watershed and then they (or their averages) may be assumed to be representative for the entire watershed. Due to this coarse treatment of variables, model calibration occurs through the adjustment of indirectly or insufficiently measured variables.

Considerable care must be taken to obtain accurate data. Proper application of the techniques of data gathering are an important feature of any data collection system. Accepted methods for direct measurement of stream flow, water quality and meteorologic data are now discussed.

### 2.3.2 Collection and Processing of Surface Water Data

The USGS has formulated standard methods for stream flow data collection.

These methods involve the general operation and maintenance of a gaging station such that data are available for establishing the stage-discharge relation and other flow characteristics at a given location on a river or stream. Accomplishing this objective includes:

- datum control to maintain the accuracy of stream flow records
- Maintenance and collection of a complete and accurate continuous stage record
- current meter measurements at a range of stages to adequately define yearly fluctuations
- development and continual verification of the stage-discharge relation to reflect current physical conditions
- computation of mean daily discharges, volumes, and peak flow discharges

2.3.2.1 Gage Datum

Maintaining gages at correct elevations requires periodic checking of all station reference marks and gages with a surveying level. Levels should be run at least once a year regardless of the apparent permanency of the gage or reference mark. Greater frequency of verification is required at stations where it is known or suspected that poor foundations or vertical movement exist.

2.3.2.2 Maintenance of a Gaging Station

Equipment maintenance is an important aspect in obtaining accurate data. A visual inspection can often identify potential problems that might prevent continuation of measurement activities. The required maintenance to resolve problems can be classed as minor or major maintenance. Minor maintenance includes the minor repairs necessary to keep the gaging station operational, safe, and to maintain its appearance. Major maintenance is defined as repair or services necessary to make the station operational after being inoperative due to vandalism, damage or major stream channel changes.

Minor repairs include, but are not limited to, replacement of defective recorders and timers which cannot be repaired in the field, replacement of outside staff gages which have been damaged by debris or vandalism, relocation of bubble-gage tubing and orifices (temporarily in order to get a continuing record, and permanently when field schedules permit), replacement of defective

floats, and repainting and repairing the shelter as required. Maintenance of shelter and surrounding area includes keeping the shelter clean, oiling hinges, locks, and hasps, clipping weeds and grass around the station and in high-water measuring section to ensure more accurate discharge measurements, removing debris, and generally keeping the area clean.

Major repairs include, but are not limited to, extensive rebuilding of the gage house, replacement of stilling wells, and complete replacement of instrumentation. If the station is destroyed, a temporary reference point should be set and a local observer hired (if possible) to take daily or more frequent gage readings until the station can be repaired. This is particularly important if the gage is inundated or destroyed by flood so that these gage readings be obtained during hte flood or on the recession to reduce the period of missing record to a minimum.

2.3.2.3 Recording and Documentation of Data

Standard recording procedures and documentation are an essential aspect of producing quality data. The data and information collected initially and throughout station servicing shall include:

a. Station name, in full.

b. Date: month (name, not number), day, and year.

c. Time: watch time using 24-hour time system.

d. Pen time of analog recorder, punch time on digital recorder.

e. Types of inside and outside gages and gage height.

f. Gage height by float tape or manometer dial, the reference gage, and the recorders.

g. Initials of contractor(s).

h. Additional remarks related to station conditions, including control conditions.

2.3.2.4 Servicing Stage Recorders

Servicing of stage recorders is performed prior to discharge measurements to insure proper operation after new tapes are installed. Following this procedure minimizes the possibility of record loss due to common mistakes (i.e.,

leaving pen up or clock stoppage after winding). The following procedures are useful as a guide to servicing analog and digital recorders:

a. Check to see if the clock and/or timer is running and mark the recorder charts.

   1. By marking the point where the pen or pencil is resting on the strip-chart recorder (adjust timer if needed or replace if timer has been malfunctioning), or

   2. By watching the instrument punch the digital tape and drawing a line across the digital tape, using the top of the punch block as the straight edge.

b. Compare gage readings and recorded gage heights and check to see if there is a malfunction of the equipment such as:

   1. If the stilling well intakes are plugged

   2. If there are any malfunctions in the gas-purge system of the bubble gage or if the orifice lines are plugged

   3. If there has been any oil loss from an oil cylinder, and

   4. If there are any inconsistencies between the recorded and reference gage heights, note them so that adjustments can be made to the <u>recorded</u> gage height. In stations equipped with a bubble gage, check the counter.

c. Records shall be removed from each recorder at intervals not to exceed two months. Change the record from each recorder as follows:

   1. Analog recorder

      a. At the time of initial inspection the time shall be indicated by a vertical mark of the pen or pencil. The float tape or cable should be grasped between the float and the float wheel and lifted a few hundredths and gradually released. The mark should not be made by rocking the float wheel because it places undue strain on the float wheel bearing. If equipped with a bubble gage, the contractor shall mark the chart by pushing the up or down switch so that the pen trace is changed a few hundredths.

      b. Advance the chart about one inch. Run a reversal mark and adjust if necessary.

      c. Blot the ink at the end of the recording to prevent smears.

      d. Identify the chart by printing the name of the station, date, time, gage height readings and initials of person.

e. Cut and remove the chart, leaving at least one full day in addition to the day of the visit on the end of the chart to provide ample room for joining the pieces in the office.

f. Wind clock or negator spring.

g. Check the amount of paper left on the supply roll and make certain that there is more than enough to last the interval between visits.

h. Flush intakes or purge orifice line.

i. Rethread the chart into take-up rolls and run reversals, read all gages again, and record all data and observations on the chart.

j. Reset pen to agree with the gage height indicated by the reference gage, and advance chart to agree with watch time, and make a vertical mark. Be certain that pen is not in reversal.

k. Check the ink supply of the pen and replenish it if necessary.

m. Unroll and examine the chart in an effort to detect any recorder malfunction or clock stoppage since the last visit, and if found, note range line.

2. Digital recorder: When arriving at a station, look at the face of the timer to see if a punch would occur in about the next five minutes, the time it would take to remove the punched record and reset the tape. If so, it would be better to wait until the punch has occurred before starting the tape removal procedure. Fill in the removal block of the inspection slip. When ready to remove the punched record, follow the steps listed below.

a. Turn the take-up roll to advance the tape about nine inches beyond the last punch, cut the tape with a knife or razor blade just above the upper paper guide bar.

b. Slip the roll of punched tape off the take-up roll.

c. Note the date, watch time, clock time and gage height on the tape just removed but do not take the time for elaborate notes until after the tape has been reset.

d. Check battery voltage or amperage and record. Replace battery if no load voltage is less than 7.0 volts.

e. Flush intakes or purge orifice line.

f. Thread the paper onto the take-up roll. Care should be exercised not to elongate the large feed holes in the tape on the pins protruding on the tape drive drum by turning the take-up roll too hard. Advance the tape until the printed line on the tape just above the punch block is about eight readings earlier than watch time. (On the 15-minute tape, this would be two hours earlier than watch time).

g. Record the station name, station number, date, time and gage height on the beginning of the new tape and start new inspection slip.

h. Reset the punch mechanism, if necessary, to agree with the gage height indicated by the reference gage.

i. Punch sufficient test punches so that the next punch caused by a properly set cam will be at the correct time.

j. Draw a penciled line across the top of the punch block so that later the test punches can be separated from the automatically recorded data. If the preset action has already taken place before the line was drawn, the line will pass through the last test punch; if not, the line will be above the last est punch. Care must be exercised not to tear the paper with the pencil.

k. After resetting the tape, record the station name and the remaining notes on the tape just removed. At this point take time to superficially examine the last portion fo the tape just removed for any obvious trouble which would call for action before leaving the station. This examination should include rolling the tape back about three feet to check damaged or poorly spaced holes in the tape or places where feed holes are skipped (these can be seen most easily by looking at the reverse side of the tape). Gross time errors and timer stoppages can be found by checking day numbers against calendar days. Attach inspection slip to removed tape with a rubber band. Prior to leaving the station, check to see that there is sufficient tape on the supply roll. If the amount of tape on the supply roll is in question, remove the left flange on the supply roll holder and measure the thickness of the paper remaining. The following table (Table 2.4) gives the approximate thickness against days of tape remaining.

m. When visiting the station but not changing tape or chart, note recorder readings and base reference gage readings on tape leader and chart, but do not advance tape or chart.

d. If the station consists of a stilling well with a float-operated recorder,

Table 2.4. Days Remaining on Supply Roll

| Thickness of remaining tape on supply roll | Days remaining on supply roll Reading Frequency | | | |
|---|---|---|---|---|
| | 5 min | 15 min | 30 min | 60 min |
| 1/4 inch | 10 | 30 | 60 | 120 |
| 7/16 inch | 20 | 60 | 120 | 240 |
| 9/16 inch | 30 | 90 | 180 | 360 |
| 11/16 inch | 40 | 120 | 240 | 480 |

1. Check the float for leaks.

2. Check the float-clamp screw to make sure that there can be no slippage of the float tape where it joins the float.

3. Check the well for unduly large accumulations of sediment and remove such material.

4. Check the depth of oil in the oil tube, if there is one, to detect any oil leaks and if any oil should be added.

5. Flush the intakes regularly if the well is equipped with a flushing system, or if there is no such system, force clean the intake with a plumber's snake, and

6. If there has been a high discharge since the last visit, check the stilling well, both inside and out, for high-water marks as a check on the peak stage shown on the recorder. If the equipment malfunctioned since the last visit, the high-water mark information is used to estimate missing record. After this check, clean the marks off to prevent confusion with later high-water marks.

e. If the station is equipped with a bubble gage sensor, there are several other checks that are necessary:

1. Inspect the bubble orifice to make sure it is not buried by sediment.

2. Keep a log of gas-feed rate, gas consumption, and gas-cylinder replacement to insure a continuous supply of gas and to help check for leaks in the system, and

3. If a high discharge has occurred since the last visit, look for a high-water mark near the base reference gage as another check on the recorded peak stage. Record gage height of outside high-water mark on measurement front sheet.

After making the necessary measurement, the initial steps (involving basic checks on the operation of the recorder) are repeated to insure operation of the recorder.

2.3.2.5 Discharge Measurements

Discharge measurements consist generally of making velocity and depth measurements at a number of verticals in a channel cross section near a stream gage. The basic equipment for most conditions includes a current meter for measuring velocity and a wading rod for measuring depths and holding the current meter or some type of hanging weight and current meter assembly when

measurements are made from a boat, bridge or cablecar. When unusual conditions prevail such as very small flows, a small flume may be used. Other conditions may best be gaged by dye dilution or float techniques. When direct discharge measurements are either missed or impossible due to flooding, indirect techniques are used such as the slope-area method.

After servicing of the gaging station, preparation for the discharge measurement begins. Sometime before the measurement begins, the contractor would have determined the method to be used (wading, cablecar, boat, bridge, etc.) beforehand so as to have all necessary equipment on hand. Possibly a specific location would have been given by the USGS. If not, a proper section must be selected by the contractor. The section where the actual measurement is to take place should: (1) be in a stable location to minimize scour and fill, (2) not be where a large amount of turbulence or backwater conditions exist, (3) be close to the gage, (4) and be in a relatively straight reach for the most uniform flow. These conditions may not all be possible, but all efforts need to be made to insure that discharge measurements are as accurate as possible.

At the beginning of the measurement, after the equipment is prepared, the stream gager prepares the discharge measurement notes. The required information includes the following:

1. Station
2. Data
3. Party
4. Meter information: date rated, spin time
5. Type of measurement (wading, boat, etc.)
6. Gage height at beginning and end of measurement (during, if stages are noted to be changing)
7. Location of section with respect to the gage
8. Quality of measurement (excellent, good, fair, poor)
9. Cross-section information (bed forms, uniformity, etc.)
10. Air and water temperature
11. Control
12. Remarks
13. Gage height of zero flow

During the measurement, depths, widths, velocities, horizontal angles, etc. are recorded.

2.3.2.6 Equipment

The current meter generally employed by the USGS is the Price AA current meter. This meter is a vertical axis meter with six cone-shaped cups which rotate with the stream velocity. Each meter has been calibrated in a test flume and a tally is made which relates the number of revolutions of the bucket wheel in a given time increment (ranging from 40 to 70 seconds) to the velocity of the flow. When shallow depths are encountered, the Price Pygmy meter can be used. It is scaled to be 2/5 as large as the AA meter and does not have a tailpiece.

The standard Price AA current meter has an eccentric cam which makes an electric contact once each revolution and a penta-gear reduction which makes contact once each five revolutions where velocities are high. This contact is heard as a click in a headphone assembly or one count on a counting box. These counts are again made over a 40 to 70 second interval which is converted to velocity by using the rating table or equation.

Current meter measurements can be made by wading, from a boat, bridge or cablecar. Wading is generally preferred since it is the easiest and fastest method, but when the product of depth times velocity ranges from 5 to 7 or higher, a person cannot safely wade a stream. The next preferred gaging method is from a cablecar. The cablecar is generally in a selected location for gaging and is perpendicular to the flow. Instead of the wading rod, a reel with cable is used to hold the current meter. A short distance below the hanging current meter a lead weight such as the Columbus sounding weights holds the cable in a near vertical position. These weights range from 15 to 300 pounds depending on flow conditions. A reel with a depth indicator is used to raise and lower the meter and weight and to measure depth.

Stream gaging from a bridge uses a similar arrangement as the cablecar method. A reel and weight system suspends the current meter. For small streams a handline can be substituted for a reel. For larger streams, one of several types of cranes or booms mounted on a truck is used to hold the reel, cable meter and weight assembly. Horizontal angle corrections need to be applied since the bridge may not be perpendicular to the flow. Discharge measurement notes can be used in determining the angle correction.

When a bridge or cablecar is not available, a boat may be used. For smaller streams, a cable may be stretched across the river and a special boom

and crosspiece is attached to the bow of the boat. This assembly attaches to the cable stretched across the river to hold the boat in place. Again a reel, cable, meter and weight arrangement is used to raise and lower the meter and measure depths.

2.3.2.7 Current Meter Measurements

A current meter measurement entails measuring the incremental width, depth and velocity at about 10 to 30 verticals in a cross section. The total discharge is then the sum of the individual areas $(a_i)$ times the velocities $(v_i)$.

$$Q = \Sigma\ (a_i v_i) \tag{2.1}$$

Widths are measured by stringing a tag line across the river or tape along a bridge or marks on the cable of a cablecar. The discharge at partial sections is computed by the midsection method as shown in Figure 2.1 (after Buchanan and Somers, 1969).

$$\begin{aligned} q_i &= v_i \left[\frac{(b_i - b_{i-1})}{2} + \frac{(b_{i+1} - b_i)}{2}\right] d_i \\ &= v_i \left[\frac{b_{i+1} - b_{i-1}}{2}\right] d_i \end{aligned} \tag{2.2}$$

where $q_i$ = partial discharge through section $i$
$v_i$ = mean velocity of location $i$
$b_{i-1}$ = distances from initial point to locations $i-1$
$b_i$ = distances from initial point to locations $i$ and
$b_{i+1}$ = distances from initial point to locations $i+1$
$d_i$ = depth at location $i$.

2.3.2.8 Velocity Measurements

The velocity of a stream generally varies logarithmically with depth. Because time constraints do not allow measuring a more complete vertical velocity profile at each site, the velocity is measured at certain depths depending on flow conditions.

Three basic methods are used under most conditions. When the depths are between 0.3 ft and 2.5 ft the velocity is measured at a depth 0.6 of the depth below the water surface or 0.4 times the depth above the bed. This depth is

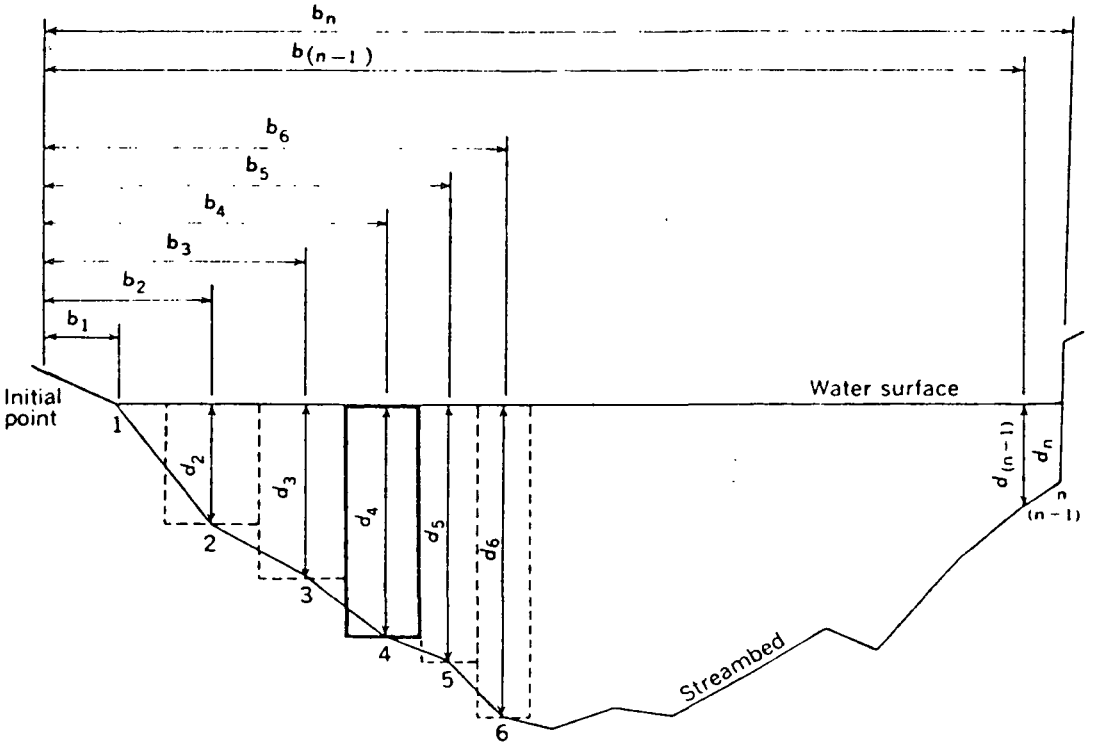


EXPLANATION

| | |
|---|---|
| 1, 2, 3, . . . n | Observation points |
| $b_1, b_2, b_3, \ldots b_n$ | Distance, in feet, from the initial point to the observation point |
| $d_1, d_2, d_3, \ldots d_n$ | Depth of water, in feet, at the observation point |
| Dashed lines | Boundary of partial sections; one heavily outlined discussed in text |

Figure 2.1. Definition sketch of midsection method of computing cross-section area for discharge measurements (after Buchanan and Somers, 1969).

used because when integrating the logarithmic velocity profile over depth to find the mean velocity, the mean velocity occurs 0.6d below the surface.

Another method is to take two velocity measurements at each vertical, one 0.2d below the surface and one 0.8d below the surface. The arithmetic mean is then computed for the mean velocity. This method is used when the depths are over 2.5 ft and is called the two-point method.

A third method incorporates the previous two where velocities are measurable at 0.2d, 0.6d and 0.8d below the surface. Generally the velocities at 0.2d and 0.8d are averaged and the result is averaged with the 0.6d measurement to compute the mean velocity. This method is used when the vertical velocity distribution is abnormal, such as when caused by obstruction on the bed.

Other modifications of these procedures may be resumed under adverse flow conditions. For example, if stages are changing rapidly, the 0.6 method may be used over depths of 2.5 ft to reduce the time of the measurement. Debris or ice may preclude the use of the 0.2 depth measurement. If the weight can't hold the meter in position at 0.8d due to high velocities and large depths, a 0.6d method or a 0.2d method with a correction may be used. When a meter cannot be used, the float technique is used to estimate discharge. Velocities are measured over a premeasured distance (100 ft at least) at various locations across the channel. Areas are multiplied by the velocities and summed to obtain the total discharge. Low-flow measurements may be made by Pygmy meter or portable flume or weir.

A few precautions must be taken in order to assure accurate discharge measurements. Allow a few seconds for the current meter to reach an equilibrium velocity after putting it in position in the stream before starting the actual measurement. When wading, keep a good distance (downstream and to the side) from the current meter with the feet and legs to minimize interference. Whenever the tagline (cablecar, bridge, etc.) is not perpendicualr to the flow, the horizontal correction must be made. Periodically, check the free spin time of the meter during the measurement to insure proper meter operation. When stream gaging an alluvial, sand-bed river, note the bed forms if at all possible and water surface conditions since often a distinct shift in the stage-discharge relation occurs when the stream bed changes from lower to upper regime. Before starting the measurement, check the chart or tape at the stream gage for rate of rise or fall of the stage. If the stage is rising

or falling rapidly, a quick 0.6d measurement may be required or at least frequent monitoring of the gage height would be necessary.

At the end of each measurement, the stream gager will check the measurement by plotting the stage and discharge on a field rating curve to see if the new measurement follows the previous trends. If a significant difference exists, a recheck of computations is performed. If the computations are correct, a remeasurement with a separate set of equipment is in order if no obvious physical reason for the discrepancy is observed. A return visit by the stream gager and supervisory personnel may be required.

2.3.2.9 Development of Rating Curves

The development of rating curves requires tabulation of the following data:

1. Measurement number
2. Date
3. By whom
4. Width
5. Area
6. Mean velocity
7. Gage height
8. Discharge
9. Rating shift
10. Percent difference
11. Method of velocity determination in vertical
12. Number of verticals
13. Gage height change
14. Measurement rating
15. Air temperature
16. Water temperatuare
17. Remarks

Following the compilation of data, the rating table of stage or gage height versus discharge can be developed. This development of the rating table follows procedures given in Surface Water Techniques of the USGS, Book 1, Chapter 12, Discharge Rating at Gaging Stations.

First the discharge versus stage is plotted from the compilation of measurements on an appropriate scale. Previous graphs at each station can

serve as a guide. The points on the curve are plotted as prescribed with a 3/32 inch circle and with a 0.8 inch guide line starting 0.2 inches from the circle at a 45° angle.

Points that don't plot within ±5 percent of the rating curve must be given attention. These points may be valid measurements indicating a shift or may be more temporary in nature. A reason for the departures should be explained. For example, when developing a rating curve for a sand-bed channel, changing bed forms can drastically change resistance to flow, which in turn changes the stage for a given discharge. The resistance to flow may be on the order of 0.035 (Manning's n) for dunes, but as flow increases and changes the bed forms to plane bed in upper regime, the n value may drop to 0.012. An example is given in Figure 2.2.

Note how the bed form observation and corresponding change in resistance to flow can explain deviations in a stage-discharge relation.

Stages or depths may also vary during the passage of a flood wave due to a lag in bed form changes due to rapidly changing hydraulic conditions as shown in a number of laboratory experiments by Simons and Richardson (1962) (see Figure 2.3). Again, relatively large changes in stage or depth can occur at a given discharge. For these reasons, all efforts should be made to observe bed forms during discharge measurements.

Dynamic effects due to unsteady nonuniform flow can create a hysteresis loop in the stage-discharge relationship. This occurs again during an unsteady flow event or when stages are rising or falling. A common method used by the USGS to correct discharge measured during a period when stages are changing is the Boyer method. The ratio of the measured discharge to the corrected discharge is found by the following equation.

$$\frac{Q_m}{Q_c} = \sqrt{1 + \frac{2}{US_c}\frac{dh}{dt}} \qquad (2.3)$$

where $Q_m$ is the measured discharge, $Q_c$ is the corrected discharge, $U$ is the velocity of the flood wave, $S_c$ is the constant stage slope for the stage at which the measurement was made and $dh/dt$ is the rate of change of stage. The velocity of the flood wave is computed by

$$U = 1.3\ V_m \frac{S_c}{S_o} + \left(1 - \frac{S_c}{S_o}\right)\sqrt{gd} \qquad (2.4)$$

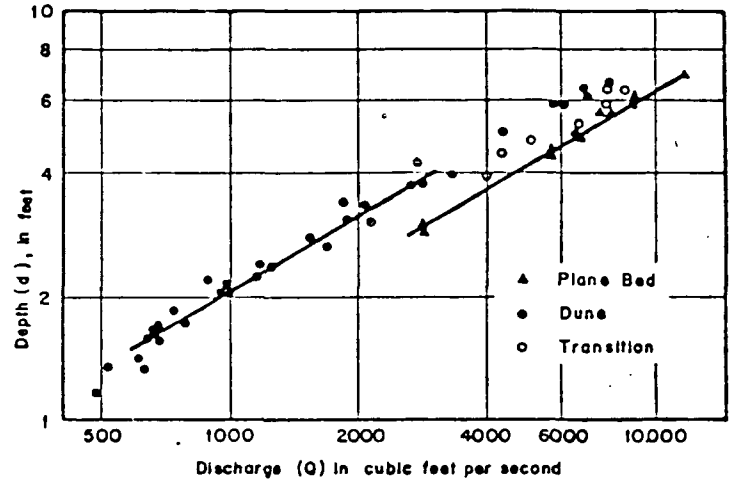


Figure 2.2. Relation of depth to discharge for Elkhorn River near Waterloo, Nebraska (after Beckman and Furness, 1962).

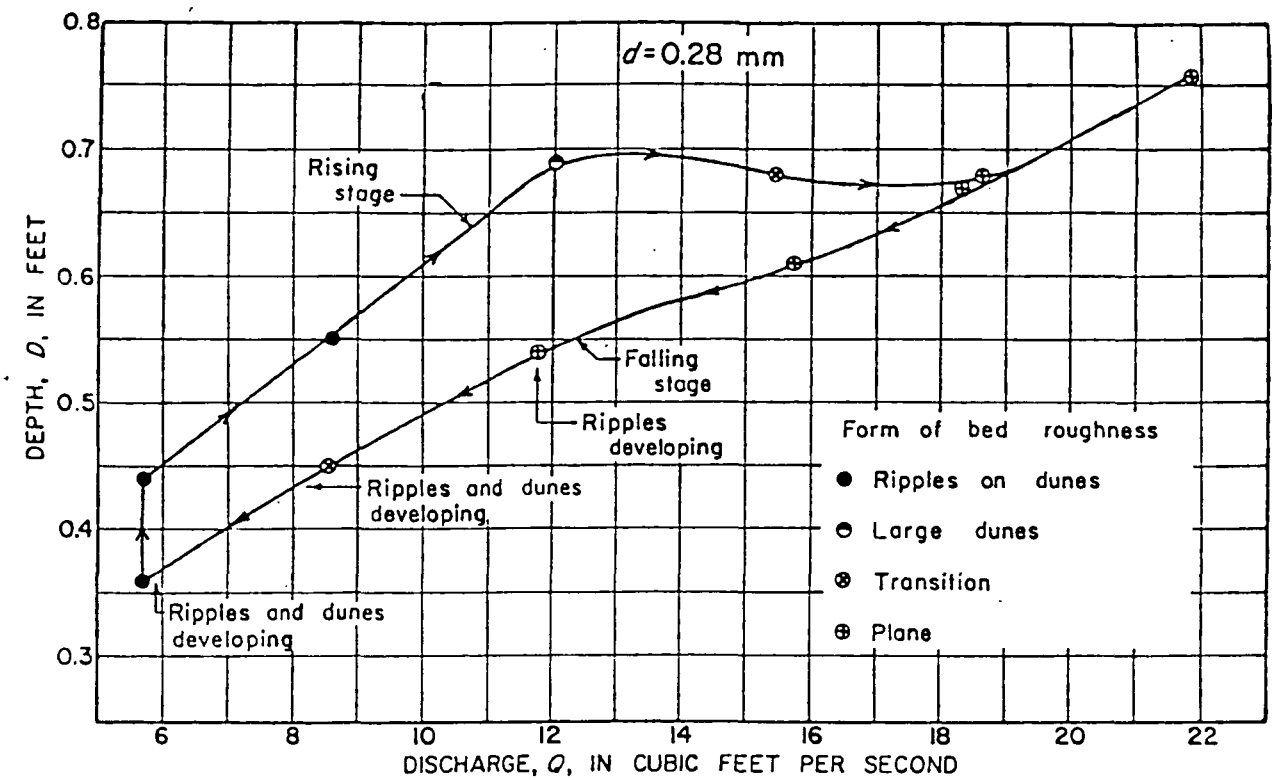


Figure 2.3 Relation of depth to discharge for lower- and upper-regime flow when the variation of slope with discharge is moderate (after Simons and Richardson, 1962).

where $S_o$ is the slope of the stream at high stages, $V_m$ is the mean velocity, $g$ is the acceleration of gravity and $d$ is the mean depth.

Another method was presented by Simons et al. (1977) which computes in more detail the relationship of stage to discharge during the passage of a flood wave to correct for the hysteresis loop due to unsteady nonuniform flow. In this method the full dynamic momentum equation given in Equation 2.5 is solved in terms of the geoemtry of the particular cross section, resistance to flow and rate of change of stage.

$$S_f = S_o - \frac{\partial y}{\partial x} - \frac{1}{gA}\frac{\partial Q^2/A}{\partial x} - \frac{1}{gA}\frac{\partial Q}{\partial t} \qquad (2.5)$$

where $S_f$ is the friction slope, $S_o$ is the channel bed slope, $y$ is the depth of flow, $x$ is the downstream distance, $g$ is the gravitational acceleration, $A$ is the cross-sectional area of flow, $Q$ is the discharge, and $t$ is the time.

Figures 2.4 and 2.5 show application of the method on the Mississippi River. Significant changes in stage can occur for a given discharge simply due to flow dynamics.

Careful consideration to physical processes such as flow dynamics, changes in bed form and of course changes in cross section due to scour and fill must be given in developing the rating curve and table for each station.

A new rating table is required when a definite shift occurs backed up by an understanding of the physical process causing the shift. After a sufficient number of new measurements is made and plotted, a manual method of developing the rating table from the curve is used. From the low end of the rating curve where the relation is usually quite curvilinear, discharges are tabulated at 0.1-ft stage increments. Where a rating curve is close to linear the discharges are read at 1.0-ft intervals. Values are then to be interpolated between the points picked from the curve. The table must then be compared at all values to the rating curve and adjustments made if needed. The rating table should be as complete as the curve and give discharge of 0.1-ft increments.

Instead of developing a new rating table whenever some natural phenomenon causes a change in a rating curve, a shifting control correction may be made. This correction involves computing the gage height that would produce the

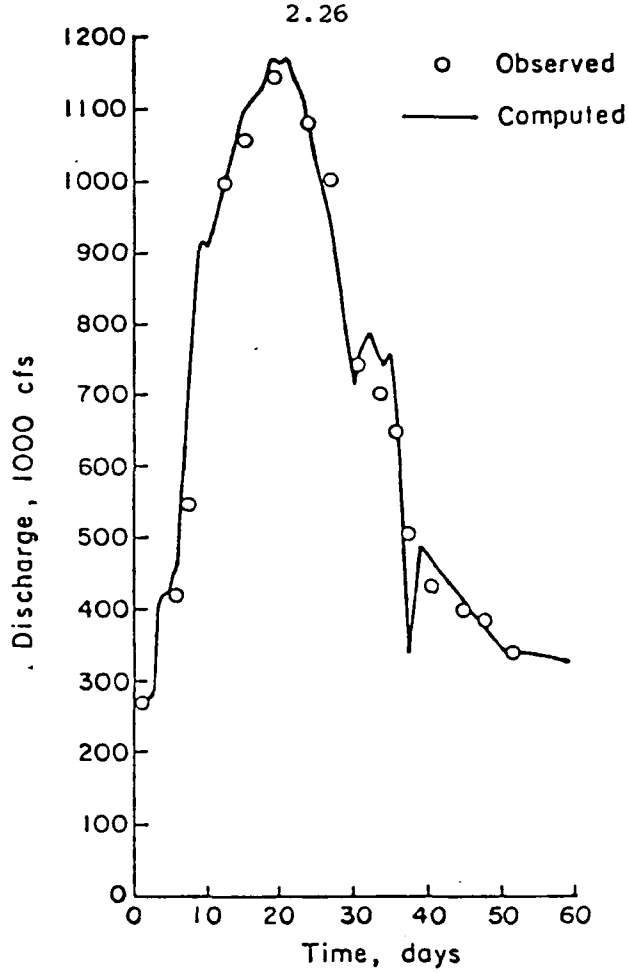


Figure 2.4. Discharge hydrograph for the Mississippi River, Tarbert Landing, LA (2/9/66 -4/11/66).

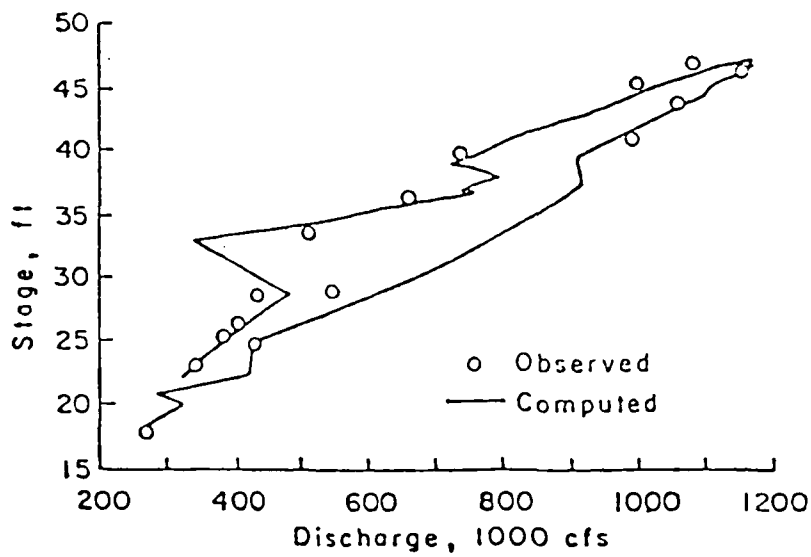


Figure 2.5. Stage-discharge relations for Mississippi River, Tarbert Landing, LA (2/9/66-4/11/66).

measured discharge from the original data. The shift is then the difference between the observed gage height and the computed gage height. Care must be taken to apply the shift with the correct sign.

If the computed gage height is less than the observed gage height, the shift is negative; if more, it is positive.

When applying shift corrections on a daily gage height record to obtain daily discharge, the shifts may be applied prorated in time or as a function of gage height or a combination of the two.

2.3.2.10 Requirement for Discharge Measurement at a Range of Stage

In order to develop a rating curve that is as complete as possible, discharge measurements should be made so as to cover as wide a range of stages as possible for given hydrologic conditions. Efforts to make measurements at high flows will be made in addition to regular monthly measurements. Such extra measurements may be made during one flood event. To accomplish this, timely and sufficient rainfall and snowmelt information must be acquired.

2.3.2.11 Operation and Maintenance of Crest-Stage Gages

A crest-stage gage marks the highest water-surface elevation that occurs between servicing by cork particles adhering to a staff gage within the gage pipe. Observations of the gage and possible changes such as debris, erosion, deposition or man-made changes are to be noted. Datum control is also important for maximum accuracy. Specific steps for site maintenance are listed.

1. If the stage at the time of inspection is below the datum pin,

   a. Remove the cap at the top of the gage pipe.

   b. Remove the staff and if cork particles indicate a peak has occurred, mark the cork line with a pencil line, then remove all cork particles. If a cork line is found at the same elevation as the vent hole, the gage may have been toppled. Always verify such a mark by outside high-water marks.

   c. Enter the date of the inspection on the penciled line and measure the distance from the line to the bottom of the staff (to the nearest 0.01 foot).

   d. Remove the lower cap and flush out any silt that might have collected; make sure all intake and vent holes are unobstructed.

e. Place one tablespoon of granulated cork in the bottom cap, and secure the cap with a pipe wrench. Caps that are easily removed are often taken by children of all ages. Make sure the intake system is positioned so that the five closely-spaced holes face upstream.

f. Replace the top cap (with a wrench), and make sure all bracket bolts and lag screws are tight.

g. Determine the present water surface at the gages (to the nearest 0.01 foot) if over-the-road flow exists.

h. Remove debris that might have collected on the gage.

i. Carefully describe and measure any debris that might have collected. Try to estimate the location of the debris at the time of the peak flow (floating, lodged in the entrance, etc.). Draw a diagram of the obstruction. Remove the debris and record any resultant change in the present water surface elevation at the gage.

j. Document the outside high-water marks and any changes in channel properties. If a peak stage has not occurred since the previous visit, the cork supply in the gage will be adequate. Never assume the gage is fully charged because ants or wind will sometimes remove the cork.

2. If the present water surface elevation is <u>higher than the datum pin</u> and the stage is falling, the above procedure should be modified as follows.

   a. Perform steps a to c above as described.

   b. Carefully pour a teaspoon of cork (half of the amount used when servicing the gage from the bottom cap) into the gage pipe. Wipe the staff completely dry and lower it very slowly into the pipe. Make it a practice to determine the present water-surface elevation by measuring outside the pipe.

   c. Perform steps g to j above as described.

3. If the water surface is <u>high and rising</u>, use the following procedure:

   a. Remove the top cap.

   b. Do not remove the staff from the gage. The removal of the staff may cause an erroneous mark if the stream is near its peak stage.

   c. Determine the present water surface by measuring the distance between the top of the gage pipe and the water surface or the datum pin, if possible.

d. Indicate the rising trend of the stream on the note sheets along with the time of day.

e. Replace the top cap and try to identify the control for the present flow.

4. The USGS Technical Officer should be notified immediately if the recorded peak stage is such as to warrant an indirect determination of peak flow. Pre-flood plans should be made as to type of indirect to be made and best location for indirect.

2.3.2.12 Discharge Measurements at Low-Flow Partial-Record Stations

Periodic seepage runs are an excellent method for explaining the significant low-flow gains or losses along an extended reach or length of stream. Accordingly, a series of discharge measurements on selected stream reaches can be used to define low-flow variations in regions of actual or anticipated coal mining development. To maximize information, seepage runs should be coordinated so that monthly inspections, discharge measurements, and sampling at other sites in the same stream basin are all made within a 36-hour period or less and during a period of uninterrupted base flow. Measurement of seepage runs follow the general techniques used for surface water discharge evaluation (Section 2.3.2.8).

The objectives of a study influence selection of a runoff measuring device. For example, if a water budget is studied in an area where runoff accounts for only about five percent of the water budget, 95 percent of the funds should not be spent on measurement of runoff. More funds should be directed to other parts of the hydrologic cycle. If the objective of a study, on the other hand, is to measure the effect of land treatment on the water supply derived from a watershed, a precalibrated runoff measuring device would be required. Fewer funds and less time should be directed to other parts of the hydrologic cycle.

Selection of a device and location for measuring runoff depends on such factors as the peak runoff rate, distribution of runoff volume by categories of flow rate, absence or presence of sediment or woody trash, or both, in the flow, whether backwater submergence will affect flow through the device, icing conditions, foundation conditions, material availability, and economics. Location of gages is also affected by the objectives of the study, site accessibility and stability and the range of discharges to be measured.

The term "runoff" normally is used to distinguish surface flows from ground water contributions to a streamflow. This distinction generally is derived through analysis of hydrographs since independent measurement is not feasible. The terms "runoff" and "streamflow" are used interchangeably here. They refer to all the flow, regardless of origin, that passes through the control at the point of measurement.

In open channels, a control is a cross section or length of reach above which the water level is a stable index of the discharge rate. All sections have equal capacity to pass a flow. In natural streams the control may shift from one point to another with changes in stage. For use as a runoff station, a control must be selected, altered, or constructed to provide a stable head-discharge relationship.

Many considerations influence selection of a control for flow measurements. The ultimate objective is to provide a stable relationship between the depth of water and the rate of flow. Since the rate of flow equals the product of average velocity and the cross-sectional area, controls should be selected for stability of cross section and such factors as slope, configuration, channel roughness, and absence of tailwater, which affects velocity.

Quantitative evaluation of flow is easier if the flow passes from subcritical to supercritical around the control section. Precalibrated devices use this advantage. Natural controls that maintain critical flow at all stages are unusual. They are selected, therefore, to provide subcritical velocities at all depths since changes in depth are approximately equal to changes in specific energy. Measurement of flow at critical depth should be avoided since it presents so many difficulties. This sometimes can be accomplished by converting to subcritical flow through impoundment or manipulation of the channel gradient. The flow subsequently can pass through critical downstream of the point of head measurement.

For some purposes the control must be located so that gaged streamflow represents the entire flow from the watershed—none escapes beneath or around the control. Cutoff walls extending vertically in impervious strata and laterally in floodplains may be needed to prevent flow from bypassing the gaging station. Bypassing flow may be unimportant for some studies and at some locations.

Other considerations in selecting a control include capacity needed for

major flows; silt, ice and debris content of expected flows; and structural requirements such as footings and protection against frost heaving. Controls are classified herein as (1) precalibrated devices, (2) existing structures adapted to calibration, and (3) natural controls, such as cross sections or channel reaches with suitable hydraulic characteristics for calibration.

Selection of sites should not necessarily be based on the assumptions of a rigid boundary channel and steady flow conditions. An additional analysis is required to answer some critical questions. First, the effect of potential bank and bed erosion on stage-discharge relations should be evaluated. Secondly, the rate of rise and fall of discharge may create a looped stage-discharge relation. The effects of loop rating curves on accuracy of flood discharge should be determined. Furthermore, the selection of sites must consider the need for erosion protection. This requires the analysis of erosion and sedimentation utilizing river mechanics and sediment transport concepts.

Analysis of potential gage sites should consider the stage-discharge relationship, including the effect of rise and fall of discharge, the effect of potential bank and bed erosion, and the sensitivity of the relationship at various levels of discharges. The analysis of potential erosion and sedimentation at a site may be particularly important. Errors in using the original stage-discharge relationship under conditions of changed channel cross section are evaluated. Stage-discharge relationships with a cutoff point above which the relationships can no longer be considered valid should be identified.

### 2.3.3 Collection and Processing of Water Quality Data

#### 2.3.3.1 General

Collection and processing of water quality data requires samples for chemical and sediment analysis. Samples collected for chemical analysis include those for laboratory analysis and those for field analysis. Laboratory samples require preparation, filtration, preservation and shipment while field samples require measurement for selected water-quality parameters and biological observations. Samples collected for sediment analysis require preparation and shipment.

Prior to collecting samples, initial observations on weather conditions, streamflow, color of the water, condition of the site, etc. must be made and documented. Current discharge measurements are required at the time of water quality data collection or at least an estimate based on stage and the rating

curve or other information.

The sampling site location is extremely important to obtaining quality data. Sections of streams that are not thoroughly mixed or where differences in composition exist should be avoided. This condition often exists downstream of the confluence of major tributaries. A good sampling section should show fairly uniform measurements or observations in the channel cross section (Middelburg, 1979) when the proper sampling technique has been applied.

2.3.3.2 Sampling Techniques

The sampling technique should produce a sample that is as representative as possible of the average condition of the water quality variables for a given time and location. Sampling techniques can be categorized as point or integrating methods. Different sampling devices or instruments are used to obtain different types of samples. The same samplers used for fluvial sediment are used for water quality with slight modifications to reduce contamination. Water sample bottles for the sampling devices must be washed and thoroughly rinsed.

The equal discharge interval technique (EDI) is one of two depth-integrated cross-sectional composite methods. The EDI method consists of the collection of equal amounts of water at the centroids of equal discharge increments of the stream. The discharge pattern must be established by measurement prior to water quality sampling, or from previous discharge measurements. For narrow streams (up to 15 meters) with good mixing, the discharge profile can be divided into three to five equal parts. For larger streams, five to ten sections are required. A depth-integrating sampler is used to get approximately an equal amount of water from the centroid of each section. The depth-integrating sampler is lowered to the bottom (or maximum depth for the sampler being used) and then raised again. The down rate does not need to equal the up rate; however, the travel rates should be constant and less than 0.4 times the velocity. The bottle should be filled 3/4 full or less. Repeated vertical transects can be used to get an adequate amount of water. The amount collected at each section depends on what is required for the analysis techniques. The proper amount can be determined by computing the amount needed for analysis plus two to three liters (for rinsing purposes and waste) divided by the number of sections. As the sampler bottle becomes full

it is composited into a larger second container. The same bottle should be used throughout the cross section to prevent the cumulative error introduced by the loss of particulate matter that is not rinsed from the sample bottle to the composite container.

The equal width increment (EWI) is the second procedure available to produce a depth-integrated cross-sectional composite sample. It can be used with or without dicharge measurements and for braided streams (the EDI should not be used for braided streams). The sampling procedures are the same as the EDI method, except equal distance is used between verticals regardless of the discharge, although the distance should be selected so that no more than ten percent of the discharge passes between two verticals. One vertical rate is used resulting in different amounts of sample collected at each cross section, depending on the depth and velocity. Therefore, it is difficult to predict how many verticals are needed. If a sufficient sample is collected, the EWI section can be repeated. The second pass can use a different cross-sectional spacing if necessary.

If the sample bottle cannot go down and back without overfilling, a point-integrating sampler must be used. Point-integrating samplers use an electric value to allow vertical transects in one direction, up to approximately 30 ft. Repeated vertical transects each covering a different depth can be used for greater depths. The point-integrating sampler can be used for either the EDI or the EWI procedures.

2.3.3.3 Field Evaluations

Field evaluations are made on samples or directly in the stream to establish certain water quality parameters prior to any potential change. Field measurements on pH, acidity, alkalinity, dissolved oxygen, specific conductance air and water temperature are generally required. The USGS has established strict procedures on these tests. These procedures are available in TWRI Book 5, Chapter A1 and "Field Measurement of Water Quality" (Middelburg, 1979). A brief review is presented below.

Field measurements of pH are often made using the glass electrode method. A water sample is taken and pH measurement is made promptly to avoid possible changes due to chemical or biological activity. Standard pH buffers used in calibration should be kept at the same temperature as the sample. A brief procedure outline follows.

1. Perform battery check.

2. Add 25 ml pH 7 buffer to a clean 50 ml beaker. Measure temperature.

3. Place electrode in buffer. Measure pH and standardize.

4. Clean electrode with distilled water and continue calibration with pH 4 and pH 10 buffers.

5. Measure pH of sample in a clean beaker or plastic cup that has been rinsed with sample water. While measuring pH set the temperature dial according to measured sample temperature.

After establishing the pH, the appropriate test for alkalinity/acidity can be performed. These tests are chemical titrations used to establish the concentrations of major constituents. The appropriate reagents to titrate with, the procedures followed and the formulas used to determine the constituents are detailed in TWRI Book 5, Chapter A1.

Dissolved oxygen can also be evaluated by chemical titration or by electrode instruments. The procedures set forth in USGS Quality of Water Branch Technical Memorandum 79.10 may serve as a guide.

Specific conductance is measured by a battery powered Wheatstone Bridge. Specific conductance should be measured in the field. After a sample is taken, the procedure is as outlined below:

1. Perform battery check
2. Clean cells
3. Check calibration
4. Rinse cell with sample water and then fill
5. Measure temperature
6. Measure conductivity
7. Correct measurement to 25°C.

Temperature is an important parameter in water quality data collection. Temperature is generally measured by thermometer or thermistor.

Air temperatures are measured using a dry thermometer in a shaded area. The thermometer should be exposed to sufficient air circulation without being subject to strong winds. Let the thermometer sit for ten or more minutes before reading. Record temperature and time of day.

Water temperatures should be measured at about five verticals in the stream and averaged to obtain a mean value. Thermistors should be allowed to stabilize for three minutes and thermometers for one. All temperature

measuring devices should be adequately calibrated to insure correct readings.

2.3.3.4 Chemical Samples

Chemical samples must be prepared, filtered, packaged, labelled and shipped by the most expedient method available on the same day of collection. USGS procedures specify volumes required for each subsample, the types of containers to be used, the type of treatment and/or preservation and the sample designation.

2.3.3.5 Sediment Sampling

The Agricultural Research branch of the U.S. Science and Education Administration has compiled many of the techniques used for monitoring sediment yields from watersheds. The following discussion is from Brakensiek et al., 1979.

Sedimentation is the detachment, entrainment, transportation, and deposition of eroded soil. Techniques and procedures described are limited to those used in fluvial sedimentation research on agricultural lands. Sedimentation in major rivers, large reservoirs, estuaries, and harbors is not considered in this manual.

Although no single phase of the sedimentation cycle can be treated as an entity, the natural sequence of the cycle is as follows: Soil erosion-transportation-deposition. Soil erosion has been defined as the detachment and movement of soil from the land surface by wind or running water.

Most of the damage caused by sediment is the result of accelerated erosion, defined as erosion in excess of the geologic norm. Accelerated erosion is usually induced by activities of man such as: deforestation, cultivation and overgrazing, reshaping the land surface for construction or mining, and disturbance of the natural drainage system.

In agriculture, sediment sources are classified as: (1) sheet and rill erosion, (2) erosion from gullies, arroyos, roads, rights of way and construction sites, and (3) channel bed and bank erosion. In most regions, sheet and rill erosion is usually the largest source of sediment.

In addition to being erosive forces, wind and water are the transporting agents for sediment. Although significant amounts of sediment are moved by wind, particularly in the arid regions, water is the major transporting agent. Sediment transported in a stream or watercourse is usually subdivided into two

categories according to the dominant mode of transport, suspended load, and bed load. Total sediment load is the sum of the two. Other paired terms such as washload, bed-material load, measured and unmeasured load, and sampled and unsampled load are also used to describe sediment transport. Figure 2.6 gives the relative location of these descriptive terms in the stream vertical.

Since sedimentation processes are completely linked to the quantity and character of runoff, it is necessary that fluvial sedimentation data be associated with corresponding runoff for many interpretive anlayses.

A variety of instruments and techniques has been developed for field measurement of soil erosion, sediment movement, and sediment deposition. In general, three basic types of measurements are required: (1) measurements of sediment in surface runoff from small experimental plots and watersheds and in stream channels, (2) measurements of eroded areas to determine the volume of material removed, and (3) measurements of the volume and density of sediment deposits. Instruments, equipment, and techniques typical of those used in sedimentation research on agricultural lands are discussed in this section.

2.3.3.6 Site Selection

The objectives of the experiment and the type of data to be obtained determine the location of the experimental site. Other considerations include the availability of land, access to the area, topography, facilities for cultivating the land if cropping practices are a part of the experiment, availability of servicing personnel, management control of the experimental area, drainage and vertical head requirements for instruments, and sampling equipment.

Generally, fractional-acre plots and small watersheds a few acres in size are used to study basic erosion rates of various soil-cover complexes which are representative of a land resource area. This requires location of the experimental area on a specific soil type with the desired topography. Vegetative cover, except forest cover, is usually easily established within a relatively short time. Replicate plots are sometimes required to obtain representative data due to such factors as inherent errors in measurement and variations within soil types. For most experiments, tenure of the land is needed for ten years or more to cover the normal range in weather patterns.

Plot shape is determined by the objective of the study and can range from a small rectangular area to a naturally shaped watershed. Plot length should

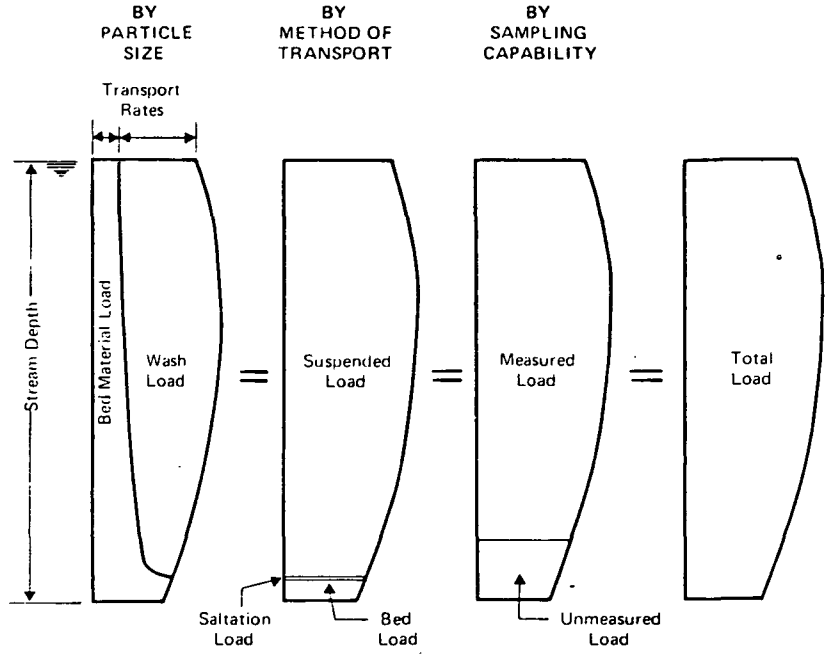


Figure 2.6 Schematic diagram of stream vertical showing relative position of sediment load terms, from Brakensiek et al, 1979.

represent the length of slope on which soil losses occur. Lengths commonly used in feet are 36.3, 72.6, 92.0, 145.2, and 400 (11, 22.1, 28, 44.3 and 122 m). Plot widths may vary from six feet (1.8 m) for hand-tilled plots to 20 feet (6 m) or more when conventional farm machinery is used. Computations of results are aided when length times width results in a simple fraction of an acre (72.6 ft (22/m) length x 6 ft (1.8 m) width = 435.6 $ft^2$ (40.5 $m^2$) = 0.01 acre (0.004 ha)).

Sites should be selected to represent the range of slopes encountered in the general farming area. Plots on natural slopes are best because reshaped slopes usually do not contain normal soil profiles. Larger plots and small watersheds may have natural slopes ranging from convex to concave. Slopes low enough to cause soil deposition above the measurement site should be avoided, unless special provision is made for measurement.

Heavy-gage sheet metal may be used for borders on small plots. Metal borders are easily removed when cultivation of the plots is required. Earthen ridges may be used on plots wide enough for farm equipment normally used in farming operations. Terrace interval plots may be used only with the terraces at the upper and lower boundaries, with a grassed waterway to route flow from the lower end of the rows to the point of measurement.

Small watersheds usually do not require borders except dikes at the lower edge to direct flow to the point of measurement. Plots of all sizes are equipped with a trough or other collecting device to route the soil-water mixture to the sampling site. Sheet metal is used for the collecting trough on small plots. A concrete channel or earth dike may be used on large plots and small watersheds. Sheet metal borders, particularly those on the lower boundary, should be installed deep enough to prevent piping and tunneling underneath by rodents.

When land use and conservation practices are to be evaluated, they must be considered when the site is selected. Cropping treatments may vary from continuous fallow (bare soil) to continuous sod or forest. Fallow soil serves as a basis for evaluating other treatments and provides a measure of the inherent erodibility of the soil. Cropping systems that employ a crop rotation patern should have all years of the rotation represented on separate plots at all times after the rotation is fully established. Conservation practices may include terraces, minimum tillage, strip cropping, contour plowing, and others.

2.3.3.7 Stream Sampling Stations

Generally, sites selected for water discharge measurements in natural channels are adequate for suspended sediment measurements. In addition to the usual requirements of access and availability, a straight channel reach with uniform velocity and sediment distribution is desirable. Consideration is also given to the construction of walkways, cables, and bridges and to the installation of sampling equipment.

Sampling equipment has not been perfected that will sample the entire depth of flow in a natural channel. Conventional depth-integrating samplers are limited to sampling the flow from the water surface to about 0.3 ft (9.1 cm) above the streambed. Therefore, artificial or natural grade controls which provide an overfall and permit sampling through the entire flow vertical are necessary if total load sampling is to be accomplished. Artificial or natural turbulence sections which uniformly suspend transported sediments also provide an alternative approach to total load sampling. Many flow-measuring devices such as weirs, rectangular notches and flumes can be designed to provide sufficient overfall for total load sampling. Highway box culverts and other hydraulic structures may also be used.

Sediment investigations in a land resource area may require measurements of sediment yield from channels, gullies, and other major sediment sources. Typical sites may not exist, but sites selected should represent local conditions as nearly as possible. There must be access to instrumentation to install and service sampling equipment. Detailed topographic surveys may be needed.

No attempt has been made to cover all sediment sampling and measuring devices and equipment. Only those used most commonly in sedimentation research on agricultural lands are discussed. Variations and adaptations of basic instruments are often made to fit local conditions.

2.3.3.8 Total Collection Devices

A simple total collection device for very small plots may be constructed to measure erosion by installing a suitable collection tank large enough to contain the total runoff (water and sediment) expected in a 24- or 48-hour period. The weight or volume, or both, of the water-sediment mixture is then determined and the material sampled for subsequent laboratory analysis and computation of the weight or volume of sediment.

Total collection devices are not generally recommended for erosion studies because runoff storage requirements are excessive even for very small drainage areas. Small drainage areas, in turn, are not normally representative of large, complex field conditions. Slot-type samplers, which collect a known portion of the runoff-sediment mixture, are preferred because they can be used on larger areas, and the sample volume is reduced to manageable quantities.

Slot-type samplers are used in basic erosion studies on small plots and watersheds. These samplers are automatic in the sense that no attendant is required during the sampling operation, and sampling is continuous during the runoff event. The samplers provide a storm-integrated or discharge weighted sample for determining sediment yield. The multislot divisor, with a stationary slot, and the Coshocton wheel sampler, with a revolving slot, have been used extensively.

The Multislot Divisor. Runoff is routed from the collector through the conveyance channel to a sludge tank where the heavier sediment particles are deposited. Overflow from the sludge tank is routed through the multislot divisor, where an aliquot sample is obtained from a single slot and routed to a sample storage tank. A second or third sample storage tank may be connected to the first if additional sample storage is needed.

Many investigators prefer to install a small, removable intertank directly below the inflow spout in the sludge and sample (aliquot) tanks. This greatly reduces the time and labor required to sample and clean up after small storms which do not overflow the small intertanks. It also improves the accuracy of volume measurements.

The size and capacity of the sampling apparatus are determined by the anticipated maximum rate and amount of runoff and sediment to be sampled. For small fraction-acre plots it is assumed for design purposes that maximum runoff rate will equal the maximum five-minute rainfall rate. Sample storage based on 100 percent runoff should be provided for a 100-year, 48-hour storm.

Sediment storage requirements vary greatly with location, soil type, land use, and climatic conditions. Sediment rates as high as 50 tons per acre have been recorded from single runoff events under adverse conditions. Bulk densities of trapped sediment may range from 40 to 100 $lb/ft^3$. The size and geometry of the collector trough and conveyance channel are determined by the maximum flow requirements. Flow velocities in conveyance channels should be

fast enough to prevent sediment deposition through a wide range of flows. Minimum velocities of 2 ft/s at flow rates of about one-fifth of the maximum will prevent excessive deposition for most soils.

The collector acts as a weir at the end of the plot. It is installed so that the elevation can be adjusted to the plot surface as erosion occurs. It is attached to an end plate which should extend at least eight inches into the soil below the collector trough. Although the collector and end plate may extend across the entire length of the plot, it is best to concentrate runoff before it reaches the collector on wide plots.

The depth is usually the same as the conveyance channel with about 0.4 foot (0.12 m) freeboard. The width may vary but should be wide enough to clean easily, 8 to 10 inches (20-25 cm). The bottom should slope to the center by at least five percent. Screens of one-half or one inch (1.3 to 2.5 cm) mesh should be installed over the collector to keep trash out of the system.

Coshocton-Type Runoff Sampler. The Coshocton-type runoff sampler is constructed to form a single unit with the small H flume. Three basic models, N-1, N-2 and N-3, have been designed for use with the 0.5, 1.0 and 1.5-foot H flumes. Models N-1 and N-2 have been used extensively in the field.

Capacities, sampling rates, and other pertinent information on Coshocton-type samplers are given in Table 2.5. Sampler size and capacity for a given experiment are determined by the capacity of the H flume required to measure peak runoff rates. Slightly oversized flumes and samplers are recommended because the sampling error increases significantly at discharges above 80 percent of flume capacity. For small plot studies the maximum runoff rate is assumed to equal the maximum expected five-minute rainfall rate. Sample storage capacity is provided for the aliquot sample from the maximum 48-hour runoff event.

#### 2.3.3.9 Suspended Sediment Samplers and Measurements

The development of suspended sediment sampling equipment and procedures and techniques for making field measurements of sediment discharge in streams and rivers has been well documented. Suspended sediment samplers currently used by most U.S. Government agencies were developed by the Federal Inter-Agency Sedimentation Project now located at the St. Anthony Falls Hydraulics Laboratory, Minneapolis, Minnesota.

Table 2.5. Size Schedule for Coshocton-type Runoff Samplers

| Sampler No. | Wheel diameter | Capacity | Head-room requirement | Aliquot | Approximate weight |
|---|---|---|---|---|---|
| | *Ft* | *Ft³/s* | *Ft* | *Pct* | *Lb* |
| N-1 | 1 | 1/3 | 1½ | 1 | 26 |
| N-2 | 2 | 2 | 2½ | ½ | 85 |
| N-3 | 3 | 5½ | 3¾ | ⅓ | 270 |

Source: Parsons

Suspended sediment samplers are designed to obtain samples of the water-sediment mixture. Two basic types have been developed; depth integrating and point integrating. Basic requirements of suspended sediment samplers have been reported as follows:

Depth-Integrating Samplers. Depth-integrating samplers are designed to continuously extract a sample as they are lowered from the water surface to the streambed and returned at a constant rate of travel. Ascending and descending speeds need not be the same, but the rate of travel must be constant in each direction. As the sample is collected, air in the container is compressed so that the pressure balances the hydrostatic pressure at the air exhaust and the inflow velocity is approximately equal to the stream velocity.

If the sampler is lowered too fast, pressurization will not equal hydostatic pressure and the inflow velocity will exceed stream velocity. Raising the sampler too rapidly will result in the opposite phenomenon. Inflow through the exhaust port may also occur. If the sampler transit speed is too slow, the sample container will overfill before the sampler is returned to the surface, circulation will occur, and the sample will be enriched. Ideally, the sample container should be from two-thirds to three-fourths full when depth integration is completed.

Point-Integrating Samplers. Point-integrating samplers are equipped with an electrically controlled rotary valve which opens and closes the sampler on command. They are designed to take a sample at any point in a stream over a short time interval. The diving bell principle is used to balance the air pressure in the sample container with the hydrostatic pressure at the nozzle to prevent an initial in rush of water when the valve is opened. With the control valve fixed in the open position, these samplers are also used to obtain depth-integrated samples. One-way depth-integrated samples may be obtained by opening the valve with the sampler at the water surface and lowering it to the streambed at constant speed. This permits sampling to greater depths.

Brief descriptions of suspended sediment samplers most frequently used by U.S. Government agencies are given in Table 2.6. All of these samplers, fabricated from cast aluminum or bronze, are streamlined with tail fins to orient the sampler so that the intake nozzle points directly into the approaching flow. Round or square glass milk bottle sample containers are

Table 2.6. Suspended Sediment Samplers from Brakensiek et al, 1979.

| Sampler designation | Type | Weight | Length | Sample nozzle sizes | Sample volume | Sampling conditions and operation | Auxiliary equipment required |
|---|---|---|---|---|---|---|---|
| | | *Lb* | *In* | *In* | | | |
| U.S. DH-48 | Depth—integrating | 4.5 | 13 | 3/16 and 1/4 | 1 pt | Wading depths & velocities. | Sampler is affixed to standard 1/2-in rod or small diameter pipe. |
| U.S. D-49 | Depth—integrating | 62 | 24 | 1/8 3/16 1/4 | 1 pt | Depths 15 to 18 ft. Low to moderate flow velocities. Sampler is usually operated from a bridge, cableway or truck-mounted rig. | 1/8-in steel cable, reel & crane. |
| U.S. DH-59 | Depth—integrating | 22 | 15 | 1/8 3/16 1/4 | 1 pt | Moderate depths & flow velocities. Sampler is usually operated from bridge or cableway. | Hand line or long suspension rod. |
| U.S. D-74 | Depth—integrating | 60 | 24 | 1/8 3/16 1/4 | 1 pt and/or 1 qt | Depths 15 to 18 ft. with 1 pt container. Usually operated from bridge, cableway or truck. | 1/8-in steel cable, reel, and crane. |
| U.S. P-61-A1 | Point—integrating | 105 | 28 | 3/16 | 1 pt and/or 1 qt | Point-integrated samples to 150 ft. Also used to obtain 2-way depth-integrated samples to 18 ft in moderate velocities. Usually operated from bridge, cableway or truck-mounted rig. | 1/8-in steel, 2-conductor electrical suspension cable, reel & crane. 48 V d.c. power source to operate sampler valve. Additional power source & electric motor to operate reel. |
| U.S. P-63 | Point—integrating | 200 | 34 | 3/16 | 1 pt and/or 1 qt | Point-integrated samples to 180 ft depth-integrated samples in deep high velocity streams. Usually operated from bridge, cableway or truck-mounted rig. | Rugged 2-conductor steel suspension cable, reel & crane. 48 V d.c. power source to operate sampler valve. Additional power source & electric motor to operate reel. |

inserted directly into the sampler body cavity. The bottles are easily removed after the sample has been collected. Plastic bottles can be used in some of these samples, but some can be equipped with teflon nozzles and bushings to minimize contact between the sample and metal surfaces.

Suspended Sediment Discharge Measurement. Sediment measurement involves sampling the water-sediment mixture to determine the mean suspended sediment concentration, particle size distribution, specific gravity, temperature of the water sediment mixture, and other physical and chemical properties of the transported solids. Suspended sediment concentration in a natural stream varies from the water surface to the streambed and laterally across the stream. Concentration generally increases from a minimum at the water surface to a maximum at or near the streambed. Vertical distribution of both sediment and flow velocity in a typical stream vertical is illustrated in Figure 2.7.

Coarse particles, sand size and larger, account for most of the variation. Fine particles, silt and clay, are usually fairly evenly distributed throughout the stream cross section. Variations and fluctuations in concentration in the vertical are affected by stream turbulence, velocity, depth, temperature, the particle size of the bed material, concentration of fine material, and some chemical properties of water. Lateral concentration in stream cross sections varies with channel geometry, slope and alignment, velocity, depth, bed form, and sediment particle size.

Suspended sediment discharge in a stream is the produce of the water discharge and the mean suspended sediment concentration. Symbolically, suspended sediment discharge, $G_{ss}$, may be defined as:

$$G_{ss} = \int_{w=0}^{w=w} \int_{y=\delta}^{y=d} C\ U\ dy\ dx = C_m Q \qquad (2.6)$$

where $w$ = the stream width

$d$ = the stream depth

$C$ and $U$ are the concentration and velocity, respectively, at any point $(x,y)$ above the streambed

$\delta$ = an indefinite point above the streambed, usually a few times the mean size of the bed sediment

$C_m$ = the mean suspended sediment concentration (discharge-weighted)

$Q$ = the stream discharge.

The suspended sediment discharge per unit width $g_{ss}$ is:

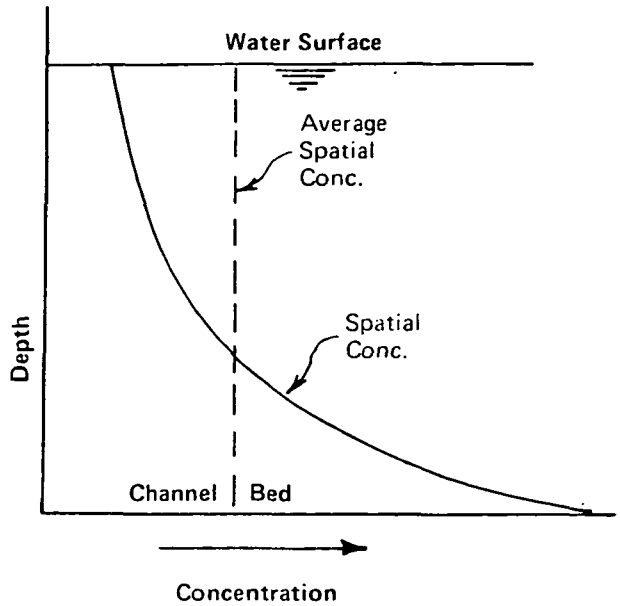


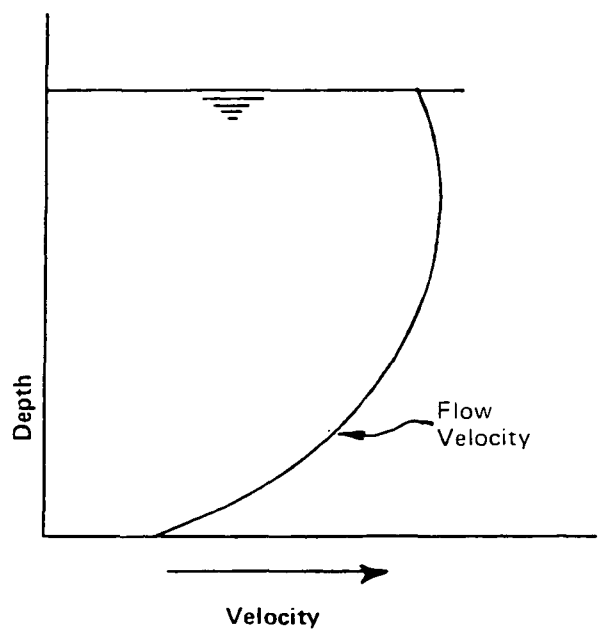


Figure 2.7. Vertical sediment concentration and flow velocity distribution in a typical stream cross section, from Brakensiek, et al, 1979.

$$g_{ss} = \int_{s}^{d} C\ U\ dy = C_m q \qquad (2.7)$$

in which $q$ is the water discharge per unit of width and $C_m$ is the suspended sediment discharge concentration (discharge-weighted) at the vertical where $C$ and $U$ were measured.

The mean spatial concentration, $C$, for the sampled zone in the stream vertical is:

$$\bar{C} = 1/(d - a) \int_{a}^{d} C\ dy \qquad (2.8)$$

in which $a$ is the distance from the bed to the lowest sampling point. By plotting the point concentration $\bar{C}$ against the position of $y$ above the bed, the mean concentration is readily determined. In the absence of a measured velocity distribution, the spatial concentration may be used as an approximation of $C_m$. However, in most field work discharge-weighted concentrations are needed for computations of sediment transport.

In most streams the sediment concentration and flow velocity vary vertically and laterally, and sometimes erratically, and samples must be collected systematically at selected points to be representative of the flow cross section.

"Equal Transit Rate Method". In this method the samples are collected at equally spaced verticals in the flow cross section. The transit rate of the depth-integrating sampler must be uniform and the same at all verticals. The composite sample from all verticals will then represent the mean (discharge-weighted) cross section concentration. Suspended sediment discharge is then computed as the product of the mean cross section concentration and the total water discharge. The number of sampling verticals required, normally 6 to 12 for most small streams, to obtain a representative sample depends upon the accuracy desired, the channel width, the velocity distribution and the sediment concentration and particle size distribution. This is the most commonly used method on small agricultural streams.

Depth-Integrated Samples at Uniformly Spaced Verticals. In this method a relatively large number of depth-integrated samples is taken at the midpoint of equal fractions of the stream width. This method gives a good indication of the distribution of sediment across the stream. Mean sediment con-

centration in the stream is determined by weighting the mean concentration in each sampling vertical with respect to stream discharge in the vertical. Suspended sediment discharge is then computed as the product of mean cross section concentration and total water discharge.

Depth-Integrated Samples at Centroids of Equal Water Discharge. This method requires depth-integrated samples at selected sampling verticals which represent areas of equal discharge across the stream as determined by water discharge measurements. The sampling vertical is then located at the centroid of each section (area). Location of the sampling verticals may be determined graphically. The water discharge for individual sections is determined and cumulated for the stream cross section. Cumulated discharge in percent of the total for various water stages is then plotted against the lateral distance of each vertical from a fixed reference point.

Table 2.7 gives the cumulative percentage of water discharge in the stream cross section for selected numbers of sampling verticals. After selecting the number of sampling intervals, the location of each interval is determined from the percentage values given in Table 2.7 and the graph of cumulated water discharge versus location in the stream cross section.

For example, if six verticals are selected, the first sampling vertical would be at the point (distance from reference point) representing eight percent of the total flow, the second vertical at the point representing 25 percent of the total flow, etc. The mean cross section concentration is the average of the concentrations of the verticals, and the suspended sediment discharge is computed as the product of mean concentration and water discharge.

Point-Integrated Samples at Selected Depths in Stream Verticals Representing Areas of Equal or Known Water Discharge. In this method, samples are taken at selected points in the stream vertical which represent areas of equal or known water discharge. Samples representing areas of equal water discharge may be averaged to determine the mean vertical concentration.

The number of point samples required to determine the mean concentration will depend upon the accuracy desired, the particle size distribution, stream velocity, and turbulence. Obviously, the accuracy of the method increases with the number of samples. Fewer samples are required for streams transporting mostly fine materials since the concentration of clays and silt will not vary significantly in the stream vertical.

Table 2.7. Cumulative Percentage of Streamflow in Cross Sections, from Brakensiek, et all, 1979.

| Number of sampling verticals | Cumulative stream discharge—percent of total | | | | | | | | | | | | | |
|---|---|---|---|---|---|---|---|---|---|---|---|---|---|---|
| | Vertical number | | | | | | | | | | | | | |
| | 1 | 2 | 3 | 4 | 5 | 6 | 7 | 8 | 9 | 10 | 11 | 12 | 13 | 14 |
| 2 | 25 | 75 | | | | | | | | | | | | |
| 4 | 12 | 38 | 62 | 88 | | | | | | | | | | |
| 6 | 8 | 25 | 42 | 58 | 75 | 92 | | | | | | | | |
| 8 | 6 | 19 | 31 | 44 | 56 | 69 | 81 | 94 | | | | | | |
| 10 | 5 | 15 | 25 | 35 | 45 | 55 | 65 | 75 | 85 | 95 | | | | |
| 12 | 4 | 12 | 21 | 29 | 38 | 46 | 54 | 62 | 71 | 79 | 88 | 96 | | |
| 14 | 4 | 11 | 18 | 25 | 32 | 39 | 46 | 54 | 61 | 68 | 75 | 82 | 89 | 96 |

Source: Federal Inter-Agency River Basin Committee on Water Resources

This method is rarely used on small upland streams. It is best suited to large streams with relatively steady flow and rated streams where cross section geometry remains relatively constant. Point sampling is not normally used for depths shallow enough for depth integration.

2.3.3.10 Bed-Material Samplers

Bed-material samplers are designed to collect samples from the bed of a stream, or from lake or reservoir deposits. Some of the most frequently used samplers for bed material, which is predominantly sand or sand and gravel, are described below. These samplers were developed by the Federal Inter-Agency Sedimentation Project, and are described in detail in Brakensiek et al. (1979).

U.S. BMH-60 Hand-Line Bed-Material Sampler. This lightweight sampler is approximately 22 inches long. If constructed from cast aluminum, it is 30 pounds. Because of its light weight, the sampler is only used in tranquil streams and moderate to slightly compacted bed materials.

A spring-loaded sampling bucket, which holds about 10.7 $in^2$ of material, is located on the bottom side of the sampler. In the cocked position the sampling bucket is fully retracted within the sampler body. It remains in this position ready for sampling as long as tension is maintained on the supporting handline. When the sampler is lowered into the stream and touches bottom, tension on the handline is released and the bucket snaps closed. In closing, it penetrates the streambed and completely encloses a sample from the top 1.5 to 2 inches of the bed matrial. Gaskets prevent the loss or contamination of the trapped sample as the sampler is raised to the surface. A safety yoke is provided to lock the sampling bucket in the open position for removing the sample.

U.S. BM-54 Bed-Material Sampler. This 100-pound, 22-inch long cast steel sampler is used to collect samples from the bed of a stream or reservoir of any depth. It is equipped with a spring-loaded scoop-type sampling bucket located on the bottom side of the sampler body. The sampler is suspended by a steel cable and raised and lowered by a suitable reel and crane. Operation is the same as that for the U.S. BM-60 sampler described above.

U.S. BM-53 Piston-Type Bed-Material Hand Sampler. This is a lightweight piston-type sampler which is used to sample bed material in streams or reservoirs shallow enough for wading. It is constructed of readily available steel

pipe and fittings. The sampling cylinder is 2 inches in diameter and 8 inches long. A handle is provided at the top of the sampler frame for pressing the cylinder into the streambed. As the sampler is forced into the streambed, a piston in the cylinder is retracted. Suction created by the piston holds the sample in place. Upon removal from the stream, the piston is used to force the sample out of the cylinder.

Bed-load Samplers. Suspended sediment samplers will only sample to a point about 0.3 foot above the streambed. The sediment transported in the unsampled zone is composed of both suspended load and bed load. The bed load portion is composed of particles having a density or grain size which precludes movement far above or for long distances out of contact with the streambed.

In wide sand-bed streams with shallow flow depths and high sand concentrations, more sediment may be transported in the unsampled zone than in the sampled zone. As flow depth increases, the proportion of sediment in the unsampled zone becomes smaller, often accounting for only a small fraction of the total sediment load.

The bed-load portion of sediment discharge in uncontrolled stream channels is the most difficult to sample. Although many portable samplers have been constructed and tested, none have proved entirely satisfactory for all conditions. For this reason and because the use of portable bed-load samplers in uncontrolled stream cross sections requires a detailed study and evaluation of the site conditions, these samplers are not discussed.

At controlled stream cross sections, fixed bed-load samplers can sometimes be developed to provide an adequate sample. The Tombstone Automatic Bedload Sampler is an example of instrumentation designed for a specific location. This sampler was designed to take a sample of bed load (sand and gravel) on the downstream side of a concrete measuring flume.

The 1-inch by 12-inch sampling slot, powered by an electric motor, traverses back and forth through half of the flow cross section extracting a sample from the bottom 12 inches of flow. The water sediment mixture passing through the slot is routed through a series of graded sieves where the coarse bed-material particles are trapped. The trapped sediment is subsequently removed, measured and packaged for laboratory analysis. The sample includes only particle sizes larger than the smallest sieve opening.

The preferred method of sampling bed load is in restricted turbulent

stream cross sections or overfalls where the total sediment load is in suspension and suspended sediment samplers can be used. The sheet piling grade control structure with footbridge and manually operated sampling device is typical of instrumentation that may be developed for total load sampling. A U.S. DH-48 suspended sediment sampler is attached to a rigid strut and raised and lowered by a cable and reel arrangement. The sampler passes through the entire flow vertical on the downstream side of the sheet piling control. It is moved across the channel on a dolly attached to the bridge hand rails.

## 2.4 Meteorological Data

The collection of meteorologic data is essential to prediction of pesticides, nutrients, sediment and water runoff as well as estimates of evapotranspiration. The following discussion is from Brakensiek (1979), which has compiled many of the basic methods of measurement for these data.

### 2.4.1 Site Requirements

A central meteorological station should be located to be as representative as possible of the macroclimate of the study area. When watershed conditions cover a wide range, such as in mountainous areas, several base stations may be needed to adequately sample the mesoscale regimes making up the watershed climate. These base stations could be supplemented with data from temporary substations on less important areas that could be correlated with from the base station. Microclimatology, the precise definition of the meteorological variables in a vertical section over a point, may be useful in special studies at the facility, but is usually not part of the routine data collection program.

In any event, most meteorological observations are point measurements that will be used to represent an area. Thus, there is an assumption of spatial conformity, more true for some variables than for others.

Exact specifications for locating a climatological station cannot be given. A site away from the immediate influence of nearby trees and buildings is necessary. It should not be on a steep slope, on a sharp ridge, or in a narrow valley. The site should be such that the exposure will not be changed over a long period. The ideal selection is an open, grassy area isolated from buildings, trees, and other obstructions by a horizontal distance of at least four times their height. In arid areas, a sparsely vegetated site would be

more natural.

Instruments at the climatological station should be installed to provide a good exposure for each instrument, primarily in terms of isolation from other instruments. Important to consider are such details as having the door of the instrument shelter open to the north, locating obstructions such as electric poles to the north of the plot to avoid shading the instruments, and maintaining a fence that will protect the site from animals.

Areas of concrete or gravel under or near instruments should be kept to a minimum. The fence should not exceed three feet in height, should be made of large mesh wire at the top with smaller mesh below, and should be supported on posts with a small cross section. A perch higher than the other instruments may attract birds that would otherwise roost on the sensors. Extra space should be reserved in the plot for installation of additional instruments not planned for when the plot was established.

Whenever feasible, recording instruments should be used in lieu of instruments requiring manual observations. These instruments furnish continuous observations over weekends and holidays—data that might be missed otherwise. Local standard time should be used for all observations. Daily averages, where required, should be for the calendar day. New stations should adopt the metric system for their observations.

A permanent record of the station should be kept in a looseleaf notebook. Such data should be entered as the latitude and longitude of the station, date established, a map showing the physical layout including electric lines and water lines, and the ground elevation of the point where the rain gage is installed. The record book should contain a series of photographs that clearly show the exposure of the plot and the relationship of the instruments to each other. A record should be kept of instruments added to or removed from the plot. Names of observers and dates of service should be noted. Notes should be kept on general operations such as dates of mowing and painting of shelters. A separate page may be reserved for each instrument, with notes on serial and model numbers used, calibration data, problems in operation and their solution, and repairs or replacements made.

Extensive climatological data compiled over the years by the National Weather Service should not be overlooked. Many meteorological readings, such as air humidity, are conservative in that the average of a series of readings taken at one location may be fairly representative of the daily average at

another location some miles away. Frequency arrays from a long-term record can be used to judge the normalcy of climate observed for a short period at a nearby experimental site if the records at the two locations are correlated. The assistance of the National Weather Service should be sought when questions on long-term records arise. A file of daily weather maps and local climatological data sheets from one or two nearby long-term National Weather Service stations will prove useful.

The instrumentation suggested in this section may be considered minimal for most facilities for watershed research. The system described herein will insure that sufficient meteorological data are collected so that the research results of a facility may be compared on a climatic basis with results of nearby National Weather Service stations or other watershed facilities. The data collected should be sufficient to enable a calculation of potential evapotranspiration on a daily basis. If further detail is needed for a special study, the installations can be expanded accordingly.

### 2.4.2 Air Temperature

Temperature of the air is one of the most commonly measured meteorological variables at a research station in agricultural hydrology. Air temperature is so intimately related to evaporation, transpiration, soil freezing and thawing, and snowmelt that its measurement is almost mandatory. Daily maximum and minimum temperatures are needed to determine mean daily air temperature, a statistic required in most methods of computing daily potential evapotranspiration. A trace of the daily march of air temperature from a thermograph or hygrothermograph is useful in studies of snowmelt and as a backup system for maximum and minimum measurements.

Separate liquid-in-glass maximum and minimum thermometers mounted on the cross board of a shelter with a thermometer support (such as those used by the National Weather Service) are recommended for obtaining daily extremes of air temperature. The maximum thermometer has a mercury-filled bulb exposed in a nearly horizontal position—the bulb end about 5° above the horizontal. The metal backing of the maximum thermometer is clamped securely to the lower (longer) shaft of the support at a point 3.5 inches from the high temperature end of the back and with the bulb end to the left. A rise in temperature forces the mercury through the constricted part of the bulb into the graduated portion. The mercury remains in this part even though the temperature falls,

thus permitting a maximum-temperature reading.

The minimum thermometer has an alcohol-filled tube exposed with the bulb end about 5° below the horizontal. The metal back of the minimum thermometer is clamped securely to the upper (shorter) shaft of the support, slightly less than half the length from the high temperature end and with the bulb end to the left. The bore of the thermometer contains a dark dumbbell-shaped piece of glass called an "index." As the temperature rises, the alcohol expands and flows around the index without displacing it. Further cooling causes the top of the column to move nearer the bulb, carrying the index with it. When the temperature rises again, the alcohol column moves toward the top of the bore without moving the index, thereby leaving the index to indicate the lowest temperature reached.

Besides the maximum and minimum thermometers, a recording hygrothermograph should be operated on the floor of the shelter house. This will furnish a continuous trace record of the air temperature and relative humidity. A weekly time scale is adequate. Temperature pen readings are checked against maximum and minimum thermometer readings made in the same shelter. Adjustments are made to the pen setting whenever its error is more than 2° F. Separate winter and summer charts are used in localities having wide ranges of seasonal air temperatures. Winter charts cover a range in temperature from -30° to 70° F, while the summer chart range is 10° to 110° F.

### 2.4.3. Air Humidity

Humidity of the air near the surface has a definite influence on the rate of evaporation from lakes and ponds and on evapotranspiration from land areas. The basic process in evaporation and evapotranspiration is the physical change of water from the liquid to the gaseous phase. This process occurs more rapidly as the difference between the saturated vapor pressure at the water surface and the actual vapor pressure of the adjacent air increases. Thus, evaporation occurs more rapidly in dry air than in air with a high relative humidity. Several techniques for computing potential evapotranspiration require a measure of air humidity such as dew point or relative humidity.

Instruments commonly used for measuring air humidity near the earth's surface fall into two general categories: (1) those using thermodynamic principles and (2) those using the change in dimensions of hygroscopic substances. Instruments using thermodynamic principles are called psychrometers.

Essentially they consist of two mercury thermometers, one of which has its bulb covered with a piece of muslin or wicking for wetting. These thermometers are mounted together on a common backing with the wet-bulb thermometer slightly lower than the dry-bulb thermometer.

Techniques for ventilating the thermometers can be classed into three general categories: (1) natural ventilation, (2) moving thermometers rapidly through the air, and (3) forcing air movement over the thermometer bulbs with a fan or other device. The first method is characteristic of simple psychrometers that are mounted in a fixed position; these are sometimes designated "hygrometers." The second method is used by the sling psychrometer, which is a widely used portable psychrometer. The third method is represented by several instruments, but the best known is the Assmann psychrometer.

The most common instrument based on the change in hygroscopic substances to measure air humidity is the hair-element hygrograph. This instrument contains a banjo set of human hair that expands and contracts with changes in atmospheric moisture. Movement caused by expansion and contraction actuates a pen that records relative humidity on a chart. This chart is rotated in time by a clock movement. Usually the hair hygrograph is coupled with a device for recording temperature on the same chart. This combination instrument is called a hygrothermograph.

Several other instruments use special animal membrane elements to measure air humidity. These usually contain a dial and a needle that is linked to the membrane and calibrated so that relative humidity can be read directly. Thus, they are designated hygrometers. All of these instruments are very difficult to calibrate and they are subject to considerable error.

### 2.4.4 Wind

Wind is important in both agriculture and hydrology. Agriculturally, excessive gusts of wind can damage many crops. Hydrologically, wind influences the magnitude of evapotranspiration. Wind speed and wind direction also influence rain gage catch and the removal and deposition of soil and snow. The total run of wind for each day is the minimum measurement of wind that should be made at a hydrologic research station. A chart trace showing the direction of wind and the variability of wind velocities throughout the day will prove useful at most stations.

Many commercially available anemometers are satisfactory for routine

measurements of wind movement. Readings should be recorded continuously so that a permanent record of velocities is available. The anemometer also should record on a counting device to eliminate the necessity of counting tick marks on the chart or integrating the chart trace to obtain a daily total.

The standard anemometer is equipped with three conical, beaded cups mounted on a rotor with a turning diameter of 17 inches. The rotor assembly drives a spindle that operates counter and a pair of wheels. The wheels are equipped with pins that close an electrical contact for every statute mile (1.6 km) of wind and every 1/60 mile (26.8 m) of wind. Electrical contacts are wired to a recorder for a continuous trace of windspeed and wind direction.

The wind transmitter operates from a 36-inch single-panel metal vane. Eight of the ten switches are used to record direction continuously to 16 points. The event recorder notes time of occurrence and duration of wind from eight directions. A simultaneous recording of two directions, such as S and SW, indicates that wind was from the intermediate direction, SSW. A separate pen records each mile of wind so that average velocity can be determined for any period. The remaining pen may be wired to record every 1/60 mile of wind or movement of wind during precipitation or other special events.

The use of a series of counters to record the total miles (or km) of wind movement on a calendar-day basis should be considered. A timing clock can be used to activate a stepping switch every midnight. The stepping switch shunts the incoming signal from one counter to the next. The time saving is considerable compared to counting tick marks from a chart.

### 2.4.5 Solar Radiation

Solar radiation provides the energy that drives regional and global hydrologic cycles. Radiation is generally the most important factor in the evaporation and transpiration processes. The energy for plant growth and production of dry matter is supplied by solar radiation.

Several methods for determining potential evapotranspiration use solar radiation data. The usefulness of such equations is being extended by studies to establish coefficients that account for stage of crop development and other plant and soil factors. These coefficients permit the conversion of calculated potential evapotranspiration to realistic estimates of actual evapotranspiration.

Evaporation and transpiration are more closely related to net radiation than to solar radiation because a fraction of solar radiation is reflected back to the atmosphere and is not used in the conversion of radiant energy to the latent heat of vaporization. In the eastern states and irrigated areas of the western states, evapotranspiration frequently uses over 80 percent of the net radiation.

The best estimates of evapotranspiration amounts, particularly for short periods, usually are obtained with equations that involve net radiation as a term. Several equations are available for predicting evapotranspiration where water is not limiting. Equations using net radiation data, plant cover, and other information are being developed to estimate actual evapotranspiration under field conditions. Evapotranspiration rates determined from meteorological measurements by the Bowen ratio method require net radiation data as an essential element.

Total incoming shortwave radiation is commonly measured with pyranometers, sometimes called solarimeters. They sense the intensity of radiation of wavelengths, less than 4μ from the sun and sky, that falls on a horizontal plane. (These instruments are often erroneously referred to as pyrheliometers. A pyrheliometer measures direct solar radiation only.)

The portion of the total radiation of all wavelengths that is transformed into other forms of energy is termed "net radiation." Net radiometers measure this difference between the incoming (downward) radiation of all wavelengths and the outgoing (upward) radiation of all wavelengths.

The electrical output from a radiation sensing device often is recorded on a strip chart recorder fitted with an integrator. Data reduction is simplified if the integrator pulses are accumulated on counters. Two or more counters per recorder should be used, with an automatic mechanism for switching integrator pulses from one counter to another at midnight. Thus, the integrated 24-hour value displayed on a counter can be read the next day at the observer's convenience. Because net radiation varies from incoming to outgoing between day and night, it is sometimes desirable to integrate these fluxes separately. This is accomplished by having separate counters for the plus and minus integrations.

Electronic integrating systems are commercially available that amplify low-level signals, integrate the resulting current, and display the amount in digital form for visual readout. These integrating systems are available with

single-stage amplification for use with circuits where the current does not vary in polarity (such as with a pyranometer) and with two-stage amplification for circuits where polarity reverses from time to time (such as with a net radiometer). They have an overall accuracy of about two percent, which is adequate for many applications.

Pyranometers and net radiometers must be installed so that the solar beam is not obstructed at any time of the day, nor during any season. The view of the horizon from the instrument location should not be obstructed by nearby objects such as trees and buildings. In addition, glare or reflections should not be directed toward the instruments.

The site over which the net radiometer is exposed should be typical of the situation under investigation. This poses problems when mixed vegetation or other nonhomogeneities exist at watershed sites. Locating the instrument high above such a site gives a representative measure of the net radiation of the heterogeneous area because of the large field of view of the instrument.

Instrument heights much greater than 3.3 ft cause some errors due to radiation divergence. These errors cause actual net radiation at instrument height to differ from that at the surface. Despite this theoretical difference, it is often best to expose net radiometers at a height of 3.3 to 9.8 ft when heterogeneous conditions exist. When the sensor is Z meters above a level surface, it receives 90 and 99 percent of its upward flux from areas with a radius of 3Z and 10Z meters, respectively.

### 2.4.6 Barometric Pressure

The need for barometric pressure measurements will be determined by the research program. Measurements are incidental to the biological processes important in agriculture and are not directly related to hydrological activities except in special situations.

An estimate of the standard barometric pressure at the facility is required in calculating potential evapotranspiration by the combination method. This value probably can be supplied by the nearest National Weather Service office with sufficient accuracy, after allowances are made for differences in elevation. A barometric pressure term appears in the psychrometric formula, but a standard barometric pressure term should be used in computing dew points unless extreme accuracy is required.

The water level in a well penetrating a confined or partly confined

aquifer may rise and fall inversely with atmospheric pressure. If this effect is possible at the facility, a recording microbarograph should be used.

Some laboratory experiments may be affected by atmospheric pressure when air is entrapped in a water column, thus necessitating the recording of barometric pressure. The value of the barometric chart in making short-range weather predictions may be enough justification for operating a barograph.

A microbarograph is recommended for routine readings of atmospheric pressure at the facility. A file of charts from which a selection of data that are pertinent to current needs should be maintained, rather than using one or two visual readings noted during a day. The microbarograph is not as reliable as a mercury barometer for indicating absolute pressure, but it gives a useful indication of pressure changes with time. It is sufficiently accurate for most hydrological and agricultural purposes. If absolute pressure values are required, they can be obtained from a mercury barometer once a day and intermediate values can be interpolated from the corrected microbarograph chart.

### 2.4.7 Rainfall Measurement

Of all the meteorological measurements, rainfall has the greatest effect on runoff from small watersheds. In its simplest form, a precipitation gage is an open-mouthed can with straight sides. Gages are installed with the open end upward and the sides vertical. Improved gages measure small amounts and record the time and intensity of precipitation. Rain gages are used in (1) climatology, in which nonrecording gages are often used, (2) hydrology, in which forecasting of runoff requires self-recording gages and totalizers, and (3) hydrometeorological studies, in which a rain gage must show rates and amounts of rainfall.

For most climatological studies, today's rain gages are adequate. For hydrological purposes, such as runoff forecasting, the recording gages are satisfactory although measurement of precipitation is limited by such factors as gage sensitivity and network density. For hydrometeorological studies in which rates of rainfall and amounts must be shown accurately for short intervals, today's networks of recording gages are frequently inadequate.

A wide variety of gages has been developed to measure precipitation; some gages were developed for a special purpose. Two types of gages (nonrecording and recording) are used primarily in the United States. The nonrecording gage

retains the total precipitation between observations; the recording gage gives the time of precipitation so that intensities can be computed.

2.4.7.1 Site Selection

Installation should be geared to conditions of operation and maintenance. Climatic factors, physical conditions of the site, and the anticipated type of observer should be considered. Usually simplicity of operation is the best guarantee of satisfactory performance. Simplicity of procedure insures adequate observations. Where procedures are complicated, the duties of the observer should be reduced to a step procedure. Provision in the installation design often can facilitate such reduction. Gage sites should be selected, designed, and located to provide unconfounded records.

The location of the gage is the primary consideration for obtaining accurate precipitation measurements. An ideal exposure would eliminate all turbulence and eddy currents near the gage. Individual trees, buildings, fences, or other small groups of isolated objects near the gage may set up serious eddy currents, especially when their height above the gage is appreciable. As a general rule, an isolated obstruction should not be closer to the gage than twice (preferably four times) its height above the gage. Obstructing objects usually provide a more accurate catch when they are so numerous and extensive that prevailing windspeed in the vicinity of the gage has been reduced and, consequently, the turbulence and eddy currents also have been reduced. The best exposures often are found, therefore, in orchards, in openings in a grove of trees or bushes, or where fences and other objects form an effective windbreak.

Sites on a slope or on ground sloping sharply away in one direction should be avoided especially if this direction is the same as that of the prevailing wind. The surrounding ground can be covered with short grass or be of gravel or shingle, but a hard, flat surface, such as concrete, causes excessive splashing and abnormally high surface temperatures.

The growth of vegetation, trees, and shrubbery, and man-made alterations to the surroundings may make an excellent exposure unsatisfactory in a relatively short time. The angle from the gage orifice to the top of any nearby object should not exceed 30°, thus allowing for growth of vegetation. Under no circumstances should an obstruction be nearer to the gage than its own height (45°). Wilson felt, however, that a small clearing in uniform forests,

having a diameter about equal to the height of the trees, was best because the measurement would gain more from the reduction of wind than it would lose from interception.

To place a gage in a forest opening of 60-foot trees, a clearing of about 1/4 acre is required. If no such openings exist on a watershed or on control watersheds where no cutting is allowed, measuring rainfall at the surface of the tree crown should be considered.

2.4.7.2 Factors Affecting Accuracy

Rain gages measure the amount of precipitation that reaches the ground. Accuracy depends on inherent inaccuracies in the gage itself, wind velocity at the orifice of the gage, and form of precipitation. Inherent errors can result from bent, damaged, or deformed knife edge and orifice, leak in storage container; inaccurate calibration of measuring container or dip stick, tilted orifice due to settling or improper installation, or evaporation between the end of precipitation and when the gage is ready.

The most common errors result from evaporation, adhesion, color, inclination of the gage, splash, wind, faulty technique in measuring catch, and physical damage to the gage. Errors in measurements have been estimated as follows:

| | Percent |
|---|---|
| Evaporation | -1.0 |
| Adhesion | -0.5 |
| Color | -0.5 |
| Inclination | -0.5 |
| Splash | +1.0 |
| Subtotal | -1.5 |
| Wind | -5.0 to -80.0 |

The greatest amount of error in rain-gage catch results from wind. Under exposed conditions, rain-gage catch generally is deficient. This error is related to windspeed and to the type of precipitation. The decrease in catch increases as wind velocity increases and is greater for light rain than for heavy rain. Wind increases pressure on the windward side of the gage, decreases pressure over the gage, and sets up eddy currents over and within the orifice. Since windspeed increases the height above a surface, the higher the gage orifice is above the ground, the greater will be catchment errors due

to exposure.

Some inherent errors are caused by the gage being out of calibration, binding or sticking parts in the weighing mechanism, bent, damaged, or malformed orifice ring, or other mechanical damage to the gage. The cause of these errors, except gage calibration, can be detected by brief inspection during routine visits to the station. The observer should watch constantly for errors and correct them as soon as possible to maintain high-quality records.

Sizable errors may occur in recording total catch. They may or may not be compensating and often change sign amount at the pen reversals. Therefore, the total catch in the bucket should be measured at the end of the storm.

A properly installed pit gage accurately measures rainfall at a point. When the rain gage is placed in a pit with its orifice at ground level, the gage no longer obstructs air movement and the effects of turbulent wind around the orifice are diminished. Conventionally exposed gages, even when shielded, catch less rainfall than pit gages. Pit gages are inadequate for snow measurements, however, because of problems with drifting snow under windy conditions. Trash and sediment also tend to collect in pit gages. For extensive rain-gage networks, increased accuracy usually does not warrant the increased cost of installing and maintaining pit gages.

The possibility of inaccurate measurements resulting from vertically placed rain gages in watersheds of steep and complex topography was pointed out by several investigators. Errors were assumed to be due to the incidence of different volumes of precipitation on sloping surfaces of several areas and exposures where wind prevented the rain from falling vertically. It was recommended that gages be placed with their orifice parallel to the slope of the land. Rain-gage catch was divided by the cosine of the gage inclination so that the volume would be on a horizontal area.

The main sources of error will be inaccurate measures or dip rods, spilling of some water when transferring it to the measure, and inability to transfer all water from the receiver to the measure.

Losses by evaporation also can occur. Evaporation errors are most serious in dry climates and in areas where gages are visited infrequently. Losses can be reduced by placing oil in the receiver (this forms a film over the water) or by designing the gage so that (1) only a small surface is exposed, (2) the ventilation is small, and (3) the internal temperature of

the gage does not become excessive. The receiving surface of the gage must be smooth so that the raindrops do not adhere to it. It never should be painted.

In winter, rains often are followed immediately by freezing weather. Damage to the receiver and subsequent loss by leakage can be prevented by adding an antifreeze solution, especially when gages are visited infrequently. Allowance for the solution added must be made when measuring the results. All gages should be tested regularly for possible leaks.

Correct timing of the recorded precipitation trace and the ability to estimate any errors in the record are important. Three causes of error that can affect timing of the record are backlash, clock rate, and change in chart dimension.

Backlash between the chart drum and the clock spindle delays the start of the record and causes a constant error once the record has started. Backlash in the timing gears can be taken up by turning the drum until the indicated time is about three hours fast and then turning it back to the correct time.

Another error may be caused by the clock rate or the use of an unsuitable time scale on the chart. If the difference is small, the rate of drum revolution can be adjusted with the clock regulator. All errors of this type probably cannot be removed by adjusting the regulator because clock rate will vary according to temperature and humidity.

Errors due to change in chart dimensions are caused by variation in humidity. Charts expand and contract as relative humidity increases and decreases, and most chart papers will change more in one direction than in another. Whether changes due to humidity are greater in the time scale or the depth scale, depending on how the paper is cut. These changes easily can exceed one percent and can amount to a 15- or 20-minute error in the time scale or several hundredths of an inch in the depth scale. Charts also creep up the drum because of expansion and contraction. Therefore, the bottom of the chart may be above the bottom flange of the drum in an amount equal to the creep.

All errors can be recognized and corrected if accurate time marks and zero checks are made when the charts are put on and taken off the drum, and at intermediate times when convenient.

#### 2.4.7.3 Nonrecording Gages

Nonrecording rain gages usually consist of a collector above a funnel

leading into a receiver. In the United States these gages have been standardized to the shape of a right circular cylinder with an eight-inch collector orifice diameter. Important requirments of nonrecording gages are:

1. The rim of the collector should fall away vertically inside and be steeply beveled outside. The gage for measuring snow should be designed to minimize errors due to constriction of the aperture. Constriction is caused by the accumulation of wet snow above the rim.

2. The area of the orifice should be known to the nearest 0.5 percent, and it should remain constant.

3. The collector should prevent rain from splashing in or out. This can be done by having the vertical wall sufficiently deep and the slope of the funnel sufficiently steep (at least 45°).

4. The receiver should have a narrow neck and should be protected sufficiently from radiation to minimize loss of water by evaporation. Rain gages used in places where daily readings are impracticable should be similar to gages used daily but should have a receiver of larger capacity.

Precipitation in nonrecording rain gages usually is measured by pouring from the gage into a calibrated container or by using a calibrated dip stick, or both.

The calibrated container should be made of clear glass with a low coefficient of expansion and should be marked clearly with the size of gage with which it will be used. Its diameter shold not be more than about one-third the diameter of the rim of the gage and can be made less than this. The graduations should be finely engraved; generally, they should be marked at 0.01, 0.05 and 0.10 inch. For accuracy, the maximum error of the graduations should not exceed 0.005 inch.

To achieve this accuracy with small amounts of rainfall, the inside of the measuring cylinder should be tapered off at its base. In all measurements, the bottom of the water meniscus should be taken as the defining line. The measure must remain vertical, and parallax errors must be avoided. It is helpful if the main graduation lines are repeated on the back of the measure.

Dip rods should be made of cedar wood or other material that absorbs little water and reduces capillarity. Wooden dip rods are unsuitable if oil has been added to the collector to suppress evaporation of the catch. Therefore, use rods of metal or other material from which oil can be cleaned. These rods should have a brass foot to avoid wear and should be graduated

according to the cross section of the gage orifice and the receiving can, allowing for displacement due to the rod itself. Marks should be shown for at least every 0.02 inch. The maximum error in the dip-rod graduation should not exceed +0.005 inch at any point.

2.4.7.4 Recording Gages

Three types of recording precipitation gages in general use are weighing, tipping bucket, and float. The only satisfactory instrument for measuring both liquid and solid precipitation is the weighing-type gage.

Several rainfall intensity recorders have been designed and used for special purposes. They are not recommended for general networks, however, because of their complexity. A satisfactory record of rainfall intensity can be determined from a float- or weigh-in-type recorder by providing the proper time scale.

Whether the rainfall recorder operates by weighing the rise of a float, the tipping of a bucket, or other method, these movements must be converted into a form that can be stored and analyzed later. The simplest method of recording is to move a time chart by a spring or electrically driven clock past a pen that moves as the float or weighing device moves. Two main types of charts are:

1. The drum chart, which is secured around a drum that should revolve once a day (exactly), once a week, or another period as desired;

2. The strip chart, which is driven on rollers past the pen arm. By altering chart speed, the recorder can operate from one week to a month, or even longer. The time scale on this chart can be large enough to calculate intensity easily.

The movement of a float, bucket, or weighing mechanism also can be converted into an electric signal. This signal can be transmitted by radio or wire to a distant receiver where records can be made from several rain recorders on data-logging equipment.

Most clocks for rain gages can be geared to provide one drum revolution in 6, 12, 24 or 192 hours. The time scale selected will depend on the storm characteristics being studied, the shortest interval to be read from the charts, and the frequency or ease of servicing gages. Table 2.8 is a guide for deciding which time scale to use. Generally, the shorter the interval, the more difficult it is to extract data from the charts because of the

Table 2.8. Guide for Selecting Time Scale for Recording Rain-gage Clocks, from Brakensiek, et all, 1979.

| Time for 1 revolution of drum (hours) | Shortest interval between chart time lines | Shortest interval on chart |
|---|---|---|
| | *Minutes* | *Minutes* |
| 6 | 5 | 1 |
| 12 | 10 | 2 |
| 24 | 20 | 5 |
| 192 | 120 | 30 |

crossing and recrossing of trace lines between chart changes. For ease in chart reading, use the longest interval that is compatible with the study objectives.

## 2.5 References

Al-Shaik-Ali, K. S., D. B. Simons and R. M. Li, 1978. Effect of sediment on resistance to flow in cobble and boulder bed rivers, Civil Engineering Department, Colorado State University, Fort Collins, Colorado, CER77-78KSA-DBS-RML-46.

Beckman, E. W., and L. W. Furness, 1962. Flow characteristics of Elkhorn River near Waterloo, Nebraska, U.S. Geological Survey Water Supply Paper 1498-B.

Brakensiek, D. L., H. B. Osborne and W. J. Rawls, 1979. Field Manual for Research in Agricultural Hydrology, Agricultural Handbook No. 224, Science and Education Administration, Washington, D.C.

Carter, R. W., and I. F. Anderson, 1963. Accuracy of current meter measurements, Journal of the Hydraulics Division, ASCE, Vol. 89, No. HY4, Proc. Paper 3572, pp. 105-115, July.

Colby, B. R., 1960. Discontinuous rating curves for Pigeon Roose and Cuffawa Creeks in northern Mississippi, U.S. Department of Agriculture, Agricultural Research Service Report 41-46, 31 pp.

Corbett, D. M., 1943. Stream gaging procedure, Geological Survey Water Supply Paper 888, U.S. Government Printing Office, Washington.

Corps of Engineers, 1968. Missouri River channel regime studies, MRD Sediment Series No. 13A, Omaha, Nebraska.

Dawdy, D. R., 1961. Depth-discharge relations of alluvial streams - discontinuous rating curves, U.S. Geological Survey Water Supply Paper 1498-C, 16 pp.

Fread, D. L., 1973. A dynamic model of stage-discharge relations affected by changing discharge, NOAA Technical Memorandum NWS Hydro 16, November.

Henderson, F. M., 1966. Open Channel Flow, MacMillan, London.

Li, R. M., G. O. Brown and D. B. Simons, 1979. Computer simulation of river stages, Colorado State University, Fort Collins, prepared for Summer Computer Simulation Conference in Toronto, Canada.

Senturk, F., 1969. Nehir hidroligi, DSI Publication No. 66/X/64, Ankara.

Simons, D. B., and E. V. Richardson, 1961. The effect of bed roughness on depth-discharge resionation in alluvial channels, Geological Survey Water Supply Paper 1498-E, U.S. Government Printing Office, Washington.

Simons, D. B., M. A. Stevens and J. H. Duke, 1973. Predicting stages of sand-bed rivers, Journal of the Waterways, Harbors and Coastal Engr. Division, ASCE, Vol. 99, No. WW2, Proc. Paper 9731, pp. 231-243, May.

Simons, R. K., 1977. A modified kinematic approximation for water and seidment routing, M.S. Thesis, Department of Civil Engineering, Colorado State University, Fort Collins, Colorado.

Simons, R. K., R. M. Li and D. B. Simons, 1977. On stage discharge relation of rivers, Proceedings Congress IAHR, Baden-Baden.

# III. SPATIAL AND TEMPORAL CORRELATION

## 3.1 Introduction

Any set of data has information stored in it and there are various ways to usurp this information. Data collected at regular intervals in time are known as a time series. A simple method to grasp overview characteristics of a time series is to simply plot the measured values versus time. In this way information such as variability and periodicity (i.e., daily, monthly, seasonal, or annual fluctuations) of the time series may be inferred. Raw statistics of the data (mean, standard deviation, skewness, etc.) are mathematical transformations of the data which result with a reduction of the total volume of data to a few numbers. Statistics of mean and standard deviation are helpful in designing and sizing structures. For example the mean organic load to a sewage treatment plant aids in the sizing of the plant's components. The mathematical transformation of data in order to compute the mean does not create any additional information, it simply reveals information which is present in the data. This concept is true for all forms of data transformation (mathematical, graphical, etc.).

Peculiar to most time series data is that the smaller the sampling interval (frequent sampling), the more similar each data point is to previously measured points. This fact indicates that a relationship exists between consecutive data points and this relationship is called the data (or process, or system) "memory." "No memory" indicates that one data point has no relationship to previous or subsequent points. An example of this is flipping a coin and recording heads or tails. Large memory means that there is a high degree of relationship between consecutive points. Average daily streamflow on the Delaware River at Philadelphia has a large memory since the average daily discharge does not considerably change over 24 hours. The degree of memory in a data series can be found by utilizing a mathematical transformation called the autocorrelation function. The autocorrelation function computes the relation (correlation) between the points of a data series. This mathematical transformation is discussed in Section 3.2.

Information which is also present in a data set is the relationship between one data set and another. An example of this type of relationship is a rating curve. The rating curve reveals the relationship between river stage and river discharge. The stage and discharge are both time series, and by plotting concurrent points of stage and discharge the familiar power function

relationship can be observed. There is a mathematical transformation for data sets which can compute the relationship or independence of the data sets and it is called the cross-correlation function. The cross-correlation function is described in Section 3.3.

## 3.2 Correlation In Time, the Autocorrelation Function

### 3.2.1 Introduction and Theory

Temporal correlation essentially is a mapping of the relationship of data of one gage with itself, when considering various time lags between data points (correlogram). Figure 3.1 depicts an observed time series and its corresponding correlogram. Autocorrelation theory has been derived for continuous as well as discrete time. Due to the fact that most hydrologic data is taken only at regular time intervals, only the discrete case will be treated herein. Errors induced by discretization of a continuous series will be treated in a later section.

The sample autocorrelation function ($r_k$) is:

$$r_k = \frac{\text{cov}\,(x_i, x_{i+1})}{\{\text{var}\,(x_i)\ \text{var}\,(x_{i+1})\}^{1/2}}$$

$$= \frac{\frac{1}{N-k}\sum_{i=1}^{N-k} x_i x_{i+k} - \left(\frac{1}{N-k}\right)^2 \left(\sum_{i=1}^{N-k} x_i\right)\left(\sum_{i=1}^{N-k} x_{i+k}\right)}{\left[\frac{1}{N-k}\sum_{i=1}^{N-k} x_i^2 - \left(\frac{1}{N-k}\right)^2 \left(\sum_{i=1}^{N-k} x_i\right)^2\right]^{1/2} \left[\frac{1}{N-k}\sum_{i=1}^{N-k} x_{i+k}^2 - \left(\frac{1}{N-k}\right)^2 \left(\sum_{i=1}^{N-k} x_{i+k}\right)^2\right]^{1/2}} \qquad (3.1)$$

where: x = observed hydrologic variable; k = the number of lags between data points; and N = the total number of observed points. Computationally, this equation can be simplified by multiplying both numerator and denominator by $(N-k)^2$. For a finite sample, as k increases, there is less data to compute the $r_k$ value (N-k values) and therefore there is less reliability in the estimates of $r_k$ for large values of k [k $\alpha$ error in estimate].

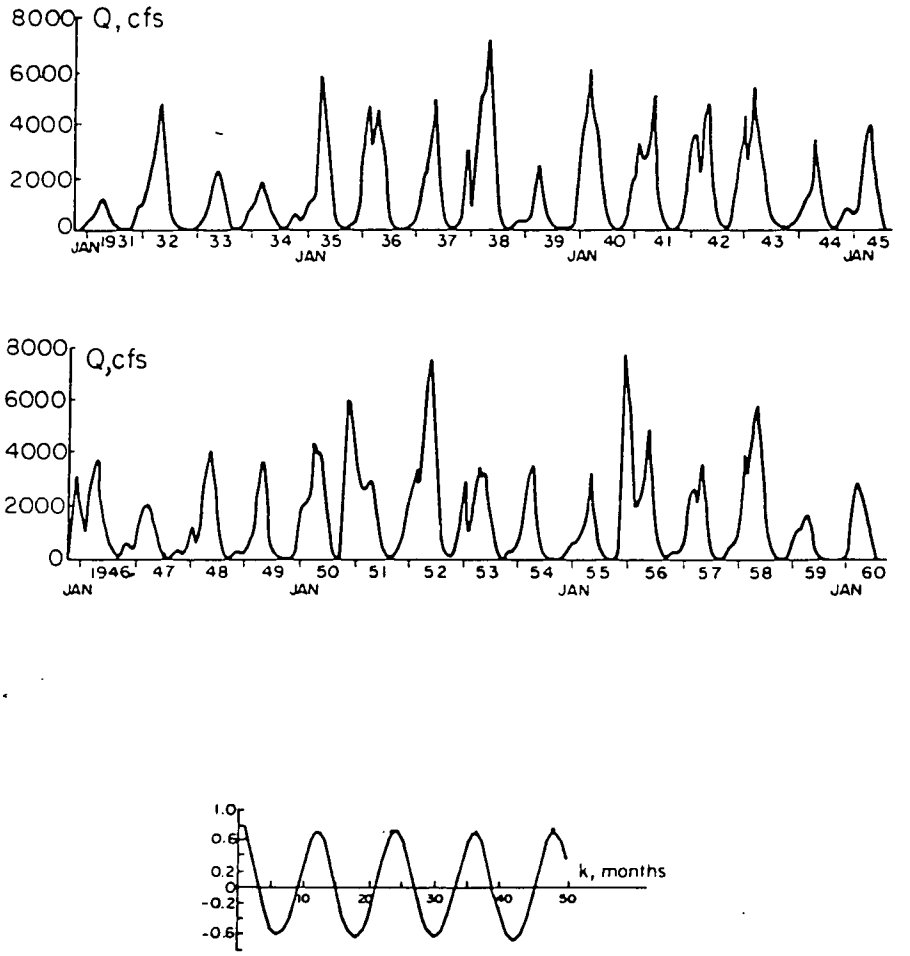


Figure 3.1. The hydrograph and correlogram of monthly river flows of the Middle Fork of the American River near Auburn, California (1931-1960)(after Yevjevich).

Significant properties of the autocorrelation plot are:

$r_o = 1.0$ ;

$r_k = r_{-k}$ .

What physically occurs during the computation of any autocorrelation coefficient (also called the serial correlation coefficient), $r_k$ , is to view the one data set as two. This is depicted in Table 3.1. Column one is simply the observation period, for the purpose of this example this can be assumed to be one day. The second column is the observed streamflow for the respective sampling period. Columns three and four represent the two series', derived from the original series in column 2, used for computing the lag zero autocorrelation coefficient $(r_o)$ . The q's are substituted for the x's in Equation 3.1, where in this case, $k=0$ . Since the two series' (columns 3 and 4) are identically the same, $cov(q_i,q_i) = var(q_i)$ , thus the numerator and denominator of Equation 3.1 are the same and $r_o=1$. This is always true. Columns five and six are the data series' used in computation of the lag one autocorrelation coefficient $(r_1)$ . Here, values from one time period are related to the values from the following time period. Since there is only a finite set of data points (N=15), the total length of the series' used for computation of $r_k$ is N-k (15-1=14). The two series are not identically the same, as they were for $r_o$ , thus $cov(q_i,q_{i+1}) \neq var(q_i)$ . In fact, $cov(q_i,q_{i+1}) < var(q_i)$ . Without loss of generality, it can be assumed that $var(q_i) = var(q_{i+1})$ . Thus the denominator of Equation 3.1 is equal to $var(q_i)$ . The numerator $(cov(q_i,q_{i+k}))$ is the relationship between how the product of two corresponding points of the correlated data series', $q_i \times q_{i+k}$ (i.e., in columns five and six, line 7, i=7, k=1, $q_i = q_7 = 18$ and $q_{i+k} = q_8 = 17$), relate to the product of the mean of each series (mean of column five times mean of column six). With perfect correlation, i.e., $r_o$, $q_i \times q_{i+k}$ is always positive (even when negative values are measured) and has the same value as $q_i^{\,2}$ . This means that $q_i$ and $q_{i+k}$ move about their respective means in perfect synchronization, thus when $q_i$ is greater than its mean, $q_{i+k}$ is greater than its mean, and vice versa. When there is not perfect correlation, $q_i$ and $q_{i+k}$ are not synchronized and thus the numerator of equation one decreases with respect to the denominator, so $|r_k| \leq 1$ for $k > 1$.

Table 3.1. Data Series' Used for Calculating the Lags Zero, One and Two Autocorrelation Coefficients.

| Observation Time | Discharge q (cfs) | Lag Zero Autocorrelation Data Series' | | Lag One Autocorrelation Data Series' | | Lag Two Autocorrelation Data Series' | |
|---|---|---|---|---|---|---|---|
| | | $q_i$ | $q_i$ | $q_i$ | $q_{i+1}$ | $q_i$ | $q_{i+2}$ |
| 1 | 10 | 10 | 10 | 10 | 12 | 10 | 17 |
| 2 | 12 | 12 | 12 | 12 | 17 | 12 | 18 |
| 3 | 17 | 17 | 17 | 17 | 18 | 17 | 18.5 |
| 4 | 18 | 18 | 18 | 18 | 18.5 | 18 | 18 |
| 5 | 18.5 | 18.5 | 18.5 | 18.5 | 18 | 18.5 | 18 |
| 6 | 18 | 18 | 18 | 18 | 18 | 18 | 17 |
| 7 | 18 | 18 | 18 | 18 | 17 | 18 | 16 |
| 8 | 17 | 17 | 17 | 17 | 16 | 17 | 15 |
| 9 | 16 | 16 | 16 | 16 | 15 | 16 | 13 |
| 10 | 15 | 15 | 15 | 15 | 13 | 15 | 11 |
| 11 | 13 | 13 | 13 | 13 | 11 | 13 | 17 |
| 12 | 11 | 11 | 11 | 11 | 17 | 11 | 22 |
| 13 | 17 | 17 | 17 | 17 | 22 | 17 | 24 |
| 14 | 22 | 22 | 22 | 22 | 24 | | |
| 15 | 24 | 24 | 24 | | | | |

Mathematically, the correlogram of various processes have been identified. The correlogram for random independent variables (Gaussian process, white noise) is very important since the disaggregation of stochastic processes is directed towards reducing a series to white noise and also other processes can be compared to this process in order to test for any significant correlation. Figure 3.2 shows the correlogram for a random process. Since the sample is only a few observations of the total population of random numbers, all $r_k$ can have non-zero values. The value of the gaussian $r_k$, for $k > 0$, will fall below error limits based upon the total number of observation and the lag. The equation for the 95% confidence bands is:

$$L_{k_{95}} = \frac{-1.0 \mp 1.96\ (N-k-1)^{1/2}}{N-k} \qquad (3.2)$$

This limit is based on the assumption that the $r_k$ are normally distributed about the population value ($\rho_k = 0$ for all $k > 0$). Recognize that the 95% confidence limit indicates that 95% of the time $r_k < L_{k_{95}}$. Therefore, for twenty computed values of $r_k$ it would be expected that one value be outside of the 95% limits. Physical consideration should be given as to whether the $r_k$ values outside of confidence limits should represent something other than sampling variability. For example $r_1$ may usually be significant for most hydrologic phenomena which are monitored at regular intervals less than one month. If a monthly measuring basis is used, it is quite possible for $r_{12} > L_{12_{95}}$, this would indicate annual cyclicity.

The correlograms of other processes have been theoretically derived, i.e., Autoregressive, Moving Average, Autoregressive Moving Average, etc., and correlograms from observed data can be compared with them to identify the underlying process by association.

### 3.2.2 Loss of Information by Discretization

The loss of information by discretizing a continuous process has been studied (2) and some of the results are presented here. Out of three types of data measuring/reporting methods, viz. discrete point sampling, average sampling, and quantization (reporting of data in class intervals analogous to measurement errors of truncation or accuracy), the information loss due to quantization sampling was negligible compared to the losses introduced when

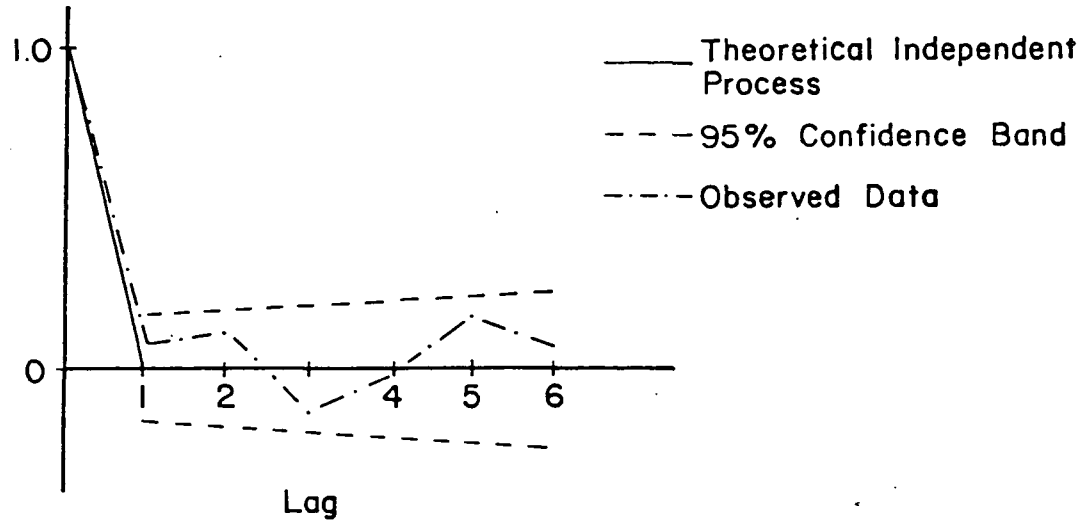


Figure 3.2. Correlogram for an independent process.

sampling in time. This implies that more frequent sampling is more important than accurately sampling.

An example of these three types of data measurement is presented here. In this case, samples are made from a continuous uniform distribution (there is equal probability of selecting any real number between zero and one. When sampling and reporting by quantizing, any sample is rounded off to the measurement accuracy, i.e., if the instrument can only measure to the nearest tenth, a sampled value of 0.1732 is reported as 0.2. Discrete sampling reports a measurement as it is measured at regular intervals. Average sampling reports the average value of a process over some time interval, i.e., average daily discharge. Six thousand data points were selected from the uniform distribution and these were considered as bi-hourly values. Every twelfth value was reported as the daily value. These two types of sampling represent discrete sampling. Every twelve values were averaged and reported for average sampling. Quantization was used on every twelfth point with two accuracy levels, accuracy to the nearest tenth (0.0, 0.1, 0.2,..., 1.0) and accuracy to the nearest hundredth (0.00, 0.01, 0.02, ..., 0.99, 1.00). The statistical results of the five sampling schemes compared to the population parameters are presented in Table 3.2 and the empirical distributions for four of the sampling schemes (exclude quantization sampling to the nearest tenth) are found in Figure 3.3.

Notice how averaging totally transforms the uniform distribution into a normal distribution. Thus it is evident that average sampling aids in estimating the mean but is actually detrimental to estimating the standard deviation. As this example worked with an independent process (no relation between two values), it has very limited application to hydrologic problems. The results of discrete and average sampling of river data is presented in the next two sections.

#### 3.2.2.1 Discrete Point Sampling

Increasing the sampling interval from 2 up to 24 hours, for river flows, does not introduce any significant information loss in estimating the mean. The same can be said about estimation of the process variation and autocorrelation with sampling intervals less than six hours, in this instance increasing to daily sampling results with about 60% loss of information. The information loss when estimating extremal events can be significant. The

Table 3.2. Statistical Results of Various Sampling Methods on the Uniform Distribution

| Sampling Method | Sampling Interval | Mean | Standard Deviation | Skew Coefficient |
|---|---|---|---|---|
| Population | Continuous | 0.500 | 0.289 | 0.000 |
| Discrete | Bi-hourly | 0.502 | 0.287 | -0.014 |
| Discrete | Daily | 0.494 | 0.296 | -0.052 |
| Average | Daily | 0.502 | 0.080 | 0.013 |
| Quantizing (0.10) | Daily | 0.491 | 0.302 | -0.032 |
| Quantizing (0.01) | Daily | 0.494 | 0.297 | -0.052 |

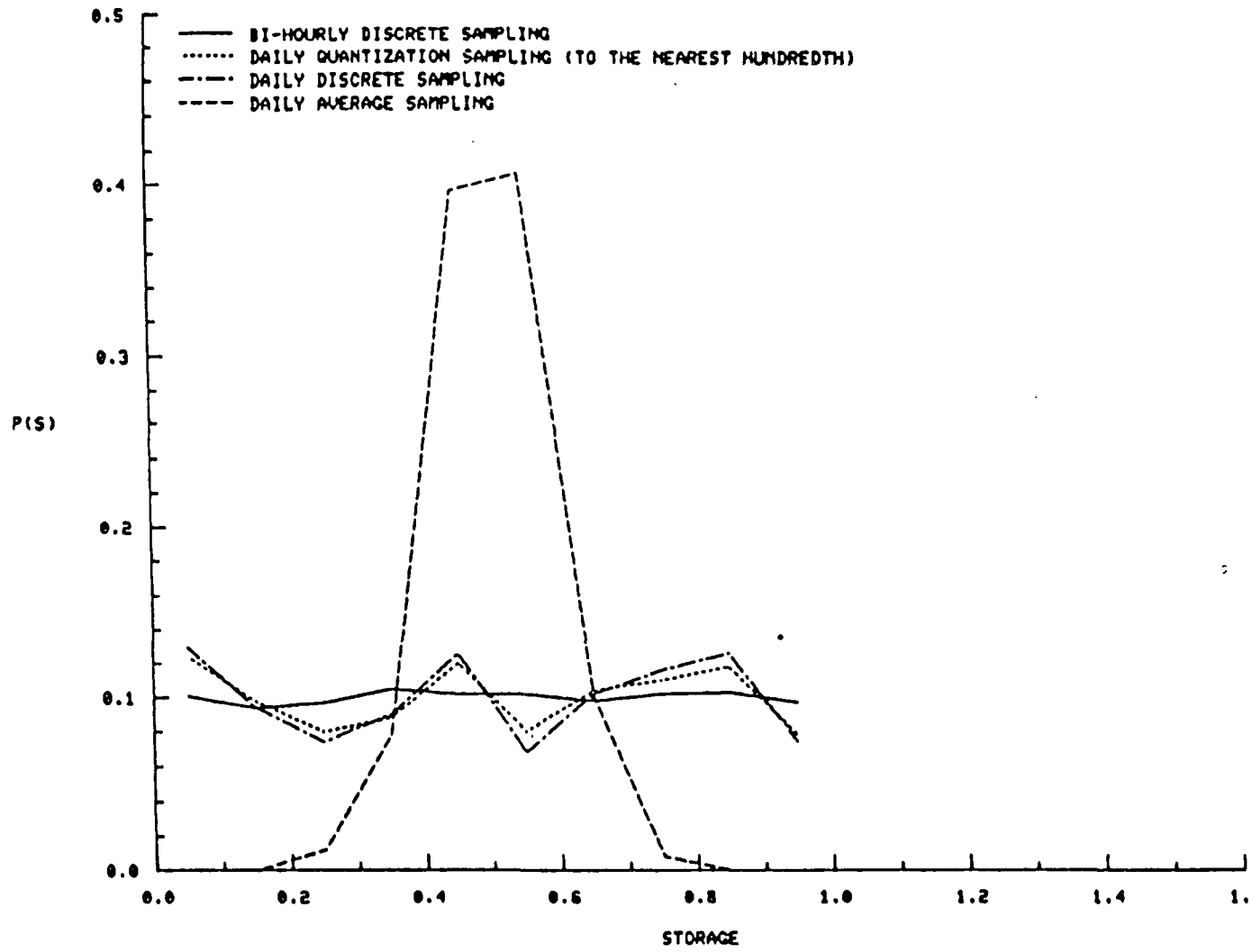


Figure 3.3. Empirical distributions from various samples of the uniform distribution between zero and one U(0,1).

marginal information loss tends to decrease with sampling intervals larger than four hours.

3.2.2.2 Average Sampling

When the mean is the only data statistic of interest, average sampling can occur in intervals up to 24 hours without significant loss of information. Unfortunately, estimation of the variance and autocovariance functions are severely impaired by average sampling. With a sampling interval of only four hours, a great degree of bias is introduced. On a daily sampling interval, the information loss in estimating the variance was three orders of magnitude larger than when using discrete point sampling.

For estimation of extreme events, an increase in the sampling interval yielded information losses similar to discrete point sampling (usually larger losses though).

3.2.3 Effect of the Sampling Interval on the Correlogram

The further apart data is taken in time, the more likely the measurements are to be independent of each other. This effect can be visualized with the aid of Figure 3.4 which plots the correlograms for the Terror River, Alaska for various sampling intervals. Recognize that the first serial correlation coefficient for monthly sampling ($r_1$) is equal on the average to the thirtieth serial correlation coefficient for the daily sampling ($r_{30}$) and also the fifteenth serial correlation coefficient ($r_{15}$) when sampling every other day. Another way of presenting the gradual independence with time is to plot the relation of the average first serial correlation coefficient, $r_1$, with sampling interval, this occurs in Figure 3.5. Interesting in Figure 3.5 is that $r_1$ for 120-day sampling is negative. This represents the seasonality of the river where there is evidently distinctive high and low flow seasons of the year. Also, there appears to be large annual correlation, possibly owing to the long season of melt-runoff ( 6 months).

As previously mentioned, the first serial correlation coefficient of annual sampling ($r_1$) is equal, on the average, to the 365th autocorrelatin coefficient ($\bar{r}_{365}$) of the daily sampling autocorrelation function. If yearly sampling were done on October 30, $r_1$ would most likely be much higher than $\bar{r}_{365}$ . This is due to normally low flows during this time of the year and thus less variation of the flow. If annual sampling were to occur on April 5,

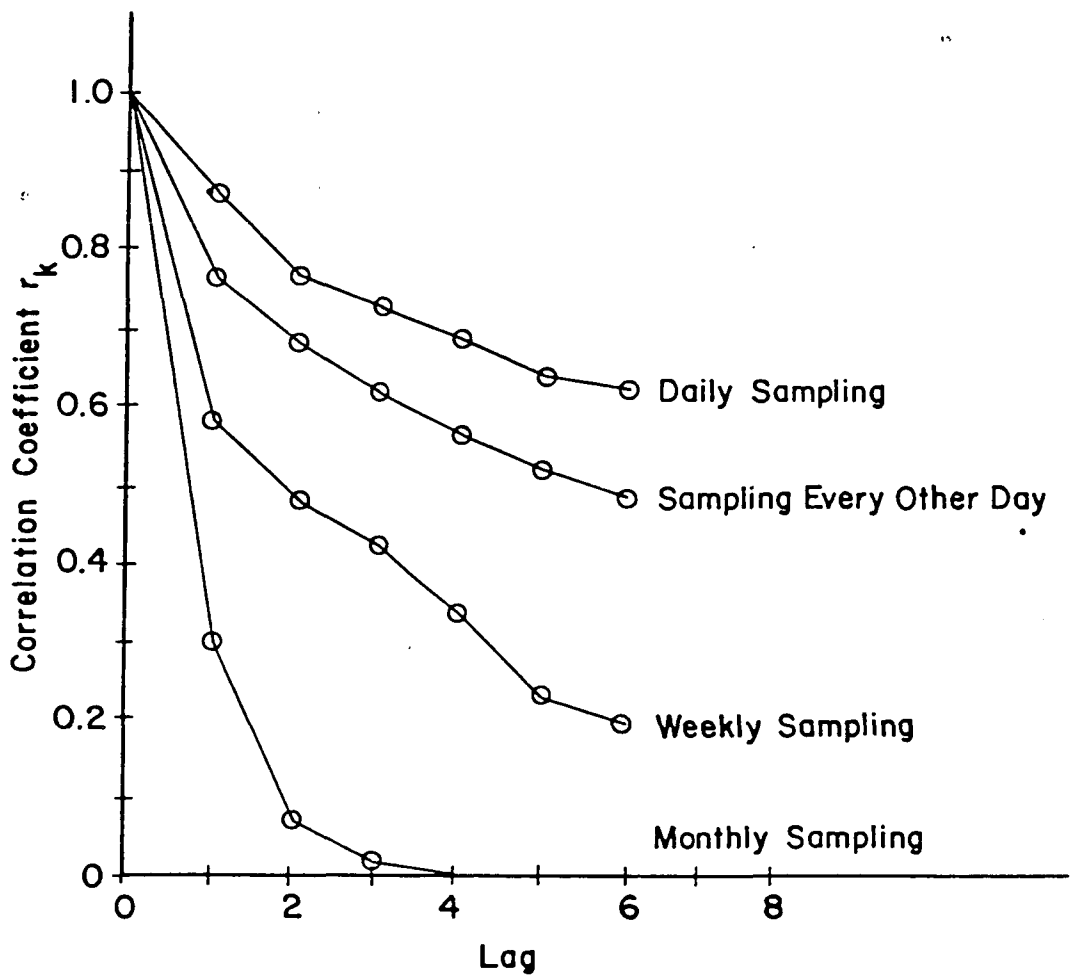


Figure 3.4. Correlograms for the Terror River, Alaska due to various sampling intervals.

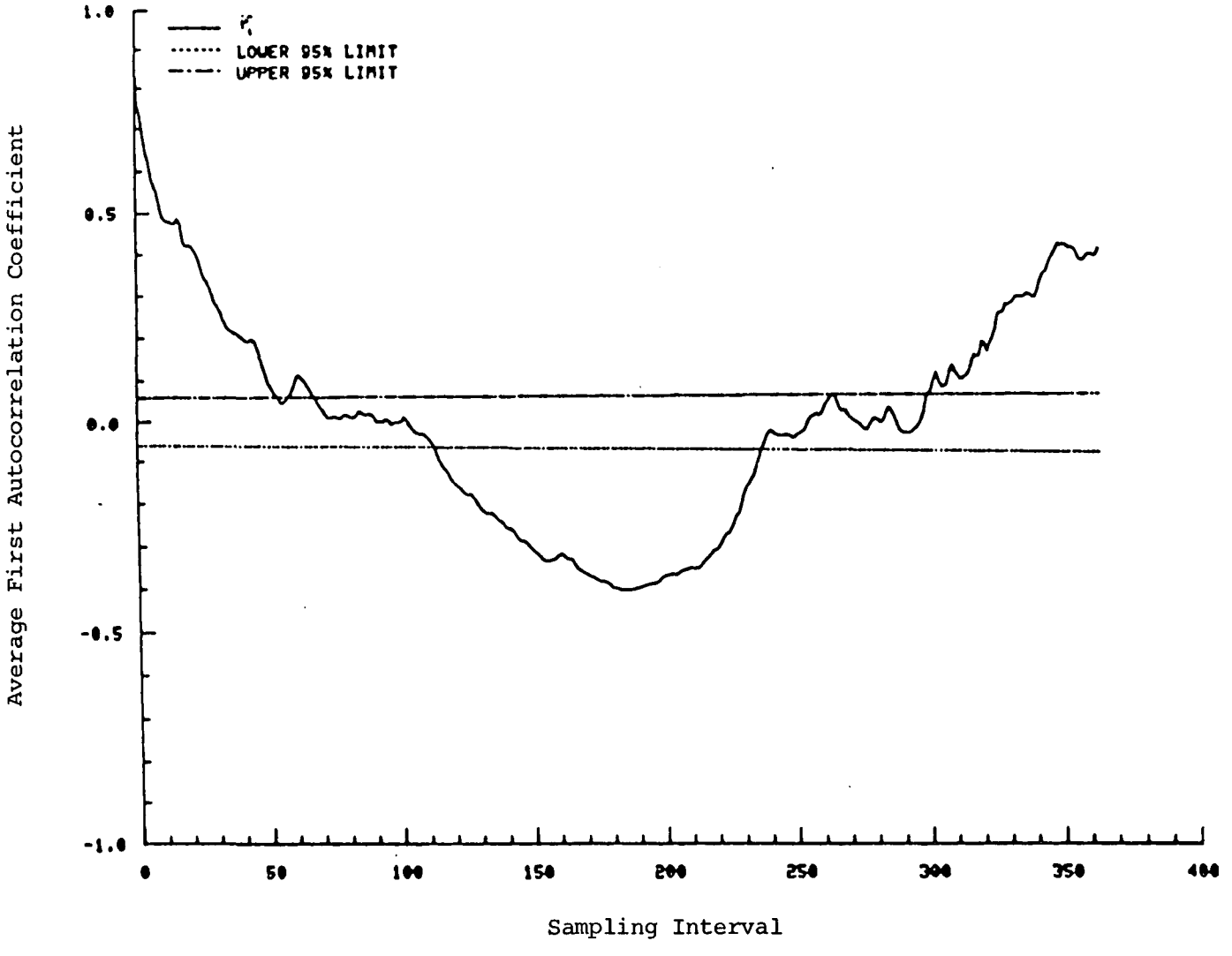


Figure 3.5. Correlogram for the Terror River daily flow series.

$r_1$ would most likely be much lower than $\bar{r}_{365}$ owing to high variability in the timing of snowmelt and the more numerous precipitation events during the spring. Thus, low variability creates high annual correlation and the converse is also true, and $\bar{r}_{365}$ for the daily series simply averages this effect for every day of the year.

### 3.2.4 Miscorrelation: Effects of the Misuse of Data and the Misinterpretation of the Autocorrelation Function

#### 3.2.4.1 Intermittent Processes

Improper use of the correlogram can lead to misinterpretation of a physical process. Take for example Figure 3.6, which plots correlograms for the Rio Puerco, New Mexico. The use of the daily flow series results in extremely high correlation structure. Recognize, though, that the Rio Puerco is an intermittant stream with an average of 205 days per year without any flow. This data produced the top most curve in Figure 3.6. If data generation were to be based on such a correlation structure, severe errors would result due to the implication of strong watershed memory. If the intermittancy was accounted for by deleting all zero flow values from the historic record, thus placing all storm hydrographs end to end, the resulting correlation structure would be smaller than the initial approach but higher than the true watershed memory. This is due to the fact that the first one or two and the last four or five values of the hydrographs are very small, causing a higher overall correlation due to effects which physically should not have any relation. A truer representation of watershed memory would be to average the $r_k$ values for each hydrograph of non-zero discharge (lowest curve in Figure 3.6). Similar types of miscorrelation may be inferred when analyzing precipitation data; water quality data with a seasonal polluter (i.e., apple processing, etc.); or any other intermittant process. A significant aid to screen such types of data is a plot of the time series itself. Such plots qualitatively indicate: mean, variability, seasonality, and intermittancy.

#### 3.2.4.2 Jumps and Trends

Data inhomoegeneity is produced by jumps and trends in the data set. A positive data jump is depicted in Figure 3.7a, and in general the jump can be positive or negative. Jumps can be caused by various factors, for example: construction of a dam, stream capture, change in measurement techniques, etc.

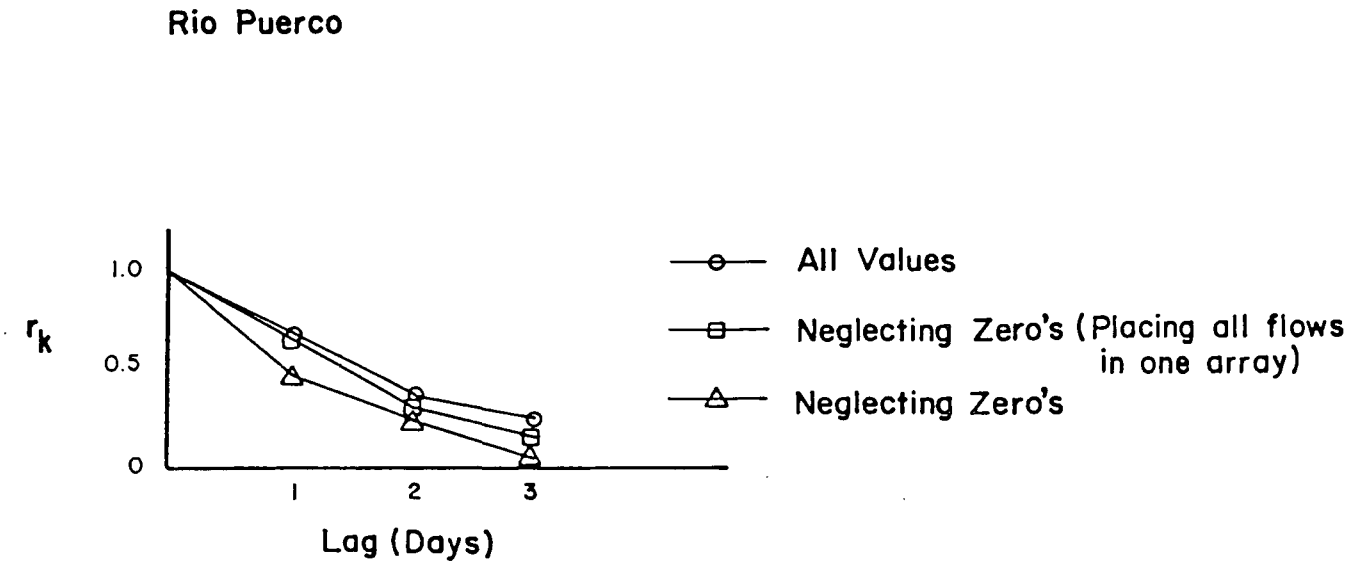


Figure 3.6. Correlograms for the daily flow series of the Rio Puerco.

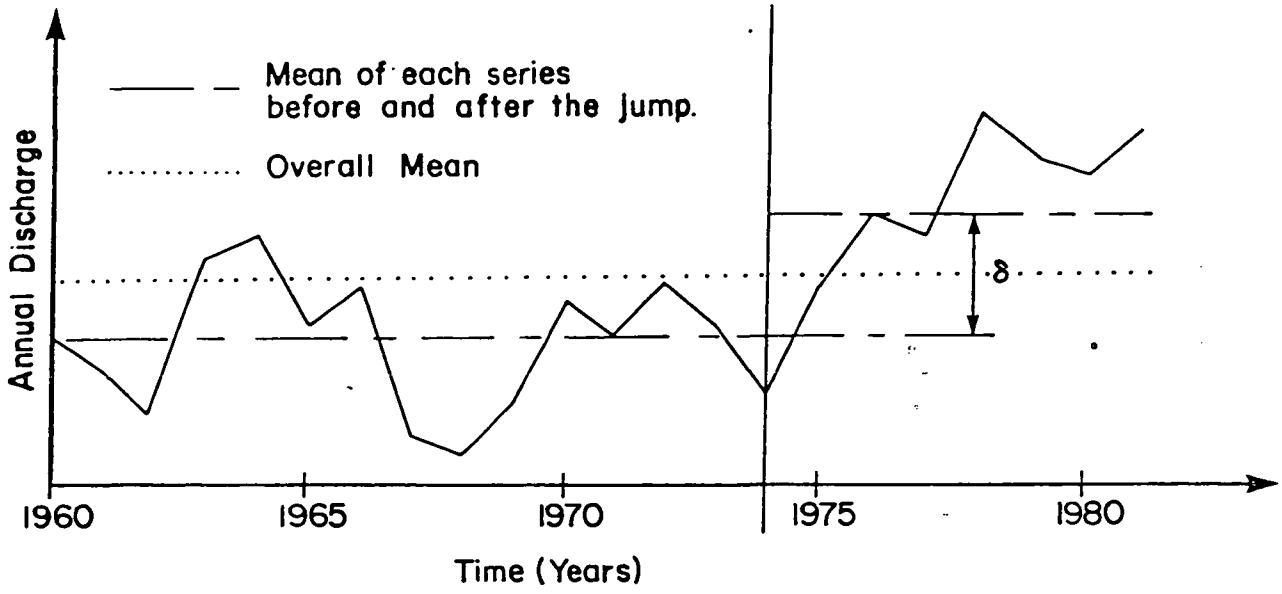


Figure 3.7a. Effect of a constant jump on an annual flow series. $\delta$ is the jump in the mean for data before and after the jump.

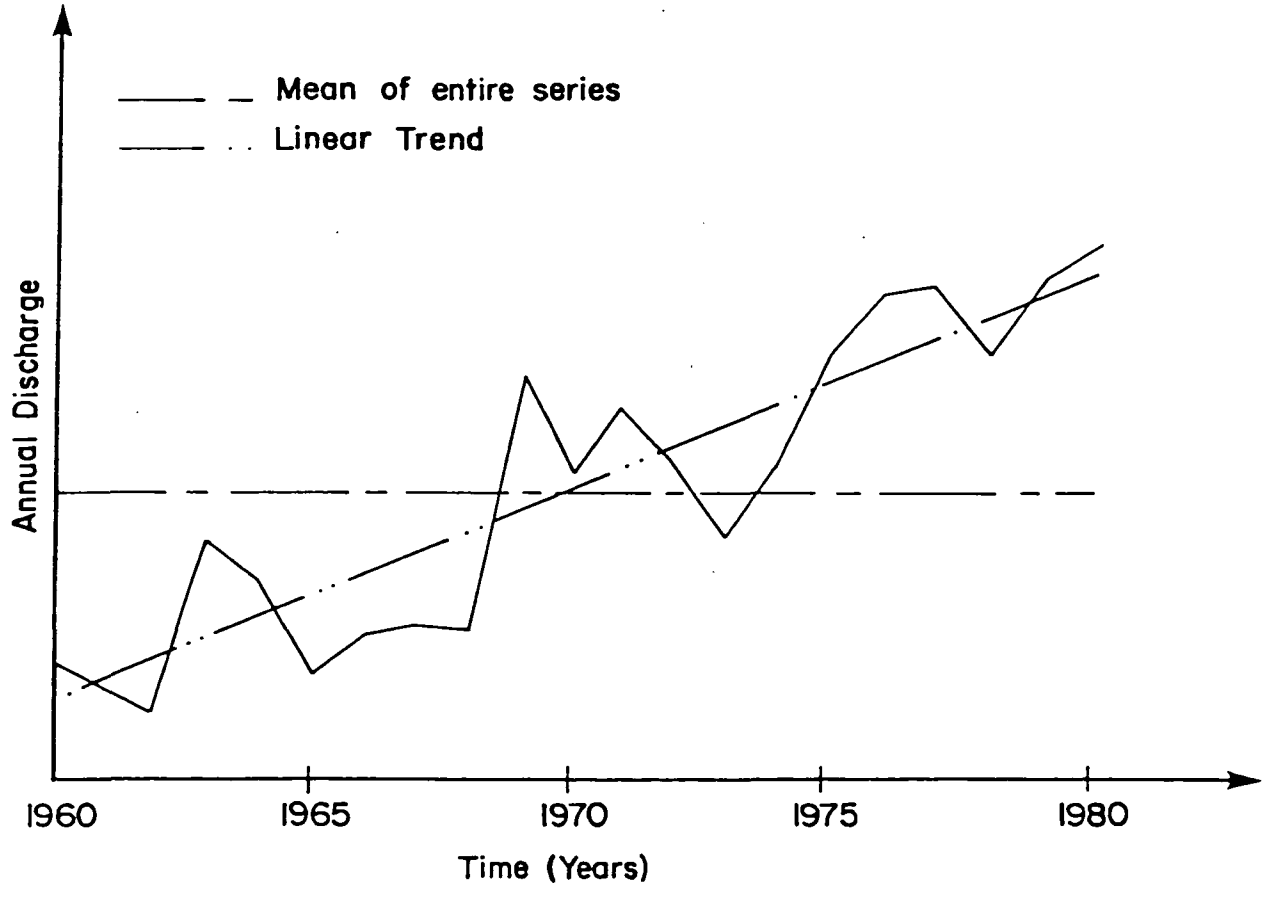


Figure 3.7b. Effect of a linear trend on an annual flow series.

A classic example of a jump is the change in the annual flow of the Nile River due to the construction of Aswan Dam. The effect of a jump on the data is to change all statistics (12), i.e., mean, standard deviation, skewness, and serial correlation. The mean changes with the type of jump (increasing jump, increasing mean) and the variance increases with the magnitude of the jump (large jump, large increase of the variance). The autocorrelation function decreases with the magnitude of the jump. A simple example of this is to visualize a jump in a constant process, here the correlogram will change from $r_k = 1.0$ for all $k \geq 1$ to $r_k < 1.0$ for all $k > 1$ .

A linear increasing trend is depicted in Figure 3.7b. The nature of trends can be increasing or decreasing and linear or nonlinear and they may be caused by various factors, i.e., watershed urbanization, industrialization, revegetation, etc. An example of a trend is the water use time series of a growing city, each year more and more water is demanded due to an increase in the number of users. Trends also change all data statistics. The mean and variance changes with a trend are the same as for the constant jump. The effect of the trend on the autocorrelation coefficients is to increase them. This increase is due to the fact that the trend represents an increase in the deterministic part of the data set, thus there is more relation between points due to the trend. Trends and jumps will be considered further in the next chapter.

3.2.4.3 Measurement Accuracy (Effect of Truncation) and Autocorrelation

There is no instrument which can exactly measure a process. Measurement errors arise from misreading, improper calibration, accuracy of the instrument, and even use of the instrument itself may disturb the process being measured such that a true reading is not possible. All of these errors, except the measurement accuracy, are random errors in the data series. The measurement accuracy is a constant error that may or may not effect the representation of the process which is being measured. Usually measurement accuracy is tied to the cost of the measuring instrument, the more accurate the measurement the more costly the instrument. If the measurement is too coarse, the process being measured is not well monitored, i.e., if one was interested in the acidic Ph fluctuations in a river in order to detect criteria violations, not much information would be obtained if the measuring instrument read either acidic or basic (as does litmus paper). Contrary to

this last example, if one wanted to measure the Mississippi River Discharge at New Orleans, it would be foolish to measure to ±0.0001 cfs since not much information would be obtained by this accuracy. Section I-B dealt with data accuracy when data sampling by quantization was discussed. In this case, accuracy can change most of the statistics of a data set. Increasing accuracy will not significantly change the mean and will slightly decrease the standard deviation, also the serial correlation coefficients will be slightly higher. A decrease in accuracy can be viewed as a process with many small jumps, here the effects on the data statistics are opposite to those of increasing accuracy.

### 3.2.5 Effects of Reservoirs on Correlation Structure

#### 3.2.5.1 Introduction

Man's influence on hydrologic variables can be quite significant, especially in the case of reservoirs. The effect of a reservoir, in a hydrologic system, is to increase water residence time. This effect results with lower water velocities (causing sediment deposition), increased mixing of water, and a decrease in the discharge range (maximum minus minimum discharge). The magnitude of the effect of reservoirs on hydrologic variables is a function of the relative size of the reservoir compared to the mean annual reservoir inflow.

#### 3.2.5.2 Water Quantity Variables

Water storage in reservoirs creates an increased correlation structure of the water quantity variables. This is due to the fact that flood peaks are stored for later release, and also that drought flows are augmented. These effects produce a very slow change in reservoir outflow from one day to the next, which may be quite contrary to the inflow time series. Figure 3.8 graphs the monthly time series' of inflows and outflows for the Bonny Reservoir which is located on the South Fork of the Republican River (SFRR) in northeast Colorado. The inflow series is a combination of the SFRR, gaged at Idalia, and Landsman Creek. Landsman Creek supplies about 9% of the total annual inflow. The reservoir outflow is gaged on the SFRR at Hale, and there is a major diversion at the dam which is not accounted for. The correlograms for each individual component and for combined components occur in Figures 3.9 and 3.10. Figure 3.9 indicates that the SFRR at Idalia does not reveal a

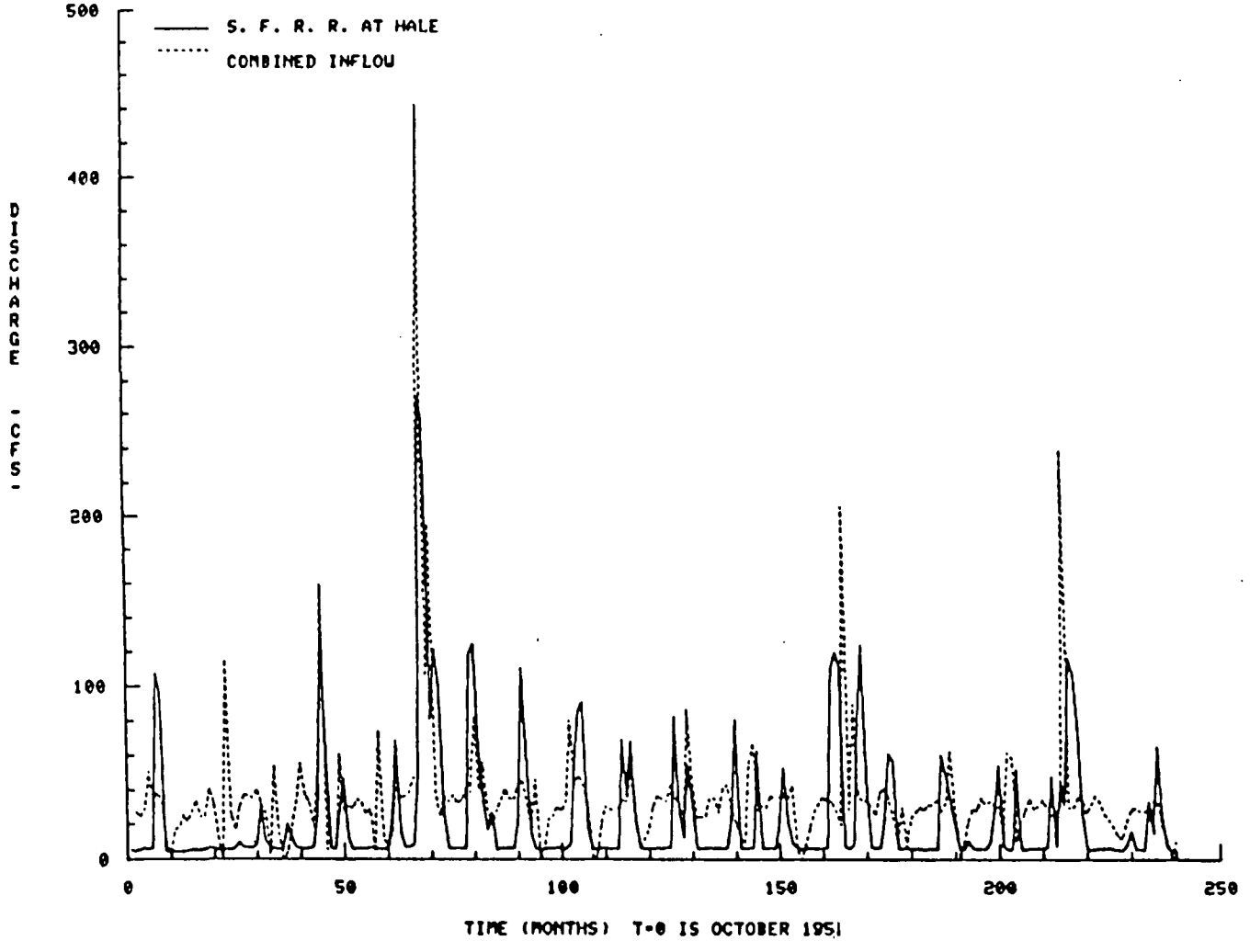


Figure 3.8. Hydrologic variables for the Bonny Reservoir.

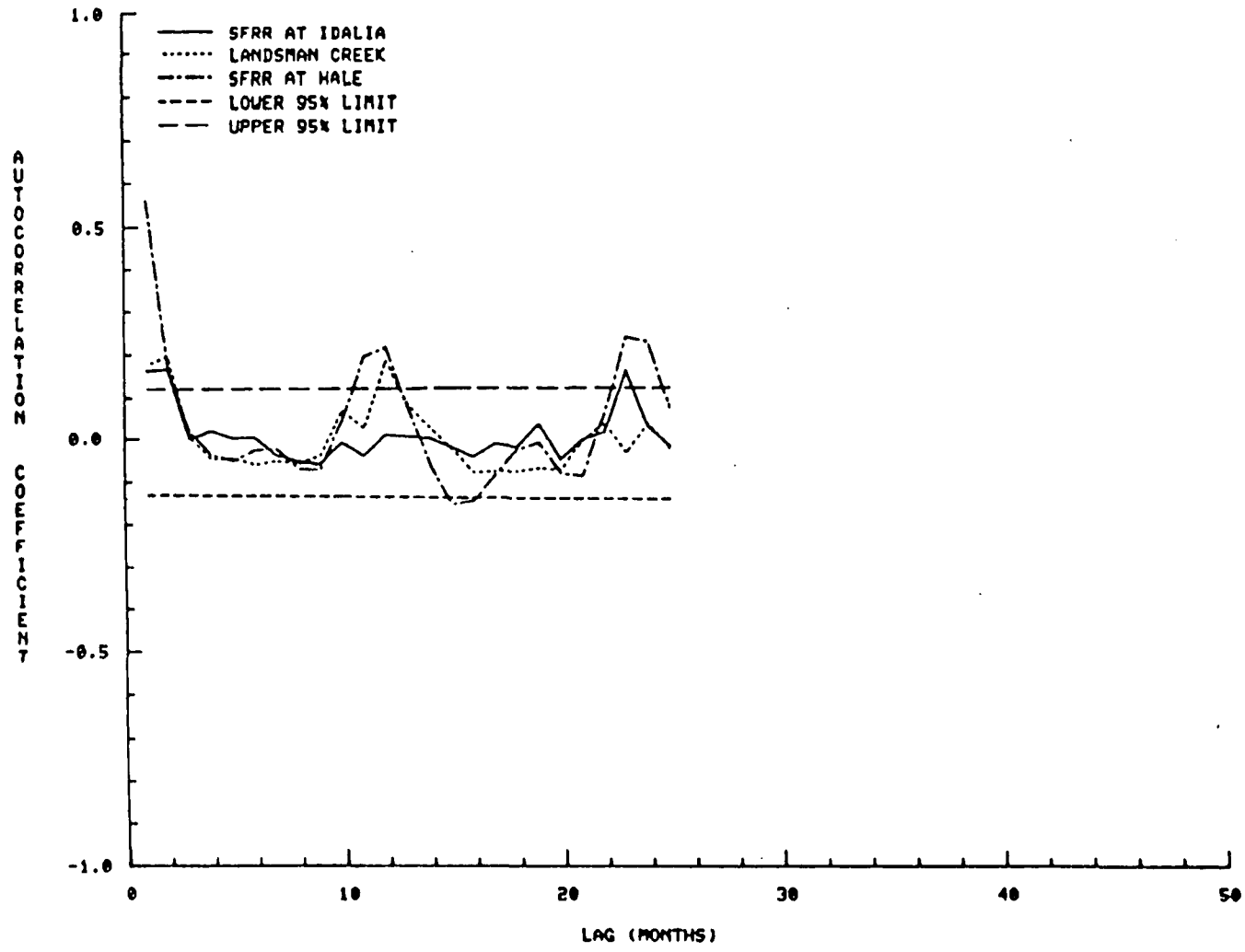


Figure 3.9. Correlograms for the Bonny Reservoir hydrologic variables.

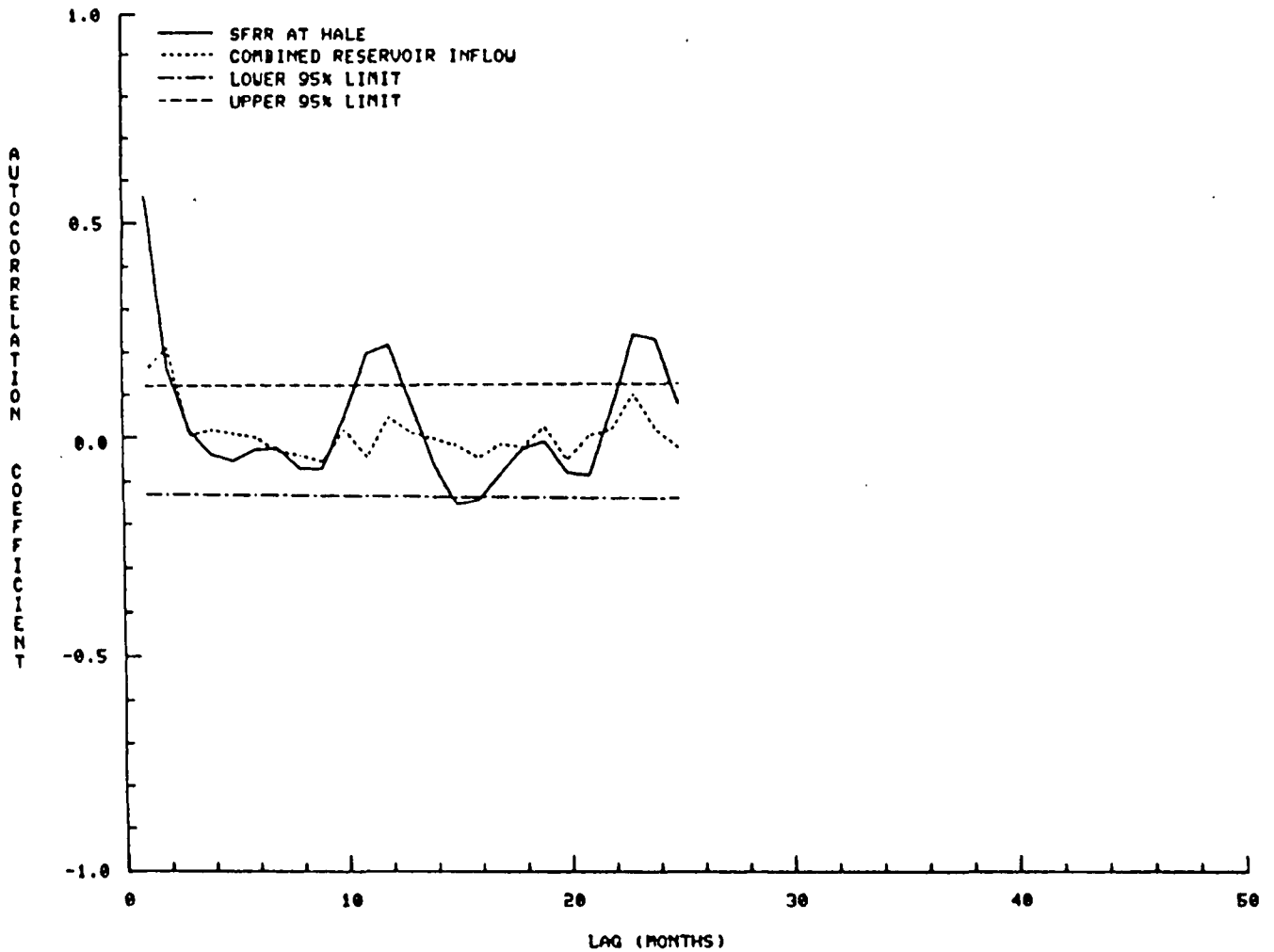


Figure 3.10. Correlogram for the Bonny Reservoir hydrologic variables.

strong seasonal component. This is due to the influence of thunder shower activity and many irrigation diversions and return flows above the gage. Contrary to this, on the smaller Landsman Creek watershed, there is definitely a seasonal factor evidenced by large $r_{12}$ and $r_{24}$. The reservoir outflows show the greatest seasonality effects and this results from seasonal operation rules for filling and emptying the reservoir. Such rules can be observed in Figure 3.8, where outflows are increased before the large inflow periods in order to reserve storage space. Bonny began filling June 6, 1950, construction was completed May 4, 1951, and it was first filled March 29, 1954. Since this time, the outflow hydrograph begins drawing down before the high inflow season and also after large flood events.

3.2.5.3 Water Quality Variables

The effect of reservoirs on water quality variables is similar to the effect on water quantity variables, and this is smoothing of the inflow series. Another effect of the reservoir, though, is to become a sink for chemicals, pollutants, etc. As previously mentioned, low reservoir water velocities result in a depositional environment for sediments. This would include insoluble chemicals as well as chemicals attached to the sediment, i.e., phosphorus, etc. In addition, the location of sedimentation may be suitable for an aquatic environment which utilizes incoming nutrients and soluble chemicals, i.e., swamps. This type of environment has been evidenced by reservoir and lake eutrophication.

Three water quality time series were selected at two stations on the Rio Grande. The Otowi Bridge gage is 26 miles upstream of Cochiti Dam and the San Felipe Gage is 15 miles below the dam. These gages are part of the USGS surveillance network and thus many chemicals, nutrients and other water quality variables are regularly monitored at each. The three variables chosen for the purposes of this analysis are Ph, total nitrogen (N) and total phosphorus (P). The Ph time series of Figure 3.11 indicate that the reservoir decreases the Ph and also introduces a lag of 1-2 months. The correlograms of these series displays a fairly independent inflow process, yet the outflow series has strong correlation extending over three months. The total nitrogen and total phosphorus series of Figures 3.12 and 3.13 indicate that the reservoir does act as a sink for these chemicals, but also there is a large loading mechanism below the dam. The correlograms, for the same figures, indicates that these

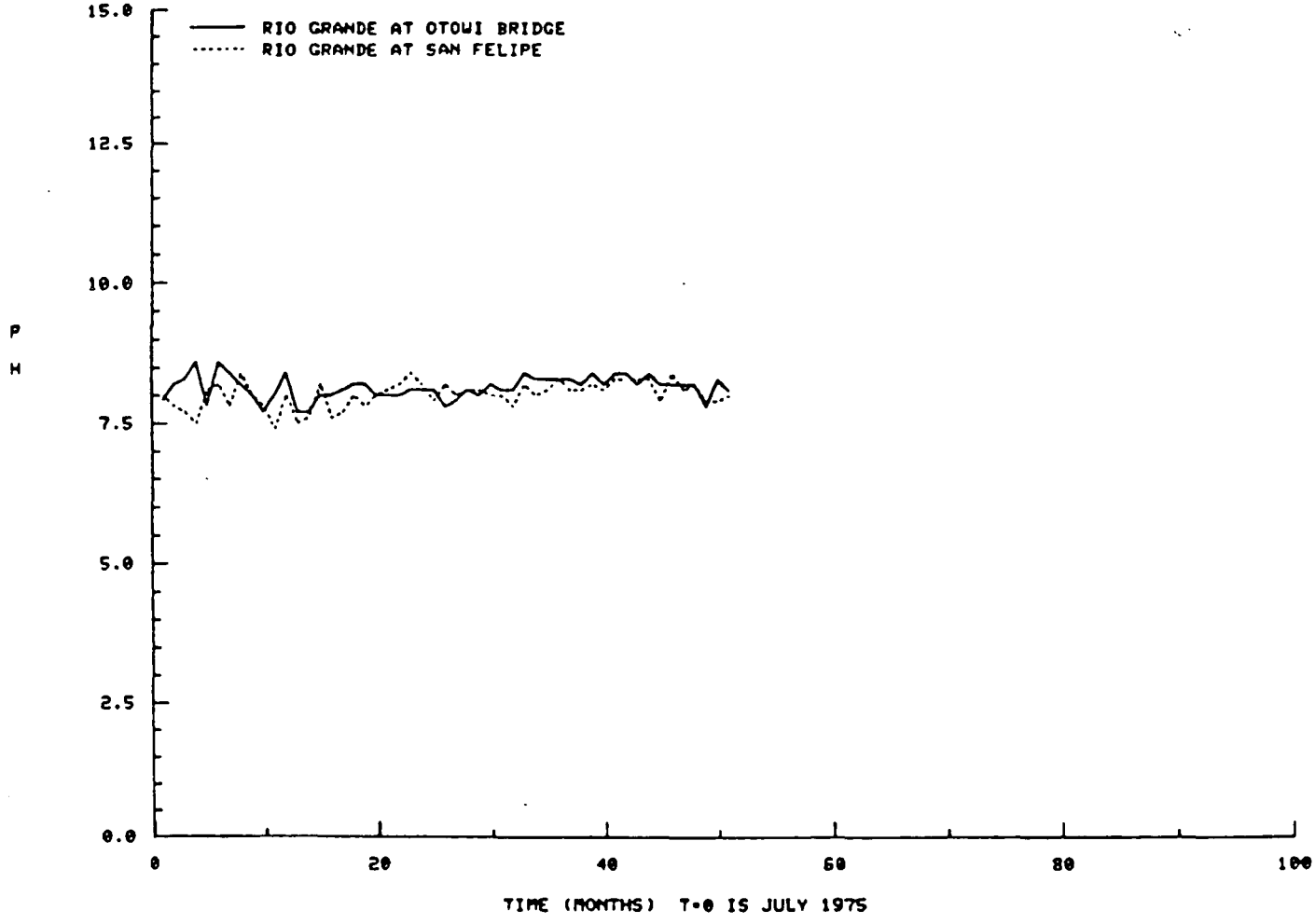


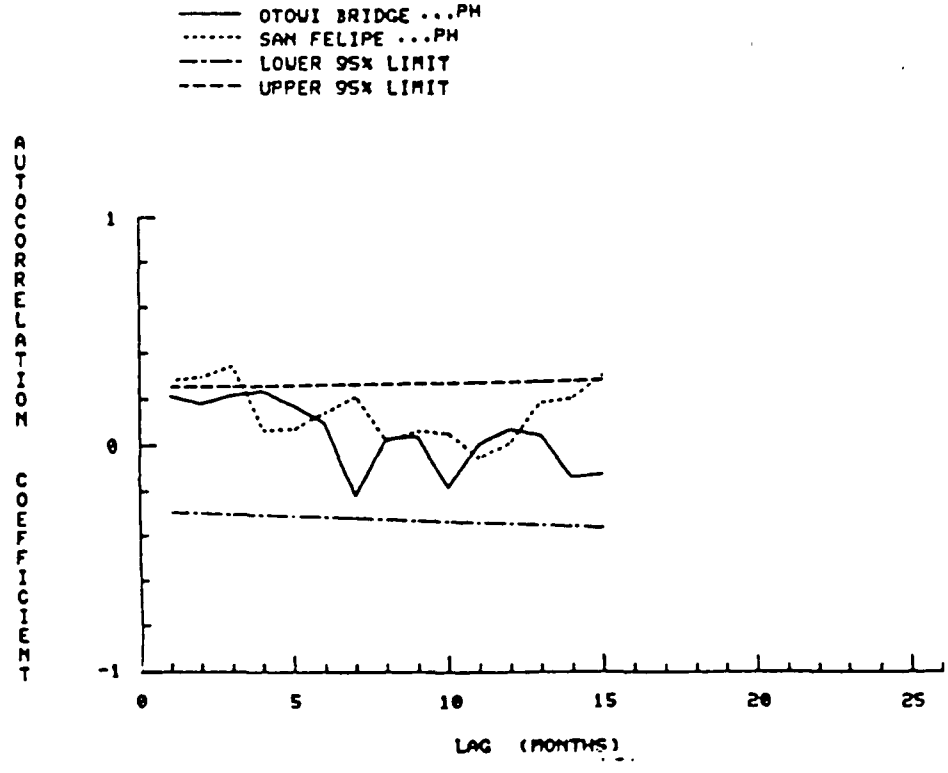


Figure 3.11. Smoothing of the Ph monthly time series of the Rio Grande due to Cochiti Reservoir.

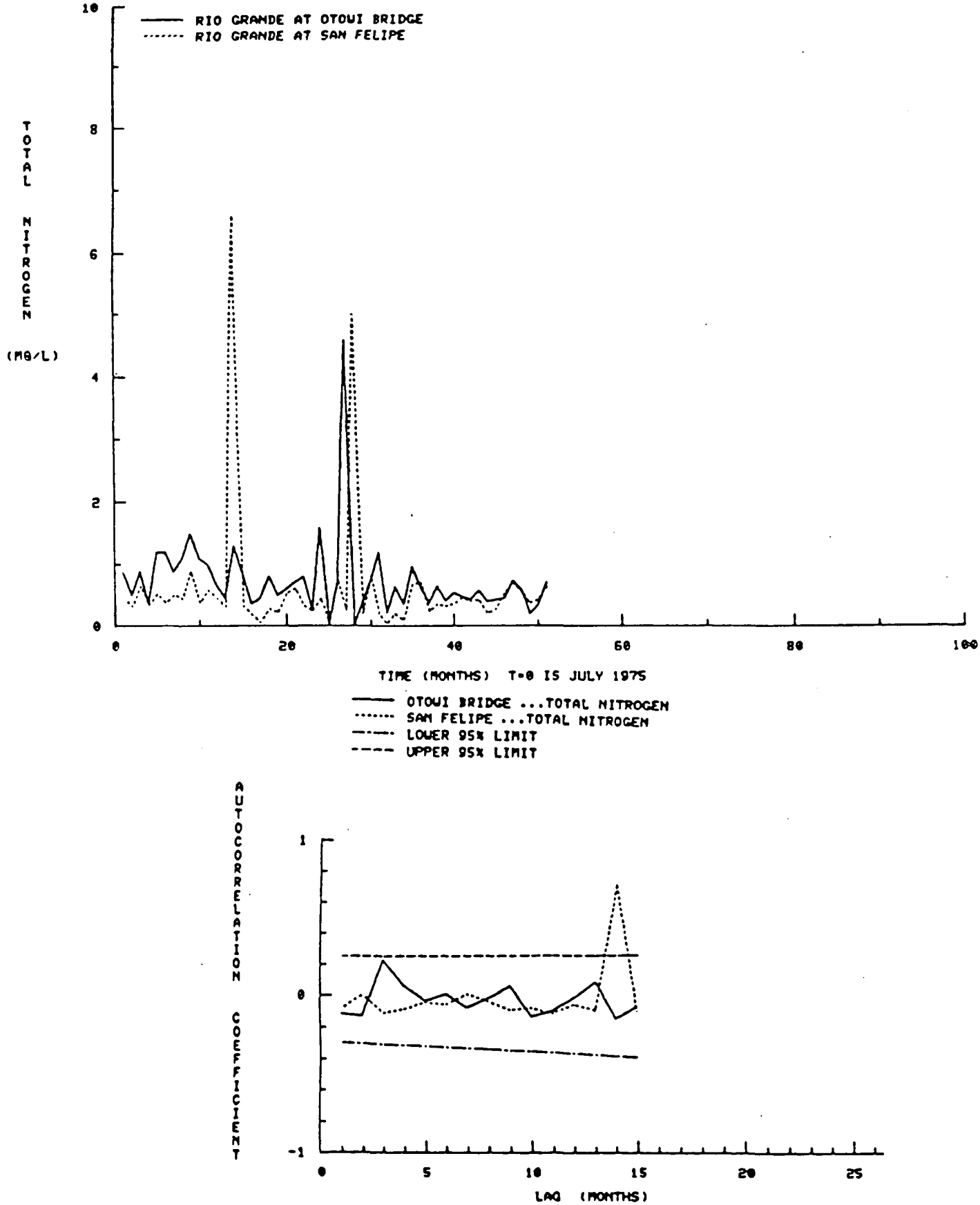


Figure 3.12. Effect of Cochiti Reservoir on the monthly total nitrogen time series.

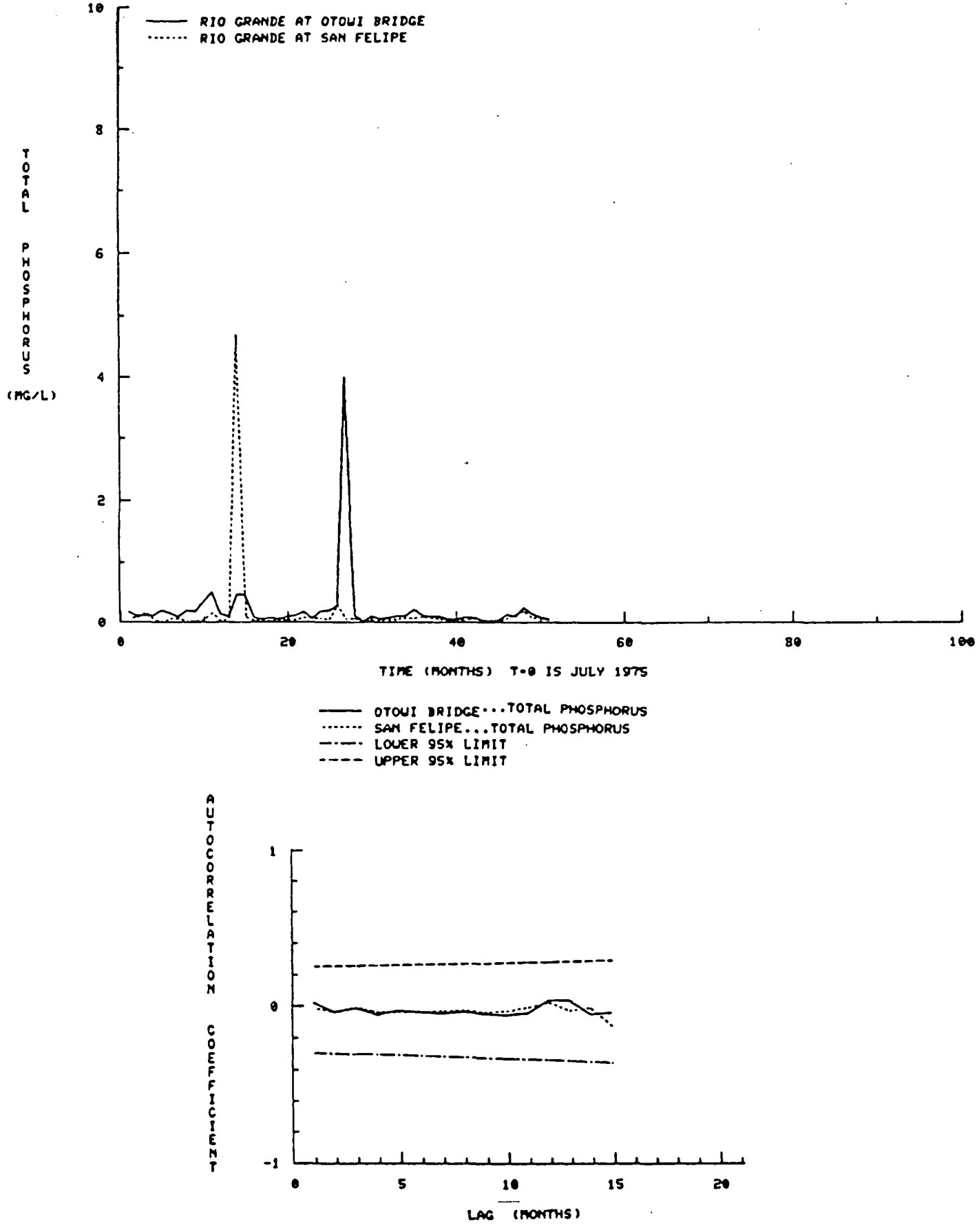


Figure 3.13. Effect of Cochiti Reservoir on the monthly total phosphorus time series.

time series are fairly independent processes. For all three variables, there does not appear to be any strong seasonal or annual cyclic component.

### 3.2.6 Note on Sampling Frequency Design

#### 3.2.6.1 Introduction

The design of any monitoring system is greatly affected by legal, logistical, political, and administrative considerations. The design and operation are further confined by economic constraints. Thus the total number of stations and the sampling interval tend to counteract each other. Many stations may not leave enough personnel and/or money for a productive sampling frequency (see Figure 3.14).

The selection of the sampling frequency itself must be related to the objective of the monitoring network itself. Examples of water quality objectives are: computation of the total load of a certain material, i.e., sediment; detection of criteria violations; maintaining effluent standards; aid in mathematical model calibration; designing temporal criteria based upon the temporal loading; identification of loading mechanisms; aid in the design of structural measures for water quality control; definition of natural background levels prior to construction or watershed management practices. Examples of water quantity objectives are: water budget identification; aid in the design of hydraulic structures; analysis of the system variability; legal partitioning of ownership; minimum stream standards; aid in calibration of hydrologic/hydraulic models; frequency analysis for design criteria.

#### 3.2.6.2 Water Quality Sampling Frequency

Pomeroy and Orlob based the design of water quality frequency on the size and water quantity variability ($Q_{maximum}/Q_{minimum}$) of watersheds. Sanders et.al. (3) have based water quality monitoring frequency on the importance of any of the three objectives of: measuring extremes; measuring trends; and measuring means and the distributions of the variables. All of Sanders' objectives can be conveniently placed on probabilistic terms and thus this method is more attractive as far as formulating sampling frequency on the water quality variables themselves rather than on water quantity variables. What the probabilistic statements enable are a direct computation of the number of samples per time period given the amount of acceptable error of the

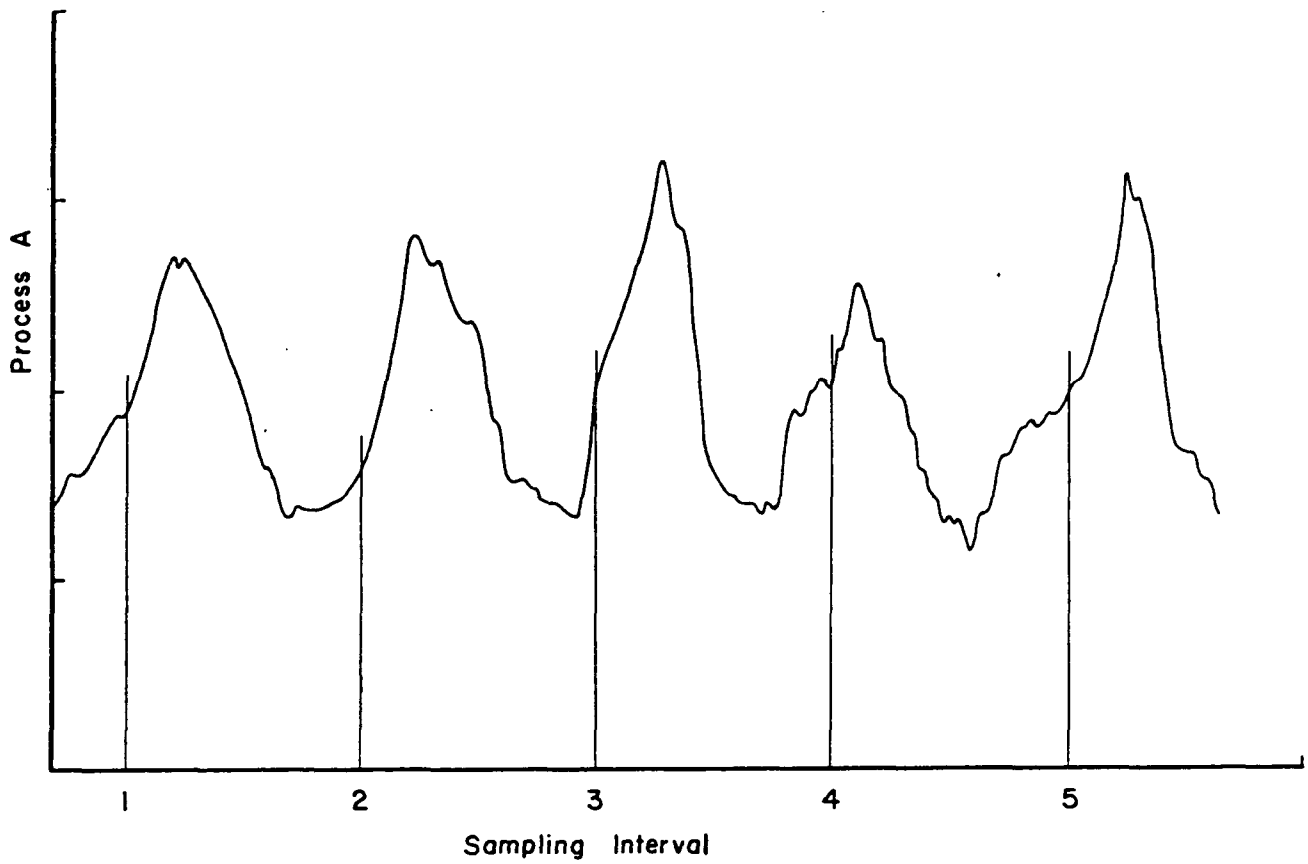


Figure 3.14. Comparison of a continuous process with its discrete time representation.

measured parameter. Unfortunately, the method requires apriori knowledge of the mean and variance of the process which is to be sampled.

#### 3.2.6.3 Concepts for Designing Sampling Frequency

It must be borne in mind that if a sampling station does not fulfill the monitoring requirements of the objective the station is almost worthless. Without any data, the sampling frequency must be determined by scrutinizing the objective. For example, if the objective is to be able to minitor the mean of a process, monthly monitoring may be feasible if the process is not a rapidly varying process. If the objective is to be able to identify periodicities, the process may have to be monitored six times a day in order to detect daily, weekly, monthly and annual cyclicities. Once the sampling frequency is set and after some data is obtained, the data may be analyzed to test whether or not it is fulfilling the objective. For example, the autocorrelation function may indicate too high a correlation between successive measurements, thus a data redundancy is present and the sampling interval could be reduced.

### 3.2.7 Conclusion for Temporal Correlation

The use of the correlogram can indicate much about a physical process. Inferences on system memory or process cyclicity can be made based upon correlograms. Also inferences of the actual time series process can be made by comparing a computed correlogram to theoretical correlograms. Data gaps in a station's records could be filled by knowledge of the underlying process and the correlation function.

## 3.3. Spatial Correlation: The Cross-Correlation Function

### 3.3.1 Introduction and Theory

Considering two separate time series (x,y), measuring one variable at two stations or measuring two different variables at one station, the cross-correlation function can identify the relationship between the two series at various time lags. A common form of cross-correlation is the usage of regression, i.e., a water discharge-sediment discharge relationship. The two time series used in regression analysis are usually regressed by using values measured at the same time, the $R^2$ value (coefficient of determination or explained variance) obtained from the regression analysis is the square of the

lag zero cross-correlation coefficient ($\sqrt{R^2} = r_o(x,y)$), which is commonly called the coefficient of correlation (r) (see Lecture 4). The cross-correlation function allows computation of the correlation between points at any desired lag, similar to the autocorrelation function. When the records of two stations are analyzed by using cross-correlation at lags other than zero, the analysis occurs over time and space.

The equation for the cross-correlation function is:

$$r_k(x,y) = \frac{\mathrm{cov}(x_i, y_{i+k})}{\{\mathrm{var}(x_i)\ \mathrm{var}(y_{i+k})\}^{1/2}}$$

$$= \frac{\frac{1}{N-k}\sum_{i=1}^{N-k} x_i y_{i+k} - \frac{1}{N^2}\sum_{i=1}^{N} x_i \sum_{i=1}^{N} y_i}{\left[\frac{1}{N}\sum_{i=1}^{N} x_1^2 - \frac{1}{N^2}\left(\sum_{i=1}^{N} x_i\right)^2\right]^{1/2} \left[\frac{1}{N}\sum_{i=1}^{N} y_i^2 - \frac{1}{N^2}\left(\sum_{i=1}^{N} y_i\right)^2\right]^{1/2}} \qquad (3.3)$$

Recognize that the records for each time series must have the same length. This equation is very similar to that of the autocorrelation function (Equation 3.1). Figure 3.15 displays the cross-correlogram for the Bonny Reservoir inflow and outflow series (found in Figure 3.8). The positive lags [$r_k(x,y)$, $k \geq 0$] relate future outflows to the present inflows, these indicate the water residence time of the reservoir. The negative lags ($r_{-k}x,y$) physically are relating the inflow series (x) to preceding values of the outflow series. Since physically there should be no relationship between outflows and inflows which have not yet occurred, the $r_{-k}(x,y)$ values are not significantly different from those of an independent series ($\rho_k(x,y) = 0$ for all k). The exception to this, in Figure 3.15, is $r_{-1}(x,y)$, which is above the 95% limit for independent x and y processes. Recall that the first serial correlation coefficient for the SFRR at Hale (the Bonny Reservoir outflows) was very large ($r_1 = 0.563$, Figure 3.10). Thus the reservoir outflow from the present period has a lot of relation to the outflow in the next period. Correspondingly, the lag zero cross-correlation coefficient between the inflow and outflow series [$r_o(x,y)$] is also very large ([$r_o(x,y) = 0.500$], Figure 3.15). Thus, with strong dependence between successive outflows and strong

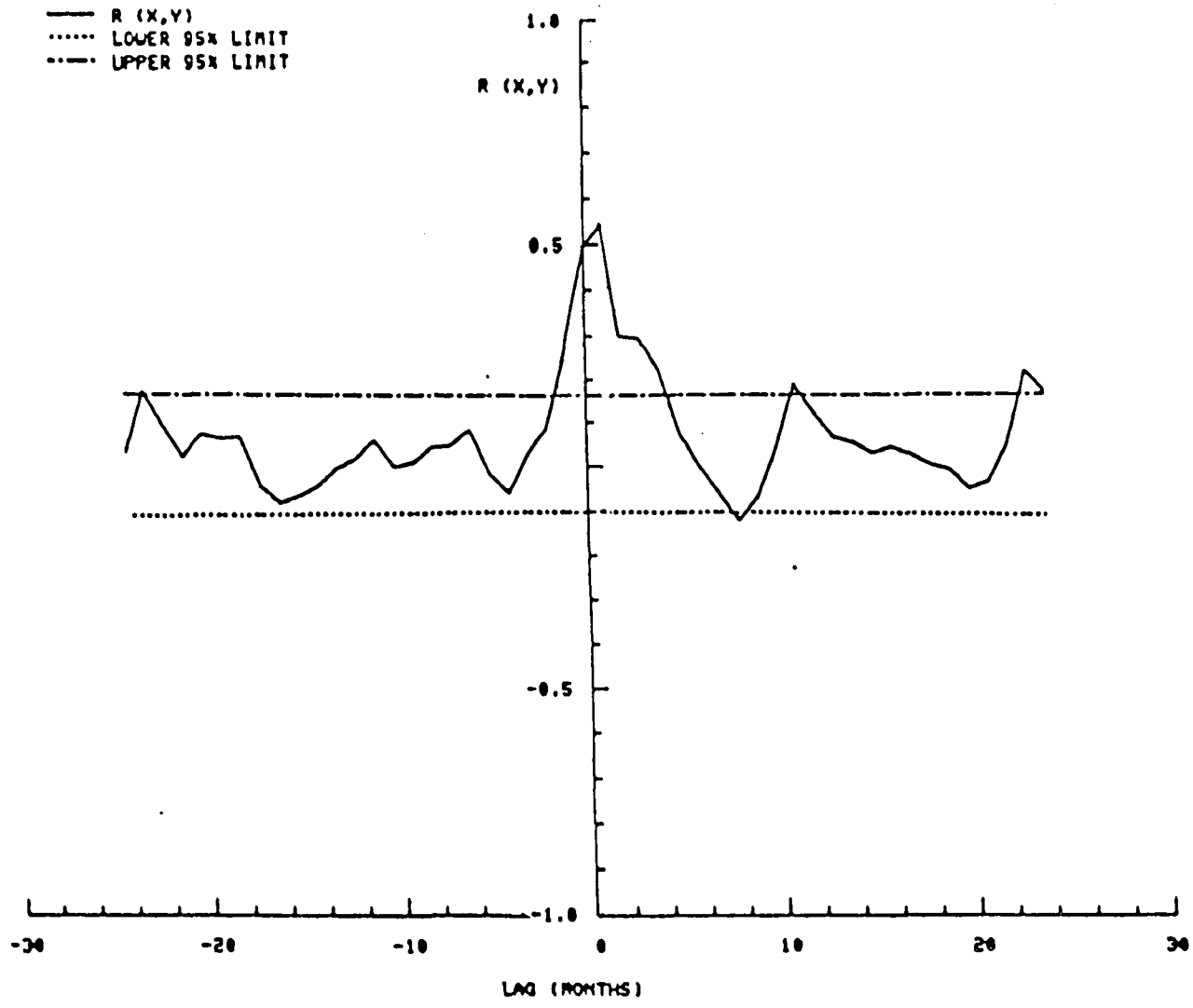


Figure 3.15. Cross-correlogram between the Bonny Reservoir inflows and outflows.

dependence of inflow and outflow at the same time period, there is some degree of dependence between present outflow and inflow of the next period due to the reservoir memory. This type of carryover relation is depicted in Figure 3.16 where strong, physical dependences are marked by solid arrows and implied dependence, caused by the reservoir memory and cross-dependence structure, is marked with a broken arrow.

It is important to note that the cross-correlation function (similarly as does the autocorrelation function) is measuring the degree of variability of points at a certain lag with their respective mean, thus there is no implication of scale or cause and effect in the cross-correlation function. Figures 3.17 and 3.18 exemplify this point. Two independent time series are depicted in Figure 3.17. Note that although the two series have a large difference in magnitude and variability, their movements about their respective means is quite similar. This latter fact is evidenced by the large lag zero cross-correlation coefficient in Figure 3.18 [$r_o(A,B) = 0.944$].

Cross-correlograms aid in identifying relationships between time series of two variables. Examples are: travel time between two locations on a river; relation between discharge and water quality variables; influence of atmospheric phenomena on streamflow, i.e., cloud cover, convective precipitation; etc. Also, cross correlograms can detect independence of two time series', i.e., sunspots and runoff; time between storm events and intensity of storms; etc.

### 3.3.2 Effect of Spatial Correlation on the Amount of Information Obtained from a Gaging Network

What any correlation coefficient indicates is the amount of information present in two sets of data.

Considering two raingages to be situated in one watershed, if the objective is to obtain the most amount of precipitation information with the two gages for use in hydrologic simulation models, the two gages should be placed far apart from each other as well as being well within the watershed boundaries. If the gages were placed right next to each other, it is farily obvious that there would be a huge redundancy of information. This would be indicated by a large $r_o(x,y)$ coefficient. The farther away the gages are placed, the lower $r_o(x,y)$ and the more information obtained on the spatial variability of rainfall. The following hypothetical example results from the

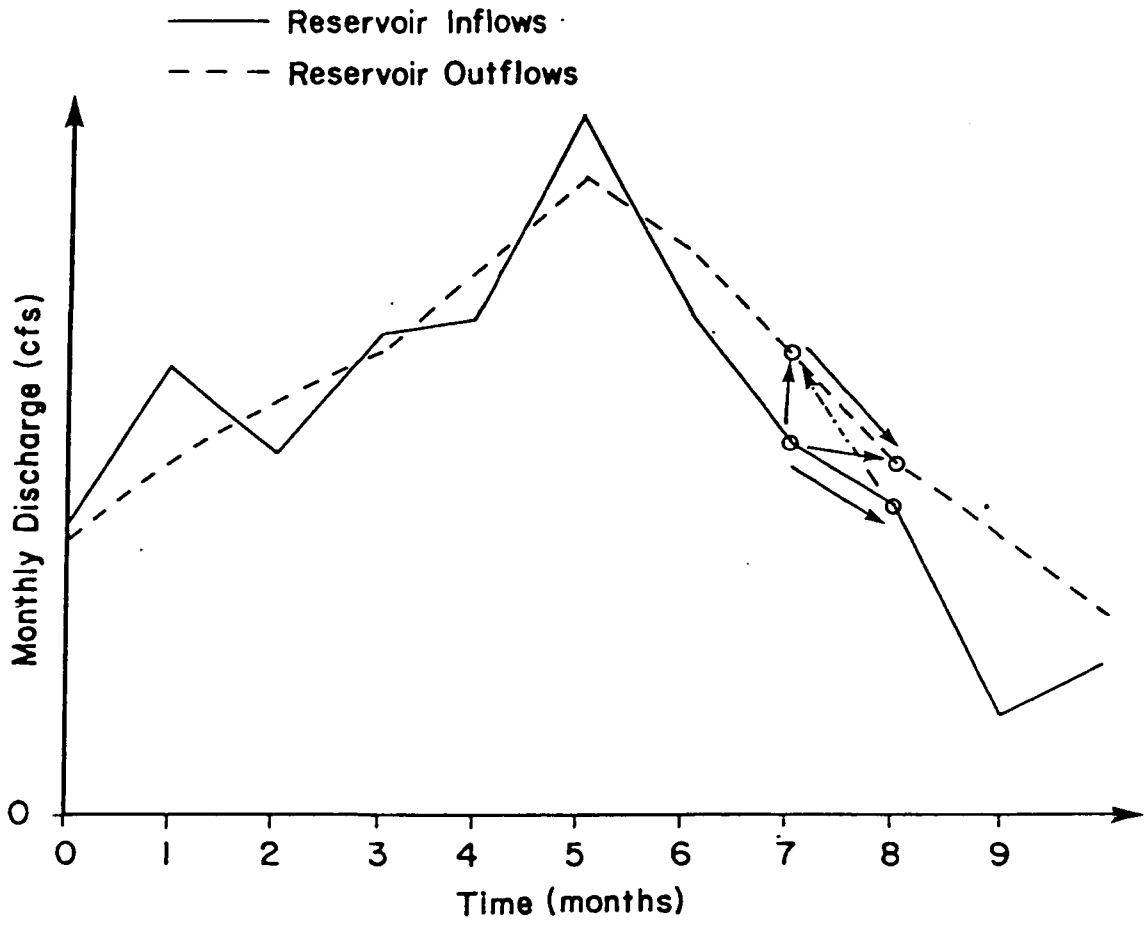


Figure 3.16. Relationship between reservoir inflow and outflow time series. Solid arrow indicates strong, physical relationships. Broken arrow indicates a relationship caused by other dependence structures.

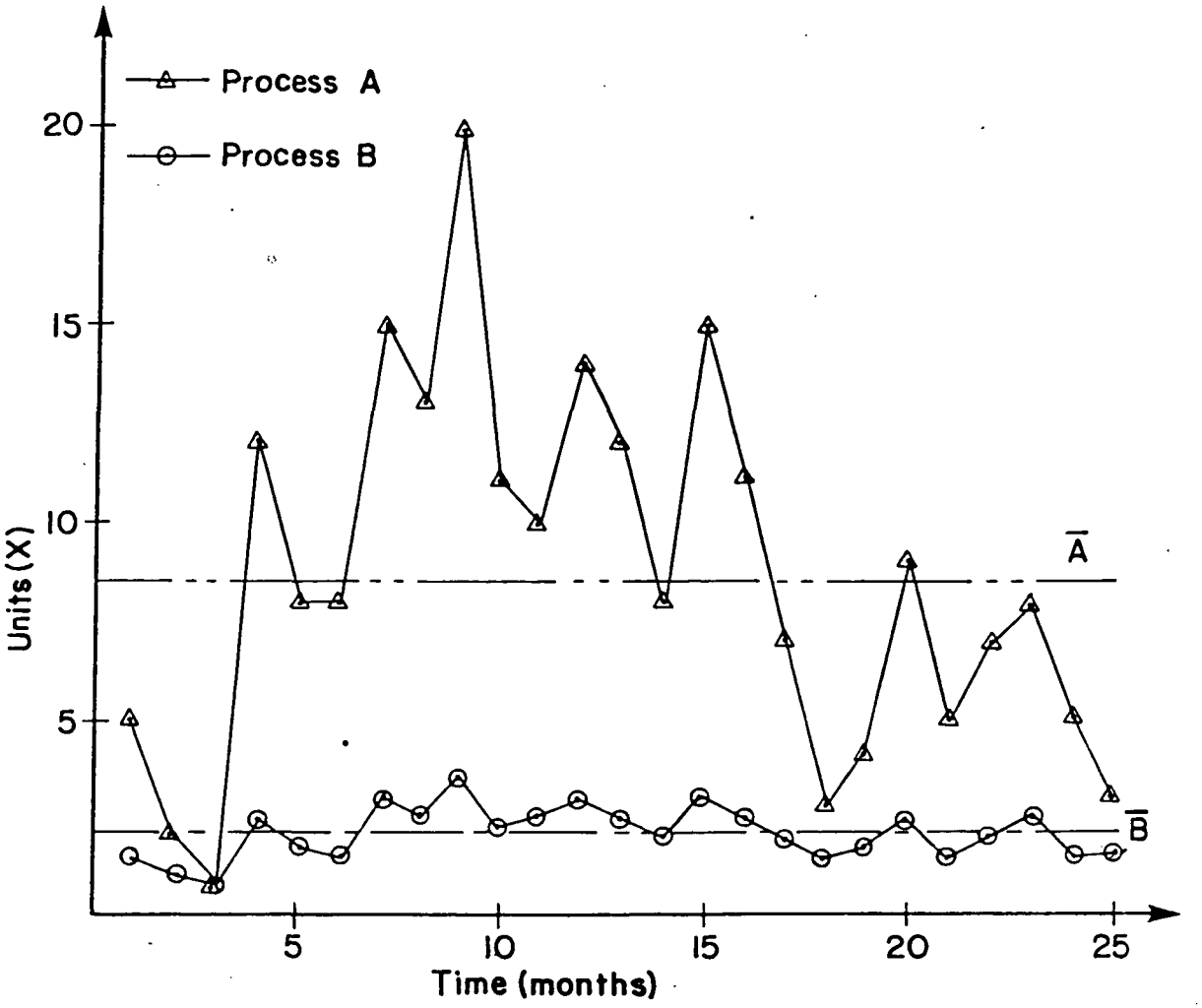


Figure 3.17. Two time series' (A,B) measured in units of x .

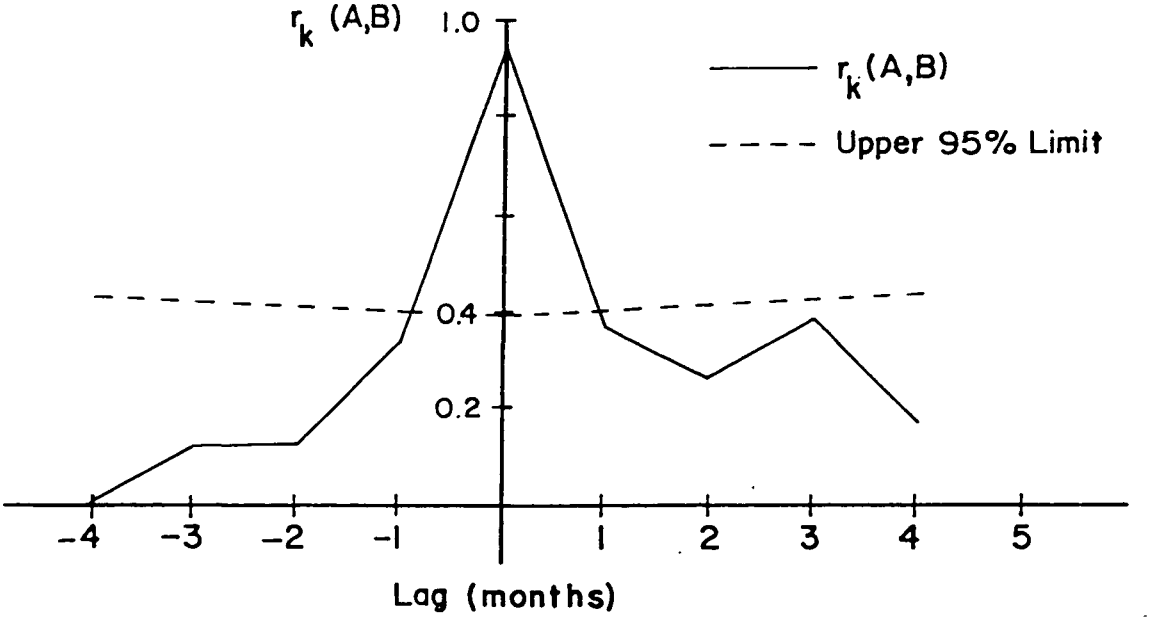


Figure 3.18. Cross-correlogram for the two time series of Figure 3.17.

work of Yevjevich and Karplus (4).

Within a fixed area, assume a network of raingages exists. Also assume that the lag zero cross-correlation coefficient between stations ($\rho_{ij}$) is uniform. Due to the interstation dependence, the information from a set number of dependent stations is equal to the same amount of information from a much smaller number of independent stations ($\rho_o(x,y) \equiv 0$). This smaller number of independent stations is known as the effective number of stations ($n_e$):

$$n_e = \frac{n}{1 + \overline{\rho_{ij}}\,(n-1)} \tag{3.4}$$

where

$n$ = the total number of stations and

$\overline{\rho_{ij}}$ = the average lag zero cross-correlation coefficient between all stations. The effect of station interdependence is found in Table 3.3 and graphed in Figure 3.19.

This last example may aid in the design of systems and this is because with the knowledge of interstation correlation, a system may be designed to obtain the maximum amount of information for the fewest number of stations. More importantly, the trade-off between the amount of obtainable information and the degree of desired interstation correlation (in order to fill data gaps, etc.) may be assessed for their separate marginal benefits with respect to the overall network and the budget for the network.

### 3.3.3 Use of Cross Correlation for Network Design and Application to a Raingage Network

#### 3.3.3.1 Introduction

Numerous studies have been conducted which deal with the spatial variability of precipitation. Precipitation, used here, refers exclusively to rainfall, although special notes are made with regards to snow. This section will be broken down in such a manner as to identify and present the factors which affect precipitation from large-scale down to small-scale or local effects. Example of the large-scale to small-scale sequence is: watershed geographic location, watershed topographic location, gage location in the watershed.

#### 3.3.3.2 Geographic Effects on the Spatial Variability of Rainfall

The spatial variability of rainfall is significantly affected by the

Table 3.3. Effect of Station Interdependence on the Effective Number of Stations ($n_e$). The Entries in the Body of the Table are $n_e$ Based on the Number of Stations, n, and the Average Interstation Lag Zero Cross-Correlation, $\overline{\rho_{ij}}$.

| | $\overline{\rho_{ij}}$ | | |
|---|---|---|---|
| n | 0.2 | 0.5 | 0.8 |
| 2 | 1.67 | 1.33 | 1.11 |
| 5 | 2.78 | 1.67 | 1.19 |
| 10 | 3.57 | 1.82 | 1.22 |
| 20 | 4.17 | 1.90 | 1.23 |
| 50 | 4.63 | 1.96 | 1.24 |

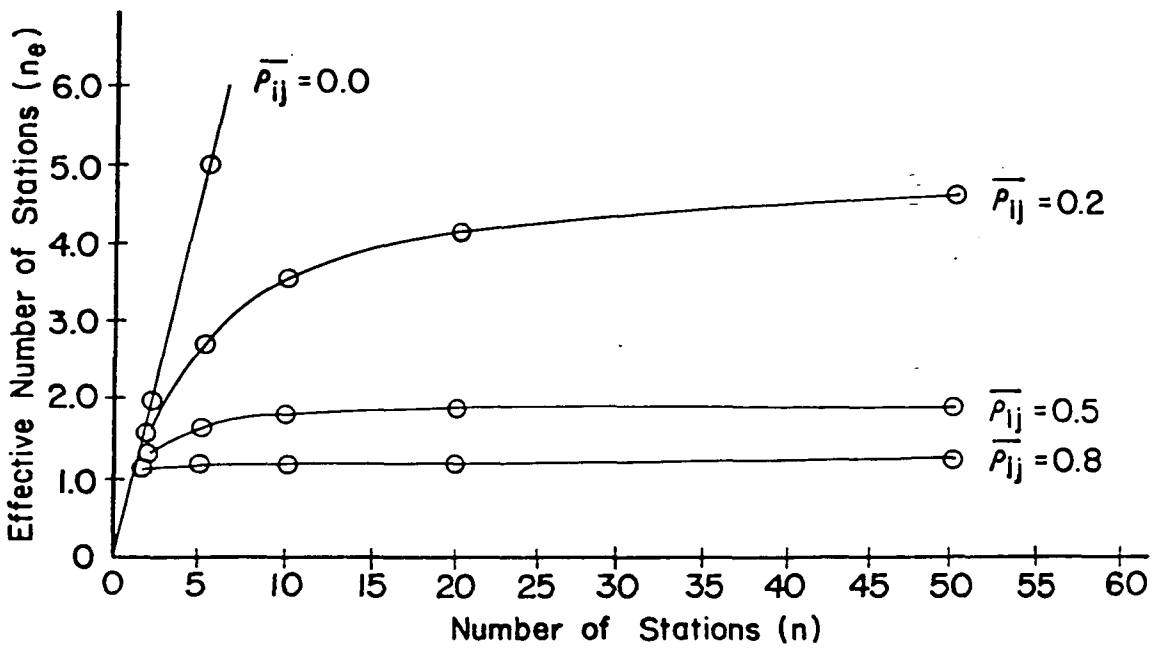


Figure 3.19. Graphical representation of Table 3.3.

location of a watershed in the continental United States. Much of this effect results from the origination and travel of moisture. Figure 3.20 depicts the origin locations of storms and their numbers and average January paths for the years of 1892-1912 (Geoff Love, personal communication). If geographic location was the sole measure of the spatial variability of rainfall, it would be expected that the least amount of spatial variation would occur along the storm paths. Orthogonal movements from the storm paths would result with the largest spatial variation of precipitation. This knowledge alone can aid in the siting of precipitation gages. For example, if a sampling network were to be designed to monitor the increse in rainfall acidity due to industrialization, the maximum effects would of course be realized in the general downwind direction, and in this direction monitoring gages can be spaced farther apart than in other directions. If the monitoring gages were placed upwind from the industrialized region, effects of industrialization may be masked by background rainfall acidity which, in upwind areas, may be as large as the degree of industrial-caused acidity.

The effect of geography on the spatial correlation of precipitation in the midwestern United States was studied by Yevjevich and Karplus (5). The study areas (Figure 3.21, Region I and Figure 3.22, Region II) have minimal topographic effects, and by observing the storm traces of Figure 3.20, it is seen that storm movements are fairly uniform over the areas. The interstation lag zero cross-correlation coefficients ($r_o(x,y)$) were computed between all precipitation stations in the study area by utilizing at least 40 years of monthly data for the correlation coefficient computations. The $r_o(x,y)$ data were then plotted against the interstation distance and ten mathematical models were analyzed for their fit to the data. An example of one of the mathematical models which was fitted to the data is presented in Figure 3.23. The three best fitting models are presented in Table 3.4 with the corresponding optimized parameters (A,n), and coefficient of determination ($R^2$) for each region. Although the mathematical fit to the data is very good, it is believed that even better fit could be made by weighting the interstation distance by its bearing (i.e., for E-W bearing the weighting coefficient is 1.0 and for N-S bearing the weighting coefficient is 1.25, then all bearings between these two bearings would have a weighting coefficient between 1.0 and 1.25).

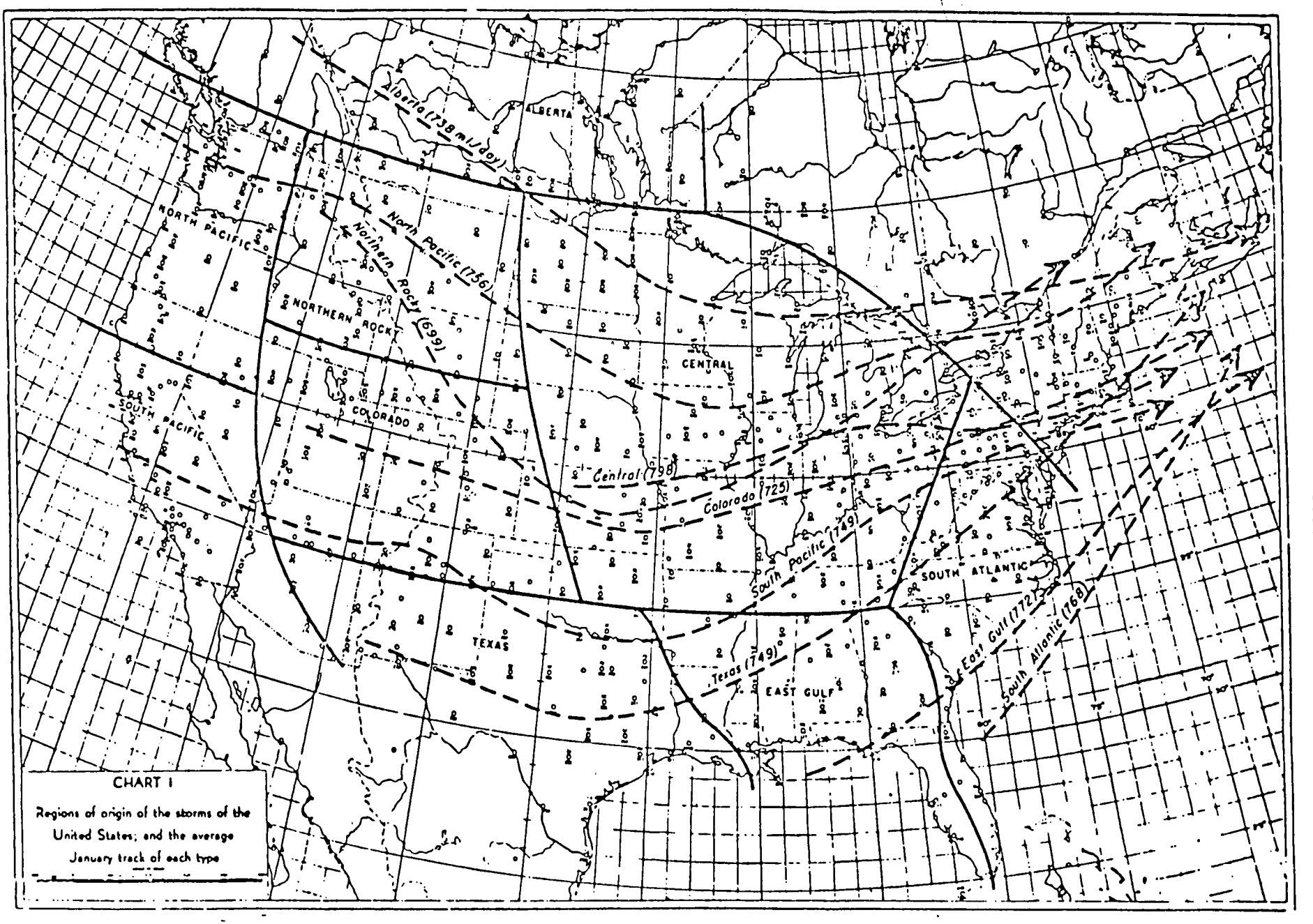


Figure 3.20. Storm tracks across the continental United States (Geoff Love, personal communication).

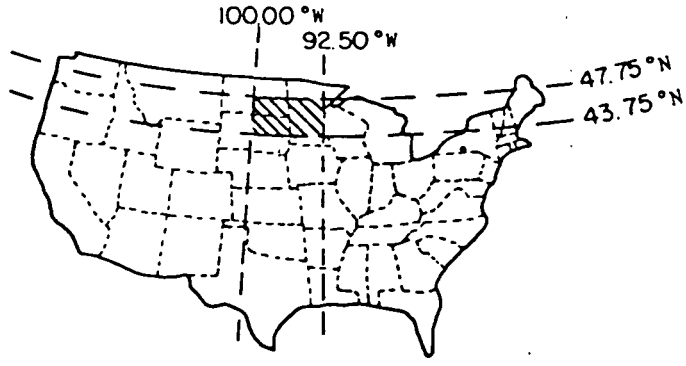


Figure 3.21. Location within U.S.A. of Region I, used as the example for the regionalization of parameters of monthly precipitation series. (after Yevjevich and Karplus)

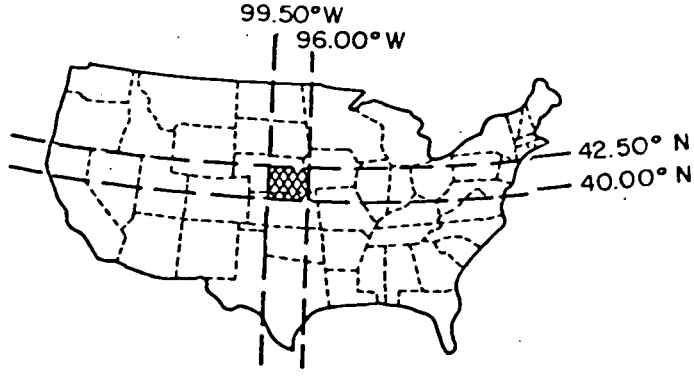


Figure 3.22. Location within U.S.A. of Region II used as the second example for the regionalization of parameters of monthly precipitation series. (after Yevjevich and Karplus)

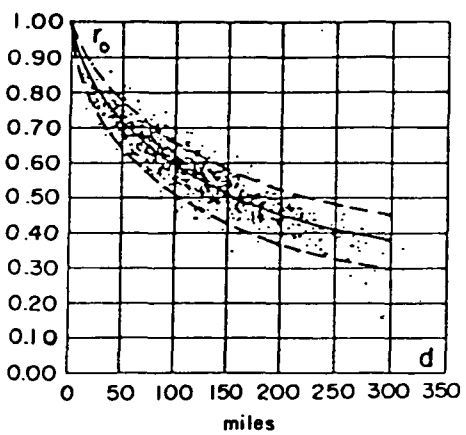


Figure 3.23. Fit of the equation $r = (1-Ad)^{-n}$ to the data for Region I (Figure 3.21), with corresponding 95% tolerance limits (after Yevjevich and Karplus.

Table 3.4. Mathematical Fit of Interstation Correlation ($r_o$) and Interstation Distance (d-miles) Data for the Midwestern United States (after Yevjevich and Karplus)

| Region | Model | $R^2$ | Fitted Coefficients A | n |
|---|---|---|---|---|
| I | $r_o = (1 + Ad)^{-1}$ | 89.8 | 0.006 | -- |
| I | $r_o = (1 + Ad)^{-n}$ | 90.8 | 0.016 | 0.534 |
| I | $r_o = (1 + Ad)^{-1/2}$ | 91.6 | 0.018 | -- |
| II | $r_o = (1 + Ad)^{-1}$ | 91.0 | 0.007 | -- |
| II | $r_o = (1 + Ad)^{-n}$ | 92.0 | 0.015 | 0.571 |
| II | $r_o = (1 + Ad)^{-1/2}$ | 92.2 | 0.018 | -- |

3.3.3.3 Topographic Effects on the Spatial Variability of Rainfall

It is a well recognized fact that precipitation variability in space is significantly controlled by the relief of the earth's surface. One common effect is the release of moisture on the windward side of mountain ranges, and a "rainshadow" on the leeward side. Physically, as moist air masses are lifted, the amount of total moisture the air mass can hold decreases. Once a lifted air parcel reaches saturation, any further lifting can result in precipitation. Thus, when incoming air masses approach the mountains, most of the moisture deposits on the windward slopes. When the air mass passes over the mountain peaks and begins descending, its total moisture has not only been reduced, but the amount of total moisture that the air can hold is increasing. Thus on the leeward mountain slopes, only strong convective or frontal systems can squeeze-out more moisture from the air. Studies of this effect for specific locations are found in references (7) and (8). The result of topography on the spatial correlation of precipitation is to modify the correlation structure prescribed by the geographic location (presented in the last section). These two effects combine to form regional spatial variability effects in precipitation.

The topographic/geographic effects on the spatial correlation of precipitation is found in Figure 3.24 (reference 6). The ellipses represent the major and minor axes of correlation, highest correlation in space is the major axis ($C_2$) and the direction of lowest correlation is the minor axis ($C_1$). The quotient of the major and minor axes ($C_1/C_2$) is written below each ellipse. A quotient of 1.0 indicates isotropic variations and as the quotient approaches zero the ellipse approaches a line. If the general moisture movement over the continental United States were assumed to be west to east, all of the ellipses would be aligned with their major axis in this direction. Topographic effects can shift this alignment a full 90°. The 90° shift can first be seen at the west coast and is attributable to the orographic influences of the Cascade, Sierra Nevada, and Coast Ranges. This alignment indicates less spatial variation in the North-South direction, perpendicular to the general moisture movement (6). A similar re-orientation of the major and minor ellipse axes occurs at the Rocky Mountains. Once these orographic controls have been passed, the orientation of the major and minor correlation ellipse axes becomes aligned to the West-East moisture flow. Exceptions to this occur near the

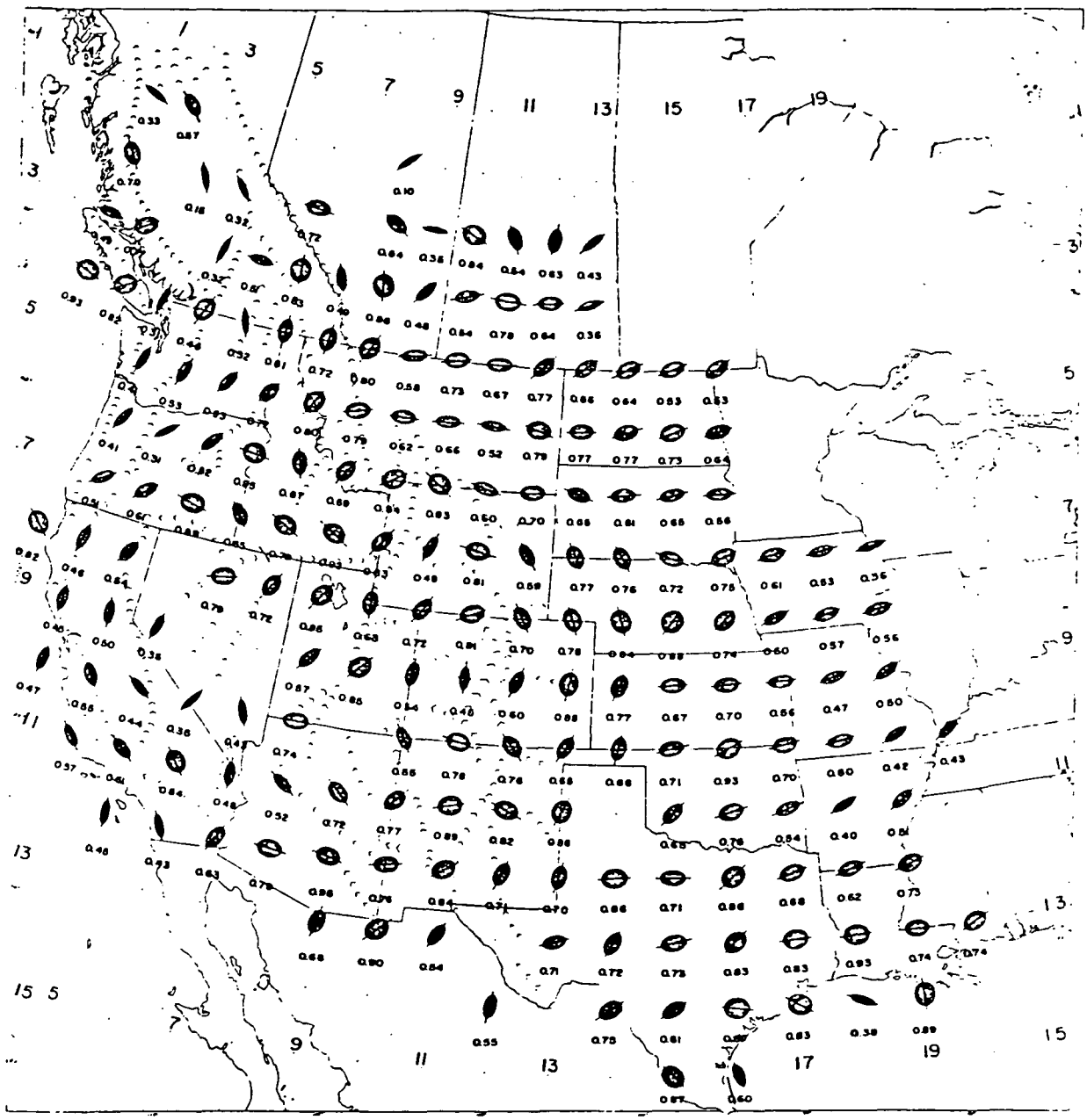

Figure 3.24. Regional distribution of the azimuths of the axes of the maximal correlation coefficients and the values of the ratio ($C_1/C_2$) for the annual precipitation variable. (after Caffey)

Great Lakes and the Gulf of Mexico, which bodies of water also act as moisture sources (6).

3.3.3.4 Small-Scale Spatial Variabilty of Precipitation

The elements causing small scale (i.e., watershed) variability in precipitation are local topography and climatic regime. Topographic influences were presented in the last section and they tend to re-orient the alignment of the spatial correlation structure set-up by the general flow of moisture. Climatic regime will be discussed in this section. Specifically, the climatic regime will deal with the various types of precipitation events which occur in a region, viz., thunderstorms, steady rains, air mass storms, etc. These climatic regimes can be further subdivided by: season (time of year); depth of rainfall; sampling interval; storm duration; etc. It would be expected large storms produce less spatial variability than small storms. For example, a thunderstorm would only affect one or two gages in a watershed whereas a tropical depression may affect all gages on a watershed. Along this line, it would be expected that longer duration and larger rainfall depth storms would produce less spatial variability than short duration and small depth storms (steady rain versus thundershowers). Two studies which have verified these observations are references 10 and 11. Huff and Shipp (10) found that the large variability of thunderstorm rainfall depth reduces the overall spatial correlation when analyzing the spatial variabiity of rainfall depth (Figure 3.25). In Figure 3.25, rainfall depths of 0.01 - 0.10 inches were mostly attributable to large scale storms producing drizzle and light, extensive rain, also the storms with a total depth greater than 1.0 inch mostly resulted from large storm systems. Thundershower activity, in general, yielded depths of 0.1 -1.0 inches. Other correlations for Illinois, found by Huff and Shipp (10), are found in Figures 3.26, 3.27, and 3.28. These figures plot the lag zero cross-correlation coefficient against the distance between raingages. All of the plots are for May through September storms. Huff and Shipp found that the cold weather precipitation events (October-April) in general yielded larger cross-correlations than the warm weather storms. For concluding remarks, they described the required interstation distance for various rainfall monitoring objectives (i.e., total rainfall depth, type of storm, fixed storm duration, etc.) given a desired interstation correlation of 0.866 (75%

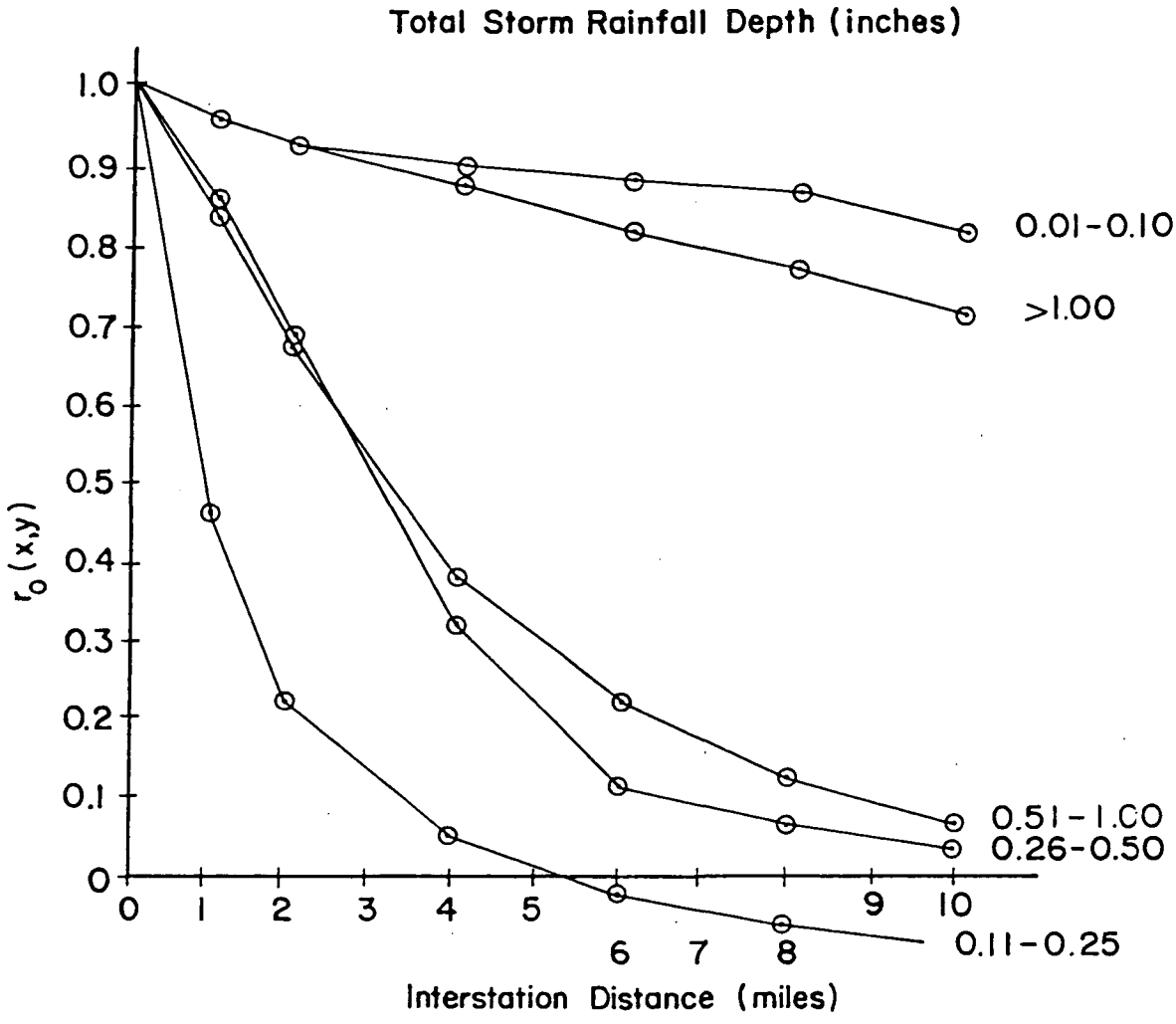


Figure 3.25. Effects of total rainfall depth with interstation correlation.

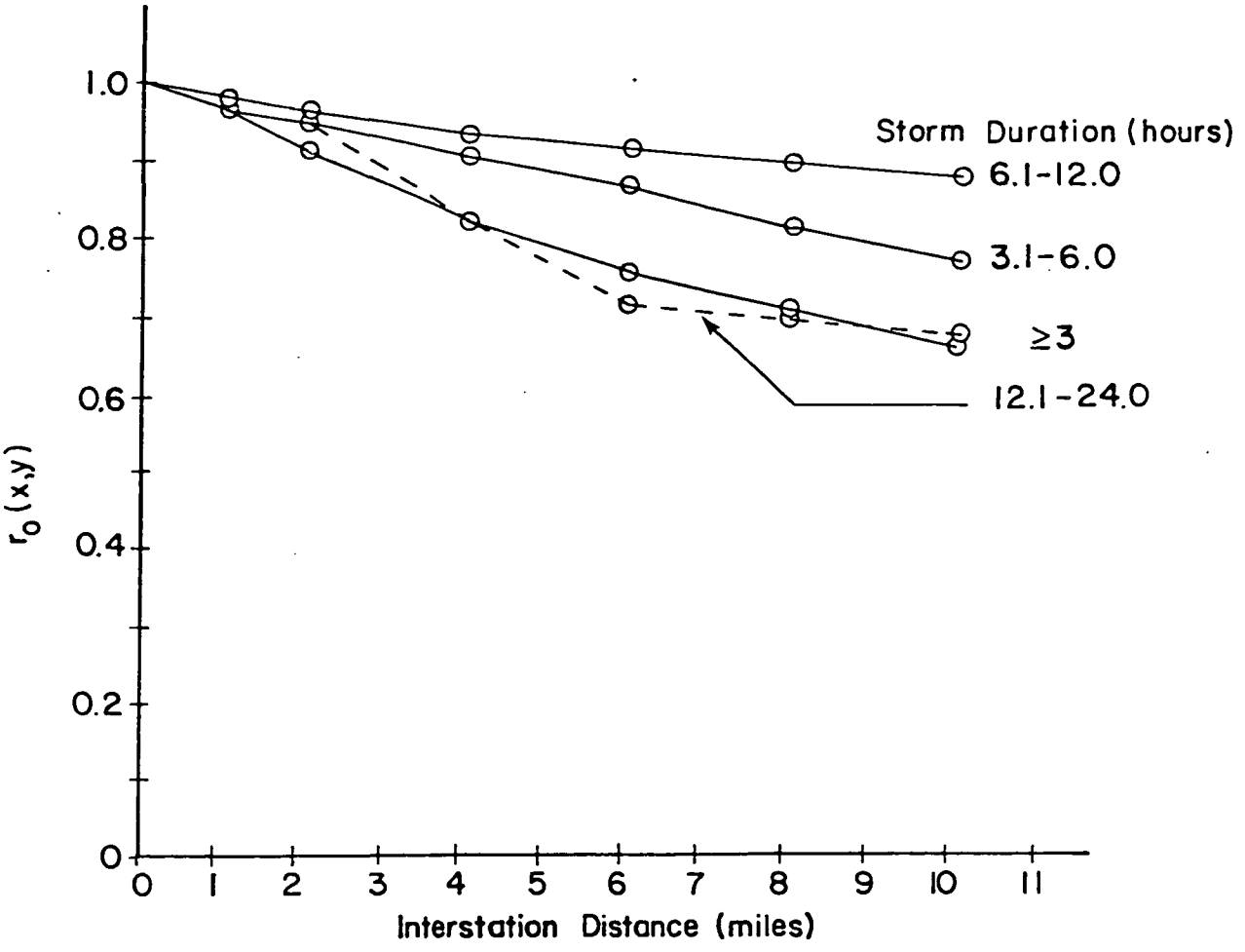


Figure 3.26. Effect of storm duration and interstation correlation for May through September storms in Illinois. (after Huff and Shipp)

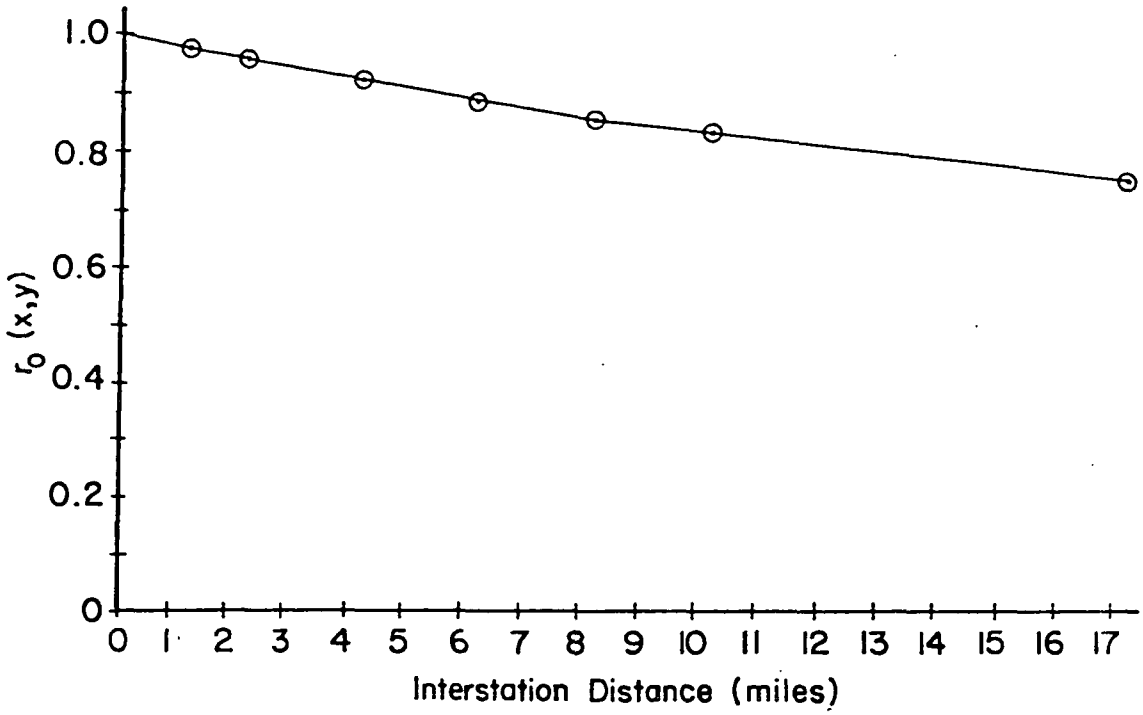


Figure 3.27. Overall spatial correlation of precipitation for May through September storms in Illinois. (after Huff and Shipp)

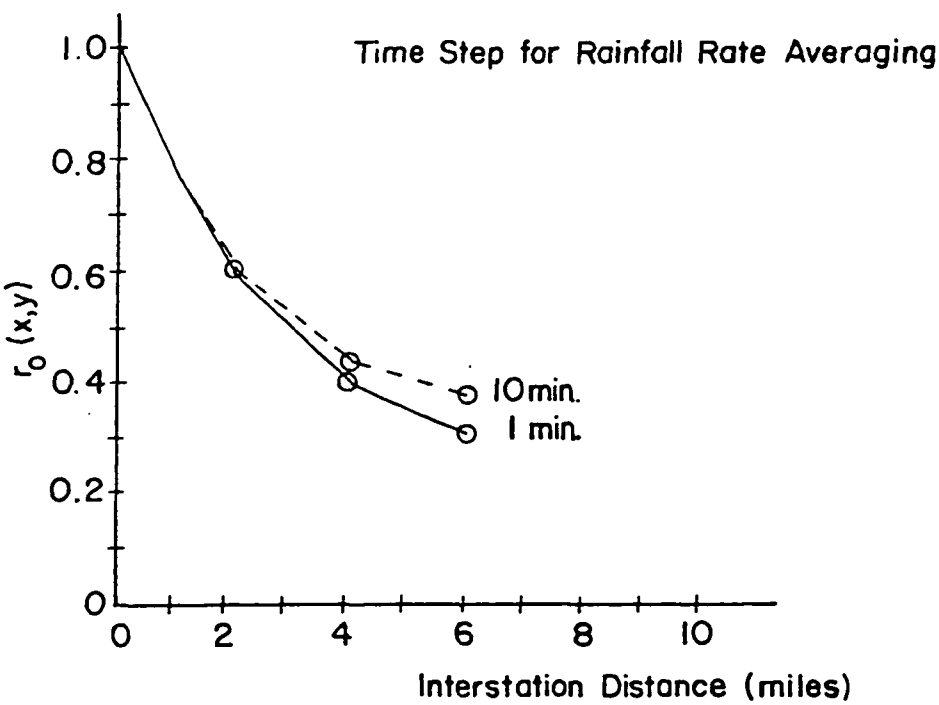


Figure 3.28. Effect of the time step for reporting average rainfall depth on the interstation correlation for May through September storms in Illinois. (after Huff and Shipp)

explained variance). Depending on the objective, raingages would then have to be spaced between 0.3 miles to 12 miles apart.

In a similar study in Vermont, Hendrick and Comer (11) found results similar to those of Huff and Shipp. Their desired interstation correlation was 0.90 (81% explained variance) and this correlation required raingages to be 2.5 to 4 miles apart (depending on the objective).

### 3.3.4 Spatial Variability of Streamflow

The spatial variability of streamflow is much smaller than that of precipitation. This is due to water storage (in rivers, on the surface, and underground) in the watershed which acts to smooth the precipitation input. This means that gages can be placed farther apart on a river and yet maintain a relatively high correlation. Depending on the sampling interval and the water velocity, the largest cross-correlation coefficient between two series may occur at any lag ($r_o(x,y)$, $r_1(x,y)$, $r_2(x,y)$, etc.) and the largest cross-correlation coefficient would indicate the travel time between gages. Recognize, that high cross-correlation between two streams on the same watershed does not indicate a cause and effect relationship (when one stream is flooding the other must also be flooding, etc.). What the high correlation means in this case is that both streams most likely have flows owing to the same type of causal factor (i.e., groundwater recharge, precipitation, snowmelt, etc.). Thus independent variables are uncorrelated, but uncorrelated variables are not necessarily independent. Dependence in correlated variables does not have to be a physical or cause and effect dependence.

### 3.3.5 Spurious Correlation

It is possible to create an apparent correlation between two variables when there is in fact no correlation present between their data sets, this is called spurious correlation. Two types of spurious correlation which can exist are data clustering and presence of one variable in both data sets. Data clustering is depicted in Figure 3.29. The overall cross-correlation between x and y is large, yet the correlation within each cluster is essentially zero. Any prediction of y by x would be dangerous since there is an implied relationship by the unpartitioned data set. An example of this may occur with water versus sediment discharge in an intermittant stream with seasonal runoff from snowmelt and thundershowers. The snowmelt runoff may

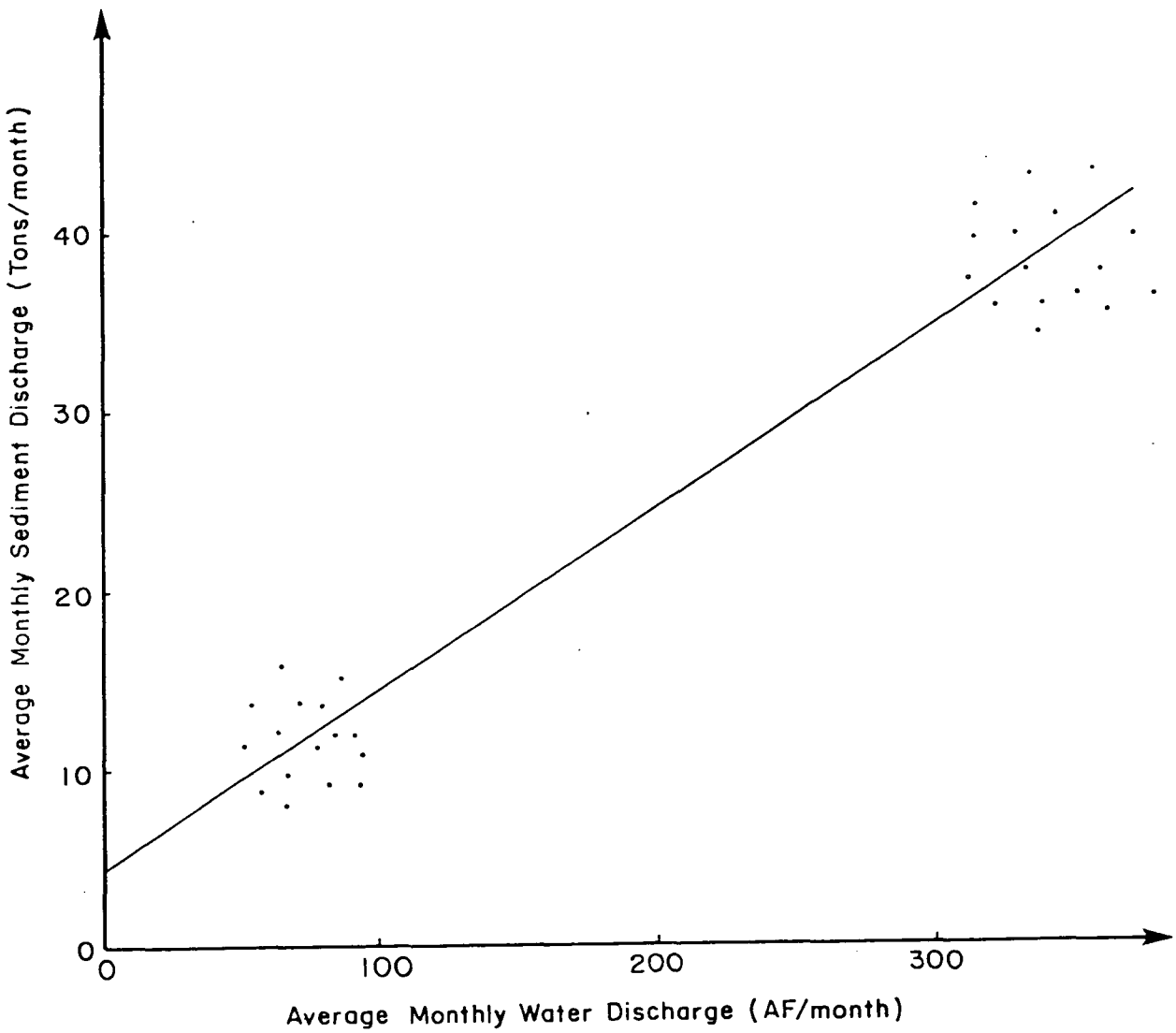


Figure 3.29. Spurious correlation caused by data clustering.

have low flows with low sediment concentrations and the thundershowers would produce highly variable flows with large sediment loads.

The second type of spurious correlation arises when data is being standardized or nondimensionalized. In these cases, two variables (X and Y) which are initially independent, may each be divided or multiplied by a third variable (Z) such that X/Z and Y/Z (or XZ and YZ) show significant correlation. This is a spurious correlation caused by a common random variable. Corrections for common variables in a correlation relationship have been determined and tabulated (such as in reference 13).

## 3.4 References

Yevjevich, V., 1972, "Stochastic Processes in Hydrology," Water Resources Publications, Fort Collins, CO.

Dyhr-Nielsen, M., 1972, Loss of Information by Discretizing Hydrologic Series, Hydrology Paper No. 54, Colorado State University, Fort Collins, CO, October.

Sanders, T. G., ed., 1980, Principals for Network Design for Water Quality Monitoring, Colorado State University, Fort Collins, CO, July.

Pomeroy, R. D. and G. T. Orlob, 1967, "Problems of Setting Standards and of Surveillance for Water Quality Control," California State Water Quality Control Commission, Pub. No. 36, Sacramento, California, May.

Yevjevich, V. and A. K. Karplus, 1973, Area-Time Structure of the Monthly Precipitation Process, Hydrology Paper No. 64, Colorado State University, Fort Collins, CO, August.

Caffey, J. E., 1965, Inter-Station Correlations in Annual Precipitation and in Annual Effective Precipitation, Hydrology Paper No. 6, Colorado State University, Fort Collins, CO, June.

Burns, J. I., 1953, "Small-Scale Topographic Effects on Precipitation Distribution in San Dimas Experimental Forest," Trans., Am. Geoph. Union, Vol. 34, No. 5, pp. 761-766, October.

Smallshaw, J., 1953, "Some Precipitation-Altitude Studies of the Tennessee Valley Authority," Trans., Am. Geoph. Union, Vol. 34, No. 4, pp. 583-588, August.

Neter, J. and W. Wasserman, 1974, Applied Linear Statistical Models, Richard D. Irwin, Inc.

Huff, F. A. and W. L. Shipp, 1969, "Spatial Correlations of Storm, Monthly, and Seasonal Precipitation," Jour. of Applied Meteorology, Vol. 8, pp. 542-550, August.

Hendric, R. L. and G. H. Comer, 1970, "Space Variations of Precipitation and Implications for Raingage Network Design," Jour. of Hydrology, Vol. 10, pp. 151-163, October.

Yevjevich, V. and R. I. Jeng, 1969, Properties of Non-Homogeneous Hydrologic Series, Hydrology Paper No. 32, Colorado State University, Fort Collins, CO, April.

Haan, C. T., 1977, Statistical Methods in Hydrology, The Iowa State University Press, Ames, IA.

# IV. QUALITY OF DATA

## 4.1 Introduction

gravitational sequence

Data quality is defined as the accuracy and homogeneity of a data set. Without exact measures of the quality of data (i.e., 99% pure, etc.), the assessment of what exactly the quality of a data set may be is difficult to describe. Some data errors may be easily discerned by looking at the physical processes involved. Other data inhomogeneities may be statistically tested for or discovered by use of a physical process model. These methods are presented in this chapter.

Data are assumed to be of good quality if they represent the measured variables, do not fluctuate so widely that they cannot be interpreted, have an acceptable level of error, and are physically realistic. Data quality is affected by several factors. These factors include: sensitivity of the measurement technique, errors in the measurements, incomplete sampling, and selection of the wrong variable to measure. An example of incomplete sampling and poor selection is encountered in rainfall measurements when only daily rainfall totals are recorded. If the selected model requires rainfall informtion by five minute increments, then the daily rainfall is incomplete indicating a poor selection of sampling interval. However, if the daily water balance is desired, then the daily total is perfectly acceptable.

If data are difficult to measure or the measurement device is insensitive, there is the possibility of significant errors and lower quality data. Hard-to-measure data may occur because of natural variability or the selected measurement technique. Natural variability of soils produces large differences in soil infiltration rates between otherwise similar sites. Therefore, infiltration rates are usually calibrated in the model using a representative starting point. Measurements are also sensitive to the technique used. For example, discharge computed from a rating curve and stage height may substantially differ from directly measured discharge if the measurement device is not responsive or sensitive enough to changes in flow depth.

Errors in measurements can occur from human, mechanical or technical sources. Human errors, such as not starting the measurement instrument correctly and without proper calibration, or missing a reading can be caused by inexperience in data collection and can usually be improved after proper training. Mechanical errors such as clock stoppage, plugging of stilling basins, or the loss of sampling equipment during large runoff events can be

minimized through proper design and maintenance. Errors caused by measurement techniques are often hard to detect unless the limitations imposed by adopted techniques are known. An example of error common in reporting discharges is created through use of average stage values. This type of error is also related to parameter sensitivity. An approach often used is to average hourly stage values for a day, then convert the stage, often adjusting for a shift, to an averge daily discharge. This approach may be unacceptable because the relationship between stage and discharge is often highly nonlinear. The stage-discharge relationship can be written as

$$Q = a\ S^b \tag{4.1}$$

where $Q$ is discharge, $S$ is stage, and $a$ and $b$ are statistically fitted parameters. Many natural channels and most flow measurement devices have $b$ parameters greater than, or equal to, 1 varying from about 1 to 4 or 5. A typical value may be from 1.5 to 3.0 to provide enough sensitivity for measurement. The relative error in $Q$ can be found from

$$\frac{dQ}{Q} \propto b\ \frac{dS}{S} \tag{4.2}$$

where $dQ/Q$ is the relative change in discharge and $dS/S$ is the relative change in stage. Because $b$ is usually greater than 1, an error in $S$ due to improper averaging is magnified to produce a greater error in $Q$. If average stages are used to determine average discharges, there may be a significant difference between that value and one obtained by computing each discharge and then averaging.

Although there are many sources of error that can affect data quality, the primary causes can be eliminated or reduced. However, complete elimination of error is practically and economically infeasible; therefore, an acceptable amount of error must be allowed. In this way, data can be of high quality at an acceptable cost.

## 4.2 Data Quality Assessment through Physical Process Analysis

As stated in the notes for the previous lecture (Spatial and Temporal Correlation), some information contained within a data set may be extracted by a simple plot of the data. This also holds true for misinformation present in data. The time series plot of data will depict any extreme (large or small)

values present in the data set. With prior knowledge of the physical characteristics of the system from which the data came, it can be qualitatively assessed as to whether or not any observed extreme values are physically possible. For example, if a large discharge value may be a reporting error, if it has also been determined that: no high water in low-lying areas was reported, no large discharges into the river occurred elsewhere, and/or no drastic watershed changes occurred.

Another form of data error is detectable by knowledge of the physical limits of the variable being measured. In such a case, a data set may look homogeneous with no extreme events, yet the entire data set may be wrong due to improper recording and/or reporting. For example, if the monthly pan evaporation for Cincinnati was reported over a five-year period with values always within a range of ten to thirty inches per month, the data is obviously wrong since calculation of the average monthly evaporation by physical models using the maximum solar radiation available could not consistently yield such high values (the average annual evaporation for Cincinnati is about 34 inches per year[1]). Many data sets can be qualitatively assessed by comparing reported values with published long-term regional average values. Knowledge of system variability will aid in determining the degree of extreme values which should occur in a data set. Also, simple calculations can be made in order to compute the general values of a process. For example, using mean annual rainfall on the rational formula to get mean annual discharge.

Of special importance in detection of data errors is the physical relationship between variables in the watershed system. Plotting two time series in one figure can reveal errors. For example, water discharge is usually related with sediment discharge, typically through a sediment rating curve. Plotting the two time series on the same graph can aid in visualizing this relationship. Physically, there cannot be any fluvial sediment discharge when there is no streamflow. In addition, there should be no sediment concentrations very much larger than the total sediment conveyance capacity for a given discharge.

These aforementioned types of qualitative assessment can be made without mathematical transformation of the data and should be included in the first phases of any modeling or data analysis procedures. It is especially important to recognize and identify the physical processes which act within the monitoring network and to assess the relative megnitude and importance of each.

Since data acquisition is usually a subset of larger objectives (i.e., watershed model, evaluation of environmental practices, etc.), errors in the data set will be present in any future usage of the data. Thus the data provides a foundation for large scale objectives and should be of as high a quality as feasible.

## 4.3 Data Inhomogeneity

### 4.3.1 Introduction

Webster's definition of homogeneity is, "like in nature or kind; uniform in structure of composition." In order to obtain relevant information from a data gathering station, the collected data should be homogeneous. Jumps and trends tend to create inhomogeneities in data. Any inhomogeneity manifested by the data is also present in any subsequent use of the data (i.e., structural design, etc.). Detection of data inhomogeneities can lead to remedial measures to form a more homogeneous data set.

The qualitative detection of data inconsistency (inhomogeneity) was described in the last section whereby knowledge of the physical process being monitored aided in detecting inconsistent or incorrect data. This section will deal with mathematical measures which are used to detect data inhomogeneities.

### 4.3.2 Testing for Data Inhomogeneities

#### 4.3.2.1 Qualitative Test for Inconsistencies

A qualitative method to isolate data inhomogeneities starts with plotting the time series data and computing the mean and standard deviation (Equations 4.3 and 4.4) of the data. [Both equations are unbiased estimates of

$$\text{Mean} = \bar{x} = \frac{1}{N} \sum_{i=1}^{N} x_i \tag{4.3}$$

$$\text{Standard Deviation} = s = \left[\frac{1}{N-1} \sum_{i=1}^{N} (x_i^2 - \bar{x}^2)\right]^{1/2} \tag{4.4}$$

the population parameters, N = total number of observations, $x_i$ = observation at time i.] Next, the mean of the data is plotted on the same graph with the time series data, and then lines one standard deviation above and below the mean are plotted. This allows identification of single extreme points, jumps

and trends. The single points must be separately assessed as to their validity and admissibility into the data set. For example, if an extremely large BOD load was recorded in the daily BOD time series, but surrounding data points were not exceptionally large, this data point would be questionable (it was found to be more than one standard deviation away from the mean daily BOD value). If it was discovered that an upstream rendering plant had dumped a large amount of organic wastes into the river due to plant malfunctions, this data point is validated. If the objective of the monitoring network is to discover criteria violations, then the data point is admissible into the data set. If the objective of monitoring is to gather data in order to model the background and typical BOD loading mechanisms, this data point may be deleted from the data set.

A jump in data observations is detected by this method in that for example, with an increasing data jump, the part of the data series before the jump will be mostly below the overall mean and the data after the jump will be mostly above the mean. The case of a decreased jump is simply the reverse of the increased jump. Trends show similar effects as jumps, only there will not be a sharp delineation as with jumps. Another way to discern a trend is to plot the running mean through time (compute a new mean each time a new observation is made) and compare this to the overall mean. A trend will have these two means equal only at the end of a record. Crossing over the overall mean by the running mean would not definitely identify a trend. This method is depicted in Figure 4.3 for an example in the next section.

#### 4.3.2.2 Testing for a Jump

Jumps may be caused by many factors, i.e., a change in a measuring technique, movement of a gage to a nearby location, a rapid and substantive change in the causal factors of the process being measured, or a change in the process itself. The major problem in detection of a jump is trying to decide whether or not the jump is significant. For instance, if a raingage were moved two feet from its original location in order to laydown some underground phone lines, the jump of data may not be detectable at all. In fact, the data set can be logically assumed to be a homogeneous set. If the gage were to be moved 300 feet and near to some large cottonwood trees, there may be quite a significant change in the data due to sheltering of the gage by the trees. In order to tell whether or not there is a significant change in data due to a

jump, the procedures described in the next paragraph should be followed.

The first step for the detection of jumps is to determine when the jump has occurred. This can be done by plotting the data and visually detecting the jump, or by knowing when the physical changes were made in the monitoring network or the process (i.e., when the gage was moved, when cloud seeding began, etc.). Once the time of the jump has been identified, the data must then be partitioned into pre- and post-jump data sets. With these two data sets, the mean and standard deviation for each is computed ($\bar{x}_1, \bar{x}_2, s_1, s_2$). What is to be done now is to test the hypothesis that both sample means ($\bar{x}_1, \bar{x}_2$) are the same. If the test fails, the means are statistically different (subject to a criterial level, i.e., at the 95% level), and if the test passes, the means are statistically the same. In other words, if the computed means are assumed to be the same (the hypothesis) and that their only difference is due to sampling variability, a test is performed to test whether the hypothesis is true or false. The mathematical formulation of the hypothesis is based on the true population parameters ($\mu$ = mean, $\sigma$ = standard deviation) of which the sample values are estimates ($\bar{x}_1$ estimates $\mu_1$, etc.). Thus the hypothesis that there is no jump and that sample statistics are derived from one population is

$$\mu_1 = \mu_2 = \mu \quad \text{and} \quad \sigma_1 = \sigma_2 = \sigma \quad . \tag{4.5}$$

The test for this hypothesis requires that all sample statistics be incorporated into one test statistic: the $t$ variable. Here,

$$t = \frac{\bar{x}_1 - \bar{x}_2}{\sigma_t \sqrt{\frac{1}{N_1} + \frac{1}{N_2}}} \quad ; \tag{4.6}$$

where $N_1$ is the subsample size of the data before the jump, $N_2$ is the subsample size after the jump, and $\sigma_t$ is the pooled variance compute with

$$\sigma_t = \sqrt{\frac{N_1 S_1^2 + N_2 S_2^2}{N_1 + N_2 - 2}} \quad . \tag{4.7}$$

The $t$ variable has special significance since its distribution is known (Student's t-distribution) and the distribution is only a function of the

number of degrees of freedom left in the data. The number of degrees of freedom (2) is equal to the sample size (N) minus the number of estimated population parameters, (k), $\nu = N-k$ . If a data set has N values, it has N degrees of freedom ($\nu = N$) as it is. When the mean is computed, by using the mean to represent the data there is one less degree of freedom ($\nu = N-1$). When the standard deviation is computed and used to represent the data, another degree of freedom is lost (one for using the mean to compute the standard deviation and one for using the standard deviation itself); thus $\nu = N-2$; and for the t statistic, $\nu = N_1 + N_2 - 2$ .

In order to use the t-statistic in a test format, the t-distribution must first be described. Figure 4.1 depicts the t-distribution with a value $t_p$ marked-off on the t-axis. The area under the entire curve is of course one. The area under the curve from $-\infty$ to $t_p$ is p, where $0 \leq p \leq 1$, and the area from $t_p$ to $+\infty$ is 1-p (or $\alpha$). Since the t-distribution is symmetric, $t_p = |-t_p|$. If the area under the curve between $-t_p$ to $t_p$ is p, each area outside of this is (1-p)/2, or the area from $-\infty$ to $-t_p$ = the area from $t_p$ to $\infty = \alpha/2$. These two concepts are important in the actual test, for what the test does is to compare Equation 4.6 to values of $t_p$. Depending upon how t compares to $t_p$ indicates acceptance or rejection of the hypothesis. There are two types of tests: a one-tailed test and a two-tailed test. The manner in which Equation 4.5 has set up the hypothesis is a two-tailed test. Here the test is to see if the two means are the same or not, and it implicitly assumes that it is not known whether the jump was an increase or a decrease. Thus t will be compared with $-t_p$ and $t_p$:

if $-t_p \leq t \leq t_p$ then the hypothesis is accepted ($\mu_1=\mu_2=\mu$);

if $|t| > t_p$ then the hypothesis is rejected ($\mu_1 \neq \mu_2$).

The power of the test is related to p. The usual values for p for strong testing are 0.95 to 0.99.

A stronger test, in the case of a suspected jump, is a one-tailed test. In the case of an increasing jump, the hypothesis can be set up the same as in Equation 4.5, but the acceptance or rejection of the hypothesis is simply:

## PERCENTILE VALUES ($t_p$)
## for
## STUDENT'S $t$ DISTRIBUTION
### with $\nu$ degrees of freedom
### (shaded area = $p$)

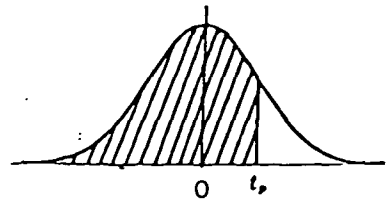


| $\nu$ | $t_{.995}$ | $t_{.99}$ | $t_{.975}$ | $t_{.95}$ | $t_{.90}$ | $t_{.80}$ | $t_{.75}$ | $t_{.70}$ | $t_{.60}$ | $t_{.55}$ |
|---|---|---|---|---|---|---|---|---|---|---|
| 1 | 63.66 | 31.82 | 12.71 | 6.31 | 3.08 | 1.376 | 1.000 | .727 | .325 | .158 |
| 2 | 9.92 | 6.96 | 4.30 | 2.92 | 1.89 | 1.061 | .816 | .617 | .289 | .142 |
| 3 | 5.84 | 4.54 | 3.18 | 2.35 | 1.64 | .978 | .765 | .584 | .277 | .137 |
| 4 | 4.60 | 3.75 | 2.78 | 2.13 | 1.53 | .941 | .741 | .569 | .271 | .134 |
| 5 | 4.03 | 3.36 | 2.57 | 2.02 | 1.48 | .920 | .727 | .559 | .267 | .132 |
| 6 | 3.71 | 3.14 | 2.45 | 1.94 | 1.44 | .906 | .718 | .553 | .265 | .131 |
| 7 | 3.50 | 3.00 | 2.36 | 1.90 | 1.42 | .896 | .711 | .549 | .263 | .130 |
| 8 | 3.36 | 2.90 | 2.31 | 1.86 | 1.40 | .889 | .706 | .546 | .262 | .130 |
| 9 | 3.25 | 2.82 | 2.26 | 1.83 | 1.38 | .883 | .703 | .543 | .261 | .129 |
| 10 | 3.17 | 2.76 | 2.23 | 1.81 | 1.37 | .879 | .700 | .542 | .260 | .129 |
| 11 | 3.11 | 2.72 | 2.20 | 1.80 | 1.36 | .876 | .697 | .540 | .260 | .129 |
| 12 | 3.06 | 2.68 | 2.18 | 1.78 | 1.36 | .873 | .695 | .539 | .259 | .128 |
| 13 | 3.01 | 2.65 | 2.16 | 1.77 | 1.35 | .870 | .694 | .538 | .259 | .128 |
| 14 | 2.98 | 2.62 | 2.14 | 1.76 | 1.34 | .868 | .692 | .537 | .258 | .128 |
| 15 | 2.95 | 2.60 | 2.13 | 1.75 | 1.34 | .866 | .691 | .536 | .258 | .128 |
| 16 | 2.92 | 2.58 | 2.12 | 1.75 | 1.34 | .865 | .690 | .535 | .258 | .128 |
| 17 | 2.90 | 2.57 | 2.11 | 1.74 | 1.33 | .863 | .689 | .534 | .257 | .128 |
| 18 | 2.88 | 2.55 | 2.10 | 1.73 | 1.33 | .862 | .688 | .534 | .257 | .127 |
| 19 | 2.86 | 2.54 | 2.09 | 1.73 | 1.33 | .861 | .688 | .533 | .257 | .127 |
| 20 | 2.84 | 2.53 | 2.09 | 1.72 | 1.32 | .860 | .687 | .533 | .257 | .127 |
| 21 | 2.83 | 2.52 | 2.08 | 1.72 | 1.32 | .859 | .686 | .532 | .257 | .127 |
| 22 | 2.82 | 2.51 | 2.07 | 1.72 | 1.32 | .858 | .686 | .532 | .256 | .127 |
| 23 | 2.81 | 2.50 | 2.07 | 1.71 | 1.32 | .858 | .685 | .532 | .256 | .127 |
| 24 | 2.80 | 2.49 | 2.06 | 1.71 | 1.32 | .857 | .685 | .531 | .256 | .127 |
| 25 | 2.79 | 2.48 | 2.06 | 1.71 | 1.32 | .856 | .684 | .531 | .256 | .127 |
| 26 | 2.78 | 2.48 | 2.06 | 1.71 | 1.32 | .856 | .684 | .531 | .256 | .127 |
| 27 | 2.77 | 2.47 | 2.05 | 1.70 | 1.31 | .855 | .684 | .531 | .256 | .127 |
| 28 | 2.76 | 2.47 | 2.05 | 1.70 | 1.31 | .855 | .683 | .530 | .256 | .127 |
| 29 | 2.76 | 2.46 | 2.04 | 1.70 | 1.31 | .854 | .683 | .530 | .256 | .127 |
| 30 | 2.75 | 2.46 | 2.04 | 1.70 | 1.31 | .854 | .683 | .530 | .256 | .127 |
| 40 | 2.70 | 2.42 | 2.02 | 1.68 | 1.30 | .851 | .681 | .529 | .255 | .126 |
| 60 | 2.66 | 2.39 | 2.00 | 1.67 | 1.30 | .848 | .679 | .527 | .254 | .126 |
| 120 | 2.62 | 2.36 | 1.98 | 1.66 | 1.29 | .845 | .677 | .526 | .254 | .126 |
| $\infty$ | 2.58 | 2.33 | 1.96 | 1.645 | 1.28 | .842 | .674 | .524 | .253 | .126 |

Figure 4.1. Percentile values ($t_p$) for student's $t$ distribution with $\nu$ degrees of freedom (shaded area = $p$).

if $t \geq -t_p$ then the hypothesis is accepted ($\mu_1=\mu_2=\mu$);

if $t < -t_p$ then the hypothesis is rejected ($\mu_1 \neq \mu_2$, in fact, $\mu_1 < \mu_2$).

Again, this decision structure is based upon an increasing jump (a decrease jump would test with $t_p$ and reject with $t > t_p$) and what is then being tested is not simply $\mu_1 \neq \mu_2$ but $\mu_1 < \mu_2$. This is because Equation 4.6 will yield a negative value of t since it is already known that $\bar{x}_1 < \bar{x}_2$ (increase jump).

To find the $t_p$ value, Figure 4.1 is used with the knowledge of the number of degrees of freedom. For the one-tailed test, $t_p$ is simply found by finding the column of the desired $t_p$ value ($t_p = t_{.95}$ for a 95% test, etc.) and then locating the row with the correct $\nu$. For example, for a one-tailed test at the 95% level and $\nu = 20$, $t_p = t_{0.95} = 1.72$. The two-tailed test requires a little manipulation in order to use the table in Figure 4.1. In this case, since there is an $\alpha/2$ rejection region at either tail of the t distribution, the desired $t_p$ value is found by looking under the column heading of $t_{p+\alpha/2}$. For example, in a two-tailed test at the 95% level with $\nu = 10$, $\alpha = 0.05$ (and thus $\alpha/2 = 0.025$), since $p = 0.95$, $p + \alpha/2 = 0.975$ and the $t_p$ value for testing is found in the $t_p = t_{0.975}$ column (here $t_{0.975} = 2.23$). Thus, the two-tailed test in this case is whether or not $-2.23 \leq t \leq 2.23$.

An example of t testing for the detection of a jump is presented here. Monthly evaporation from April through October has been recorded at the Bonny Lake gage since 1949. The original type of recording instrument was the standard USWB 4-foot diameter sunken pan. From 1965 through 1976, the measuring device was a sunken 3-foot diameter pan which was painted black. The location of the Bonny Lake gage is in northeast Colorado (Figure 4.2). The time series of the monthly pan evaporation data is found in Figure 4.3, and it appears that either regional evaporation has decreased sometime near when the gage was changed or the change in the gage technique affected the data collection. Comparing the Bonny data with long-term average regional evaporation values (2) revealed that there was no significant deviations from the long-term monthly means. After the instrument change, the running mean in Figure 4.3 decreased and started to level off in 1971. The records at the nearby Enders Dam gage (Figure 4.4) show that during this time, evaporation showed a slight decrease. This decrease is not found in the data of the nearby Tribune 1W

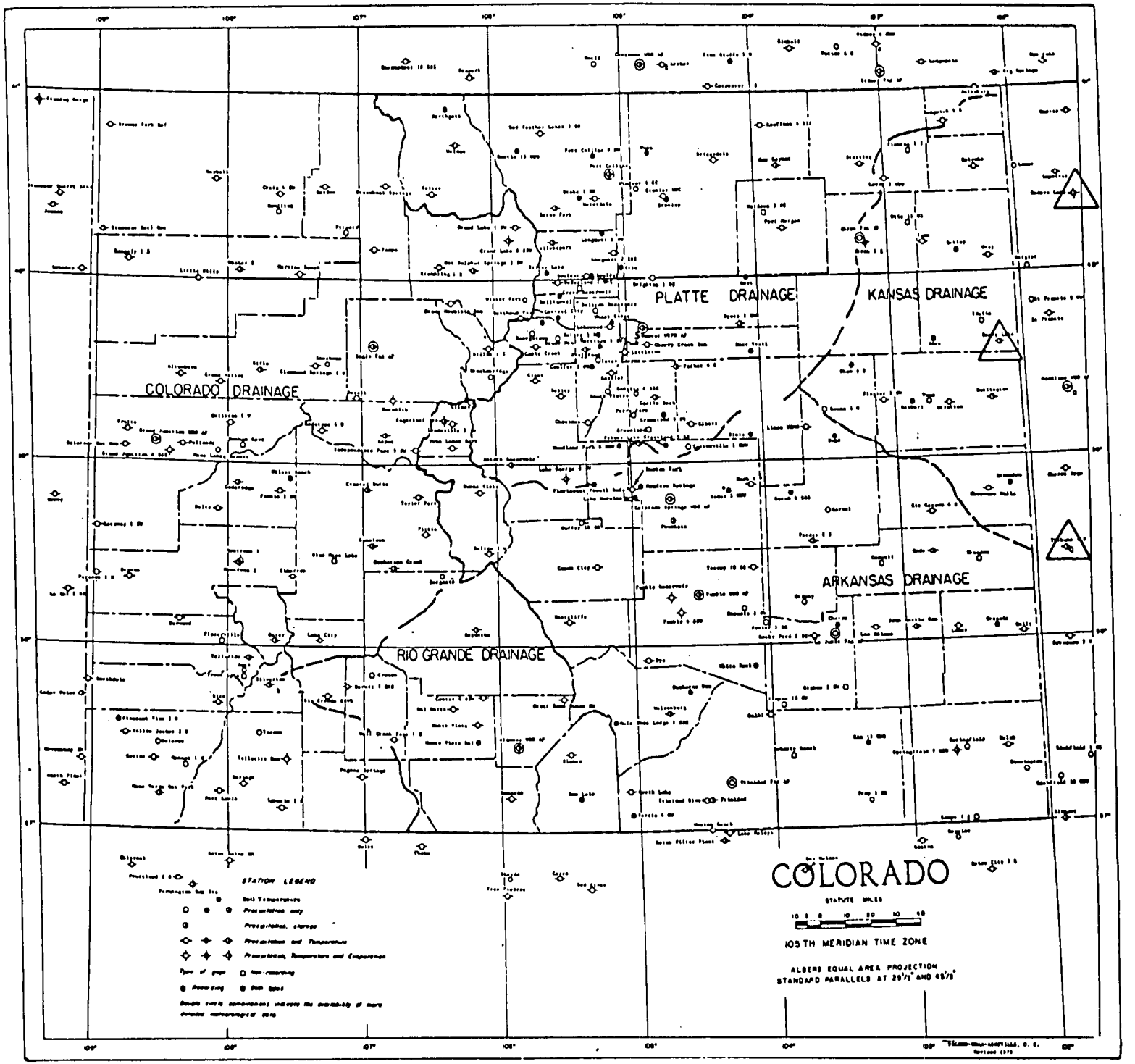
PLATTE DRAINAGE
KANSAS DRAINAGE
COLORADO DRAINAGE
ARKANSAS DRAINAGE
RIO GRANDE DRAINAGE
COLORADO
STATUTE MILES
105TH MERIDIAN TIME ZONE
ALBERS EQUAL AREA PROJECTION
STANDARD PARALLELS AT 29 1/2° AND 45 1/2°
STATION LEGEND

Figure 4.2.

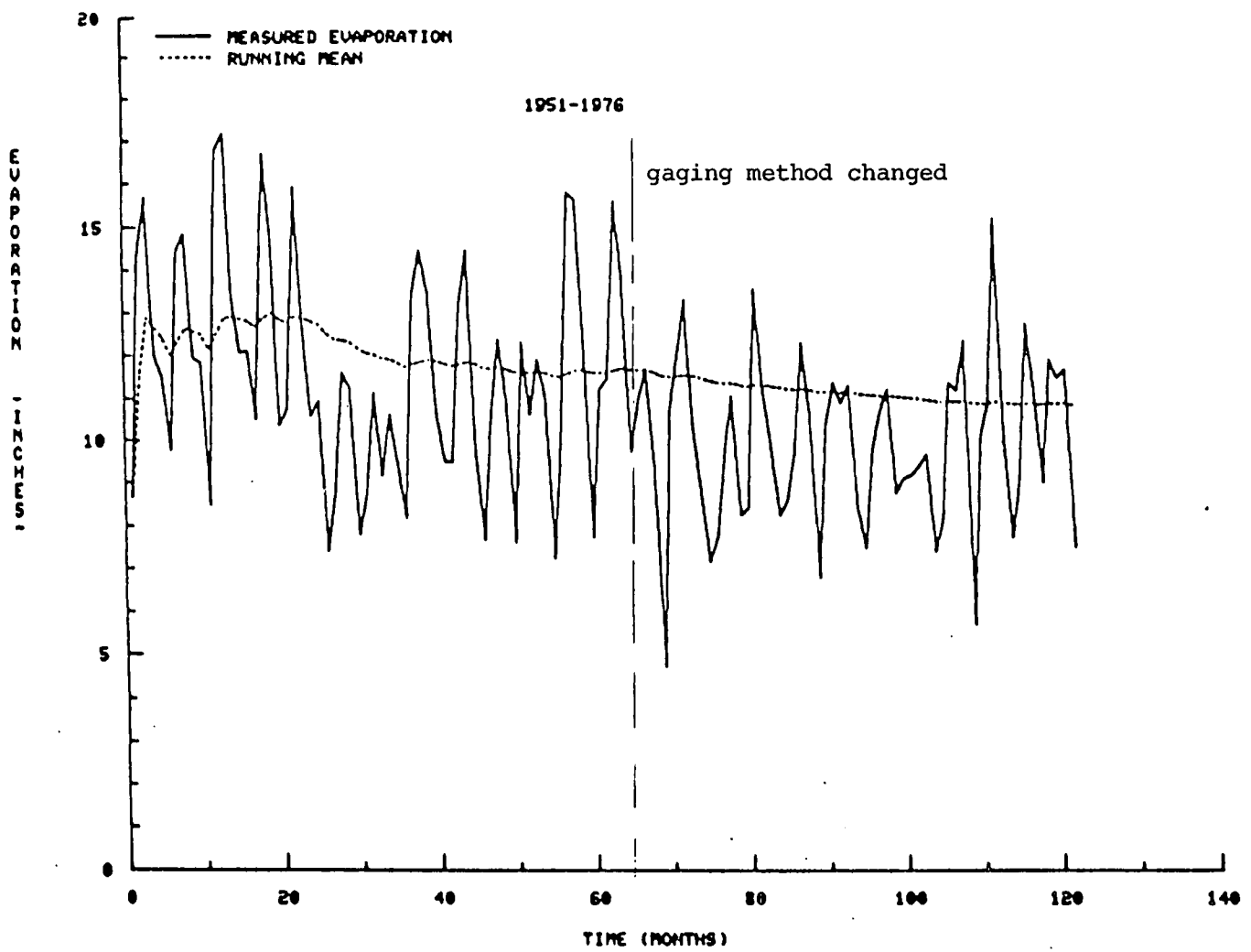


Figure 4.3. Bonny Dam evaporation series.

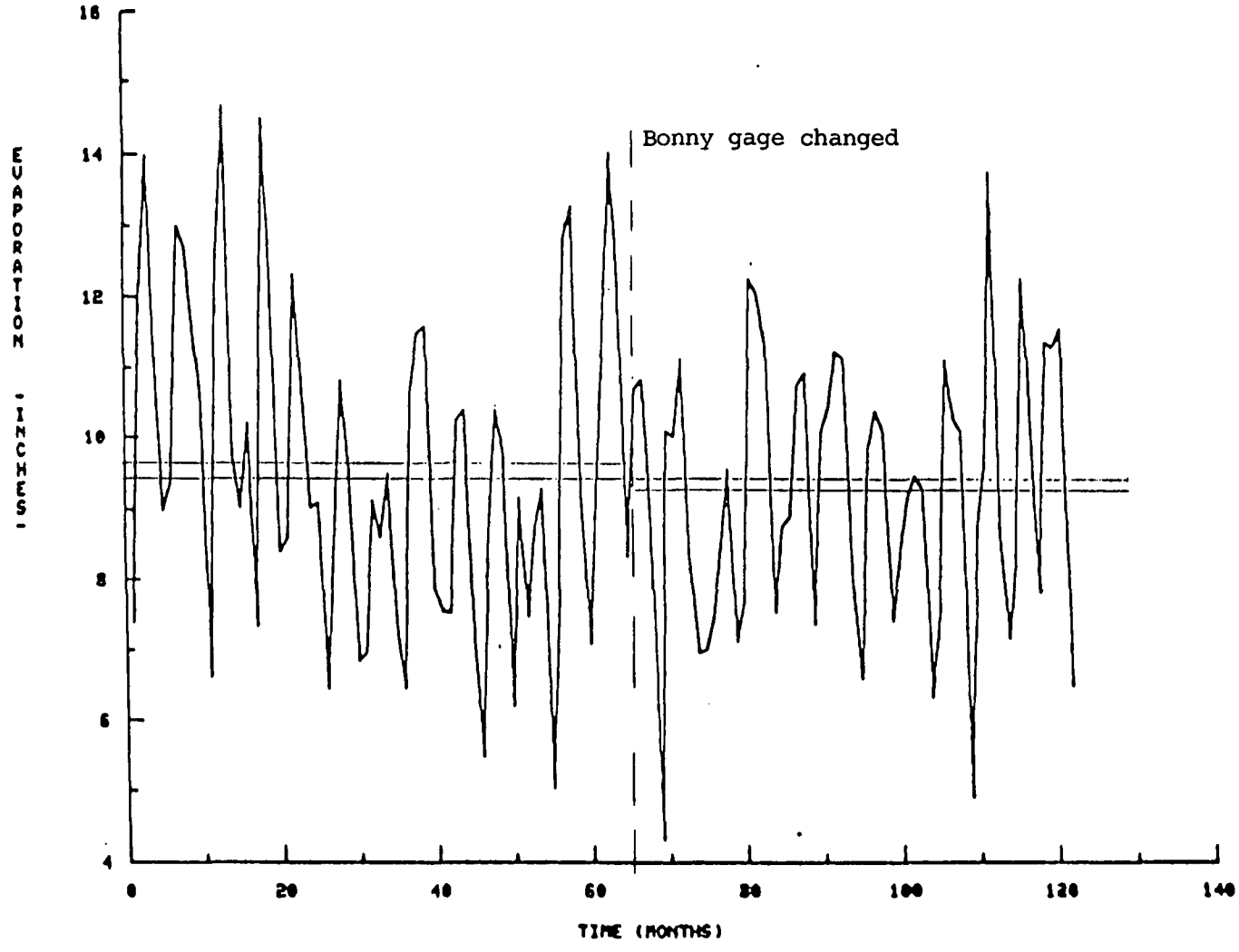


Figure 4.4. Pan evaporation for the Enders Dam gage during the growing season.

gage (Figure 4.5). Thus, with evidence from nearby gages that there was no significant decrease in evaporation, the Bonny Lake gage shows a decrease jump during the time after the monitoring equipment was changed. A one-tailed test was then performed on the two subsamples of before and after the gage change. The two means of each data subset are found plotted in Figure 4.6. Calculations for the one-tailed test are found on below.

Bonny Lake Evaporation Test for a Data Jump

| | Mean | Standard Deviation | Sample Size |
|---|---|---|---|
| Before Change | 11.63 | 2.58 | 65 |
| After Change | 9.93 | 1.96 | 57 |

$\sigma_t = 2.330$ and $t = 4.02$

$t_{0.99} = 2.36$

since $t = 4.02 > t_{0.99} = 2.36$ the means are statistically different at the 99% level.

This test means that the data before and after the change are essentially from two different populations and thus the data set is inhomogeneous.

Since the Enders Dam gage also showed a small decrease jump during the same time, this data set was tested simlarly to the Bonny Lake data in order to see if the decrease might be some type of regional trend:

| | Mean | Standard Deviation | Sample Size |
|---|---|---|---|
| Before Change | 9.62 | 2.30 | 65 |
| After Change | 9.24 | 1.93 | 57 |

$\sigma_t = 2.153$ $t = 0.973$ $t_{0.99} = 2.36$

since $t = 0.973 < t_{0.99} = 2.36$ the means are statistically the the same at the 99% level.

The conclusion is that the Bonny Lake evaporation data is not a homogeneous set due to the change in the measuring device in 1965. The decrease jump in the Bonny data was also found to not be due to a regional decrease in evaporation.

Another way to show that there was no regional decrease in evaporation after 1965 is to plot the concurrent data of the Bonny gage against that of a nearby gage. If there were a regional factor causing lower evaporation, the

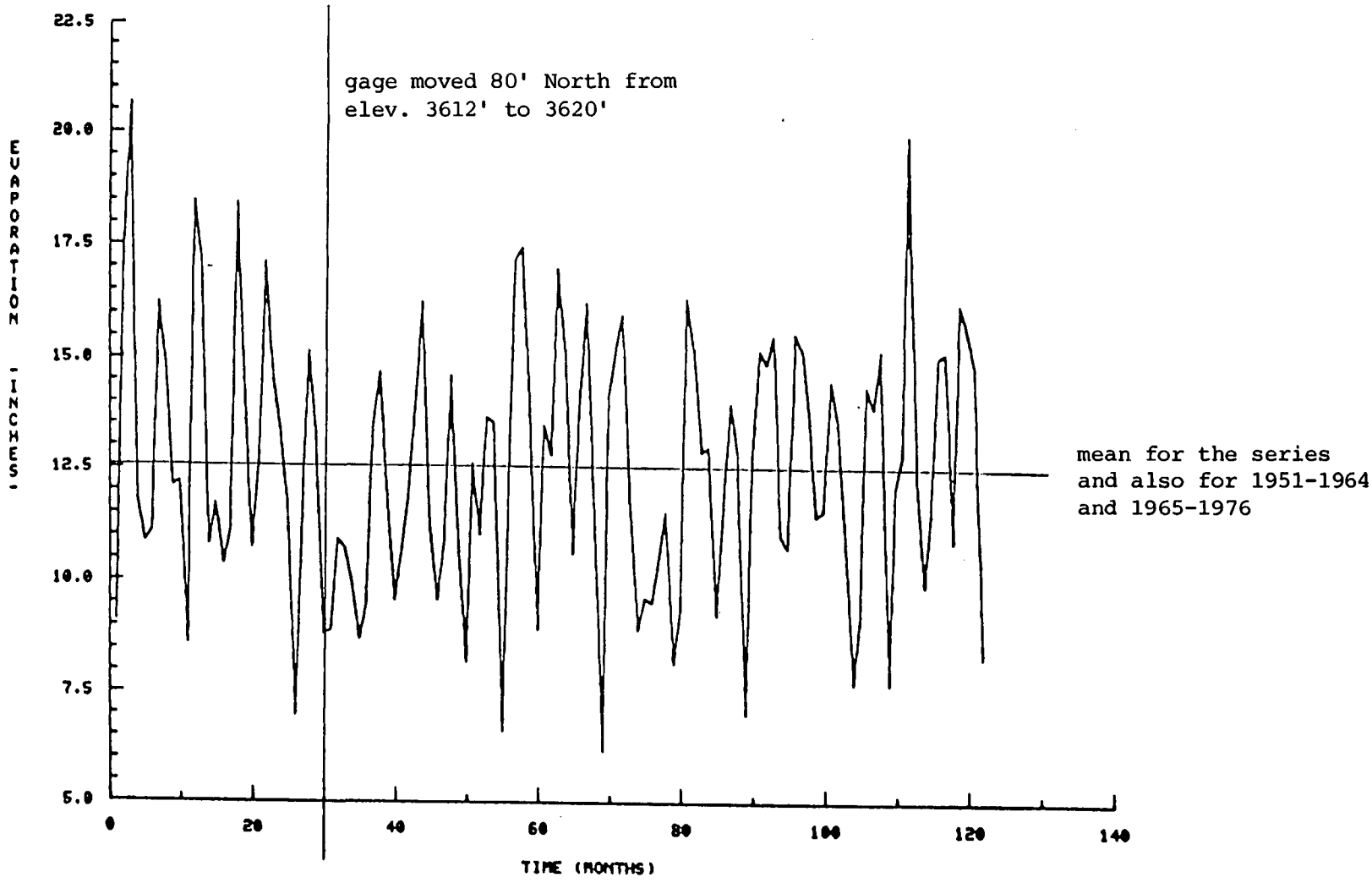


Figure 4.5. Pan evaporation for the tribune 1W gage during the growing season.

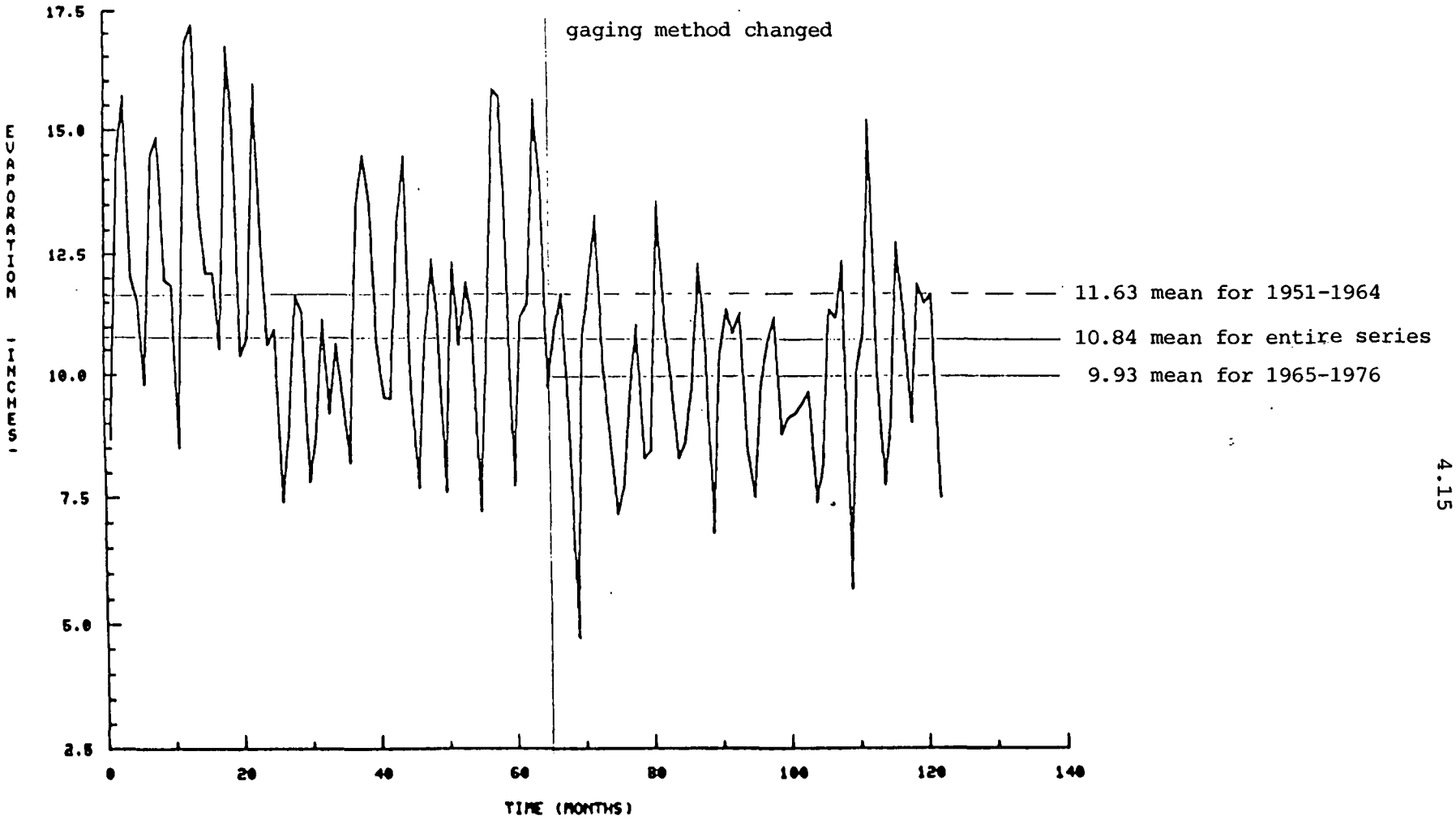


Figure 4.6. Pan evaporation for the Bonny Dam gage during the growing season.

points of this plot will be randomly scattered about a regression line through all of the data. If there is no regional factor for the evaporation decrease and the decrease was only due to the change of the Bonny gage, then data about a regression line will be partitioned into two sets: most points above the regression line will be from before the change and most points below the regression line will be after the change. This partitioning results from the fact that the Bonny gage will have a lower evaporation value for a post-change value of the Enders or Tribune gages than a pre-change value. This effect can be observed in Figure 4.7 for the Bonny Lake and Tribune 1W data. More evidence of the partitioning is found in the coefficient of determination ($R^2$) for all data compared to $R^2$ values for each data subset (Table 4.1).

The t test is one of the best methods to test the significance of a jump. It is based on sampling theory and gives a level of accuracy of the test itself.

There are many ways to detect a jump and they are: plotting of the data, computation and plotting of the running mean, interstation plots (such as Figure 4.7), knowledge of the movement of a gage or change in the gaging method. Another general method to detect jumps is the double mass analysis, and this method will be presented in the next section, dealing with trends.

#### 4.3.2.3 Detection of Trends

A trend in a process (see Figure 3.7b of the last lecture) is found in the systematic and continuous change over an entire sample of that process. This produces a systematic and continuous change in the estimated parameters of that process. The trend can be viewed as an added deterministic (predictable) component in any hydrologic process, i.e., the increase in water demand through time due to population growth can be predicted, but exact values cannot be predicted due to random variations. The effects of trends on sample statistics was discussed in Section 2.4.2 of the last lecture.

A simple qualitative method to detect trends is to plot the time series, its overall mean, and its running mean. A series with a quantity trend will have a running mean which continuously changes in a consistant manner (i.e., always increasing, etc.). There are trends in which the mean can stay constant yet the standard deviation changes. There will be no crossing-over of the running and overall means (except for the first three of four values) with a quantity trend in the data. The trend causing a change in the mean

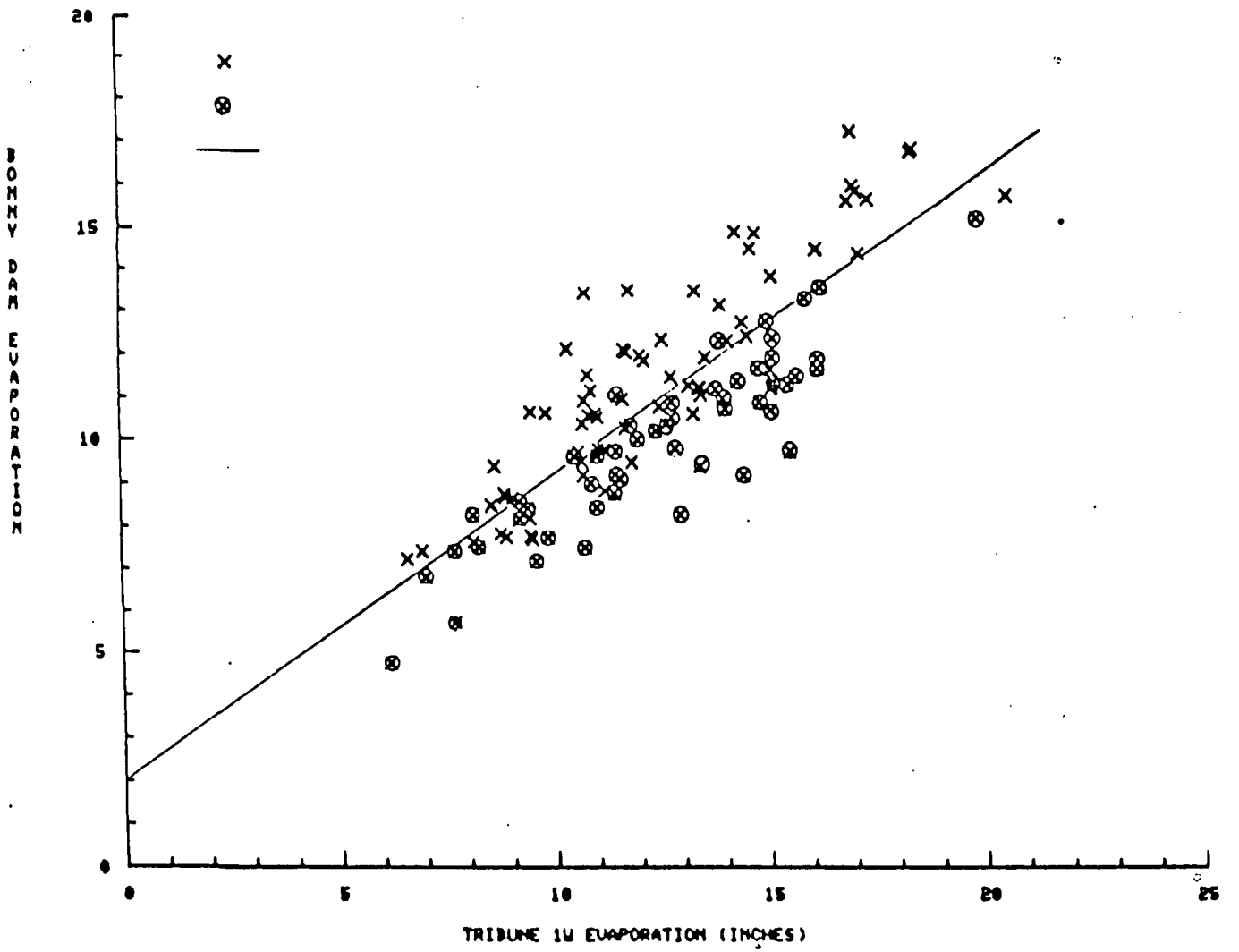


Figure 4.7. Regression of Bonny Dam evaporation on tribune 1W evaporation.

Table 4.1. Linear Regression Equations and Coefficients of Determination ($R^2$) for the Data of Figure 4.7 [Bonny Evaporation = $a_0 + a_1$ (Tribune 1W Evaporation)]

| | $a_0$ | $a_1$ | $R^2$ |
|---|---|---|---|
| All Data (1951 - 1976) | 2.01 | 0.70 | 0.707 |
| Before Bonny Gage Change (1951 - 1964) | 1.95 | 0.77 | 0.816 |
| After Bonny Gage Change (1965-1976) | 2.18 | 0.62 | 0.812 |

will be exclusively analyzed from this point on. The implication of the trend by plotting the mean should be verified by an inspection of the causal factors which could produce such data. If the trend is due to measurement errors, a trend in the process does not truly exist. It is not altogether uncommon for hydrologic processes to have trends. A more quantitative method to assess the degree of a trend is the use of the doublemass analysis.

The doublemass analysis (DMA) essentially assesses interstation relationships in order to detect data inhomogeneities at one station. This is done by computing and then plotting the cumulative value of data through time for the station in question versus a group of nearby or strongly correlated stations. If there were no data inhomogeneities, the plot would be fairly linear (some scatter may exist due to the variaiblity of most hydrologic processes), see Figure 4.8a. If there was an isolated data inhomogeneity (i.e., the reporting of a very large rainfall at only one station, on one day), there would be a noticeable jump in the relationship between the one station and the group of stations (Figure 4.8b). If there were many isolated inhomogeneities, the DMA may not actually indicate an inhomogeneous data set, but rather imply poor correlation between the gage in question and the group of gages (Figure 4.8c). In the case of a data jump, the DMA will show two distinct lines which intersect at the point in time when the jump began (Figure 4.8d). Finally, for a trend, the DMA will show a progressive movement away from the linear relationship (Figure 4.8e).

The major drawback to the doublemass analysis is that there is no test of significance associated with it. Weiss and Wilson (1953) use an analysis of variance technique to discern whether or not slope changes from a DMA are significant or simply due to chance. This method would require severe slope changes to detect a trend or jump with only one or two points, and this may not be true with most trends.

Once a trend is discovered in data, the physical process and its causal factors should be analyzed in order to ascertain whether or not the trend is physially based (i.e., watershed management causing slow decrease of sediment dishcarge, tree growing near a precipitation gage causing a decrease in precipitation records, surface mining within the watershed causing gradual river pH changes, etc.). The trend may be tested by partitioning the data set into three groups: Zone I, unaffected, homogeneous data subset; Zone II, transition data subset; Zone III, subset of obvious trend (Figure 4.9). With this

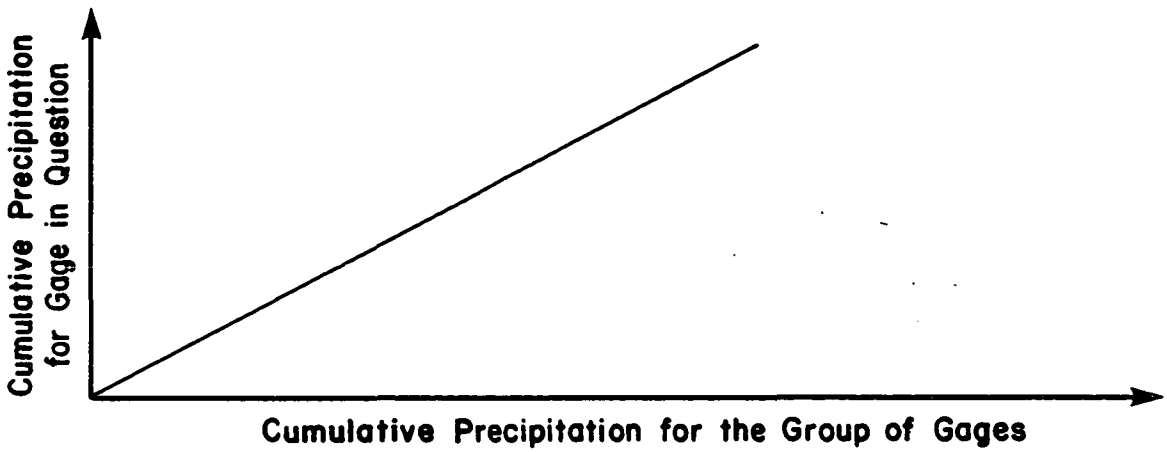


Figure 4.8a. Double mass curve for well correlated stations indicating homogeneous data sets.

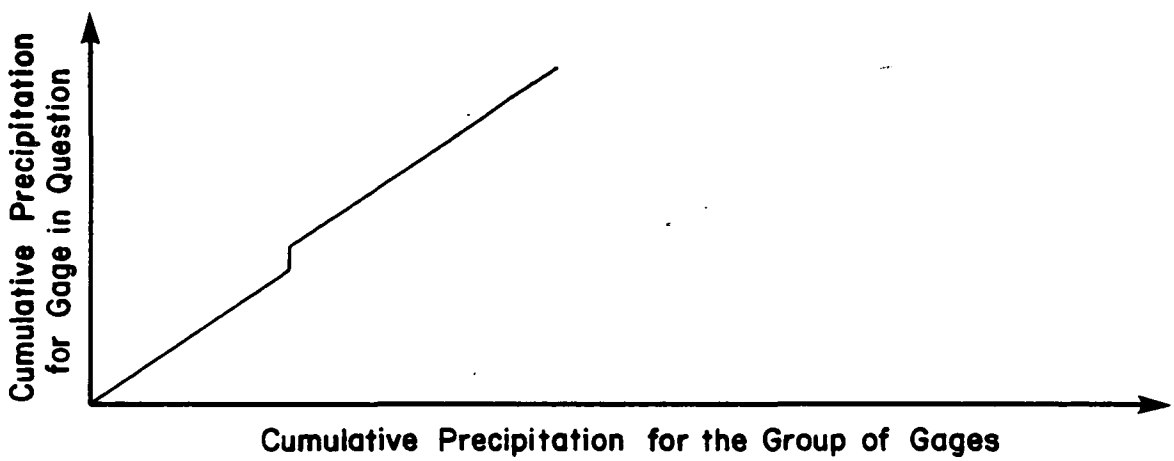


Figure 4.8b. Double mass analysis indicating an isolated inhomogeneity.

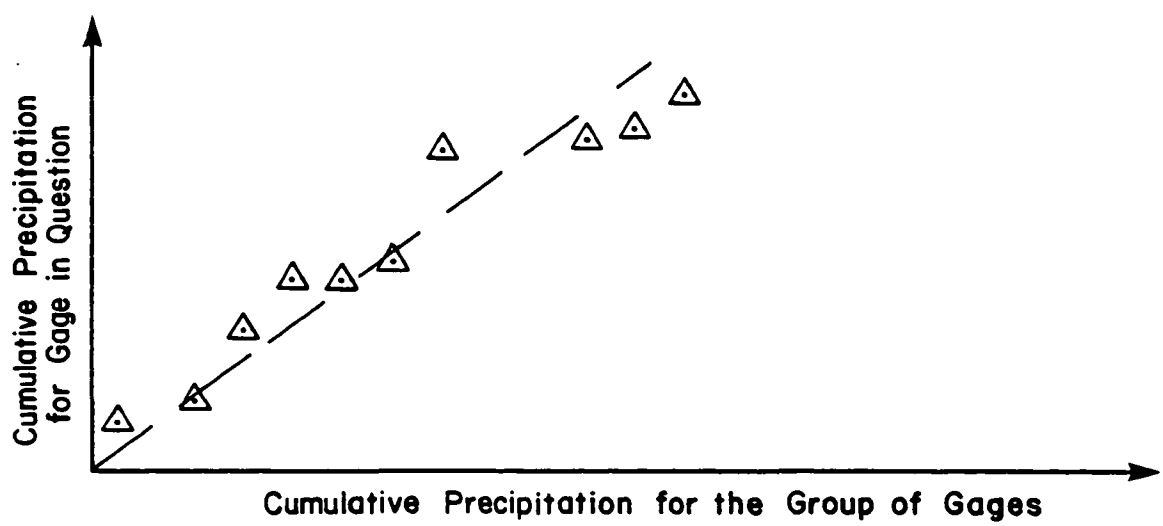


Figure 4.8c. Double mass analysis indicating poorly correlated stations.

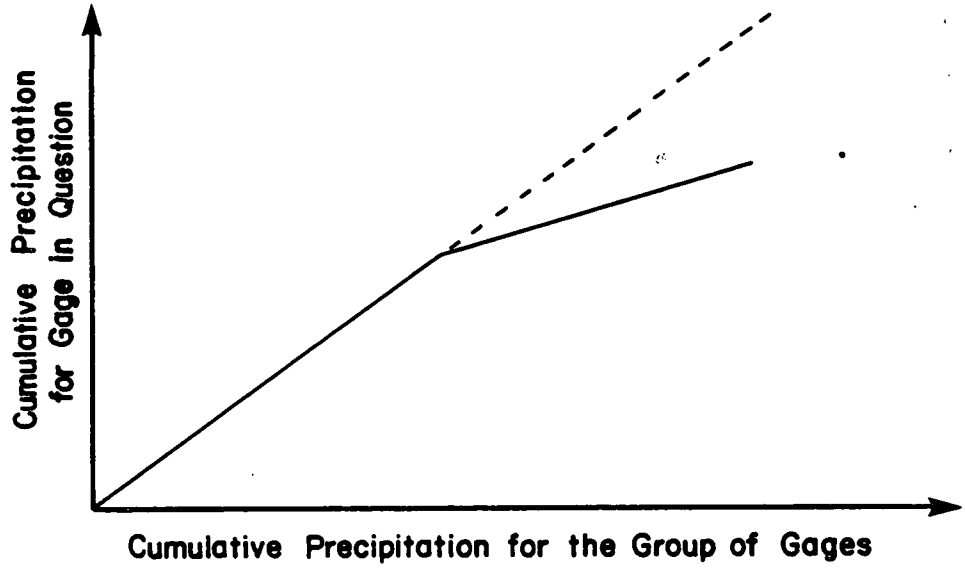


Figure 4.8d. Double mass analysis indicating a jump.

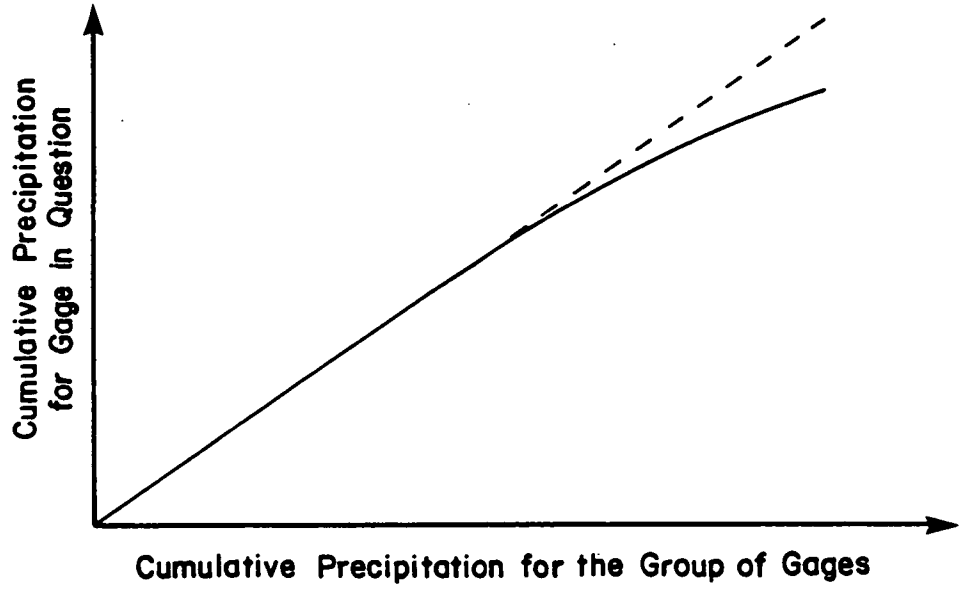


Figure 4.8e. Double mass analysis indicating a trend.

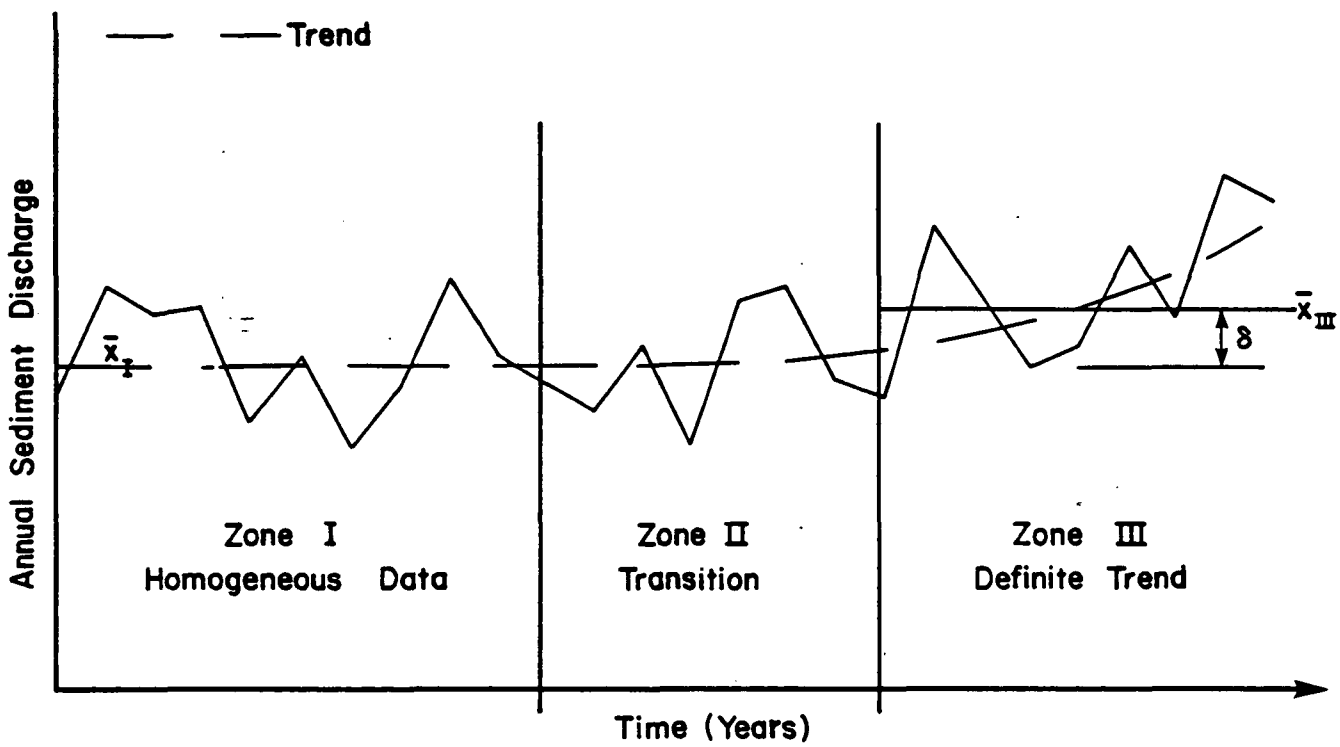


Figure 4.9. Triple partition of a data set for testing of a trend.

partitioning, the data sets before and after the transition region can be tested as a jump would be tested. It must be emphasized that there should be at least ten points in the trend and unaffected series, otherwise the $t_p$ values will be very large, thus producing tests which cannot significantly detect statistical differences due to too little data.

## 4.4 Correction of Data Inhomogeneities

### 4.4.1 Introduction

Data inhomogeneities may be corrected by various techniques. Any specific technique selected for correction of data inhomogeneities is a function of the type of inhomogeneity, the data available and the availability of physical process models. If it is known that an isolated data inhomogeneity is due to simple recording error (i.e., reading water stage as 13.72 feet and reporting it as 3.72 feet), the correction procedure may be quite obvious, especially if the values from previous and successive observations were all consistently below or above the suspected observation and there is a large memory in the process. If a stream gage were knocked out during a flood event, it would be possible to estimate the flood hydrograph with a watershed model, or backing into the flood peak with information on the high-water marks and use of a slope-area backwater technique. In the absence of a physical process model, data may be estimated with the aid of data from a nearby station that has high interstation correlation with the knocked out gage. The methods for correction of an inhomogeneous data set are presented in this chapter.

### 4.4.2 Filling of Missing Data

Data gaps represent a specific type of data inhomogeneity in which data for certain time periods is missing from the data set. Physical process models can fill data gaps by modeling the causal factors of a process. Knowledge of system inputs and use of the physical process model allow a reproduction of data points surrounding the data gap as well as points in the gap itself. For example, if a flood hydrograph was not recorded, a watershed model can be run with knowledge of antecedent storm conditions (baseflow, antecedent moisture, etc.), watershed pre-storm physical characteristics (vegetative cover, impervious area, soil type, etc.), and the rainfall hyetograph in order to reproduce the flood hdyrograph. When the data required for the physical process model is unavailable or gaps also exist in the input

data (i.e., malfunctioning rain gage, etc.), reasonable estimates must be made for the input data, or it may be possible to use statistical methods to fill these data gaps. Physical process modeling is to be covered in the next two lectures.

With strong interstation correlation, it is possible to transfer the information from other gages to fill data gaps. This is very similar to regression relationships. Here, an analysis is performed between one or more variables to find the relationship between the variables (i.e., linear relationship between nearby raingages, power function relationship between water and sediment discharges, etc.). This regression relationship allows prediction of one variable by the other variable(s) in the regression relationship; thus when data for one variable are missing, the regression relationship is used to predict the missing data. Regression with one independent variable will be treated here. Descriptions and examples of the use of multiple regression can be found in any of the many books on regression, such as Reference 4.

Regression analysis produces the statistical relation between two variables. Unlike a functional relation (i.e., $y = 3x + 5$), the statistical relation is not perfect. The statistical relation has a functional part and a random part (i.e., $y = 2x + 1 + \varepsilon$, where $(2x + 5)$ is the functional (deterministic) part and $\varepsilon$ is the random part). A regression analysis finds the best fitting functional part and the random part is described by the degree of correlation (coefficient of determination - $R^2$) between the two variables in the analysis. If the functional part is very strong compared to the random part, a high correlation exists. If the random part is much larger than the functional part, a very low correlation exists. A special note here is that if the functional part is strong, yet the form of the regression relationship is improperly chosen, the correlation will be very low. A classic example is trying to fit the data from a perfect circle by a linear regression relation, in this case the correlation is zero because the data were fitted by an equation of the form $y = a_0 + a_1 x$ ($a_0$ and $a_1$ are constants) instead of the equation $y^2 = a_1 - x^2$. An aid to picking the correct regression relation is to either physically analyze what the relation should be (i.e., the relation between two nearby precipitation gages should be linear since meteorologic events usually cover an area in a uniform fashion; theoretically sediment discharge is a function of velocity to some power,

therefore a power function for sediment discharge versus water discharge is expected) or to plot the data and see what type of graphical transformation (i.e., plotting on log paper, etc.) best linearizes the data.

The linear regression function for the dependent variable $y$ regressed on the independent variable $x$ is:

$$y_i = a_0 + a_1 x_i + \varepsilon_i \tag{4.8}$$

where $a_0$ and $a_1$ are constants and $\varepsilon$ is a random error term which is independent and normally distributed with mean zero and variance of $\sigma_\varepsilon^2$ which is equal to the variance of $y$ (reference 4, page 31). Figure 4.10 describes the significance of each term in Equation 4.8. The estimates of $a_0$ and $a_1$ are

$$a_1 = \frac{\sum_{i=1}^{N} x_i y_i - \frac{\sum_{i=1}^{N} x_i \sum_{i=1}^{N} y_i}{N}}{\sum_{i=1}^{N} x_i^2 - \frac{\sum_{i=1}^{N} x_i^2}{N}} \tag{4.9}$$

$$a_0 = \frac{1}{N} \left( \sum_{i=1}^{N} y_i - a_i \sum_{i=1}^{N} x_i \right) \tag{4.10}$$

where $N$ is the total number of data points. The use of the linear regression equation as a predictor takes the form

$$\hat{y}_i = a_0 + a_1 x_i \tag{4.11}$$

where $\hat{y}_i$ is the predicted value of $y$ at time period $i$ given the observed value of $x_i$. The measure of the goodness of fit of a regression relation is the coefficient of determination $R^2$. $R^2$ is a ratio of the explained variation (by the regression equation) to the total variation (variation of $y$ to its own mean). If every data point were to be exactly predicted by the regression equation, the explained variation would be equal to the total variation and $R^2$ would equal unity (in this case the unexplained variance is zero). $R^2$ is computed by Equation 4.12.

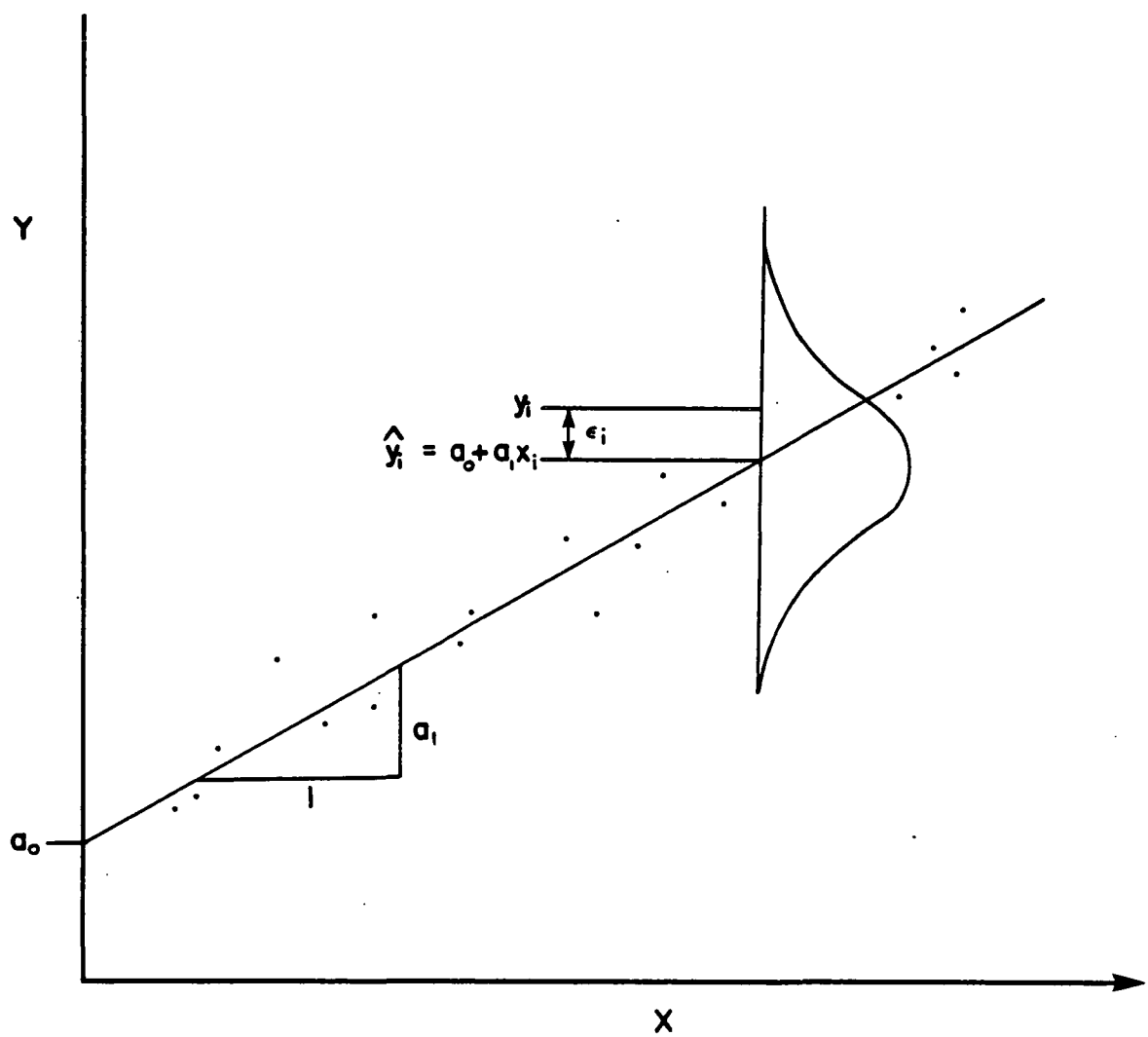


Figure 4.10. Example of a linear regression fit to data ($\hat{y}_i = a_o + a_1 x_i$) and the actual scatter of the data about the regression line.

$$R^2 = \frac{\sum_{i=1}^{N} \left(\hat{y}_i - \frac{\sum_{i=1}^{N} y_i}{N}\right)^2}{\sum_{i=1}^{N} \left(y_i - \frac{\sum_{i=1}^{N} y_i}{N}\right)^2} \qquad (4.12)$$

An example of the use of linear regression between two stations was presented in Section B.2 for the Bonny Lake and Tribune 1W evaporation gages (Table 4.1, Figure 4.7).

Other forms of nonlinear regression relations may be found in books covering the regression topic.

### 4.4.3. Measurement or Recording Errors

If a measurement or recording error has been determined as an inhomogeneity in a data set (i.e., 20 inches of rain on a cloudless day), the inhomogeneity may be adjusted with the knowledge of how the error might have been made, or the inhomogeneity may simply be treated as a data gap.

Knowledge of how the error was made can be obtained by checking back with the original records or by analyzing the values of correlated variables during that time (i.e., a discharge of 19,700 cfs at a time when river stage was not above bankfull, a stage that allows only 2000 cfs, indicates that the actual discharge may have been 1970 cfs; the complete hydrograph should be plotted to verify the correct value though).

If the data homogeneity is treated as a data gap, a physical process model or a regression relationship may be able to fill the gap.

### 4.4.4 Jumps

The effect of a jump is to essentially be monitoring two different processes. What is needed is to extract information from the data set in spite of the jump. The treatment of data, in light of a data jump, is based upon the specific objective of the monitoring network. For example, if a monitoring network is to detect water quality criteria violations, the jump may have resulted from better treatment practices, but the data set need not be changed in any way to account for the jump. Contrary to this, if a river discharge data set showed an increased jump and the data were to be used for the design of a flood control project, use of the entire data set can lead to

significant underdesign. In this last example, the easiest method to correct for the data inhomogeneity is to neglect the first part of the data. In such a case, though, the information contained within the pre-jump data is discarded and this results in a design on less data, resulting in hydraulic structures with less reliability in regulating the system. Thus, in the case of jumps, the information contained in the entire data set is very useful in satisfying design objectives. The abstraction of the information from an inhomogeneous data set is performed by first converting the data set to homogeneous form.

As with measurement and recording errors, data jumps may be handled by treating the unrepresentative portion of the data as a data gap. In this case, the data gap may be filled by a physical process model or by regression relations. The physical process model can be calibrated on the representative data subset, and then reproduce data for the unrepresentative data subset with knowledge of the input parameters during that time. For regression relations, it would probably be best to use the form of the regression equation which includes the random component term (i.e., Equation 4.8) and then to generate many equally likely traces of the missing data. In this manner, structures can be designed in a probabilistic framework.

The last form of correction of data inhomogeneity due to a jump is to transform the unrepresentative data subset to conform to the representative subset. This is done by reducing the unrepresentative data to just its random part by removing the deterministic components. This is termed standardizing the data. The most common form of standardization is to subtract the mean from each value in a data set and then divide these values by the standard deviation (Equation 4.13):

$$\xi_i = \frac{x_i - \bar{x}}{s_x} \tag{4.13}$$

where $\xi_i$ is the residuals which are usually normally distributed with mean zero and variance of one. For a jump, the mean and standard deviation are computed for each subset (before and after the jump). The residuals from the unrepresentative subset are then multiplied by the standard deviation of the representative subset and added to the representative subset mean. Now the entire data set is in homogeneous form. This method is presented in the

following example.

The evaporation data for the Bonny Reservoir gage (1952-1976) has been determined to have a jump (1965-1976) due to the change in the type of gage (III-B-2). The post-jump data (1965-1976) yield lower evaporation readings than the pre-jump data (1952-1964) and the post-jump data are the unrepresentative data subset since the common USWB sunken pan was not used during this time. The subset statistics for pre- and post-jump data are presented in Table 4.2, and these statistics were used to standardize the post-jump data and then transform it to a form more homogeneous to that of the pre-jump data. The two time series are then plotted in Figure 4.11. Statistics of the entire data sets (before and after correction for the jump) are found in Table 4.3. This type of reconstructed record can be used to check the results of a physical process model.

### 4.4.5 Trends

Once a trend has been identified, the part of the data which is affected by the trend can be deleted and then this period may be treated as a data gap (just as the jump was). Thus, physical process or regression models may be employed to fill this gap.

It is possible to treat all of the data as one homogeneous set when the trend is removed. This is done by recognizing the trend as a deterministic component in the time series (Equation 4.14):

$$x_i = T_x + D_x + E_i \tag{4.14}$$

where $x_i$ is the value of the stochastic process at time $i$, $T_x$ is the trend in $x$ (constant increase, nonlinear change, etc.), $D_x$ is the deterministic part of $x$ (seasonal mean, annual mean, etc.), and $E$ is the random component for time period $i$. With Figure 4.9 in mind, it is easy to see that for a homogeneous data set $T_x = 0$. This is also true for the part of the data set unaffected by the trend. Thus, an inhomogeneous data set caused by a trend can be made homogeneous by simply removing the trend component from the part of the data which owns the trend.

## 4.5 References

Linsley, R. K. Jr., M. A. Kohler and J. L. H. Paulhus, 1975, Hydrology for Engineers, Second Edition, McGraw-Hill Book Company, New York, New York, page 173.

Table 4.2. Historic Statistics for the Bonny Reservoir Evaporation Time Series

| | $\bar{x}$ | s |
|---|---|---|
| All data (1951 - 1976) | 10.84 | 2.46 |
| Before (1949 - 1964) Jump | 11.63 | 2.58 |
| After (1965 - 1976) Jump | 9.93 | 1.96 |

Table 4.3. Comparative Statistics for the Bonny Reservoir Evaporation Time Series When Correcting for Data Inhomogeneity

| | $\bar{x}$ | s |
|---|---|---|
| All data (inhomogeneous set) | 10.84 | 2.46 |
| All data (homogeneous set) | 11.63 | 2.57 |

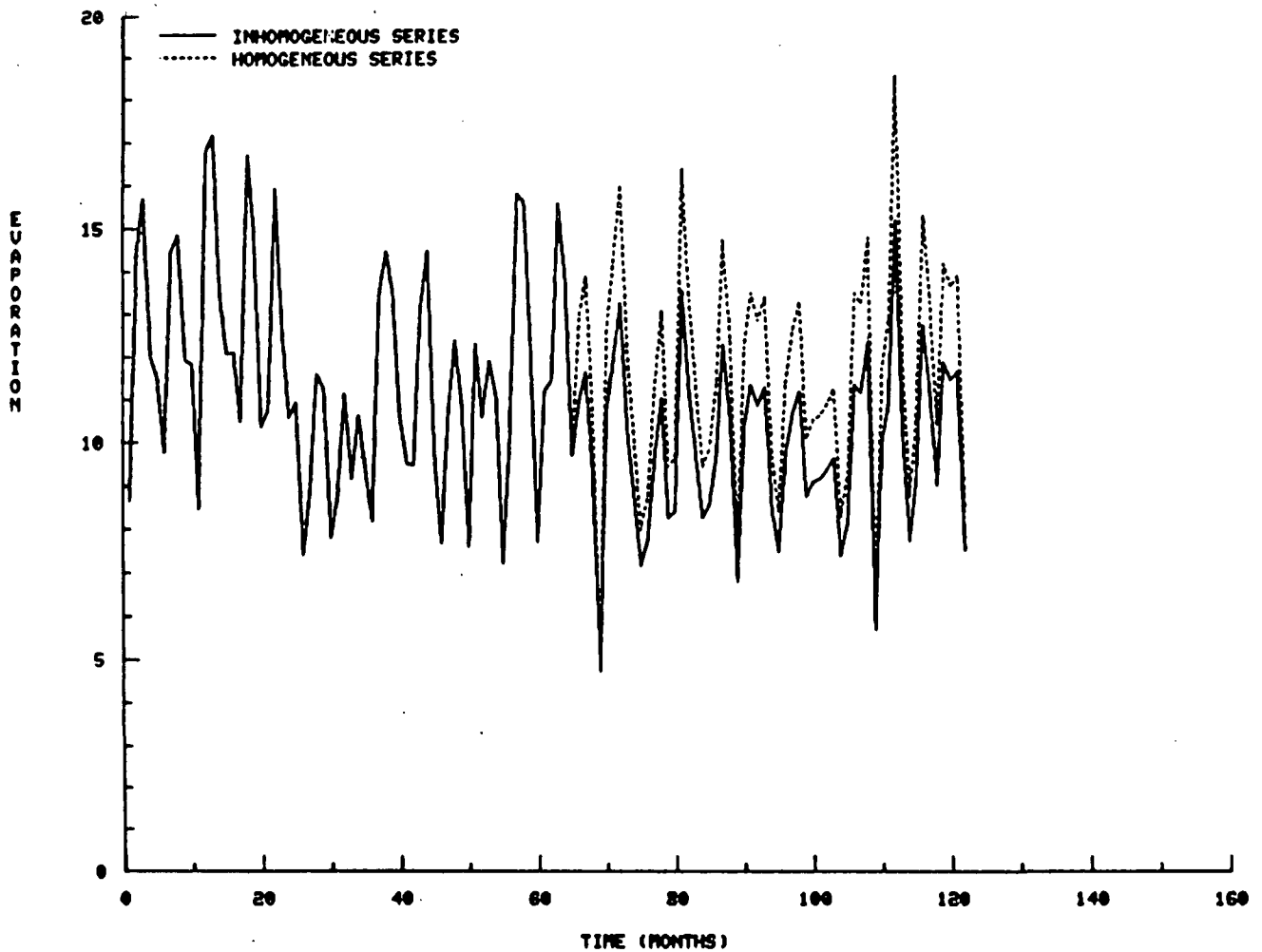


Figure 4.11. Evaporation (in.) series for Bonny Reservoir 1952-1976 (Apr-Sep).

Meyer, A. P., 1942, Evaporation from Lakes and Reservoirs, Minnesota Water Resources Commission, St. Paul, Minn., June.

Neter, J., and W. Wasserman, 1974, Appleid Linear Statistical Models, Richard D. Irwin, Inc., Homewood, Illinois.

Weiss, L. L., and W. T. Wilson, 1953, "Evaluation of Slope Changes in Double-Mass Curves," Transactions of the American Geophysical Union, Volume 34, No. G, December, pages 893-896.

# V. PHYSICAL PROCESS SIMULATION: I. WATER AND SEDIMENT ROUTING

## 5.1 Introduction

A variety of simulations may be used to evaluate and extend data collection systems. The primary requirement for such a model is that it must represent the physical process active in the watershed. Such a model is sensitive to management activities in the simulation area and can be expected to correctly reflect at least trends in watershed response with a minimum of data for calibration. A model meeting these requirements was developed at Colorado State University and at Simons, Li & Associates, Inc. for the purpose of examining a variety of nonpoint source pollution problems. Elements of this mode have been implemented for the purpose of this short course.

The data base and collection system examined as a case study for this short course was the Four Mile Creek Watershed near Traer, Iowa. Data was available from this watershed for the years 1976-1978 (Johnson, 1977; 1978). For the purposes of this course, the processes simulation were water and sediment runoff, and nonpoint source loading from pesticides. Conclusions drawn regarding these processes are by and large applicable to the problem of estimating non-conservative processes such as nutrient loading as well as conservative processes such as pesticide yields. In particular, the characterization of runoff hydrology and sediment transport are key elements in a proper understanding of the transport of all water quality constituents. Synthesis of water quality and quantity records can require not only the calculation of water and sediment hydrographs, but the estimation of interstorm phenomena such as evapotranspiration and soil water movement as well. Interstorm processes are of considerable importance to the modeling of nutrient and pesticide processes through the estimation of soil moisture changes.

Therefore, the elements of nonpoint source pollution modeling discussed here in detail are as follows:

1. Water runoff, including
   - o interception
   - o infiltration
   - o overland and channel routing
2. Sediment runoff, including
   - o erosion processes
   - o sediment transport

- o aggradation and degradation

3. interstorm processes
   - o evapotranspiration
   - o vertical soil moisture movement
4. pesticide yields
   - o pesticide uptake by runoff
   - o pesticide incorporation in soil.

The chapter will present the theoretical foundation for the water and sediment runoff model and in this short course. The following chapter will present the interstorm process model which in combination with the water and sediment model and other nonpoint source pollutants (NPS) models constitute the NPS model used in this short course. Nonpoint source components are driven by the routing and interstorm models in a roughly similar manner. A pesticide routing component is used as an example of such a component. It is felt that conclusions reached about the quality and appropriateness of data with respect to the above mentioned components encompass most of thos applicable to other water quantity and quality components.

## 5.2 Water and Sediment Routing

In order to correctly represent the processes encountered in estimating water and pollutant runoff from watersheds, a runoff event model was implemented. This model may be incorporated into (or "driven" by) an interstorm model such as the one to be described in the next chapter to form a continuous time simulation. However, simulation of transport of materials from watersheds requires careful attention to the hydraulics of water and sediment runoff. The runoff model used here was developed by Li, et al., 1979 and has been refined to its present form by Fullerton, 1980. It is incorporated into a group of programs called MULTSED, which consists of 3 subprograms, MSED1, MSED2 and MSED3.

### 5.2.1 Formulation of the Water and Sediment Model

The theoretical background for physical process components used in MULTSED is presented below. In the derivation of the basic equations used in the model, the following assumptions are made:

1. Subwatersheds may be represented by an "open book" approximation (see Figure 5.1).

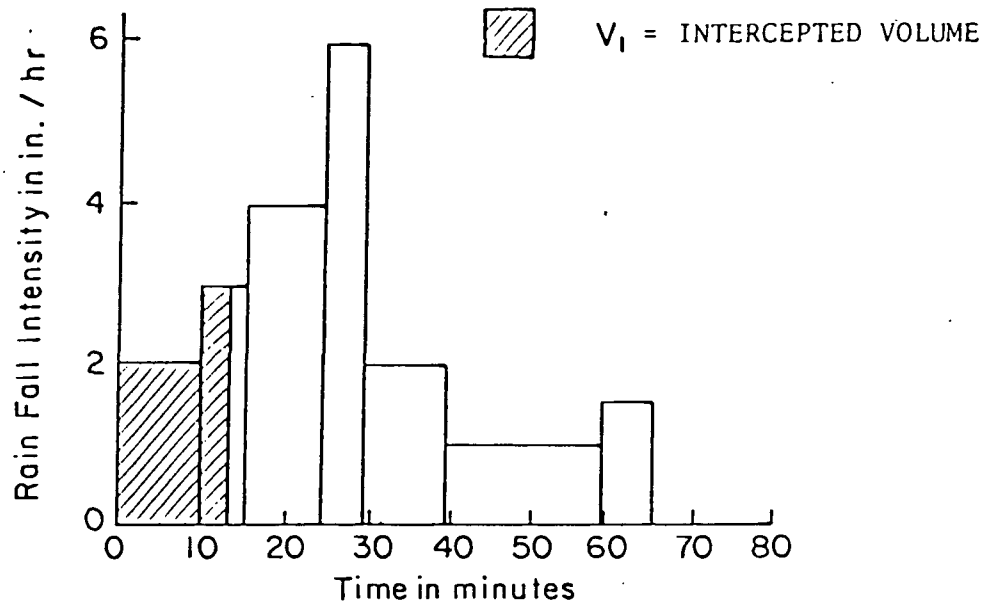


(a) Original hyetograph.

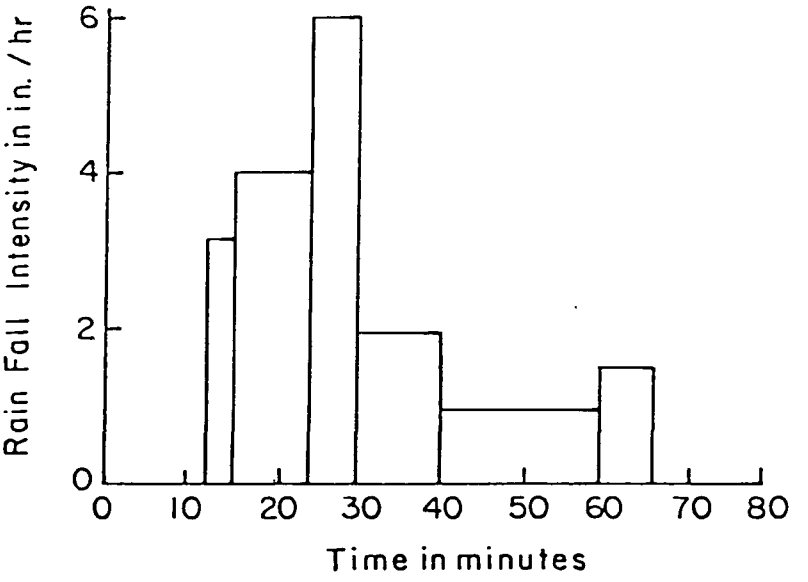


(b) Rainfall reaching the ground.

Figure 5.1. Effects of interception on rainfall hyetograph.

2. Soil characteristics are isotropic and homogeneous for a single unit (or side of a subwatershed).
3. Canopy cover and ground cover are homogeneous for a single unit (or side of a subwatershed).
4. Rainstorm events are spatially homogeneous within a unit and cover the entire plane or subwatershed unit.
5. Initial conditions such as soil moisture are uniform within a unit (or side of a subwatershed).
6. Evaporation processes are neglected for the runoff event.
7. Streams within the watershed are ephemeral, and the movement of subsurface flow and ground water flow are negligible as far as surface water runoff is concerned.
8. The kinematic-wave approximation for flow routing is valid, i.e., the gradients due to local and convective accelerations are negligible and the energy slope is nearly equal to the bed slope. (If an appropriate estimate of the energy slope can be made, it may be substituted for the bed slope to relax this restriction.)
9. Water and sediment yield simulation are based on a single storm.

### 5.2.2 Formulation of Excess Rainfall Calculations for MSED1

Much of the rain falling during the first part of a storm is intercepted by the ground cover. Precipitation intercepted by vegetation or other ground cover eventually evaporates, and the amount of rainfall reaching the soil surface is less than the recorded amount. The amount of interception loss depends on the percentage of the ground that is covered by canopy and ground cover, and their respective water holding capacities. The total intercepted volume can be written as:

$$V_i = C_c V_c + C_g V_g \tag{5.1}$$

where $V_i$ is the total potential intercepted volume per unit area, $C_c$ is the canopy cover density $(0 \leq C_c \leq 1)$, $V_c$ is the potential storage volume per unit area of canopy cover interception, $C_g$ is the ground cover density $(0 \leq C_g \leq 1)$, and $V_g$ is the potential storage volume per unit area of ground cover interception. The values of $V_c$ and $V_g$ are a function of types of vegetation and corresponding leaf area.

The interception volume given by Equation 5.1 is subtracted from the rainfall hyetograph. This is done by assuming that no rainfall is available for infiltration or overland flow until the total interception volume has been filled. Effects of interception on the rainfall hyetograph are shown in Figure 5.1.

A portion of the rainfall reaching the ground moves through the soil surface into the soil by infiltration. The model used to simulate this process is based on the Green and Ampt (1911) infiltration equation. Development of the infiltration model is based on the following assumptions:

1. The effect of the displacement of air from soil has negligible effect on the infiltration process.
2. Infiltration may be regarded as purely vertical, and the movement of water through the soil may be described by a distinct piston wetting front (Figure 5.2).
3. Soil compaction due to rainfall impact is neglected.
4. Hysteresis effects in the saturation-desaturation process may be neglected.
5. Depth of overland flow is sufficiently small that it has little influence on the infiltration process.

The derivation is essentially the same as presented by Eggert (1976), with minor changes. Under the assumptions stated, Darcy's Law may be applied. That is

$$V_z = -K_w \frac{dh}{dz} \tag{5.2}$$

where $V_z$ is the water velocity in the vertical direction, $K_w$ is the hydraulic conductivity in the wetted zone, $h$ is the piezometric head and $z$ is the vertical dimension.

Due to the assumed piston wetting front shown in Figure 5.2, the piezometric head may be expressed as

$$h = -z_o - \psi \tag{5.3}$$

where $z_o$ is the gravitational head and $\psi$ is the capillary suction head.

Darcy's Law can be rewritten as

$$V_z = K_w \frac{(z_o + \psi)}{z_o} \tag{5.4}$$

Further, by continuity, it is easy to see that

$$f = V_z \tag{5.5}$$

where $f$ is the rate of infiltration that is defined in the following equation:

$$f = \frac{dF}{dt} \tag{5.6}$$

where $F$ is the total volume of infiltration at time $t$.

The value of $z_o$ (Figure 5.2) can be written as

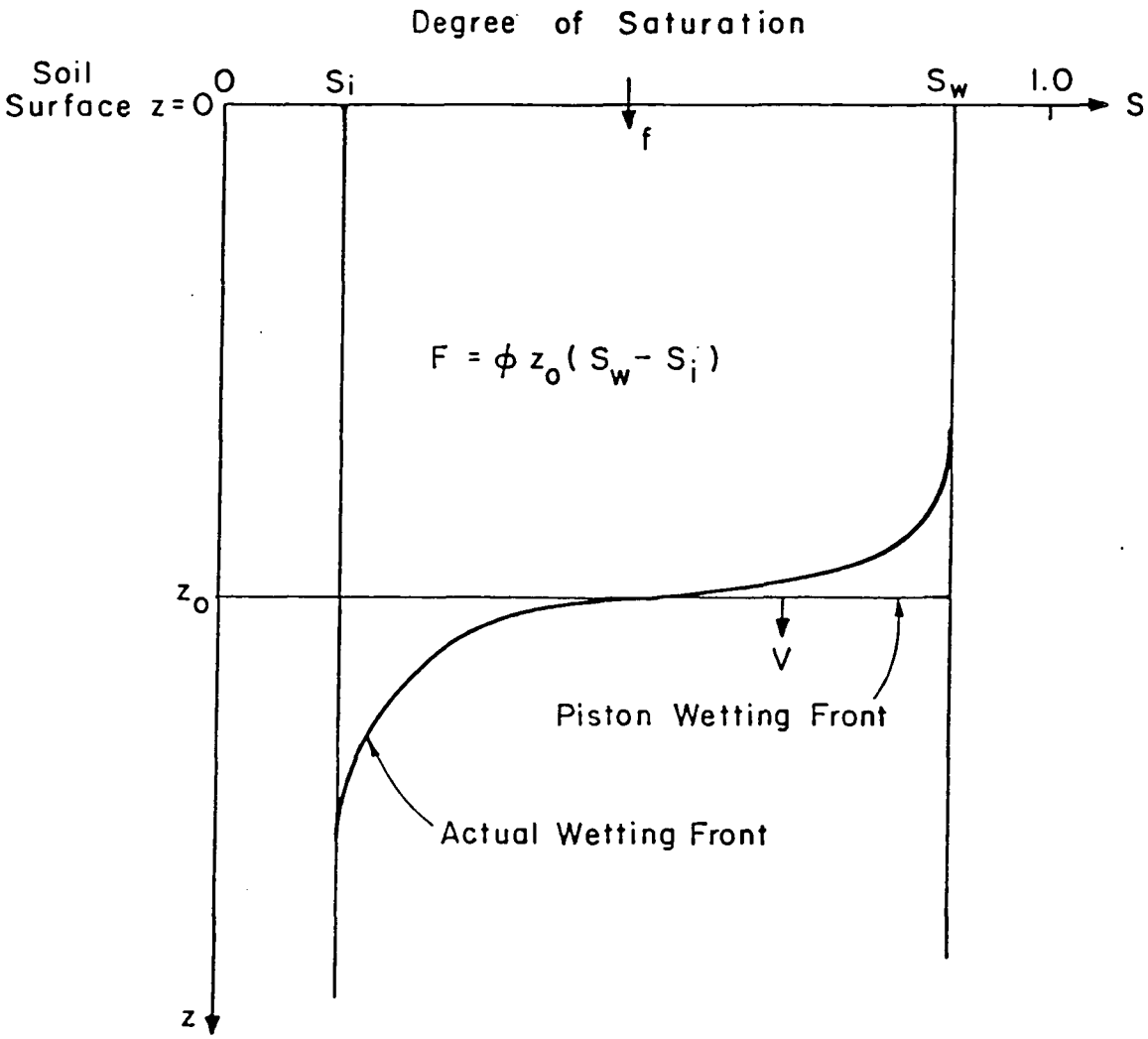


Figure 5.2. Approximation of soil moisture profile.

$$z_o = \frac{F}{\phi\,(S_w - S_i)} \tag{5.7}$$

where $\phi$ is soil porosity, $S_w$ is the degree of soil saturation in the wetted zone, and $S_i$ is the initial degree of saturation. Using Equations 5.5, 5.6 and 5.7, Equation 5.4 may be rewritten as

$$\frac{dF}{dt} = K_w\,(1 + \frac{\gamma}{F}) \tag{5.8}$$

where $\gamma$ is defined as

$$\gamma = \psi\,\phi\,(S_w - S_i) \tag{5.9}$$

This is essentially the equation proposed by Green and Ampt (1911).

Equation 5.8 can be rearranged so

$$\frac{F\,dF}{(F + \gamma)} = K_w\,dt \tag{5.10}$$

Integrating this equation between zero and a time $t$ results in

$$\frac{F}{\gamma} - \ell n\,(1 + \frac{F}{\gamma}) = \frac{K_w}{\gamma}\,t \tag{5.11}$$

If at any time $t$ the infiltrated volume is $F(t)$, then at some later time $t + \Delta t$ the infiltrated volume is

$$F(t + \Delta t) = F(t) + \Delta F \tag{5.12}$$

in which $\Delta F$ is the change in infiltrated volume that occurs during the time increment $\Delta t$. An expression for $\Delta F$, obtained from Equation 5.12, is

$$\Delta F = F(T + \Delta t) - F(t) \tag{5.13}$$

Substituting $F[(t) + \Delta t]$ for $F$ in Equation 5.11 results in

$$\frac{F(t + \Delta t)}{\gamma} - \ell n\quad 1 + \left[\frac{F(t + \Delta t)}{\gamma}\right] = \frac{K_w}{\gamma}\,(t + \Delta t) \tag{5.14}$$

Substituting $F(t)$ for $F$ in Equation 5.11 and subtracting this equation from Equation 5.14 yields

$$\frac{F(t + \Delta t) - F(t)}{\gamma} - \ell n\,\frac{1 + \frac{F(t + \Delta t)}{\gamma}}{1 + \frac{F(t)}{\gamma}} = \frac{K_w}{\gamma}\,\Delta t \tag{5.15}$$

The above equation can be simplified, by using Equation 5.13, to the following form:

$$\frac{\Delta F}{\gamma} - \ell n\,[1 + \frac{\Delta F}{\gamma + F(t)}] = \frac{K_w}{\gamma}\,\Delta t \tag{5.16}$$

Equation 5.16 gives a relationship between the infiltrated volume $F(t)$ and time, but due to its implicit nature, the equation is very difficult to use. An explicit solution can be obtained by using a power series expansion to approximate the logarithmic term in Equation 5.16. The result is

$$\ln\left(1 + \frac{\Delta F}{\gamma + F(t)}\right) = \ln 1 + \frac{\dfrac{2\Delta F}{\gamma + F(t)}}{2 + \dfrac{F(t)}{\gamma}} + \ldots \tag{5.17}$$

Truncating Equation 5.17 after the second term and substituting into Equation 5.16, one obtains

$$\frac{\Delta F}{\gamma} - 2\left[\frac{\dfrac{\Delta F}{\gamma + F(t)}}{2 + \dfrac{\Delta F}{\gamma + F(t)}}\right] = \frac{K_w}{\gamma}\Delta t \tag{5.18}$$

Equation 5.18 is simplified into the following quadratic equations for $\Delta F$:

$$\Delta F^2 + [2F(t) - K_w \Delta t]\,\Delta F - 2\,K_w\,\Delta t\,[\gamma + F(t)] = 0 \tag{5.19}$$

which has a solution with

$$\Delta F = \frac{-[2F(t) - K_w\Delta t] + [(2F(t) - K_w\Delta t)^2 + 8K_w\Delta t\,(\gamma + F(t))]^{1/2}}{2} \tag{5.20}$$

Since only the positive root of Equation 5.19 has any physical meaning, the negative root is ignored. Equation 5.20 provides an explicit function for infiltration with respect to time. The infiltration $\Delta F$ occurring during time $\Delta t$ can be determined knowing the soil characteristics ($K_w$ and $\gamma$) and the previous infiltration volume $F(t)$.

Once interception and infiltration have been calculated, the final rainfall excess can be determined. The following discussion presumes the rainstorm considered is spatially uniform over each subwatershed or plane unit but varies in time. This type of storm can be represented by a hyetograph as shown in Figure 5.1a. After the effects of interception have been subtracted from the rainfall hyetograph (Figure 5.1b), the average rainfall intensity occurring during a time increment $\Delta t$ is compared to the average infiltration rate $f$. Then the average infiltration rate or $f$ can be found by dividing the change in infiltrated volume $\Delta F$ given in Equation 5.20 by a time increment $\Delta t$ or

$$\bar{f} = \frac{\Delta F}{\Delta t} \tag{5.21}$$

This average infiltration rate is the maximum of potential average rate that occurs when there is a continuous supply of water, i.e., when there is more water available than can be infiltrated. The actual infiltration rate depends on the rainfall intensity and has a range from a minimum of zero to a maximum equal to the potential rate. If the rainfall intensity exceeds the potential rate $f$ (Equation 5.21), excess rainfall is generated. The actual average infiltration rate $i$ is given by

$$\bar{i}_j = \bar{f}_j \qquad \text{if} \qquad r_j > \bar{f}_j \tag{5.22}$$

$$\bar{i}_j = \bar{r}_j \qquad \text{if} \qquad r_j < \bar{f}_j \tag{5.23}$$

where the subscript $j$ denotes the jth time increment of a storm hyetograph and $r_j$ is the jth rainfall intensity in units of length per unit time. The excess rainfall intensity during the jth time increment can be calculated as

$$e_j = r_j - \bar{i}_j \tag{5.24}$$

The infiltration process continues after the termination of rainfall until all available water has either run off or been infiltrated. To approximate this process, the excess rate is set to the negative of the hydraulic conductivity in the wetted zone. In other words, the water continues to infiltrate at a rate equal to the hydraulic conductivity. The method of characteristics can easily handle the negative excess as long as it is the last excess.

### 5.2.3 Derivation of Analytical Kinematic Wave Equations for MSED1

This portion of the section clarifies the analytical kinematic routing component of the watershed model. The derivation is essentially the one given by Harley, Perkins, and Eagleson (1970), or Simons, Li, and Eggert (1976). This routing procedure is used for the plane and subwatershed units of MSED1 to determine the upstream and lateral inflows into the channel units of MSED3.

A single routing procedure is presented to compute both overland flow (used by the plane and subwatershed units), and channel flow (used only by the subwatershed units). Other than a few minor changes needed to switch the procedure between overland and channel flow, the derivations are identical.

The analytical solution to the kinematic wave approximation is based on the continuity and momentum equations in the absence of all dynamic interac-

tion. The continuity equation for overland flow is

$$\frac{\partial q}{\partial x} + \frac{\partial y}{\partial t} = e \tag{5.25}$$

where $q$ is the discharge per unit width, $x$ is the downstream dimension, $y$ is the depth, $t$ is time and $e$ is the lateral inflow. In this case, $e$ is the excess rainfall function presented earlier.

The Darcy-Weisbach resistance equation for overland flow is

$$S_f = f \frac{q^2}{8gy^3} \tag{5.26}$$

where $S_f$ is the friction slope, $f$ is the Darcy-Weisbach friction factor and $g$ is the acceleration due to gravity. By neglecting dynamic effects, the momentum equation for a kinematic wave becomes

$$S_f = S_o \tag{5.27}$$

in which $S_o$ is the average land slope. (For slopes in excess of 20 percent, the sine of the slope angle, not the tangent, should be used).

Substituting Equation 5.26 into Equation 5.27 and rearranging, the following expression for discharge as a function of depth is

$$q^2 = \frac{8gS_o}{f} y^3 \tag{5.28}$$

Many researchers, most recently Chen (1976), have shown that $f$ may be represented as

$$f = \frac{K}{R_e} \tag{5.29}$$

where $R_e$ is the Reynolds number and $K$ is a constant directly dependent on resistance. The Reynolds number may be expressed as

$$N_r = \frac{q}{\nu} \tag{5.30}$$

where $\nu$ is the kinematic viscosity of water. Equations 5.29 and 5.30 may be substituted into Equation 5.28 to give

$$q = \frac{8gS_o}{K\nu} y^3 \tag{5.31}$$

Discharge is often assumed to be a power function of depth.

$$q = \alpha y^{\beta} \tag{5.32}$$

Therefore, in the case of overland flow $\beta = 3$ and $\alpha$ is expressed as

$$\alpha = \frac{8gS_o}{K\nu} \tag{5.33}$$

Substituting Equation 5.32 into Equation 5.25 yields

$$\alpha\beta y^{\beta-1} \frac{\partial y}{\partial x} + \frac{\partial y}{\partial t} = e \tag{5.34}$$

This partial differential equation may be solved by the method of characteristics. The total differential of $y(x,t)$ is given by:

$$dy = \frac{\partial y}{\partial t} dt + \frac{\partial y}{\partial x} dx \tag{5.35}$$

Equations 5.34 and 5.35 form a system of two equations in two unknowns, and may be written in matrix form as:

$$\begin{bmatrix} \alpha\beta y^{\beta-1} & 1 \\ dx & dt \end{bmatrix} \begin{bmatrix} \frac{\partial y}{\partial x} \\ \frac{\partial y}{\partial t} \end{bmatrix} = \begin{bmatrix} e \\ dy \end{bmatrix} \tag{5.36}$$

The characteristic paths along which the solution is valid are found by determining the loci of indeterminancy of the solution. These loci are obtained by equating the determinant of the coefficient matrix with zero. The resulting characteristic equation is

$$\frac{dx}{dt} = \alpha\beta y^{\beta-1} \tag{5.37}$$

Integrating Equation 5.37 with respect to time yields

$$x - x_o = \alpha\beta \int_{t_o}^{t} y^{\beta-1} dt' \tag{5.38}$$

The invariants of this solution are found by substituting the right-hand side of Equation 5.36 for each column of the coefficient matrix and equating the determinant of the resulting matrix to zero. The invariants are

$$\frac{dy}{dt} = \frac{dq}{dx} = e \tag{5.39}$$

or by integrating Equation 5.39

$$y - y_o = \int_{t_o}^{t} e dt' \tag{5.40}$$

or

$$q - q_o = \int_{x_o}^{x} e dx' \tag{5.41}$$

By substituting Equation 5.40 into Equation 5.38, the following expression for the characteristic path is obtained.

$$x - x_o = \alpha\beta\left(\int_{t_o}^{t}\int_{t_o}^{t'} e d\sigma + y_o\right)^{\beta-1} dt' \tag{5.42}$$

Theoretically, if the functional form of $e(t)$ is known, then Equation 5.42 will give the characteristics in the $xt$ plane. When $e(t)$ is a histogram, then with reference to Equation 5.40, Equation 5.42 may be evaluated in pieces.

The procedure that calculates the characteristic paths is illustrated in Figure 5.3. From any point $(x_i, t_i)$ on characteristic $C$, the value of $x_{i+1}$ on $C$ corresponding to time. $t_{i+1}$ may be calculated by Equation 5.42 expressed as

$$x_{i+1} = x_i + \alpha\beta \int_{t_i}^{t_{i+1}} [e_{i+1} (t' - t_i) + y_i]^{\beta-1} dt' \tag{5.43}$$

From Equation 5.40 it may be seen that

$$y_{i+1} = y_i + e_{i+1} (t_{i+1} - t_i) \tag{5.44}$$

Integrating Equation 5.43 yields

$$x_{i+1} = x_i + \frac{\alpha}{e_{i+1}} [(y_i + e_{i+1} (t_{i+1} - t_i))^{\beta} - y_i^{\beta} ] \tag{5.45}$$

For a given plane of length $L$, values of $x_{i+1}$ are calculated until $x_{i+1} > L$. Time of arrival of the characteristic at the downstream boundary $t_L$ is found by solving Equation 5.45 for $t_L$ in terms of $t_j$ and $x_j$.

$$t_L = t_j + \frac{1}{e_{j+1}} \left[\frac{e_{j+1}(L-x_j)}{\alpha} + y_i^{\beta}\right]^{1/\beta} - y_j \tag{5.46}$$

For cases where $e_{j+1} = 0$, Equations 5.45 and 5.46 may be rederived from Equation 5.42, yielding

$$t_L = \frac{L - x_j}{\alpha\beta y_j^{\beta-1}} + t_j \tag{5.47}$$

and

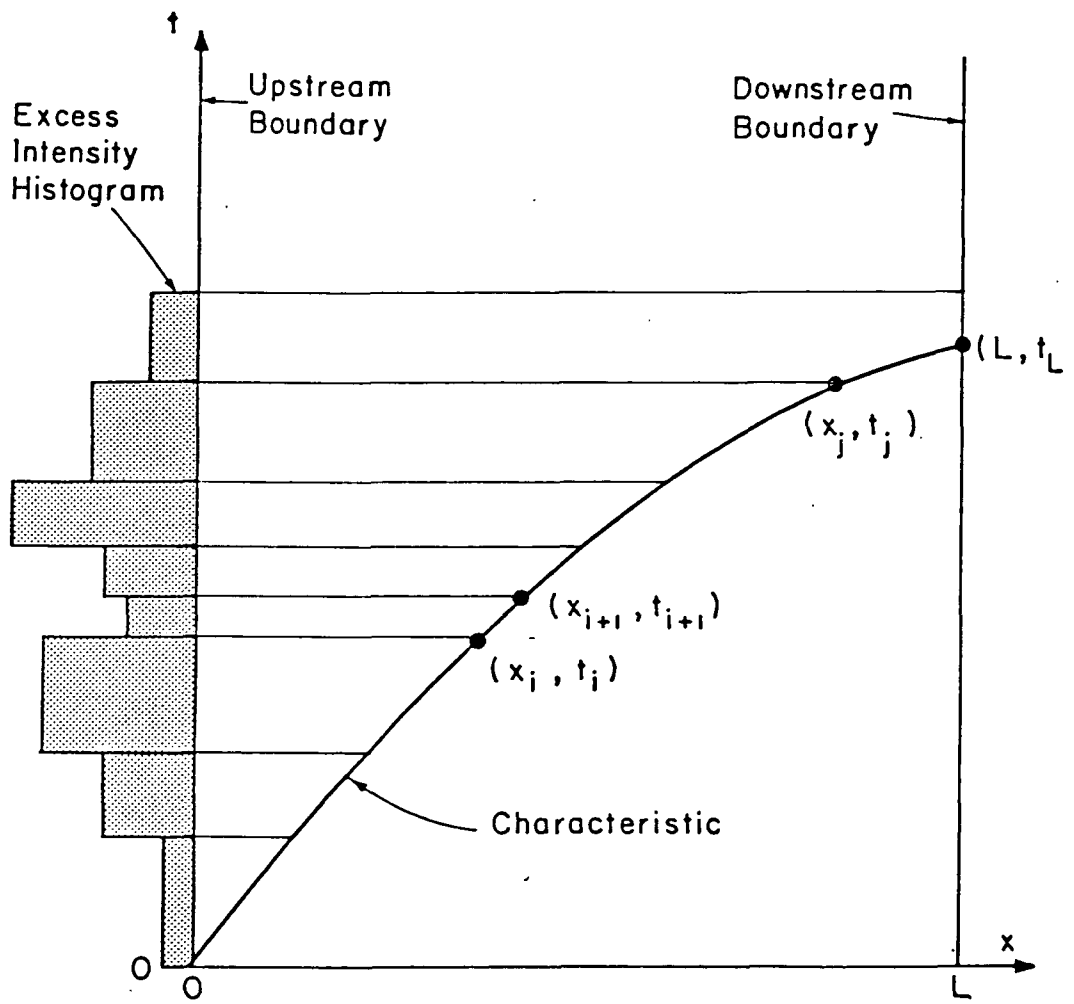


Figure 5.3. Method of characteristics solution domain illustrating calculation of characteristics in downstream direction.

$$x_{i+1} = x_i + \alpha\beta y_i^{\beta-1} (t_{i+1} - t_i) \tag{5.48}$$

Equations 5.45 through 5.48 are used serially, until a characteristic reaches the downstream boundary after the final time of interest for the hydrograph. At this time, additional characteristics are not required. If a characteristic contains the final negative excess, it may never cross the downstream boundary. This happens when the infiltration process is given sufficient time to remove all the excess surface water, after the termination of rainfall. The characteristic path in this case is represented by an upward slope until it eventually reaches vertical. At this point all runoff has been infiltrated. For the case when this occurs before the final time increment of the hydrograph, the time when the last characteristic reaches the boundary is estimated by an iterative procedure. The remaining portion of the storm hydrograph is set equal to zero. Figure 5.4 illustrates the characteristic solution domain.

As previously stated, the channel routing for the subwatersheds scheme is nearly identical to the overland flow routing. The continuity equation for channel flow is

$$\frac{\partial Q}{\partial x} + \frac{\partial A}{\partial t} = q_\ell \tag{5.49}$$

where $Q$ is the total discharge, $A$ is the cross-sectional area of the channel and $q_\ell$ is the lateral inflow to the channel.

When using Manning's equation, the kinematic wave approximation to the momentum equation can be written as

$$S_o \cong S_f = \frac{n^2 Q^2}{2.21\ R^{4/3} A^2} \tag{5.50}$$

in which $S_o$ is bed slope, $S_f$ is energy slope, $n$ is Manning's roughness coefficient, $g$ is the gravitational acceleration and $R$ is the hydraulic radius. By definition the hydraulic radius is:

$$R = \frac{A}{P} \tag{5.51}$$

in which $P$ is the wetted perimeter and usually can be represented as a power function of flow area, or

$$P = a_1 A^{b_1} \tag{5.52}$$

in which $a_1$ and $b_1$ are constants that vary with the shape of a cross-

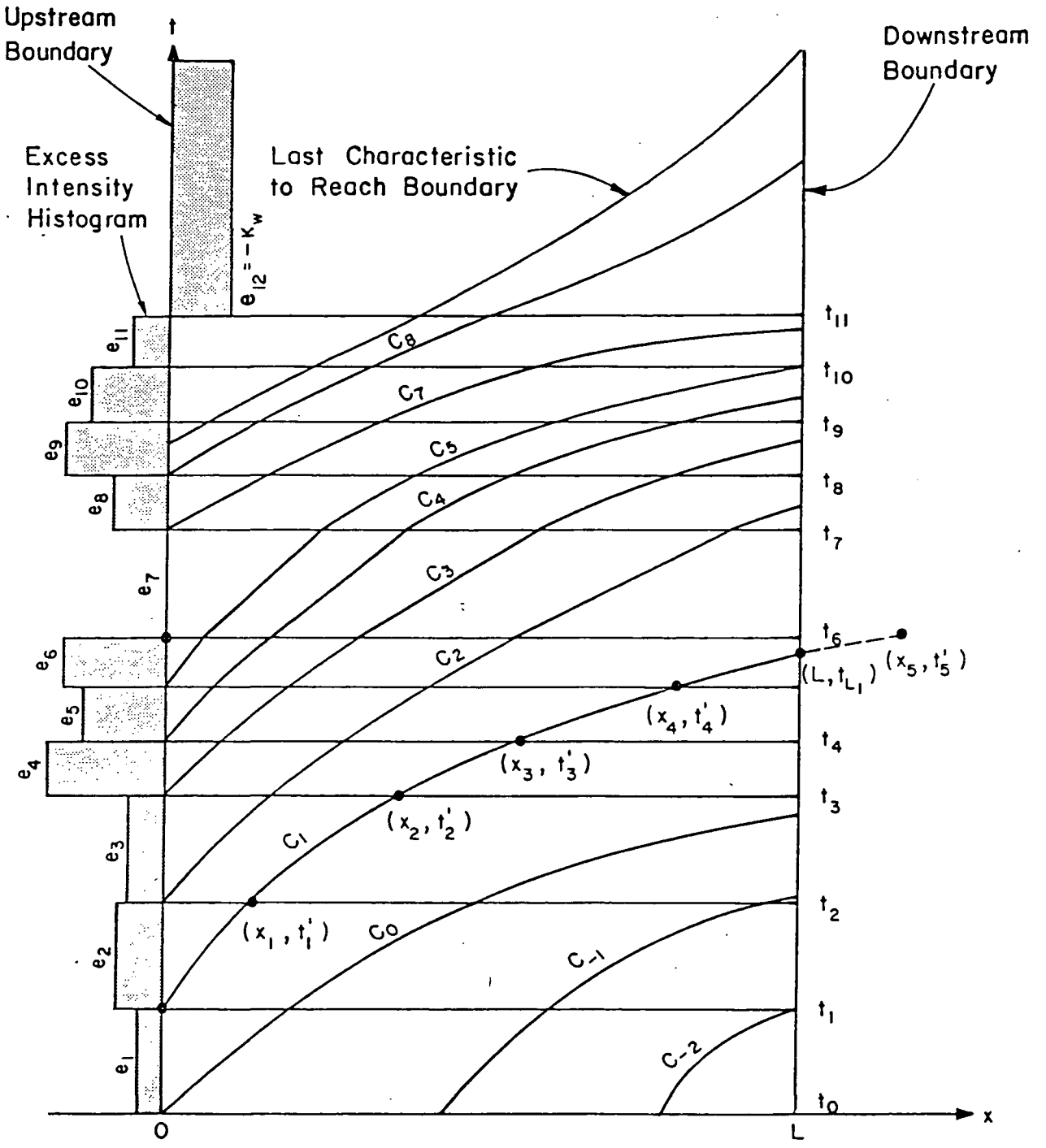


Figure 5.4. Method of characteristics solution domain illustrating a set of characteristics for an arbitrary excess rainfall histogram.

sectional area. Simons, Li and Ward (1977) devised a computer program to estimate $a_1$ and $b_1$ providing the cross section of the channel is known.

If the Chezy relationship is employed, the momentum equation becomes

$$S_o \cong S_f = \frac{Q^2}{A^2 C^2 R} \tag{5.53}$$

in which $C$ is the Chezy coefficient.

The flow cross-sectional area can be expressed as a power function of discharge

$$Q = \alpha A^{\beta} \tag{5.54}$$

in which $\alpha$ and $\beta$ are coefficients with values dependent on channel shape, roughness and slope.

If Manning's equation is applied, the corresponding $\alpha$ and $\beta$ are determined by using Equations 5.50, 5.51, 5.52 and 5.54. The values are

$$\alpha = \left[\frac{S_o(2.21)}{n^2 \; a_1^{4/3}}\right]^{1/2} \tag{5.55}$$

and

$$\beta = \frac{5 - 2b_1}{3} \tag{5.56}$$

If the Chezy relationship is used, the $\alpha$ and $\beta$ values are determined using Equations 5.51, 5.52, 5.53 and 5.54. The values are:

$$\alpha = \left(\frac{S_o C^2}{a_1}\right)^{1/2} \tag{5.57}$$

and

$$\beta = \frac{3 - b_1}{2} \tag{5.58}$$

The user may also assume that the two planes of the Wooding watershed configuration meet to form a triangular channel. The wetted perimeter of that channel $P$ (Figure 5.5) may be expressed as

$$P = \frac{A}{R} = r_1' + r_2 = [y^2 + t_1^2]^{1/2} + [y^2 + t_2^2]^{1/2} \tag{5.59}$$

where the subscripts refer to plane 1 and plane 2. Since $t_1$ and $t_2$ may be expressed as

$$t_1 = \frac{y}{S_1} \quad ; \quad t_2 = \frac{y}{S_2} \tag{5.60}$$

Equation 5.59 may be written:

$$P = y \left[ \left( 1 + \frac{1}{S_1^{\,2}} \right)^{1/2} + \left( 1 + \frac{1}{S_2^{\,2}} \right) \right]^{1/2} \tag{5.61}$$

Referring to Figure 5.5, the cross-sectional area of the channel may be expressed:

$$A = \frac{1}{2}\, y\, [t_1 + t_2] \tag{5.62}$$

or

$$A = \frac{1}{2}\, y^2 \left(\frac{1}{S_1} + \frac{1}{S_2}\right) \tag{5.63}$$

Solving Equation 5.63 for $y$ and substituting the result into Equation 5.61 yields the following expression for $P$ in terms of A:

$$P = a_1\, A^{1/2} \tag{5.64}$$

allowing

$$a_1 = \left( \frac{2}{\frac{1}{S_1} + \frac{1}{S_2}} \right)^{1/2} \left[ \left( 1 + \frac{1}{S_1^{\,2}} \right)^{1/2} + \left( 1 + \frac{1}{S_2^{\,2}} \right) \right]^{1/2} \tag{5.65}$$

$$b_1 = 1/2 \tag{5.66}$$

The $a_1$ and $b_1$ calculated in this manner may then be used to obtain $\alpha$ and $\beta$ by substitution into either Equations 5.55, 5.56, 5.57 or 5.58. If $a_1$ and $b_1$ are not input to the program, they will be calculated in MULTSED as in Equations 5.65 and 5.66.

Equations for water routing are again Equations 5.45 through 5.48. Excess $e$ is replaced by lateral inflow or discharge per unit width $q_\ell$. The parameters $\alpha$ and $\beta$ are defined above, and $y$ and $q$ are replaced by $A$ and $Q$, respectively. Since there are two planes, lateral inflow to the channel consists of the sum of the two overland flow discharge hydrographs.

A problem in constructing an open-book catchment simulation using the method of characteristics solution for kinematic wave routing lies in the timing of the overland flow feeding the channel. In order to preserve as much generality as possible, the two planes must be allowed to differ in geometric and hydraulic properties. When using the method of calculating charac-

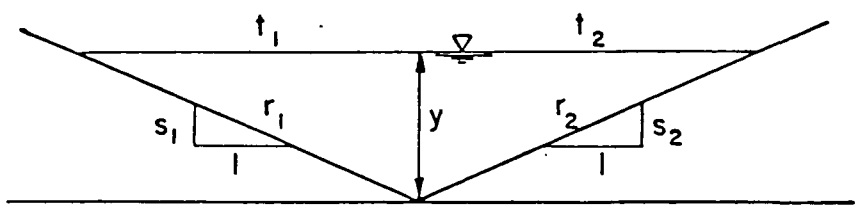


Figure 5.5. Definition sketch of triangular channel.

teristics, one selects a time on the upstream boundary of the solution domain, $t_o$ (Figure 5.4) and proceeds to determine points on the characteristic until the downstream boundary is reached. Time of arrival of that characteristic at the downstream boundary $t_L$ is a function of the lateral inflow and the hydraulic and geometric properties of the plane. Therefore, for the selection of the same set of $t_o$'s, different planes produce different sets of $t_L$'s.

This situation poses no particular difficulty until it is desired to combine the overland flow discharges to produce the lateral inflow for channel routing. It might be suggested that the difficulty may be easily handled by simply interpolating each onto a common time line. This solution is valid, though an unknown amount of error in each discharge occurs due to interpolation. If, on the other hand, it is possible to pick the time on the downstream boundary and then calculate $t_o$ on the upstream boundary, the two overland flow hydrographs could simply be added, time by time, to obtain the desired lateral inflow to the channel. Further, in this case, there would be no error included in forming the inflow hydrograph. A subroutine was developed to find the $t_o$ corresponding to a selected $t_L$, and it is based on the theory presented below.

The equation for a general characteristic path is:

$$\frac{L}{\alpha\beta} = \int_{t_o}^{t_L} \left[ \int_{t_o}^{t'} [q_\ell \ (\sigma \ d\sigma]^{\beta-1} \right] dt' \qquad (5.67)$$

where $L$ is the length of the slope being routed and $t'$ and $\sigma$ are dummy variables of integration. The problem here is to solve Equation 5.67 for $t_o$ when everything else is known. Lateral inflow $q_\ell$ is generalized; therefore, Equation 5.67 may be used for both overland and channel flow. For simplicity of discussion, the method will continue to be developed for overland flow; however, it will be directly applicable to channel flow simply by specifying the appropriate $\alpha$, $\beta$ and $q_\ell$. For overland flow, the lateral inflow $q_\ell$ is defined as the excess rainfall after satisfying infiltration and interception, $e$. This function is assumed to exist in the form of a histogram and is displayed vertically along the upstream boundary in Figure 5.4.

Since $e(t)$ has the form of a histogram, excess rainfall during the jth time increment $t_j - t_{j-1}$ is constant. In addition, the form of Equation 5.67 may be simplified by noticing the inner integration, i.e., the integra-

tion of $\sigma$ is simply the difference between the cumulative excess at time $t_L$ and the cumulative excess at time $t_o$. That is,

$$\int_{t_o}^{t_L} e(\sigma)\, d\sigma = E(t_L) - E(t_o) \tag{5.68}$$

where $E$ represents the cumulative excess.

With this notation in mind and taking advantage of the histogram form of $e(t)$, Equation 5.67 may be rewritten as

$$\frac{L}{\alpha\beta} = \int_{t_k}^{t_L} [e_{k+1}t' - e_{k+1}t_k + E_k - e_{j+1}t_o + e_{j+1}t_j - E_j]^{\beta-1}\, dt'$$

$$+ \sum_{i=j+2}^{k} \int_{t_{i-1}}^{t_i} [e_i t' - e_i t_{i-1} + E_{i-1} - e_{j+1}t_o + e_{j+1}t_j - E_j]^{\beta-1}\, dt'$$

$$+ \int_{t_o}^{t_{j+1}} [e_{j+1}t' - e_{j+1}t_j + E_j - e_{j+1}t_o + e_{j+1}t_j - E_j]^{\beta-1}\, dt' \tag{5.69}$$

Equation 5.69 consists of nothing more than a series of simple integrations of the form

$$\int (at' + b)^{\beta-1}\, dt' = \frac{1}{\alpha\beta}(at' + b)^{\beta} \tag{5.70}$$

Integrating as in Equation 5.70 and introducing $A_i$ as defined below,

$$A_i = -e_i\, t_{i-1} + E_{i-1} + e_{j+1}\, t_j - E_j \tag{5.71}$$

Equation 5.69 may be written as:

$$\frac{L}{\alpha\beta} = \frac{1}{e_{k+1}\beta}[e_{k+1}\, t' + A_{k+1} - e_{j+1}\, t_o]^{\beta}\Bigg|_{t_K}^{t_L}$$

$$+ \sum_{i=j+2}^{k_1} \frac{1}{e_i\beta}[e_i\, t' + A_i - e_{j+1}\, t_o]^{\beta}\Bigg|_{t_{i-1}}^{t_i}$$

$$+ \frac{1}{e_{j+1}\beta}[e_{j+1}t' - e_{j+1}\, t_o]^{\beta}\Bigg|_{t_o}^{t_{j+1}} \tag{5.72}$$

Since Equation A-72 may be explicitly differentiated with respect to $t_o$,

a Newton-Raphson technique can be used to obtain a solution. The subroutine developed uses a second-order routine to speed convergence. The routine proceeds by rewriting Equation A-72 as

$$f(t_o) = -\frac{L}{\alpha\beta} + \frac{1}{e_{k+1}^{\beta}}\left[e_{k+1}t' + A_{k+1} - e_{j+1}t_o\right]^{\beta}\Bigg|_{t_k}^{t_L}$$

$$+ \sum_{i=j+2}^{k} \frac{1}{e_i^{\beta}}\left[e_i t' + A_i - e_{j+1}t_o\right]^{\beta}\Bigg|_{t_{i-1}}^{t_i}$$

$$+ \frac{1}{e_{j+1}^{\beta}}\left[e_{j+1}t' - e_{j+1}t_o\right]^{\beta}\Bigg|_{t_o}^{t_{j+1}} \qquad (5.73)$$

The first and second derivatives of $f(t_o)$ with respect to $t_o$ are, respectively,

$$f'(t_o) = -\frac{e_{j+1}}{e_{k+1}}\left(e_{k+1}t_L + A_{k+1} - e_{j+1}t_o\right)^{\beta-1}$$

$$- \left(e_{k+1}t_k + A_{k+1} - e_{j+1}t_o\right)^{\beta-1}$$

$$- \sum_{i=j+2}^{k} \frac{e_{j+1}}{e_i}\left(e_i t_i + A_i - e_{j+1}t_o\right)^{\beta-1}$$

$$- \left(e_i t_{i-1} + A_i - e_{j+1}t_o\right)^{\beta-1}$$

$$- \left(e_{j+1}t_{j+1} - e_{j+1}t_o\right)^{\beta-1} \qquad (5.74)$$

and

$$f''(t_o) = \frac{e_{j+1}^2}{e_{k+1}}(\beta-1)\left(e_{k+1}t_L + A_{k+1} - e_{j+1}t_o\right)^{\beta-2}$$

$$- \left(e_{k+1}t_k + A_{k+1} - e_{j+1}t_o\right)^{\beta-2}$$

$$+ \sum_{i=j+2}^{k} \frac{e_{j+1}^2}{e_i} (\beta-1) \quad (e_i t_i + A_i - e_{j+1} t_o)^{\beta-2}$$

$$- (e_i t_{i-1} + A_i - e_{j+1} t_o)^{\beta-2}$$

$$+ (\beta-1)(e_{j+1}) \; (e_{j+1} t_{j+1} - e_{j+1} t_o)^{\beta-2} \tag{5.75}$$

The second-order Newton's method is based on truncating a Taylor's series expansion of $f(t_o)$ about a trial value of $t_o$, defined as $t_o^*$, after the third term. Thus, $f(t_o)$ is written as

$$f(t_o) \cong f(t_o^*) - (t_o - t_o^*) \, f'(t_o^*) + \frac{(t_o - t_o^*)^2}{2} f''(t_o^*) \tag{5.76}$$

Roots of $f(t_o)$ are then obtained by setting $f(t_o) = 0$ in Equation 5.76 and solving the resulting quadratic for $t_o$. This value of $t_o$ becomes the new estimate of the root, and interactions continue until

$$\left| \frac{f(t_o^*)}{\frac{L}{\alpha\beta}} \right| < \eta \tag{5.77}$$

where $\eta$ is some arbitrarily small convergence increment.

In this manner, $t_o$'s can be calculated corresponding to selected $t_L$'s. The values of $t_o$ contain some error due to the Newton method approximation; however, this error, unlike the error due to interpolation, may be precisely controlled by the specification of $\eta$.

The number of terms in the summation appearing in Equations 5.73, 5.74 and 5.75 are determined by using the histogram of the lateral inflow to subdivide the solution domain. This subdivision is accomplished by calculating the characteristics arising at the beginning of each new histogram element (Figure 5.6). Since the applications for which these routines are intended never exhibit kinematic shock, no characteristics in the solution domain intersect. Therefore, the characteristics calculated serve as a minimum set of bounds for those to be calculated by Equation 5.77. The number of terms in Equations 5.73 through 5.75 are immediately known by simply counting the number of histogram units crossed by the regions that are bounded by the characteristics having $t_L$'s on either side of the $t_L$ selected (Figure 5.6). Thus, the values of $k$ and $j$ for a given $t_L$ in Equations 5.73 through 5.75

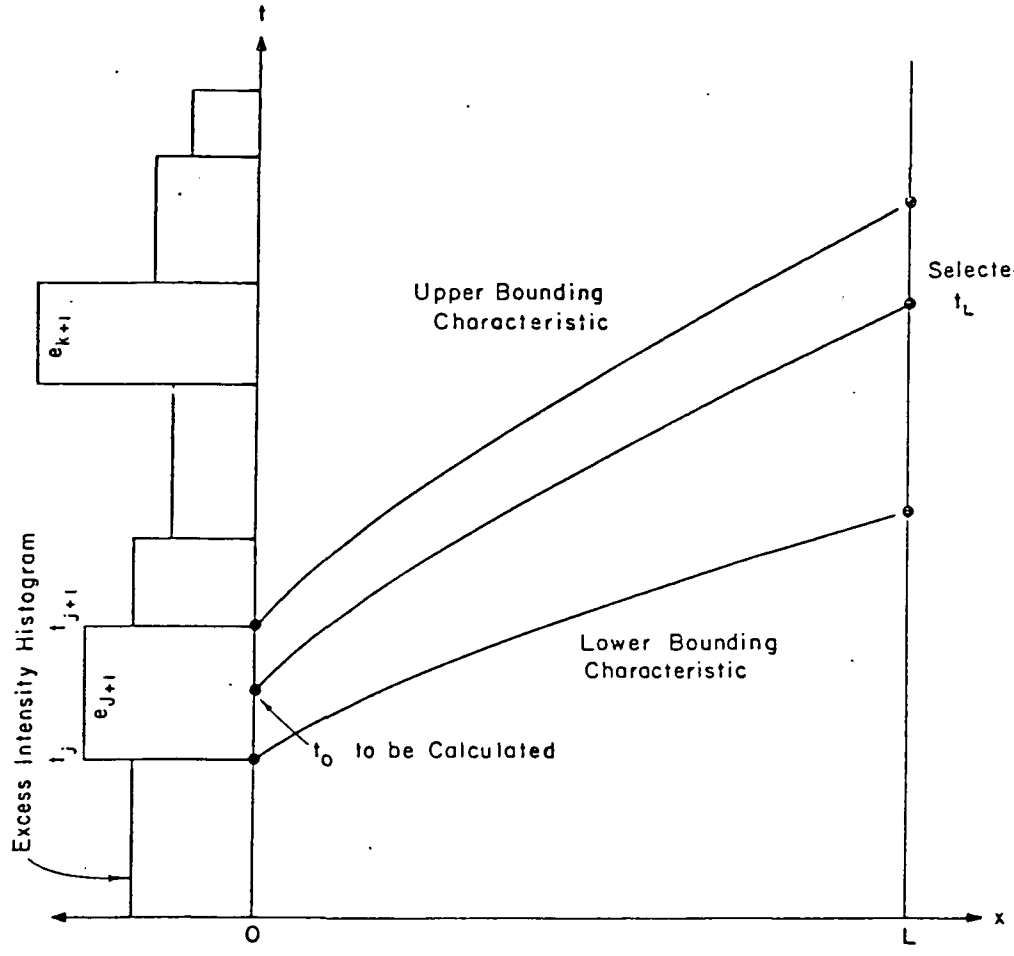


Figure 5.6. Method of characteristics solution domain illustrating upstream calculation of characteristics between bounding characteristics previously calculated in downstream direction.

are known.

This technique provides a rapid means of finding $t_o$'s corresponding to a given $t_L$. Three iterations of Newton's method have seemed sufficient for $\eta = 0.001$. Knowing $t_o$ and $t_L$, the depth may be evaluated at the downstream boundary at time $t_L$ by using Equation 5.40. This depth is used to determine the discharge at the downstream boundary at time $t_L$ by using Equation 5.32.

### 5.2.4 Sediment Determination for MSED1

Erosion and sediment yields are processes of balancing soil erosion rates and transporting rate of the transporting medium. Generally, sediment yield from a watershed can be divided into processes related to the flow conditions, such as overland flow and channel flow. The following is a discussion of sediment supply due to erosion by both rainfall and runoff, and the transporting rate by overland flow and channel flow in upstream subwatersheds.

#### 5.2.4.1 Overland Sediment Transport Capacity

After a runoff rate $q$ is known, the overland sediment transport capacity rate can be calculated. This is accomplished after determination of several intermediate steps. First, the overall flow resistance is assumed to be:

$$K_g = K_\ell + (K_h - K_\ell)\, C_g^2 \tag{5.78}$$

where $K_g$ is the parameter describing the overall flow resistance associated with ground cover effects, $K_\ell$ is the parameter describing the maximum resistance for the area $(C_g = 1.0)$, and $C_g$ is the percent of ground cover. An increase in $C_g$ produces a rapid increase in $K_g$, as seen in Figure 5.7. These values closely agree with those found in Woolhiser's (1975) work in unsteady overland flow modeling.

Both $q$ and $K_g$ are then used to find the average flow depth as

$$y = \left(\frac{qK_g v}{8gS_o}\right)^{1/3} \tag{5.79}$$

where $y$ is the flow depth, $v$ is the kinematic viscosity of water, $g$ is the acceleration of gravity and $S_o$ is the slope of the ground surface.

The mean flow velocity is

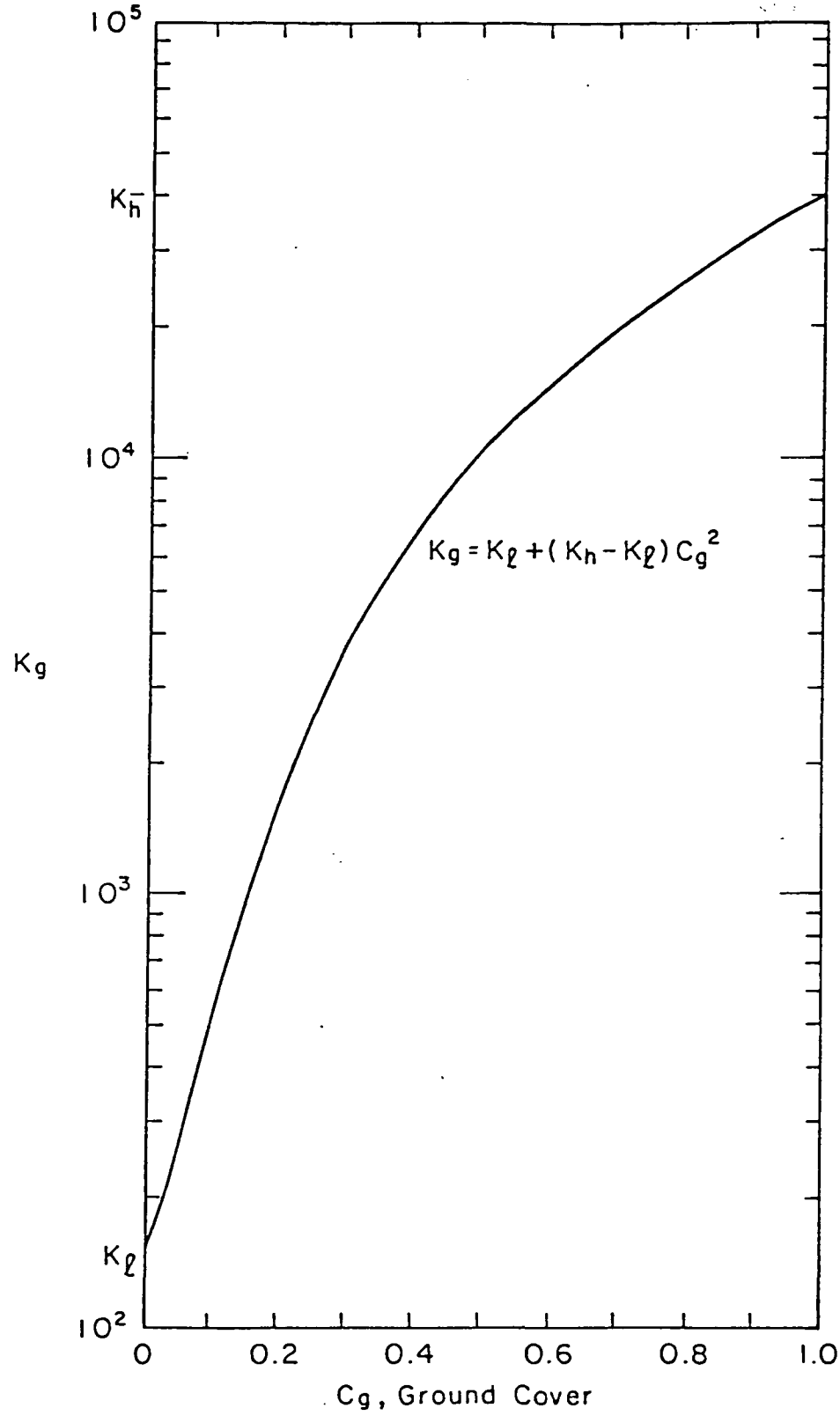


Figure 5.7. Assumed variation of overall resistance with ground cover.

$$V = \frac{q}{y} \tag{5.80}$$

The flow parameters calculated above are then used to determine sediment transport capacity. The procedure for determining sediment transport capacity given by Simons, Li and Stevens (1975) is used in this report.

The first sediment transport parameter that should be determined is the tractive force or boundary shear stress. Effective boundary shear stress acting on a grain can be determined by

$$\tau = \frac{1}{8} f\rho V^2 = \frac{1}{8} \frac{K_o}{q} \nu\rho V^2 \tag{5.81}$$

where $\tau$ is the effective boundary shear stress, $f$ is the Darcy-Weisbach friction factor for grain resistance, $\rho$ is the density of water and $K_o$ is the parameter describing grain resistance.

The boundary shear stress $\tau'$, considering total resistance (form and grain resistance), is

$$\tau' = \gamma y S_o \tag{5.82}$$

where $\gamma$ is the specific weight of water. It should be noted that $\tau'$ is usually much larger than $\tau$. The shear velocity $U_*$ is then

$$U_* = \sqrt{\frac{\tau'}{\rho}} \tag{5.83}$$

The sediment transport capacity rate is an integral of all the individual sediment size transport rates or in discrete form

$$q_t = \sum_{i=1}^{N} (q_{ti} i_s) \tag{5.84}$$

where $q_t$ is the total transport capacity rate, $q_{ti}$ is the potential transport rate for each size, $i_s$ is the percentage of each sediment size of bed material and $N$ is the total number of sizes considered. Each individual size transport $q_{ti}$ is composed of bed-load transport $q_{bi}$ and suspended load transport $q_{si}$, or

$$q_{ti} = q_{bi} + q_{si} \tag{5.85}$$

The bed-load transport rate can be calculated using the Meyer-Peter, Muller formulation (USBR, 1960) as

$$q_{bi} = \frac{12.85}{\sqrt{\rho}} (\tau - \tau_c)^{1.5} \tag{5.86}$$

where $\tau_c$ is the critical shear force for the given particle size. Though

the Meyer-Peter, Muller equation was used here, other suitable bed-load formulations could be easily substituted into the model. The critical shear force for particle movement is determined by the Shields criteria of

$$\tau_c = \delta\gamma(S_s - 1)\, d_{si} \tag{5.87}$$

where $\delta$ is the parameter depending on flow conditions, $S_s$ is the specific gravity of the sediment, and $d_{si}$ is the sediment size in question. The value of $S_s$ usually ranges from 2.60 to 2.70, but $\delta$ is dependent on flow conditions and should be calibrated to the actual field situation. If $\tau_c$ is greater than $\tau$ there is no sediment movement.

For steep slopes, the critical shear stress must be reduced to account for the lessened component of gravity in the direction normal to the land surface. This correction factor is expressed as

$$k = \cos\theta \sqrt{1 - \frac{\tan^2\theta}{\tan^2\phi}} \tag{5.88}$$

The variable $\theta$ is the slope angle of the land surface, $\phi$ is the angle of repose of the material (assumed to be 40°), and $k$ is the correction factor. The critical shear stress is multiplied by this factor.

The suspended load is determined using the Einstein method (1950), or

$$q_{si} = C_a U_* a \frac{S^{w-1}}{(1-S)^w} \left[\left(\frac{V}{U_*} + 2.5\right) J_1 + 2.5\, J_2\right] \tag{5.89}$$

where $C_a$ is the sediment concentration at distance $a$ above the land surface, and $S$, $A$, $a$, $J_1$ and $J_2$ are given below.

The concentration term is related to the bed-load transport as

$$q_{bi} = 11.6\, C_a U_* a \tag{5.90}$$

The distance $a$ is assumed to be 0.2 feet for particles which are less than 0.1 foot in diameter. For larger particles, the distance $a$ is set equal to twice the particle size. The 0.2-foot value was chosen based on a calibration with Colby's method for sand sizes. If twice the sediment diameter is used for small particles, such as sand, the transport rates become unrealistically large. The dimensionless parameters relate flow depth to sediment size as

$$S = \frac{a}{y} \tag{5.91}$$

The dimensionless parameter $w$ relates the in-water settling velocity of the

sediment to the shear velocity, or

$$w = \frac{V_s}{\kappa U_*} \tag{5.92}$$

where $V_s$ is the settling velocity of the sediment and $\kappa$ is von Karman's number, taken as 0.40.

Settling velocities are a function of particle size and water properties and can be formulated (ASCE, 1975) as

$$V_s = \frac{2.9517\ d_{si}^{\ 2}}{v} \quad \text{when} \quad d_{si} < 0.0002 \text{ feet} \tag{5.93}$$

or

$$V_s = \frac{(36.064\ d_{si}^3 + 36v^2)^{1/2} - 6v}{d_{si}} \quad \text{when} \quad d_{si} > 0.0002 \text{ ft}$$

The terms $J_1$ and $J_2$ are integrals resulting from integration of the equation describing the vertical concentration of sediment in the flow. The first integral $J_1$ is given as

$$J_1 = \int_S^1 \left(\frac{1-\sigma}{\sigma}\right)^w d\sigma \tag{5.94}$$

where $\sigma$ is a dimensionless relative position,

$$\sigma = \frac{\varepsilon}{\gamma} \tag{5.95}$$

and $\varepsilon$ is the distance above the land surface in the flow. The other integral is similar and is given as

$$J_2 = \int_S^1 \ln\sigma \left(\frac{1-\sigma}{\sigma}\right)^w d\sigma \tag{5.96}$$

These two integrals can be evalauted by successive integrations of a power series expansion given by Li (1974). Rearranging Equation 5.89 and substituting into Equation 5.88 gives a simpler form or

$$q_{si} = \frac{q_{bi}}{11.6} \frac{S^{w-1}}{(1-S)^w} \left[\left(\frac{V}{U_*} + 2.5\right) J_1 + 2.5\ J_2\right] \tag{5.97}$$

The total potential transport rate, Equation A-85, becomes

$$q_t = \sum_{i=1}^{N} (q_{si} + q_{bi})\ i_s \tag{5.98}$$

The potential transport capacity can be found as

$$V_t = \frac{T}{\gamma S_s} \int_0^{\Delta t} q_t \, dt \tag{5.99}$$

where $T$ is the top width of the channel, $\Delta t$ is the duration of runoff and $V_t$ is the nonporous volume of potential transport.

Channel Sediment Transport Capacity

After the overland flow runoff is known, the sediment transporting capacity of the channel can be calculated. Although the physics of sediment transport for the channel are much the same as those for overland flow, relations describing channel sediment capacity are altered.

The resistance factor $f$ is calculated for each sediment size based upon the ratio of sediment diameter to hydraulic radius. The expression used is

$$f = [1.69 + 2 * \log (2 * R/d_{si})]^{-2} \tag{5.100}$$

in which $R$ is the hydraulic radius. This is an empirical expression shown to be valid for calculating flow resistance in open channels when the flow is in the turbulent range. According to the equation, for a given depth the larger particles will have a larger resistance. Since the resistance on a selected particle size also depends on the size of the particles surrounding it, the resistance factor is not allowed to fall below half the value computed for the largest sizes. In addition, the friction factor is not allowed to fall out of the range between 0.1 and 0.01.

5.2.4.3 Determination of Sediment Supply

Potential sediment transport represents the capacity of the system. Supply of sediment comes from two mechanisms: detachment by raindrop splash and detachment by overland and channel flow. For a plane of width and length $L$, raindrop splash detachment can be formulated as a simple power function of rainfall intensity (Meyer, 1971):

$$V_r = a_1 i^2 \, LW \, (1 - \phi) \, A_b \tag{5.101}$$

where $V_r$ is the nonporous volume of detached material by raindrop splash, $a_1$ is an empirically determined constant describing erodibility of the soil, and $A_b$ is an area reduction factor.

The variable $A_b$ represents the fraction of unprotected or bare soil in

the area and is given as

$$A_b = 1 - C_g - C_c + (C_g C_c) \tag{5.102}$$

where $(C_g C_c)$ accounts for areas of cover overlap. Sediment supply by overland flow detachment is determined by

$$V_f = D_f \, (V_t - V_r) \tag{5.103}$$

where $V_f$ is detachment by overland flow and $D_f$ is the flow detachment coefficient. An equation similar to that used in overland flow detachment is used for channel flow detachment. For many cases, however, the flow detachment coefficient for channels is assumed to be zero due to natural armoring, riprap or other forms of bed and bank protection. This is especially true for man-made channels.

If $V_t < V_r$ there is no flow detachment because the transport rate is limited by the transporting capacity. The total available sediment supply $V_a$ is

$$V_a = V_r + V_f \tag{5.104}$$

5.2.4.4 Determination of Sediment Yield

Once the supply and capacity for each size fraction has been calculated and summed over the entire event, the actual sediment yield can be determined. This is done by comparing the transporting capacity and supply for each size fraction. If the transporting capacity is greater than the total available sediment supply, $V_t > V_a$, then the sediment yield for that size fraction is equal to $V_a$. However, if $V_t < V_a$, then the yield for that size fraction is equal to $V_t$.

5.2.5 Mathematical Derivation of the Numerical Kinematic Routing Procedure for MSED3

The numerical and analytical kinematic wave routing schemes are governed by the same equations: the equation of continuity, the momentum equation and the equations describing channel geometry and flow resistance. The following numerical kinematic routing procedure is used by MSED3 for the channel units.

The derivation for the discharge-area relationship is slightly different. In MSED3 the relationship is expressed as

$$A = \alpha' \, Q^{\beta'} \tag{5.105}$$

instead of

$$Q = \alpha A^{\beta} \tag{5.106}$$

as in MSED1. This is due to the use of the numerical method in MSED3. Usually $\beta'$ is less than 1.0 and has a value of 1/3 for Reynolds numbers less than 900. Consequently, if discharge is computed incorrectly, the relative error in the flow area is smaller than the relative error in the discharge. On the other hand, the error in the discharge estimation is magnified if the numerical computations are performed on the flow area (Li, Simons and Stevens, 1975). In the case of MSED1 it is more convenient to compute discharge as a function of flow area.

If Manning's equation is applied, the corresponding $\alpha'$ and $\beta'$ are

$$\alpha' = \left(\frac{a_1^{4/3} n^2}{2.21\ S_o}\right)^{\left(\frac{3}{10-4b_1}\right)} \tag{5.107}$$

and

$$\beta' = \frac{3}{5-2b_1} \tag{5.108}$$

If the Chezy relationship is used, the $\alpha'$ and $\beta'$ values are

$$\alpha' = \left(\frac{a_1}{C^2 S_o}\right)^{[1/(3-b_1)]} \tag{5.109}$$

and

$$\beta' = \frac{2}{3-b_1} \tag{5.110}$$

The water continuity equation for the channel can be expressed as

$$\frac{\partial Q}{\partial x} + \frac{\partial A}{\partial t} = q_\ell \tag{5.111}$$

in which $Q$ is water discharge, $x$ is the downslope distance, $A$ is the flow area, $t$ is time and $q_\ell$ is the lateral inflow. The lateral inflow rate $q_\ell$ for the channel units is obtained from the overland flow in the adjacent plane units calculated in MSED1.

The problem of water routing becomes a matter of solving Equations 5.105 and 5.111. A nonlinear scheme with an iterative procedure was used in this study. A linear scheme was used to obtain the initial estimate of the unknown discharge for the nonlinear scheme. The linear scheme may be used as is, with no iterations, to solve for the unknown discharge if the accuracy is

satisfied.

The finite difference form of Equation 5.111 can be represented as

$$\frac{Q_{j+1}^{n+1} - Q_j^{n+1}}{\Delta x} + \frac{A_{j+1}^{n+1} - A_{j+1}^{n}}{\Delta t} = \frac{1}{2}\left(q_{\ell_{j+1}}^{n+1} + q_{\ell_{j+1}}^{n}\right) \tag{5.112}$$

in which $Q_j^n$ is the quantity $q$ at grid point $x = j\Delta x$ and $t = n\Delta t$, where $\Delta x$ is the space increment and $\Delta t$ is the time increment. The rectangular network shown in Figure 5.8 illustrates the $x$-$t$ grid system.

Unknowns in Equation 5.112 are $(Q_{j+1})^{n+1}$ and $(A_{j+1})^{n+1}$, but the discharge bears a definite relation with the flow area, as indicated by Equation 5.105. With two equations, the values of the two unknowns can be obtained.

Substitution of Equation 5.105 into Equation 5.112 yields

$$\frac{\Delta t}{\Delta x} Q_{j+1}^{n+1} + \alpha'(Q_{j+1}^{n+1})^{\beta'} = \frac{\Delta t}{\Delta x} Q_j^{n+1} + A_{j+1}^{n} + \frac{\Delta t}{2}\left(q_{\ell_{j+1}}^{n+1} + q_{\ell_{j+1}}^{n}\right) \tag{5.113}$$

The right side of Equation 5.113 contains known quantities and is denoted by $\Omega$ which can be expressed as

$$\Omega = \frac{\Delta t}{\Delta x} Q_j^{n+1} + A_{j+1}^{n} + \frac{\Delta t}{2}\left(q_{\ell_{j+1}}^{n+1} + q_{\ell_{j+1}}^{n}\right) \tag{5.114}$$

If

$$r = Q_{j+1}^{n+1}$$

and

$$\theta = \frac{\Delta t}{\Delta x}$$

then the left side of Equation 5.113 is expressed as

$$f(r) = \theta r + \alpha' r^{\beta'} \tag{5.115}$$

The solution of Equation 5.113 satisfies the condition

$$f(r) = \theta r + \alpha' r^{\beta'} = \Omega \tag{5.116}$$

An approximate solution to this nonlinear equation is obtained by the following iterative scheme.

If $r^k$ is the value of $r$ at the kth iteration, the Taylor Series expansion of the function $f(r)$ around $f^k$ is

$$f(r) = f(r^k) + (r - r^k)\, f'(r^k) + \frac{1}{2}(r - r^k)^2 f''(r^k) + \frac{1}{6}(r - r^k)^3 f'''(r^k) + \ldots \tag{5.117}$$

in which $f'(r^k)$ and $f''(r^k)$ are values of the first and second derivatives

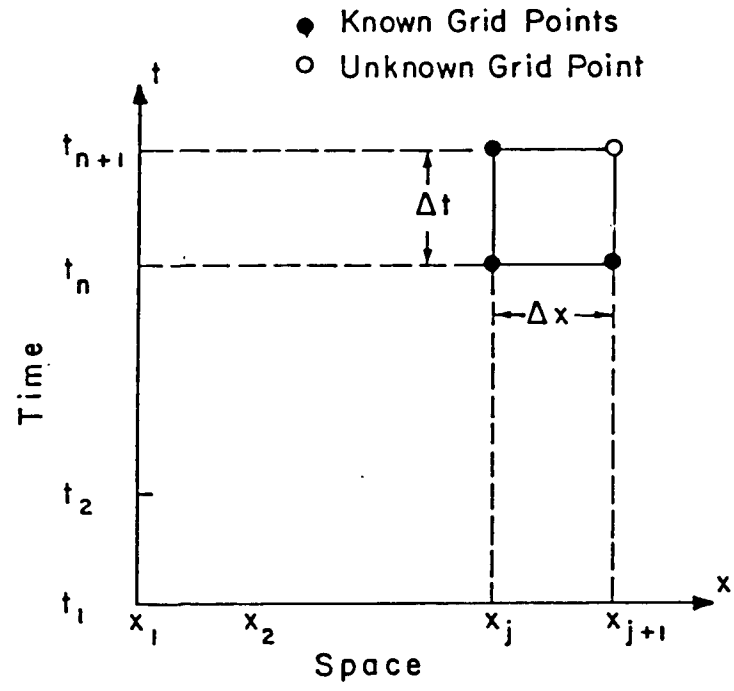


Figure 5.8. Definition sketch for channel water and sediment finite difference routing scheme.

of the function at $r^k$. Dropping the terms higher than the second order, one obtains

$$f(r) \cong f(r^k) + (r - r^k)\, f'\,(f^k) + \frac{1}{2}\,(r - r^k)^2\, f''\,(r^k) \qquad (5.118)$$

The purpose of iteration is to force $f(r^{k+1})$ to approach the value of $\Omega$ or

$$\Omega \cong f(r^k) + (r^{k+1} - r^k)\, f'\,(r^k) + \frac{1}{2}\,(r^{k+1} - r^k)^2\, f''\,(r^k) \qquad (5.119)$$

The solution of Equation 5.119 is

$$r^{k+1} = r^k - \frac{f'(r^k)}{f''(r^k)} \pm \sqrt{\frac{f'(r^k)}{f''(r^k)}^{\,2} - \frac{2[f(r^k) - \Omega]}{f''(r^k)}} \qquad (5.120)$$

in which

$$f(r^k) = \theta r^k + \alpha'(r^k)^{\beta'} \qquad (5.121)$$

$$f'(r^k) = \theta + \alpha'\beta'\,(r^k)^{\beta'-1} \qquad (5.122)$$

and

$$f''(r^k) = \alpha'\beta'\,(\beta'-1)\,(r^k)^{\beta'-2} \qquad (5.123)$$

There are two solutions to Equation A-120. It is advisable to choose the solution that gives the smaller value of $|f(r^{k+1})-\Omega|$. The above iteration is continued until the absolute error $|f(r^{k+1})-\Omega|$ is less than a preassigned tolerance $\eta$. The termination criteria can be written as

$$|f(r^{k+1}) - \Omega| < \eta \qquad (5.124)$$

An appropriate value for $\eta$ is $0.01\Omega$. However, it may be changed according to the purpose of individual problems.

The scheme represented by Equation 5.112 has proved to be unconditionally stable and can be used with a wide range of time-to-space increment ratios without loss of significant accuracy (Li, Simons and Stevens, 1975). However, the initial guess $r°$ is the key to the speed of convergence to the correct numerical solution. The best way of determining $r°$ is to use a linear scheme.

The term $\partial A/\partial t$ in Equation 5.111 can be expressed as

$$\frac{\partial A}{\partial t} = \frac{\partial A}{\partial Q}\,\frac{\partial Q}{\partial t} \qquad (5.125)$$

Also, from Equation 5.105

$$\frac{\partial A}{\partial Q} = \alpha'\beta' Q^{\beta'-1} \qquad (5.126)$$

Substituting of Equations 5.125 and 5.126 into Equation 5.111 yields

$$\frac{\partial Q}{\partial x} + \alpha'\beta' Q^{\beta'-1} \frac{\partial Q}{\partial t} = q_\ell \tag{5.127}$$

The finite difference form of Equation 5.127 is given by the expression

$$\frac{Q_{j+1}^{n+1} - Q_j^{n+1}}{\Delta x} + \alpha'\beta' \left(\frac{Q_{j+1}^{n} + Q_j^{n+1}}{2}\right)^{\beta'-1} \frac{Q_{j+1}^{n+1} - Q_{j+1}^{n}}{\Delta t}$$

$$= \frac{1}{2}\left(q_{\ell_{j+1}}^{n+1} + q_{\ell_{j+1}}^{n}\right) \tag{5.128}$$

so that

$$r^\circ = Q_{j+1}^{n+1} = \frac{\theta Q_j^{n+1} + \alpha'\beta' Q_{j+1}^{n} \left(\frac{Q_{j+1}^{n} + Q_j^{n+1}}{2}\right)^{\beta'-1} + \frac{\Delta t}{2}\left(q_{\ell_{j+1}}^{n+1} + q_{\ell_{j+1}}^{n}\right)}{\theta + \alpha'\beta' \left(\frac{Q_{j+1}^{n} + Q_j^{n+1}}{2}\right)^{\beta'-1}} \tag{5.129}$$

Equation 5.129 uses a linear scheme to provide the best initial estimate of $r^\circ$ for the nonlinear scheme. However, Equation 5.129 is not applicable if both $Q_{j+1}^{n}$ and $Q_j^{n+1}$ are zero. When both are zero, $\beta' = 1$ is used in Equation 5.115 and then

$$r^\circ = \frac{\Omega}{\theta + \alpha'} \tag{5.130}$$

### 5.2.6 Channel Infiltration Routine for MSED3

The channel infiltration routine is similar to the layered infiltration scheme described earlier in the report, but with one difference. Since the depths of flow in the channels are normally much greater than those for overland flow, the depth of the water is not ignored. Thus, the equations are the same except for the addition of head due to the depth of flow.

### 5.2.7 Sediment Routine for MSED3

The sediment routing in MSED3 uses the same principle as the sediment yield calculations in MSED1, the process of balancing supply and capacity for each sediment size.

The sediment calculations in MSED3 are different in that the numerical method used allows for the sediment to be routed through the channels at each time increment and then integrated over the time increments to arrive at a total yield for each size fraction. The method used in MSED1 can only provide a total yield for each size fraction, but cannot truly route the sediment

through the channel. MSED3 is able to route the sediment because the balancing of transporting capacity and supply can be compared at each time and space increment along the channel due to the use of the numerical scheme. The method used in MSED1 does not allow for this, since only conditions at the downstream end of the channel are calculated.

Since MSED3 uses the numerical method, which requires actual transport rates at each time increment, and it needs to use the yields calculated in MSED1 as upstream and lateral inflows, the yields in MSED1 must be transformed into sediment hydrographs. This is accomplished by distributing the yields from MSED1 in proportion to the water discharge at each time increment. MSED3 could easily be modified to distribute the yields from MSED1 by various other schemes.

The remainder of this section will be devoted to the governing equations for sediment routing and the development of the numerical routing technique.

5.2.7.1 Governing Equation for Sediment Routing

In the channel units the processes which govern sediment routing are the continuity for sediment, the transport capacity, sediment flow detachment and armoring. The continuity equation for sediment size $i$ is

$$\frac{\partial G_{si}}{\partial x} + \frac{\partial C_i A}{\partial t} + \frac{\partial T Z_i}{\partial t} = g_{si} \tag{5.131}$$

in which $i$ is the size fraction index, $G_{si}$ is the total sediment transport rate by volume per unit time, $C_i$ is the sediment concentration by volume, $Z_i$ is the depth of loose soil, $T$ is the channel top width, and $g_{si}$ is the lateral sediment inflow. ($Z$ is in terms of nonporous soil. To correct for porosity $Z$ is divided by one minus the porosity.)

The concentration of sediment for a sediment size $i$ is

$$C_i = \frac{G_{si}}{Q} \tag{5.132}$$

The total concentration of sediment at a cross section is

$$C_T = \sum_{i=1}^{N} C_i \tag{5.133}$$

and the total loose soil available is

$$Z_T = \sum_{i=1}^{N} Z_i \tag{5.134}$$

The sediment transport capacity equations are the same as those used for the channel in MSED1 and described earlier. The only difference is the transport capacity is calculated at segments along the channel at each time increment instead of at the downstream end of the channel.

The amount of soil detachment by channel flow is determined by comparing the total sediment transport capacity to the total available amount of loose soil. The total sediment transport capacity is

$$G_c = \sum_{i=1}^{N} G_{ci} \tag{5.135}$$

Assuming the total sediment transport capacity $G_c$ is equal to the transport rate, the total potential change in loose soil can be determined from Equation 5.131 as

$$\Delta Z^P = \frac{\partial Z}{\partial t} \Delta t \tag{5.136}$$

If $\Delta Z^P > -Z$, the loose soil storage is enough for transport and there is no detachment of soil by surface runoff. Soil is detached if $\Delta Z^P < -Z$. The amount of detachment can be computed by

$$D = D_f(\Delta Z^P + Z) \tag{5.137}$$

in which $D$ is the total amount of detached soil and $D_f$ is a detachment coefficient which varies from 0.0 to 1.0 depending on soil erodibility. If the channel bed is cemented together by cohesive material, $D_f$ is equal to zero. In a river which has no cohesive material, the value for $D_f$ is one.

Two limitations are placed on the loose soil layer. The first states that when the loose soil layer has become greater than one foot, the detachment process is controlled by the sediment size with the lowest relative transport rate (this will be the largest size present). The reasoning which justifies this procedure is when the loose soil layer has grown as large as one foot, the flow cannot effectively interact any deeper; therefore, it must remove the less transportable sediment before it can move the more easily transportable sediment. As a result, the detachment process becomes limited to the rate at which the largest sizes can be detached. Although the bed is not armored, the transport rate has become retarded by the larger sizes when this occurs.

The other limitation is when a nontransportable size exists, the detachment cannot be larger than the amount of material that must be removed to

leave behind a layer of nontransportable particles with a thickness of twice the nontransportable diameter. If there is enough nontransportable material in the loose soil layer at the beginning of the time increment, then no detachment at all can occur.

The accepted value for the soil detachment is the lower of the values computed by Equation 5.137, or the two limitations just described. The new amount of loose soil is then

$$Z_i = Z_i + D\ F_i \tag{5.138}$$

in which $Z_i$ is calculated for each size fraction of sediment.

5.2.7.2 Numerical Procedure for Sediment Routing

A numerical routing procedure is adopted for determining the sediment transport rate for each sediment size. In this procedure, the sediment continuity equation is solved for each size. Equation 5.131 is rewritten in finite difference form and combined with Equation 5.132 to yield

$$\Delta Z_i = \frac{1}{T}\ [(G^{n+1}_{si_j} - G^{n+1}_{si_{j+1}})\ \frac{\Delta t}{\Delta x} - G^{n+1}_{si_{j+1}}\ A^{n+1}_{j+1}/Q^{n+1}_{j+1}$$

$$+ C^n_{i_{j+1}}\ A^n_{j+1} + \frac{\Delta t}{2}\ (g^{n+1}_{si_{j+1}} + g^n_{si_{j+1}})] \tag{5.139}$$

The sediment transport rate for each size at the outlet of the reach for the time increment of interest can be approximated by

$$G^{n+1}_{si_{j+1}} = \frac{Z^{n+1}_{i_{j+1}}}{Z^n_{T_{j+1}}}\ Q^{n+1}_{si_{j+1}} \tag{5.140}$$

in which $(Q_{si_{j+1}})^{n+1}$ represents the theoretical transport capacity of the ith sediment size if the bed was made only of that size material. The other term represents an approximation of the fraction of sediment of the ith size in the loose soil layer at the end of the time increment. It is an approximation since the denominator is the total loose soil depth for the previous time increment and not the present. The approximation is good as long as the loose soil layer does not change greatly during the time increment.

The change in the loose soil layer can be rewritten as

$$\Delta Z_i = Z^{n+1}_{i_{j+1}} - Z^n_{i_{j+1}} \tag{5.141}$$

Combining equations 5.139 through 5.141, the new loose soil layer can be solved for directly by the equation

$$Z^{n+1}_{i_{j+1}} = [Z^{n}_{i_{j+1}} T + G^{n+1}_{si_j} \frac{\Delta t}{\Delta x} + C^{n}_{i_{j+1}} A^{n}_{j+1} + \frac{\Delta t}{2} (g^{n+1}_{si_{j+1}} + q^{n}_{si_{j+1}})]/[T + (Q^{n+1}_{si_{j+1}} / Z^{n}_{T_{j+1}}) (\frac{\Delta t}{\Delta x} + A^{n+1}_{j+1}/Q^{n+1}_{j+1})] \quad (5.142)$$

All the terms on the right-hand side of Equation 5.142 are known and as a result $(Z_{i_{j+1}})^{n+1}$ is determined. Knowing the new loose soil depth, the transport rate can be solved for by Equation 5.140.

When Equation 5.142 predicts aggradation (an increase in the loose soil layer) the amount of aggradation is checked against that which is feasible given the flow conditions and the settling velocity of the sediment particles. This is extremely important for the routing of fine materials that will not settle out in relatively short reaches of a channel even if the transport capacity is much smaller than the supply.

The fraction of sediment that can settle out based on ideal settling and assuming a simplified sediment concentration profile (uniform), is given by

$$S_{f_i} = V_{s_i} T\Delta x/(2\ Q^{j+1}_{n+1}) \quad (5.143)$$

A factor of 2 is included to account for turbulence. The total amount of aggradation predicted by 5.142 and 5.143 is compared and the lesser value chosen. If $S_{f_i}$ is greater than one, settling cannot lessen the aggradation process.

When Equation 5.143 controls, the transport rate is corrected by including the fraction of sediment that was predicted to be deposited by Equation 5.142, but could not settle.

### 5.2.8 MSED2

MSED2 mentioned above acts as in interface between the MSED1 and MSED3 components of MULTSED and is necessary to make efficient use of computer time and storage. As described, MSED1 uses an analytical routing method which calls for the results for each unit (plane or subwatershed) to be calculated for the whole event before proceeding to calculate any results for the next unit in the computational sequence. However, MSED3 uses a numerical procedure

which works most efficiently when the results for a single itme increment of the event are calculated for all units before proceeding to the next time increment. Since MSED1 provides the lateral and upstream inflows for MSED3 the space time orientation of the results must be switched. MSED2 reads the files created in MSED1 and then executes the switch. In addition, MSED2 separates the discharge hydrographs from the sediment yield results.

## 5.3 Water and Sediment Input Data Requirements

Data requirements for the water and sediment routing model are summarized in the list below. Other mechanistic water and sediment models require similar data input and therefore this list of inputs summarizes the data that must be provided in order to provide a data base for simulating water and sediment impacts from man's activities in the watershed.

Geometry and Channel Data

- Watershed area
- Length of overland slopes
- Width of overland slopes
- Gradients of overland slopes
- Length of channel sections
- Gradient of channel sections
- Measured, representative channel cross sections
- Extent of impervious areas

Soil Data

- Distribution of soils
- Types of soils
- Initial water content of soil
- Saturated hydraulic conductivity of soil
- Porosities of soil
- Specific gravity of sol
- Grains size analysis of soil and channels
- Rainfall storm hyetographs

Hydrologic and Hydraulic Data

- Storm and daily runoff hydrographs
- Overland flow resistance

Channel flow resistance
Storm sediment yield
Grain size and analyses of sediment
Sediment detachment coefficient for rainfall and runoff

Vegetation Data
Types
Distribution
Density of ground cover
Density of canopy cover
Storage of ground cover
Maximum and minimum storage of canopy cover

Climatic Data
Average daily temperature

## 5.4 References

American Society of Civil Engineers, 1975, Sedimentation Engineering, prepared by the ASCE Task Committee of the Hydraulics Division.

Einstein, H.A., 1950, The Bed Load Function for Sediment Transportation in Open Channel Flows, USDA Technical Bulletin No. 1026, Washington, D.C.

Fullerton, W.T., 1980, Water and Sediment Routing Model for Complex Watersheds and Its Application, unfinished Masters Thesis, Department of Civil Engineering, Colorado State University, Fort Collins, Colorado.

Green, W.H. and G. A. Ampt, 1911, "Studies on Soil Physics, Part I: The Flow of Air and Water through Soils," Journal of Agriculture Science, May.

Harley, B.M., F.E. Perkins, and T.S. Eagleson, 1970, A Modular Distributed Model of Catchment Dynamics, Massachusetts Institute of Technology, Hydrodynamics, Report No. 133.

Johnson, R., N. Crawford, P. Grimsrud, T. Barnwell, and L. Mulkey, 1979, Hydrologic Simulation Program-Fortran Workshops, sponsored by the Environmental Protection Agency and Hydrocomp Inc., Mountain View, California.

Li, R.M., 1974, Mathematical Response from Small Watersheds, Ph.D. Dissertation, Department of Civil Engineering, Colorado State University, Fort Collins, Colorado.

Li, R.M., D.B. Simons, W.T. Fullerton, K.G. Eggert, and B.E. Sprank, 1979, "Simulation of Water Runoff and Sediment Yield from a System of Multiple Watersheds," XVIII Congress International Association for Hydraulic Research, Cagliani, Italy.

Li, R.M., D.B. Simons, and M.A. Stevens, 1975a, "A Nonlinear Kinematic Wave Approximation for Water Routing," Water Resources Research, Vol. 11.

Meyer, L.D., 1971, "Soil Erosion by Water on Upland Areas," in River Mechanics, Vol. II, ed. by H.W. Shen, Fort Collins, Colorado.

Simons, D.B., R.M. Li, and K.G. Eggert, "Storm Water and Sediment Runoff Simulation for Upland Watersheds Using Analytical Routing Technique," Volume I--Water Routing and Yield, Colorado State University Report CER77-78DBS-RML-DGE16, prepared for USDA Forest Service, Rocky Mountain Forest and Range Experiment Station, Flagstaff, Arizona, April 1977.

Simons, D.B., R.M. Li, and M.A. Stevens, 1975, Development of Models for Predicting Water and Sediment Routing and Yield from Storms on Small Watersheds, prepared for USDA Forest Service, Rocky Mountain Forest and Range Experiment Station.

Simons, D.B., R.M. Li, and T.J. Ward, 1977a, Estimation of Parameters for Describing Channel Geometry for Watershed Modeling, prepared for the USDA Forest Service, Rocky Mountain Forest and Range Experiment Station, Flagstaff, Arizona.

United States Bureau of Reclamation, 1960, "Investigation of Meyer-Peter, Muller Bedload Formulas," Sedimentation Section, Hydrology Branch, Division of Project Investigations, U.S. Department of Interior, Washington, D.C.

Woolhiser, D.A., 1975, "Simulation of Unsteady Overland Flow," in Unsteady Flow in Open Channels, ed. by K. Mahmood and V. Yevjevich, Water Resources Publications, Fort Collins, Colorado.

# VI. PHYSICAL PROCESS SIMULATION: II. INTERSTORM AND PESTICIDE MODELS

## 6.1 General

This chapter discusses two physical-process simulations, an interstorm model for simulating soil moisture changes, and a pesticide loading model for predicting pesticide yields and residues from managed fields. The interstorm model may be used in conjunction with the water and sediment model, as well as water quality components such as the pesticide model, in two ways. First, the simulation of soil moisture levels is important for determination of initial moisture condition for runoff and pesticide yield. Secondly, knowledge of the variation in soil moisture with time is required for modeling of nutrient changes. The case study to be discussed in the next two chapters largely deals with the final use of the interstorm model, and therefore the following discussion will emphasize the use of the interstorm model for estimation of moisture condition between storms.

The pesticide model chosen for the purposes of this course was developed by the Science and Education Administration - Agricultural Research (Leonard and Wanchope, 1980), and presented in Knisel (1980). This loading model was chosen as appropriate for the data available and represents a mechanistically based approach to computation of pesticide yields and residues. It is coupled to the water and sediment routing model which provides required runoff and sediment yield calculations.

## 6.2 Interstorm Process

Teare (1977) observed that two significant advances in describing plant-water relationships occurred in this century. One advance was the realization that the movement of water from cell to cell within a plant is not wholly controlled by osmotic pressure gradients, but rather by gradients in total water potential. The second advance was the recognition of the analogy between electrical circuits and the flow of water in the soil-plant-atmosphere system. The analogy is a natural outgrowth of the form of the steady-state equations for flux density of a quantity through a medium. This relationship has the form

$$J_i = -K \frac{\partial \phi_i}{\partial s} \tag{6.1}$$

where $J_i$ is the flux density of quantity $i$, $K_i$ is the conductivity of the

medium for $i$, and $\partial\phi_i/\partial s$ is the gradient of $i$ in the direction of $s$. For example, if quantity $i$ is heat, then Equation 6.1 is known as the Fourier heat conduction law, usually expressed,

$$q = -K \frac{\partial T}{\partial s} \tag{6.2}$$

where $q$ is the flux density of heat through the medium, $K$ is the Fourier thermal conductivity of the medium, and $\partial T/\partial s$ is the temperature gradient.

Equations having the form of Equation 6.1 are used to model a variety of physical phenomena, including the flow of electrical energy. If Equation 6.1 is rewritten as follows

$$J_i = (\frac{\delta s}{K_i}) = -\delta\phi_i \tag{6.3}$$

the analogy to Ohm's laws is apparent. The quantity $J_i$ is analogous to current, $\delta s/K_i$ to resistance, and $-\delta\phi_i$ to the electrical voltage drop. This analogy has been applied to the daily water balance processes by a number of authors, notably Cowan (1965), Sutcliffe (1968), Huff et al. (1977), and Goldstein and Mankin (1972). The code for the water balance components of the simulation was in large part taken from that developed by Goldstein, Mankin and Luxmoore (1974). Their code directly implements the basic theory to follow. Some special assumptions and computational details of their implementation will be discussed later.

### 6.2.1 Evaporation

As pointed out by Eagleson (1970), evaporation is a combination of diffusive and convective processes. In the presence of an absolutely still atmosphere, vapor transport away from the free surface would be entirely a diffusion process. Fick's first law of diffusion has the form of Equation 6.1, where $\partial\phi_i/\partial s$ is the concentration gradient of substance $i$ in a medium and $K_i$ is the molecular diffusivity of substance $i$ into the medium. In a diffusion process, $K_i$ is a property of the substance and the medium, and a function of their physical state. However, under other than laboratory conditions, evaporation seldom occurs by pure diffusion.

Heating of the earth's surface and the interaction of wind motion with surface roughness combine to introduce vertical air motion. The presence of turbulence in the layer of air above that immediately adjacent to the earth or

the evaporating surface means that water vapor is convected away from the surface. Convection in general transports materials orders of magnitude more quickly than diffusion alone. Therefore, convection is the dominant process when the atmosphere may not be assumed at rest. Convective processes may also be modeled using equations having the form of Equation 6.1. The flux density of material $i$ is still represented by $J_i$, and $\partial\phi_i/\partial s$ still represents the concentration gradient of $i$. However, in this case the constant of proportionality $K_i$ may be shown to depend on the flow of the transporting medium as well as of the medium. Prandtl's mixing length theory may be viewed as an example in which $K_i$ is a function of turbulent structure.

For convective processes, the constant $K$ is usually called an eddy diffusivity, and in general its value, not being purely properties of the medium, is not known. However, examination of the flow may be used to calculate values of the eddy diffusivity. Another quantity transferred by convection is momentum. The flux of momentum is generally known as the Reynolds stress, and is given by

$$\tau = \rho K_m \frac{\partial u}{\partial z} \tag{6.4}$$

where $\tau$ is the Reynolds stress, $\rho$ is the density of air, $u$ is the horizontal wind speed, $z$ is distance measured vertically and $K_m$ is the kinematic eddy diffusivity. Using the Reynolds stress as an example, and assuming adiabatic (neutral or nonbuoyant) conditions,

$$\frac{\partial u}{\partial z} = \frac{u_*}{\kappa z} \tag{6.5}$$

where $\kappa$ is the von Karman number ($\kappa = 0.41$), and $u_*$ is the shear velocity, given by

$$u_* = \sqrt{\frac{\tau}{\rho}} \tag{6.6}$$

Integrating Equation 6.5 gives the familiar logarithmic velocity profile

$$u_2 - u_1 = \frac{u_*}{\kappa} (\ln \frac{z_2}{z_1}) \tag{6.7}$$

In integrated form, Equation 6.4 may be written as

$$\tau = \rho K_m \frac{u_2 - u_1}{z_2 - z_1} \tag{6.8}$$

and by combination with Equation 6.6,

$$u_*^2 = K_m \frac{u_2 - u_1}{z_2 - z_1} \tag{6.9}$$

By solving Equation 6.7 for $u_*$, and substituting the result into Equation 6.9, the following expression for $K_m$ may be obtained:

$$K = \frac{\kappa^2 (u_2 - u_1)(z_2 - z_1)}{(\ln \frac{z_2}{z_1})^2} \tag{6.10}$$

Therefore, the kinematic eddy diffusivity for momentum may be directly related to measurable properties of the flowing air.

The relevance of Equation 6.10 to the evaporation process may be seen by assuming that water vapor is transported in proportion to momentum, and the eddy diffusivity of water vapor $K_v$ may be equated to the kinematic eddy diffusivity $K_m$. Therefore, evaporation flux density $E$ given by

$$E = -\rho K_v \frac{\partial q}{\partial z} \tag{6.11}$$

where $q$ is the specific humidity of the air, may be written

$$E = - \frac{\rho\kappa^2 (u_2 - u_1)(z_2 - z_1)}{(\ln \frac{z_2}{z_1})^2} \frac{\partial q}{\partial z} \tag{6.12}$$

In integrated form, Equation 6.12 is written

$$E = - \frac{\rho\kappa^2 (u_2 - u_1)}{(\ln \frac{z_2}{z_1})^2} (q_2 - q_1) \tag{6.13}$$

Equations of the form given by Equation 6.13 have been used to estimate potential evapotranspiration. Equations of this type represent the profile method of estimating vapor flow. The utility of Equation 6.13, however, is limited by the necessity to measure $q_1$, the specific humidity at the leaf surface. This difficulty may be avoided by use of the energy balance and an expression

for the heat (and mass) transfer from leaf surfaces.

Since energy must be conserved, the energy equation provides a mathematical means to calculate energy available for evaporation. Ignoring such small terms as energy storage in the canopy, the energy equation may be written on a daily basis as

$$R_n + \lambda E + G + A = 0 \tag{6.14}$$

where $R_n$ is the net daily radiation input to the evapotranspiration surface, $\lambda$ is the latent heat of vaporization of water, $G$ is the energy used in heating the soil, and $A$ is the sensible heat or heat convected from the surface of the atmosphere. Equation 6.14 is written for daily flux density to a surface that is assumed a uniform, homogeneous site of evaporation. For cropped surfaces, the surface represents an integration of the leaf area. In a forest, the surface must represent leaf area as well as ground area subject to evaporation.

The net radiation $R_n$ may be calculated from

$$R_n = R_s(1 - A_v) + R_L \tag{6.15}$$

where $R_s$ is the incoming shortwave energy, $A_v$ is the albedo of the vegetation, and $R_L$ is the net longwave or re-radiated energy input to the surface. Net radiation $R_n$ may be calculated by measuring $R_s$ and calcualting $R_L$ from temperature measurements, or it may be measured directly by using a net radiometer (Reifsnyder and Lull, 1965). The energy transferred daily to the soil may be estimated by functions such as given by Van Wijk and DeVries (1963),

$$G = G_m + G_r \sin\left(\frac{2\pi\ (D-\eta)}{365}\right) \tag{6.16}$$

where $G_m$ is the mean daily heat flux to the soil, $G_r$ is the maximum daily variation of $G$ from the mean, $D$ is the Julian day number and $\eta$ is a phase shift to compensate for the cycle not being at value $G_m$ on the first day of the year.

The sensible heat transfer is a convective process and may be expressed by:

$$A = -\rho c_p\ K_h\ \frac{T_2 - T_1}{z_2 - z_1} \tag{6.17}$$

where $c_p$ is the specific heat of air at constant pressure, $K_h$ is the eddy diffusivity of heat, $T_2$ is the temperature of air at distance $(z_2-z_1)$ from the surface, $T_1$ is the temperature of the surface, and $z_1$ is the height of the surface relative to some datum. Again by assuming that the heat transferred to the atmosphere is in proportion to the momentum transfer, $K_h$ may be taken as equal to the kinematic eddy diffusivity, allowing sensible heat transfer to be estimated as a function of atmospheric conditions. However, as in the case of the specific humidity of the surface, the temperature of the surface is usually not known. Transport equations such as Equations 6.4, 6.11 and 6.17 may be placed in a more useful form by assuming further that the flow is steady. Under this condition $K_m$, $K_v$ and $K_n$ may be assumed constant, and using the flow of sensible heat as an example, Equation 6.17 may be written as:

$$A = \frac{\rho c_p (T_1 - T_2)}{r_a''} \tag{6.18}$$

where $r_a''$ is known as the diffusion resistance to heat transport and is equal to $(z_2-z_1)/K_h$. The form of Equation 6.18 may also be used for Equation 6.13, resulting in

$$E = \rho \frac{q_1 - q_2}{r_a} \tag{6.19}$$

or

$$E = \frac{\rho_{v_1} - \rho_{v_2}}{r_a} \tag{6.20}$$

where $\rho_v$ is vapor density. Equations 6.18 and 6.20 still contain surface temperature and humidity, which are difficult to measure. However, a combination of Equations 6.20 and 6.14 is often used to predict potential evapotranspiration, PE, which is the maximum amount of water that can be evaporated and transpired for the given set of micrometeorological conditions and energy available. The necessity of measuring the state of vapor at the surface is avoided by assuming there are no horizontal gradients and that the energy entering a control volume at height $z_1$ is equal to that leaving at height $z_2$. The energy balance is therefore written for a control volume in

close proximity to the evapotranspiration surface, as observed by Van Bavel (1966) and Tanner and Pelton (1960). It is possible to eliminate the necessity of measuring at two points above the surface by using the aerodynamic arguments introduced in the derivation of $K_m$. This result is very advantageous since it allows calculation of evaporation by using only standard meteorologic measurements.

### 6.2.2 Evapotranspiration (ET)

From the standpoint of simulating soil moisture losses through evapotranspiration, two problems still remain: (1) evapotranspiration seldom proceeds at the potential rate, and (2) the formulations presented are not sensitive to plant type. In ET calculations the actual evapotranspiration $E_t$ rate is usually related to the potential rate by a multiplicative crop-soil factor. That is,

$$E_t = C_{et}PE \tag{6.21}$$

The difficulty with this approach is the estimate of $C_{et}$ and predicting its sensitivity to management activities. Further, $C_{et}$ depends on the moisture status of the plants and soils. In order to address this problem, several authors (Tanner and Pelton, 1960, and Slatyer, 1967) have proposed linking the energy and aerodynamic methods with a mechanistic leaf model.

A detailed discussion of the structure of plant leaves is beyond the scope of this discussion; however, a brief description of a mesophyte leaf is useful for hydraulic analysis. As pointed out by Slatyer (1967), the leaf of most mesophytes (plants having intermediate water requirements) is usually between 100 and 200 μ in thickness, and consists of between 10 and 15 cell layers. The upper and lower surfaces of the leaf are formed by the cuticle layer of waxy substance known as cutin that is essentially impervious to vapor transport. Immediately below the cuticle is a layer of epidermal cells whose outer walls are also impregnated with cutin. The cuticle and epidermis completely sheath the leaf except for many small openings called stomata.

The stomata are pores in the sheath that permit air to ventilate the leaf interior. A stoma is formed by a pair of guard cells, and the size of the individual stoma depends on the turgor of the guard cells. During periods when there is insufficient water for plant needs, guard cells lose turgor and the stomata may completely close. When water is plentiful, the guard cells

are fully hydrated and the stomata are open. Therefore, the stomata functions as a type of valve sensitive to plant moisture stress.

The actual site of evaporation in a leaf is the mesophyll tissue inside the epidermis. The liquid flow of water is conducted along the cell walls and through the cell cytoplasm. Mesophyll tissue consists of a sponge-like structure of cells and interconnects air passageways. Evaporation occurs on the interface between the cells and air. Since the mesophyll also contains most of the plant chlorophyll, it is also the site of most plant photosynthesis. Therefore, the regulation of water vapor, oxygen, and carbon dioxide by the stomata is vital to plant life functions.

The flow of water from the plant occurs largely in the vapor phase. However, the water enters the leaf in liquid form via the petiole or through leaf sheaths. Liquid water is distributed throughout the leaf to the mesophyll by a system of veins and vascular strands, branding into progressively smaller dimensions. The capillary tensions developed in the leaf may reach values lower than -100 bars, which combined with the cohesive nature of water, explains the ability of very tall trees to lift water to great heights.

From this very brief description of leaf morphology, it may be seen that the stomata exert considerable control over the evapotranspiration process. Therefore, models such as Equation 6.20 are inadequate, since they do not incorporate the plant's ability to regulate transpiration. Researchers including Slatyer (1967), Cowan (1965), and Cowan and Milthorpe (1968) have presented equations having the form

$$E = \frac{\rho_{v_1} - \rho_{v_2}}{r_\ell + r_a} \tag{6.22a}$$

where site 1 is within the leaf and $r_\ell$ is the resistance of the leaf to vapor flux back through the cuticle and through the stomata. Since the stomatal aperture is a function of plant water status, the evapotranspiration rate as given by Equation 6.22a is a function of atmospheric as well as plant water status.

The vapor concentration adjacent to the evaporation surface within the leaf, $\rho_{v_1}$, is usually somewhat less than the saturated vapor pressure at ambient conditions; however, the relative humidity within the spongy mesophyll is seldom less than 0.80 and is likely to be greater than 0.95 in non-

transpiring plants (Slatyer, 1967). Therefore, the assumption that $\rho_{v_1}$ is equal to the vapor density at saturation $\rho_{s_1}$ is justified. Equation 6.22a may be restated as

$$E = \frac{\rho_{s_1} - \rho_{v_2}}{r_\ell + r_a} \tag{6.22b}$$

The diffusive resistance to vapor transport $r_a$ may be approximated using heat transfer analysis as follows. If Equation 6.17 is written in the form

$$A = k_h \ (T_1 - T_2) \tag{6.23}$$

$k_h$ is defined as a local heat transfer coefficient, and may by equating terms with Equation 6.17 be expressed as

$$k_h = \frac{\rho c_p K_h}{z_2 - z_1} \tag{6.24}$$

As presented in Holman (1972), the nondimensional Nusselt number may be used to describe convective heat transfer. The Nusselt number for flow in the $x$ direction $N_{u_x}$ is described as follows:

$$N_{u_x} = \frac{k_h x}{k} \tag{6.25}$$

where $k$ is the thermal conductivity of the convecting fluid, in this case air. For a flat plate heated over its entire length, the Nusselt number may be represented as

$$N_{u_x} = 0.332 \ P_r^{1/3} \ R_{e_x}^{1/2} \tag{6.26}$$

where $P_r$ is the Prandtl number, $P_r = \nu/D$, $\nu$ being kinematic viscosity and $D$ being thermal diffusivity; and $R_{e_x}$ is the Reynolds number in the $x$ direction. Combining Equations 6.23 and 6.24 gives an expression for $k_h$

$$k_h = \frac{k}{x} \ (0.332 \ P_r^{1/3} \ R_{e_x}^{1/2}) \tag{6.27}$$

Or, for a plate of down-wind length $b$,

$$k_h = 4.57 \times 10^{-5} \frac{u^{1/2}}{b^{1/2}} \tag{6.28}$$

where $u$ is the wind speed and the constant reflects units of $cal/cm^{-2}\ sec^{-0.5}\,{}^{\circ}C^{-1}$. The average value of $k_h$, $\bar{k}_h$, is twice the local value, or

$$\bar{k}_h = 9.15 \times 10^{-5} \frac{u^{1/2}}{b^{1/2}} \tag{6.29}$$

Slatyer (1967) noted that a cylindrical body perpendicular to the flow has an average heat transfer coefficient of

$$\bar{k}_h = 1.03 \times 10^{-4} \frac{u^{1/3}}{(2r)^{2/3}} \tag{6.30}$$

where $r$ is the radius of the cylindrical body in centimeters.

From Equations 6.18 and 6.23 it may be seen that

$$k_h = \frac{\rho c_p}{r''_a} \tag{6.31}$$

or

$$r''_a = \frac{\rho c_p}{k_h} \tag{6.32}$$

Further, the resistance to heat transfer may be related to water vapor transfer by noting that

$$r''_a = \frac{d}{D} \tag{6.33}$$

where $d$ is the thickness of the boundary layer next to the surface. Similarly, the resistance to water vapor transfer may be expressed as

$$r_a = \frac{d}{D_w} \tag{6.34}$$

where $D_w$ is the diffusivity of water vapor in air. Therefore,

$$r_a = \frac{D}{D_w} r''_a \tag{6.35}$$

and finally, using Equation 6.29 with $r_2$ for the constant

$$r_a = \frac{D}{D_w} \frac{\rho c_p}{r_2} \left(\frac{b}{u}\right)^{1/2} \tag{6.36}$$

The values of $D$, $D_w$, $\rho$ and $c_p$ are constant at normal temperatures, so that Equation 6.36 may be written

$$r_a = r_1 \left(\frac{b}{u}\right)^{1/2} \tag{6.37}$$

Cowan and Milthorpe (1968) presented an additional function for randomly oriented leaves having the form of Equation 6.37.

$$r_a \cong 2.6 \frac{A^{0.25}}{u^{0.5}} \tag{6.38}$$

where $A$ is the individual leaf area and the units are in cgs system. Goldstein, Mankin and Luxmoore (1974) used

$$r_a = 3.3 \frac{\ell^{0.3}}{u^{0.5}} \tag{6.39}$$

where $\ell$ is a representative leaf length. This expression is currently used in the simulation.

Using expressions developed above, vapor flux to the atmosphere may be directly related to commonly measured meteorologic data and plant moisture status (noting that Equation 6.22 includes the leaf resistance to vapor flux which is itself a function of leaf hydraulic potential). Combining Equations 6.22, 6.18 and 6.14 and assuming that $r_a''$ is essentially equal to $r_a$, the following expression for ET flux to the atmosphere may be derived by eliminating $\rho_1^*$ and $T_1$,

$$E = \frac{\left\{\frac{(R_n - G_s) r_a \Delta}{\rho c_p} + (\rho_2^* - \rho_2)\right\}}{\left\{\frac{r_a \Delta \lambda}{\rho c_p} + (r_a + r_\ell)\right\}} \tag{6.40}$$

where

$$\Delta = \frac{T_1 - T_2}{\rho_1 - \rho_2} \tag{6.41}$$

Assuming the air and water vapor mixture behaves like an ideal gas,

$$\Delta = \frac{T_1 - T_2}{\rho_1 - \rho_2} \cong \frac{d\rho^*}{dT} = \frac{1}{R_v T} \frac{de^*}{dT} \tag{6.42}$$

where $R_v$ is the gas constant for water vapor and $e^*$ is the saturation vapor pressure. Several expressions for saturation vapor pressure and the slope of the saturation vapor pressure curve exist as functions of ambient temperataure $T_2$, the Goff-Gratch equation being among the most accurate (Smithsonian Institute, 1966). Equation 6.42 is similar in form to that presented by Monteith (1965) for latent heat transfer.

The resistance of leaves to vapor release is a combination of stomatal resistance, cuticle resistance, cellular transport, and resistance within the leaf itself (Cowan and Milthorpe, 1968). Leaf resistance has been successfully related to xylem hydraulic potential, water vapor deficit, incident radiation, leaf temperature, and intercellular $CO_2$ concentration (Ehleringer and Miller, 1976; Running, Waring and Rydell, 1975; Running, 1976; Slatyer, 1967; and Jarvis, 1976). The subject has inspired considerable research in the last two decades since it appears that stomata regulation exerts the greatest control over plant transpiration of all plant processes (Thompson and Hinckley, 1977; Slatyer, 1967). Of all the factors that affect stomatal resistance, leaf water potential is the most attractive for simulation, since if it dominates stomatal aperture, the coupling of the atmospheric considerations discussed above to a hydraulic plant and soil model would be complete. Unfortunately, stomatal resistance is apparently a complex function of all of the above factors (Jarvis, 1976). However, many researchers have successfully shown that stomatal resistance can be related to leaf water potential, although with considerable scatter. Goldstein and Mankin (1972) used a function of the form

$$r_\ell = r_{min} + (r_{max} - r_{min})\, e^{p(\Psi_c - \Psi_\ell)}, \quad |\Psi_\ell| < |\Psi_c| \tag{6.43}$$

where $r_{min}$ is the minimum leaf resistance assumed to represent resistance when stomata are fully open, $r_{max}$ is the maximum value of resistance when

stomata are closed, $\Psi_c$ is the critical leaf water potential at which the stomata are closed, and $p$ is an empirical factor.

An equation of this form incorporates most of the essential features of stomatal response to moisture stress, if not the exact mechanism. At high moisture stress ( $|\Psi_\ell| > |\Psi_c|$ ), the guard cells lose turgor and close. Under this condition the flux of water vapor continues, but at a greatly reduced rate, since it must pass through the leaf cuticle. Cuticle resistance $r_{max}$ and critical leaf water potential $\Psi_c$ are available in the literature for a number of species. Under conditions of full hydration the guard cells fully open the stomata and the flux of vapor is predominantly along that path. The resistance $r_{min}$ represents this flow condition.

A similar equation has been presented by Reed and Waring (1975), for stomatal resistance as a function of leaf infiltration pressure. Running, Waring, and Rydell (1975) show a figure relating pre-dawn plant moisture stress to leaf conductance for conifers that would fit an equation like Equation 6.43. However, the best models of leaf resistance as a function of a single variable are based on $CO_2$ concentration or vapor pressure deficit (Tan, Black and Nuyamak, 1977; Slatyer, 1967). Also according to Slatyer (1967), transpiration estimates based on water potential alone in general give good first approximation results. Further, intercellular $CO_2$ concentration and vapor pressure deficit require a more basic physiological model including plant photosynthesis processes. Therefore, Equation 6.43 is judged to give a reasonable or first-order approximation for stomatal control of transpiration.

### 6.2.3 Electrical Analogue

The remaining details of the soil-plant interaction were developed by Goldstein, Mankin, and Luxmoore (1974), and for clarity they are presented in this section. The basic concept of the soil and plant flow model is that this part of the system may be modeled by an electrical circuit analogue. While the details of this part of the simulation were developed by Goldstein and Mankin (1972), the analogue concept has been presented by many authors, including Cowan (1965), Cowan and Milthorpe (1968), Sutcliffe (1968) and Slatyer (1967).

The central assumption is that there is not storage in the plant in particular at the interface between the atmosphere and the plant tissues containing liquid water. Under this assumption the leaf water potential appears

as the independent variable in both the atmospheric analysis presented above and the electrical soil-plant analogue described below. If there is no storage at the liquid-vapor interface, the mass flow of vapor by ET flux from the interface must be equal to the delivery mass flow rate to the interface. A method therefore is established by which the leaf potential may be calculated as a function of measurable atmospheric conditions and known soil moisture status. The expressions are written for the flux of water to the ET surface in terms of the potential of the soil layers and the unknown potential of the ET surface. As discussed above, the flux away from the ET to the atmosphere is calculated using combined aerodynamic and energy balance approach. The flux away from the surface is also a function of the liquid-vapor interface potential $\Psi_\ell$ through the expression for resistance to vapor flux from the ET interface. If the mass flux to the interface is called $H(\Psi_\ell)$, and the flux to the surface is assumed to be equal to the flux away from the surface, then

$$E(\Psi_\ell) = H(\Psi_\ell) \tag{6.44}$$

$H(\Psi_\ell)$ represents a function of $\Psi_\ell$ derived by circuit analysis of the representative soil-plant electrical analog. An example of the function $H(\Psi_\ell)$ is derived below for the current model implementation. From the functional form of $H(\Psi_\ell)$ and $E(\Psi_\ell)$, from Equations 6.40 and 6.43 it will be clear that Equation 6.44 is a nonlinear expression for $\Psi_\ell$. In addition, it is functionally desirable to separate the expressions for vapor flux away from the ET interface and water flow to the interface so that their forms may be altered to fit the application. Therefore, Equation 6.44 is solved numerically by a linear fractional iteration scheme. This scheme seeks to find a zero of the function $F(\Psi_\ell)$ where

$$F(\Psi_\ell) = H(\Psi_\ell) - E(\Psi_\ell) \tag{6.45}$$

The model provides for up to five soil layers. The current model formulation assumes that there are five layers but the four lowest layers are assumed to have the same properties due to a lack of data. As stated earlier, the form of $H(\Psi_\ell)$ is dependent on the electrical analog used to represent the soil-plant system. The current form is based on the representation shown in Figure 6.1. The resistance definitions for Figure 6.1 appear in Table 6.1. Here the plant roots are assumed to be distributed only in the top two soil

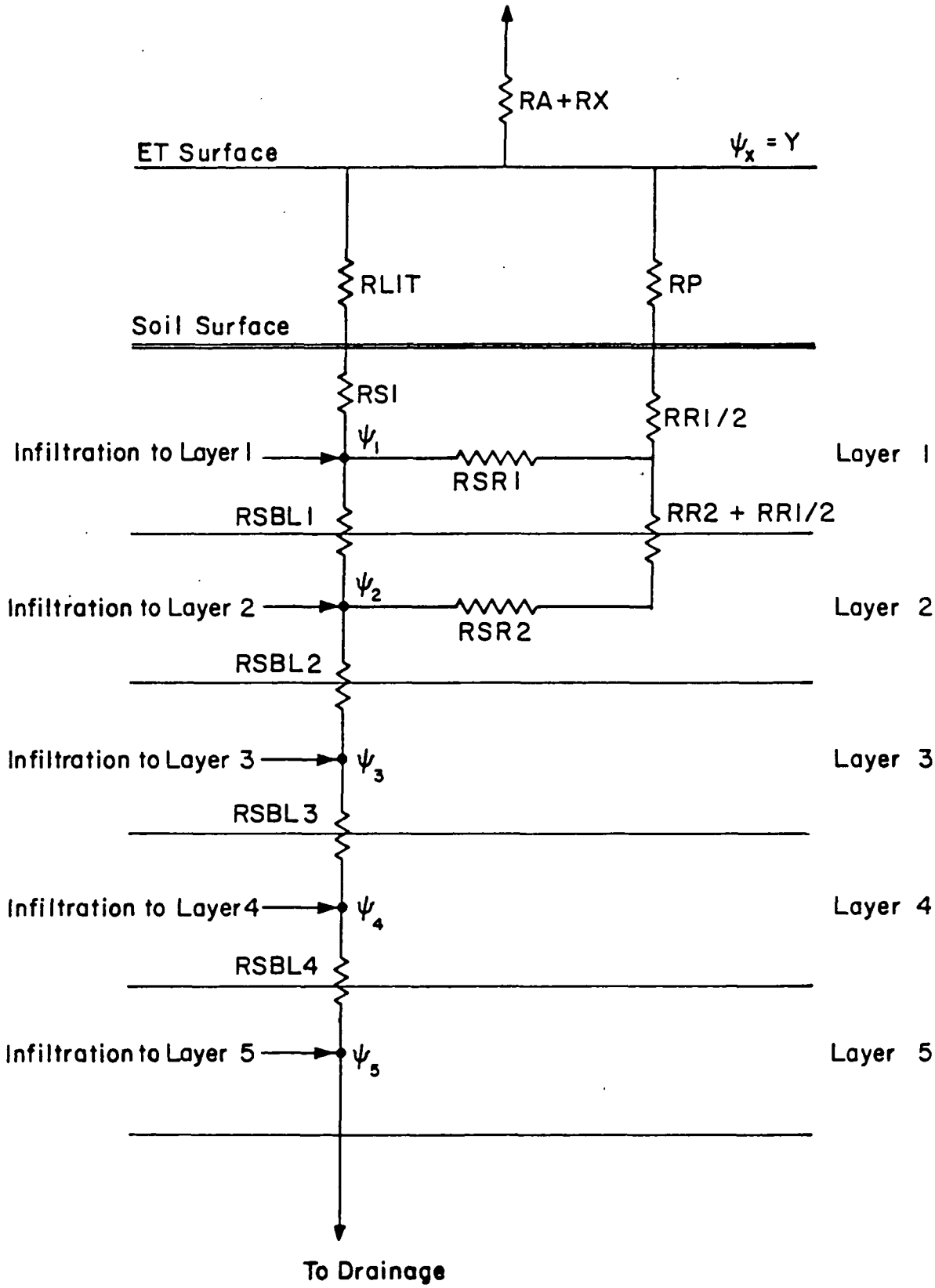


Figure 6.1. Electrical analogue for water balance calculations.

Table 6.1. Resistance Definitions for Figure 6.1

| Resistance | Resistance in Figure 2 | Verbal Description | Defining Expression or Resistance Value in Current Implementation |
|---|---|---|---|
| $r_\ell$ | RLIT | resistance of litter layer | 200,000 |
| $r_{s1}$ | RS1 | resistance to soil layer 1 | $\frac{d_1}{2\ K_1}$ |
| $r_{s2}$ | RS2 | resistance to soil layer 2 | $\frac{d_2}{2\ K_2}$ |
| $r_{r1}$ | RR1 | resistance of roots in layer 1 | $\frac{d_1}{2\ A_{r1}K_{r1}}$ |
| $r_{r2}$ | RR2 | resistance of roots in layer 2 | $\frac{d_2}{2\ A_{r2}K_{r2}}$ |
| $r_{sr1}$ | RSR1 | resistance to soil water uptake by roots in layer 1 | $\frac{d_1A_{r1}}{f_1A_IK_1}$ |
| $r_{sr2}$ | RSR2 | resistance to soil water uptake by roots in layer 2 | $\frac{d_2A_{r2}}{f_2A_IK_2}$ |
| $r_p$ | RP | above ground plant resistance | 5,000 |

layers of a five-layer soil column. The schematic of Figure 6.1 may be redrawn as shown in Figure 6.2a with resistance values as defined below and in Table 6.1. In Table 6.1 $d_i$ is the thickness of soil layer $i$, $K_i$ is hydraulic conductivity of soil layer $i$, $f_i$ is the fraction of roots in soil layer $i$, $A_{r_i}$ is the cross-sectional area of roots in layer $i$. The conductivity of roots in layer $i$ is assumed to be linearly related to the soil conductivity by

$$K_{r_i} = C_1 K_i \tag{6.46}$$

where $C_1$ is an empirically derived constant having the value of $10^4$ in the current implementation. The resistance to water flow between soil layers is represented by $RSBL_i$ in Figure 6.1. To simplify the resistance expressions the above resistances are regrouped as illustrated in Figure 6.2a. Resistance equivalences between Figure 6.1 and Figure 6.2a are as follows:

$$\begin{aligned} R1 &= RSBL1 \\ R2 &= RSR2 + (RR2 + RR1/2)\ g(A_I) \\ R3 &= RS1 \\ R4 &= RP + RR1/2 \\ R5 &= (RSR1)\ g(A_I) \end{aligned} \tag{6.47}$$

The numerical value of 200,000 for $r_\ell$ was obtained by calibration by Goldstein, Mankin and Luxmoore (1974). The value of 5000 appearing in this expression for the above-ground plant resistance $r_p$ was obtained from Cowan (1965). Both values represent possible calibration parameters for ET flux.

A $\Delta$-Y transformation is performed on the lower $\Delta$ of Figure 6.2a to produce the equivalent circuit of Figure 6.2b. The $\Delta$-Y transform gives an equivalent circuit element with resistances given by

$$\begin{aligned} RT1 &= \frac{R1\ R5}{R1 + R5 + R2} \\ RT2 &= \frac{R1\ R2}{R1 + R5 + R2} \end{aligned} \tag{6.48}$$

and

$$RT4 \equiv RT3 - RR = \frac{R5\ R2}{R1 + R5 + R2} \tag{6.49}$$

or

$$RT3 = \frac{R5\ R2}{R1 + R5 + R2} + RR \tag{6.50}$$

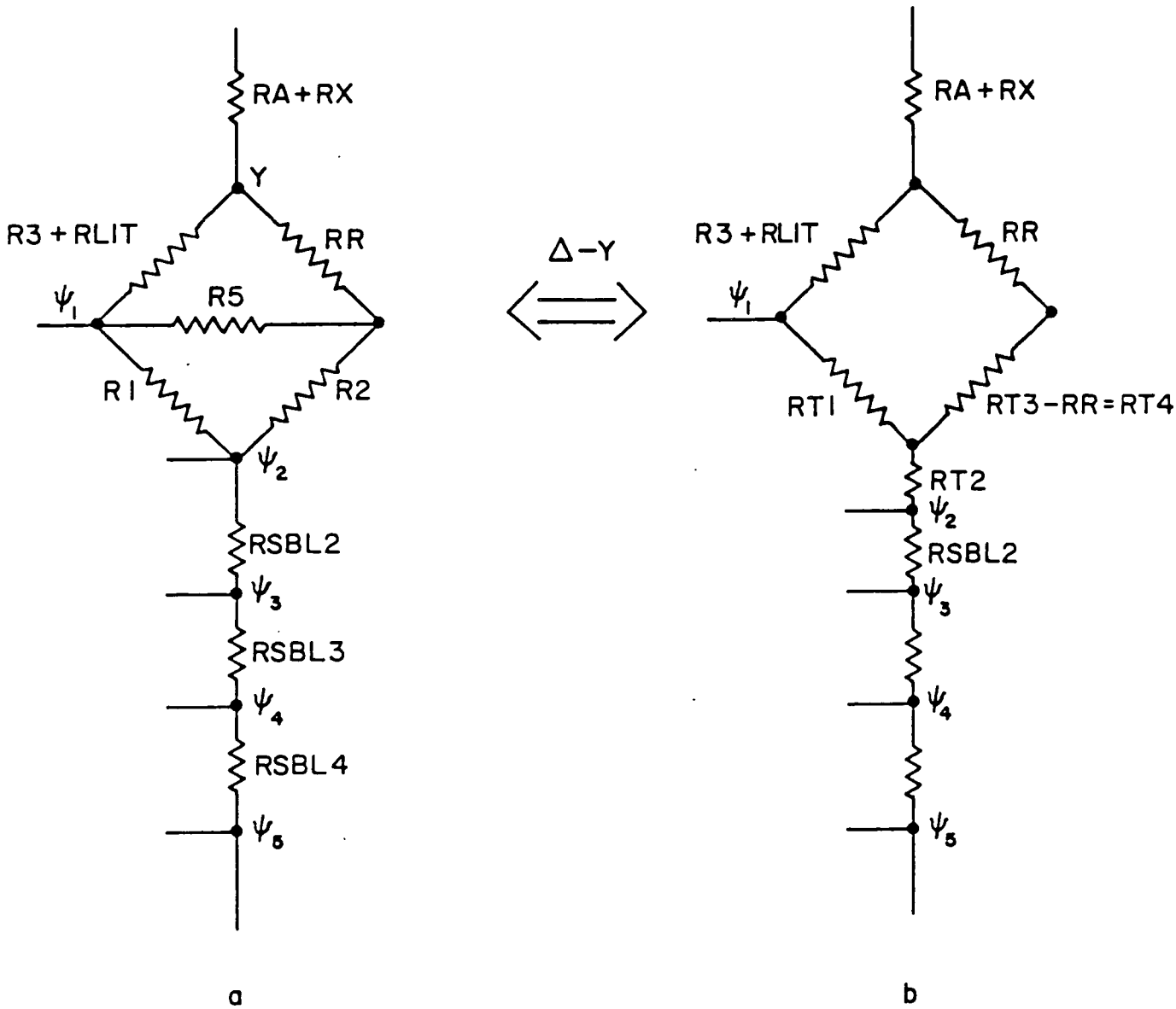


Figure 6.2. Circuit diagram of Figure A-1 and first Δ-Y transformation.

Noting that the loop of the circuit of Figure 6.2b may be redrawn as Figure 6.3a, another $\Delta$-Y transformation may be applied again to give the final equivalent circuit shown in Figure 6.3b. Equivalent resistances are given by

$$RRA = \frac{RT3\ RT1}{RT1 + RT3 + R3 + RLIT} + RT2 \tag{6.51}$$

$$RRB = \frac{(R3 + RLIT)\ RT3}{RT1 + RT3 + R3 + RLIT} \tag{6.52}$$

$$RRC = \frac{(R3 + RLIT)\ RT1}{RT1 + RT3 + R3 + RLIT} \tag{6.53}$$

Knowing potentials $\Psi_1$ and $\Psi_2$ from the previous calculation, the flux to the ET surface, $H(\Psi_\ell)$ may be expressed in terms of ET surface potential Y by Kirchoff's current law applied at node A (Figure 6.3). Allowing $\Psi_A$ to represent the potential at node A, and using the convention the flux away from the node is negative,

$$H(\Psi_\ell) = \frac{\Psi_A - \Psi_1}{RRC} + \frac{\Psi_A - \Psi_2}{RRA} \tag{6.54}$$

However, from Ohm's Law,

$$H(\Psi_\ell) = \frac{\Psi_\ell - \Psi_A}{RRB} \tag{6.55}$$

Therefore,

$$H(\Psi_\ell) = \frac{(RRA + RRC)\Psi_\ell - RRA\ \Psi_1 - RRC\ \Psi_2}{RRC\ RRA + (RRA + RRC)\ RRB} \tag{6.56}$$

or

$$H(\Psi_\ell) = \frac{\Psi_\ell - \frac{RRA}{D}\Psi_1 - \frac{RRC}{D}\Psi_2}{\frac{RRA\ RRC}{D} + RRB} \tag{6.57}$$

where $D = RRA + RRC$. This is the form of $H(\Psi_\ell)$ found in subroutines EVAL and SUBEV. This derivation is presented to indicate how the form of $H(\Psi_\ell)$ depends on the circuit representation and may be used as a guide if a different representation such as three or more soil layers of differing properties is desired.

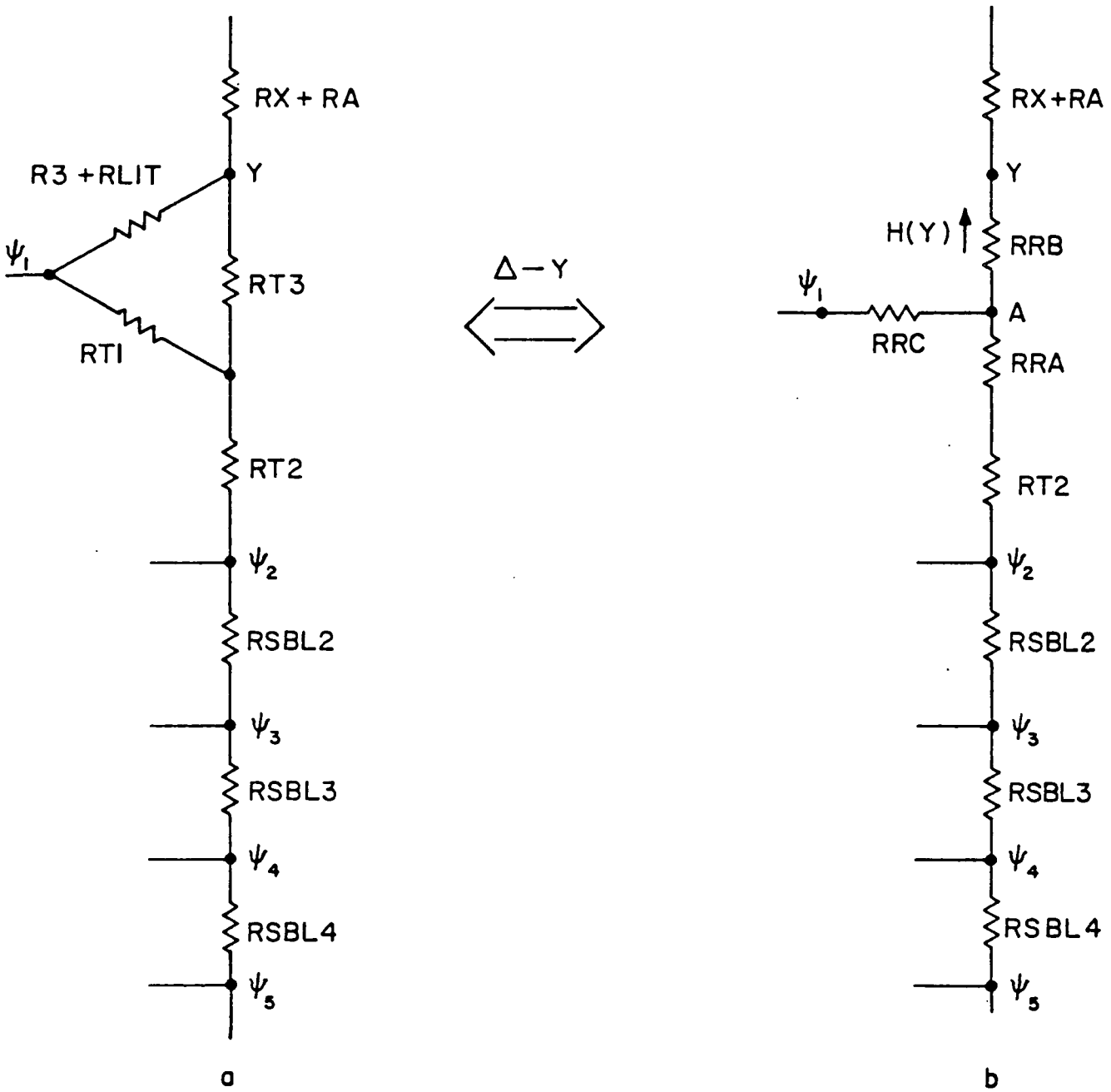


Figure 6.3. Second Δ-Y transformation.

6.2.4 Heat Transfer by Convection

The rate of transfer of heat energy by convection $A$ from the evapotranspiration surface is given by

$$A = \left[\sigma C_p \rho (T_1 - T_2)\right]/r_a \tag{6.58}$$

where $C_p$ is the specific heat of air at constant pressure, $\rho$ is the density of air, $T_1$ is the temperature of the evapotranspiration (ET) surface, $T_2$ is the ambient air temperature, and $r_a$ is the resistance to the transfer of sensible heat from the evapotranspiration surface to the atmosphere. All of these parameters have been defined above with the exception of $\sigma$, the ratio of convection area to evapotranspiration area. For this implementation, $\sigma$ is given by

$$\sigma = 1 + \frac{A_I}{A_{Imax}} \tag{6.59}$$

where $A_I$ is the current leaf area index and $A_{Imax}$ is the maximum value of $A_I$.

Convection occurs throughout the canopy. Since the evapotranspiration surface is a combination of soil surface, litter surface and leaf area, the evapotranspiration surface does not reflect the vertical structure of the canopy. Therefore, $\sigma$ is given this simple form to allow for greater convection than would be possible from a simple plane and relates convection area to canopy growth.

6.2.5 Implementation Specific to Vegetation Type

The parameters of Equation 6.43 are evaluated internally. Stomatal resistance at full hydration is given by

$$r_{min} = 6 - \left(\frac{L_I}{L_{Imax}}\right)\left(5 - \frac{2\ (T - T_{on})}{(T_{off} - T_{on})}\right) \tag{6.60}$$

where $T$ is the Julian day number, $T_{on}$ is the Julian day the canopy has emerged 50 percent, and the $T_{off}$ is the Julian day the canopy has fallen below 50 percent emergence.

It should be noted that the expression for $r_\ell$, the resistance to vapor flux from the evapotranspiration surface, is related to canopy growth through the expression for $r_{min}$. This functional relationship can account for obser-

vations that the number of open stomata varies during the year and that minimum stomatal resistance per unit area varies with leaf area. Therefore, if changes to this function are made, these variations may need to be considered.

Swift et al. (1975) modified the energy flux equation originally implemented by Goldstein, Mankin and Luxmoore (1974) to account for leaf area being much greater than ground surface area. However, the leaf area index is not directly used since not all of the canopy is equally effective in evapotranspiration at any given time. An effective leaf area function $f(A_I)$ is implemented to compensate for this effect. This variable has the form

$$f(L_I) = \frac{L_I}{1 + \frac{L_I}{3}} \tag{6.61}$$

In addition, $f(L_I)$ is used in the energy balance calculation of evapotranspiration flux given by

$$R_N = [f(L_I) + 1]\ \lambda E + [\sigma f(L_I) + 1]\ A + G \tag{6.62}$$

where $R_N$ is the net incoming solar radiation, $\lambda$ is the latent heat of vaporization of water, $A$ is the convective heat flow, $E$ is the vapor flux, and $G$ is the daily change in soil heat storage. The functional form of $f(L_I)$ was selected for experimental data obtained at the Coweeta Hydrological Laboratory and is discussed in Swift et al. (1975). If such data are available in the area to be modeled, the formulation could be changed.

The electrical analog representation discussed below assumes that plant transpiration characteristics may be lumped into a single resistance to water flux for each watershed plane. Therefore, active roots, stems and leaves are assumed to be homogeneously distributed across the plane. This assumption is probably most valid under the condition of a closed canopy. However, for management activities such as crop growth in agricultural watersheds, timber replacement and regrowth, or under natural conditions of low canopy cover, a closed canopy cannot be assumed. Since number of transpiration paths per unit ground area is reduced for low values of leaf area index, the resistance to transpiration water flux should increase during these periods. Swift et al. (1975) presented a function of the form

$$g(L_I) = \frac{k\ L_I^2}{(A_1^2 + L_I^2)} \tag{6.63}$$

where $A_1$ and $k$ are calibrated parameters, to accomplish the increase in resistance. The transpiration resistances are therefore divided by $g(L_I)$.

## 6.3 Interception and Infiltration

### 6.3.1 Interception

The processes of interception and infiltration have been discussed in Chapter 5; however, some modifications of these routines are incorporated into the interstorm model. When coupling the event water and sediment model with the interstorm model, the interstorm routines perform more sophisticated interception and infiltration calculations in order to generate excess rainfall on any given day. The interception process is modified to incorporate evaporation. The infiltration model is reformulated to provide for layered soils.

A portion of rainfall is intercepted by canopy foliage, ground cover, and forest litter. Part of this water eventually reaches the ground by stem flow or by dripping from vegetation; however, the water that is held on these surfaces never reaches the soil and is for the most part lost to evaporation. In many conditions of light rainfall or in dense forests this process cannot be ignored. For this purpose of this simulation the intercepting area is taken to be equal to the area of the evapotranspiration surface. Maximum and minimum values of interception storage per unit canopy-covered area are assumed to be provided data, and therefore potential interception storage is a volume of water related to evapotranspiration surface size and the amount of water already existing in interception storage.

On a day when rainfall occurs, an amount of water equal to the available interception storage or the volume of rainfall, whichever is smaller, is removed from the storm water available for infiltration. Some or all of this water is evaporated during the day. Any water left in interception storage decreases the amount of interception potential for the next day to the difference between the maximum potential storage and the amount of water left in storage. In addition, since the storage of energy available for evaporation in the forest environment is assumed negligible with respect to the daily

energy fluxes, the energy required to evaporate water from interception storage should be deducted from the daily influx of solar radiation before evapotranspiration is calculated. This approach works well for determining daily water balance; however, it must be augmented in order to modify the rainfall hyetographs into throughfall needed for infiltration and subsequent surface water routing calcualtions, particularly when a storm lasts for more than one day.

In order to modify the rainfall histogram, the following procedure is adopted. On the day the rainfall begins, a volume of water equal to that day's potential interception volume is removed from the beginning of the rainfall hydrograph. Of course, if this volume is greater than the day's precipitation volume, no throughfall will occur on this day, and the remaining interception volume, after evaporation, forms a part of the potential interception volume for the next day. The rationale for removing the interception volume from the beginning of the storm on the first day of the event is based on the concept that at the beginning of a storm the potential interception volume represents a reservoir that must be filled before throughfall can reach the ground. Processes of stemflow and dripping are ignored for the purposes of this simulation. If there is insufficient rainfall volume to satisfy the interception volume on the first day of the storm, all of that day's rainfall is intercepted. The remaining unfilled interception volume is added to the day's evaporation loss from interception, and this volume becomes the potential initial interception loss for the next day, and so forth through the storm. The change in the beginning of the storm to reflect initial interception losses is illustrated in Figure 6.4.

If the storm lasts for more than one day, significant changes in potential interception volume may occur as a result of evaporation. Evaporation losses from the interception storage are assumed to be made up by interception on the following day. Since evaporation losses are distributed throughout the day, these losses are not subtracted from the beginning of that day's rainfall, but are assumed to be made up uniformly during the next day. The distribution of interception storage losses and the subsequent modification of rainfall after the initial storage is satisfied as illustrated in Figure 6.4.

Equations 6.64 and 6.65 below are used to calcualte the initial and distributed evaporation interception volumes per unit area, respectively.

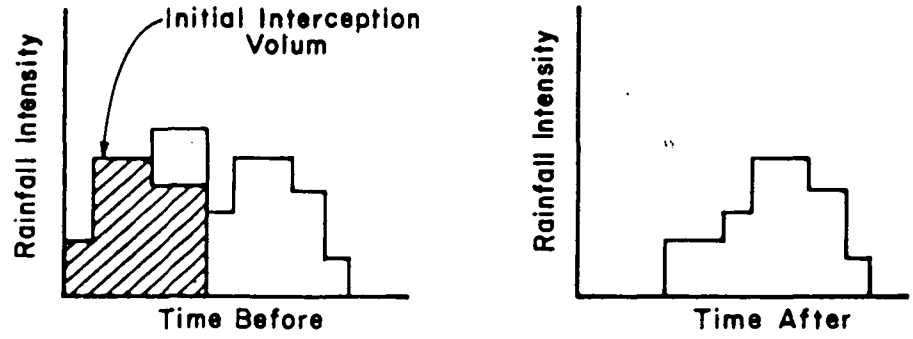


(a) Initial Interception

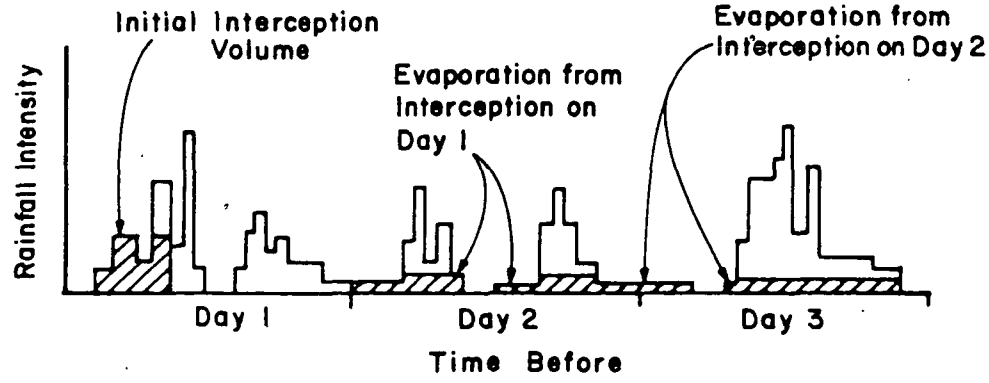


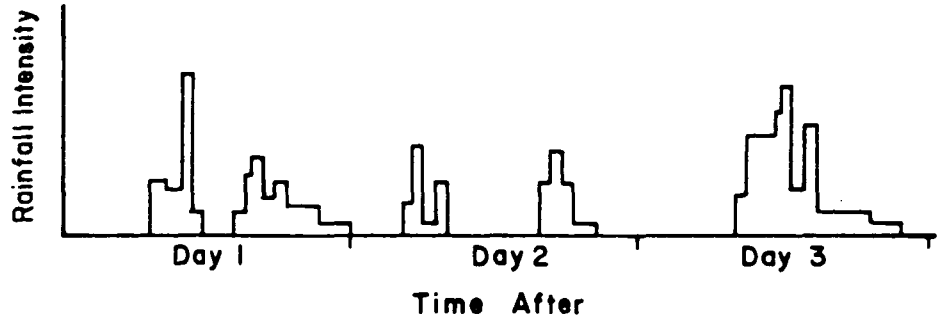


(b) Multiple Day Storms

Figure 6.4. Transformation of hyetograph by interception process.

$$V_I = [\frac{L_I}{L_{Imax}} V_{Imax} C_c + V_{Imin} (1 - C_c)] - V_{I_i} \tag{6.64}$$

$$V_I = (\frac{E_I}{D_s}) D_s \tag{6.65}$$

where $V_I$ is the potential interception volume per unit watershed area, $V_{Imax}$ is the potential interception volume per unit area completely covered by canopy, $V_{Imin}$ is the potential interception volume per unit area not covered by canopy, $L_I$ is the canopy leaf area index, $L_{Imax}$ is the maximum value of $L_I$, $C_c$ is the fraction of watershed area covered by canopy, and $V_{I_i}$ is the residual water stored in interception as a result of insufficient evaporation on the previous day. The residual interception $V_{I_i}$ is assumed to be evenly distributed between canopy covered and uncovered ground. Since $V_I$ varies with canopy leaf area index, it is mathematically possible that case $V_I$ is assumed to be zero.

In Equation 6.65, $E_I$ is the daily evaporation loss from interception storage and $D_s$ is the duration of the non-zero portion of a storm on a given day. Equation 6.65 appears unsimplified to illustrate that the intensity $(E_I/D_s)$ is subtracted from the hyetograph intensities to provide for a uniform distribution in time of the evaporation losses from interception. Evaporation losses are assumed to be evenly distributed between leaf area and uncovered ground.

A short comment on the definition of some of the above quantities is relevant at this point. Leaf area index is usually defined as the ratio between the total watershed leaf area and the watershed ground area. Leaf area index as a function of time may be viewed to give the growth curve for the plan tspecies. Some authors, e.g. Rutter (1967), have used leaf area index to describe species-specific response. The difficulty with the definition as it usually appears is that if strictly interpreted, it would also be affected by cover density. For crops and dense forests, there usually is no problem, since crown closure may be assumed. However, where cover densities are significantly less than one, that is, where there are clearings in the forest or thinning has been performed, a more rigid definition is necessary. For the purposes of this model, leaf area index as measured in a closed canopy will be assumed to be the same as the ratio between the leaf area of an individual and

the ground covered by that individual. This definition effectively makes the leaf area index function-specific to the plant type and not to the particular watershed. This assumption is imperfect as well, since it does not allow for species response to different environments; however, it provides a more workable definition.

Secondly, that definition of canopy cover density for current purposes needs some clarification. The present simulation is made up of watershed response subunits consisting of planes and channels. Precise detail of parameter distributions within the planes is not made. That is, the cover density is taken to be uniformly distributed across the plane. For example, an 80 percent canopy cover is taken to mean that at any given point in the plane, there is an 80 percent probability of being covered by canopy. This applies to a representation of a real watershed having 80 percent of its surface continuously covered with closed canopy and 20 percent continuous clearing, as well as a closed canopy that has been 20 percent thinned. This definition also extends to ground cover and allows expressions of set theory to be applied to combinations of cover.

### 6.3.2 Infiltration

The infiltration scheme chosen is a time-explicit formulation for the Green and Ampt infiltration equation as presented by Eggert, Li and Simons (1979). This method is an extension to layered soils with hydraulically homogeneous layers of a time-explicit formulation presented by Eggert (1976). The derivation of the layered scheme for layered soils parallels that for a homogeneous soil. For clarity the derivation will be briefly discussed. Modern interpretation of the Green-Ampt (1911) formulation as provided by Mein and Larson (1973), assumes that as rainfall infiltrates the soil, a wetting front advances like a piston so that the rate of change of volume behind the wetting front equals the infiltration rate at the surface. The situation is illustrated by Figure 6.5. Here the location of the wetting front at time $t$ is shown by the dashed line of depth $z$ from the surface. At the beginning of the storm, the wetting front is assumed to be at the surface. It moves downward through the soil column as water infiltrates, filing the volume of pore space not already occupied by water initially in the layers at the beginning of throughfall.

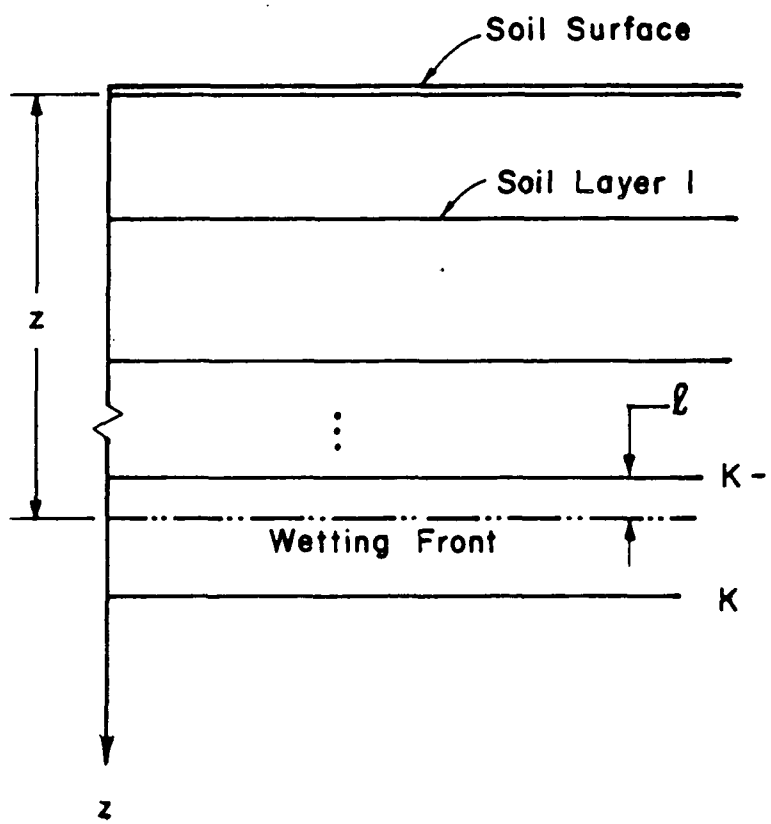


Figure 6.5. Definition sketch for infiltration process.

To formulate the equation of infiltration, it is assumed that the wetting front as mentioned before is already at depth $z$ as shown in Figure 6.5. The total hydraulic head at depth $z$ is

$$h_T = \sum_{i=1}^{k-1} \Delta h_i + \Delta h_k \tag{6.66}$$

where $h_T$ is the total head at $z$, $\Delta h_i$ is the head loss in the $i^{th}$ fully-wetted layer, and $\Delta h_k$ is the head loss in the $k^{th}$ layer containing the wetting front. For flow above the wetting front, Darcy's law for the $i^{th}$ layer may be written

$$\frac{Q}{A_G} = q = K_i \frac{\Delta h_i}{\Delta z_i} \tag{6.67}$$

where $Q$ is the total volume inflow of water per unit area, $A_G$ is the ground area, $q$ is the Darcian velocity, $K_i$ is the hydraulic conductivity in the wetted zone of the $i^{th}$ layer, $\Delta h_i$ is the change in head in the $i^{th}$ layer, and $\Delta z_i$ is the thickness of the $i^{th}$ layer. Solving Equation 6.67 for $\Delta h_i$ for each $i = i,k$ and substituting the results into Equation 6.66 yields an expression for the total hydraulic head at $z$ as a function of the Darcian flux $q$

$$h_T = q \left( \sum_{i=1}^{k-1} \frac{\Delta z_i}{K_i} + \frac{\ell}{K_k} \right) \tag{6.68}$$

where $\ell$ is the distance that the wetting front has penetrated the $k^{th}$ layer. However, the total hydraulic head may also be written as the sum of the gravitational and capillary suction heads such that

$$h_T = \underbrace{\sum_{i=1}^{k-1} \Delta z_i + \ell}_{\text{gravitational head}} + \underbrace{\bar{\Psi}_k}_{\text{capillary pressure head}} \tag{6.69}$$

where $\bar{\Psi}_k$ is the capillary suction head across the wetting front in the $k^{th}$ layer. Therefore, Equation 6.69 may be substituted into Equation 6.68 yielding an expression for $q$, that is,

$$q = \frac{\sum_{i=1}^{k-1} \Delta z_i + \ell + \overline{\Psi}_k}{\sum_{i=1}^{k-1} \frac{\Delta z_i}{K_i} + \frac{\ell}{K_k}} \tag{6.70}$$

If $F$ is allowed to be the total infiltrated water volume above the wetting front at $z$, it may be expressed as

$$F = \sum_{i=1}^{k-1} \phi_i \, \Delta S_i \, \Delta z_i + \phi_k \, \Delta S_k \ell \tag{6.71}$$

where $\phi_i$ is the porosity of the $i^{th}$ layers and $\Delta S_i$ is the difference between the percent of pore space in the $i^{th}$ layer filled with water at saturation and the percent of pore space filled with water initially or the initial degree of saturation deficit of the $i^{th}$ layer. The product of porosity and degree of saturation deficit is the potential change of dimensionless water content or for the $i^{th}$ layer, $\Delta\theta_i = \phi_i \Delta S_i$. Allowing the summation term of Equation 6.71 to be represented as $F_{k-1}$, the length $\ell$ may be expressed as

$$\ell = \frac{F - F_{k-1}}{\Delta\theta_k} \tag{6.72}$$

Using Equations 6.71 and 6.72 and noting that $q = dF/dt$ by continuity, Equation 6.70 may be written as

$$\frac{dF}{dt} = \frac{z_{k-1} \, \Delta\theta_k + F - F_{k-1} + \overline{\Psi}_k \, \Delta\theta_k}{W_{k-1} \, \Delta\theta_k + \frac{F - F_{k-1}}{K_k}} \tag{6.73}$$

where

$$z_{k-1} = \sum_{i=1}^{k-1} \Delta z_i$$

and

$$W_{k-1} = \sum_{i=1}^{k-1} \frac{\Delta z_i}{K_i}$$

In order to simplify algebra it may be noticed that for flow in the $k^{th}$ layer

$$\Delta\theta_k \, (z_{k-1} + \bar{\Psi}_k) - F_{k-1} = c_k = \text{constant}$$

$$W_{k-1} \, \Delta\tilde{\theta}_k - \frac{F_{k-1}}{K_k} = d_k = \text{constant} \tag{6.74}$$

Therefore, for flow in the $k^{th}$ layer, Equation 6.73 may be written as

$$\frac{dF}{dt} = \frac{c_k + F}{d_k + \frac{F}{K_k}} \tag{6.75}$$

Suitable rearrangement of Equation 6.75 and integration within the $k^{th}$ layer yields the following nonlinear expression for $F$:

$$(d_k - \frac{c_k}{K_k}) \ln (1 + \frac{F}{c_k}) - (d_k - \frac{c_k}{K_k}) \ln (1 + \frac{F_{k-1}}{c_k}) + \frac{F - F_{k-1}}{K_k} = t - t_{k-1} \tag{6.76}$$

where $t$ is the time after the beginning of the event when the total infiltrated volume equals $F$, and $t_{k-1}$ is the time when the total infiltrated volume was $F_{k-1}$ (or when the wetting front was at $z = z_{k-1}$). In order to obtain an approximate solution to Equation 6.76, it is noted that within the $k^{th}$ layer the infiltrated volume at some time $t + \Delta t$ may be expressed as

$$F(t + \Delta t) = F(t) + \Delta F \tag{6.77}$$

where $\Delta F$ is the change in $F$ occurring between $t$ and $t + \Delta t$. If Equation 6.76 is written for $F(t + \Delta t)$ and $F(t)$ and subtraction is performed, an expression for $\Delta F$ as a function of $F(t)$ results:

$$(d_k - \frac{c_k}{K_k}) \ln [1 + \frac{\Delta F}{c_k + F(t)}] + \frac{\Delta F}{K_k} = \Delta t \tag{6.78}$$

The logarithmic term may be expressed using a standard series expansion for $\ln(a+x)$,

$$\ln(a+x) = \ln a + 2 \, [\frac{x}{2a + x} + \frac{1}{3} (\frac{x}{2a + x})^3 + \ldots] \tag{6.79}$$

If only the first two terms of Equation 6.79 are used, insignificant error

results (Li, Simons and Stevens, 1976). Noting that $a = 1$, Equation 6.78 may be approximately rewritten and simplified to become

$$\Delta F^2 + [2K_k d_k + 2F(t) - K_k \Delta t]\ \Delta F$$

$$- 2K_k \Delta t\ [c_k + F(t)] = 0 \qquad (6.80)$$

Equation 6.80 may be immediately recognized as a quadratic equation for $\Delta F$. All other quantities in Equation 6.80 are known at time $t + \Delta t$; therefore the change in infiltrated volume between time $t$ and $t + \Delta t$ may be calculated from

$$\Delta F = \frac{-\beta \mp \sqrt{\beta^2 - 4\gamma}}{2} \qquad (6.81)$$

where

$$\beta = 2K_k d_k + 2F(t) - K_k \Delta t$$

$$\gamma = -2K_k \Delta t[c_k + F(t)]$$

and only the positive root is physically meaningful.

Equation 6.81 provides a time-explicit formulation for the change in infiltrated volume occurring between $t$ and $t + \Delta t$. The formulation is written for flow in the $k^{th}$ layer. However, this presents no computational problems since initially $F = 0$ and the flow is in the first layer. As the event proceeds in time, water enters the upper soil surface of the soil and the wetting front travels down through the soil. One need only keep track of the location of the wetting front at any time and appropriately update the values of $F(t)$, $W_{k-1}$, $Z_{k-1}$, $\widetilde{\Delta\theta}_k$, $\bar{\Psi}_k$, $F_{k-1}$, and $K_k$ depending on the location of the wetting front. The only apparent difficulty is the implicit nature of the problem, since the depth of the wetting front at any time is directly related to the infiltrated volume. However, the problem is easily solved due to the explicit nature of Equation 6.81. The change in infiltrated volume $\Delta F$ given by Equation 6.81 represents a potential volume that will infiltrate if there is sufficient supply of water at the surface. If there is insufficient throughfall during $\Delta t$ to satisfy the potential volume, then the infiltration is controlled by rainfall and

$$\Delta F = i\ \Delta t \qquad (6.82)$$

### 6.3.3 Infiltration Parameters

The Green-Ampt layered infiltration model described above is essentially a two-parameter model: (1) $K_i$ the hydraulic conductivity in the wetted zone of the $i^{th}$ layer and (2) $\Psi_i$ the average capillary suction head of the $i^{th}$ layer. A possible third parameter is the porosity of the $i^{th}$ soil layer $\phi_i$, but this parameter is bound to the initial saturation deficit $\Delta S_i$ which is discussed below, and is assumed not to change as a function of moisture content. The hydraulic conductivity of the soil layer is a function of the layer moisture content. However, the Green-Ampt formulation is based on the saturated conductivity of the wetted zone $K_s$. This parameter does not appreciably vary with moisture content. The average suction head, however, is a direct function of initial degree of saturation. This parameter is evaluated by taking the weighted mean of the capillary suction between the initial degree of saturation and the final degree of saturation using the relative conductivity as a weighting function. The approach was suggested by Mein and Larson (1973). The equation for average head takes the form

$$\bar{\Psi}_k = \int_{k_k(S_i)}^{k_k(S_w)} \Psi dk_k \qquad (6.83)$$

where $k$ is the relative hydraulic conductivity of the $k^{th}$ layer; that is, $k_k(S) = K_k(s)/K_{S_k}$ where $K_{S_k}$ is the saturated hydraulic conductivity of the $k^{th}$ layer, and $K_k(S)$ is hydraulic conductivity of the $k^{th}$ layer at saturation $S$; $S_w$ is the final or wetted soil degree of saturation, usually taken as 1.0, and $S_i$ is the initial degree of saturation. As examples, graphs of $\bar{\Psi}$ as a function of $S_i$ are shown in Figure 6.6. For degrees of saturation near 1.0, $\bar{\Psi}$ is obviously a sensitive function of $S_i$. For this reason the value of $\bar{\Psi}_i$ is updated based on the value of $S_i$ on the day prior to the storm by reevaluating Equation 6.83. Therefore, the initial degree of saturation serves as an initial condition affecting the saturation deficit $\Delta S_i$ and the average suction head. All of the parameters mentioned above are determined by a soil routine of the daily water flux model or are supplied as changing inputs from daily moisture content calculations.

The soil routine for initially determining the soil moisture-soil tension and soil moisture relative conductivity terms is borrowed from the Goldstein, Mankin and Luxmoore (1974) model. This routine uses theory presented by Green

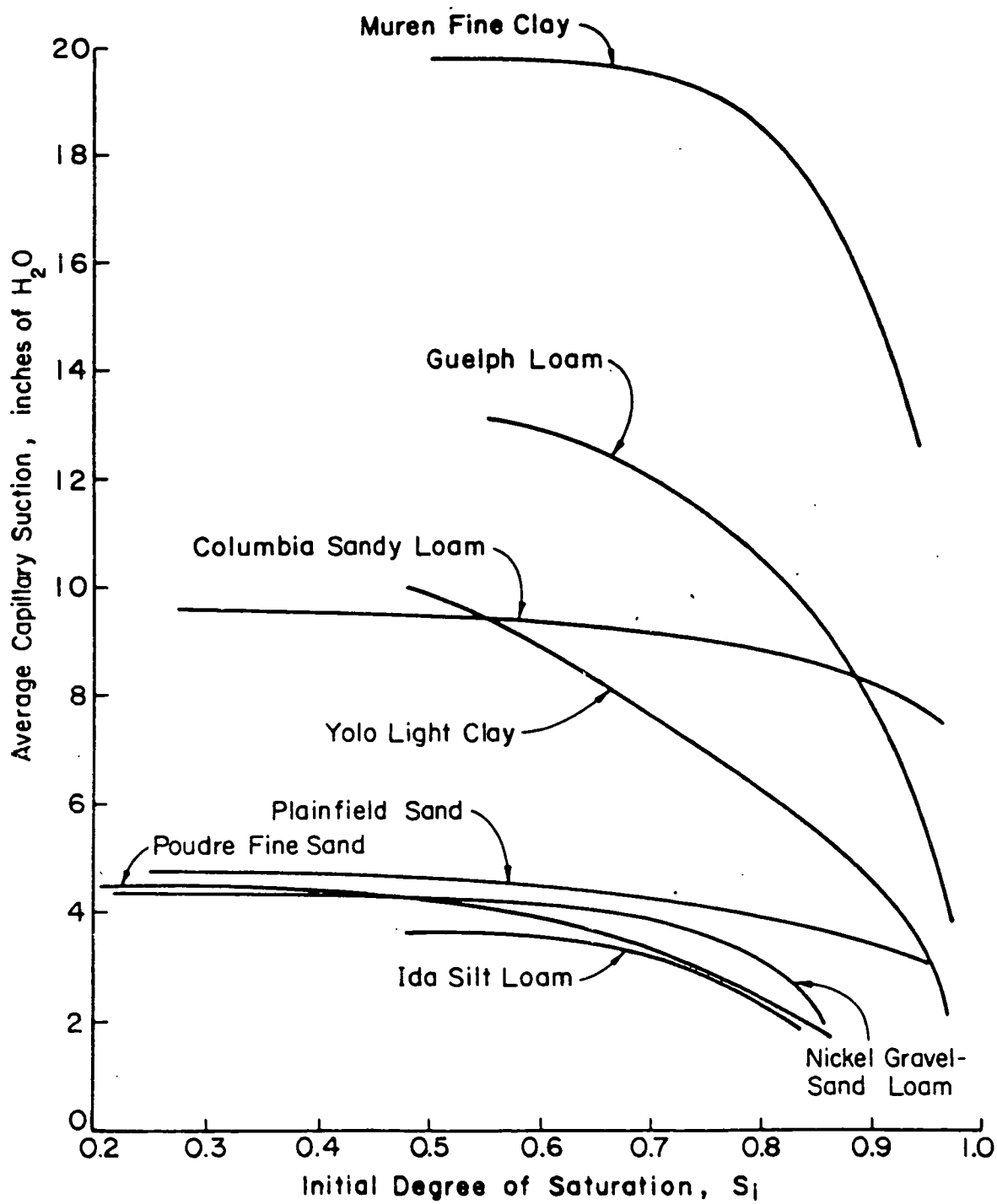


Figure 6.6. Average capillary suction head as a function of initial moisture content.

and Corey (1971). The method allows calculation of full soil hydraulic properties from the porosity and a simple laboratory tensiometer-moisture content experiment.

The above discussion with reference to Appendix A completes a description of the portion of the model necessary to simulate evapotranspiration, soil water balance, interception, and infiltration. In short, those routines necessary to calculate time-dependent excess rainfall function on a continuous basis. This model may be used to simulate on a daily basis any period of time for which environmental data are provided.

## 6.4 Data Requirements for Interstorm Model

Simulation of the interstorm processes requires a variety of data. Measurements of soil, meteorological, geometric and vegetative parameters are required for input and calibration. Usually daily values are necessary for meteorological variables used in obtaining meaningful estimates of soil moisture variation. The following list details the data requirements for simulation of daily soil moisture.

Geometry and Channel Data

- Length of overland slopes
- Width of overland slopes
- Elevation of watershed

Soil Data

- Distribution of soils
- Types of soils
- Number of soil layers
- Thickness of layers
- Initial water content of layers or top layer
- Saturated hydraulic conductivity of each layer or top layer
- Tensiometer measurements (desorption curve) for each layer
- Temperature for tensiometer data
- Field moisture capacity for each layer
- Porosities of soil layers on top layer

Vegetation Data

- Types
- Distribution
- Density of ground cover
- Density of canopy cover
- Storage of ground cover
- Maximum and minimum storage of canopy cover
- Albedo of vegetation
- Yearly growth cycle of canopy
- Average leaf length of dominant species

Maximum and minimum leaf area
Root cross-sectional area per unit area of soil in each layer
Fraction of roots in each layer

Climatic Data
Daily solar radiation
Average daily temperature
Average daily humidity or vapor pressure
Total daily precipitation
Average wind speed

Climatic Data
Air pressure—for year as function of altitude
Specific heat of air
Rainfall storm hyetographs

Hydrologic and Hydraulic Data
Storm and daily runoff hydrographs

Man's influence may affect all of the physical qualities controlling water runoff, sediment yield, and nutrient transport from watersheds. The effects can be quantified by assessing the impact of man's activities on the different measurable variables.

## 6.5 Pesticide Loading

The pesticide model chosen for this study is a simple mechanistically based model developed by the Science and Education Administration - Agricultural Research (Knisel, 1980). It is directly coupled to the water and sediment yield model through the use of water and sediment runoff volumes as inputs. The model also requires an estimate of the initial moisture deficit in the soil, therefore, the interstorm model may be used to generate daily changes in initial moisture content. The following discussion is taken from Leonard and Wanchope, 1980 (Knisel, 1980).

The pesticide submodel was developed on simplified concepts of processes and designed to be responsive to different management options. Foliar- and soil-applied pesticides are separately described so that different decay rates can be used for each source of the same chemical if necessary. Usually pesticide residing on foliage dissipates more rapidly than that from soil. Also decay rates can be made site specific if information is available. Movement of pesticides from the soil surface as a result of infiltrating water is estimated using differences of rainfall and runoff for the storm and pesticide mobility parameters. Pesticide in runoff is partitioned between the solution or water phase and the sediment phase. This aspect is particularly important

when examining management options that limit sediment yield.

A simple conceptualization of the runoff system is shown in Figure 6.7. The primary source of pesticide available to enter the runoff stream is visualized as a surface layer of soil defined arbitrarily as having a depth of one centimeter. This definition is based on observations by Leonard et al. (1979) that runoff concentrations of both dissolved and adsorbed pesticides were strongly correlated with pesticide concentrations in this layer. Actually the thickness of this layer depends on many factors. Pesticide extraction by raindrop splash and interrill soil movement may occur in a very shallow layer, whereas extraction from rills may extend several centimeters deep. In models by Bruce et al. (1975) and Frere et al. (1975), rill and interrill extractions were described separately, but here the process was conceptually combined for simplicity. Others have defined this effective thickness to be about 0.5 cm and 2.5 cm (Crawford and Davigan, 1974; Steachius and Walter, 1978).

Washoff of pesticide applied to foliage is another source that may enter the runoff stream. In this model, the fraction of applied pesticide intercepted by foliage is specified initially. Dislodgeable residue remaining on the foliage at the time of rainfall is estimated from information given in Knisel (1980). The fraction of this dislodgeable residue removed by rainfall is then added to the soil surface 0 to 1 cm zone and a new concentration for this zone is computed for the runoff event.

Pesticide dissipates from the surface zone primarily by degradation and volatilization processes. During rainfall events, pesticide may move below the surface zone in the infiltrating water and across the surface in runoff. In the model, initial concentrations of unincorporated pesticides are computed as if they were uniformly incorporated into the 0 to 1 cm depth. Concentrations of incorporated pesticides are computed based on their incorporation depth and efficiency of incorporation. A simplified schematic of the pesticide submodel is shown in Figure 6.8.

As stated previously, the source zone for extraction into runoff was arbitrarily defined as the 0 to 1 cm depth increment of the soil surface. Concentrations are computed in units of micrograms/gram or parts per million. For pesticides applied directly to the soil surface the concentration resulting from the application, $C_1$, is

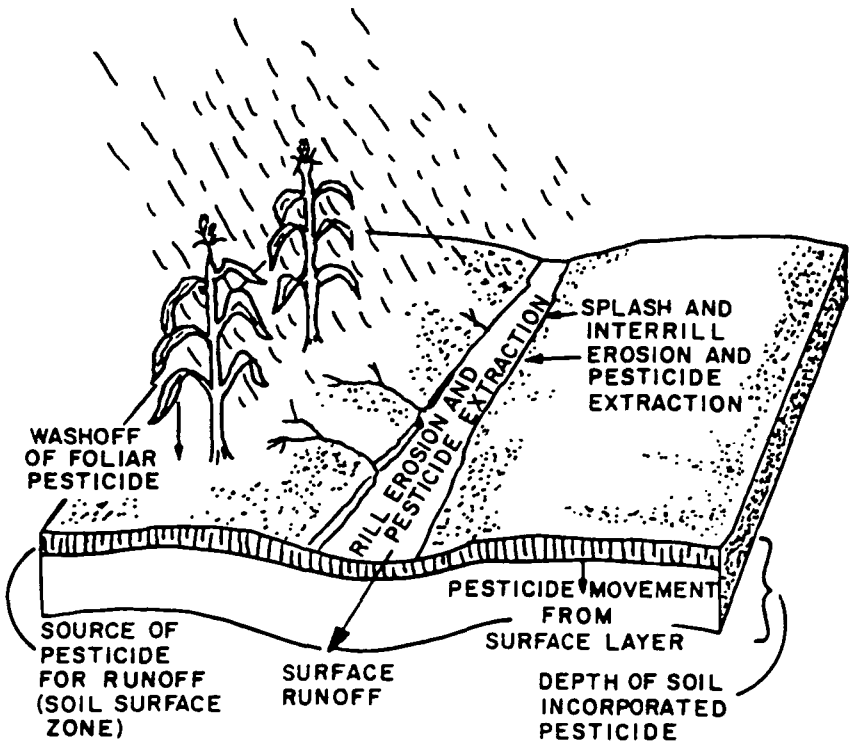


Figure 6.7. Schematic representation of the conceptualized runoff process. (from Leonard and Wanchope, 1980)

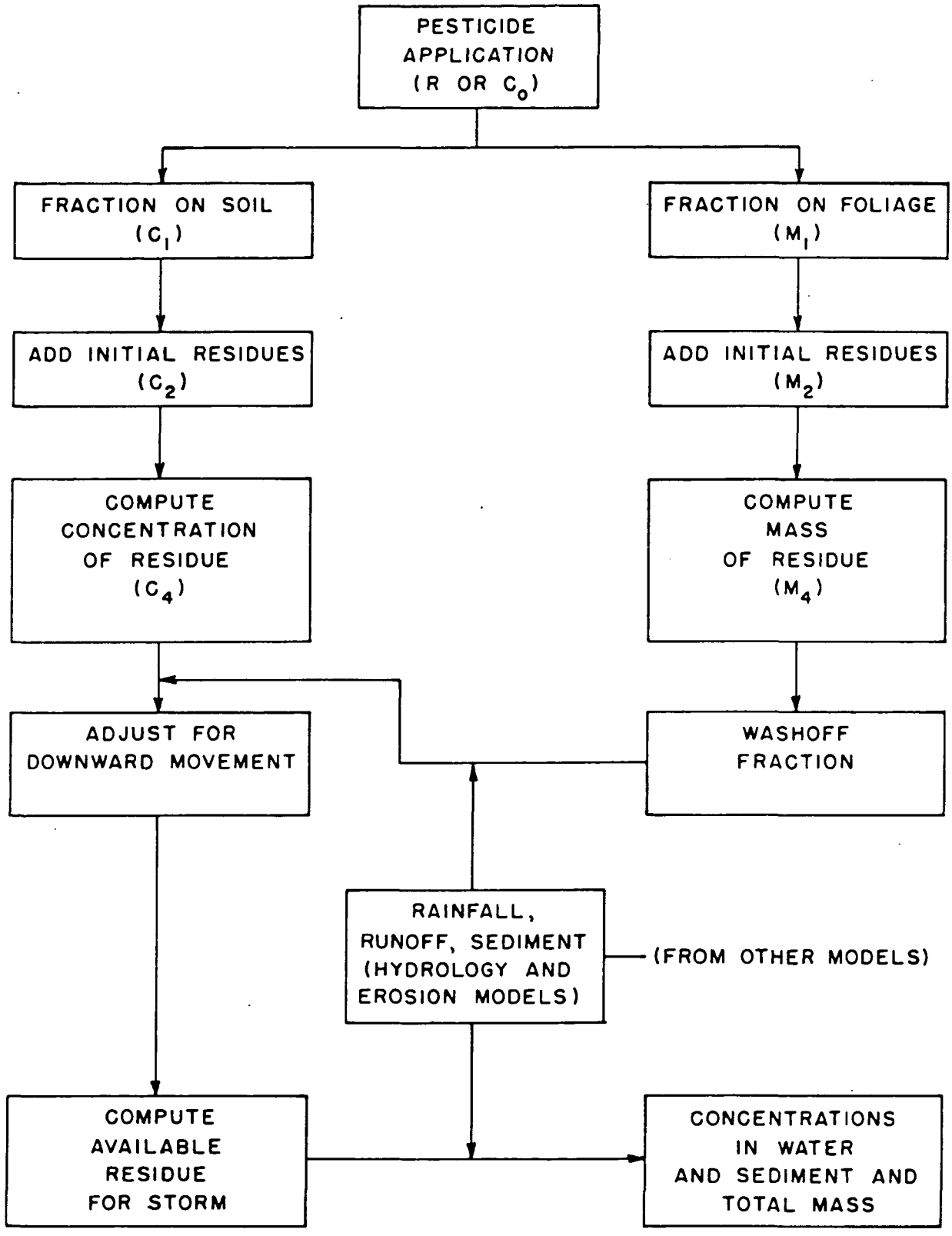


Figure 6.8. Simplified schematic representation of the pesticide model.

$$C_1 = R \times \frac{10}{BD} \tag{6.84}$$

where BD is the bulk density of the surface soil layer and R is the application rate in units of kilograms/hectares. Assuming an average BD of 1.5,

$$C_1 = R \times 6.7 \tag{6.85}$$

For soil incorporated pesticides,

$$C_1 = 6.7\ R \times EF/ID \tag{6.86}$$

where EF is a unitless factor to compensate for nonuniform incorporation and ID is the incorporation depth. If uniform mixing is assumed, EF = 1; however, experience has shown that uniform mixing is rarely achieved (Smith et al., 1978). Concentrations in the surface 0 to 1 cm layer are usually higher than computed assuming uniformity so that EF probably ranges from 1 to 3. In situations where pesticide is injected or banded below the soil surface, EF may be less than 1. A range of 0.5 to 1 is suggested. Normally EF would be assigned a value of 1 unless information is available on the incorporation pattern in a specific situation of interest. If some pesticide residue, $C_2$, was initially present in the soil at the time of application, the total or net concentration wold be $C_3 = C_2 + C_1$.

When pesticides are applied to foliage, the areal concentration expressed in units of milligrams/square meters is

$$M_1 = R \times FF \times 100 \tag{6.87}$$

where FF is the fraction of the application intercepted by the foliage. M is not concentration on the leaf surface, but a concentration based on the projected ground area. Unless the canopy is dense with complete closure, a fraction of the application, SF, will also be intercepted by the soil surface. Soil concentration resulting from this application is computed as above as $C_1 = R \times SF$. When aerial applications are made, losses by drift and volatilization may occur so that FF + SF will not equal one.

Residues of the same pesticide from previous applications, if present in either the soil or foliage compartment, are added to that resulting from the new application for the total residue level. At the beginning of the model application period, any initial residues present are specified. When pesticide residues are redistributed in the soil by major tillage, a new model

application period should be begun, with the resultant surface concentration input as initial residue for this period. The surface concentrations at the beginning of the period may be estimated from the residue remaining and the tillage depth.

A simple exponential dissipation rate is assumed for both soil and foliar residues throughout the model application period. For soil residue, $C_4$, the concentration remaining at time $t$ in days after application of the pesticide or in days after specifying the concentration of initial residue is:

$$C_4 = C_3 e^{-k_s t} \tag{6.88}$$

Likewise, mass remaining on foliage, $M_4$, at time $t$ is:

$$M_4 = M_3 e^{-k_f t} \tag{6.89}$$

or

$$M_4 = M_3 e^{-\left(\frac{0.693t}{C_{1/2}}\right)} \tag{6.90}$$

where $C_{1/2}$ is the "half life" or half concentration time of the foliar residue in days. In the model, the mass of foliar pesticide of concern is that "dislodgeable" or potentially removed by rainfall.

Little information is available in patterns of pesticide removal by rainfall. In the model, the assumption is made that once rainfall exceeds a threshold value corresponding to the amount that can be retained as droplets on the canopy, the fraction potentially dislodgeable is removed during the event. This amount is then added to the soil pesticide residue present at the time of the event. For computation of concentrations consistent with the conceptual thickness of the soil surface, this mass is distributed evenly in the 0 to 1 cm zone. In reality, washoff may occur during the storm such that foliar contributions may fall directly into the runoff stream and be transported off the field. Also, spatial patterns of washoff are likely not uniform and washoff may fall into rills under the plant formed by previous rainfall. Therefore, the assumptions made may tend to underestimate the foliar contribution to runoff.

Some pesticides, particularly dust formulations, may reach the soil surface by dry fall between runoff events. Also, drop losses from heavy dew may remove pesticide from foliage.

Runoff potential of mobile pesticides is reduced as infiltrating water moves some of the pesticide below the soil surface (Baldwin et al., 1975). Pesticide mobility in soil has been studied extensively using thin-layer chromatography technique (Davidson et al., 1975). With this technique, mobility is expressed relative to the movement of water ($R_f$ values). $R_f$ values are related to $K_d$, a coefficient describing distribution of pesticide between the solution phase and the soil phase, defined as a constant for a simple linear adsorption isotherm as:

$$K_d = \frac{C_s}{C_w} \tag{6.91}$$

where at equilibrium $C_s$ is the concentration, micrograms/gram, in the soil or solid phase and $C_w$ is the concentration in solution, micrograms/milliliter. Other procedures for estimating $K_d$ for a number of common pesticides in soil, along with limitations and possible inherent errors in its use, are also discussed in Knisel (1980).

The following algorithm was developed to estimate vertical movement of pesticide from the soil surface.

The rate of change of pesticide mass $Z$ in the soil surface is

$$-dZ = C_w \, f \, dt \tag{6.92}$$

where $C_w$ is the pesticide concentration in water or mobile phase and $f$ is the water flux. At saturation,

$$Z = C_w \, p + C_s \, (1 - p) \, D \tag{6.93}$$

where $p$ is the soil porosity, $C_s$ is the concentration of the adsorbed or immobile phase, and $D$ is the particle density. Introducing $C_s = K_d C_w$ and rearranging the equation above becomes:

$$C_w = \frac{Z}{p + DK_d(1-p)} \tag{6.94}$$

The rate equation can now be written:

$$-dZ = \frac{Z \, f}{p + DK_d(1-P)} dt \tag{6.95}$$

and integrated between limits of $Z_o$, $t_o$ and $Z$, $t$ to yield

$$Z = Z_o e^{-\left(\frac{f\ t}{DK_d(1-p) + p}\right)} \tag{6.96}$$

where $Z_o$ is the mass of pesticide present per unit volume of soil surface at the beginning of the storm. The water flux through the surface during a storm is

$$f = \frac{RF - RO - S}{t} \tag{6.97}$$

where RF is the amount of rainfall, RO is runoff, S is the surface storage or initial abstraction to reach saturation, and t is the storm duration. Making the substituting for f, t can be eliminated so that

$$Z = Z_o e^{-\left(\frac{RF - RO - S}{DK_d(1-p) + p}\right)} \tag{6.98}$$

The value of S is estimated from porosity and the average soil water content plus canopy stored water. In the model, $C_4 \times BD = Z_o$ and $Z = C_{AV} \times BD$ where $C_{AV}$ is the runoff available pesticide concentration and $C_4$ is as previously described.

Where pesticide is foliar applied, the amount assumed to reach the soil by washoff is added to the surface pesticide residue before estimation of vertical translocation. This method provides only a crude approximation of the process compared to other methods (Genuchten et al., 1974). However, it is developed for use where only total storm rainfall and runoff amounts are available. Its primary function is to reduce surface concentrations of those compounds with high soil mobility. Since the amount of vertical translocation will be small in a single storm for relatively insoluble compounds, this calculation is bypassed in the model if the compound solubility is $< 1$ μg/g.

The source zone supplying pesticide to runoff was defined as the surface (0 to 1 cm) depth increment. At the time of runoff, this increment of soil contains a pesticide residue specified in the model as the concentration of "available residue." This is the concentration computed using the appropriate decay functions, adding any foliar washoff, and allowing for vertical translocation. The concentration units are expressed in micrograms/gram of dry soil as is the convention when a soil sample is removed and analyzed for its pesticide content.

Pesticide is extracted by water flowing over the surface and by dispersion and mixing of the soil material by the flow and by raindrop impact. Instantaneous pressure gradients at the surface caused by raindrop impact on a water-saturated soil could also contribute to exchange of pesticide between the soil water and the flowing water. At the interface between the soil matrix and the runoff stream, some mass of soil is "extracted" or is effective in supplying pesticide to some volume of runoff. The mass of pesticide in this mass of soil is:

$$Y = B\ C_{AV} \tag{6.99}$$

where $B$ is the soil mass per unit volume and $C_{AV}$ is the concentration of available residue. As this soil mass mixes or "equilibrates" with the runoff stream

$$Y = (C_w\ V) + (C_s\ B) \tag{6.100}$$

where $C_w$ is the pesticide concentration in the water, $V$ is the volume of water per unit volume of runoff interface, and $C_s$ is the pesticide concentration remaining in the soil or solid phase. Ignoring the volume occupied by the soil mass compared to the larger volume of water, that is, $V =$ total unit volume of runoff interface = 1,

$$C_w + C_s\ B = B\ C_{AV} \tag{6.101}$$

By assuming that the distribution between the solution and the soil is approximated by the equilibrium expression:

$$K_d = \frac{C_s}{C_w} \tag{6.102}$$

$$C_w = \frac{B\ C_{AV}}{1 + B\ K_d} \tag{6.103}$$

or

$$C_s = \frac{B\ C_{AV}\ K_d}{1 + B\ K_d} \tag{6.104}$$

In these expressions it can be seen that when $K_d = 0$, then $C_w = B\ C_{AV}$; e.g., if 100 g of soil containing 1 μg/g of pesticide that partitions completely to the solution phase is extracted by or is dispersed in one liter of water, $C_w = 100$ μg/l. Also, as $K_d$ becomes larger, $C_s = C_{AV}$. The

numerical value of the parameter B in the above equation cannot be obtained by direct measurement, and probably is dependent on runoff conditions. However, it will be shown later that the value ranges from 0.05 to 0.2, with 0.1 giving adequate fit in most situations.

As material flows from the field, it is assumed that the pesticide concentration in the runoff solution is equal to $C_w$. However, not all the affected soil material will become sediment at the field edge. The coarser soil material will be deposited or left in place. As a result, the transported soil will have a higher per unit mass adsorptive capacity and adsorbed pesticide concentration than that of the whole soil. Therefore, an enrichment factor is required.

Total storm loads are computed as: mass in solution phase = $C_w$ x storm runoff volume, and mass in sediment phase = $C_s$ x enrichment factor x sediment yield.

The approach taken by these procedures differs from other models in that the runoff stream is not forced to equilibrate at the soil/water ratio determined by the composition of the saturated soil matrix (Frere et al., 1975) nor at a ratio determined by the concentration of the transported sediment, assuming sediment has the same adsorptive capacity as the soil (Crawford and Donigan, 1974). The weakest assumption, probably, is that associated with using $K_d$ to partition between the solution and the soil phase. In addition to the limitations discussed in Knisel (1980) the runoff process is dynamic, and true equilibration is probably never reached. Also, pesticide apparently partitions differently depending on time of contact with the soil (Smith et al., 1978); that is, the "apparent $K_d$" based on observed partitioning in runoff from experimental watersheds differs from the laboratory determined values and increases throughout the observation period. For this reason, $K_d$ may be best used to differentiate between behavior of pesticide classes, with $K_d$ ranges differing perhaps by orders of magnitude, that is, 1 to 10, 10 to 100, and so forth.

## 6.6 Data Requirements for Pesticide Model

Hydrologic inputs required are rainfall and runoff volume. These are obtaiend from the hydrology model or input as observed data. Sediment yield is also obtained from the model, experimental observations, or other

estimates. The other data requirements are detailed as follows. Most are specific to the chemical applied.

Application Rate. The desired pesticide rate for a given application usually is specified within certain limits by the registration data on the label or is obtained as recommendations from the supplier or extension specialists. The number of applications for some pesticides, particularly foliar-applied insecticides, will depend on extent of insect infestation or established spray schedules. Application rate is input in units of kilograms/hectare.

Depth of Pesticide Incorporation. Pesticides often are incorporated by double-disking, rotary tillers, and other equipment for harrowing or smoothing the soil surface. Depth of pesticide incorporation will depend on the type of tillage equipment used and soil conditions. Depth of incorporation normally ranges from about 8 to 15 cm (3 to 6 inches). When the pesticide is incorporated, select the depth based on the tillage equipment used. For surface-applied chemicals, a value of 1 cm is input as the incorporation depth since the surface is defined arbitrarily as having a depth of 1 cm.

Efficiency Factor for Incorporation. Most incorporation devices do not mix the applied pesticide uniformly throughout the entire depth. The concentration remaining at the surface may be significantly higher than at lower depths. Injected pesticides may have a low surface concentration due to their placement below the surface. The efficiency factor can be used to adjust the surface concentration based on known patterns of incorporation. If an incorporation device leaves a concentration in the surface of twice that achieved by uniform mixing, for example, an efficiency factor equal to half the incorporation depth could be used. For injected pesticides, an efficiency factor of less than one will reduce the surface concentration in proportion. Since this type of information usually is unavailabale, a value of 1 would be input with the assumption that uniform mixing was achieved.

Fraction on Soil and Foliage. When crops are treated with pesticides applied to the plant canopy, some of the application, depending on degree of canoy closure, will reach the surface of the soil directly, some will remain on the foliage, and the rest will be lost by drift and volatilization. At full canopy, about 75$\pm$20 percent and 50$\pm$20 percent of the ground and aerial applications, respectively, reach the canopy. If the amounts reaching soil directly are assumed negligible at full canopy, about 25 to 50 percent can be lost by drift and volatilization during application. For incomplete canopy,

the fraction reaching soil should be somewhat proportional to the extent of ground cover, although insufficient information is available to provide any functional relationship. The actual distribution between soil, foliage, and off-target loss will be highly variable and dependent on atmospheric conditions, path of application, and canopy characteristics. If site-specific information is unavailable, at full canopy closure use 0.4 to 0.6 on foliage for aerial applications and 0.7 to 0.8 on foliage for ground applications. Assume an insignificant fraction reaching the soil. For less than full closure, use a fraction for soil interception in proportion to exposed ground surface. For example, suppose an aerial application is made to cotton that, on projection, covers 50 percent of the ground surface. The fraction on foliage would be 0.3 and the fraction on soil would be 0.3, with the rest, 0.4, assumed as off-target losses.

Initial Foliar Residues. Pesticides normally dissipate from foliage such that a residue will not be present at the beginning of a model application period. This option is provided, however, so that the model can be applied on any date. To estimate an initial residue from a previous application, assume interception fraction, as was suggested, and use equations given in Knisel (1980) to estimate dissipation with time. Rates of foliar dissipation are discussed in a following section. The value input should be in units of milligrams of pesticide per square meter of ground surface. Initial residue can be determined best by direct measurement, but this procedure usually is not practical except for research.

Initial Soil Residue. As for foliar residue, the amount of pesticide present in soil at the beginning of a model application period is best determined by sampling and analysis. Little residue of nonpersistent pesticides would be expected at the beginning of a growing season. When persistent pesticides, such as organochlorines, have been used for several years on a site, however, a significant residue will be present. If sampling and analysis cannot be accomplished, published data should be sought on residues in the soils of the area. The input value should be in units of micrograms per gram (ppm). If the initial residue cannot be determine by measurement or cannot be estimated from published information such as that found in the Pesticide Monitoring Journal, levels of initial residue may be estimated by using the values in Kniser (1980).

The initial residue parameter also provides a service for updating the

concentration of pesticide in the surface of the soil as a result of redistribution caused by major tillage. Persistent pesticide may accumulate at the soil surface during an application season. This accumulated residue would be predicted as output from the model. At the time of tillage, a new value for the concentration at the surface of the soil can be computed, based on the accumulated residue and tillage depth, and can be entered as an initial soil residue for a new model application period.

Foliar Washoff Threshold. This parameter estimates the amount of rainfall required to exceed the capacity of the canopy to intercept and retain rainfall as droplets on the leaf surfaces. Once this amount of rainfall is exceeded, pesticide washoff is assumed. The value of this parameter probably ranges from about 0.1 cm to 0.3 cm for a dense crop canopy.

Washoff Fraction. Little information is available on extent and patterns of pesticide washoff from foliage. The efficiency of the washoff process may be related to several factors. Information in Knisel (1980) suggests that rainfall can remove about 60 percent of the dislodgeable residue of most pesticides. Organochlorines, and possibly other pesticides, however, are exceptions. Less than 10 percent of these compounds is removed by rainfall. Values of 0.6 to 0.7 are suggested, therefore, for all except the organochlorines, where values in the range of 0.05 to 0.1 should be used.

Water Solubility. Pesticide solubilities can be found in many handbooks on pesticide properties. In the model, solubility serves two functions. If solubility is < 1 ppm, the vertical transport computation is bypassed. Secondly, the predicted runoff concentration in solution is compared to solubility. If solubility is exceeded, the solution concentration is limited to the water solubility. Solubility is, therefore, a critical input parameter only for the relatively insoluble pesticides.

Foliar Residue Half Life. Knisel (1980) presented estimates for half-life values of pesticides on foliage. Pesticides generally are not as persistent on foliage as in soil.

Extraction Ratio. This parameter describes the efficiency of the runoff stream in removing or extracting pesticide. Conceptually, it is the ratio of soil:water in the mixing zone. Tests with the model indicate that values in the range of 0.05 to 0.2 are needed—the higher values for conditions of excessive runoff and erosion. Predicted runoff concentrations of those pesticides transported entirely in solution vary in direct proportion to the value

of the extraction ratio. As sediment transport becomes more significant, sensitivity to this parameter decrases. A value of 0.1 gives adequate prediction in most situations.

Soil Decay Constant. Value sof rate constants, $k_s$, are tabulated (Knisel, 1980) for the assumed expoential decay function applied to several pesticides and conditions. Because dissipation rates are affected by climatic factors, the results of individual experiemnts also should be reviewed before making a final selection. Many pesticides dissipate more rapidly at the surface of the soil than from the soil bulk. The $k_s$ values for surface dissipation are more appropriate for runoff prediction, but more results have been reported on persistence in the soil bulk. Where $k_s$ values are given for soil bulk but not for surface, differences reported for similar compounds maybe used in making a subjective judgment on how the surface $k_s$ might differ from the reported bulk soil $k_s$.

Additional information is provided in Knisel (1980) on how $k_s$ values can be estimated based on properties of the pesticides and their environment. In addition to a better perspective of factors influencing dissipation rates, methods are provided by which $k_s$ values can be estimated where little experiemntal data are available.

In some instances, the first-order decay equation poorly describes dissipation of a pesticide. No direct method is provided in the present model for substituting these equations for the first-order decay equation. The $k_s$ values can be updated, however, using different values for different times after application. A best-fit equation could be used to compute $k_s$ values for shorter time segments of the linear log c vs t relationship assumed.

Distribution Coefficient $K_d$. Knisel (1980) discusses how $K_d$ is determined, the factors affecting its value for different pesticides and soils, and how to estimate $K_d$ for a specific situation. Tables are presented that list mean $K_d$ with standard deviations for several pesticides. These tables also provide for estimating $K_d$ as a function of soil texture and organic matter content, thus tying $k_d$ to both the pesticidal properties and controlling site-specific characteristics of the soils. Additional relationships for estimating $K_d$ are based on observed soil thin-layer chromatography and pesticide solubility.

Some assumptions are discussed for using $K_d$ to predict distribution of pesticide between solution and adsorbed phases. Users should compare

potential errors due to linearity and other assumptions in relation to the accuracy of required output to achieve the objectives of their simulation. Since the effect of these assumptions on the validity of model output is uncertain, $K_d$ values for an order of magnitude mgiht be warranted when distinguishing major behavioral differences. Expressing $K_d$ values explicitly as per reference may be useful to analyze certain problems or situations, using model simulations to compare effects of different management alternatives on the same site.

## 6.7 References

Baldwin, F.L., P.W. Santelmann, and J.M. Davidson, 1975, "Movement of Fluometuron across and through the Soil," Journal of Environmental Quality, 4:191-194.

Bruce, R.R., L.A. Harper, R.A. Leonard, W.M. Snyder, and A.W. Thomas, 1975, " A Model for Runoff of Pesticides from Small Upland Watersheds," Journal of Environmental Quality, 4:541-548.

Cowan, I.R., 1965, "Transport of Water in the Soil-Plant Atmosphere System," Journal of Applied Ecology, 2:221.

Cowan, I.R. and F.L. Milthorpe, 1968, "Plant Factors Influencing the Water Status of Plant Tissues," in Water Deficits and Plant Growth, Vol. I, ed. by T.T. Kozlawski, Academic Press, New York.

Crawford, N.H. and A.S. Donigian, Jr., 1974, "Pesticide Transport and Runoff Model for Agricultural Lands," Hydrocomp, Inc., Palo Alto, California, prepared for U.S. Environmental Protection Agency, Athens, Georgia, Publication No. EPA-600/2-74-013, 211 pp.

Davidson, J.M., G.H. Brusewitz, D.R. Baker, and A.L. Wood, 1975, "Use of Soil Parameters for Describing Pesticide Movement through Soils," U.S. Environmental Protection Agency, Publication No. USEPA-660/2-75-009, 149 pp.

Eagleson, P.S., 1970, Dynamic Hydrology, McGraw-Hill, New York.

Eggert, K.G., 1976, Modeling the Unsteady Infiltration Process, Master's Thesis, Department of Civil Engineering, Colorado State University, Fort Collins, Colorado.

Eggert, K.G., R.M. Li, and D.B. Simons, 1979, "The Explicit Formulation of the Green-Ampt Infiltration Equation," 18th Congress of International Association for Hydraulic Research, Vol. 5, Cagliari, Italy, pp. 145-152.

Ehleringer, J.R. and P.C. Miller, 1975, "A Simulation Model of Plant Water Relations and Production in the Alpine Tundra, Colorado," Oceologia, Vol. 19, pp. 177-193.

Frere, M.H., C.A. Onstad, and H.N. Holtan, 1975, ACTMO, An Agricultural Chemical Transport Model, U.S. Department of Agriculture, Agricultural Research Service, Headquarters, ARS-H-3, 54 pp. (Series discontinued; Agricultural Research Service now Science and Education Administration-Agricultural Research.)

Genuchten, M.Th.van, J.M. Davidson, and P.J. Wierengen, 1974, "An Evaluation of Kinetic and Equilibrium Equatins for the Prediction of Pesticide Movement through Porous Media," Soil Science Society of America Proceedings, 38:29-35.

Green, R.E. and I.C. Corey, 1971, "Calculation of Hydraulic Conductivity: A Further Evaluation of Some Predictive Methods," Soil Science Society of America Proceedings, Vol. 35, pp. 3-8.

Green, W.H. and G.A. Ampt, 1911, "Studies on Soil Physics, Part I: The Flow of Air and Water through Soils," Journal of Agriculture Science, May.

Huff, D.D., R.J. Luxmoore, J.B. Mankin, and C.L. Begovich, 1977, TEHM: A Terrestrial Ecosystem Hydrology Model, Oak Ridge National Laboratory, EDFB/1BP-76/8, Oak Ridge, Tennessee.

Jarvis, P.G., 1976, "The Interpretation of the Variations in Leaf Water Potential and Stomatal Conductance Found in Canopies in the Field," Phil. Trans. Royal Soc. Lond., Vol. 273, pp. 593-610.

Knisel, W.G., 1980, "A Field Scale Model for Chemicals, Runoff, and Erosion from Agricultural Management Systems," for U.S. Department of Agriculture, Conservation Research Report #26.

Leonard, R.A., G.W. Langdale, and W.G. Fleming, 1979, "Herbicide Runoff from Upland Piedmont Watersheds - Data and Implications for Modeling Pesticide Transport, Journal of Environmental Quality, Vol. 8, pp. 223-229.

Leonard, R.A., R.D. Wanchope, 1980, "The Pesticide Submodel," in U.S. Department of Agriculture, Conservation Research Report #26.

Li, R.M., M.A. Stevens, and D.B. Simons, 1976, "Solutions to Green-Ampt Infiltration Equation," Journal of Irrigation and Drainage, ASCE, Vol. 102, pp. 239-248.

Mein, R.G. and C.L. Larson, 1973, "Modeling Infiltration During a Steady Rain," Water Resources Research, Vol. 9.

Monteith, J.L., 1965, "Evaporation and Environment," Symposium Society of Environmental Biology, Vol. 19, pp. 206-234.

Reed, K.L. and R.H. Waring, 1975, "Coupling Environment to Plant Response," Ecology, Vol. 55, pp. 62-72.

Reeves, M. and E.E. Miller, 1975, "Estimating Infiltration for Erratic Rainfall," Water Resources Research, Vol. 11, No. 1, pp. 102-110.

Reifsynder, W.E. and H.W. Lull, 1965, Radiant Energy in Relation to Forests, U.S. Department of Agriculture Technical Paper No. 1344, Washington, D.C.

Running, S.W., 1976, "Environmental Control of Leaf Water Conductance in Conifers," Canadian Journal of Forest Research, Vol. 6, No. 1, pp. 104-112.

Running, S.W., R.H. Waring, and R.A. Rydell, 1975, "Physiological Control of Water Flux in Conifers," Oceologia, Vol. 18, pp. 1-16.

Rutter, A.J., 1967, "An Analysis of Evaporation from a Stand of Scots Pine," Forest Hydrology, ed. by W.E. Sopper and H.W. Lull, Pergamon Press, Oxford, England, pp. 403-415.

Slatyer, R.O., 1967, Plant-Water Relationships, Academic Press, New York.

Smith, C.N., R.A. Leonard, G.W. Langdale, and G.W. Bailey, 1978, "Transport of Agricultural Chemicals from Small Upland Piedmont Watersheds," U.S. Environmental Protection Agency, Athens, Georgia, and U.S. Department of Agriculture, Watkinsville, Georgia, Final Report on Interagency Agreement No. D6-0381, Publication No. EPA 600/3-78-056, 363 pp.

Smithsonian Institute, 1966, Smithsonian Meteorological Tables, Vol. 69, No. 1, Washington, D.C.

Steenhuis, T.S., and M.F. Walter, 1978, "Closed Form Solution for Pesticide Loss in Runoff Water," American Society of Agricultural Engineers Technical Paper No. 78-2031, presented at the 1978 summer meeting of the American Society of Agricultural Engineers, Logan, Utah, June 27-30.

Sutcliffe, J., 1968, Plants and Water, Studies in Biology No. 14, Institute of Biology, St. Martins Press, New York.

Swift, L.W., Jr., W.T. Swank, J.B. Mankin, R.J. Luxmoore, and R.A. Goldstein, 1975, "Simulation of Evapotranspiration and Drainage from Mature and Clear-Cut Deciduous Forests and Young Pine Plantation," Water Resources Research, Vol. II, No. 5.

Tan, C.S., T.A. Black, and J.V. Nuyamak, 1977, "Characteristics of Stomatal Diffusion Resistance in a Douglas Fir Forest Exposed to Soil Water Deficits," Canadian Journal of Forest Research, Vol. 7, pp. 595-604.

Tanner, C.B. and W.L. Pelton, 1960, "Potential Evapotranspiration Estimate by the Approximate Energy Balance Method of Penman," Journal of Geophysical Research, Vol. 7, pp. 400-409.

Thompson, D.R. and T.M. Hinckley, 1977, "A Simulation of Water Relations of White Oak Based on Soil Moisture and Atmospheric Evaporative Demand," Canadian Journal of Forest Research, Vol. 7, pp. 400-409.

Van Bavel, C.H.M., 1966, "Potential Evaporation: The Combination Concept and Its Experimental Verification," Water Resources Research, Vol. 2, pp. 455-467.

Van Wijk, W.R. and D.A. DeVries, 1963, "Periodic Temperature Variations in a Homogeneous Soil," in Physics of Plant Environment, ed. by W.R. Van Wijk, North-Holland Company, Amsterdam.

## VII. APPLICATION OF EVALUATION PROCEDURES

### 7.1 Introduction

The methodologies described previously were applied to an agricultural watershed in Iowa. This watershed is located near Traer, Iowa, and is called Four-Mile Creek (Figure 7.1). The watershed covers an area of 19.51 square miles and contains several smaller watersheds and numerous data measurement sites. The watershed is characterized by glacial till covered by loess up to 35 feet thick. Average temperature is about 47.6°F and annual precipitation averages 32.4 inches. The watershed is about 90 percent agriculture with 65 percent row crop and 25 percent pasture, meadow, and small grains. There are three U.S. Geological Survey gages in the watershed, designated as Four-Mile Creek near Traer, Four-Mile Creek near Lincoln, and Half-Mile Creek near Gladbrook. In addition, Iowa State University (ISU) in cooperation with the U.S. Environmental Protection Agency (EPA) has installed and is currently collecting data at three field size watersheds ranging in size from about 14 to 19 acres, and two larger sites about 370 and 700 acres each. There are five recording rain gages in the total watershed. A weather station with a recording rain gage is located just outside the watershed boundary. Fifteen permanent channel cross section measurement sites are maintained in the main channel and one additional cross section site is located on Half-Mile Creek. In addition to these typical measurement sites, ISU maintains tile drain sampling stations, nutrient and herbicide soil collection stations, pump smaplers for collecting sediment, nutrient, and herbicide outflow with runoff, vegetation observation points, and erosion markers. Details of the entire collection system were presented in two annual reports (Johnson, 1977; 1978), and are not repeated in this study. Application of the data network evaluation methodology to Four-Mile Creek is presented in the following sections. Each piece of data was not evaluated because of time and financial limitations. However, every data type was examined using some or all of the techniques presented herein.

### 7.2 Data Availability and Data Gaps

Model requirements for data listed in Table 2.1 were compared to those available as outlined in the previously cited annual reports. Of the 69 items listed, available data was identified for 35 (Table 7.1). Although 35 items were identified, this does not indicate these data were accurate or sufficient

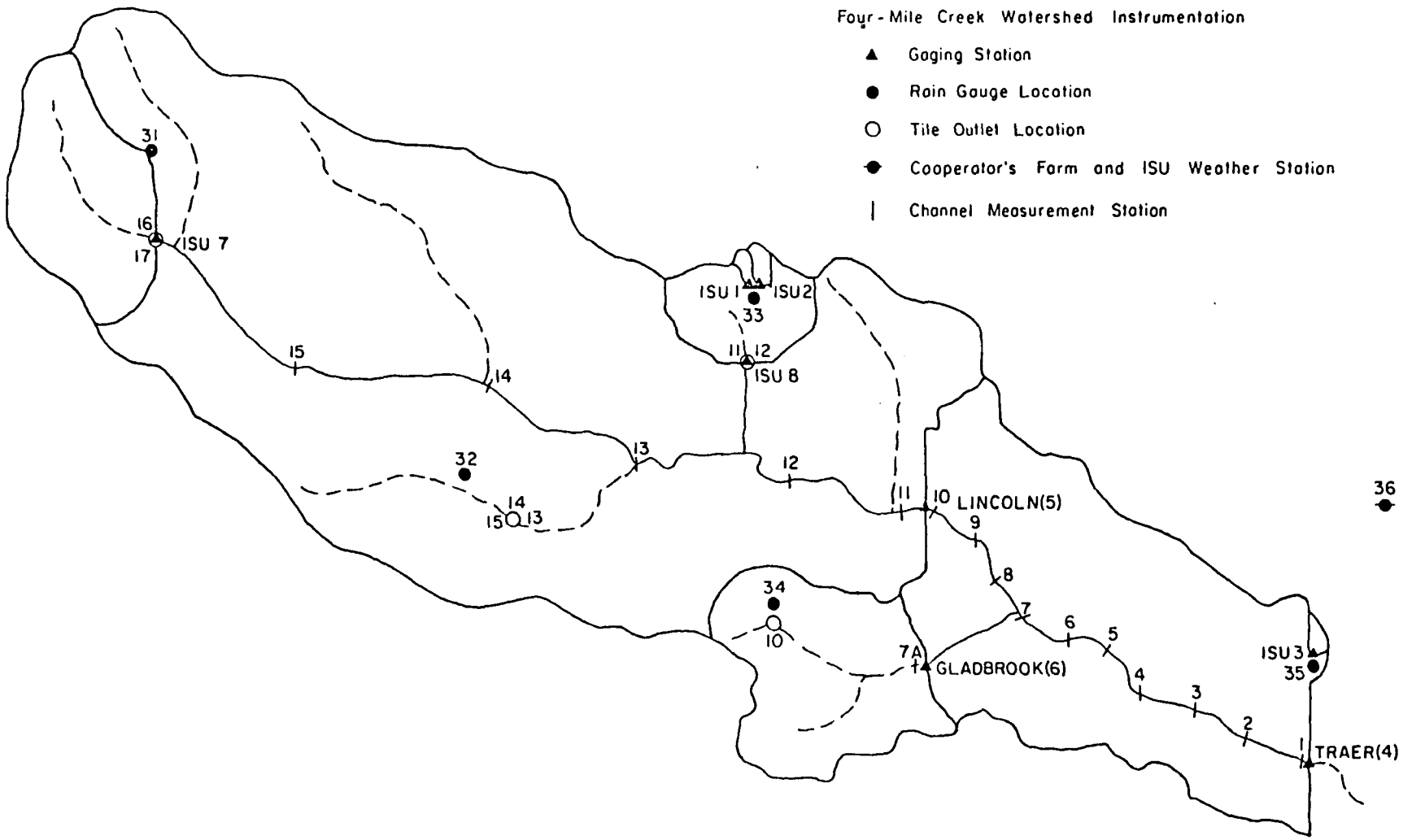


Figure 7.1. Sampling sites in the Four-Mile Creek Watershed.

Table 7.1. Available Data for Colorado State University Physical Process Models

| Data groups | Data availability* |
|---|---|
| Geometry and channel data | |
| Watershed area | + |
| Length of overland slopes | + |
| Width of overland slopes | + |
| Gradients of overland slopes | + |
| Length of channel sections | + |
| Gradient of channel sections | + |
| Measured, representative channel cross sections | + |
| Elevation of watershed | + |
| Soil data | |
| Distribution of soils | + |
| Types of soils | + |
| Number of soil layers | + |
| Thickness of layers | + |
| Initial water content of layers or top layer | + |
| Saturated hydraulic conductivity of each layer or top layer | - |
| Tensiometer measurements (desorption curve) for each layer | - |
| Temperature for tensiometer data | - |
| Field moisture capacity for each layer | - |
| Intrinsic permeability of top layer | - |
| Porosities of soil layers o top layer | - |
| Specific gravity of soil | - |
| Temperature of top layer | + |
| Thermal conductivity of soil | - |
| Grain size analysis of top layer | - |
| Concentrations of nitrogen and phosphorus species in soil layers | + |

Table 7.1. Available Data for Colorado State University Physical Process Models (continued)

| Data groups | Data availability* |
|---|---|
| Vegetation data | |
| Types | + |
| Distribution | + |
| Density of ground cover | - |
| Density of canopy cover | + |
| Storage of ground cover | - |
| Maximum and minimum storage of canopy cover | - |
| Albedo of vegetation | - |
| Yearly growth cycle of canopy | + |
| Average leaf length of dominant species | - |
| Maximum and minimum leaf area | - |
| Root cross-sectional area per unit area of soil in each layer | - |
| Fraction of root in each layer | - |
| Annual litter input to ground surface | - |
| Litter layer thickness | - |
| Average litter temperature | - |
| Nitrogen content of litter | - |
| Phosphorous content of litter | - |
| Specific gravity of litter | - |
| Climatic data | |
| Daily solar radiation | + |
| Average daily temperature | + |
| Average daily humidity or vapor pressure | + |
| Total daily precipitation | + |
| Average wind speed | + |
| Air pressure--for year as function of altitude | - |
| Specific heat of air | - |
| Rainfall storm hyetographs | + |
| Nitrogen species input from rainfall | - |
| Surface water temperature | - |

Table 7.1. Available Data for Colorado State University Physical Process Models (continued)

| Data groups | Data availability* |
|---|---|
| Hydrologic and hydraulic data | |
| Storm and daily runoff hydrographs | + |
| Overland flow resistance | - |
| Channel flow resistance | - |
| Storm sediment yield | + |
| Sediment yield from litter layer | - |
| Runoff temperature | - |
| Grain size and analyses of sediment | + |
| Sediment detachment coefficient for rainfall and runoff | - |
| Dissolved oxygen content in runoff | - |
| Nutrient concentration in runoff | + |
| Rate of addition of BOD in runoff | - |
| Man's influence | |
| Cropping patterns | + |
| Land use changes | + |
| Timbering activities | - |
| Modification of drainages | + |
| Nitrogen application | + |
| Phosphorus application | + |

* + Yes, this item has been identified in the annual reports
- No, this item has not been identified in the annual reports

for modeling. For example, although cropping patterns were detailed for the small field sized plots, only very generalized information for the entire watershed was provided. More detailed descriptions of data accuracy and adequacy are included for each data category. In general, the data base as it now exists is deficient in some key items. This makes model application difficult. The model may still be applied but with "best estimates" of the missing data.

## 7.3 Analysis of Existing Data Network

Data can be subdivided into several groups as evidenced by Table 7.1. To facilitate discussion, groupings of data will be utilized and analysis of selected specific data is presented for illustrative purposes.

### 7.3.1 Geometry and Channel Data

This group of data is complete because most of the measures can be acquired from topographic maps. U.S. Geological Survey 7-1/2 minute quadrangle sheets were used to define most of the data listed within this group, excpet for determination of channel cross sections. In addition, topographic maps for the three field size watersheds were included in the annual reports. These topogaphic maps yielded the detail necessary for the small watersheds. A complete description of the geometric measures is included in the model application section.

The detail on the topographic maps proved to be sufficient to satisfy requirements at this time.

Channel cross-sectional measurements taken at the 16 collection sites show a substantial change in channel shape between 1967 and 1977. These types of changes must be taken into account if water and sediment routing is to be correctly computed. An example of the changes that occurred over a shorter period can be found by comparing the 1977 measurements to those of 1978. It is appropriate to compare those measures of the channel cross-sectional geometry that are used in the proposed model. In this instance the parameters $a$ and $b$ of the wetter perimeter $(P)$ and flow area $(A)$ relationship:

$$P = a\,A^{b} \tag{7.1}$$

are considered. Theory and experience show that $a$ and $b$ are inversely related. In addition, $b$ usually ranges from 0.3 to 0.6 for many channels,

whereas a can be quite variable. As cross sections change with time and location on the stream, so do the a and b parameters. Figure 7.2 shows variation in these parameters as a function of distance from the outlet of Four-Mile Creek. Note that parameter b increases toward 0.5, a value associated with swale or triangular sections, but parameter a decreases in the upsteam direction. Similar trends are seen in Figure 7.3 which can also be compared to Figure 7.2. Changes in a and b parameters between 1977 and 1978 measurements indicate the channel is relatively active in the lower and middle portions, as might be expected, but less active near the upper end of the channel. Although the changes are relatively small in absolute values, they can significantly effect water routing and sediment transport. In this case, the a and b parameters are used in the water routing portion of the model to find flow area A from discharge Q. An error in parameter a of 10 percent, for example, creates a similar error in the flow area, whereas an error in b may be magnified several times depending on flow conditions (Simons, Li and Ward, 1978). Fortunately, b is less variable than a for most channels. It is important, then, that the a and b parameters be accurately evaluated. In the Four-Mile Creek channel, the downstream and yearly changes in cross-sectional geometry suggest the need for additional measurement sites that may be maintained on an annual or semi-annual schedule. These additional stations and shorter sampling interval may help indicate channel changes and necessary model adjustments.

Watershed geometry data is relatively good. Some additional emphasis on cross section measurements can help in selecting proper model parameters and making correct adjustments with time and distance. In addition, reproduction of cross section plots in the annual summaries was poor in some cases making it difficult to correctly choose distances and elevations.

### 7.3.2 Soil Data

Soil data were examined with respect to hydrologic properties, sedimentologic characteristics, and nutrient and herbicide-pesticide indices. Silt loam soils predominate in the watershed, primarily derived from the loess deposits. Their distribution and types for the small field size watersheds are presented in the annual reports. However, soils distribution maps for the entire watershed were not presented. Depth information from the nutrient and herbicide-pesticide sampling sites can be used. However, these measurements

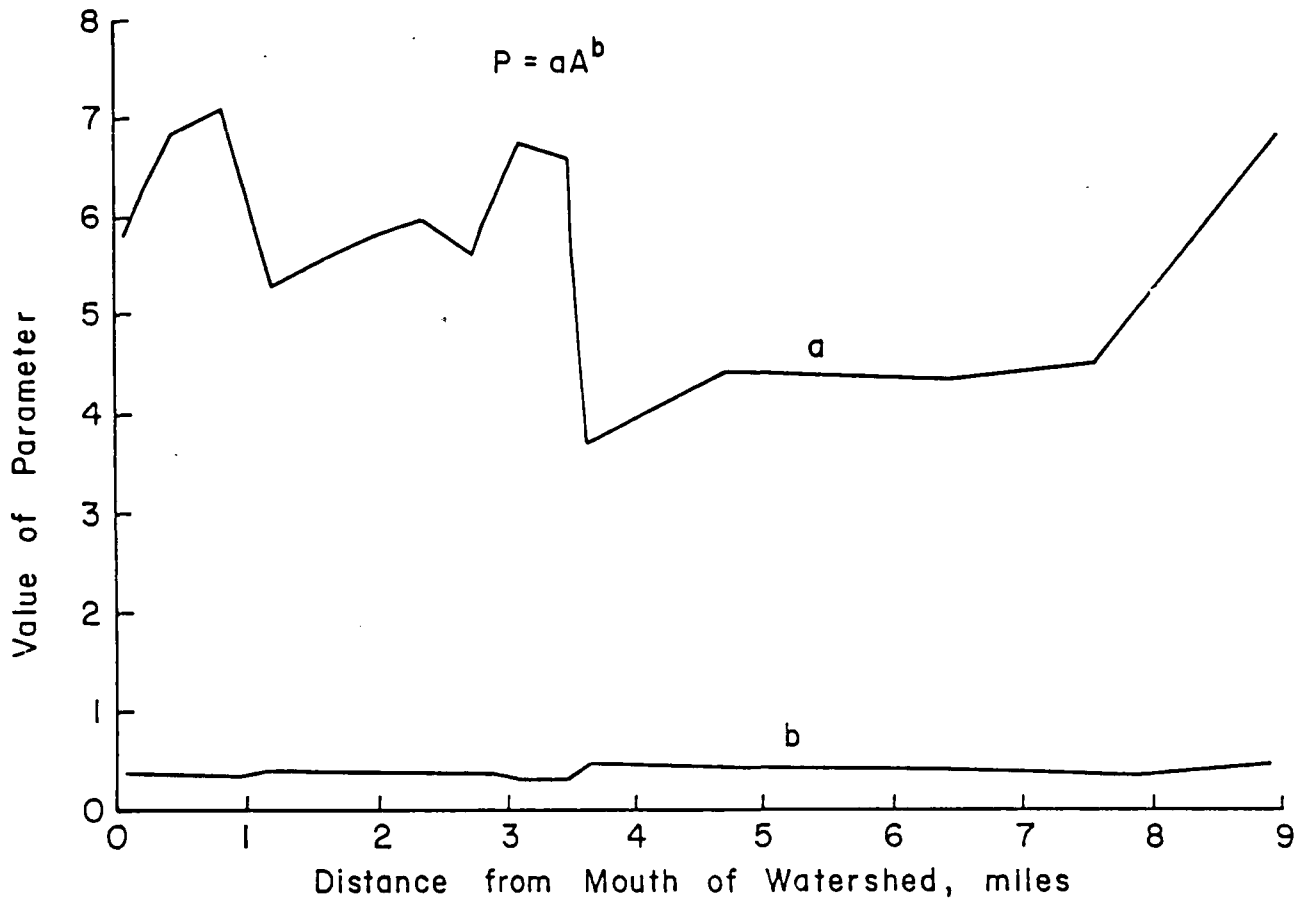


Figure 7.2. Cross section parameters a and b for 1976-1977 measurements.

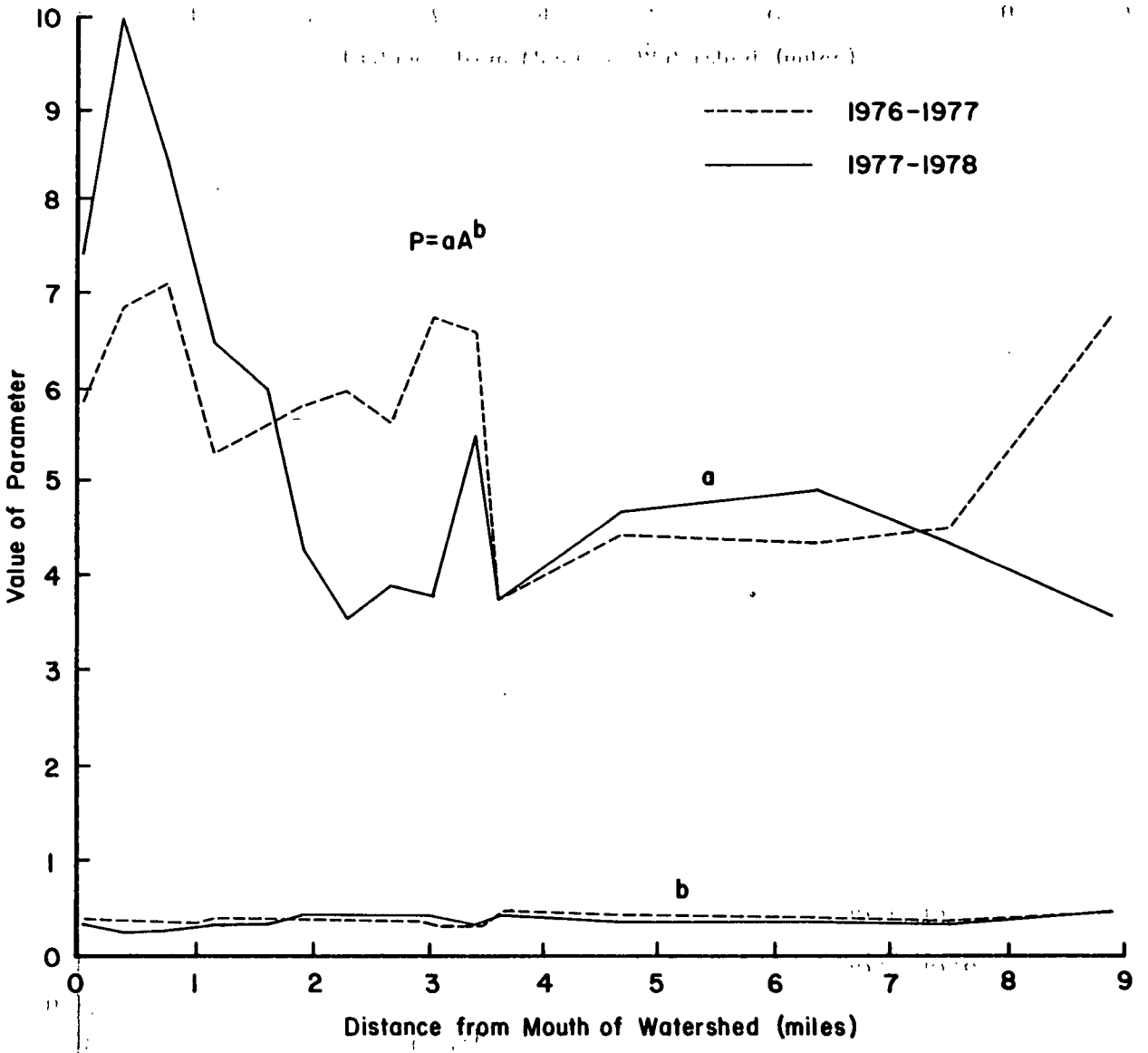


Figure 7.3. Cross section parameters a and b for 1976-1978 and 1978-1979 measurements.

are taken to a depth of only 60 inches. This is probably adequate for most modeling unless deep ground water flow is analyzed, then a better measure of soil depth is needed. In addition, the sampling, by necessity, is done at preselected depth ranges that may or may not be related to specific soil horizons if there are any. A better description of a typical soil profile for each type would be useful in determining from which horizon or layer the soil samples are taken. Although such information may be available elsewhere, a summarized description would be helpful.

One useful piece of information derived from nutrient and herbicide-pesticide soil measurements is the water content of the soil layers. This type of information, for the small watersheds at least, can be used to determine antecedent conditions needed for infiltration computations. The model being developed at Colorado State University for predicting the effects of best management practices can use soil moisture measurements as a check to keep simulated interstorm soil moisture levels realistic. Soil temperature data is collected at the ISU weather station (number 36) at several depths. Similar measurements have been made at Site 1 (field watershed) and based on a very limited winter sampling, the measurements indicate that both sites have similar temperature profiles. More data is needed before conclusions about the correlation of these two stations can be made.

Additional soil temperatures for the surface 1 to 2 cm of depth were made for pesticide studies. These temperatures are also beneficial since they depict the diurnal variations in surface conditions. Concentrations of nutrients and herbicides-pesticides in the soil are also necessary for modeling the origin and fate of these constituents. One type of information that is valuable is the change in constituent concentrations with depth. Figures 7.4a, b and c show the changes in concentration of the herbicide paraquat with depth for three sample sites in field watershed 1 (ISU 1). These figures show the spatial distribution in two directions: planar and with depth; and the temporal variations. The concentrations are plotted at the midpoint of the soil layer sampling interval. These figures show that the concentration of Paraquat generally increases then decreases with depth. This is important because Paraquat readily absorbs to and is transported on soil particles. If the surface layers have lower concentrations than the subsurface layers, this should be considered in soil loss and pesticide loss modeling. If the soil is disturbed to a depth of 15 cm, more paraquat may be

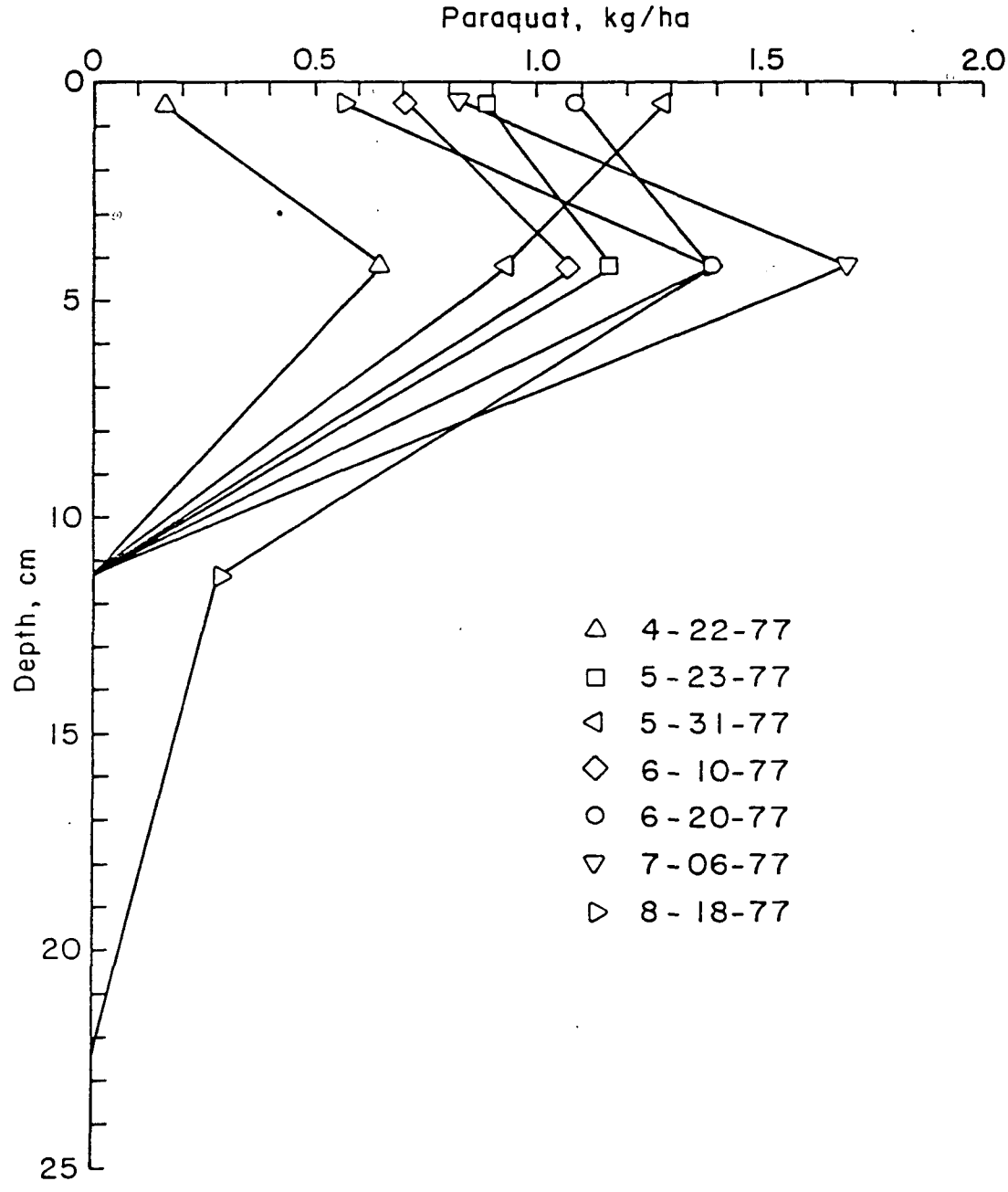


Figure 7.4a. Temporal and spatial variation of Paraquat site 1-1 corn, 1977.

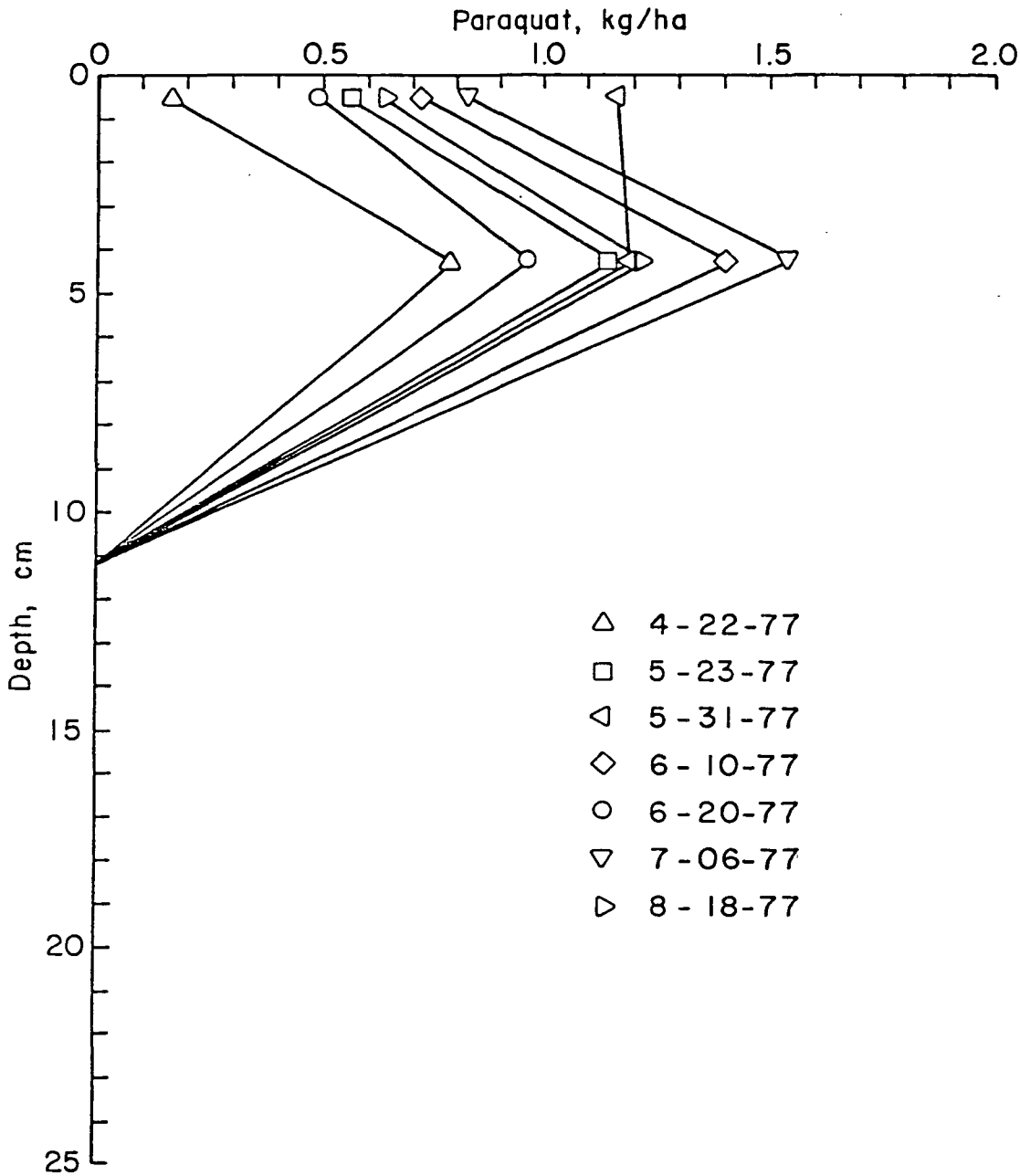


Figure 7.4b. Temporal and spatial variation of Paraquat site 1-2 corn, 1977.

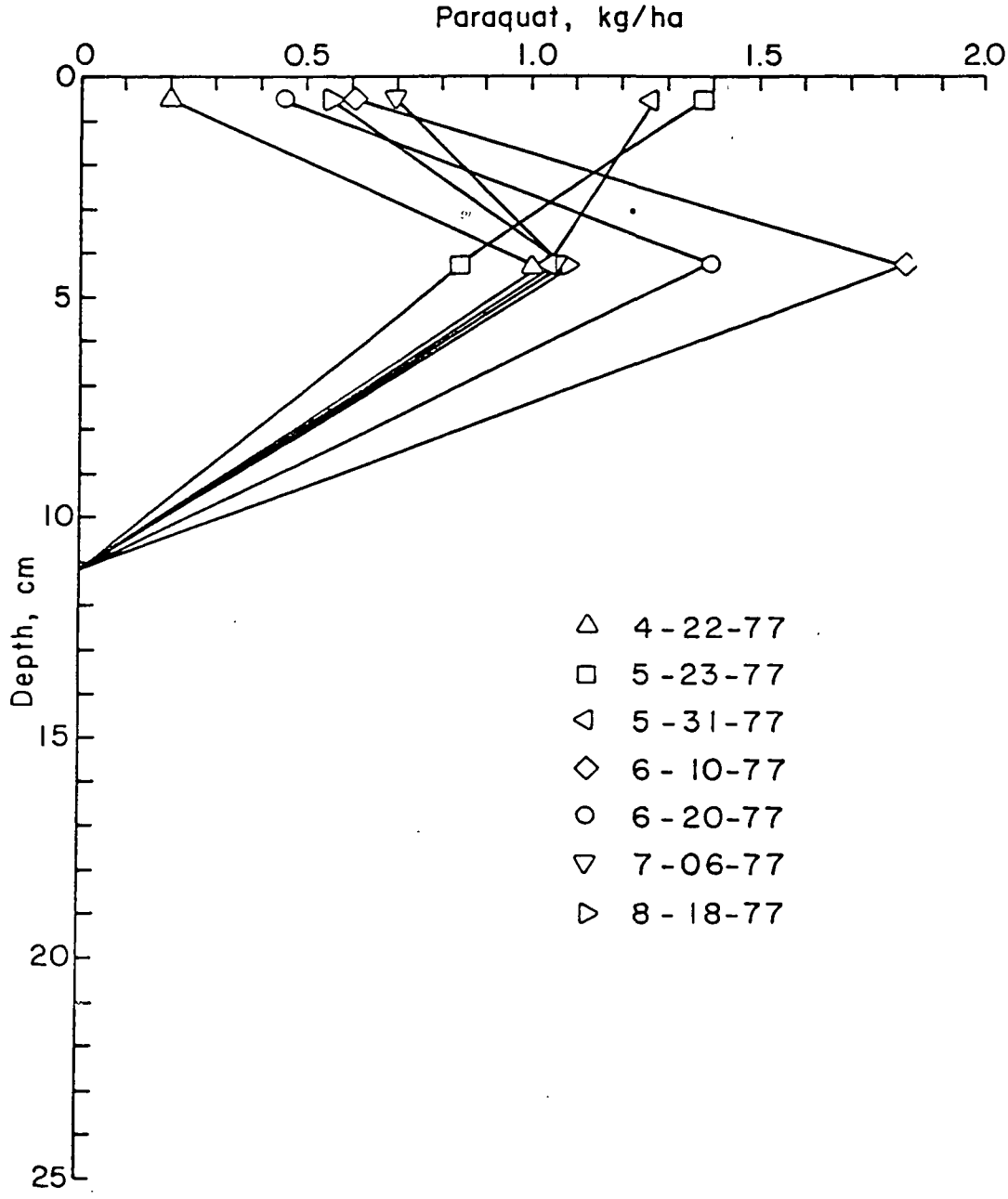


Figure 7.4c. Temporal and spatial variation of Paraquat site 1-3 corn, 1977.

lost during erosion events. Similarly, soil loss during certain times of the year will have more effect on paraquat concentrations than others. Figure 7.4a shows that the paraquat concentration is more than twice as high in July than in April for the 7.5 to 15 cm soil layer, but more than four times higher in the surface layer. Such information is needed for correctly estimating the timing of constituent movements. More discussion on nutrients and herbicides-pesticides is presented in a later section.

Key soil measures missing from the data base are those related to the hydrologic properties. These have previously been identified in Table 7.1 and include hydraulic conductivity, tensiometer data, specific gravity, grain size distribution, and porosity. Such information is essential for determining infiltration and sediment transport parameters. Some of this information may be contained in other publications unavailable for review in this study. It typcially is not included and therefore needs to be collected to provide better estimations of key model parameters. Infiltrometer tests, carefully collected soil samples, sieve analyses, and saturation-desaturation tests need to be conducted. As stated in the 1977-1978 annual report, sediment size analyses for the on-site soil sampels are being conducted for inclusion in the data base. Other sedimentalogical aspects of the soil are covered in a later section.

### 7.3.3 Vegetation Data

Vegetation data, like soils information, is rather sparse in certain areas. Considerable effort has been expanded in monitoring canopy cover growth for the field size watersheds. Spatial and temporal changes in leaf canopy for watersheds 1 and 2 are shown in Figures 7.5 and 7.6 for 1976 and 1977. These plots show the increase in leaf area during the growing season and the plant litter left after harvest, basic information necessary when modeling. Such detailed work has not been expended on other sub-watersheds nor on the entire watershed. This creates a problem when modeling the responses of the entire watershed, particularly when canopy and ground cover changes can significantly affect water and sediment yields. The extent of the description of vegetation for the entire watershed is limited to percent areas of different crops grown during the year. A complete vegetation distribution map for the entire watershed is not available, however, using physical process models it is possible to transfer parameters from one watershed to another.

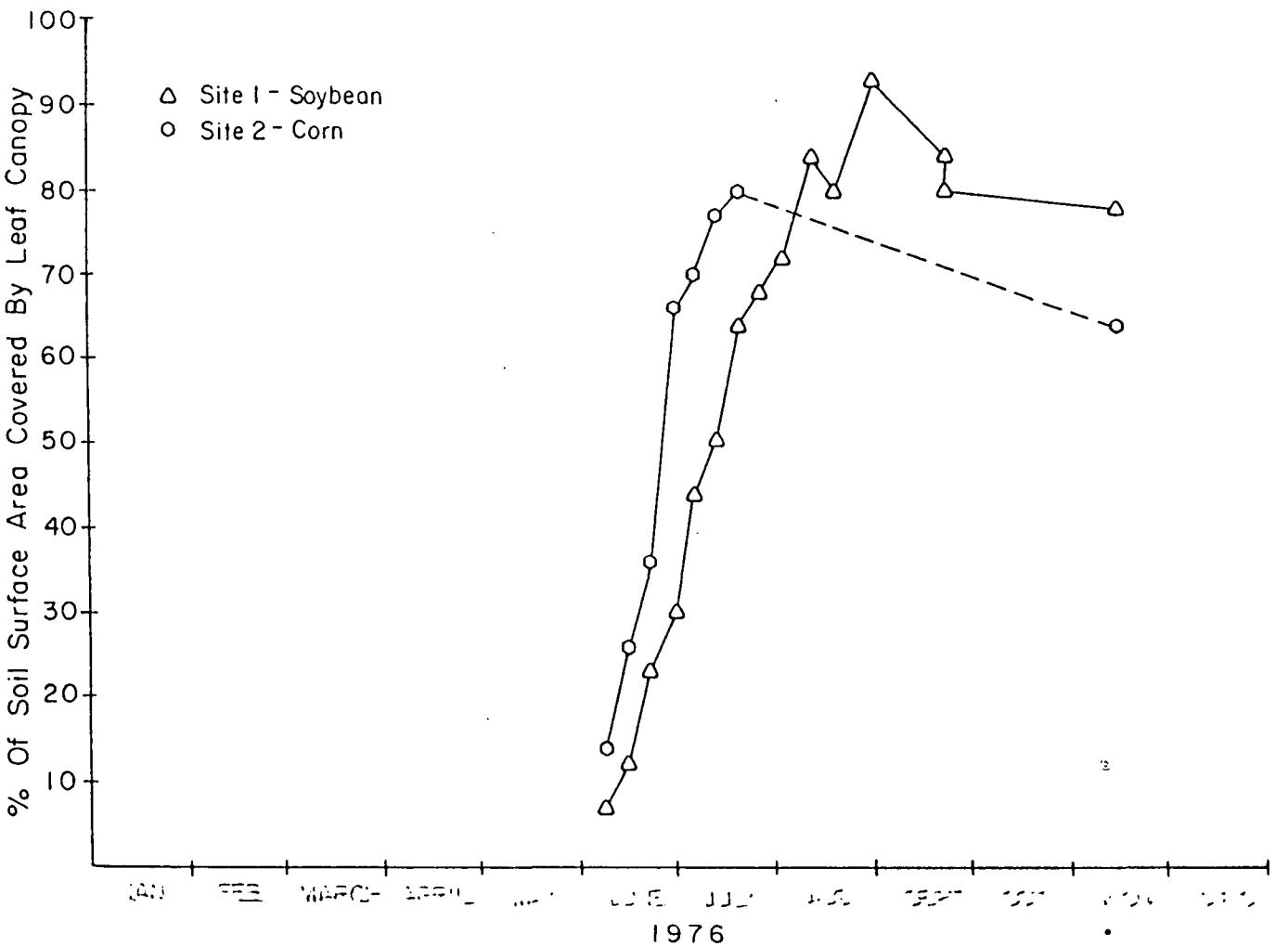


Figure 7.5. Variation of leaf canopy cover for 1976, sites 1 and 2.

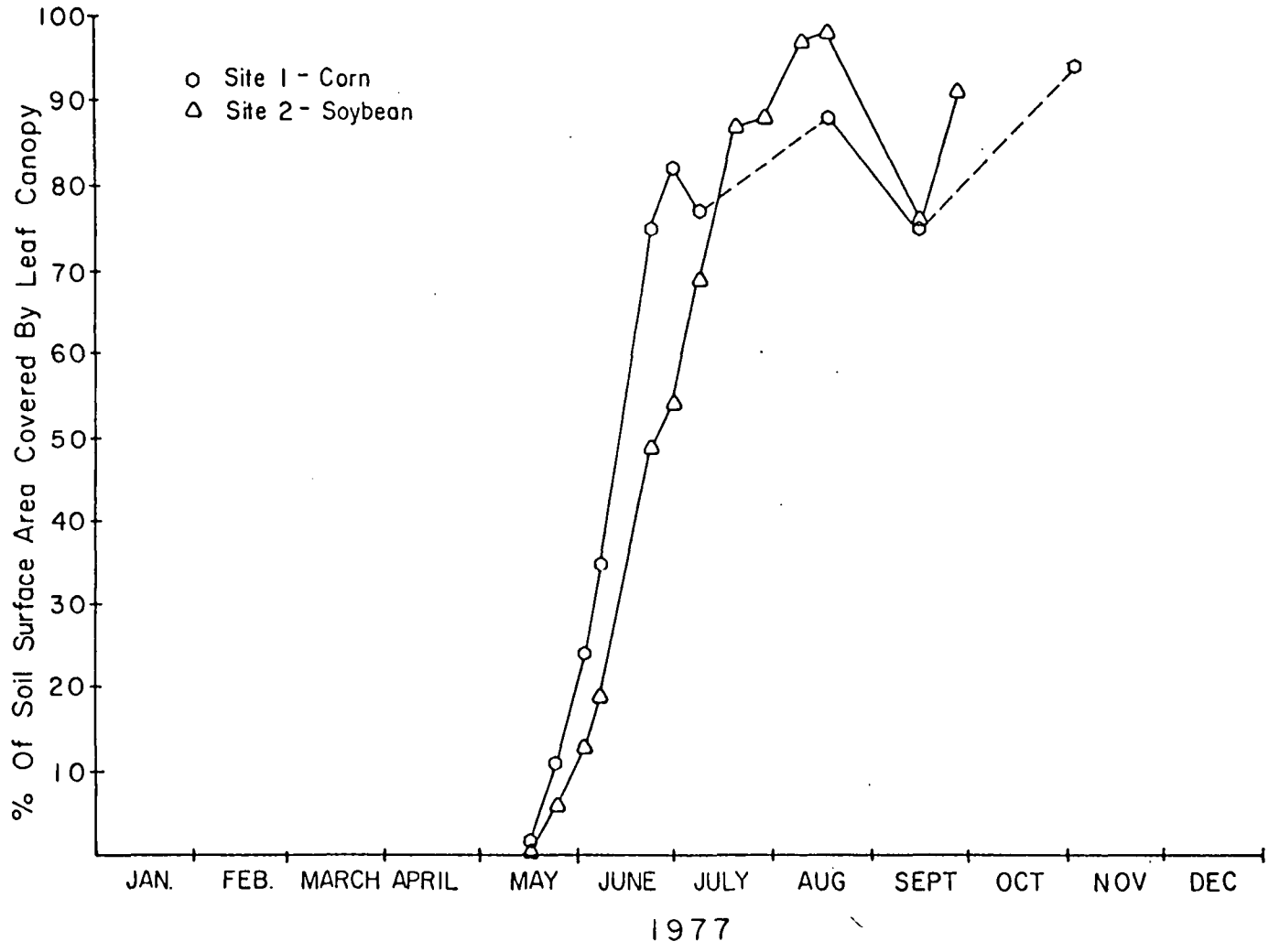


Figure 7.6. Variation of leaf canopy cover for 1977, sites 1 and 2.

This can be done for soils, vegetation, and other data types. Unfortunately, there is a limit to the amount of transferability that can be attained. If the vegetation types and patterns are similar between watersheds, then such a transfer can be made with acceptable reason. Conversely, if the watersheds are dissimilar such a transfer is risky. More detail on transferability is presented in the model application.

Information is needed on the specific characteristics of each vegetation type, specifically the growth characteristics, transpiration rates, amount of litter produced, and interception properties. Much of this information can probably be derived from published sources. However, additional critical information, may need to be collected for accurate model applications.

### 7.3.4 Climatic Data

Of all data types, climatic data is usually the most abundant, but not necessarily the most complete or accurate. Primary climatic data for modeling include precipitation, temperature, solar radiation, humidity, and wind speed. Considerable effort has been spent in collecting climatic data for the Four-Mile Creek watershed. Six recording rain gages are in use for measuring precipitation, specifically rainfall events. In addition to these gages, one site (Number 36) has been instrumental for measurement of several climatic variables including daily maximum and minimum temperatures, solar radiation, average wind speed, relative humidity, and pan evaporation.

Because of numerous rainfall events in the area, rainfall records are the most numerous type of data available for climatic information. Two types exist, daily total rainfall and storm accumulations. The storm accumulation records can be analyzed to yield volume-duration or hyetograph values that may be used in modeling. Analyses of rainfall records should compare stations both temporally and spatially. Daily rainfall values are often a key input to water yield models. Therefore extensive daily records are collected at all six stations. However, simple spatial correlations of daily rainfall between the stations indicated that the readings were very similar. Results of these correlations are shown in computer produced figures (Figures 7.7, 7.8, 7.9, 7.10, 7.11 and 7.12) for each of the stations. The lowest correlation is between stations 31 and 34 as seen in Figures 7.7 and 7.8 with a correlation value of about 0.79. The highest correlation are for gage 32 (Figure 7.8). Key gage numbers 33 and 36 also have correlations usually greater than 0.85.

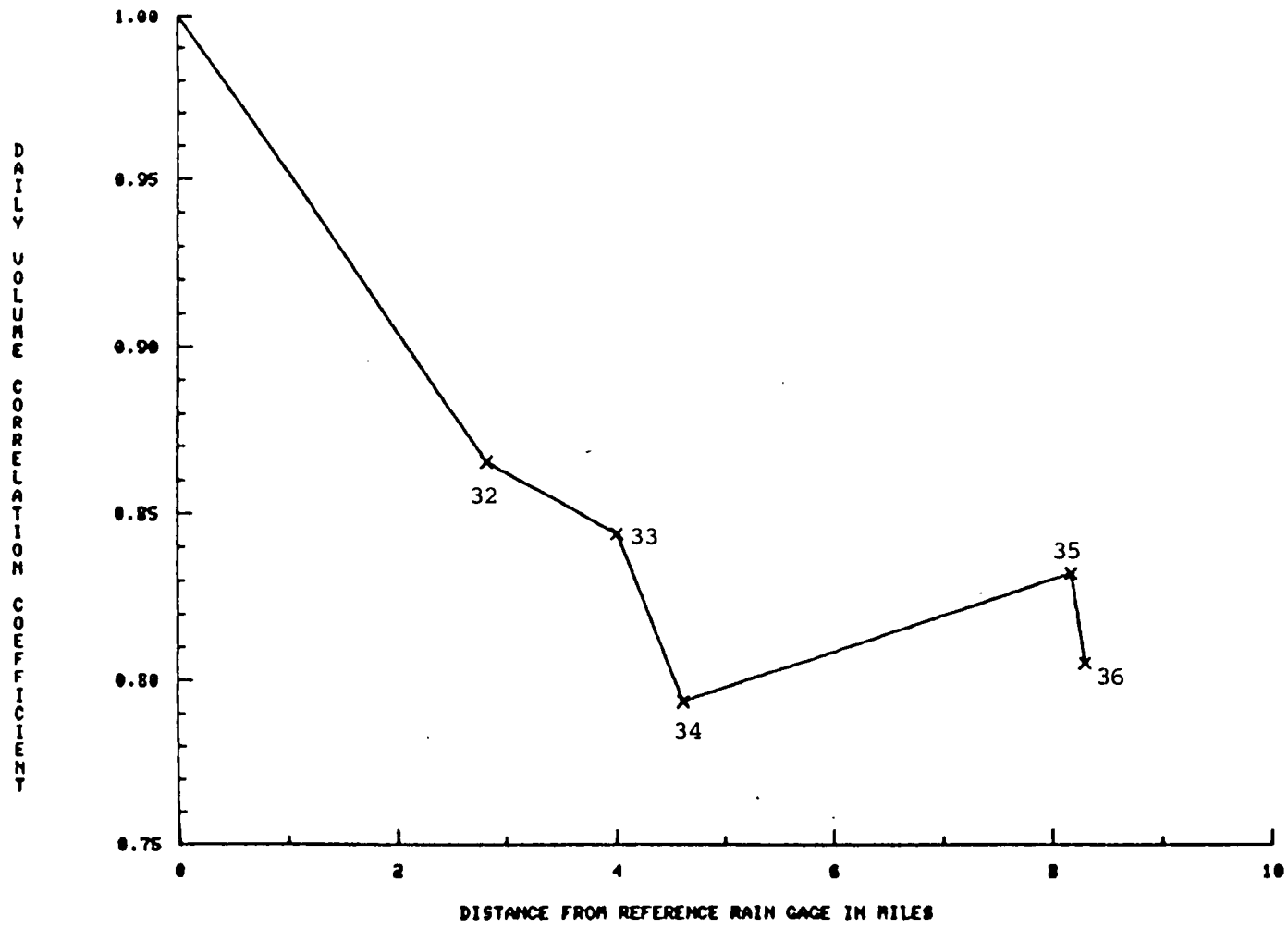


REFERENCE GAGE FOR THIS FIGURE IS NUMBER 31

Figure 7.7. Spatial correlation of daily rainfall volumes between base gage (number 31) and other gages.

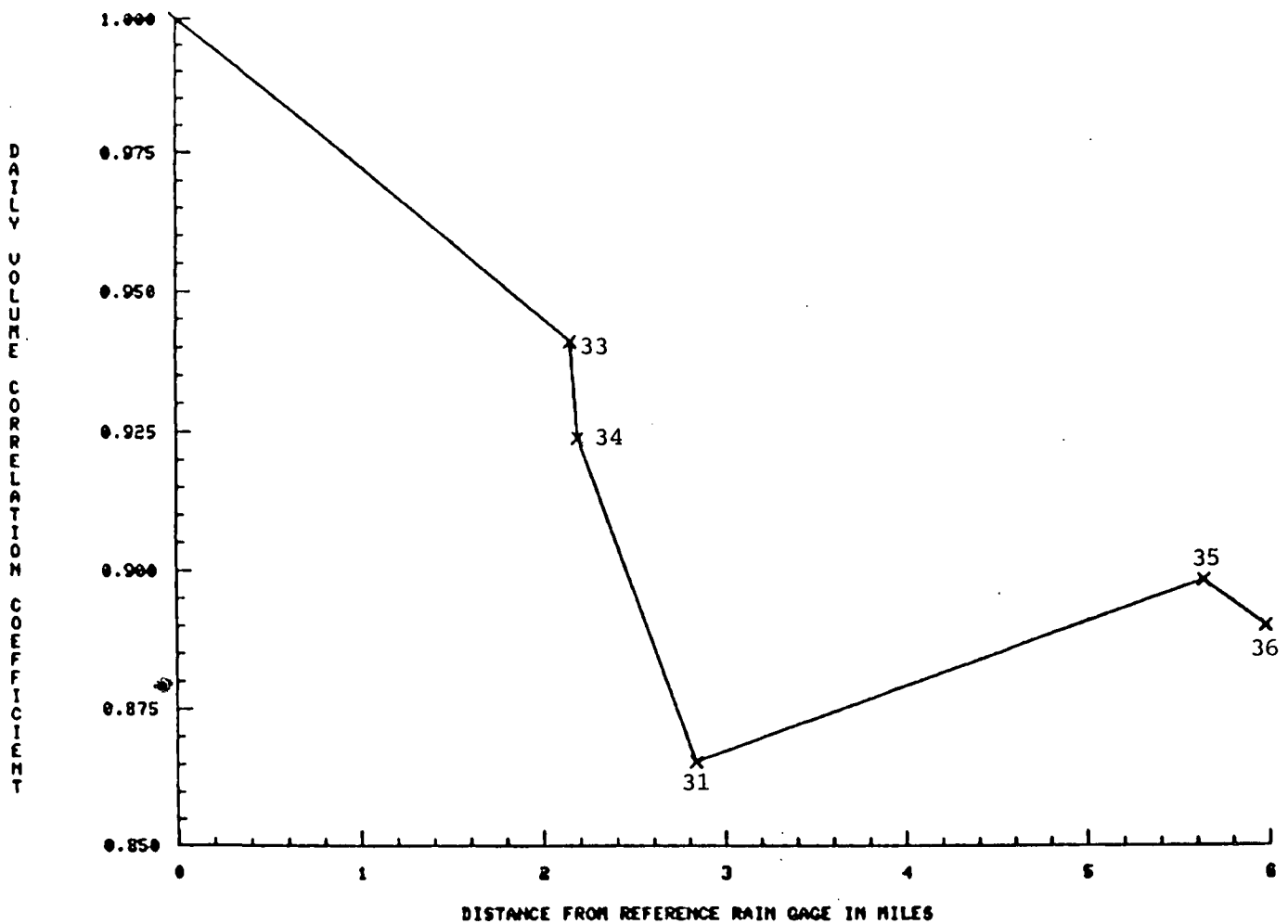


REFERENCE GAGE FOR THIS FIGURE IS NUMBER 32

Figure 7.8. Spatial correlation of daily rainfall volumes between base gage (number 32) and other gages.

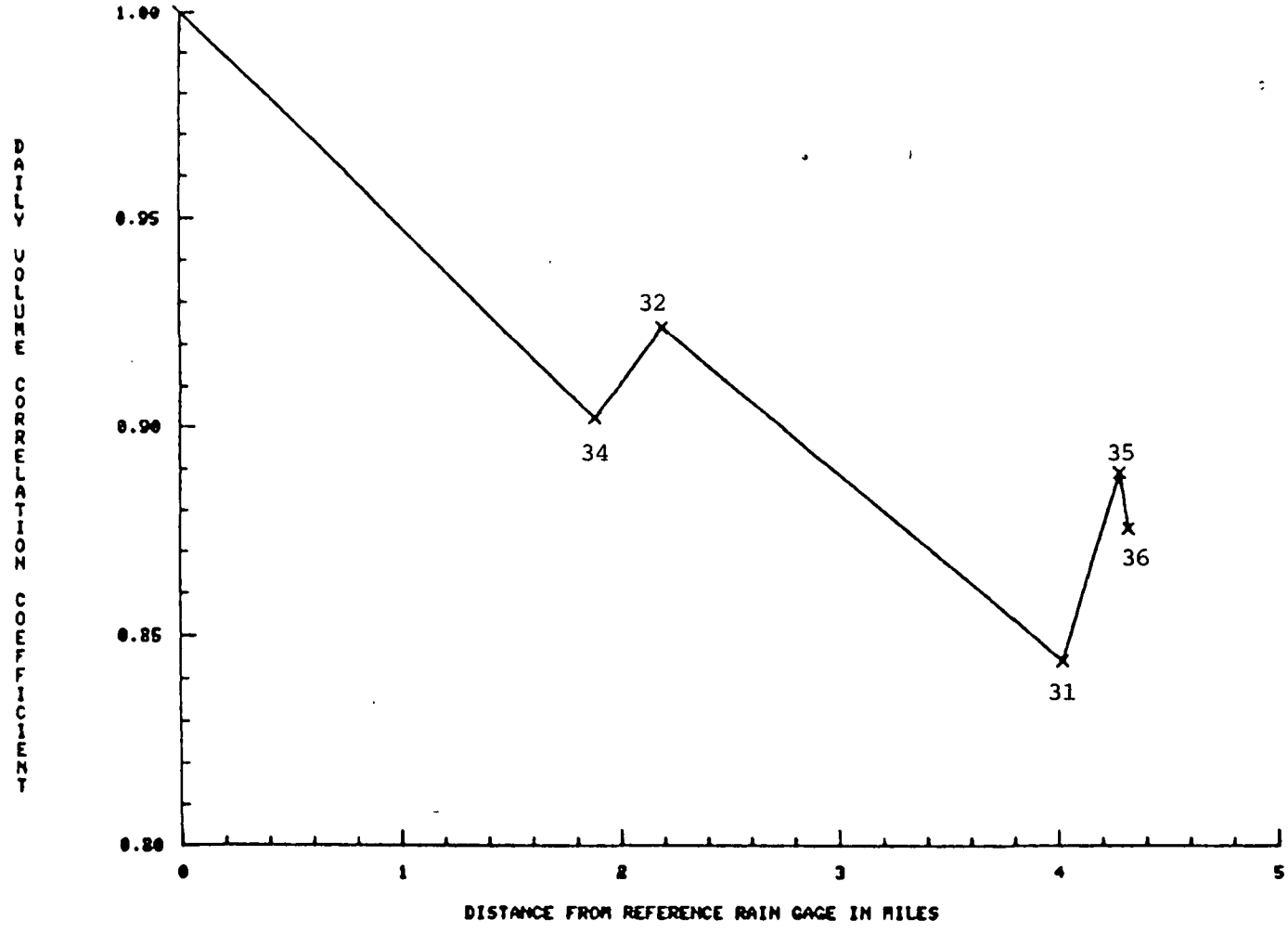


REFERENCE GAGE FOR THIS FIGURE IS NUMBER 33

Figure 7.9. Spatial correlation of daily rainfall volumes between base gage (number 33) and other gages.

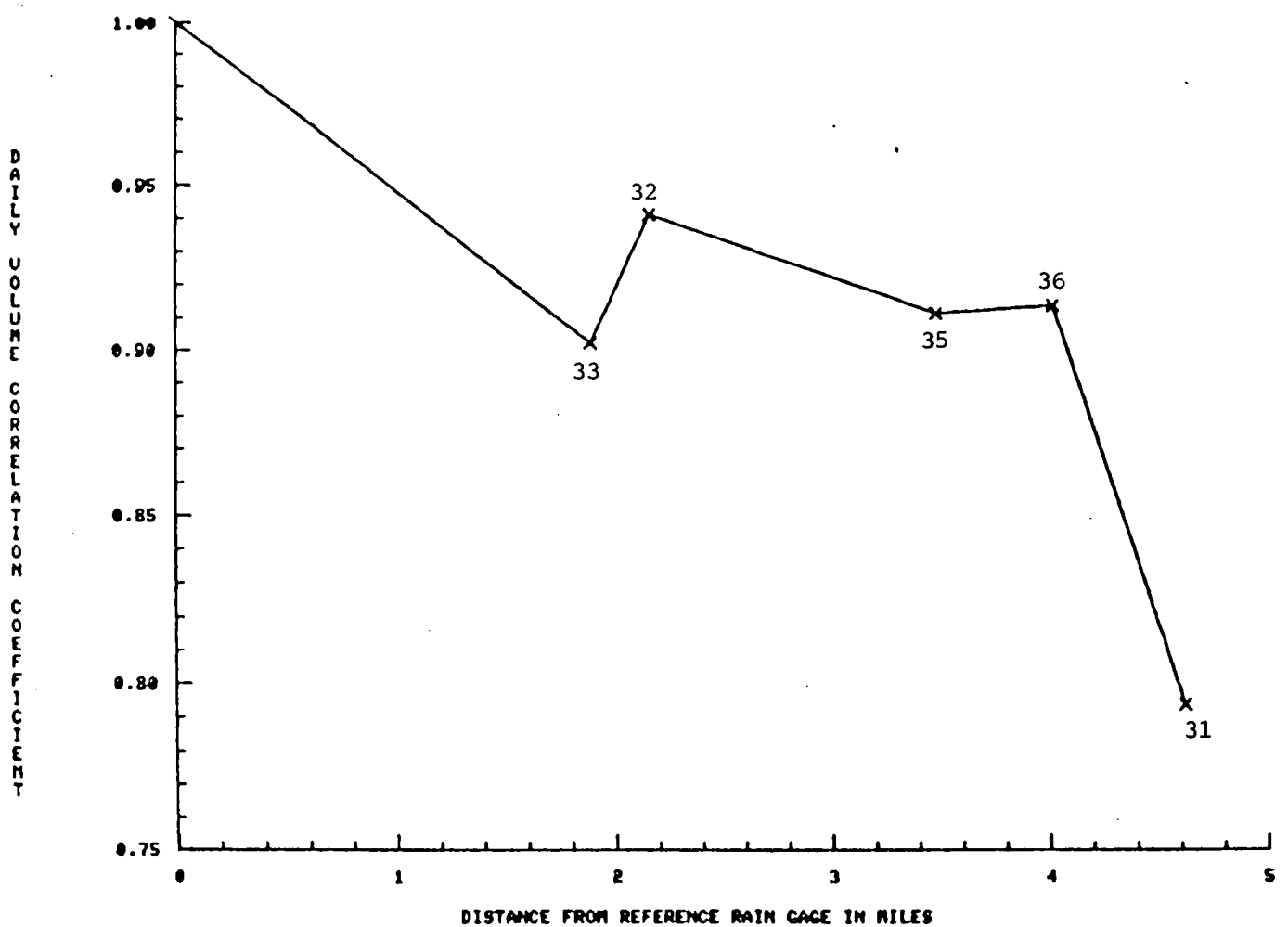


REFERENCE GAGE FOR THIS FIGURE IS NUMBER 34

Figure 7.10. Spatial correlation of daily rainfall volumes between base gage (number 34) and other gages.

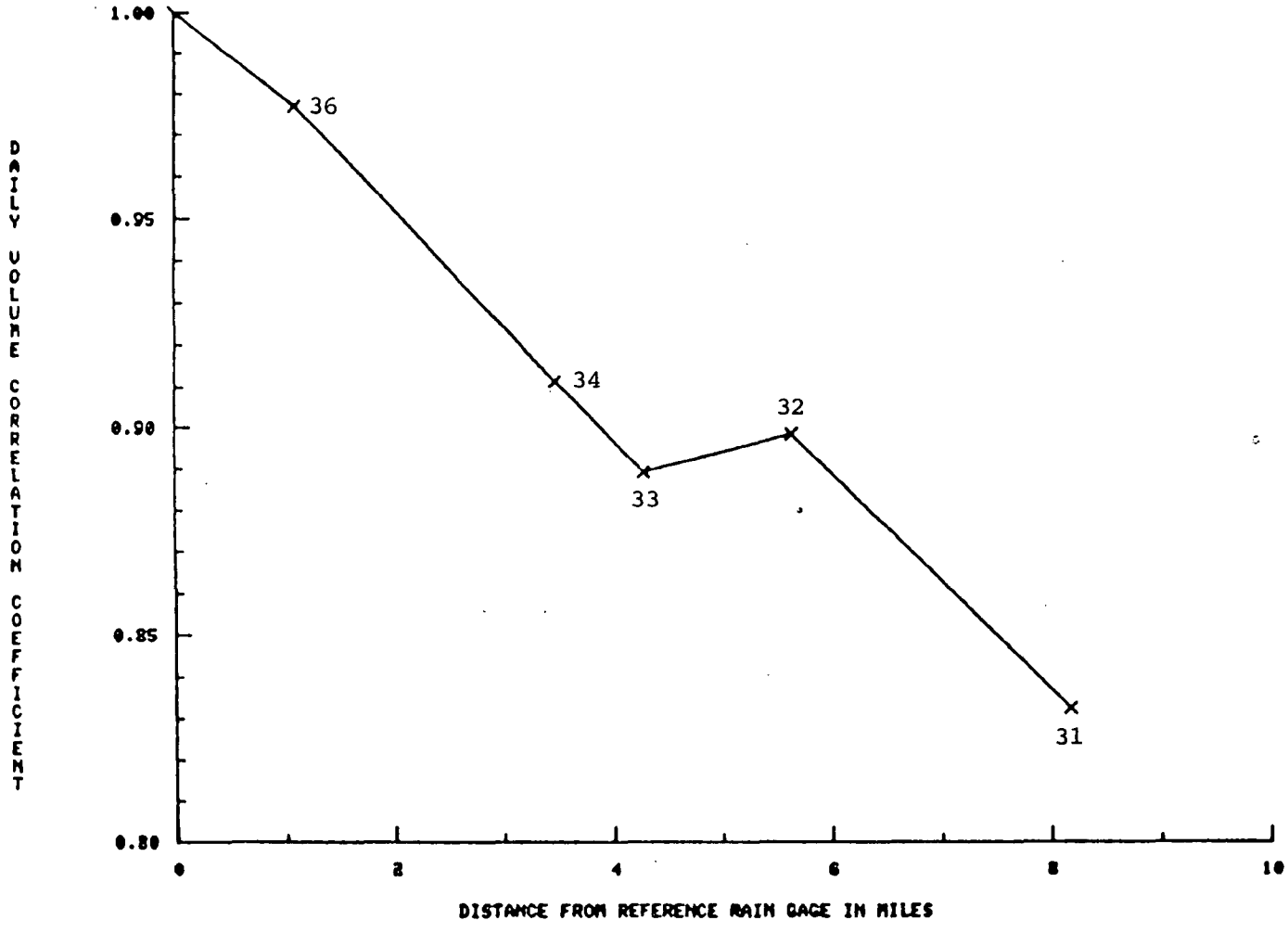


REFERENCE GAGE FOR THIS FIGURE IS NUMBER 35

Figure 7.11. Spatial correlation of daily rainfall volumes between base gage (number 35) and other gages.

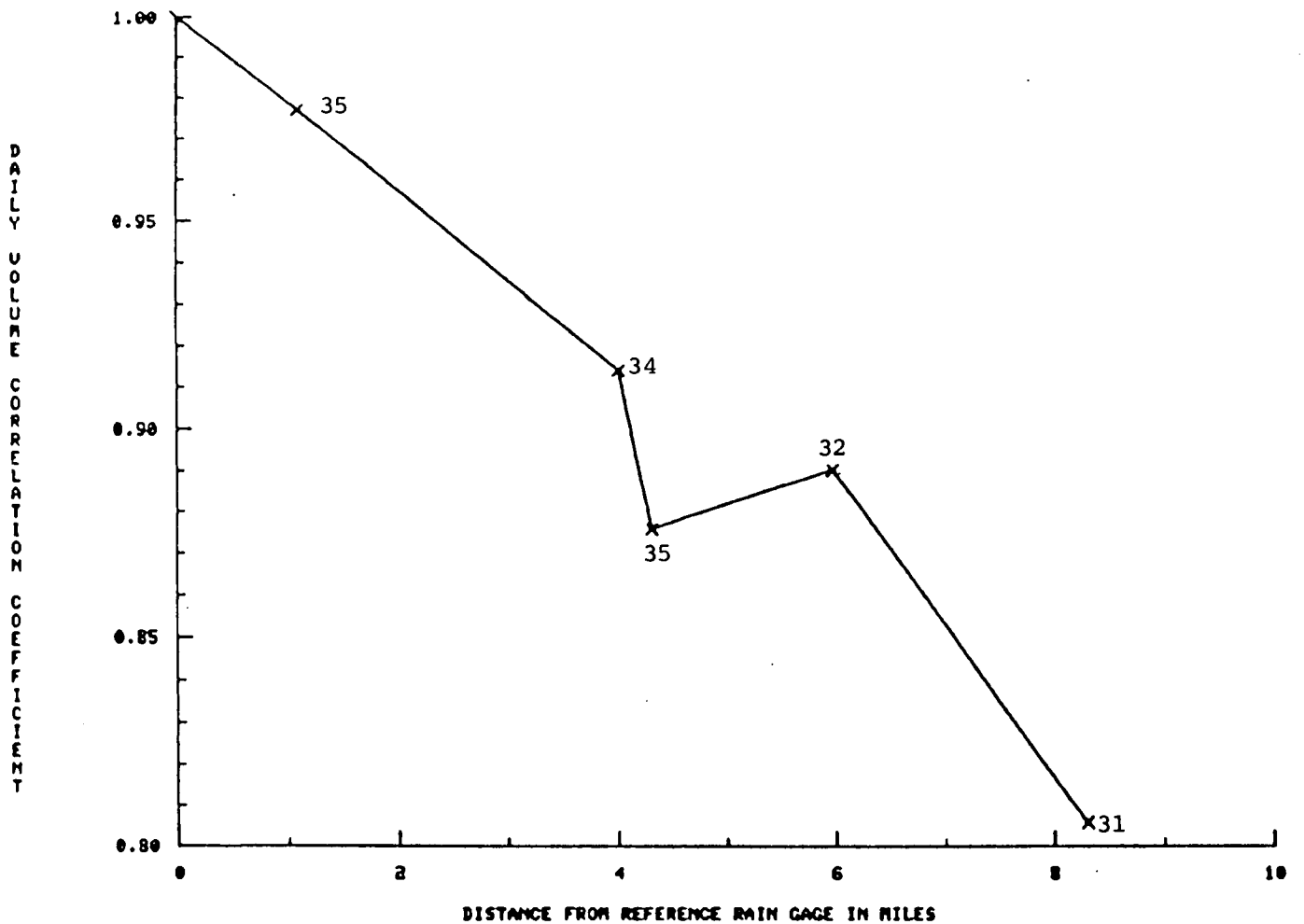


REFERENCE GAGE FOR THIS FIGURE IS NUMBER 36

Figure 7.12. Spatial correlation of daily rainfall volumes between base gage (number 36) and other gages.

This analysis indicates two things. First, gage 32 should be maintained to help fill missing records, and second, the high corelations suggest a redundancy in measurements for daily rainfall totals. This does not suggest that certain stations be abandoned, as following analyses show, only that there is oversampling of daily rainfall with the present network. Another comparison of daily snowfall amounts for stations 33 and 36 produced a correlation of 1.0. Apparently, this strong relationship was also noted by ISU personnel as station 33 was discontinued for snowfall measurements.

Storm events were too numerous for complete analyses. Therefore about five storms with the highest volumes at station 33 were selected for each year (1976, 1977, 1978) as a comparison basis. The first noticeable result was that of the 15 storms; only four had records at all six stations (Table 7.2). Station 32 which was previously identified as being highly correlated was missing eight of fifteen records. Table 7.2 indicates that the variability in rainfall volumes and length of storm can be quite large for the watershed. Table 7.3 lists the statistics of the 15 storms. Ranges where all six gage records are available, particularly for the storm of 5/28/76, demonstrate the need for a good network of recording gages. Interestingly, the patterns of the storms at the six gages were very similar as shown in Figures 7.13, 7.14, 7.15 and 7.16. The 5/28/76 storm exhibits an advanced-delayed pattern with periods of low intensity or no rainfall. Normally such a storm would be subdivided into two parts if the intermittent break were larger than two hours. It is included in total here for demonstration purposes. The 5/12/78 storm is of an intermediate pattern as shown in Figure 7.15, while Figures 7.14 and 7.16 indicate that the 6/13/76 and 6/20/78 storms have patterns typical of thunderstorm events. Although durations and volumes vary from station to station, the dimensionless time-volume distribution is similar between stations for a particular storm. This is helpful if recordings are lost and must be synthesized. No attempt was made to correlate storm values or durations because of lack of complete six station data sets.

In order to better understand the characteristics of storms over the watershed, 95 storms at station 33 were analyzed for key statistics of volume and duration. The mean volume was 0.508 inches with a standard deviation of 0.448. The range was 0.01 to 2.55 inches. For duration, the mean was 4.558 hours, the standard deviation was 4.359 hours, with a range of 0.01 to 23.17 hours. Figures 7.17 and 7.18 show that the distribution of volume and

Table 7.2. Characteristics of Fifteen Large Rainfall Storms

| | GAGE NUMBER | | | | | | | | | | | | | | | | | |
|---|---|---|---|---|---|---|---|---|---|---|---|---|---|---|---|---|---|---|
| | 31 | | | 32 | | | 33 | | | 34 | | | 35 | | | 36 | | |
| Date | B | E | V | B | E | V | B | E | B | B | E | V | B | E | V | B | E | V |
| 04-17-76 | No Record | | | No Record | | | 17.75 | 7.38 | 38.35 | No Record | | | 17.67 | 4.58 | 29.89 | No Record | | |
| 04-20-76 | Not Complete | | | No Record | | | 11.75 | 1.00 | 26.35 | No Record | | | No Record | | | 11.17 | 20.67 | 30.48 |
| 05-28-76 | 19.42 | 7.4 | 21.84 | 22.75 | 7.93 | 16.0 | 19.5 | 7.67 | 37.34 | 22.33 | 7.6 | 13.97 | 22.25 | 8.0 | 37.85 | 22.5 | 8.0 | 27.18 |
| 06-13-76 | 18.32 | 22.22 | 36.83 | 18.42 | 22.33 | 43.69 | 18.3 | 21.58 | 35.56 | 18.47 | 22.42 | 35.36 | 18.5 | 23.5 | 37.59 | 18.58 | 23.0 | 40.64 |
| 07-28-76 | 2.0 | 7.33 | 33.53 | 2.45 | 9.08 | 22.61 | 2.22 | 6.5 | 27.94 | 2.55 | 4.93 | 26.42 | 2.47 | 7.55 | 25.15 | No Record | | |
| 07-28-77 | No Record | | | No Record | | | 16.6 | 19.08 | 29.97 | 16.55 | 19.33 | 41.66 | 16.58 | 18.67 | 40.64 | 16.58 | 18.42 | 39.37 |
| 08-15-77 | 17.83 | .67* | 47.75 | No Record | | | 18.00 | .88* | 37.85 | 18.00 | .50* | 37.34 | 18.17 | 1.17* | 36.32 | 18.17 | .67* | 36.31 |
| 08-27-77 | 19.8 | 9.33 | 21.39 | No Record | | | 19.97 | 10.17 | 28.19 | 19.87 | 8.58 | 28.96 | 19.93 | 9.42 | 35.31 | 19.98 | 9.25 | 35.56 |
| 09-17-77 | 19.12 | 22.93 | 34.62 | No Record | | | 19.33 | 23.20 | 28.05 | 19.33 | 22.90 | 49.53 | 19.25 | 22.97 | 60.68 | 19.30 | 23.03 | 60.28 |
| 10-07-77 | No Record | | | 7.00 | 18.00 | 22.86 | 7.42 | 20.58 | 27.43 | 7.42 | 19.08 | 27.18 | 7.33 | 21.17 | 28.7 | 7.33 | 20.83 | 28.7 |
| 04-05-78 | 13.85 | 18.45 | 19.78 | No Record | | | 11.72 | 2.00 | 27.94 | 11.75 | 1.42 | 29.21 | 11.25 | 1.37 | 31.5 | 11.25 | 2.00 | 31.24 |
| 04-17-78 | 11.67 | 6.83* | 59.18 | No Record | | | 11.83 | 6.83* | 63.96 | 11.83 | 7.00* | 60.20 | 10.50 | 5.67* | 67.51 | 10.73 | 5.57* | 60.15 |
| 05-12-78 | 19.90 | 6.90* | 36.07 | 19.92 | 6.97* | 35.81 | 19.83 | 7.00* | 36.83 | 20.17 | 7.17* | 37.08 | 19.75 | 6.38* | 50.80 | 19.75 | 6.38* | 45.72 |
| 05-27-78 | No Record | | | 16.08 | 17.00 | 26.67 | 16.40 | 17.23 | 28.45 | 16.00 | 17.22 | 31.50 | No Record | | | No Record | | |
| 06-20-78 | .35 | 4.58 | 29.21 | .30 | 5.83 | 38.10 | .58 | 4.58 | 30.23 | .53 | 4.33 | 32.00 | .47 | 6.33 | 42.16 | .83 | 5.67 | 39.12 |

* = next day, B = beginning time (military time in decimal hours), E = ending time, V = volume in mm of depth

Table 7.3. Statistics of Fifteen Large Rainfall Storms

| Date | # of gages | Duration (hr) | | | Rainfall (in.) | | |
|---|---|---|---|---|---|---|---|
| | | Mean | Std. dev. | Range | Mean | Std. dev. | Range |
| 04-17-76 | 2 | 12.50 | 2.24 | 10.91-14.08 | 1.34 | .24 | 1.18-1.50 |
| 04-20-76 | 2 | 11.63 | 3.01 | 9.50-13.75 | 1.12 | .11 | 1.04-1.20 |
| 05-28-76 | 6 | 10.31 | 1.38 | 9.18-12.17 | 1.01 | .406 | .55-1.49 |
| 06-13-76 | 6 | 4.08 | .58 | 3.28- 5.00 | 1.59 | .178 | 1.40-1.86 |
| 07-28-76 | 5 | 4.74 | 1.57 | 2.38- 6.63 | 1.07 | .160 | .89-1.32 |
| 07-28-77 | 4 | 2.30 | .42 | 1.84- 2.78 | 1.49 | .212 | 1.18-1.64 |
| 08-15-77 | 5 | 6.67 | .25 | 6.50- 7.00 | 1.54 | .190 | 1.43-1.88 |
| 08-27-77 | 5 | 12.86 | 1.36 | 10.61-14.20 | 1.18 | .232 | .84-1.40 |
| 09-17-77 | 5 | 3.74 | .11 | 3.57- 3.87 | 1.84 | .585 | 1.10-2.30 |
| 10-07-77 | 5 | 12.63 | 1.23 | 11.00-13.84 | 1.06 | .095 | .90-1.13 |
| 05-05-78 | 5 | 13.67 | 1.29 | 11.45-14.75 | 1.13 | .135 | .91-1.24 |
| 04-17-78 | 5 | 19.07 | .15 | 18.84-19.17 | 2.45 | .137 | 2.33-2.66 |
| 05-12-78 | 6 | 10.99 | .18 | 10.63-11.17 | 1.59 | .249 | 1.41-2.00 |
| 05-27-78 | 3 | .99 | 1.01 | .83- 1.22 | 1.14 | .096 | 1.05-1.24 |
| 06-20-78 | 6 | 4.71 | .85 | 3.80-5.87 | 1.38 | .211 | 1.15-1.66 |
| | | Mean 8.72 | Std. dev. 5.19 | | Mean 1.40 | Std. dev. .382 | |

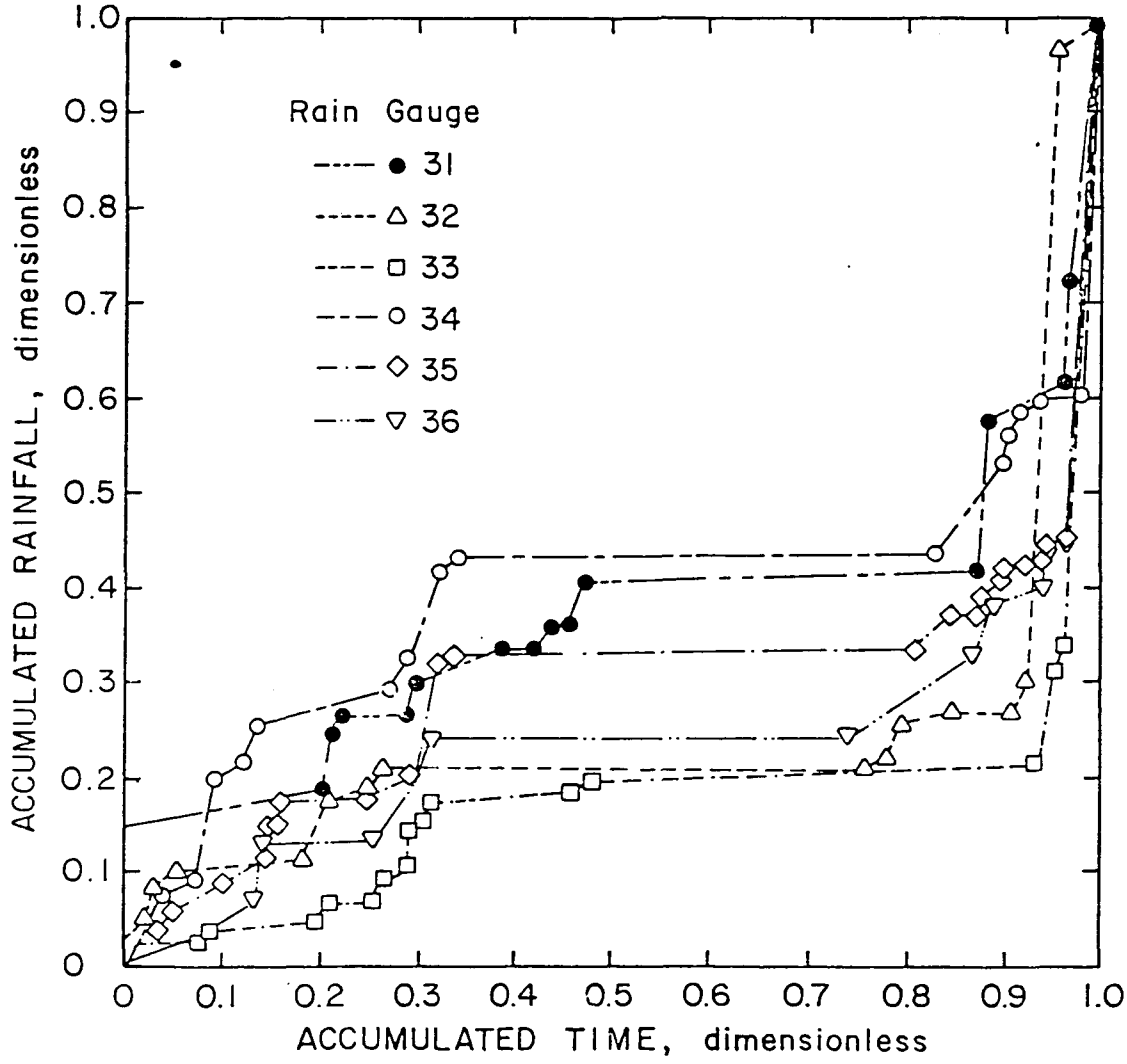


Figure 7.13. Dimensionless mass accumulation curve for rainfall event of 5/28/76.

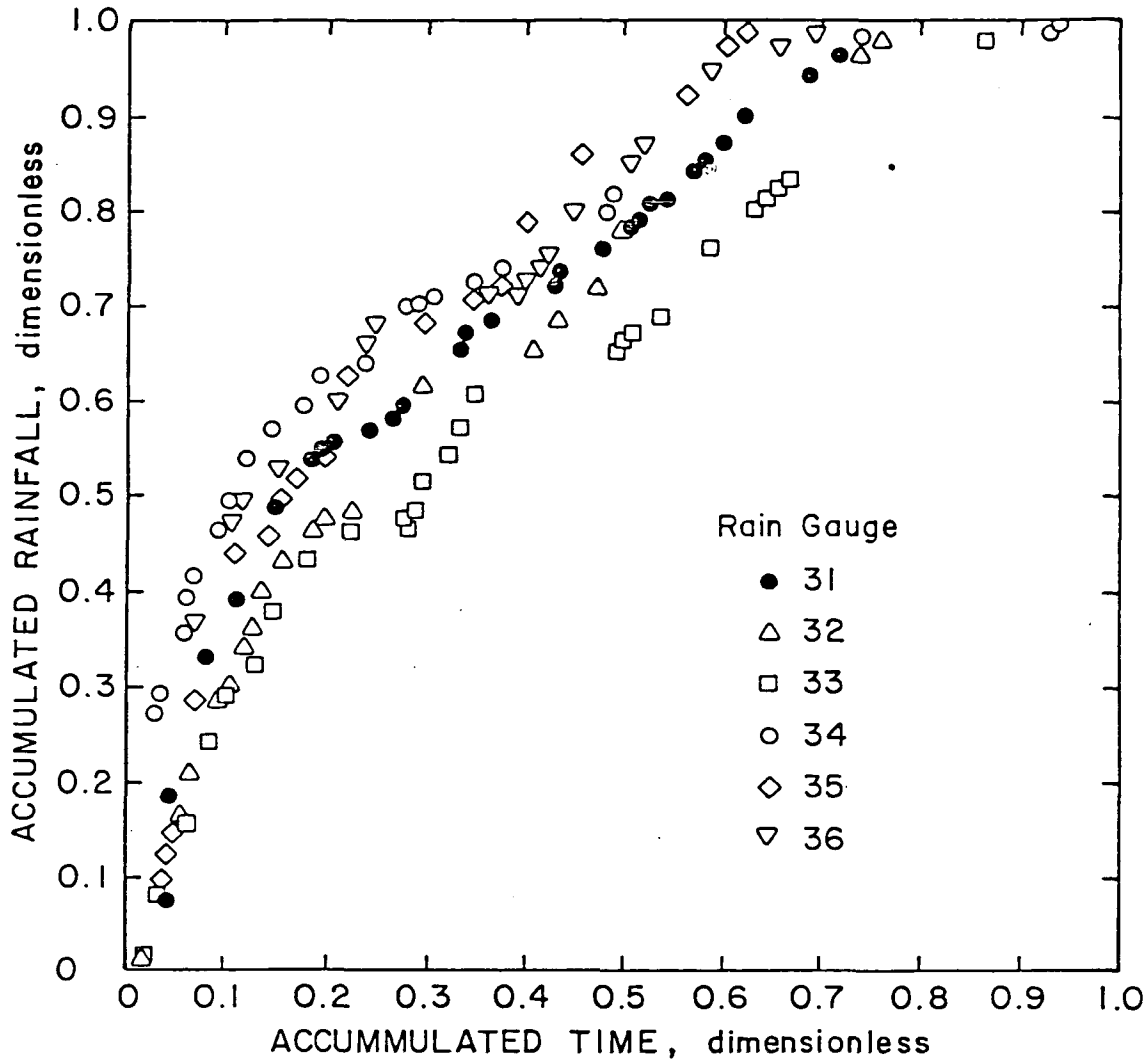


Figure 7.14. Dimensionless mass accumulation for rainfall event of 6/13/76.

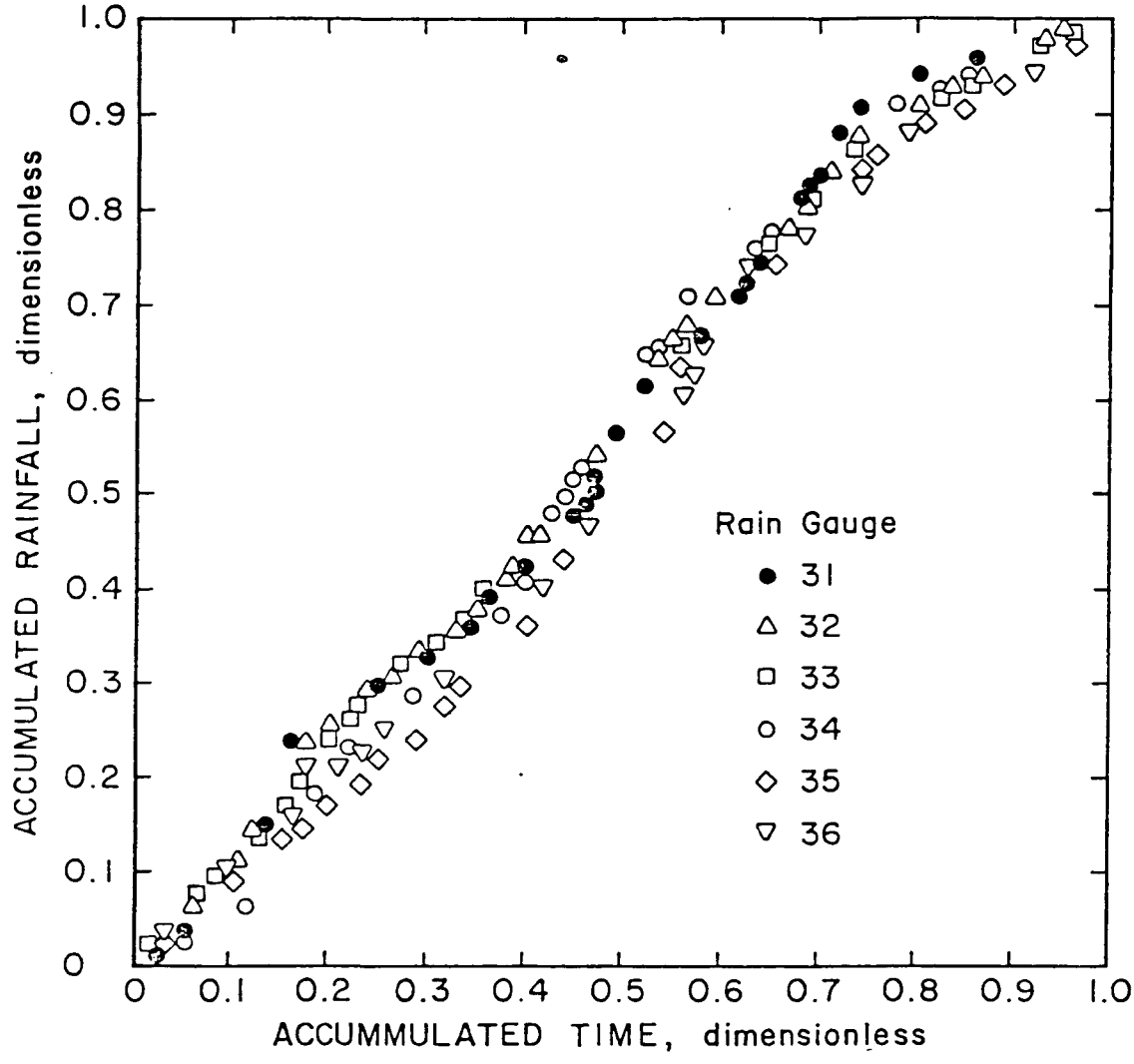


Figure 7.15. Dimensionless mass accumulation for rainfall event of 5/12/78.

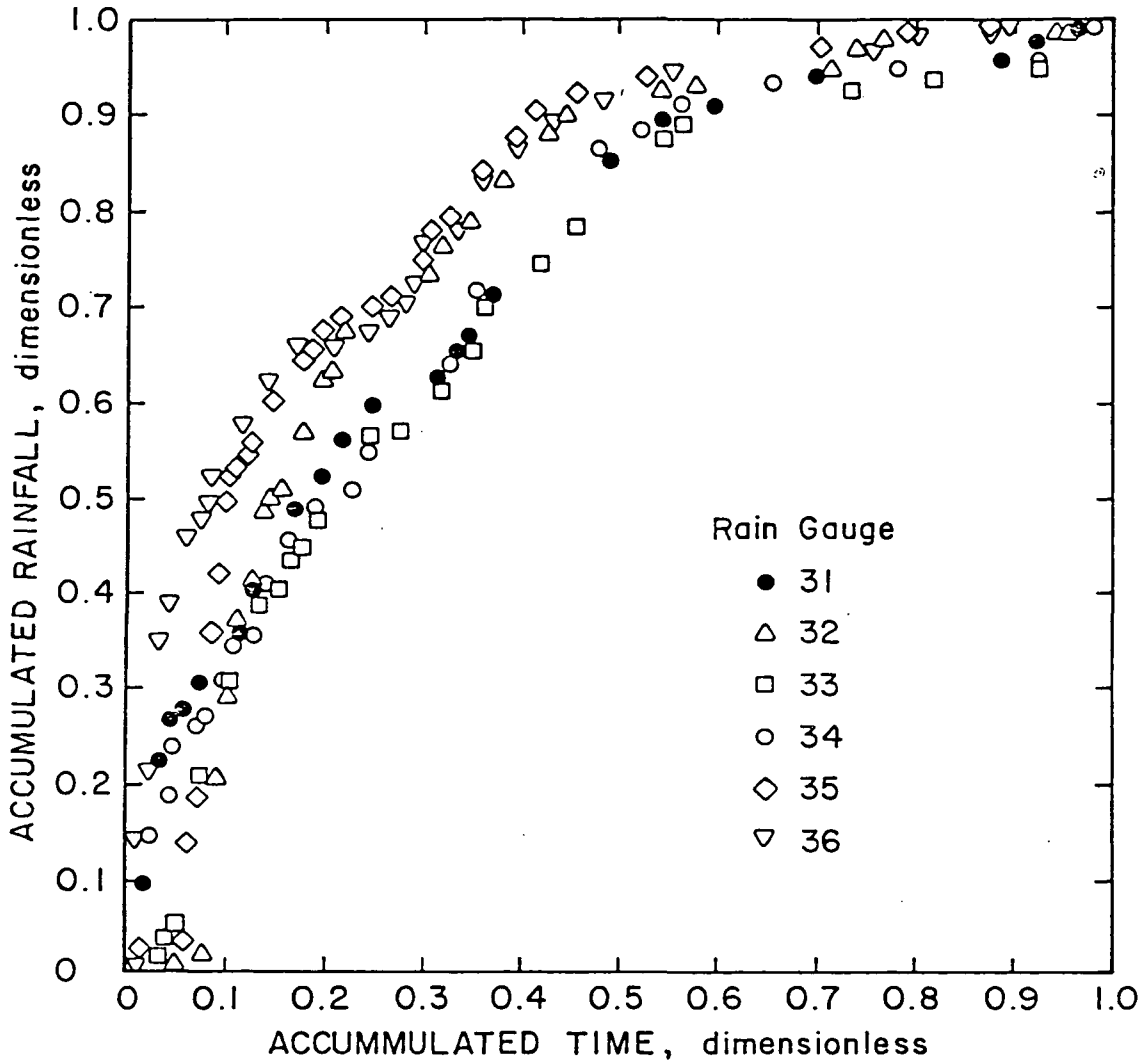


Figure 7.16. Dimensionless mass accumulation for rainfall event of 6/20/78.

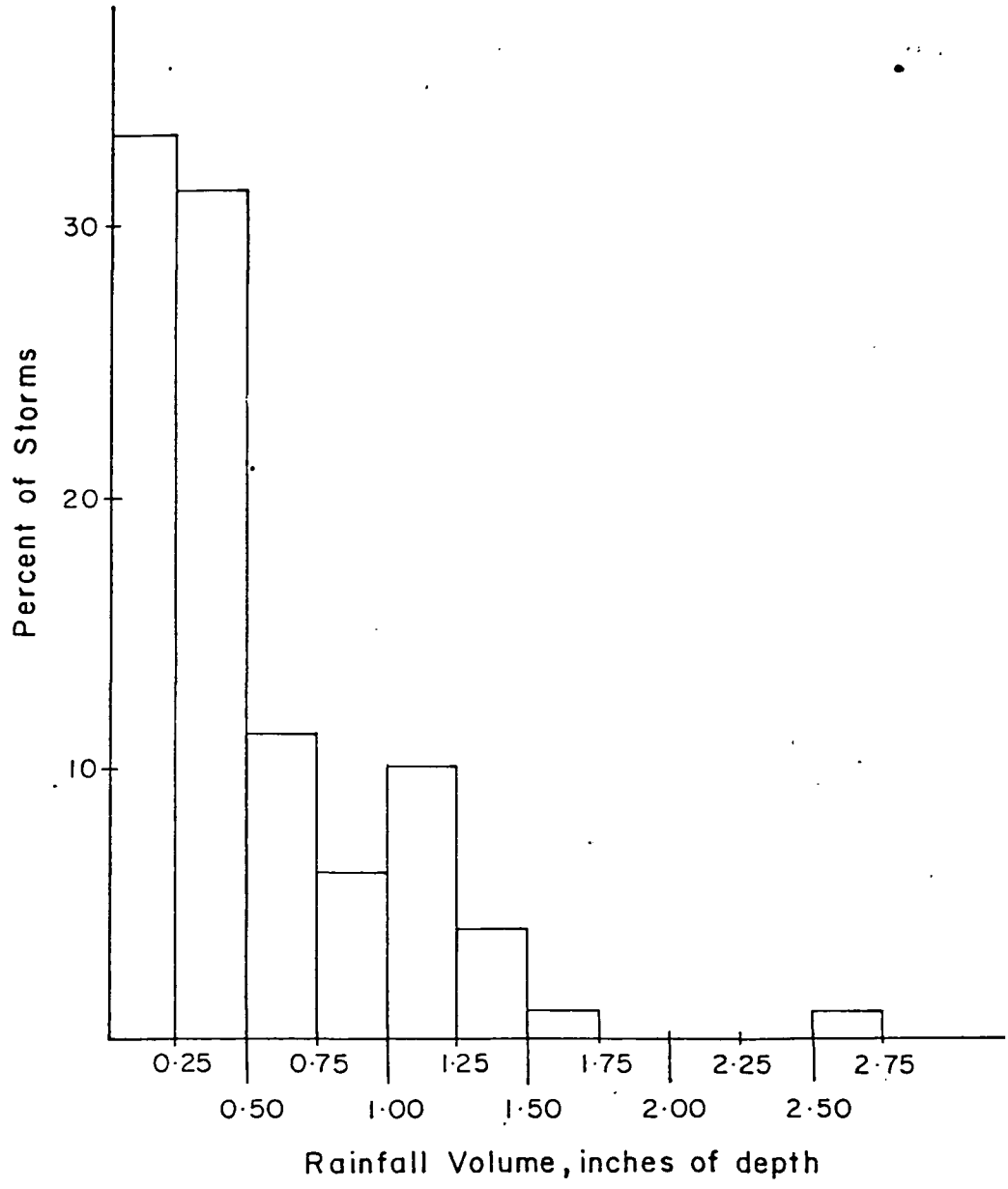


Figure 7.17. Distribution of rainfall volumes by depth classes.

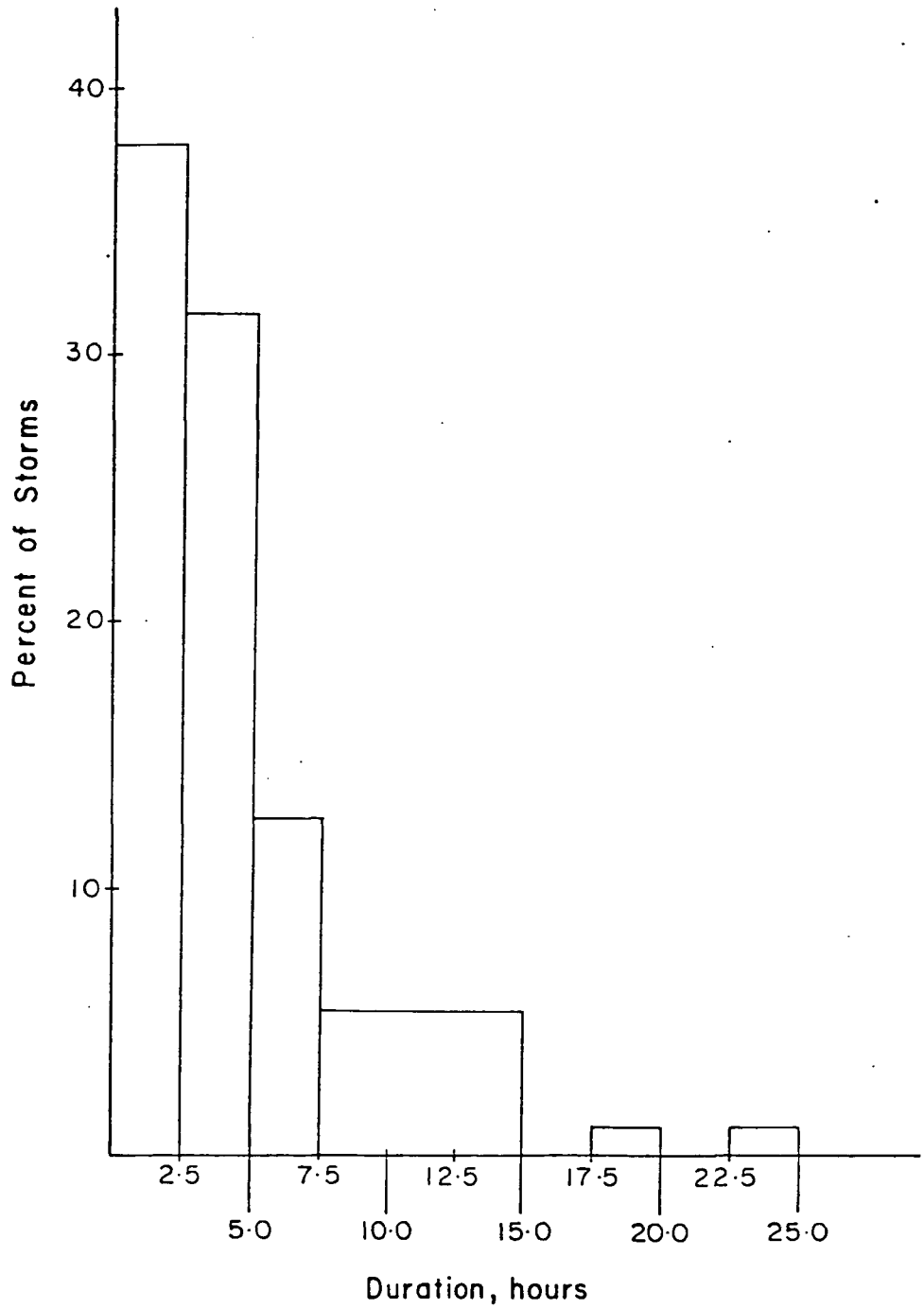


Figure 7.18. Distribution of rainfall durations by hour classes.

duration are skewed towards zero or smaller durations and amounts. These two distributions are independent and a short duration storm may produce a large rainfall volume.

In general the rainfall data are fairly complete. Problems do arise when gages malfunction and only partial coverage results. However, the close correlation for daily volumes and similar storm patterns suggest that synthesized data may be used to fill gaps. Not much can be said about snowfall data except that daily volumes appear adequate at this time.

Other climatic data of temperature, wind, humidity, and pan evaporation appear realistic and reasonable. Unfortunately, solar radiation does not. Several times the reported langleys per day were well over 1000, such as 6/13/77 (3047), 3/30/78 (2086), and 4/25/78 (2657). As a comparison the maximum solar radiation at the top of the atmosphere for the latitude of Four-Mile Creek is about 1000 (Eagleson, 1970). Therefore, the several values above that level are suspect if not completely false. For water balance modeling more care is needed in solar radiation collection. The other data listed in Table 7.1 are specific types and must be measured as needed.

### 7.3.4 Hydrologic and Hydraulic Data

Whereas climatic data include the inputs to models, these data include the output against which models are checked or calibrated. Of particular interest are the daily and storm hydrographs, how they are measured, and sedimentation characteristics.

There are not enough gaging stations in the watershed to conduct an extensive correlation analysis of the flow. Daily discharges and storm runoff must be examined. Simple analysis of the daily discharge values at the three U.S. Geological Survey gaging sites (numbers 4, 5, and 6 in Figure 7.1) help define discharge characteristics of the watershed. A large portion of the volume of runoff occurs during the winter snowmelt and spring rainfall months as indicated by Figure 7.19 for Four-Mile Creek near Traer, the basin outlet. It is interesting to note that the last few years were relatively dry, as evidenced by lower flows; indicating that recent efforts may be during a non-typical runoff regime and not representative of a wide spectrum of conditions. Comparison of average daily discharges for all three stations (a measure of water yield) shows there is significant watershed runoff contribution in the lower portion of the watershed (Figure 7.20), as would be expected. This is

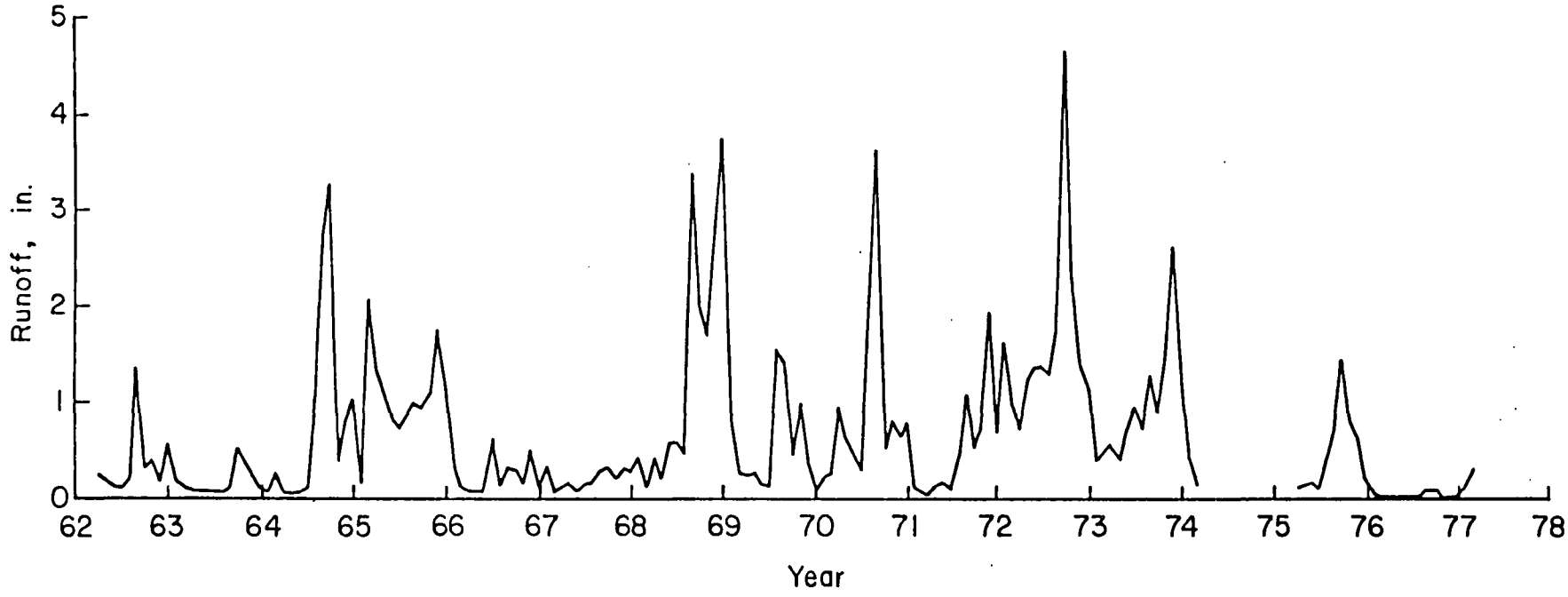


Figure 7.19. Four-Mile Creek near Traer, Iowa monthly runoff in inches.

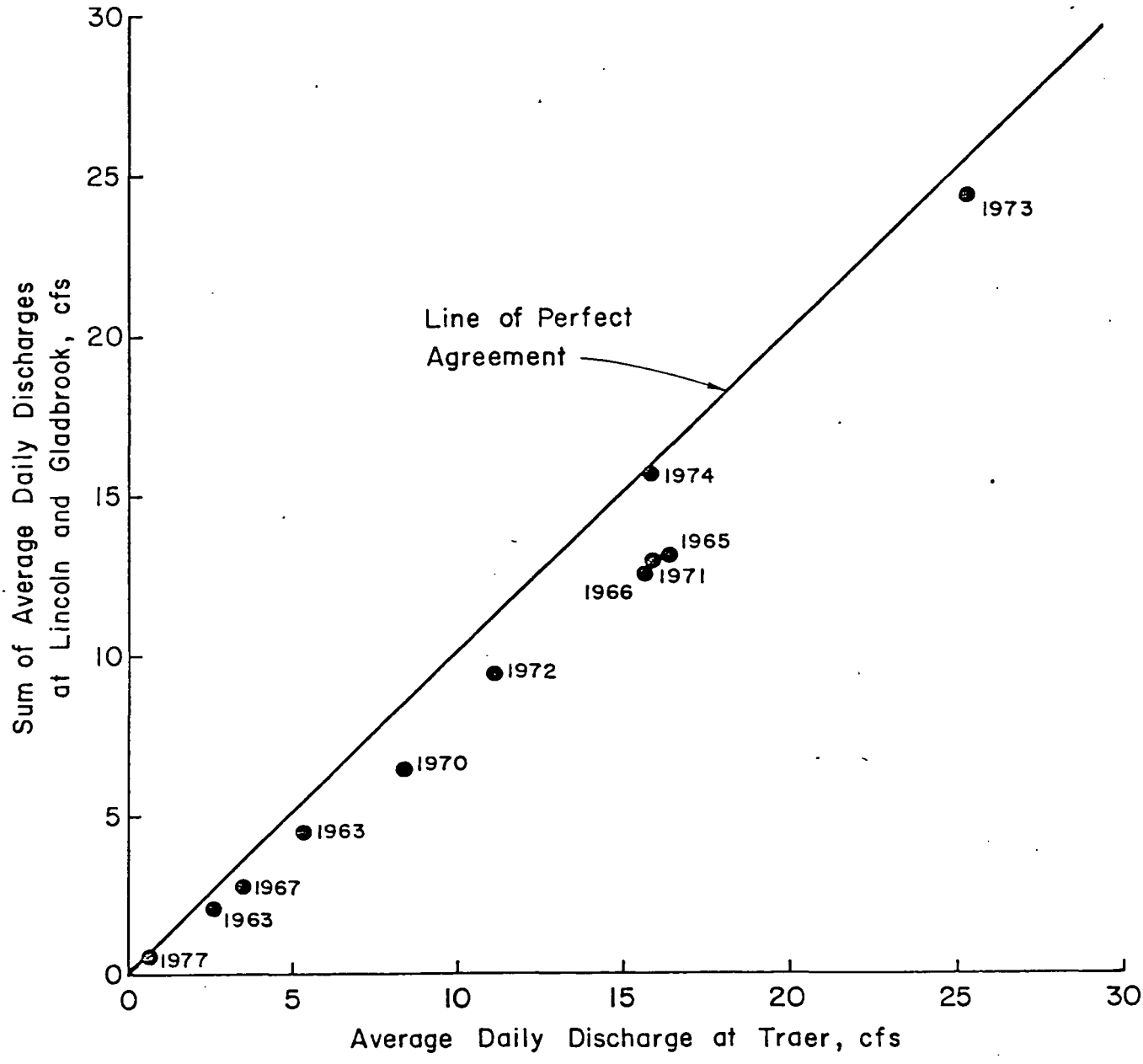


Figure 7.20. Comparison of upstream contributions to downstream flows.

consistent with other watersheds. Peak discharge records are affected by many factors including overland flow contributions, channel flow resistance, and the reliability of the gaging station. Original graphical comparisons of peak discharges for the upstream Lincoln and downstream Traer sites based on U.S. Geological Survey gaging records indicated some discrepancies. In particular the Lincoln peaks were greater for six of eleven discharges. Although this difference may have been a result of attenuation of intense, short duration storms, it actually was gaging errors that were corrected in the 1977-1978 annual report.

Figure 7.21 shows the relationship between the corrected yearly instantaneous peaks at Traer and at Lincoln. Of the eleven events, four did not occur on the same day and one was higher at Lincoln than at Traer (1963). In this case, attenuation of the flood peak or its location may have caused the lower downstream discharge. Graphical analysis helped pinpoint the fact that there were mistakes in the peak discharge records. Whenever a graphical analysis shows a trend or relationship that appears different than expected, the records should be rechecked.

The interrelationship of daily flow at Lincoln and Traer and the relationship between stations were checked for an "average" water year based on the Traer gage. An average year is defined here as one in which the annual mean daily flow is nearly the same as the long term mean daily flow. As of the end of the water year (WY) 1977 (October 1 to September 30), the long term 14 year mean daily flow was 11 cfs. Water year 1972 almost matched that with a 11.1 cfs mean daily flow and consequently was chosen for analysis. A more complete analysis would require encoding all data for Lincoln, Gladbrook, and Traer; a task that was beyond the scope fo this project. However, this analysis using WY 1972 can be extended if the data obtained in a reasonable format. Figures 7.22 and 7.23 show the autocorrelation plots or correlograms for Lincoln and Traer with a maximum 14 daily lags (two weeks). There is a similarity in shape. Of particular interest is the sharp drop in correlation between zero lag and lag 1 (same day and previous day). This indicates there is only a moderate relationship between daily flow values due to large watershed precipitation variability, irrigation diversion and return flows. In a large system such as the lower Mississippi River, changes occur more slowly so the correlation at lag 1 is expected to be higher. Another interesting observation is the rise in correlation at lag 6 (six days). This may be particular

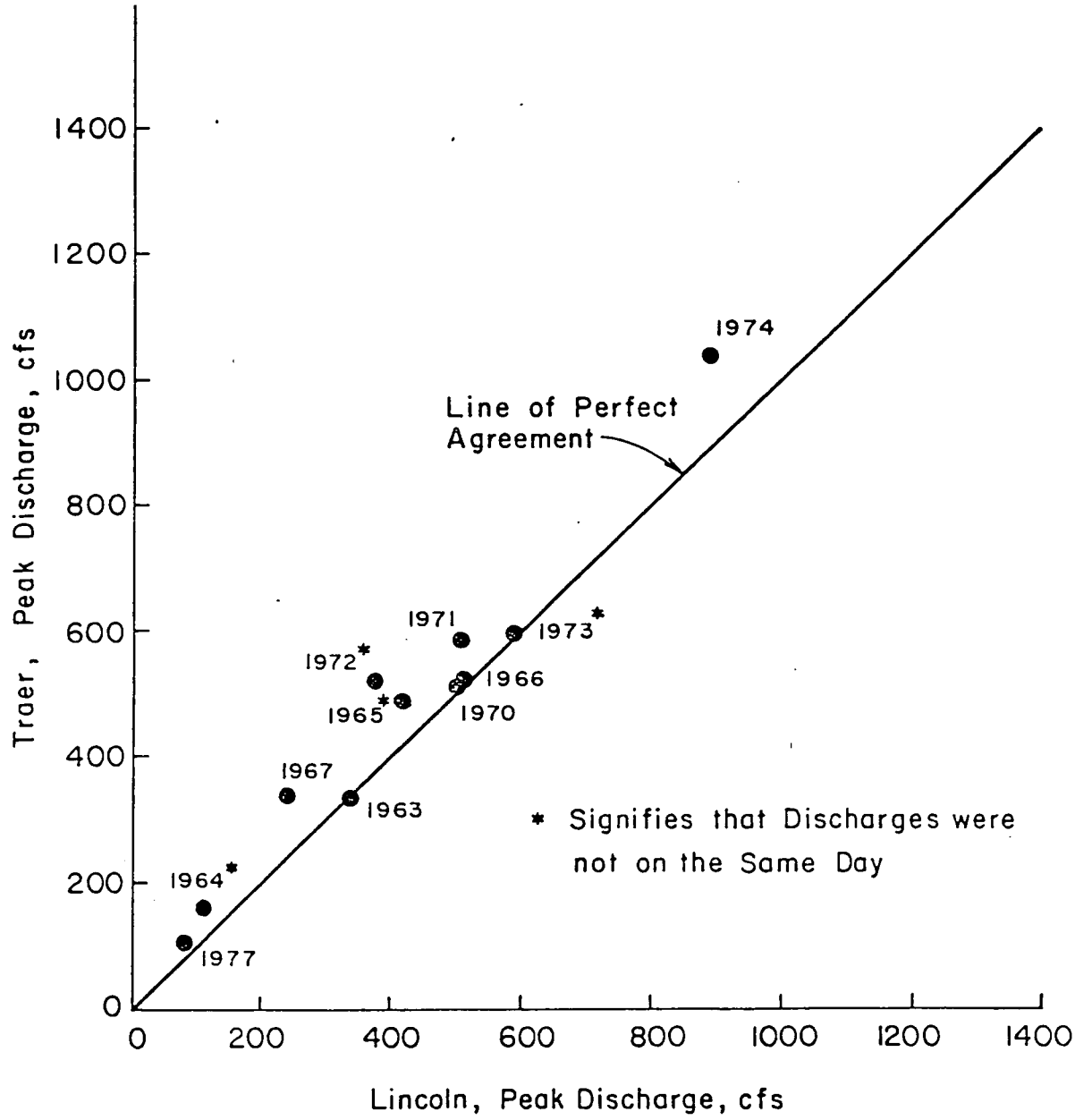


Figure 7.21. Comparison of peak discharges at downstream Traer and upstream Lincoln gages.

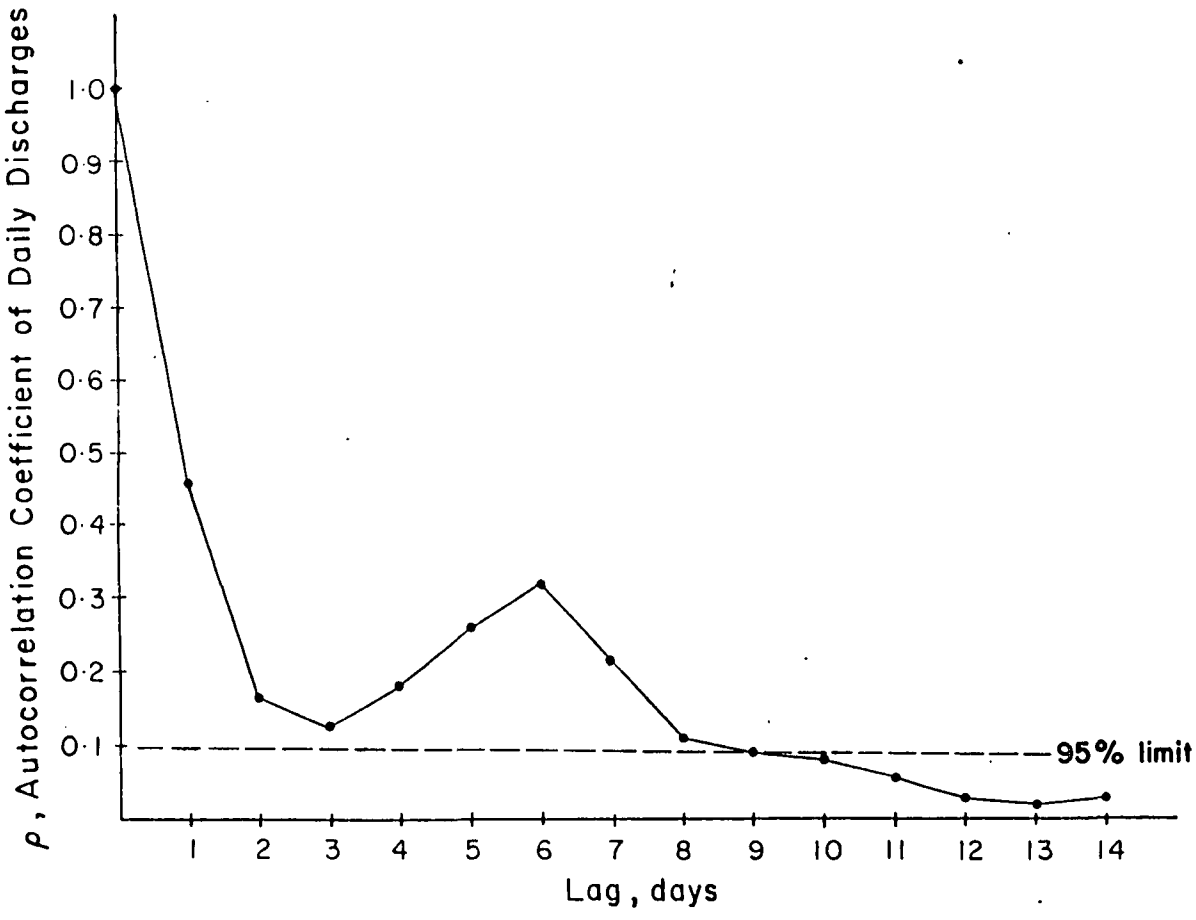


Figure 7.22. Autocorrelation for Four-Mile Creek near Lincoln, WY 1972 daily discharges.

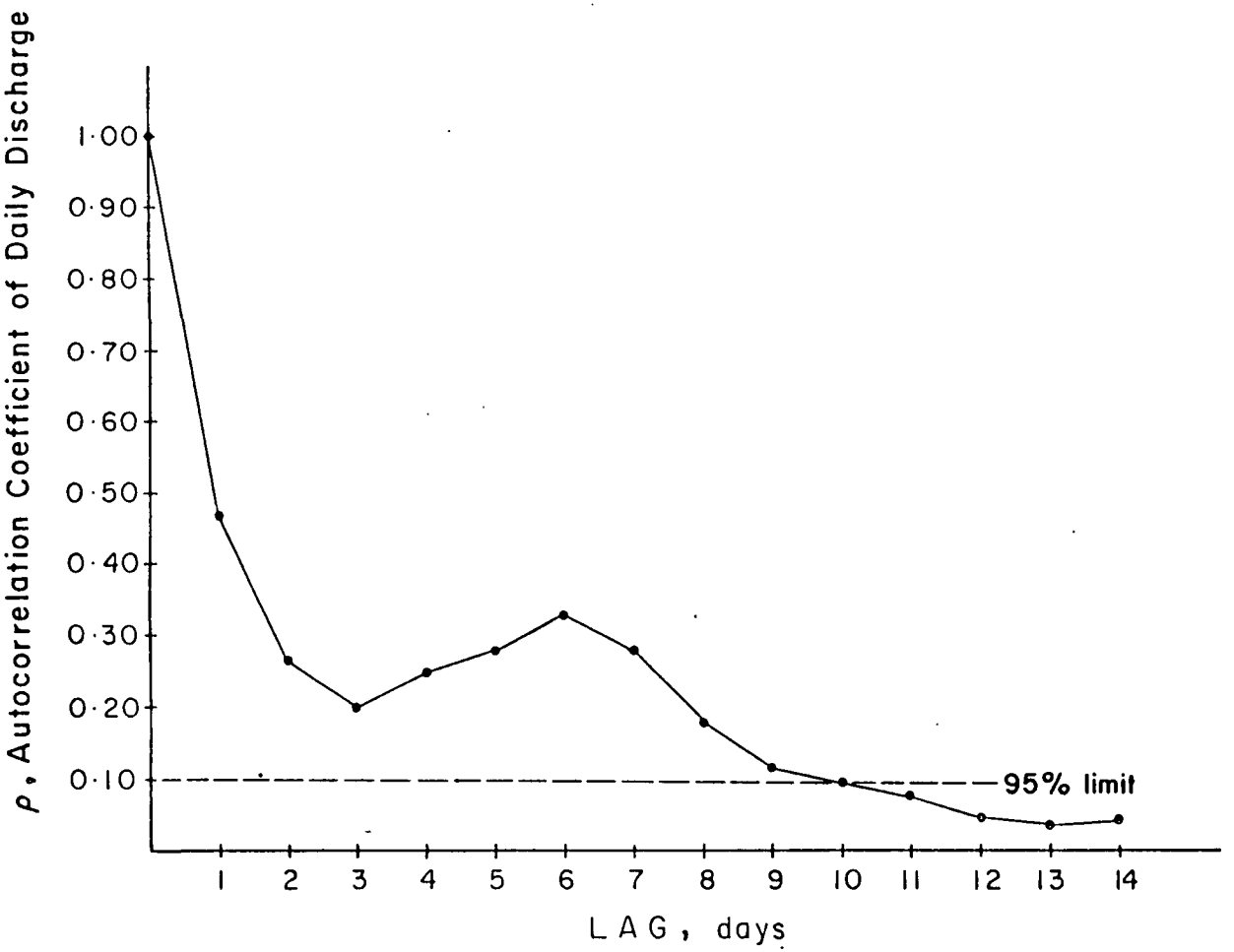


Figure 7.23. Autocorrelation for Four-Mile Creek near Traer, WY 1972 daily discharges.

to WY 1972 but may also indicate some physical process such as ground water effluent flow. Another cause for this relationship is the correlation of the flows at the beginning and end of storm hydrographs. This analysis shows that daily flows may not be the best method for characterizing system response because they cannot be correlated well enough with previous records, i.e., information may be lost. Cross-correlations have similar results (Figure 7.24) with the zero lag being quite high and lag 1 dropping appreciably. This analysis shows that the use of daily flow to characterize discharge is a choice that may lead to problems. Correlation at lag 6 increases similar to the autocorrelation and this is due to the carryover effect of the large autocorrelation at this lag for each gage.

The cross-correlation of the Traer and Lincoln gages with a gage outside of the Four-Mile watershed was next assessed. This was done to assess the degree of correlation of the causal factors for streamflow and also to be able to transfer data in case the need arose. The Hudson stream gage on Blackhawk Creek was selected for this correlation. The gage monitors 303 sq. mi. and is located twenty miles northeast of the Lincoln gage. The lag zero cross-correlation coefficient for monthly data is 0.937 and 0.902 for the Hudson-Lincoln and Hudson-Traer gages respectively. This high interwatershed correlation indicates that the causal processes for runoff are fairly uniform over this area.

Interpolation of the correlograms indicates a time lag of about one hour at the 0.8 correlation level. This coincides with time of travel estimates for the channel based on historic flood records, typical channel cross sections ($a$ and $b$ parameters), channel slope, and Manning's $n$ value. The equation used to determine time of travel was:

$$V = a_1 Q^{b_1}$$

where $V$ is average velocity, $Q$ is discharge, and $a_1$ and $b_1$ are parameters estimated from channel characteristics. This equation was derived from Manning's formula. Several flood discharges were used to estimate travel times. These discharges roughly correspond to 2, 5, 10, 25, 50, and 100 year return period flows (based on short records). The parameters used were slope of 0.0014, Manning's $n$ of 0.04, average $a_1$ value (from wetted perimeter-flow area relationship) of 5.9, and average $b_1$ value of 0.38. The time of

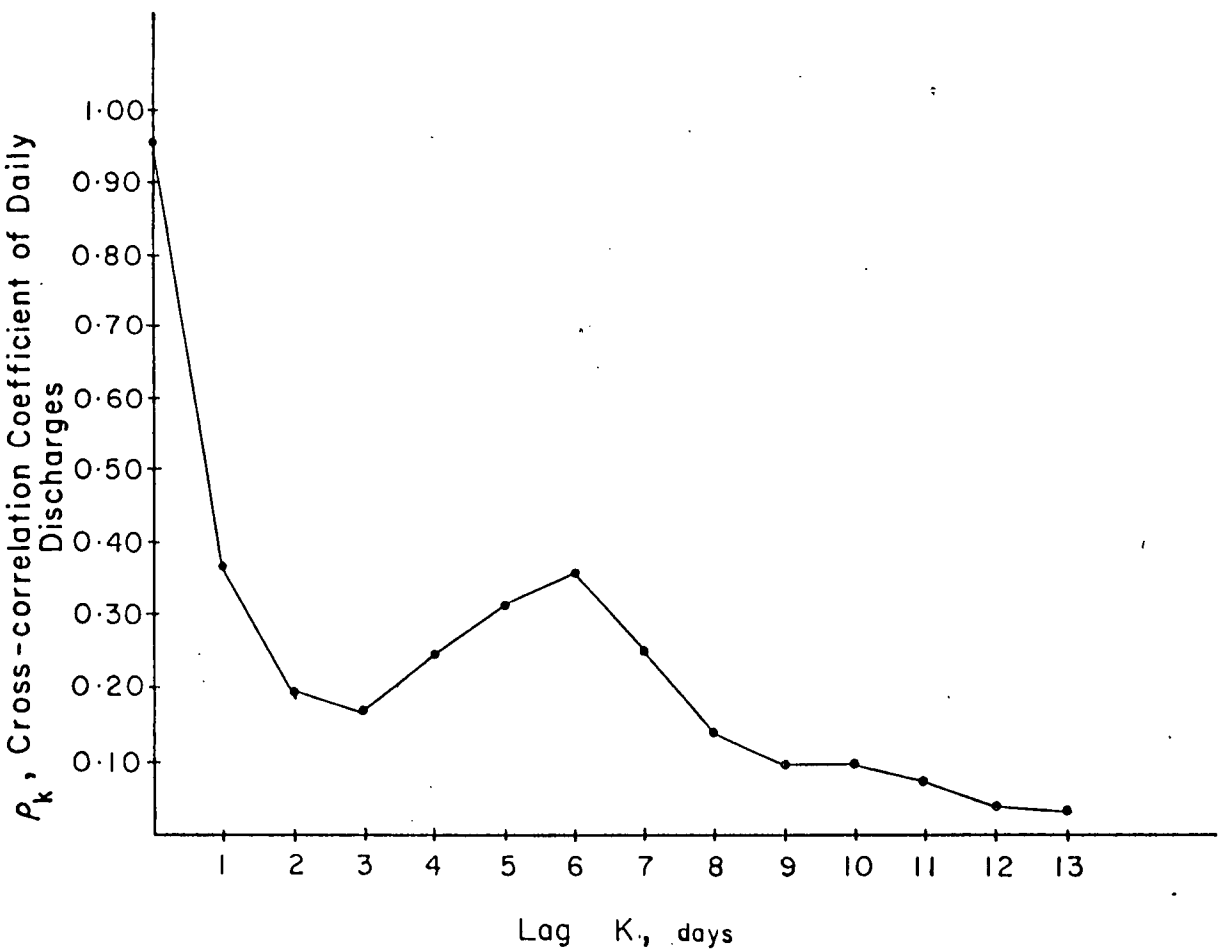


Figure 7.24. Cross-correlation between Four-Mile Creek near Lincoln and near Traer, WY 1972 daily discharges.

travel for the 3.41 miles between Lincoln and Traer for a 2 year return period discharge of 400 cfs is about 1.6 hours while the 100 year peak of 2,000 cfs requires only one hour. These values are comparable with the lag times required to yield a high cross correlation as seen in Figure 7.24. Computations show that a one hour, or preferably shorter, sampling interval is needed to correspond to the movement of the flood wave. Because flooding is not a major concern of the watershed data collection system, such a requirement may be excessive. However, the above analyses do show there may be a need for re-evaluating the sampling interval at these stations.

Similar comparisons of peaks can be made for ISU 1 and ISU 8. These two watersheds were chosen because ISU 1 lies inside ISU 8 and records exist for both. In addition, raingage 33 which represents conditions in both areas is considered as a key gage site from which other analyses can be conducted. Figure 7.25 shows a plot of peak discharge per unit area at ISU 1 and 8 for eight events. As this figure indicates, there is some consistency between the peaks at each of the stations. However, it also suggests that at this watershed scale, there is a certain degree of "noise" or natural variability in rainfall and runoff that creates the scatter seen in this figure. Figure 7.26 shows a comparison of time to peak runoff from the beginning of rainfall for the same eight storms. Although there is a trend towards closer values as time to peak increases, it appears, using Figure 7.25, that these are not associated with resistance effects as much as location of storm cells and movement of the storm. For example, events 7 and 8 had similar magnitudes of peak discharge for ISU 1, but almost an order of magnitude difference for ISU 8. This would indicate that these runoff events may be heavily controlled by the spatial distribution of the rainfall. Inspection of the rainfall record confirms this suspicion as event 7 was only 43 minutes in duration while event 8 lasted four hours. This would suggest that event 7 may be a more localized, high-intensity short duration event, whereas event 8 may be more uniform in nature. Such comparisons help in modeling to determine when certain assumptions, such as homogeneity of rainfall, are invalid.

In addition to discharge, there is available information for a brief analysis of sediment data. Figure 7.27 shows the variation of bed material with distance along the stream. For the coarse fraction larger than 62 microns, there is no trend along the channel indicating the material has not been sorted by stream action. These coarse sizes indicate that sediment sampling

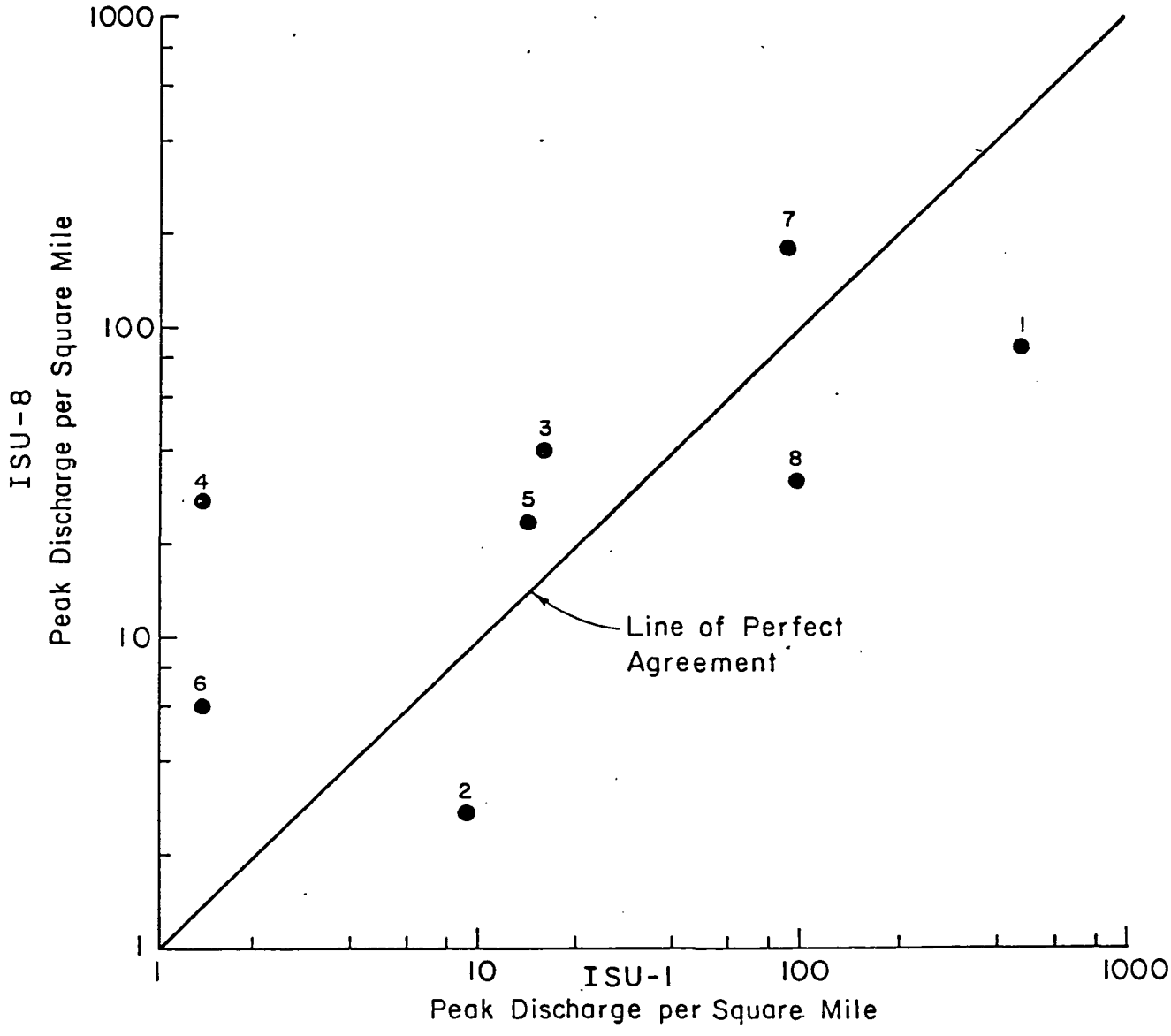


Figure 7.25. Comparison of peak discharge per square mile for ISU 1 and ISU 8 watersheds.

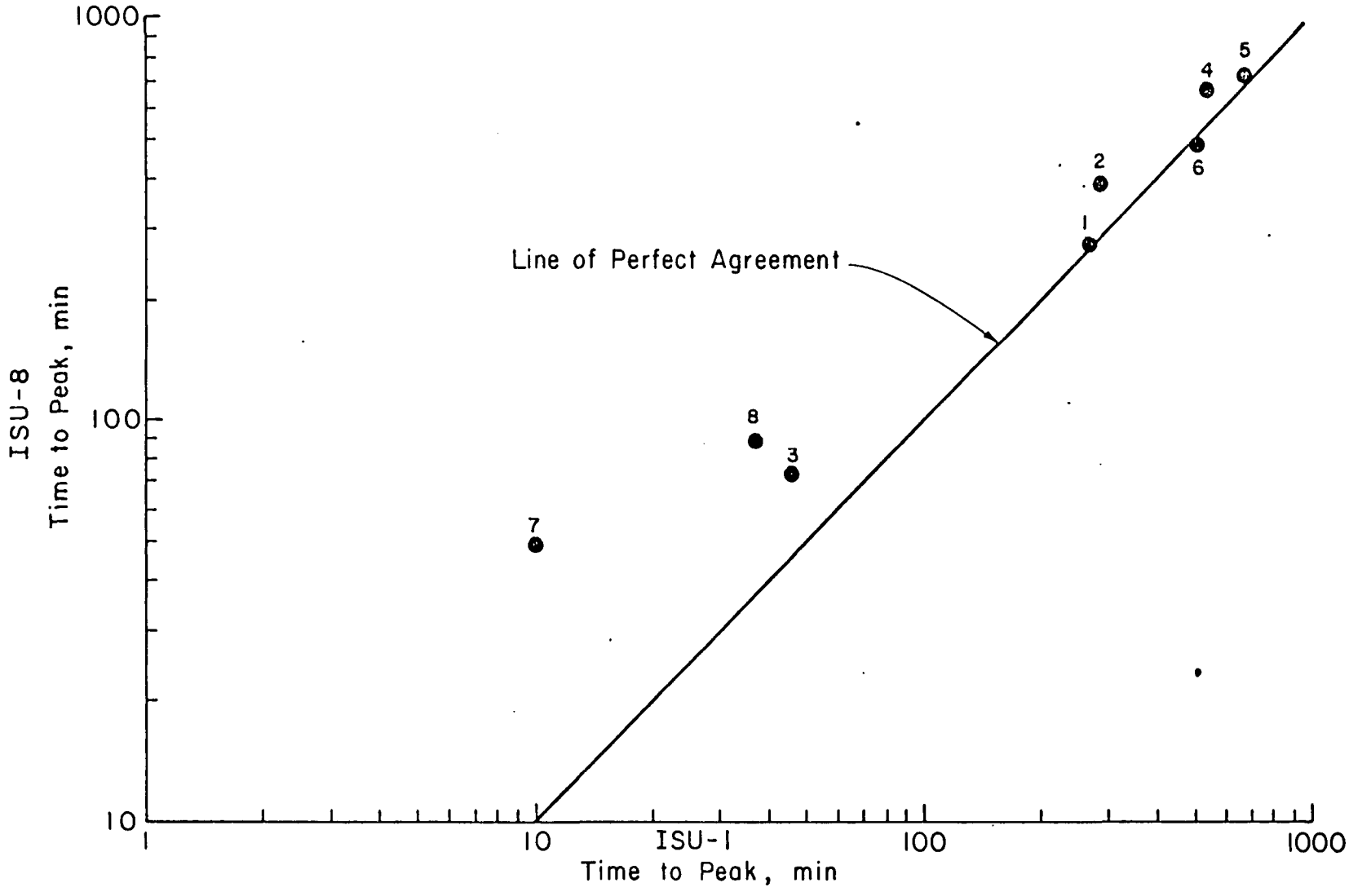


Figure 7.26. Comparison of time to peak discharge for ISU 1 and ISU 8.

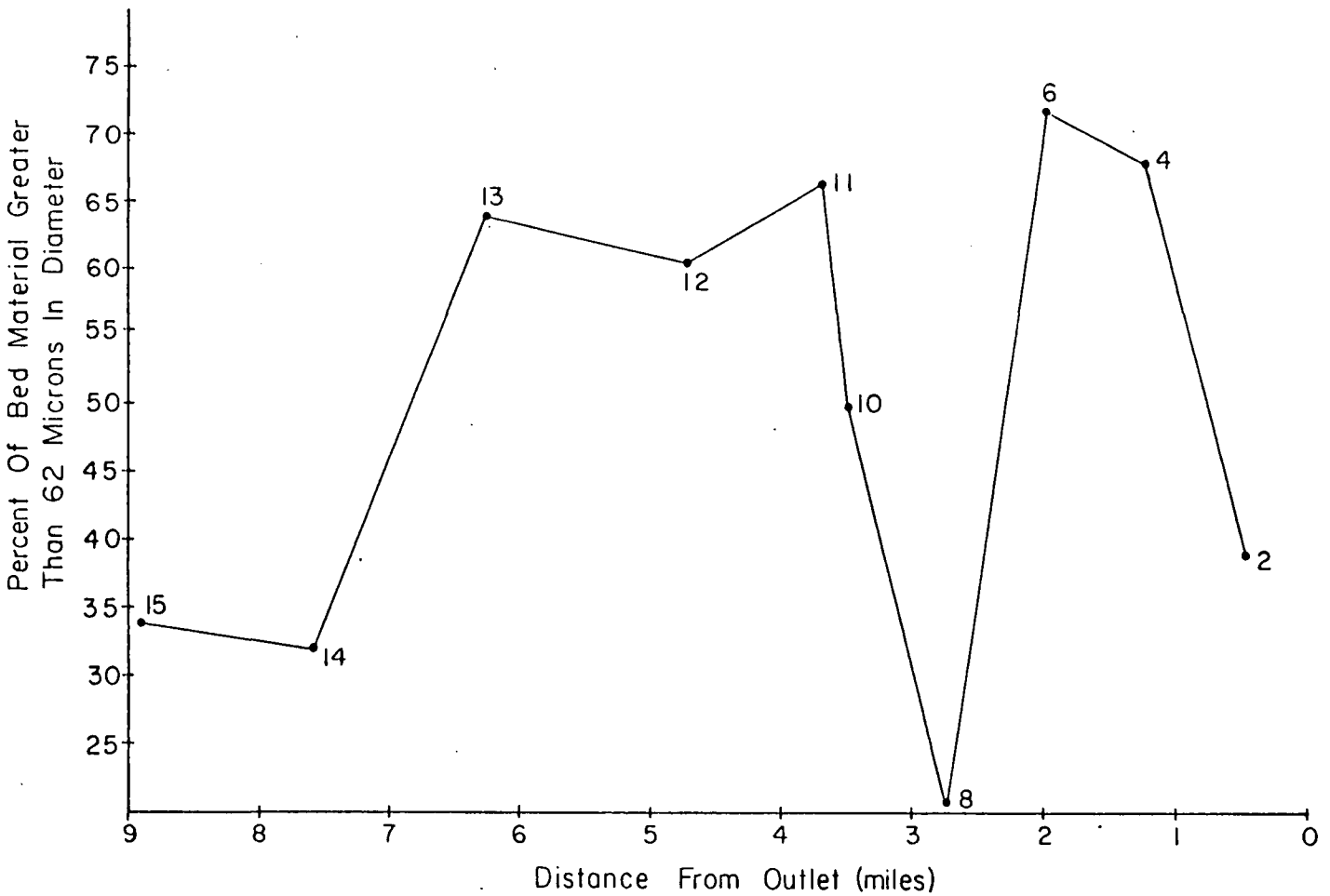


Figure 7.27. Changes in bed material size along main channel.

devices may be needed to collect sand size particles. This graph also shows that a significant portion of sediment is composed of fines (less than 0.62 mm in diameter) as might be expected for the loessial soils. Buried, vertical channel chains and field sediment discs are efficient ways of checking the aggradation and degradation at certain locations. Field discs are flat pieces of plastic that are placed in the field to detemrine the amount of aggradation in an area. For the field discs, sieve samples have only shown that most of the deposited sediments are silt size and smaller. However, sieving will determine when larger particles move and are deposited. A better understanding of field sediment processes will be provided by continuation of sieve samples. Likewise, the chain surveys and sieve analyses are useful for determining channel transport and aggradation and degradation. Use and testing of the sedigraph 5000 for measuring concentrations of fines should be continued because it appears to be an acceptable method.

A rating curve of sediment transport rate versus water discharge is sometimes developed to help in determining sediment outflow. Figures 7.28 and 7.29 show rating curves for ISU 1 and the entire watershed. The relationship is scattered up to some threshold discharge after which there is a rise in sediment outflow with increasing discharge. Although there is a very strong linear trend for the higher discharges at ISU 1 (Figure 7.28), there is much more randomness at Traer. As the data base improves, more information may substantiate these preliminary relationships. However, there is a complex relationship between the transport capacity of the discharge and the sediment supply that must be better understood if the watershed is to be properly modeled. Such relationships cannot be adequately explained by a simple sediment transport rate-water discharge relationship.

One other important aspect of the hydrologic measurements in the watershed is the rating curves used for converting stage readings to discharge. Each of the U.S. Geological Survey stations is a meter rated section. The ISU watersheds 1, 2, and 3 have four foot H flumes and watersheds 7 and 8 have rated culverts. For comparison, the rating curves for each of these devices was converted to an equation of the form

$$Q = a\ S^b$$

as discussed in an earlier section. Here $S$ is either the actual stage or it has been adjusted by a constant value so that $Q \cong 0$ when $S \cong 0$. This con-

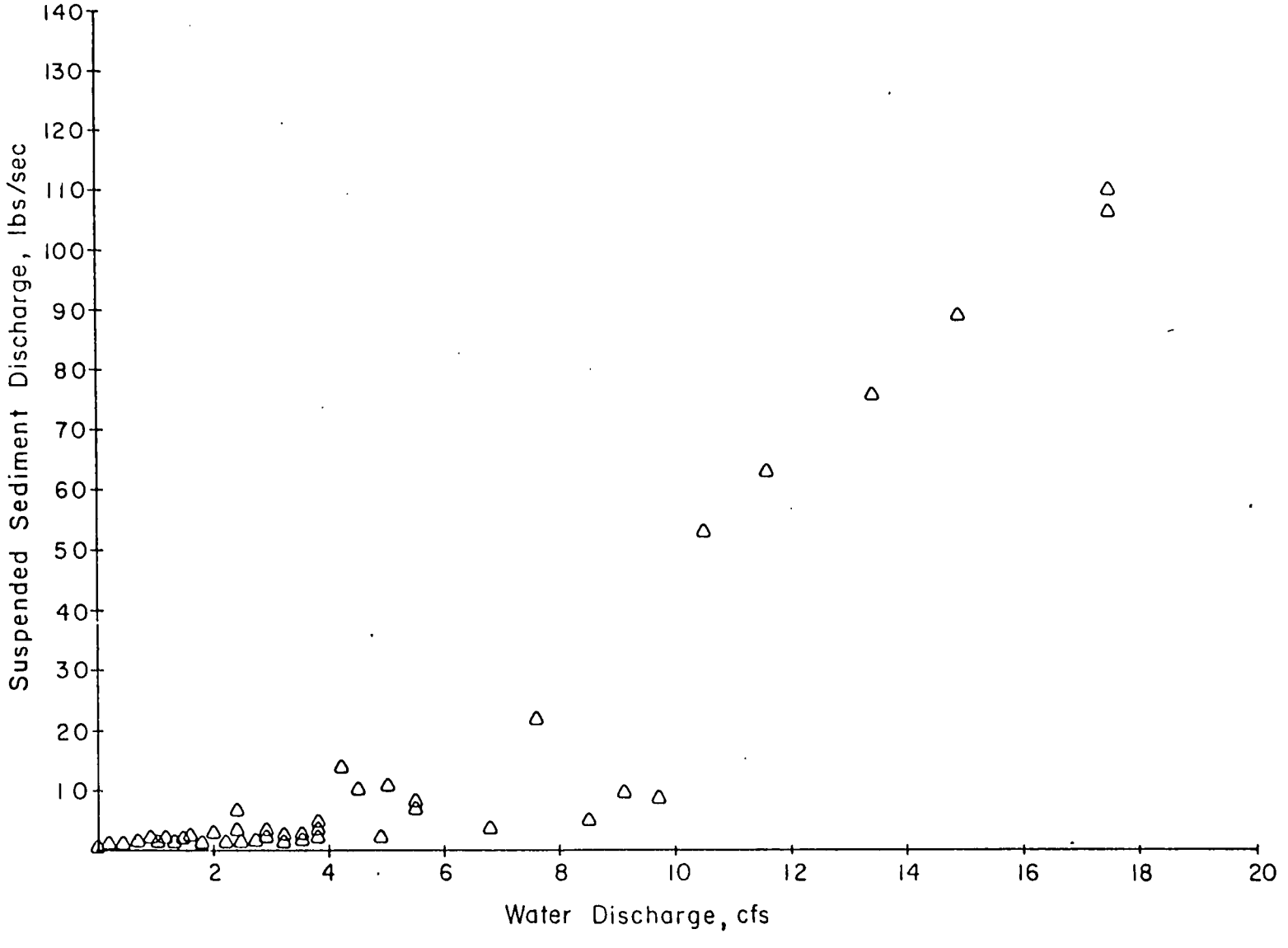


Figure 7.28. Suspended sediment discharge and water discharge at ISU 1.

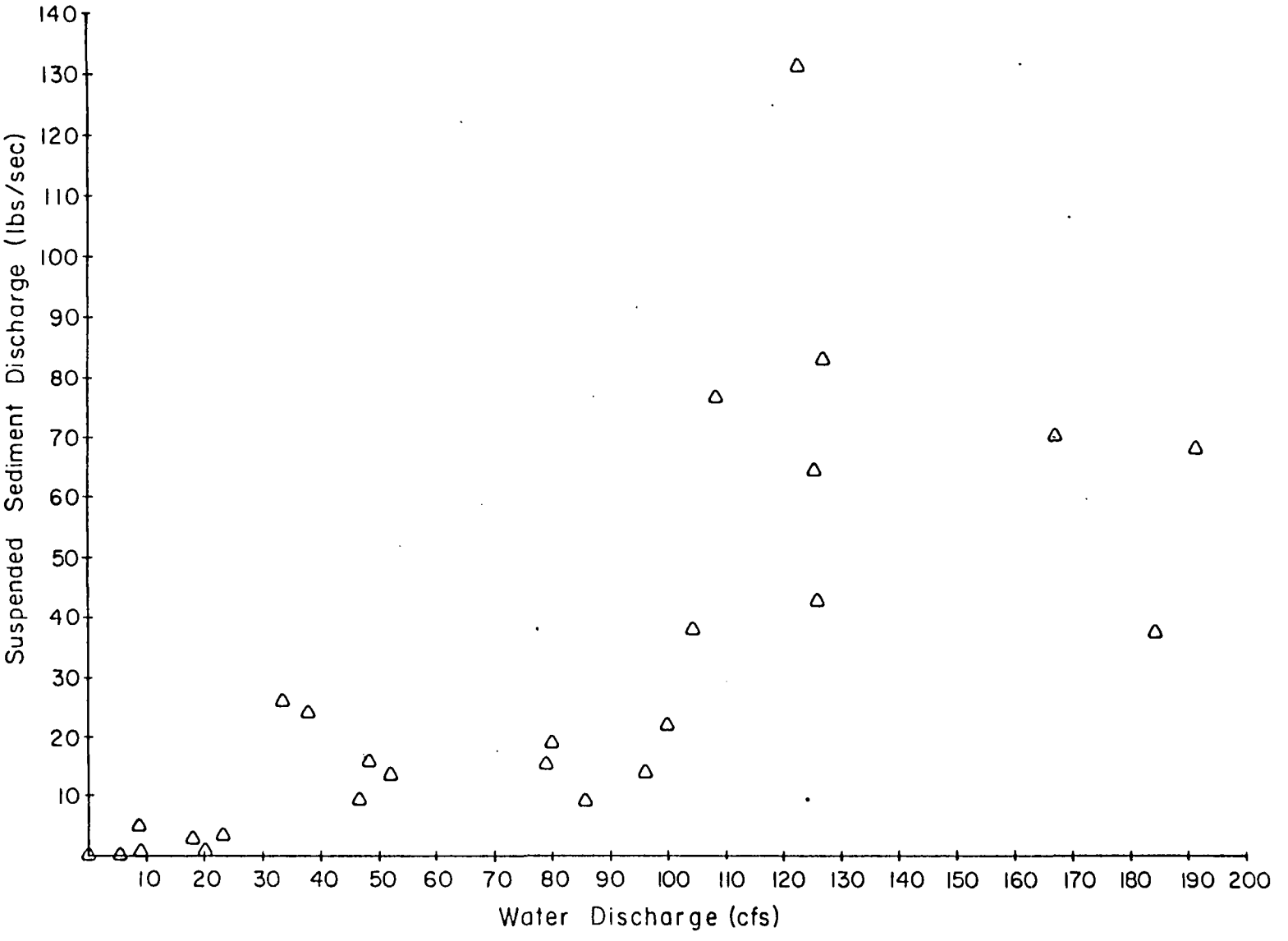


Figure 7.29. Suspended sediment discharge and water discharge at Four-Mile Creek near Traer.

version makes comparisons of a and b parameters meaningful. All of the points in the published rating curves were not used in this analysis, only selected points that help define the relationship. Figures 7.30, 7.31, and 7.32 show examples of these curves. The lines shown are for definition only and are not computed from the equations. The listed parameters should not be used to compute discharge from stage readings. Instead, the parameters in Table 7.4 show the relative magnitude of the coefficient and, more significantly, the power b parameters.

As previously discussed, the larger the b value, the more sensitive the computed discharge is to the change in stage. This will be beneficial if low flows with minor head changes are being gaged. However, such benefits can be minimized if small errors in gage measurements produce significantly large errors in computed discharges. It is interesting to note that the ISU 8 gage with a power of b of about 1.02 is the least sensitive and almost linear.

In general, the discharge and sediment information is acceptable for testing the model. However, there are some problems with regard to the timing of measurements for short-term events that should be resolved.

### 7.3.6 Nutrients and Herbicides-Pesticides

Nutrient (i.e., fertilizers) and herbicide-pesticide data are not grouped separately in Table 7.2. The general types of data available for these man-introduced chemicals are concentration measurements in the on-site soils and in the runoff and in the water transported sediments. This information is collected to show the sources and downstream occurrence of chemicals in the hydrologic cycle.

#### 7.3.6.1 Nutrients

On-site soil samples were taken from selected depths at different sites in the field size watersheds. These samples were collected at various times during the year. Combinations of these data illustrate a sequential change in concentration with time and depth at a site as previously shown. Samples are analyzed for $NH_4$-N, $NO_3$-N, $PO_4$-P, EXT N, available P, and water content. Unfortunately, there are no corresponding pH measurements, important information when modeling chemical reactions and transport. Nutrient outflows at the stream gaging sites and tile drains are measured to indicate the amounts lost to hydrologic processes. These data are presented in a site, Julian day,

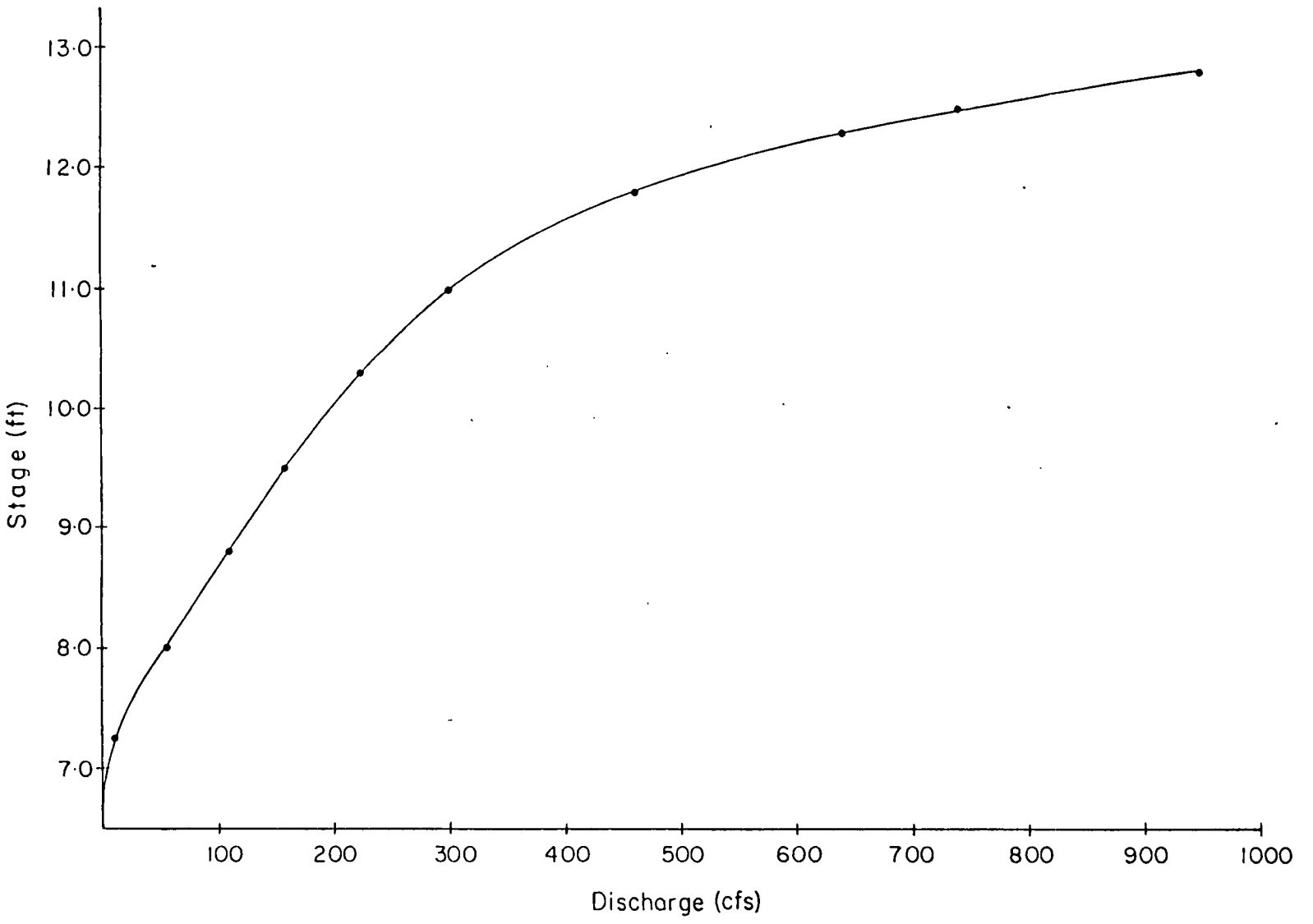


Figure 7.30. Stage-discharge relationship for Four-Mile Creek near Traer.

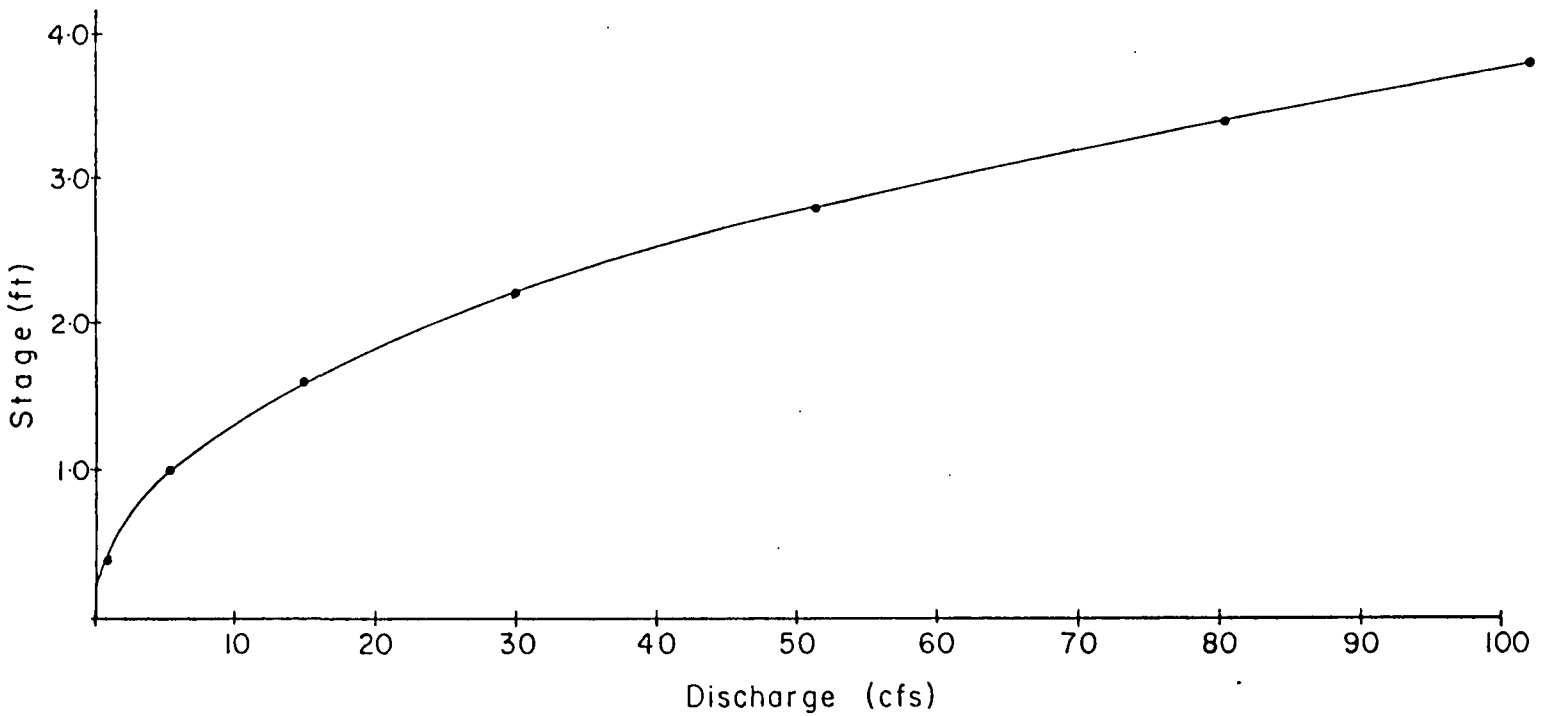


Figure 7.31. Stage-discharge relationship for 4-foot H flumes.

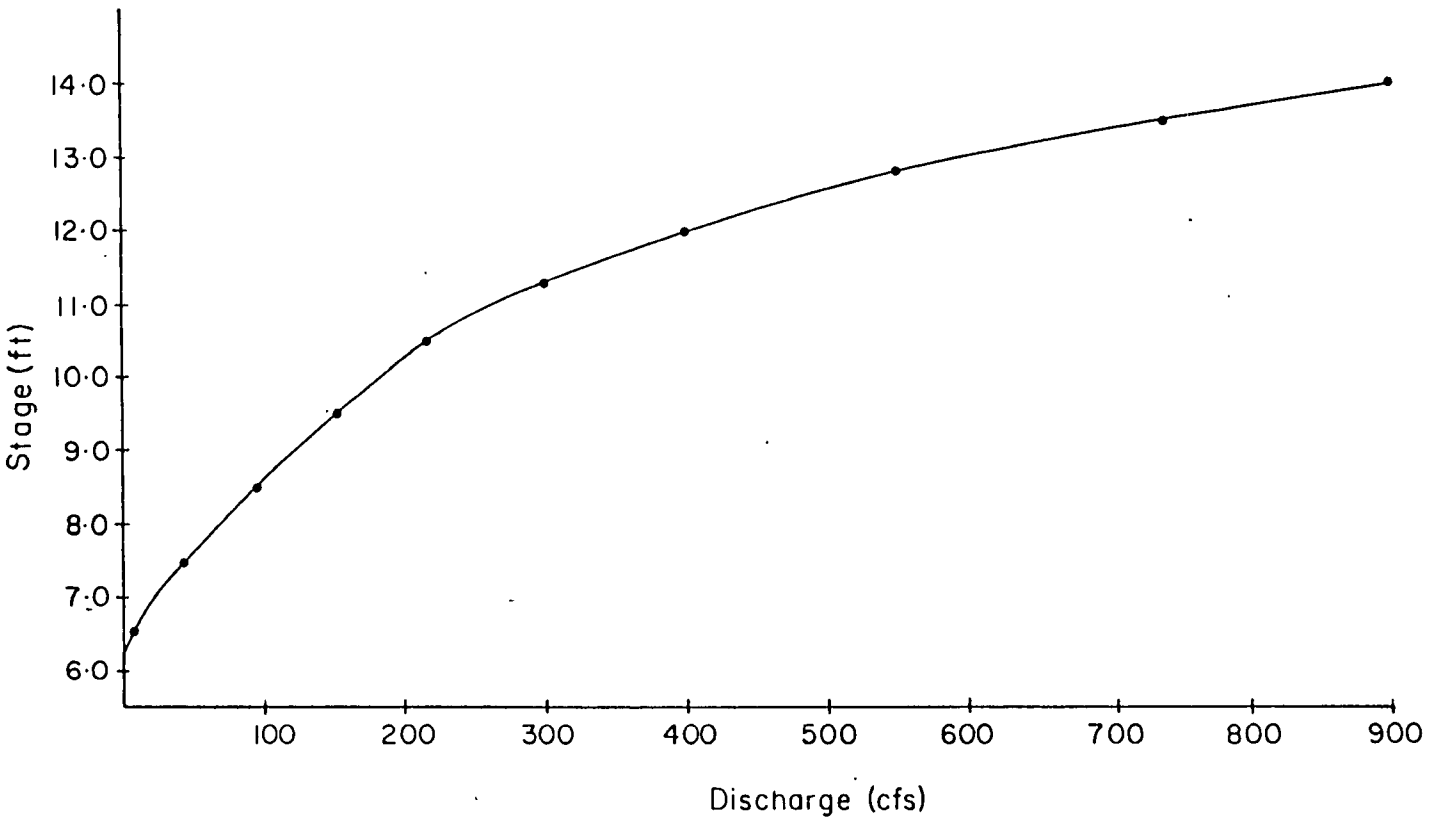


Figure 7.32. Stage-discharge relationship for Four-Mile Creek near Lincoln.

Table 7.4. Comparative Rating Curve Parameters Based on Selected Values from the Four-Mile Creek Watershed

| Location | Device | Preliminary parameters in $Q = a\ S^b$ | | Remarks |
|---|---|---|---|---|
| | | a | b | |
| ISU 1,2,3 | 4-ft H flume | 6.08 | 2.06 | -- |
| Traer | Rated Section | 6.78 | 2.50 | Stage reduced by 6 ft |
| Lincoln | Rated Section | 10.51 | 2.00 | Stage reduced by 5.5 ft |
| Gladbrook | Rated Section | 14.51 | 2.00 | Stage reduced by 3 ft |
| ISU 7 | Box Culvert | 21.19 | 1.60 | -- |
| ISU 8 | Headwall and Culvert | 69.39 | 1.02 | -- |

and time format. They also include $NH_4$-N, $NO_3$-N, $PO_4$-P, TDS, TDS plus sediment, and chloride measurements in ppm. These data are useful in showing the temporal and spatial variations in surface and ground water water quality. However, it lacks a key element in that the flow rate at the time the water is sampled is not specified. Without this information it is difficult to determine concentration changes affected by flow changes and total yields of the chemical being measured. There are some monthly flow concentration data available as shown in Figure 7.33. However, such information only shows general responses and is not sufficiently detailed for use in modeling.

7.3.6.2 Herbicides-Pesticides

Herbicides were measured similarly to the nutrients. Five herbicides were used and sampled in soils and water. These were (by their common (trade) names): Alachlor (Lasso), Cyanazine (Blandex), Metribuzin (Sencor/Lexane), Paraquat (Ortho Paraquat), and Propachlor (Ramrod). The solubilities of these herbicides ranges from 171 to 1220 mg/1 at 20°C, except for Paraquat which readily attaches to positive ions in the soil. Paraquat is seldom detected in water, unlike the other herbicides that are associated with water and sediment. Like the nutrient samples, soil concentrations are measured at several sites and depths at various times. Likewise, water outflow at sites 1, 2, and 8 are sampled. Again, there is no corresponding discharge data presented with the concentration data. However, the 1976-1977 Annual Report did present limited data for one event, that of 6/13/76, for sites 1 and 2. Figures 7.34, 7.35 and 7.36 show the variablity in flow and concentrations from site 1. This type of data is extremely valuable in modeling. Although data sets for some events may be obtained piecemeal from various data sections, these sets should be self-contained in the pesticide section. In general, the herbicide-pesticide information lacks detail for model application. As indicated above, there is some ambiguity with the runoff rate and sampled concentration. This information, particularly for event-based models, is necessary. The frequency of soil sampling and water chemistry analyses should be better assimilated to show the relationship between the two and to check consistency. Another missing item is measurements of $NH_4$-N and $PO_4$-P attached to the transported sediment. This information helps pinpoint a key source of loss for these chemicals. Finally, the loss of chemicals from the soil is a function of temperature and pH, both of which are missing from the soil sample data.

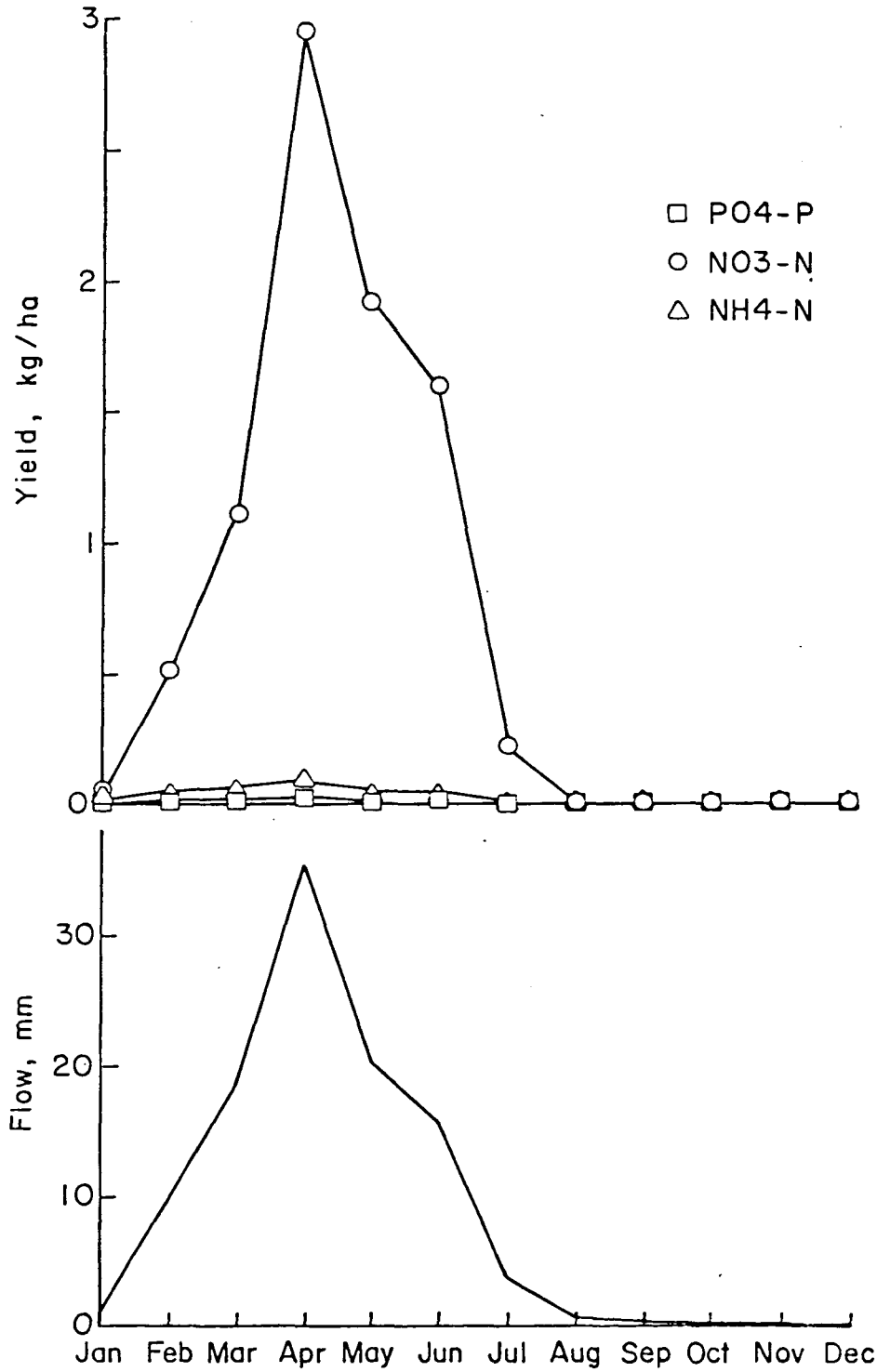


Figure 7.33. Four-Mile Creek near Traer, monthly yields of selected chemicals.

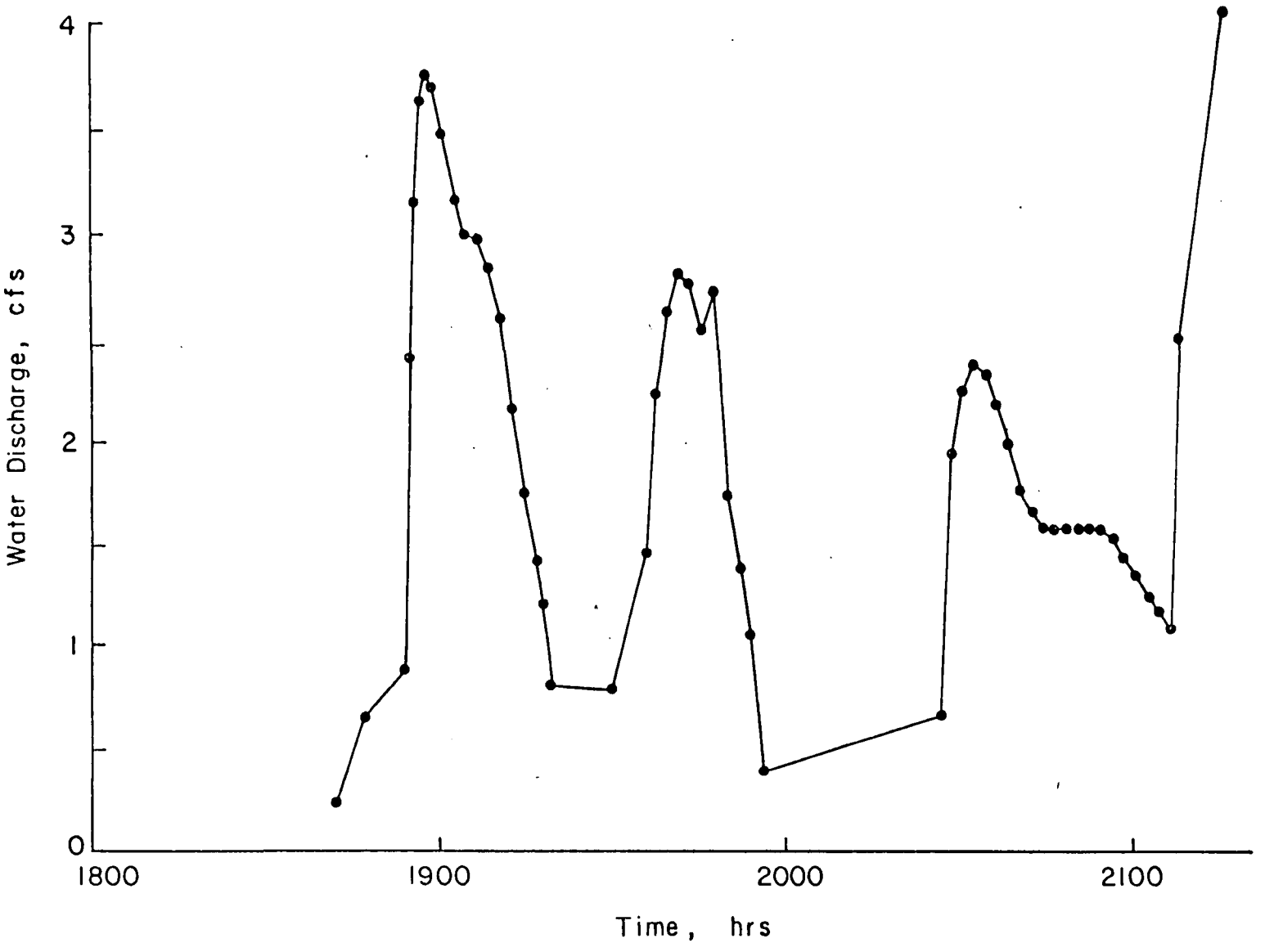


Figure 7.34. ISU 1 water discharge from rainfall storm of 6/13/76.

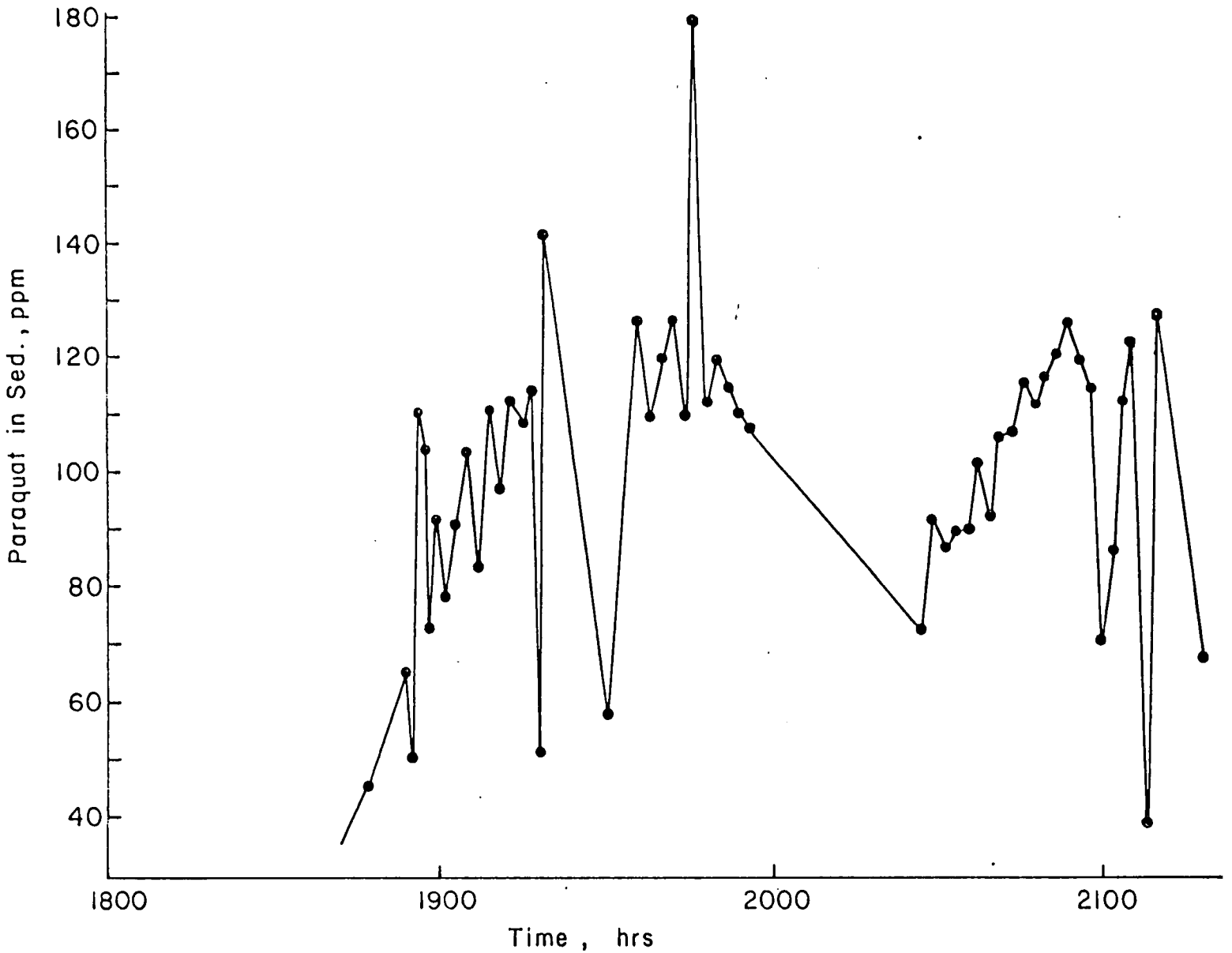


Figure 7.35. ISU 1, Paraquat concentration in sediment from rainfall storm runoff of 6/13/76.

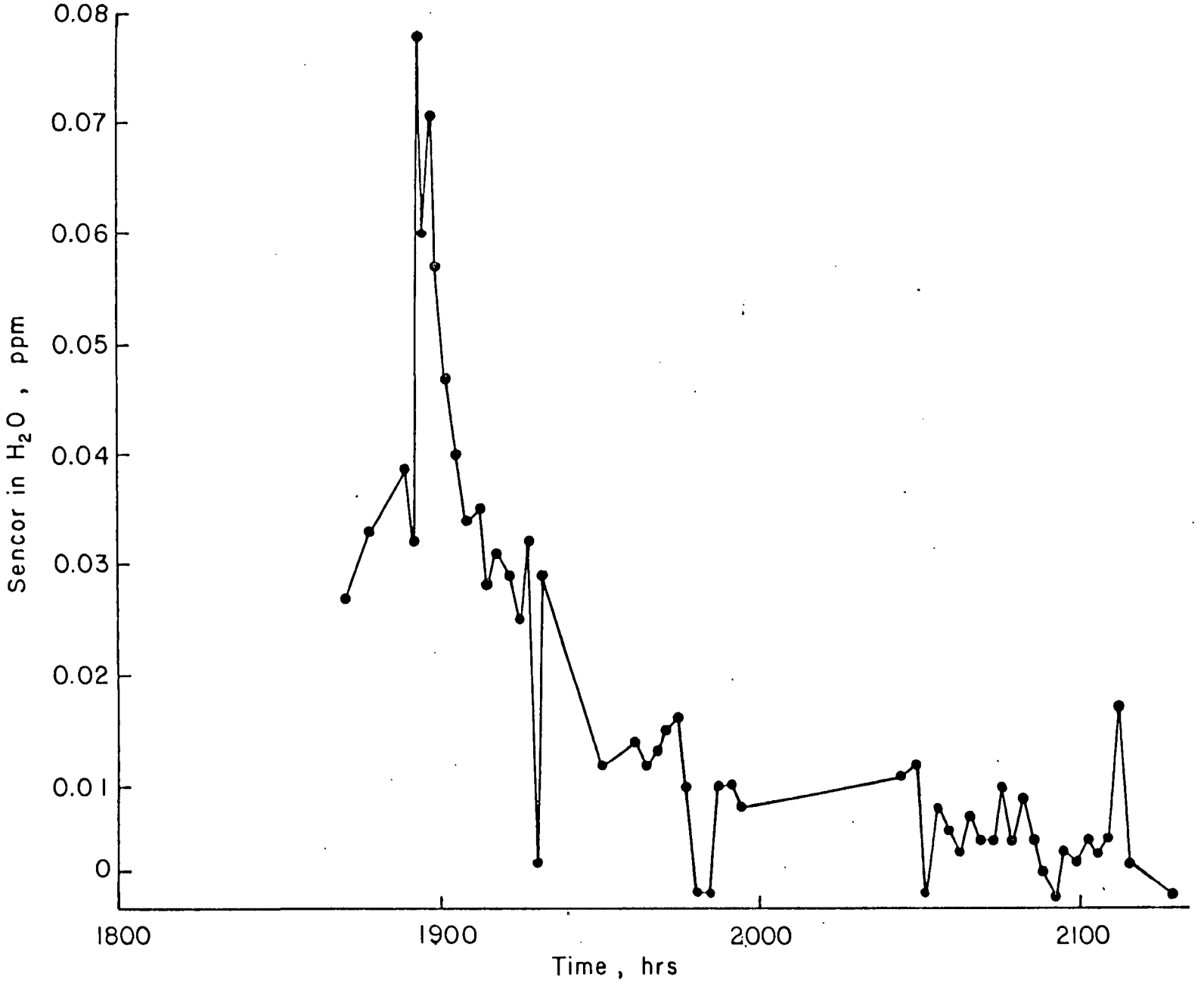


Figure 7.36. ISU 1, Sencor concentration in water from rainfall storm runoff of 6/13/76.

## 7.4 References

Simons, D.B., R.M. Li, and T.J. Ward, 1978, "Methods for Estimating Parameters that Describe Channel Geometry," prepared for U.S. Forest Service, Rocky Mountain Forest and Range Experiment Station, Flagstaff, Arizona.

Johnson, H..P., 1977, "Development and Testing of Mathematical Models as Management Tools for Agricultural Nonpoint Source Pollutants," Annual Report 1976-1977, Department of Agricultural Engineering, Iowa State University, Ames.

Johnson, H.P., 1978, "Development and Testing of Mathematical Models as Management Tools for Agricultural Nonpoint Source Pollutants," Annual Report 1977-1978, Department of Agricultural Engineering, Iowa State University, Ames.

# VIII. CASE STUDY II: APPLICATION OF A PHYSICAL PROCESS MODEL

## 8.1 General

An important aspect of data network evaluation requires use of physical process models. Since the core of the previously discussed primary model is rainfall-runoff simulation, this part is selected for example application. The processes that simulate the production of sediment and nonpoint source pollutants are dependent on the results of the rainfall and runoff. In order for the former to provide reasonable results, the routing model must provide realistic results.

This evaluation uses the multiple watershed rainfall-runoff simulation model (MULTSED) (Li, et al., 1979) to help analyze the data collection system at Four-Mile Creek. MULTSED is used in three areas. First, a comparison is made of recorded and simulated hydrographs obtained from the available data to determine the adequacy of the data collected. Simulations are carried out on two sizes of watershed within Four-Mile Creek, small (ISU 1) and medium (ISU 8) sized subwatersheds with areas of 18.83 acres and 369.6 acres, respectively. Next, the model is tested for sensitivity to the various input parameters to determine the quality of the data being collected, to reduce the errors in the simulation results, and to help with the calibration of the model. Finally, the creation of hydrographs utilizing the model for storms of specified duration and return periods (not available from recorded data) are then used in the spatial and temporal analysis of the system.

## 8.2 Data Needs

The physical process model MULTSED requires data that represents the phenomena being simulated. To entirely model the processes would be impractical due to the immense amount of data required and the resulting complexity of the model. Simplifying assumptions must be made to make the model manageable. Details of the model are presented in Li, et al. (1979) or Simons, et al. (1979). The physical processes modeled are interception, infiltration, overland flow, channel flow, erosion, sediment transport, aggradation and degradation. With the model formulated in this manner, the data needs are specified as listed in Table 8.1.

## 8.3 Available Data and Gaps

From the annual reports and several supplemental sources, such as the

Table 8.1. Input Data for MULTSED Program

I. Geometry
   1. Number of subdivision
   2. Slope, length, and area for each plane and subwatershed unit
   3. Slope and length for channel units
   4. Relationships of: a) wetted perimeter vs. cross-sectional area, and b) top width vs. cross-sectional area for each of the channel units

II. Soil Characteristics
   1. Effective hydraulic conductivity
   2. Porosity
   3. Initial and final soil moisture
   4. Average suction head
   5. Temperature
   6. Rilling ratio
   7. Sediment size distribution
   8. Plastic index

III. Vegetative Cover
   1. Density
      a. Percent canopy cover
      b. Percent ground cover
   2. Cover storage
      a. Canopy cover
      b. Ground cover

IV. Rainfall Data
   1. Rainfall hyetographs that are spatially consistent over each subdivision

V. Overland Flow and Channel Flow Data
   1. Duration of hydrograph
   2. Time increment used for the calculation of the hydrograph

VI. Erosion Data
   1. Overland flow detachment coefficient
   2. Channel flow detachment coefficient
   3. Detachment coefficient for rain drop impact

U.S. Geological Survey topographic maps and U.S. Weather Service records, most of the data needs listed in Table 8.1 are satisfied. Data gaps that exist are listed in Table 8.2.

Some data can be estimated by calibration. This is accomplished by realistically varying the parameter in question until the simulated hydrographs are similar to the recorded hydrographs. Missing data for soil characteristics and resistance parameters are supplemented by this method. The technique requires detailed recorded hydrographs which are available for the small and medimum sized watersheds, but not for the entire watershed. Therefore, the parameters calibrated in the two smaller watersheds were extended to cover the entire watershed. The validity of this procedure cannot be tested due to the absence of detailed, recorded hydrographs. However, the parameters calibrated for ISU 1 were used directly for ISU 8 as a check.

## 8.4 Model Application and Results Using Collected Data

### 8.4.1 General

The watershed must be divided into subwatershed units, plane units, and channel units. A schematic map of the Four-Mile Creek watershed is presented in Figure 8.1. The simplified geometry data are presented in Table 8.3.

### 8.4.2 Small Watershed Simulation

The small watershed selected was ISU 1 with an area of 13.83 acres. This site was picked because of a recording raingage location near it, available vegetative cover data, and a recording discharge measurement device located on its outlet. Representative storms during 1977 and 1978 which produced measurable runoff were chosen for simulation. The storms and their respective rainfall depths and durations are listed in Table 8.4.

The soil parameters were adjusted in an attempt to match the recorded hydrographs. The results are listed in Table 8.5. Several of the events did not model well because of minimal runoff. It was difficult to calibrate the model using these events and still produce reasonable agreement with the larger events. Because the larger events are usually more significant in terms of water runoff, sediment, and nutrient losses, they were used for parameter calibration.

Table 8.2. Data Gaps Identified for MULTSED

I. Geometry
   1. No gaps, good quality

II. Soil Characteristics
   1. Effective hydraulic conductivity
   2. Porosity
   3. Initial and final soil moisture
   4. Average suction head

III. Vegetative Cover
   1. Data are present, but are not given for the entire watershed, therefore, extrapolation methods must be utilized.

IV. Rainfall Data
   1. No gaps

V. Overland Flow and Channel Flow Data
   1. Resistance for channel units
   2. Resistance to flow for overland units

VI. Erosion Data
   1. Parameters may be estimated.

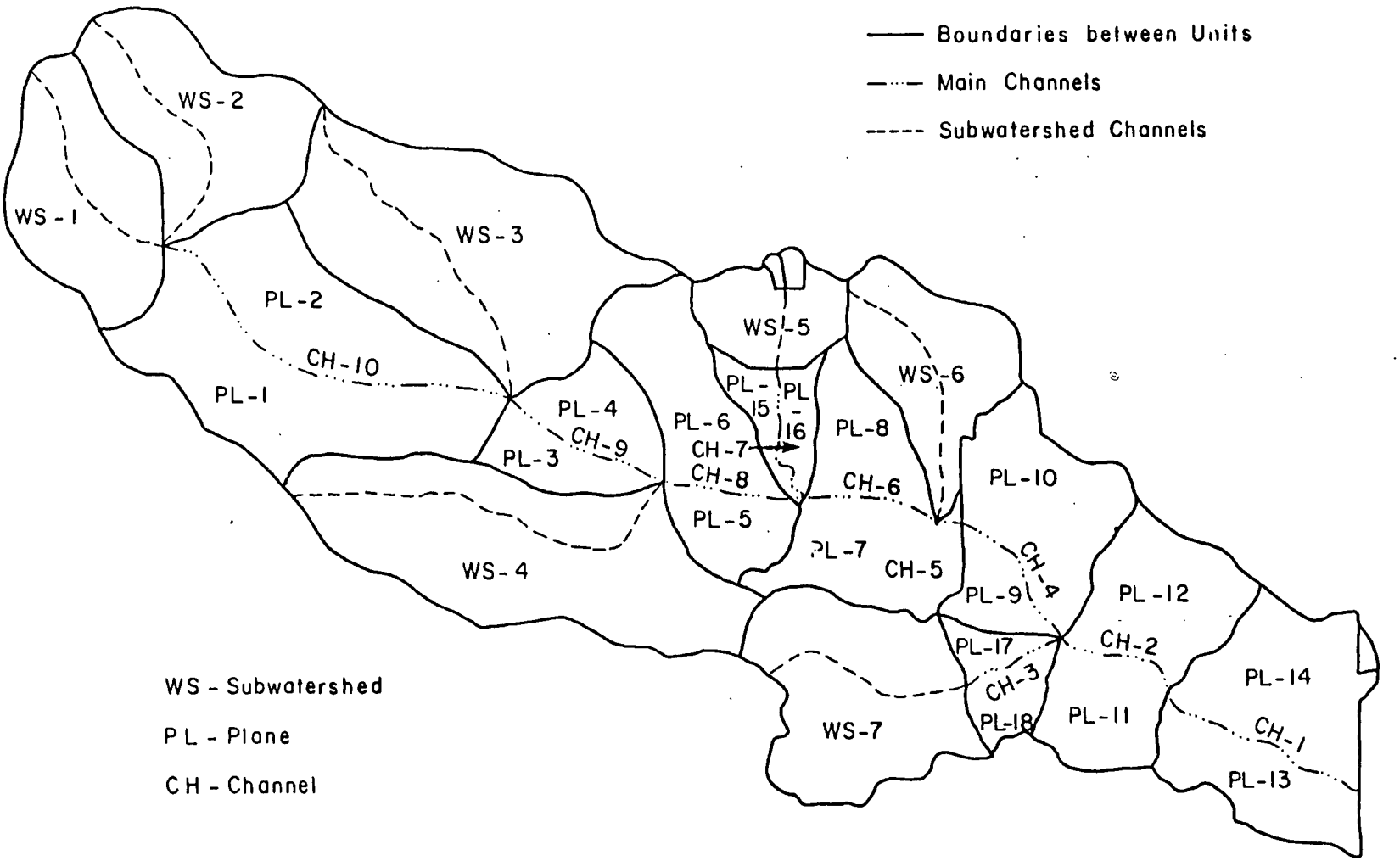


Figure 8.1. Four-Mile Creek map showing subdivisions for modeling.

Table 8.3. Watershed Geometry for Four-Mile Creek

| Unit | Length (feet) | Width (feet) | Slope | Area (acres) |
|---|---|---|---|---|
| WS-1L | 6200 | 3131 | .0147 | 446 |
| WS-1CH | 6200 | | .00629 | |
| WS-1R | 6200 | 1890 | .0123 | 269 |
| WS-2L | 7200 | 1768 | .0162 | 292 |
| WS-2CH | 7200 | | .00542 | |
| WS-2R | 7200 | 2869 | .0170 | 474 |
| WS-3L | 11000 | 1611 | .0278 | 407 |
| WS-3CH | 11000 | | .00691 | |
| WS-3R | 11000 | 3508 | .0253 | 886 |
| WS-4L | 13000 | 3553 | .0266 | 1061 |
| WS-4CH | 13000 | | .00623 | |
| WS-4R | 13000 | 1388 | .0277 | 414 |
| WS-5L | 3000 | 2645 | .0330 | 182 |
| WS-5CH | 3000 | | .0183 | |
| WS-5R | 3000 | 2282 | .0326 | 157 |
| WS-6L | 9000 | 1199 | .0455 | 248 |
| WS-6CH | 9000 | | .0122 | |
| WS-6R | 9000 | 1781 | .0440 | 368 |
| WS-7L | 7400 | 3184 | .0355 | 541 |
| WS-7CH | 7400 | | .0115 | |
| WS-7R | 7400 | 1970 | .0381 | 335 |
| PL-1 | 12500 | 2961 | .0322 | 850 |
| CH-10 | 12500 | | .00264 | |
| PL-2 | 12500 | 2294 | .0239 | 658 |
| PL-3 | 6267 | 1395 | .0412 | 201 |
| CH-9 | 6267 | | .00303 | |
| PL-4 | 6267 | 1626 | .0316 | 234 |
| PL-5 | 4133 | 2056 | .0367 | 195 |
| CH-8 | 4133 | | .00218 | |
| PL-6 | 4133 | 4970 | .0242 | 472 |
| PL-7 | 7066 | 2890 | .0388 | 469 |
| CH-6 | 7066 | | .00170 | |
| PL-8 | 7066 | 1887 | .0431 | 306 |
| CH-5 | 7066 | | .0017 | |
| PL-9 | 5400 | 1335 | .0573 | 166 |
| CH-4 | 5400 | | .00148 | |
| PL-10 | 5400 | 3677 | .0488 | 456 |
| PL-11 | 4800 | 2769 | .0534 | 305 |
| CH-2 | 4800 | | .00146 | |
| PL-12 | 4800 | 3406 | .0454 | 375 |
| PL-13 | 7400 | 2253 | .0653 | 383 |
| CH-1 | 7400 | | .00135 | |
| PL-14 | 7400 | 4523 | .0495 | 768 |
| PL-15 | 2933 | 1318 | .0557 | 89 |
| CH-7 | 2933 | | .0443 | |

Table 8.3. Watershed Geometry for Four-Mile Creek (continued)

| Unit | Length (feet) | Width (feet) | Slope | Area (acres) |
|---|---|---|---|---|
| PL-16 | 2933 | 948 | .0400 | 64 |
| PL-17 | 3467 | 1034 | .0652 | 82 |
| CH-3 | 3467 | | .0433 | |
| PL-18 | 3467 | 1580 | .0488 | 126 |
| ISU-Site 1L | 574.50 | 494.21 | .0453 | 6.52 |
| ISU-Site 1CH | 574.50 | | .0174 | |
| ISU-Site 1R | 574.50 | 554.50 | .0456 | 7.31 |

Abbreviations:

PL - Plane
CH - Channel
WS - Subwatershed
L - Left
R - Right

Table 8.4. Selected Storms for Simulation

| Date | Depth (inches) | Duration (minutes) |
|---|---|---|
| August 15, 1977 | 1.48 | 413 |
| September 17, 1977 | 1.10 | 232 |
| April 17, 1978 | 2.56 | 1390 |
| May 12, 1978 | 1.43 | 670 |
| May 27, 1978 | 1.12 | 50 |
| June 20, 1978 | 1.19 | 240 |

Table 8.5. Comparison of Simulated and Recorded Hydrographs for the Small Watershed

| Date | Peak Discharge (cfs) | | Volume (acre-ft) | | Time to Peak (min) | |
|---|---|---|---|---|---|---|
| | Recorded | Sim. | Recorded | Sim. | Recorded | Sim. |
| 8/15/77 | 10.1 | 10.1 | .22 | .36 | 20:28 | 22:30 |
| 9/17/77 | .34 | .39 | .01 | .09 | 20:06 | 20:24 |
| 4/17/78 | .31 | 1.4 | .06 | .10 | 23:15 | 23:20 |
| 5/12/78 | Negligible recorded runoff - no simulated runoff | | | | | |
| 5/27/78 | 2.01 | 7.06 | .05 | .25 | 16:49 | 16:48 |
| 6/20/78 | 2.15 | 1.67 | .16 | .14 | 9:12 | 1:14 |

8.4.3 Medium Watershed Simulation

The medium sized watershed selected was ISU 8 with a planimetered area of 369.6 acres. (ISU annual report states 749 hectares or 368.03 acres). It was chosen for the same reason as ISU 1. In addition, ISU 1 lies within its boundaries so that the parameters calibrated for ISU 1 could be transferred. No calibration was done on the simulations for ISU 8; the paramters from ISU 1 were directly applied. The same events as those for ISU 1 were also used. The results were presented in Table 8.6. Again, events that cannot be modeled well are those with little runoff. The amount of runoff being produced is smaller than the resolution capability of the model, but for larger events the results do show that the model can simulate the rainfall-runoff response adequately with the available and transferred data.

## 8.5 Use of the Model for Data Synthesis and Evaluation

8.5.1 Time of Concentration Determination

The time of concentration is an important characteristic when designing a gaging system because it provides insight into the watershed's response to a given rainfall and helps determine at which intervals readings should be taken. Rainfalls with specified return periods were calculated using a regression method developed from information in the U.S. Weather Service Technical Paper No. 40 (Hershfield, 1963). The equation and results are listed in Table 8.7.

In order to reach a time of concentration, it is expedient to assume a constant rainfall excess. Since interest is in the time it takes for the water to travel from the furthest point of the watershed to the outlet, the infiltration and interception model components for the time of concentration simulations are not used. To account for infiltration and interception losses the actual rainfall rate was multiplied by a factor ranging from 0.1 to 0.4 to account for losses. The 0.1 factor is used for the one year storm and the 0.4 factor was used for the 100 year storm. The factors for storms with return periods between these values are calculated by linearly interpolating between the one and 100 year volumes according to the storm's actual volume. For example, if the one year actual storm has a volume of one inch and the 100 year storm has a volume of two inches, a 50 year storm with a rainfall volume of 1.5 inches will have a factor of 0.25 to determine its excess. The results of the runs of ISU 1 and ISU 8 are presented in Table 8.8 and in Figure 8.2.

Table 8.6. Comparison of Simulated and Recorded Hydrographs for the Medium Sized Watershed

| Date | Peak Discharge (cfs) | | Volume (acre-ft) | | Time to Peak (min) | |
|---|---|---|---|---|---|---|
| | Recorded | Sim. | Recorded | Sim. | Recorded | Sim. |
| 8/15/77 | 51.40 | 100.70 | 4.12 | 8.43 | 22:38 | 22:45 |
| 9/17/77 | 23.60 | 8.40 | 1.42 | 2.10 | 20:32 | 22:33 |
| 4/17/78 | 14.50 | 1.56 | 5.61 | 1.28 | 23:24 | 23:29 |
| 5/12/78 | 0.98 | No runoff | 0.30 | No runoff | 4:07 | No Runoff |
| 5/27/78 | 108.40 | 95.28 | 3.32 | 5.94 | 16:55 | 16:59 |
| 6/20/78 | 18.84 | 17.23 | 2.25 | 3.21 | 1:55 | 2:24 |

Table 8.7. Four-Mile Creek Watershed Synthetic Rainfalls Using the Regression Method Developed From "TP-40"

| Duration (hour) | Return period (years) | | | | | | |
|---|---|---|---|---|---|---|---|
| | 1 | 2 | 5 | 10 | 25 | 50 | 100 |
| 0.5 | 1.01* | 1.22 | 1.50 | 1.72 | 2.00 | 2.22 | 2.43 |
| 1.0 | 1.29 | 1.57 | 1.94 | 2.22 | 2.59 | 2.87 | 3.15 |
| 1.5 | 1.45 | 1.77 | 2.19 | 2.51 | 2.93 | 3.25 | 3.57 |
| 2.0 | 1.57 | 1.91 | 2.37 | 2.72 | 3.17 | 3.52 | 3.86 |
| 2.5 | 1.66 | 2.02 | 2.51 | 2.88 | 3.36 | 3.73 | 4.09 |
| 3.0 | 1.73 | 2.12 | 2.62 | 3.01 | 3.51 | 3.90 | 4.28 |
| 3.5 | 1.79 | 2.19 | 2.72 | 3.12 | 3.64 | 4.04 | 4.44 |
| 4.0 | 1.85 | 2.26 | 2.80 | 3.21 | 3.76 | 4.17 | 4.58 |
| 4.5 | 1.90 | 2.32 | 2.88 | 3.30 | 3.86 | 4.28 | 4.70 |
| 5.0 | 1.94 | 2.37 | 2.94 | 3.37 | 3.94 | 4.38 | 4.81 |
| 6.0 | 2.01 | 2.46 | 3.06 | 3.50 | 4.10 | 4.55 | 5.00 |
| 9.0 | 2.18 | 2.66 | 3.31 | 3.80 | 4.44 | 4.93 | 5.41 |
| 12.0 | 2.29 | 2.81 | 3.49 | 4.00 | 4.68 | 5.20 | 5.71 |
| 24.0 | 2.58 | 3.15 | 3.92 | 4.50 | 5.27 | 5.85 | 6.43 |

*Rainfall in inches

$$PPT = 1.2870 + 0.453\ (\ell nY) + (0.4040 + 0.1360\ (\ell nY))\ \ell nT$$

PPT = precipitation in inches
Y = storm duration in hours
T = return period in years

Table 8.8. Time of Concentration Results, Four-Mile Creek

| | Return Period (year) | Duration Duration (min) | Rainfall Intensity (in/hr) | Time of Concentration (min) |
|---|---|---|---|---|
| ISU 1 | | | | |
| | 100 | 30 | 1.94 | 16 |
| | 50 | 30 | 1.58 | 18 |
| | 25 | 30 | 1.24 | 20 |
| | 20 | 30 | 0.86 | 24 |
| | 5 | 30 | 0.61 | 30 |
| | 5 | 60 | 0.40 | 39 |
| | 2 | 60 | 0.23 | 57 |
| | 1 | 120 | 0.079 | 112 |
| ISU 8 | | | | |
| | 100 | 30 | 1.94 | 23 |
| | 50 | 60 | 1.02 | 43 |
| | 25 | 60 | 0.08 | 51 |
| | 10 | 60 | 0.56 | 60 |
| | 10 | 120 | 0.341 | 79 |
| | 5 | 120 | 0.243 | 96 |
| | 2 | 120 | 0.138 | 120 |
| | 2 | 180 | 0.103 | 162 |
| | 1 | 180 | 0.058 | 200 |

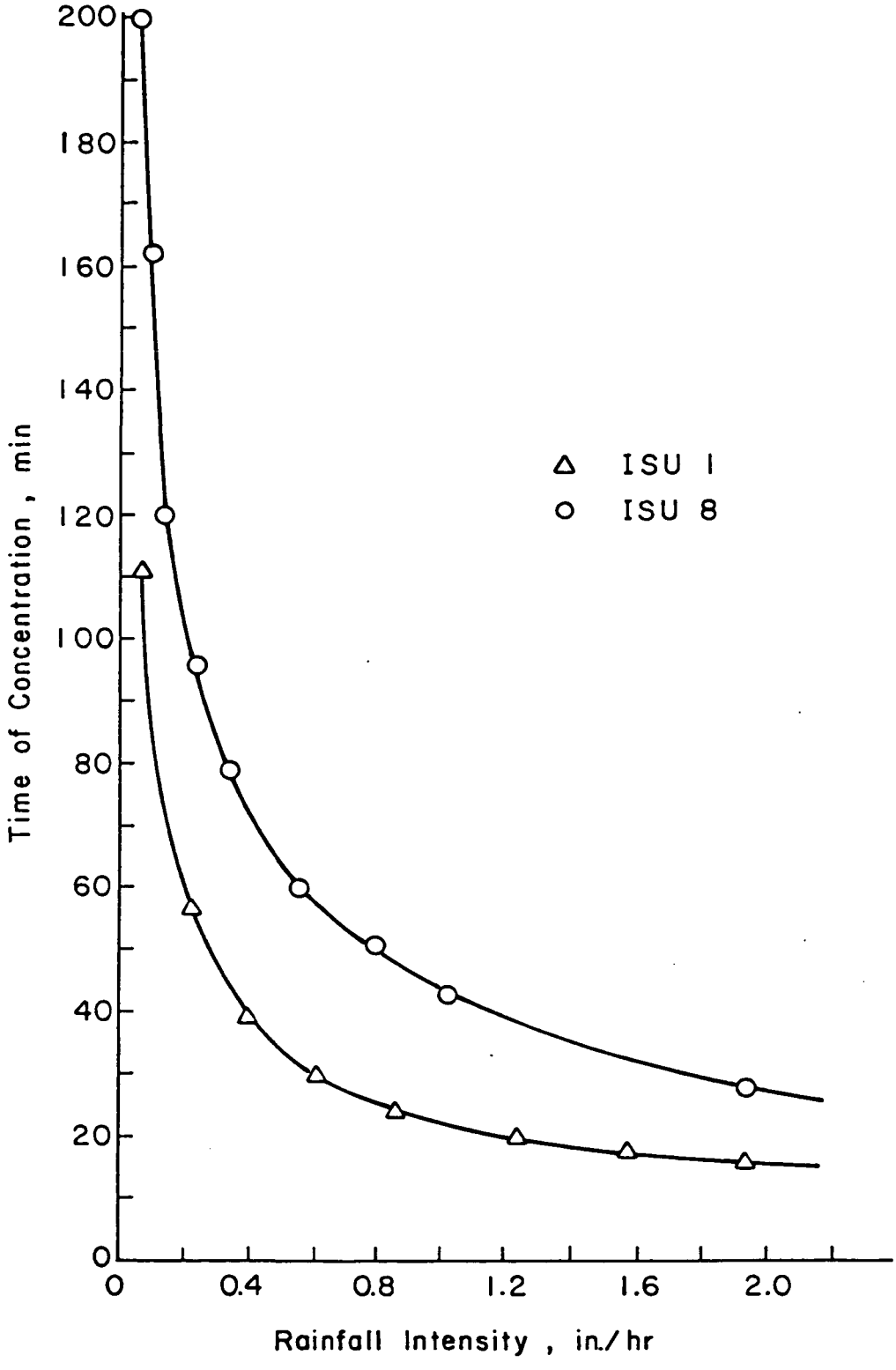


Figure 8.2. Simulated time of concentration for ISU 1 and ISU 8 for different rainfall intensities.

Considering the entire Four-Mile Creek watershed, the rainfall intensities are such that the time of concentration is never reached for any of the durations or return periods.

The simulated time of concentration for ISU 1 varies between 16 and 112 minutes and for ISU 8 between 28 and 200 minutes depending on the storm's return period. An estimate of the time it takes the watershed to completely respond to a rainfall input is important. Depending on the number of intermediate points desired between the start of rainfall and the time of concentration an idea of the time interval and when discharge reading should be taken is provided.

### 8.5.2 Sensitivity Analysis

A sensitivity analysis is necessary for two reason. The analysis is important in determining the quality of the various data needed in order to keep errors within acceptable limits. It is also a useful aid in the calibration process in that it gives the user an idea about how the simulated hydrographs response to changes in the parameters being calibrated.

The sensitivity analysis was carried out on the medium sized watershed (ISU 8) for two storms. The storms occurred on May 27, 1978 and on August 15, 1977. These storms are used since they represent two distinct types of rainfall that occur at the site. The first storm was of short duration, high intensity and the second was of long duration, low intensity.

In the analysis, the parameters required as input to the model are varied one at a time at various percentages of their original values while leaving all other parameters constant. The results are graphed in Figures 8.3 and 8.4 for peak flows only. Volume and duration are similarly affected. Results show that the most sensitive parameters are the soil characteristics and the overland flow resistance which is governed by the percentage of ground cover and the resistance factor. This could be signficiant since these two areas have little data collected for these parameters. However, the calibration process can fill in these gaps and still produce reasonable simulations as was noted earlier.

Similar sensitivity analysis was performed for sediment yield (Figures 8.5, 8.6). Changes in parameters such as permeability (or hydraulic conductivity) and overland flow resistance are shown to exert considerable influence on sediment yield as was the case for water yield. This result is

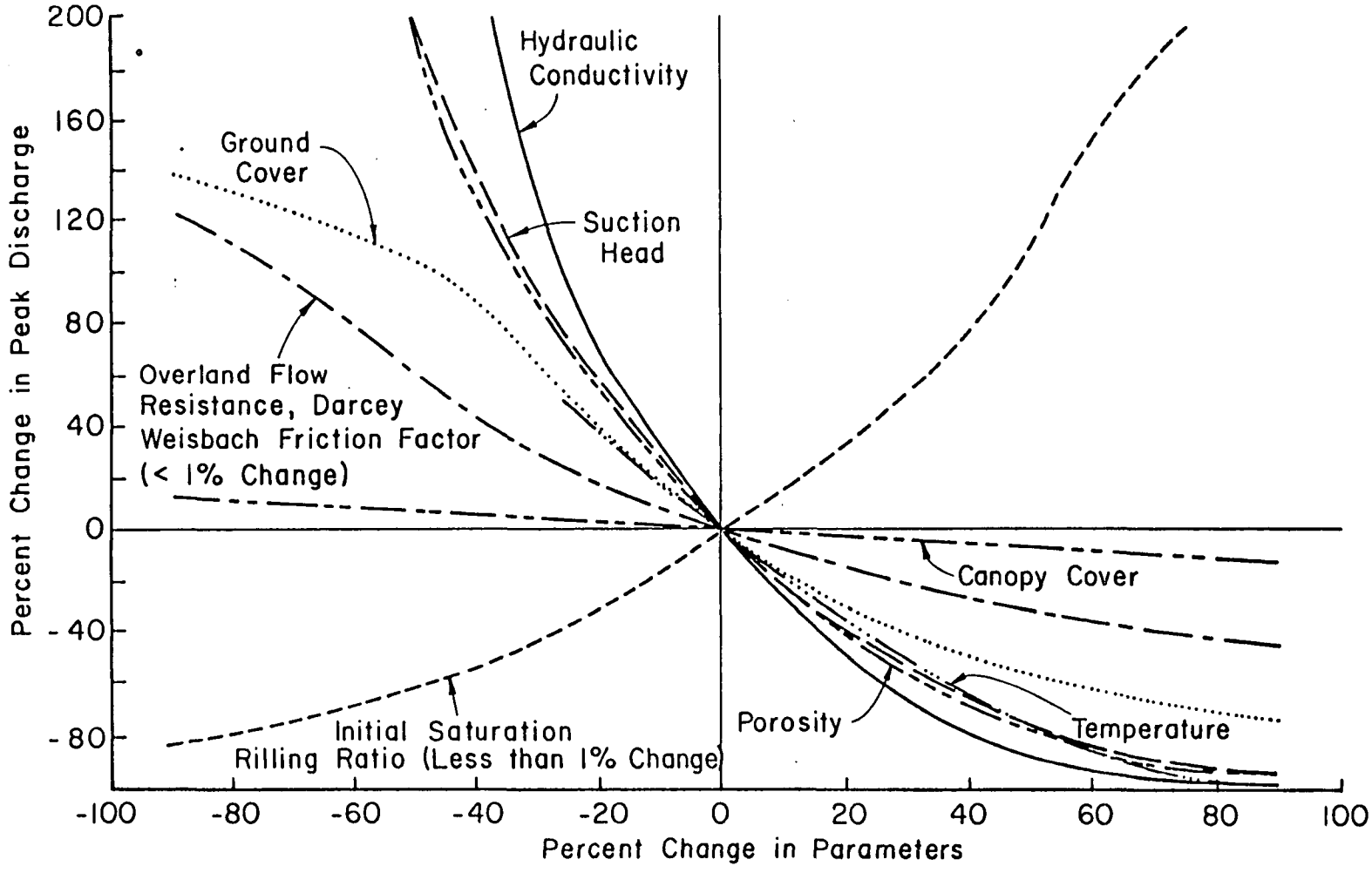


Figure 8.3. Peak discharge sensitivity analysis for watershed ISU 8, storm of May 27, 1978.

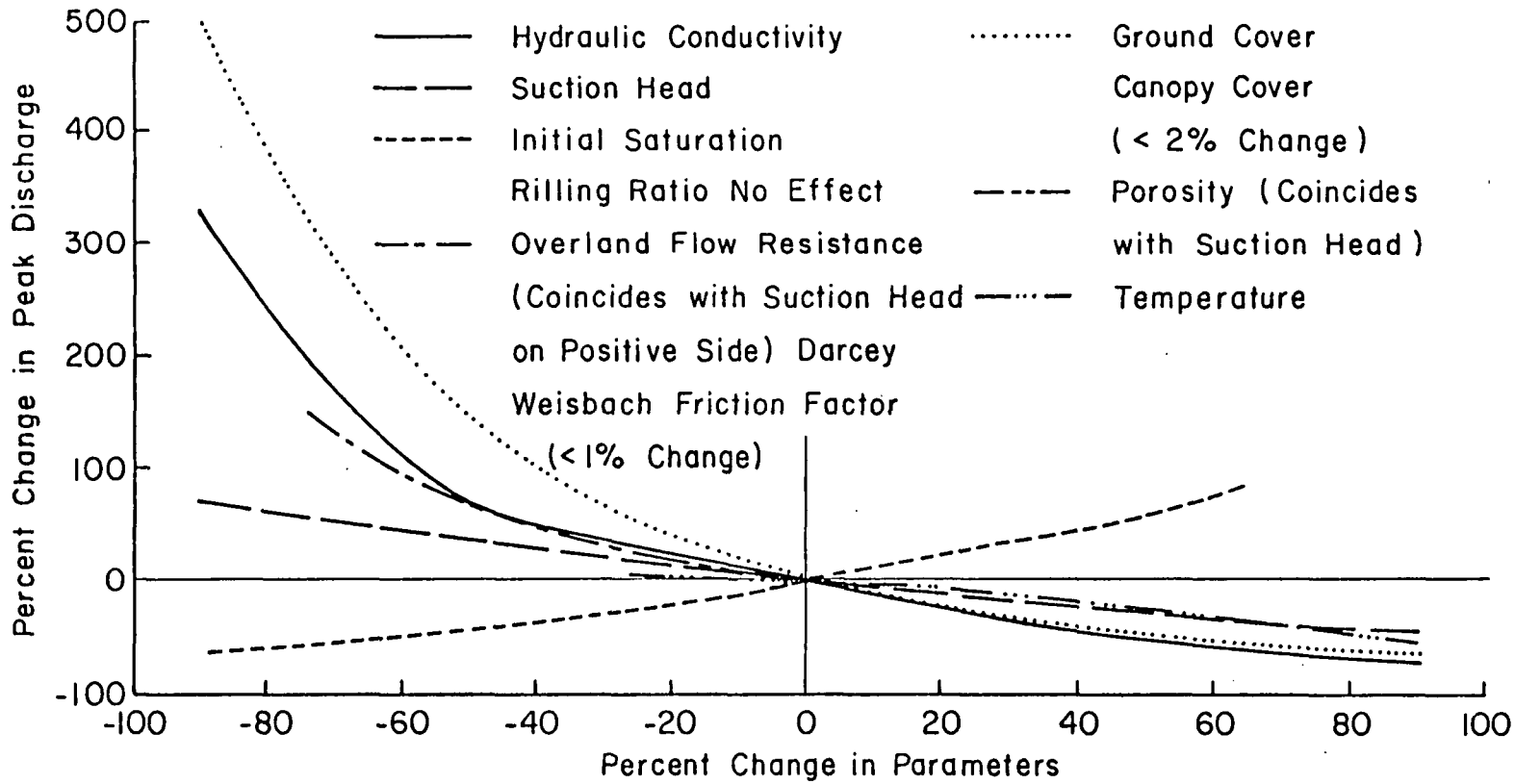


Figure 8.4. Peak discharge sensitivity analysis for watershed ISU 8, storm of August 15, 1977.

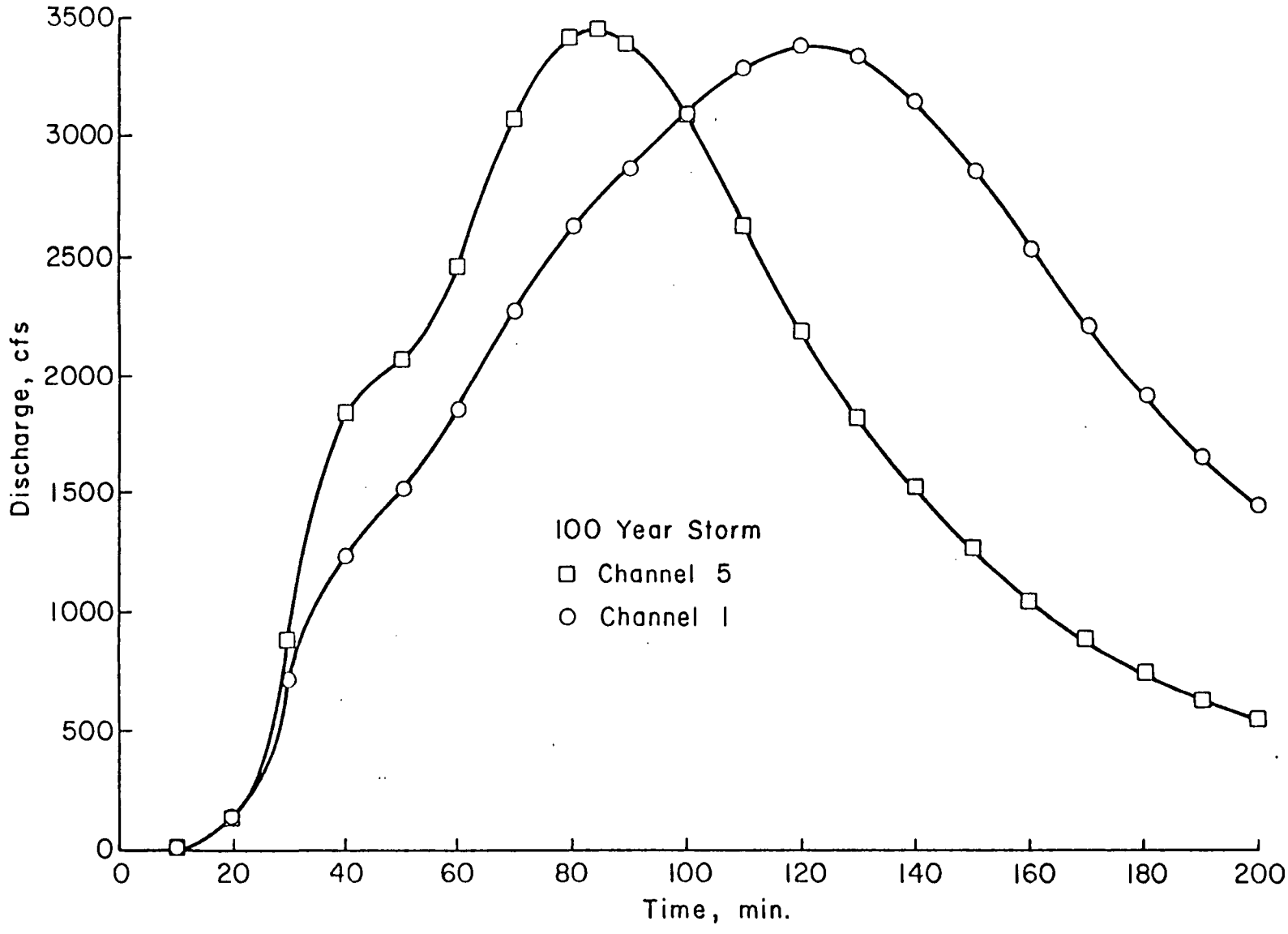


Figure 8.5. Simulated hydrographs for 30 minute, 100 year storm. (Time is real time.)

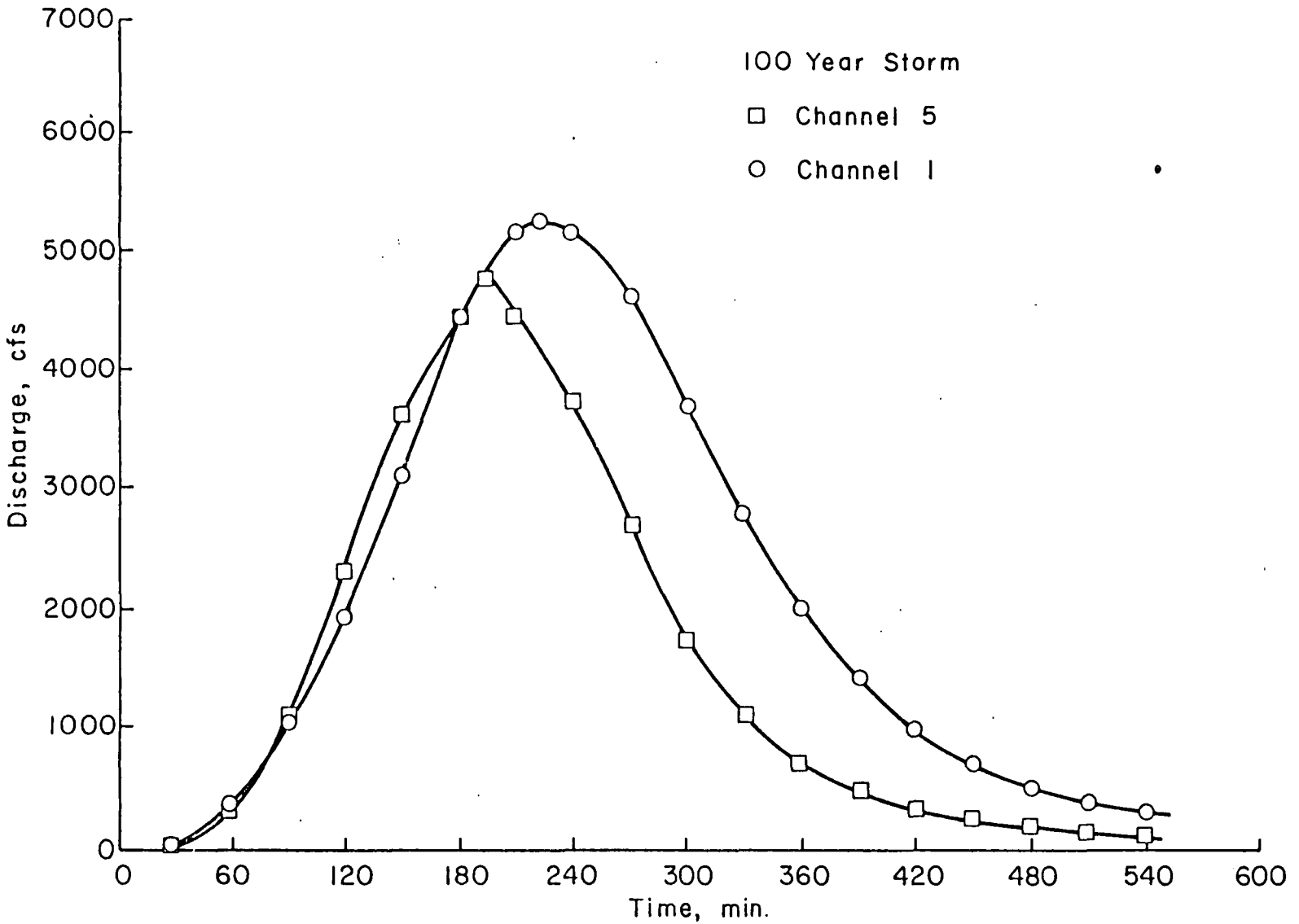


Figure 8.6. Simulated hydrographs for 3 hour, 100 year storm. (Time is real time.)

not surprising as the hydraulics of flow determines sediment transport, however, it does further emphasizes the importance of accurate measures of these parameters. Figure 8.5 indicates effects of changes in parameters largely related to overland flow on sediment yield. Figure 8.6 displays a similar sensitivity plot for channel patterns based on the same event. The channel sensitivity analysis indicates that considerable attention should be given to these parameters since errors in their estimation can cause considerable differences in estimates of sediment yield. Since these parameters are usually guided by calibration within physically reasonable bounds, measured sediment yields and hydrographs or concentration records are required.

### 8.5.3 Correlation in Simulated Runs

To help assess the required spatial and temporal design for the water discharge gaging stations in the entire watershed, correlations were determined as to how the discharge varies in space and time. The available discharge records along the main channel are such that they are inadequate in providing the data necessary to make such correlations on a basis any finer than hourly. Since most of the events are less than a day in length, this information is important. Thus, in order to provide information for such correlations, the runoff results from the 100-year storm for the entire watershed were substituted for actual data. These hydrographs are simulated for the downstream end of the watershed (channel 1 in the simulation model) and a point further upstream (channel 5 in the model). These points correspond to the U.S. Geological Survey gaging station at Traer and Lincoln, respectively. The hydrographs are presented in Figures 8.7 to 8.10.

Autocorrelations and lagged cross-correlations were made for the hydrographs. The lag time was varied to determine how the discharge at different time intervals is correlated. This was done to help assess the time increment that would be most useful for taking readings. For example, if readings are taken at highly correlated time intervals, little information is gained by each and excessive data are collected. However, if readings are recorded at intervals that have very low correlation, the data is too sparse. Results are shown in Figures 8.11, 8.12, and 8.13. Interestingly enough, the time increment for a 0.8 correlation is on the order of one hour for the two and three hour storms. This value is similar to that interpolated from the

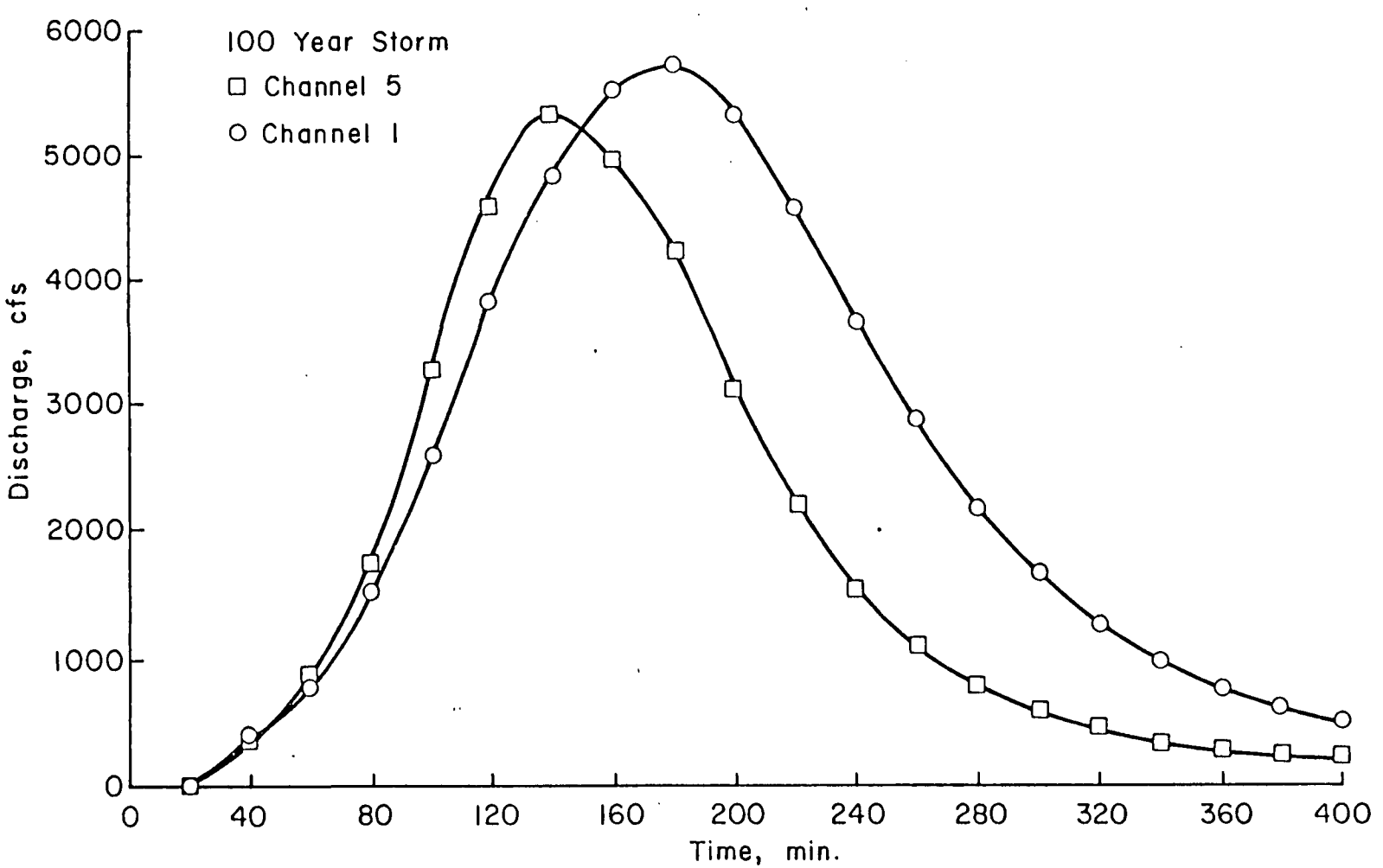


Figure 8.7. Simulated hydrographs for 2 hour, 100 year storm. (Time is real time.)

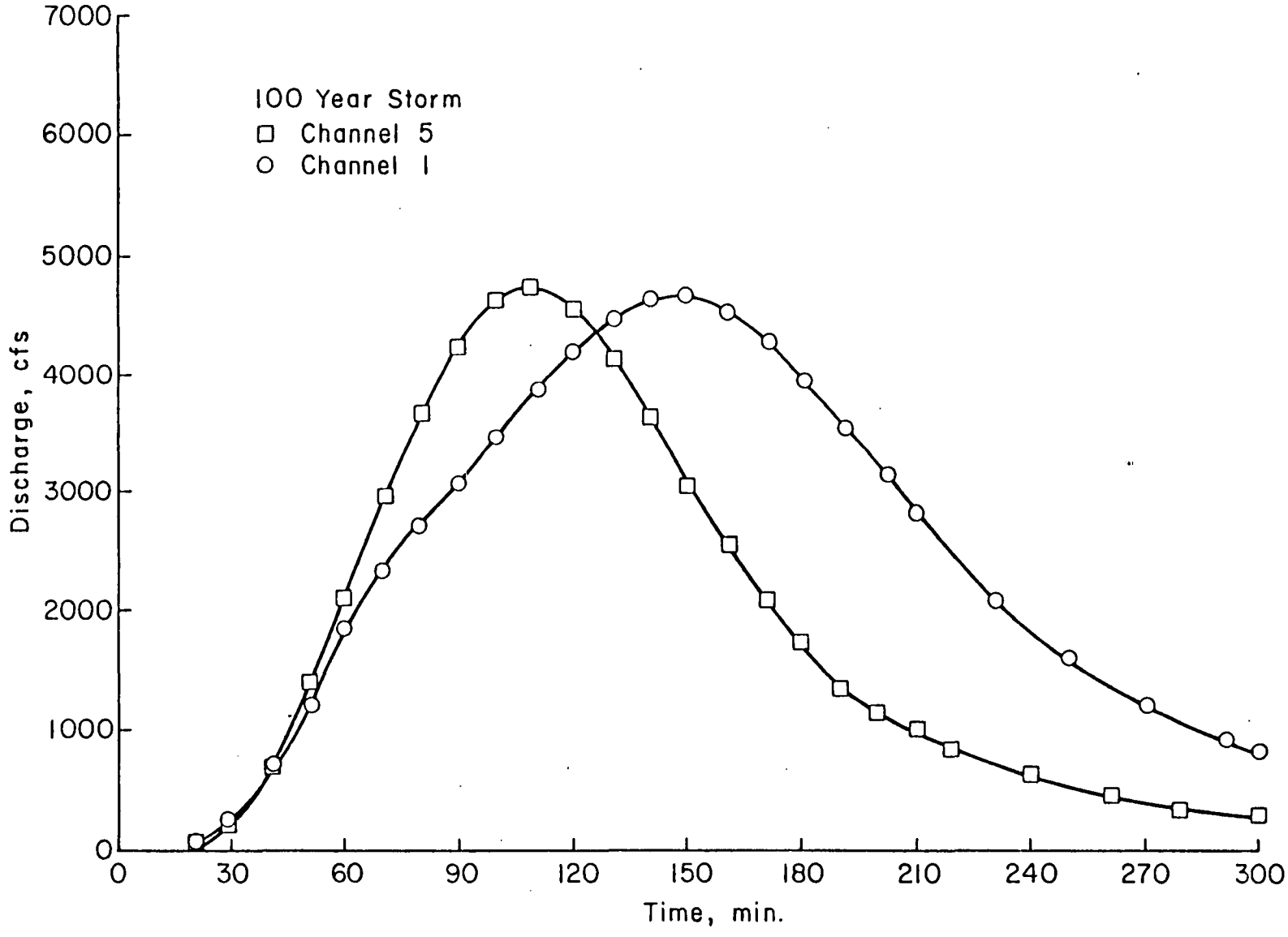


Figure 8.8. Simulated hydrographs for 1 hour, 100 year storm. (Time is real time.)

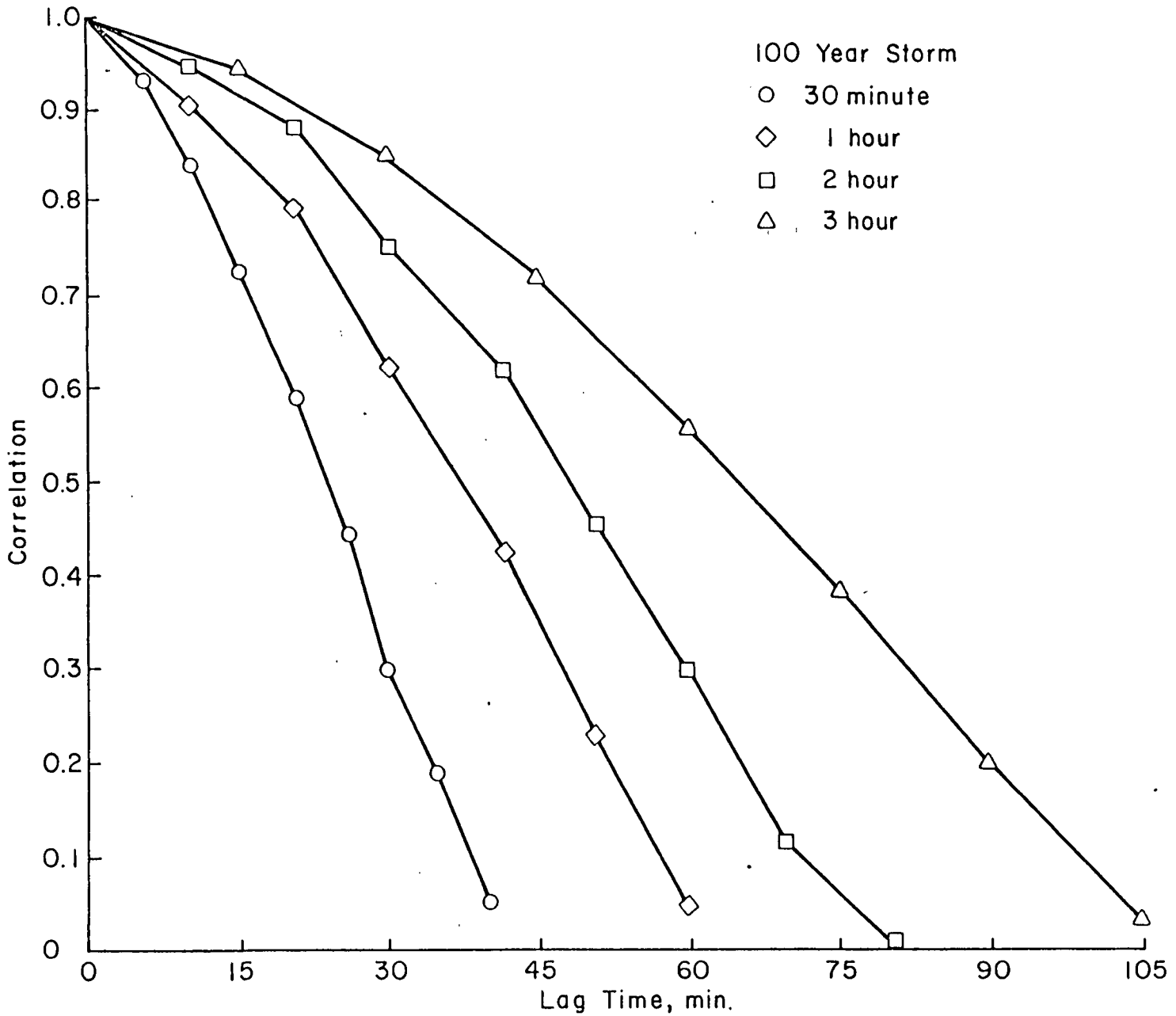


Figure 8.9. Autocorrelation for channel 5.

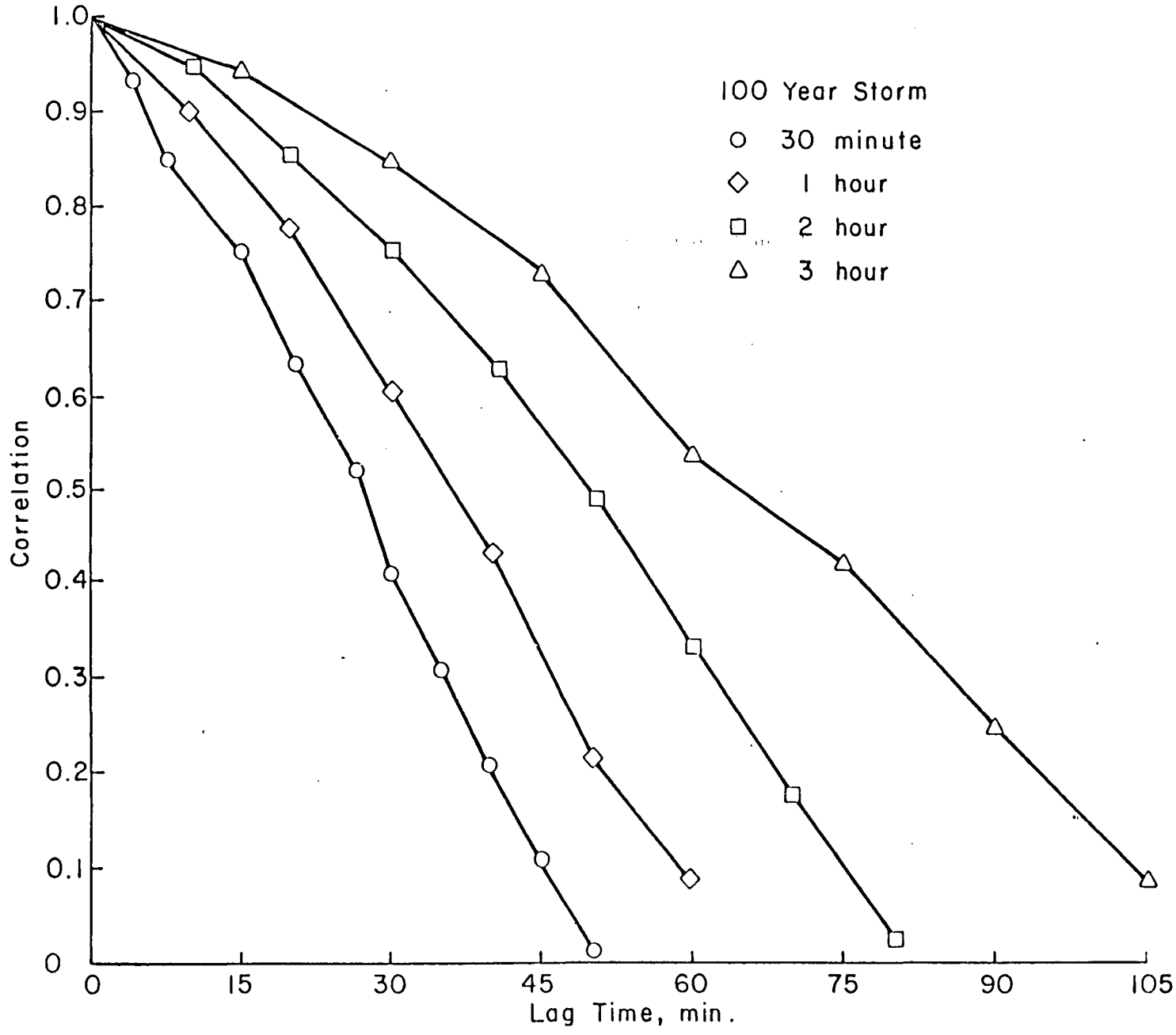


Figure 8.10. Autocorrelation for channel 1.

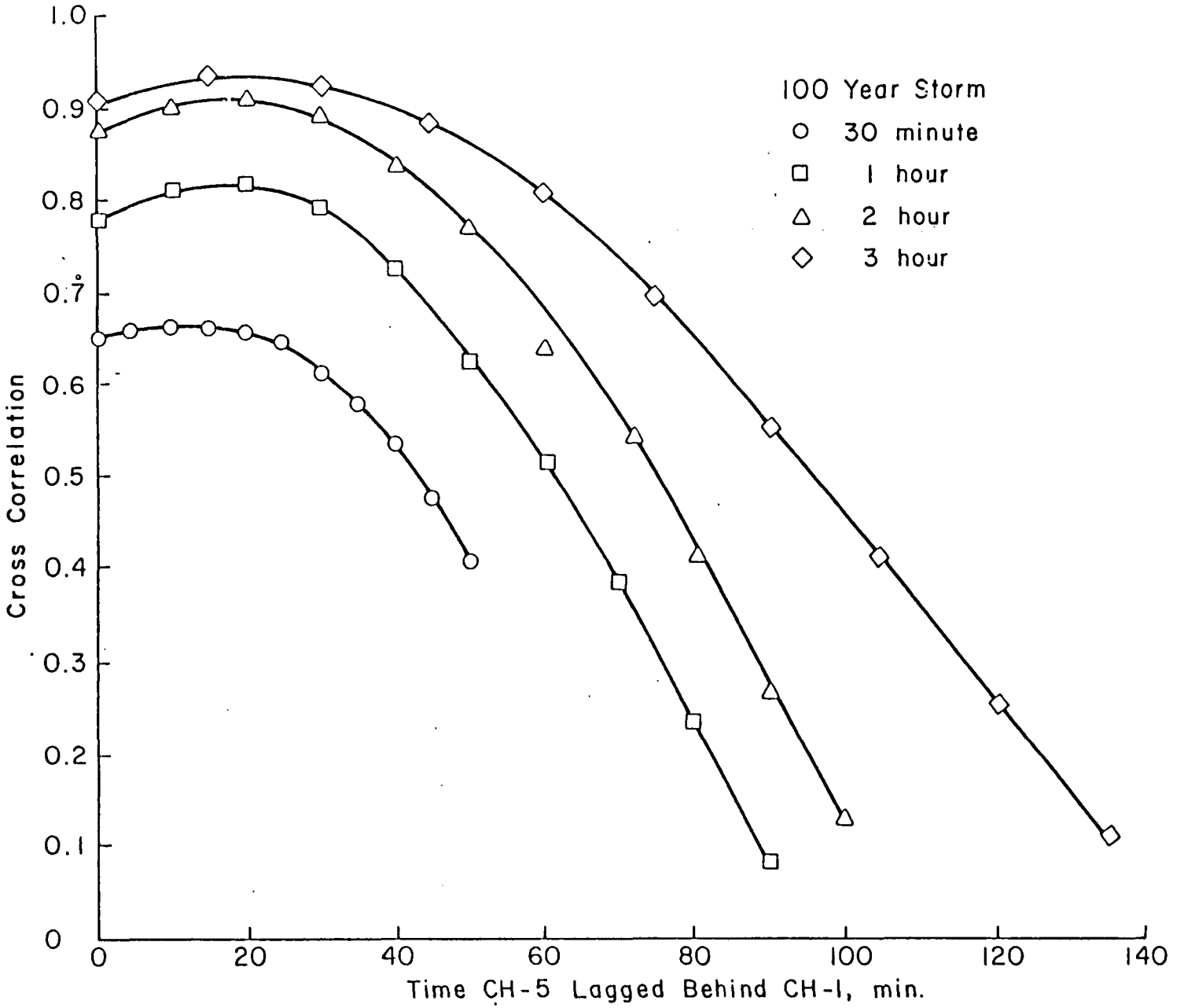


Figure 8.11. Lagged cross-correlation of simulated hydrographs.

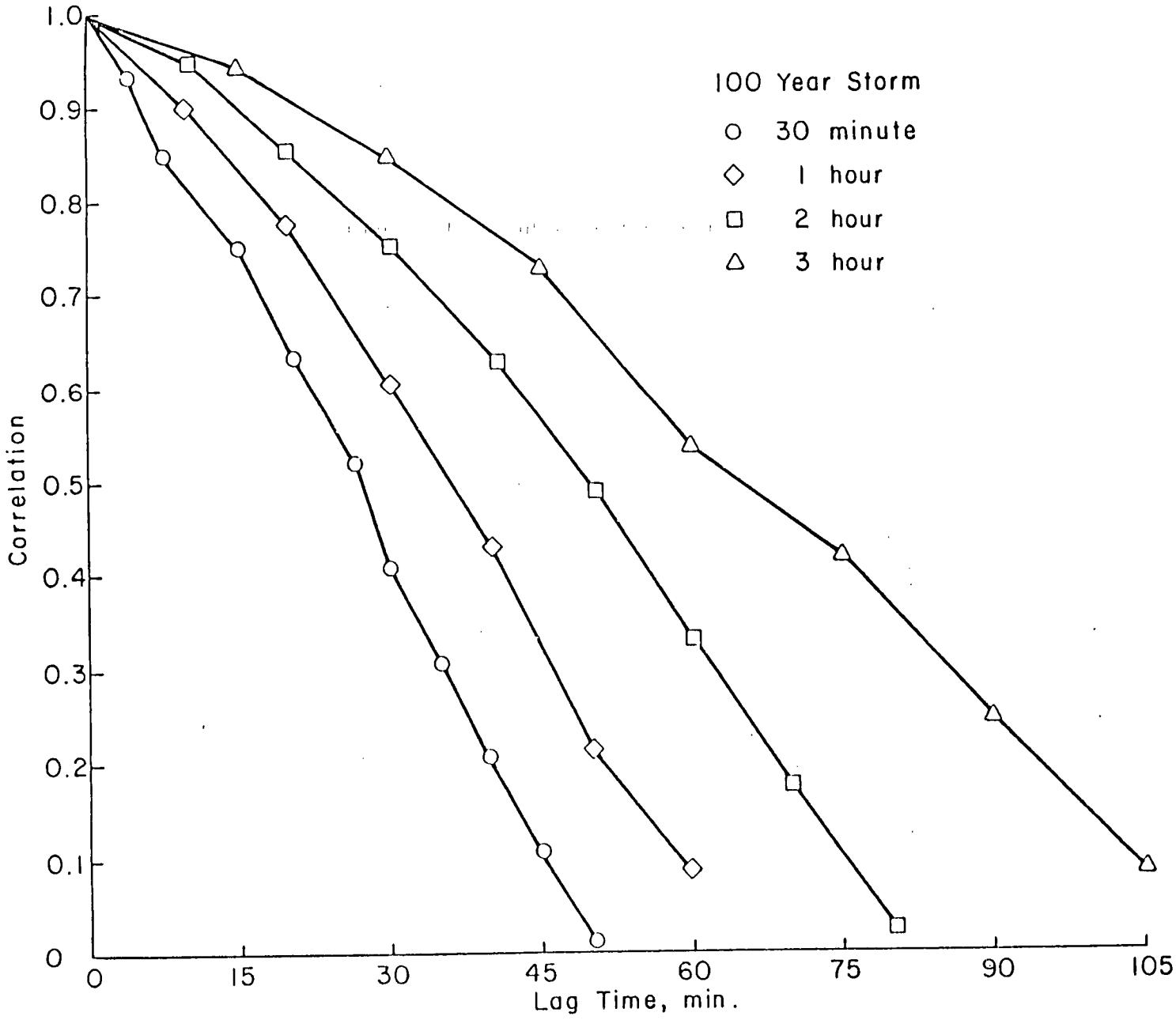


Figure 8.12. Autocorrelation for channel 1.

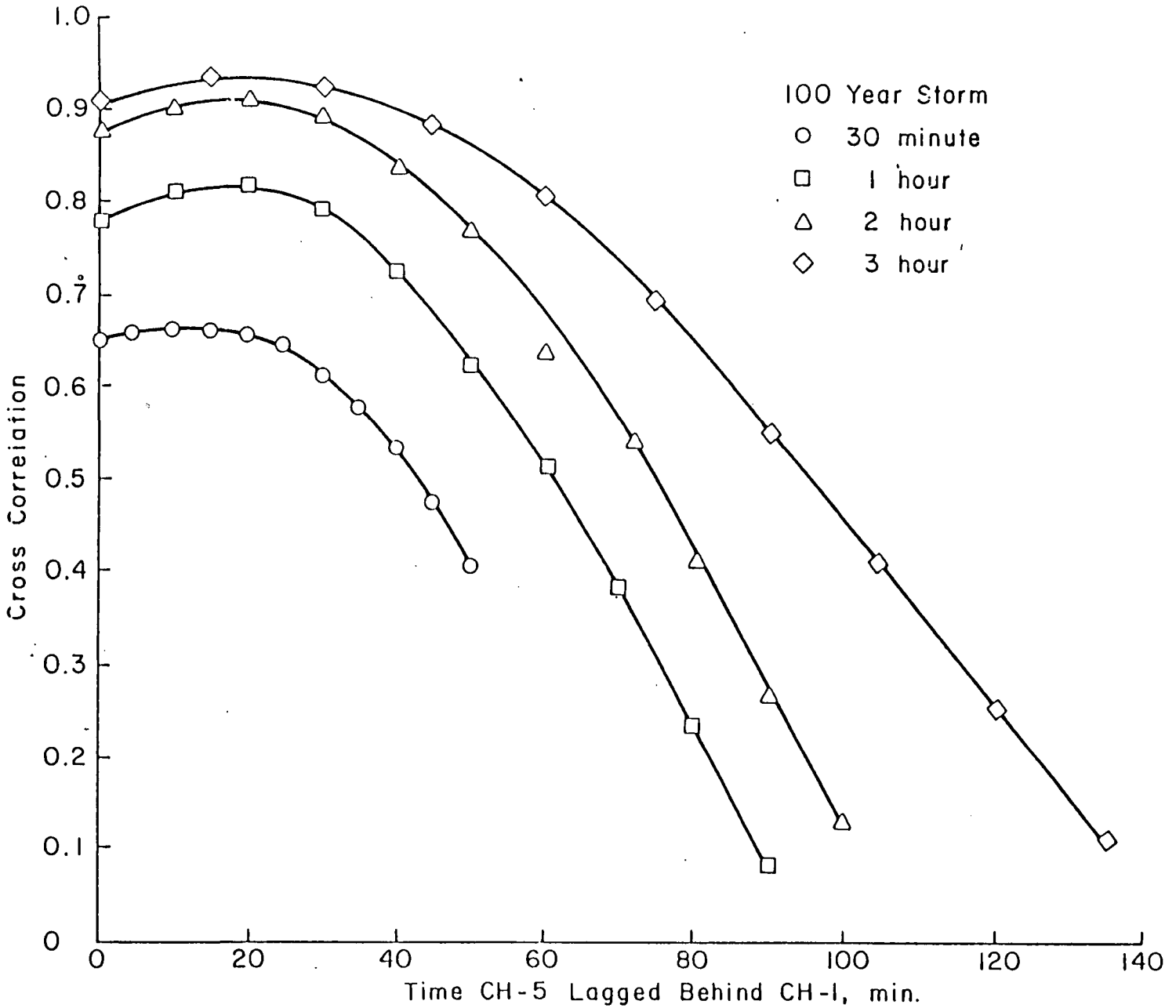


Figure 8.13. Lagged cross-correlation of simulated hydrographs.

daily discharge correlograms previously shown.

Similar autocorrelation analysis was performed on the sediment hydrographs (Figures 8.14 to 8.17) for channels 1 and 5. The results of the analysis in the form of correlograms appear in Figures 8.18 and 8.19. The correlation is similar to that performed for water hdyrographs indicating that a similar sampling frequency may be used for both water and sediment.

As stated before, there should be an upper and lower "correlation band" where sample timing and station spacing occurs. The upper correlation may be about 0.8. The lower correlation can be estimated using statistical techniques. Using a "t" test, the value of correlation below which there is no significance can be calculated. At the 95 percent level of significance, the limiting values of the correlation coefficients range between 0.44 for the 30 minute storm with ten time lags and 0.31 for the three hour storm with no time lag. To maintain correlation, the readings should be taken at some increment that provides a correlation greater than 0.44. The 30 minute storm provides a basis for design of the gaging system because this type of short duration-high intensity storm causes high discharges which in turn may result in large sediment and nonpoint pollutant yield. This will result in more data being taken for longer storms, but it may not be adequate to design the system for longer storms and then collect poor data for important short storms. The system should be designed with higher correlation than the lower limit calculated so that bad data can be identified using nearby stations or data gaps filled if a station malfunctions.

## 8.6 Summary

Use of physical process models can aid in the design and analysis of data collection systems. Process models can be used as a basis for identifying data gaps and checking data quality. They can also be used to simulate data that can be utilized in correlation analyses and design modification. Use of models in this fashion allows a more efficient, better conceived collection network. Model results indicate that:

1. The math model can be used to estimate water discharge from the small and medium sized watersheds,
2. Data is transferable between sites,
3. Sampling intervals are reasonable for the watershed stage recorders,
4. Flood peaks may be higher at the watershed mouth than previously

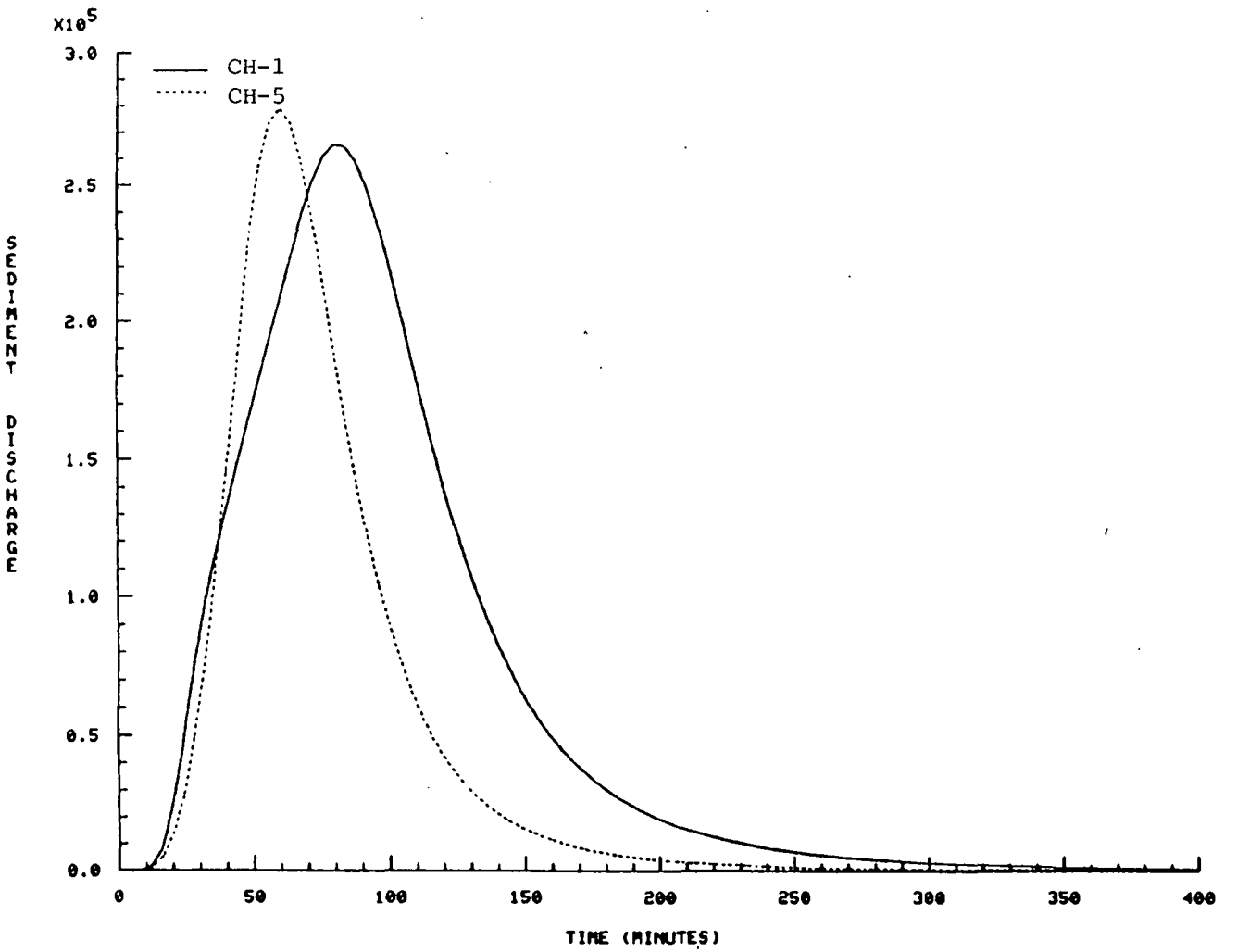


Figure 8.14. Simulated sediment hydrographs for the 30 minute, 100 year storm.

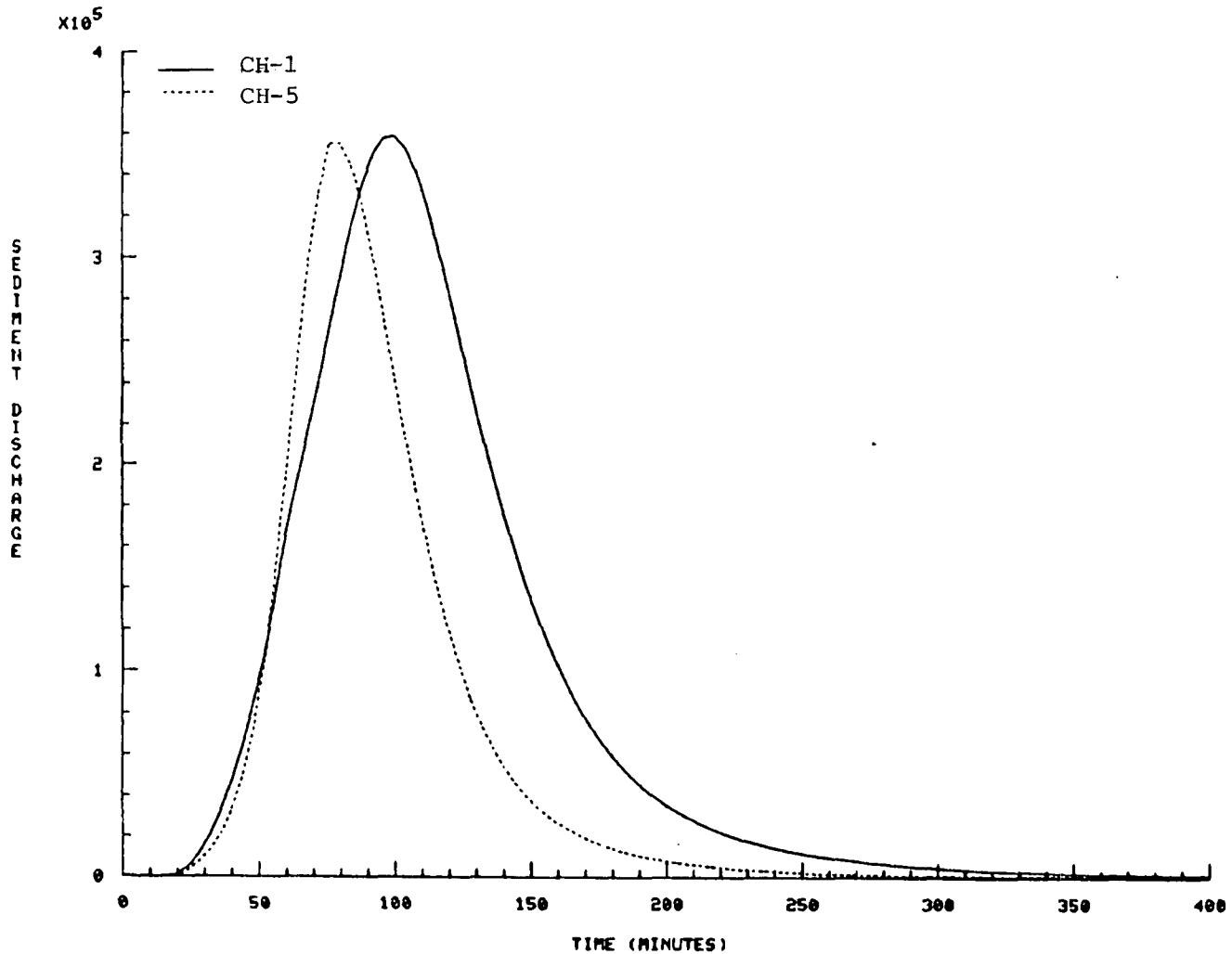


Figure 8.15. Simulated sediment hydrographs for the 1 hour, 100 year storm.

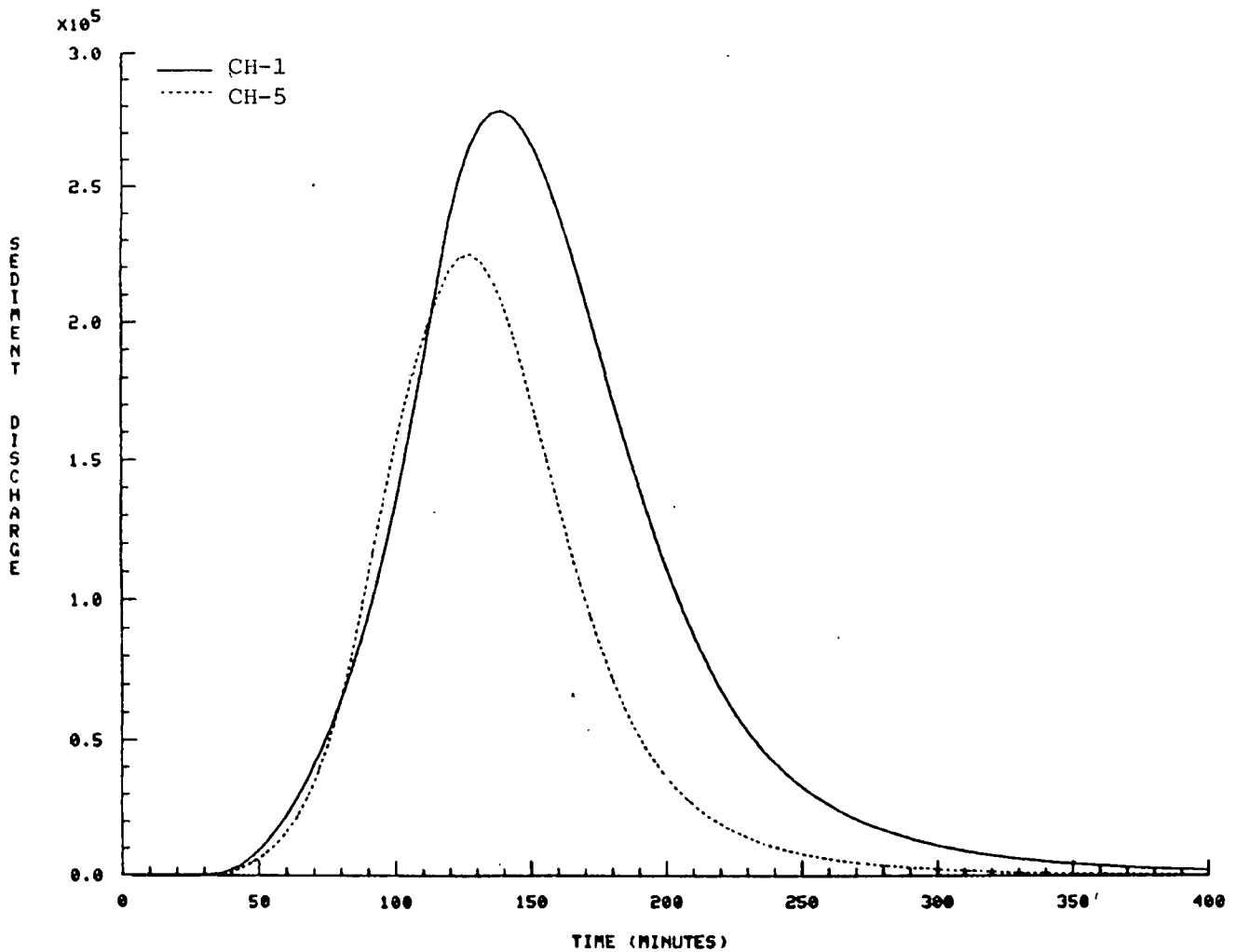


Figure 8.16. Simulated sediment hydrographs for the 2 hour, 100 year storm.

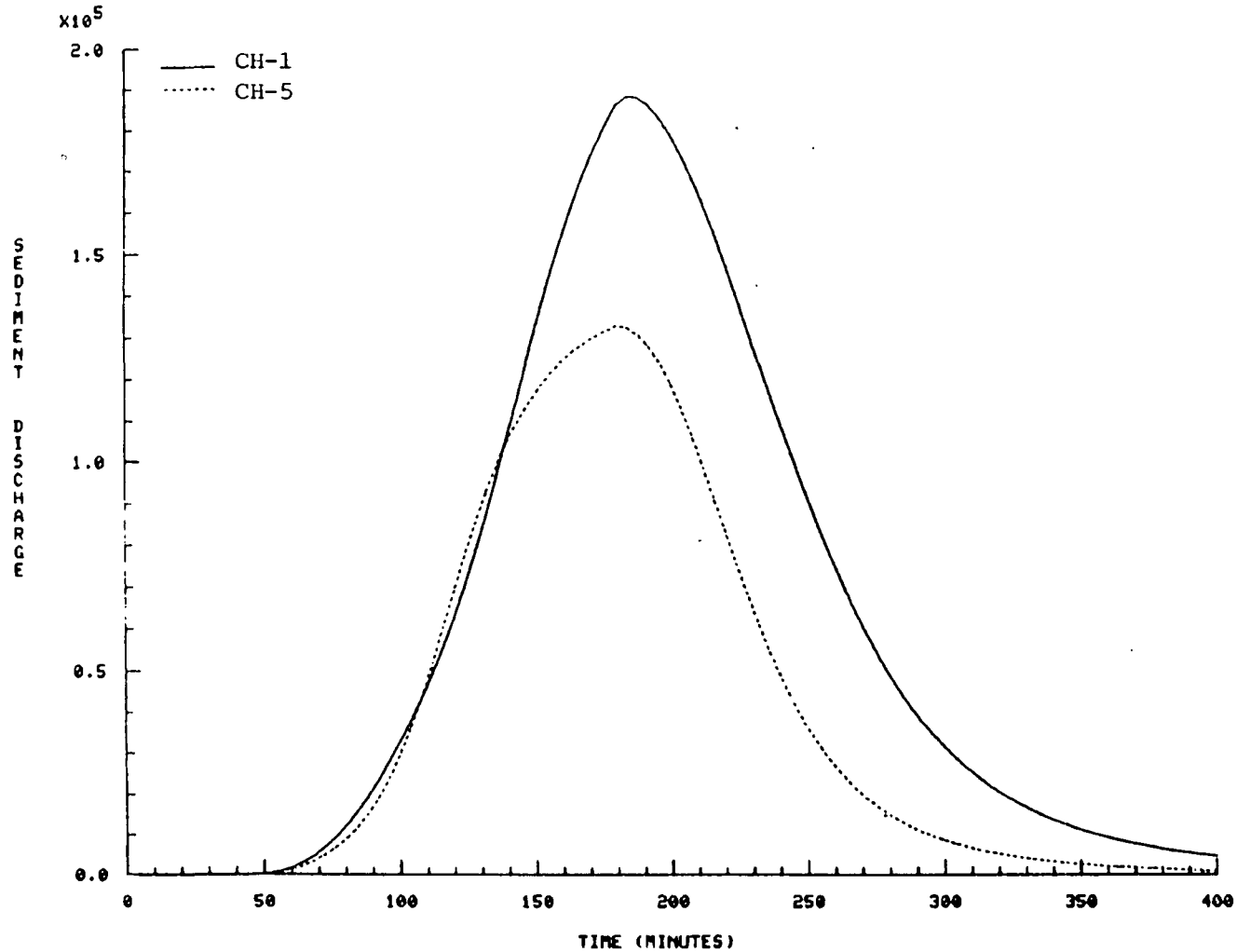


Figure 8.17. Simulated sediment hydrographs for the 3 hour, 100 year storm.

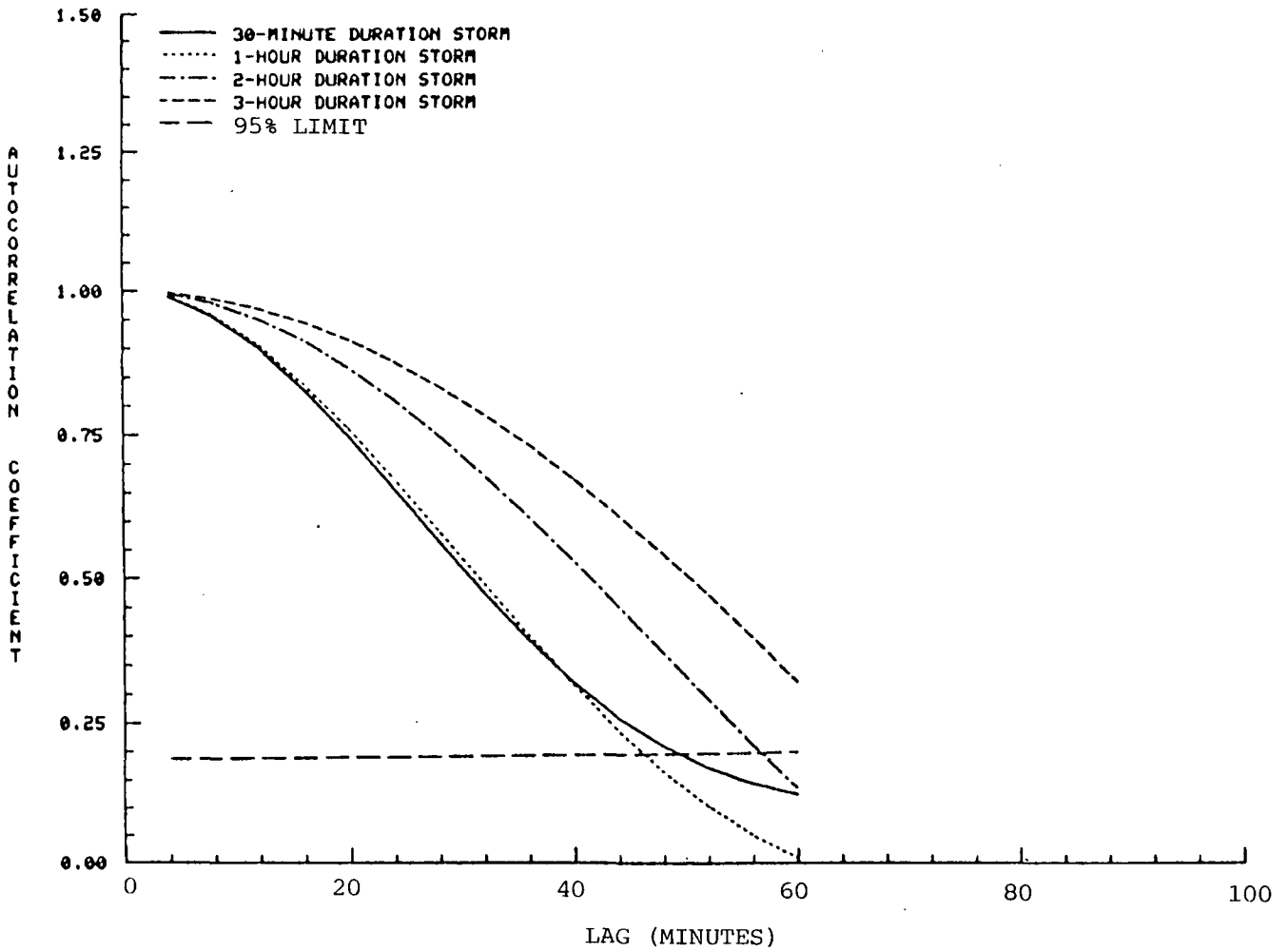


Figure 8.18. Autocorrelogram for channel 5 sediment discharge.

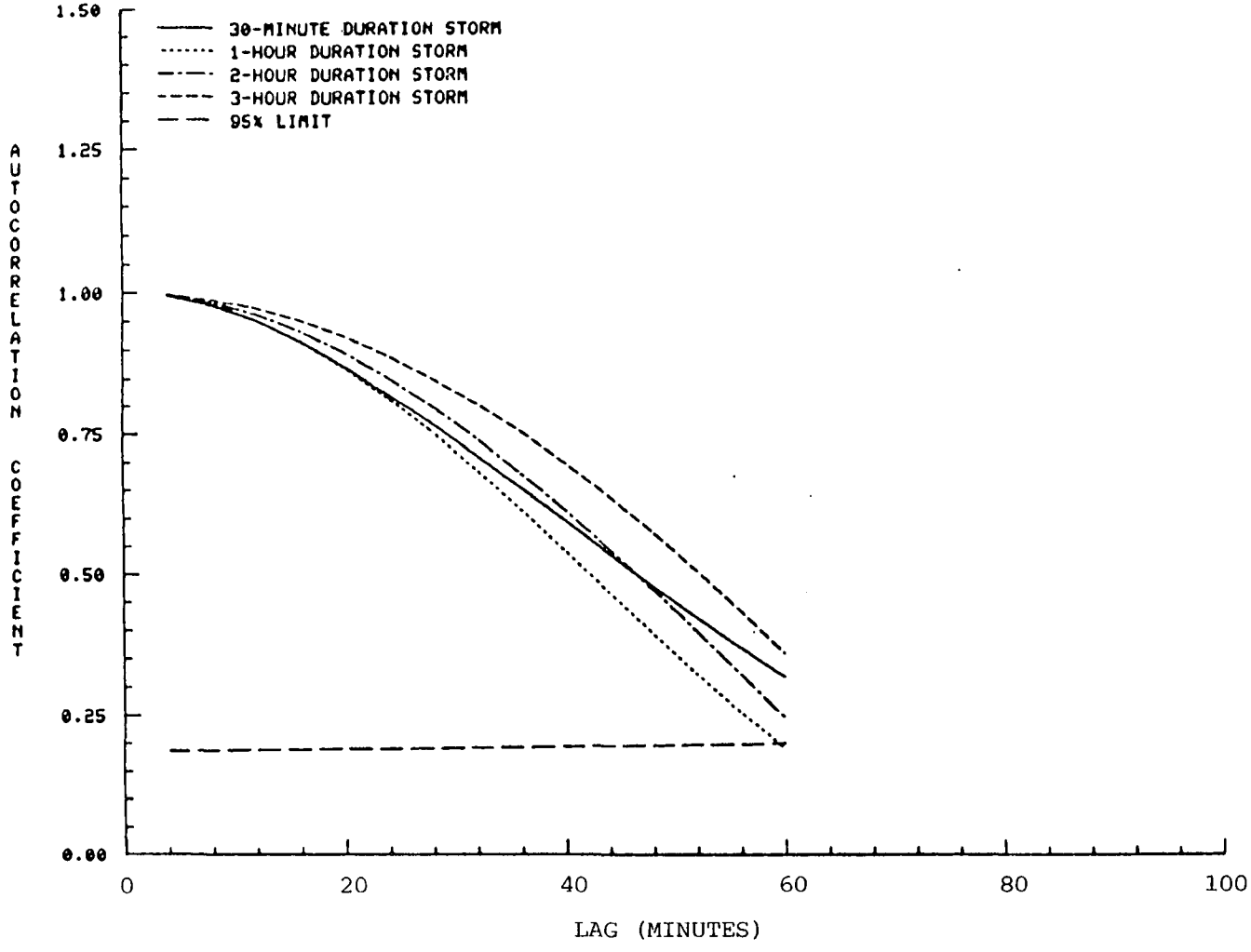


Figure 8.19. Autocorrelogram for channel 1 sediment discharge.

recorded,

- Sampling intervals on U.S. Geological Survey gages should be no longer than one hour and preferable 30 minutes for smaller events, and
- A thirty minute storm may aid in designing future measurement installations.

## eferences

ield, D.M., 1963, "Rainfall Frequency Atlas of the United States for ıration from 30 Minutes to 24 Hours and Return Periods from 1 to 100 ears," Tech. Paper No. 40, U.S. Weather Bureau.

n, H.P., 1978, "Development and Testing of Mathematical Models as anagement Tools for Agricultural Non-Point Pollution Control," for epartment of Agricultural Engineering, Iowa State University, Ames.

M., D.B. Simons, W.T. Fullerton, K.G. Eggert, and B.E. Sprank, 1979, Simulation of Water Runoff and Sediment Yield from a System of Multiple atersheds," XVIII Congress International Association for Hydraulic esearch, Cagliani, Italy.